GREENHOUSE GASES – EMISSION, MEASUREMENT AND MANAGEMENT

Edited by **Guoxiang Liu**

INTECHWEB.ORG

Greenhouse Gases – Emission, Measurement and Management
Edited by Guoxiang Liu

Published by InTech
Janeza Trdine 9, 51000 Rijeka, Croatia

Publishing Process Manager Maja Bozicevic
Technical Editor Teodora Smiljanic
Cover Designer InTech Design Team

First published March, 2012
Printed in Croatia

A free online edition of this book is available at www.intechopen.com
Additional hard copies can be obtained from orders@intechweb.org

Greenhouse Gases – Emission, Measurement and Management, Edited by Guoxiang Liu
p. cm.
ISBN 978-953-51-0323-3

Contents

Preface

Greenhouse gases, such as carbon dioxide, nitrous oxide, methane, and ozone, play an important role in balancing the temperature of the Earth's surface by absorbing and emitting radiation within the thermal infrared range from the source. However, with the enormous burning of fossil fuels from the industrial revolution, the concentration of greenhouse gases in the atmosphere has greatly increased. The increase has most likely caused serious issues such as global warming and climate change. Such issues urgently request strategies to reduce greenhouse gas emissions to the atmosphere. The main strategies include clean and renewable energy development, efficient energy utilization, transforming greenhouse gases to nongreenhouse gases/compounds, and capturing and storing greenhouse gases underground.

The book entitled Greenhouse Gases - Emission, Measurement and Management contains two parts, a total of 22 chapters. The first 12 chapters (Part 1) discuss the emissions of greenhouse gases, which cover the sources, measurements, and analysis. The last ten chapters (Part 2) cover the effects and management of greenhouse gases, which contain climate changes related to local and global effects, arctic sea ice decline, and environmental performance.

I would like to thank all of authors for their significant contributions on each chapter, providing high-quality information to share with worldwide colleagues. I also want to thank the book managers, Maja Bozicevic and Viktorija Zgela, for their help during the entire publication process.

Guoxiang Liu, Ph.D.
Energy & Environmental Research Center,
University of North Dakota,
USA

Part 1

Greenhouse Gases Emission and Measurement

1

Emissions of Nitrous Oxide (N_2O) and Di-Nitrogen (N_2) from the Agricultural Landscapes, Sources, Sinks, and Factors Affecting N_2O and N_2 Ratios

M. Zaman, M.L. Nguyen, M. Šimek, S. Nawaz,
M.J. Khan, M.N. Babar and S. Zaman
Ballance Agri-Nutrients Limited, Tauranga,
New Zealand

1. Introduction

Nitrous oxide (N_2O) is one of the key greenhouse and ozone (O_3) depleting gas, constituting 7% of the anthropogenic greenhouse effect. On a molecular basis, N_2O has 310 and 16 times higher global warming potential than that of CO_2 and CH_4 respectively over a 100-year period. To develop mitigation tools for N_2O emissions, it is imperative to understand the processes of nitrogen (N) transformation and N_2O and di-nitrogen (N_2) production in soils as influenced by different land uses, management and environmental conditions. The aim of our chapter is to examine the current information and understanding of the sources of N_2O and N_2 production and the factors affecting N_2O:N_2 ratio from the agricultural landscapes. Nitrous oxide concentration has increased by 20% from 270 ppbv since 1750 to a current level of 322 ppbv and continues to increase currently by 0.3% per year. Intensification of agricultural and human activities, such as the increased use of synthetic fertilizer (103 M ton of N worldwide in 2010), increasing human population and changes in their diet, inefficient use of irrigation water, increased crop production, deposition of animal excreta (urine + dung) from grazing animals, excessive application rates of farm effluents and animal manures to croplands and pastures, and management practices that enhance soil organic N mineralization and C decomposition including cultivation, residues removal or burning, and following no crop rotation are to be blamed for the increased N_2O emissions of 17.7 T g of N per year to the atmosphere. This book chapter focuses on the following sub-sections including nitrogen transformations, processes of N_2O and N_2 production across the agricultural landscape, challenges in N_2O measurements and estimates across the agricultural landscape, factors affecting N_2O and N_2 emissions and possible mitigating options, conclusions and references.

2. Nitrogen transformations

Nitrogen is an essential nutrient controlling the diversity, dynamics, and functioning of many terrestrial, freshwater and marine ecosystems. Agricultural ecosystems rely on N

inputs from a variety of sources including synthetic chemical fertilizers, predominantly urea which accounts for more than 50% of the total world N consumption, organic wastes (farm dairy effluent, animal excreta, plant residues and sewage sludge) and atmosphere (biological fixation of atmospheric N through symbiotic and non-symbiotic microorganisms) to sustain productivity. A detailed description of N cycling in agricultural ecosystems is beyond the scope of this chapter and for details on N transformations, N dynamics, sources of N inputs, and losses, the readers are referred to research papers, articles and review written by these authors (Ledgard et al., 1999; Saggar et al., 2004b, 2005, 2009, 2011; deKlein & Eckard 2008; Ledgard & Luo 2008; Luo et al., 2010); however a brief description of the various microbial and enzymatic processes involved in N cycling is given below.

2.1 A brief biochemistry of N mineralization

Nitrogen transformations within soil-plant-water and atmospheric systems refer to N cycling. As will be discussed in section 3, N cycling provides precursors like ammonium (NH_4^+) and nitrate (NO_3^-) for the production of N_2O and N_2 in soil. A simple schematic diagram of the N inputs, losses and transformation processes is presented in Fig. 1 The key N transformation processes within soil, plant and atmospheric systems include mineralization (gross and net), immobilization, nitrification (gross and net), denitrification, ammonia (NH_3) volatilization, NH_4^+ fixation and NO_3^- leaching. The first four processes (i.e. mineralization, immobilization, nitrification and denitrification) are of microbial and enzymatic origin (biotic), while the last three (i.e. NH_3 volatilization, NH_4^+ fixation and NO_3^- leaching) involve only chemical and physical processes (abiotic). Nitrogen mineralization is a sequence of microbial and enzymatic activities which involves the conversion of organic N (eg. protein, amino acids, amines, amides, urea, chitin and amino sugars) into an inorganic form of N (mainly NH_4^+), which then serves as a substrate for a diverse group of micro-organisms and for nitrification (Zaman et al., 1999 a, b; 2004; Zaman & Change, 2004). The

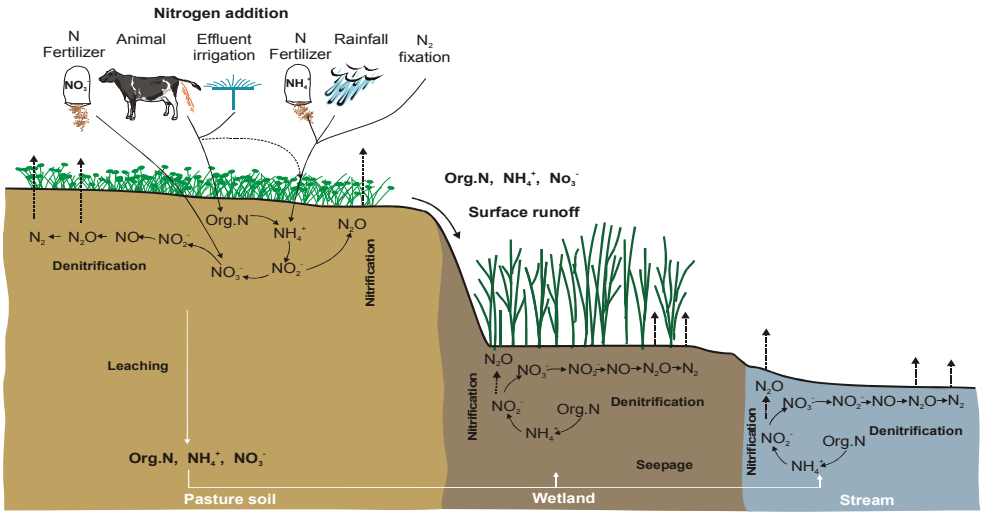

Fig. 1. N inputs, losses and transformation processes across the agricultural landscape (Zaman et al., 2008b).

immobilization process is the opposite of mineralization, where mineral N (NH_4^+ and NO_3^-) and even organic N (amino acids) are consumed by a diverse group of microorganisms to synthesize their protein and grow in number. These diverse groups of microorganisms are mostly heterotrophic (consume organic C) bacteria, fungi, and actinomycete, which produce a wide variety of extracellular and intra-cellular enzymes (e.g. protease, deaminase and urease) in soil. They then carry out the hydrolysis of high molecular weight organic compounds like protein into low molecular weight organic compounds such as amino acids, as shown in Eq. 2.1.1

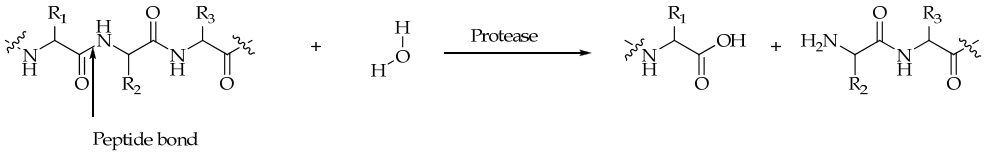

(2.1.1)

The low molecular weight organic compounds such as amino acids, amines and amides produced after proteolytic decomposition or after the application of organic residues or wastes are then subjected to microbial and enzymatic decomposition such as deamination which is carried out either by extracellular deaminase (Ladd & Jackson, 1982; Zaman et al., 1999 a, b) or by direct assimilation within the microbial cell (Barak et al., 1990; Barraclough, 1997). A large number of heterotrophic microorganisms are capable of carrying out the deamination of amino acids, both within and outside the microbial cell. Deaminases hydrolyse the NH_2-N attached to the α-C of an amino acid to NH_3 and CO_2. The amino acids are deaminated at different rates through four different reactions, depending on their side chains, as shown below in Eq. 2.1.2. Some amino acids are reported to be readily mineralized, while others take longer to mineralize (Alef & Kleiner, 1986).

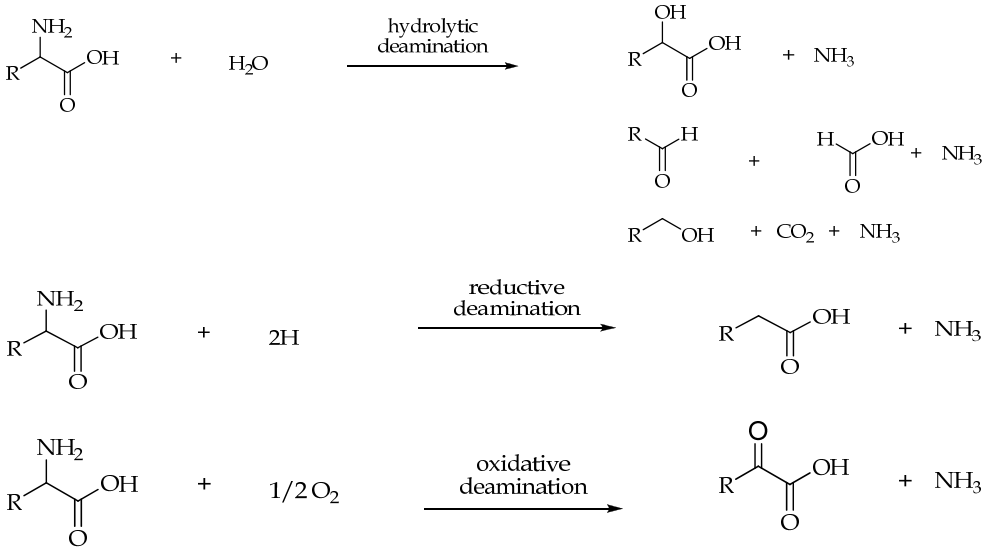

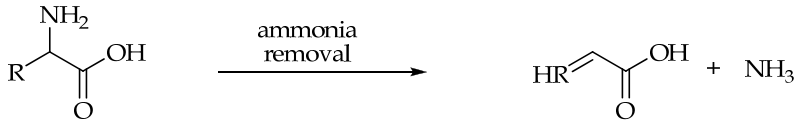

(2.1.2)

Whether an amino acid is used for an energy source by microorganisms or as a building block for protein synthesis depends on the available N and soluble organic C at the micro-site where the microbial reaction occurs (Mengel, 1996). After deamination has occurred within the cell, the removal of NH_4^+ is carried out by enzymes such as glutamate dehydrogenase and coenzyme nicotine adenine dinucleotide (NADH). Ammonium produced by deamination is always associated with the production of new microbial biomass, and the extent of NH_4^+ immobilization or accumulation in the soil depends on the micro-organism's C:N ratio (Mengel, 1996; Paul & Clark, 1996) and the available soil mineral N and organic C. The turnout of microbial biomass is reported to be fast and the new microbial biomass die after reaching a certain limit, thus serving as a substrate for enzymes and other groups of microorganisms. This turnover of microorganisms releases the NH_4^+ again. Thus the dead biomass, which is prone to biological decomposition (Jenkinson & Ladd, 1981), serves as the main source of NH_4^+ production in soil (Azam et al., 1986). The non-proteinaceous cell wall constituents of bacteria and fungi, such as amino sugar and chitin, are first depolymerised by chitinase to glucose amines. These are then attacked by kinases, and this process finally releases the NH_4^+ in soil as shown in Eq. 2.1.3.

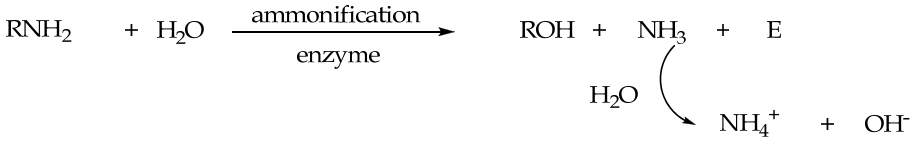

(2.1.3)

Similarly urea ($CO(NH_2)_2$, from (i) urine deposition of grazing animals, (ii) the application of urea fertilizer or (iii) from production of hydrolytic decomposition of proteinaceous materials in soil, undergoes fast hydrolysis (Zaman et al., 2008a & 2009) and the hydrolysis is usually completed within 1 to 2 days by urease enzymes. These ubiquitous enzymes are found in soils, many plants and plant litters (Freney & Black, 1988) and in most species of bacteria, yeast and fungi (Sumner, 1953). Urease catalyzes the hydrolysis of urea to NH_4^+ (Eq. 2.1.4) and carbamate ions, which result in the production of carbon dioxide (CO_2) and NH_4^+.

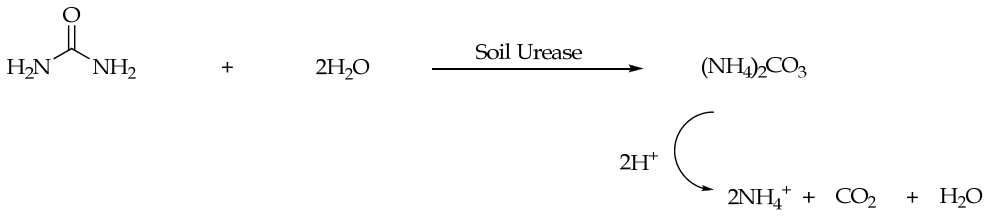

(2.1.4)

The active site of urease contains two-nickel (II) atoms, which are linked by a carbamate bridge. Two imidazole N atoms are bound to each Ni atom; a carboxylate group and a water molecule fill the remaining coordination site of the metal ion. The ability to hydrolyze urea is found to vary from 17 to 70% for soil bacteria and from 78 to 98% for soil fungi (Lloyd & Sheaffe, 1973; Roberge & Knowles, 1967). Although soil urease is considered to be of microbial origin (Skujins, 1976), there is evidence to suggest that some urease activity may be derived from plants (Frankenberger & Tabatabai, 1982). However, there is no direct evidence for the production of urease by plant roots (Estermann & McLaren, 1961).

3. Processes of N_2O and N_2 production across the agricultural landscape

Gaseous N emissions from the agricultural landscape (arable, pasture and wetland soils) occur as NH_3, nitric oxide (NO also called nitrogen oxide), nitrogen dioxide (NO_2), N_2O and N_2. Quantifying N_2O emission is of particular interest to those countries, which are signatories to the Kyoto Protocol, since it is one of the key greenhouse gases constituting 7% of the anthropogenic greenhouse effect. On a molecular basis, N_2O has 310 and 16 times higher global warming potential than that of CO_2 and methane (CH_4) respectively over a 100-year period (IPCC, 2007). The global atmospheric concentration of N_2O has increased from 270±7 in the pre-industrial-period (1750) to a current level of 322 ppbv representing a 20% increase. Over the last two decades a nearly linear increase of 0.26% in the concentration of N_2O has been measured (Saggar et al., 2009). Moreover, due to its relative stability, (150 years) after emission from the soil surface and transport through the troposphere, N_2O acts as a source of NO in the stratosphere, and thus indirectly accelerates depletion of ozone (O_3), a substance that protects the biosphere from harmful ultraviolet (UV) radiation (Crutzen, 1981; Duxbury, 1994). The total estimated emissions of N_2O are about 17.7 Tg N per year, but there are large uncertainty ranges in each of the individual sources. About 70% of N_2O emissions come from the bacterial breakdown of N in soils and in the oceans. Globally, soils in areas of natural vegetation, especially in the tropics, and the oceans account for N_2O emissions of about 6.6 and 3.8 Tg N per year respectively; while human activities account for the remaining 30% of N_2O emissions, or about 6.7 Tg N per year (Denman, 2007). Factors blamed for the increased N_2O emissions of 17.7 T g of N per year to the atmosphere include; a rapid increase in human population (according to the latest United Nations population estimates, 77 million more people each year are being added to the current world population of 6.98 billion), intensification of agricultural and human activities, such as the increased use of synthetic fertilizer (103 million ton of N worldwide in 2010) (IFA 2011), inefficient use of irrigation water and N fertilizers (both synthetic and organic), increased grassland areas for livestock which cover 117 million km^2 of vegetated lands that provide forage for over 1800 million livestock units and wildlife (World Resources Institute 2000). The other factors include increased animal stocking rates (>3 cows per ha) and intensive gazing, which results in deposition of huge amounts of N via animal excreta (urine + dung), farm management practices that enhance soil organic N mineralization and decomposition of organic C (deep cultivation, crop residues removal or burning, and following no crop rotation) and the increased consumption of dairy products worldwide especially in fast growing economies like China and India (Robertson et al., 1989; Duxbury et al., 1993; Šimek & Cooper, 2001; Rochester, 2003; Denman et al., 2007; IPCC, 2010; Zaman & Blennerhassett., 2010; Zaman & Nguyen., 2010). Nitrous oxide can also be produced during nitric acid production and fossil fuel combustion, but the amount of N_2O

from fossil fuel varies with the fuel type and technology. Fossil fuel combustion and industrial processes are responsible for N_2O emissions of around 0.7 Tg N per year (Denman, 2007). Other important sources include human sewage and the burning of biomass and biofuels.

Across the agricultural landscape, several microbial processes can occur simultaneously to produce harmful N_2O and non-greenhouse N_2 in soils (pasture and arable) and sediments (drain, ditch, wetland and stream). These microbial processes are regulated by various soil, environmental and management factors, therefore making it difficult to control the rates of N_2O and N_2 production and their ratios (Paul & Beauchamp, 1989; Stevens et al., 1997; Zaman et al., 2007, 2008 b,c; Zaman & Nguyen, 2010). The aim of our review is to examine current information and understanding of the sources of N_2O and N_2 production and factors affecting N_2O:N_2 ratio in agricultural landscape, to enable management practices to be devised that minimize N losses as N_2O emission to the atmosphere.

Soil microbial processes, which account for major N_2O production include; nitrification (Inubushi et al., 1996), denitrification (Tiedje, 1988; Firestone & Davidson, 1989; Smith, 1990; Cavigelli & Robertson, 2001) and dissimilatory NO_3^- reduction to NH_4^+ (DNRA) (Silver et al., 2001). These three microbial processes may occur in soils and sediments across the landscape depending on the physical (moisture contents or O_2 level) and chemical conditions [N form (i.e. NH_4^+ and NO_3^-), pH and C contents] in their micro-sites. Details of each of these processes are given below:

3.1 Nitrification

Autotrophic nitrification, a strictly aerobic process, is carried by chemolitho-autotrophic bacteria which use O_2 as a terminal electron acceptor. In the first step, NH_4^+ is oxidized to NO_2^- by ammonia oxidizing species of the genus *Nitrosomonas,* while in the second step, NO_2^- oxidation to NO_3^- is facilitated by *Nitrobacter* and *Nitrococcus* (Bremner & Blackmer, 1981; Watson et al. 1981) as shown in Eq. 3.1.1 Other genera including *Nitrosococus, Nitrosospira* and subgenera *Nitrosobolus, and Nitrosovibrio* also have the ability to autotrophically oxidize NH_3 to NO_2^-:

$$2NH_4^+ + 3O_2 \xrightarrow{\text{Nitrosomonas}} 2NO_2^- + 2H_2O + 4H^+$$

$$NO_2^- \xrightarrow{\text{Nitrobacter}} 2\,NO_3^- \qquad (3.1.1)$$

In addition to NO_2^- production during the first stage of autotrophic nitrification, several intermediate and unstable compounds such as hydroxylamine (NH_2OH) and nitroxyl (NOH) are also formed. Ammonia oxidizers consume relatively large amounts of molecular O_2 during this first stage, causing anaerobic conditions in the microsites, which then lead to a reduction of NO_2^- to N_2O and N_2 (Poth & Focht, 1985; Firestone & Davidson, 1989; Zart & Bock, 1998; Colliver & Stephenson, 2000) as shown in Eq. 3.1.2.

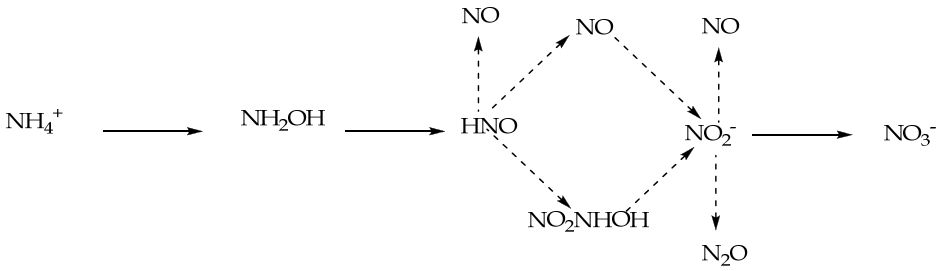

(3.1.2)

Broken lines show the unconfirmed pathways of the biological reaction.

Heterotrophic nitrification, the oxidation of reduced N compounds or NH_4^+ to NO_3^- in the presence of O_2 and organic C, can also produce N_2O from NO_2^- and typically occurs in acidic soils (Wood, 1990). However, high rates of heterotrophic nitrification relative to autotrophic nitrification have been measured in a riparian wetland soil with a pH close to 7, which was exposed to O_2 (Matheson et al., 2003). Production of N_2O via heterotrophic nitrification is poorly understood because autotrophic and heterotrophic nitrification can occur simultaneously in a given soil and it is difficult to separate the end products of these two processes without using ^{15}N tracers (Matheson et al., 2003). Sufficient soil O_2 levels [(optimum at water filled pore space (WFPS) of 60%)], adequate NH_4^+ concentrations, a favorable soil temperature above 5°C (optimum 25 to 35°C), and soil pH above 5 (optimum 7 to 9) are among the known soil and environmental conditions which control the rate of autotrophic nitrification (Linn & Doran 1984; Grundmann et al., 1995; Whitehead, 1995; Zaman et al., 1999a; Šimek., 2000; Zaman & Chang, 2004; Zaman et al., 2007; Saggar et al., 2009; Zaman et al., 2009; Zaman & Nguyen, 2010). Among these factors, NH_4^+ and O_2 concentrations are considered the most critical factors affecting autotrophic nitrification (Zaman et al., 2007). Thus autotrophic nitrification is expected to be a dominant N transformation process in well-drained pastoral or arable systems, where soils are oxygenated (at or around field capacity or at 60% WFPS) and NH_4^+ is abundant [(e.g., excreta deposition after animal grazing, after the application of organic wastes, and NH_4^+-based synthetic fertilizer like urea, di-ammonium phosphate (DAP), ammonium sulphate, and liquid ammonia or as a result of increased mineralization of soil organic N compounds)] (Zaman et al., 1999a,b; Zaman & Chang, 2004; Zaman et al., 2007; 2008a; 2009; Zaman & Nguyen 2010). However, nitrification can also occur in waterlogged areas at a slower rate where wetland vegetation releases O_2 from roots (Armstrong, 1964). At the sediment-plant root interface, nitrifying bacteria are supplied with O_2 from plants and NH_4^+ from the surrounding sediment. There is evidence to suggest that autotrophic denitrification can proceed at a pH around 4, because soil aggregates protect bacterial cells against nitrous acid toxicity (De Boer et al., 1991).

3.2 Denitrification

Denitrification is predominantly a microbial process by which NO_3^- and NO_2^- are reduced to N_2O and N_2 in a respiratory metabolism. During respiratory denitrification, denitrifiers couple reduction of N-oxides to oxidation of organic C under anaerobic conditions and

produce adenosine tri-phosphate (ATP) by phosphorylation (Firestone, 1982; Linn & Doran, 1984; Tiedje, 1988, Smith, 1990; Cavigelli & Robertson, 2001). Four different reductase enzymes are involved in a complete denitrification reaction. These enzymes are usually distributed in different microorganisms as shown in Eq. 3.2.1.

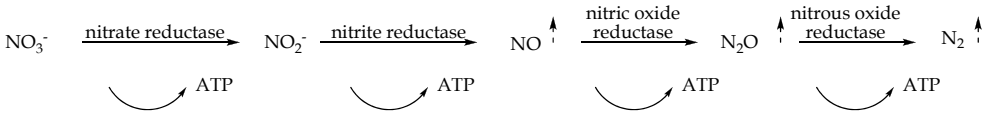

(3.2.1)

Denitrifiers are usually aerobic bacteria; however they prefer to use N-oxides at a low O_2 level (Tiedje, 1988). Biological denitrification thus requires; NO_3^- as a substrate (more than 2 mg NO_3^--N per kg of soil) as an electron acceptor, absence of O_2, which is related to a high soil moisture content >60% WFPS, available organic C as an electron donor, suitable soil pH, which generally ranges from 5 to 8 (optimum at 7) and a soil temperature range between 5 and 30 ^oC (optimum 25 ^oC) (Ryden & Lund, 1980; Ryden, 1983; Goodroad & Keeney, 1984; Scholefield et al., 1997; Barton et al., 1999; Swerts et al., 1997; Aulakh et al., 2001; Zaman et al., 2004; Zaman et al., 2007, 2008 b c, 2009; Zaman & Nguyen, 2010). However, the most critical factors are the NO_3^- concentrations, anaerobic conditions and the availability of soluble organic C (Zaman et al., 2007; 2008bc). Thus denitrification is expected to be an important N transformation process in areas where soils and sediments are subject to water logging (making them anaerobic), where they contain sufficient organic C and intercept inputs of NO_3^- or NO_2^- in groundwater or where there is excess nitrate after application of nitrate based fertilizers, or after nitrification (eg. 3.1.1). These areas include; urine patches in grazed pastures, where up to 1,000 kg N ha^{-1} can be found (Saggar et al., 2009; Zaman & Blennerhassett., 2010), riparian wetlands (Nguyen et al., 1999; Matheson et al., 2003), drains and ditches, and stream or river channels (Garcia-Ruiz et al., 1998; Bronson & Fillery, 1998; Mcmahon & Dennehy, 1999; Walker et al., 2002; Groffman et al., 2002; Zaman et al., 2008b&c, Zaman & Nguyen, 2010). However denitrification can also occur in less obviously waterlogged areas within the agricultural landscape due to the existence of anaerobic micro-sites such as in the center of soil aggregates (Parkin, 1987) or in areas of localized high O_2 consumption (hot spots), which are created by decaying organic C (Burton et al., 1999; Godde & Conrad, 2000; Khalil et al., 2002; Mosier et al., 2002). Depending on soil physical and chemical conditions, other processes like chemo-denitrification can result in substantial production of N_2O.

3.3 Dissimilatory NO_3^- reduction to NH_4^+ (DNRA)

DNRA is the 3rd biological process, which is known to produce considerable amounts of N_2O as a byproduct under anaerobic conditions (Tiedje, 1988; Silver et al., 2001) as shown in Eq. 3.3.1

Conditions required for DNRA are similar to those required for denitrification and besides anaerobiosis include available NO_3^- and organic C (Tiedje, 1988). DNRA has been found in anaerobic sludge and animal rumen, and also in lake littoral sediments, riparian wetland soil (Matheson et al., 2002) and tropical forest soils (Silver et al., 2001). Matheson et al., (2002) has also shown that DNRA is likely to be a more important process of NO_3^-

transformation relative to denitrification under more reducing (O_2 limited) conditions, since the microbes capable of DNRA are fermentative, and are able to grow in the absence of O_2 contrary to predominantly aerobic denitrifiers. Silver et al. (2001) reported that in upland tropical forest soils, DNRA accounted for 75% of the turnover of the NO_3^- pool and N_2O emission rates via DNRA, were 3 times greater than the combined N_2O and N_2 fluxes from nitrification and denitrification. Within the agricultural landscape, DNRA is likely to be an important N transformation process in wetland or stream sediments but may also occur in slow-draining upland soils where anaerobic sites are prevalent.

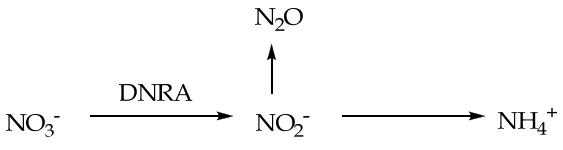

(3.3.1)

As discussed above, while nitrification and DNRA produce only N_2O, denitrification produces both N_2O and N_2. Stevens and Laughlin (1998) hypothesized that N_2O produced by various processes might form one common pool before being reduced to N_2 by nitrous oxide reductase. However, there is limited information available about the bulk reduction of N_2O to N_2.

4. Challenges in N_2O measurements and estimates across the agricultural landscape

Nitrous oxide emission and estimation across the different agricultural landscapes (arable, pasture, and wetland) is extremely variable (both spatially and temporally), thus posing the greatest challenge to researchers, modellers and policy makers to accurately predict N_2O emissions. Among the different field and laboratory methods, the static chamber method has most widely been used to determine the rate of N_2O emissions from soil because these chambers are easy to design, portable, compact, easy to install, and can be readily adapted to take gas measurements in the presence of animals and growing crops (Saggar et al., 2009). Readers are referred to Saggar et al (2009) for detailed information on the static chamber method. Other methods, including the sub-surface measurement of N_2O emissions (Arah et al., 1991; Gut et al., 1998; Clark et al., 2001), the Push and Pull technique of Addy et al. (2002) modified by Zaman et al., 2008b to quantify N_2O and N_2 emissions from wetland soils and the estimation approach of the Intergovernmental Panel on Climate Change (IPCC) have also been used to quantify N_2O emissions.

Few studies have carried out simultaneous measurements of N_2 and N_2O across the agricultural landscape. This is probably due to a lack of robust, easy and less expensive measurements and analytical methods. The most commonly used methods for measuring production of N_2 and N_2O in and their emission from the soils, include a technique based on the acetylene (C_2H_2) inhibition of N_2O reduction (Tiedje et al., 1988) and methods using substrates enriched in ^{15}N which allow subsequent ^{15}N gas determination by isotope-ratio mass spectrometry (Mosier & Klemedtsson, 1994). These methods are not only expensive but far from perfect and have some serious biological implications. For example, C_2H_2 inhibition method needs paired soil samples (with or without C_2H_2), which is not only time

consuming and expensive to analyze but a small amount of C_2H_2 (1%) can block nitrification and thus underestimates denitrification in NO_3^- limited soils. Denitrifiers after repeated exposure to C_2H_2 adapt to C_2H_2 and use it as a source of C, which stimulates denitrification rates. Therefore both paired soil samples need to be discarded after 24 hrs of incubation to avoid this problem. In addition, acetone, which is added to C_2H_2 as stabilizer, also acts as a source of C for denitrifiers (Gross & Bremner, 1992) and needs to be removed before injecting C_2H_2 into soil cores or incubation jars. The most problematic step of this technique however, is to successfully achieve a uniform distribution of the desired concentration of C_2H_2 in microsites inhabited by denitrifiers if intact soils cores are used (Zaman & Nguyen, 2010). Similarly a lack of inhibitory effect of C_2H_2 on *Nitrosospira briensis*, one of the common ammonia-oxidizing bacteria in soils, observed by Wrage et al., (2004) also poses a challenge, especially in soil treated with ammonium-based fertilizer where N_2O production via nitrifier-denitrification is likely to be overestimated. Thus although the technique of C_2H_2 inhibition has been widely used in laboratory conditions, when sieved soils or small monoliths were deployed, it has rarely been used in field conditions. To avoid the inhibitory effects of C_2H_2 on nitrification and denitrification, recently there has been an increasing interest in developing isotopic methods, which enable researchers to measure both N_2O and N_2 concurrently and identify the source of N_2O production from various microbial processes including nitrification, denitrification and DNRA (Stevens et al., 1997; Matheson et al., 2003; Sutka et al., 2006). N_2O production during nitrification and denitrification involves significant isotopic discrimination (ε = 35–60‰ and 28–33‰, respectively) (Robinson, 2001). Tilsner et al. (2003) reported that N_2O emitted during denitrification under controlled laboratory conditions was highly depleted in ^{15}N (–40.8 ± 5.7‰). Similarly Stevens et al. (1997) differentially labelled the NH_4^+ and NO_3^- pools simultaneously with ^{15}N, and periodically measured their individual ^{15}N enrichments and N_2O emission. A random distribution of ^{15}N in N_2O indicated a single source of origin whereas a non-random distribution indicated the two or more sources of N_2O origin. Despite the fact that the isotopic method permits the fractional contribution of each pathway to N_2O production and concurrent measurements of both N_2O and N_2, few researchers have used this method due to the high cost of ^{15}N-substrates and ^{15}N gases analyses, limited access to gas chromatograph with isotope-ratio mass spectrometers, and the difficulties associated with the uniform labeling of N pools in drier soils. Recently Mondini et al (2010) developed a robust automated dynamic closed chamber technique for concurrent measurement and analysis of N_2O, CO_2 and CH_4 under laboratory conditions. In their system, a gas chromatograph is connected to a fully computerised sampling system composed of 16 sample jars and 2 multiposition valves. For further details on these various methods, the readers are referred to the above mentioned papers.

In the estimation approach, the IPCC divides N_2O emissions from the agricultural landscape into direct and indirect emissions. Direct N_2O emission refers to N_2O derived from applied fertilizer and manure N, which is believed to increase with fertilizer use. Under the United Nations Framework Convention for Climate Change (UNFCCC), the majority of the countries use the IPCC default value of the 1% as emission factor (EF) (IPCC, 2006) from agricultural soils receiving synthetic fertilizers, farm dairy effluents (FDE), organic wastes and N fixed via biological fixation by leguminous crops (Bouwman et al., 2002; Stehfest & Bouwman 2006). However, a wide range of direct N_2O emissions (i.e. 3 to 22% of applied N) across the agricultural landscape have been reported in the literature (Corre et al., 1996;

Lovell & Jarvis, 1996; Velthof et al., 1996; Jambert et al., 1997; Goossens, et al., 2001; De Klein et al., 2003**;** Zaman et al. 2007; 2008b, c; Saggar et al., 2007b; Zaman & Nguyen, 2010) which is greater than the 1% EF value of the IPCC. A comprehensive review collected by Saggar et al., (2009) indicated that N_2O emissions from synthetic fertilizers range between 0.1 and about 2% of applied N. The large variations in the EF could be related to differences in soil types, time of fertilizer application, climatic conditions, weather patterns and form of synthetic fertilizers (ammonium and nitrate-based chemical fertilizers), animal urine and different protocols of N_2O measurement such as static chambers, C_2H_2 inhibition, micrometeorological, and isotopic methods. Crutzen et al (2007) also reported that the IPCC methodology seriously underestimates N_2O emissions from agriculture. Their estimates, using known global atmospheric removal rates and concentration growth of N_2O, show an overall EF of 3–5%, whereas the EFs estimated for direct and indirect emissions using IPCC methodology cover only part of these emissions. Saggar et al (2009) further argued that the IPCC approach is limited by a number of uncertainties in emission factors, and in indirect emissions, limited data on the type and amount of N excreted by grazing animals, and in spatial and temporal variability of N_2O emissions. Furthermore, the IPCC methodology does not allow for any mitigation options such as the use of urease or nitrification inhibitors and others. It is therefore critical to collect more data to validate the IPCC emission factor for N_2O emission from agricultural soils, which may enable us to accurately predict the global N_2O budget.

According to the IPCC, indirect N_2O emission consists of 3 parts; N_2O emissions associated with atmospheric N deposition [N_2O (G)], human waste [N_2O (S)], and with N lost via surface runoff and leaching [N_2O (L)]. Indirect N_2O emissions represent 1/3 of the total agricultural emissions, and the majority (75% of the total indirect emission) come from riparian zones (riparian wetlands, drainage ditch and stream sediments), where NO_3^- in leachate and NH_4^+ in runoff from farmland are microbially converted to N_2O and N_2 (Groffman, 2002; Zaman et al., 2007; Zaman et al., 2008b,c Zaman and Nguyen, 2010). N_2O emission rates from riparian wetlands are generally higher than those of agricultural soils (Lowrance et al., 1984; Pinay et al., 1993; Zaman et al., 2008c) which could be attributed to the higher C in riparian soils and enriched NO_3^- inputs from surrounding areas via seepage and groundwater flow to riparian zones. Given the potentially higher N_2O emission rates from wet soils c.f. dry soils in agricultural landscapes, and the general lack of data from wet soils, there is a clear need for more data on N_2O emission rates from riparian wetlands. Limited studies have been conducted to measure the rate of N_2O emissions from streams and rivers. Garcia-Ruiz et al. (1999) found that N_2 production ranged from 0.05-0.27 μmol N m^{-2} h^{-1} in the Swale-Ouse River system to 570 μmol N m^{-2} h^{-1} in the River Wiske. In the River Wiske, N_2O production accounted for up to 80% of total N gas production. Using the current IPCC methodology, approximately 40% of indirect N_2O emissions (emissions not accounted for from direct N sources such as fertilizers and applied animal urine) are derived from streams, rivers and estuaries.

5. Factors affecting N_2O and N_2 emissions and possible mitigating options

As reviewed in Section 3 (Processes of N_2O and N_2 production across the agricultural landscape), autotrophic and heterotrophic nitrification and DNRA produce only N_2O; while

denitrification produces both N_2O and N_2. The emissions of N_2O and N_2 and their ratios are affected by various soil and management factors, including mineral N concentration, available C, soil pH, soil aeration status, soil temperature and their interactions as shown in Table 5.1.

Factors	Management	Impact	Management practices
Soil NH_4^+ & NO_3^- concentration	Decrease	Reduce nitrification & denitrification and lower N_2O:N_2	Use urease and nitrification inhibitors to enhance fertilizer use efficiency; split N fertilizer application to synchronize plant N demand and to minimize N losses; avoid over grazing; manipulation of animal diet; use of constructed or natural riparian wetland, improving water use efficiency to avoid anaerobicity
Soil organic C	Increase	Improve soil health, facilitate denitrification and thus lower N_2O:N_2	Sequester more C by adopting management practices including zero or minimum tillage, retention of crop residues, mulching, application of organic and farm wastes, biochar, and applying chemical fertilizers with organic amendments
Soil pH	Increase	Facilitate nitrification and denitrification and thus lower N_2O:N_2	Regular liming each year or if possible with every N fertilizer application
Soil aeration and water status	Improve	Facilitate nitrification and denitrification and thus lower N_2O:N_2	Improving soil structure via C sequestration, avoiding soil compaction; improving soil drainage condition and also water use efficiency

Table 5.1. Factors affecting N_2O and N_2 emissions and their ratios.

In the section below, an attempt has been made to discuss these soil and management factors. Understanding these factors may help us to design mitigating tools to reduce the rate of N_2O production and to lower N_2O:N_2 ratios.

5.1 Soil NH_4^+ and NO_3^- concentrations

The amount of mineral N, both NH_4^+ and NO_3^-, are critical for the production of N_2O, N_2 and their ratio. The amount of NH_4^+ in soil under aerobic soil conditions, and hence its availability for nitrification, can directly regulate N_2O emission via nitrifier-denitrification (Webster & Hopkins, 1996; Wrage et al., 2001; Dalal et al., 2003; Ma et al., 2007), while NO_3^- is used as a substrate by both denitrification and DNRA and thus affects N_2O production (Webster and Hopkins, 1996; Zaman et al., 2008c). A higher level of NO_3^- in soil is also known to result in incomplete denitrification and thus higher N_2O:N_2 due to suppression of nitrous oxide reductase activity, the enzyme responsible for microbial conversion of N_2O to N_2 (Eq. 3.2.1). To mitigate N_2O emissions, researchers during the past two decades focused mainly on reducing the rate of nitrification while little work has been done to exert control on the denitrification level. For example, to reduce N_2O emissions from applied urea, ammonium based fertilizers or urine N, researchers have developed different mitigation technologies including the use of N inhibitors to reduce the entry of mineral N from applied fertilizer/urine into the available N pool, application of soil amendments like zeolites to capture soil NH_4^+ and controlled release and split applications of N fertilizers to match crop N demand. Among these options, coating chemical fertilizers with N inhibitors or applying N inhibitors on their own to treat urine patches in grazed pastures have received the most attention. The two major classes of N inhibitors are urease inhibitors (UIs) and nitrification inhibitors (NIs). Urease inhibitors retard the hydrolysis of soil-applied urea and delay the entry of urea-N into the NH_4^+ pool, which is likely to produce less N_2O via nitrification due to the limited availability of NH_4^+ (Watson, 2000; Xu et al., 2000; Zaman et al., 2008a; Zaman et al., 2009) as shown earlier in Eq. 2.1.4. Such a reduction in urea hydrolysis also limits the opportunity for nitrite (NO_2^-) accumulation in the soil, which is known to produce N_2O (Eq. 3.1.2).

Decisions about N fertilizer application are usually dependent on the availability of water, and the N application rate is determined by crop growth stage and the productivity goals. Fast urea hydrolysis starts within hours of urea fertilizer application or after deposition of urine from grazing animals and is completed within 1 to 3 days, during which time a significant amount of NH_3 (up to 30% of the applied N) is lost. UI like N-(n-butyl) thiophosphoric triamide (nBTPT) or Agrotain® applied at a very low concentration (0.01%) with urea fertilizer is reported to delay such fast urea hydrolysis by 7 to 9 days (Watson et al., 2008), which has implications for worldwide urea use in pasture and cropping systems where there is a high risk of NH_3 loss due to low moisture and high temperature, especially during summer or early autumn. Such a delay in urea hydrolysis allows more time for rainfall or irrigation water to wash the applied urea from surface soil and thus minimizes the risk of NH_3 emissions. After application, nBTPT is quickly converted to its oxygen analog N-(n-butyl) phosphoric triamide) (NBPT) (Eq. 5.1.1), which is the actual UI (McCarty et al., 1989; Christianson et al., 1990; Creason et al., 1990), and it is bound and moves along with urea molecule in the soil (Christianson & Howard, 1994). The conversion of nBTPT to NBPT is rapid, occurring within minutes/hours in aerobic soils (Byrnes & Freney, 1995), but can take several days in the floodwater of tropical soils. NBPT forms a tridentate ligand with the urease enzyme, blocking the active site (Manunza et al., 1999).

In addition to reduced nitrification, Agrotain is also known to reduce N_2O emission indirectly through reduced NH_3 volatilization (Watson et al., 1990; 1994 a & b, 1998, 2008;

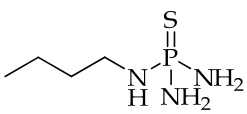

N-(*n*-butyl)thiophosphoric triamide
(*n*BTPT)

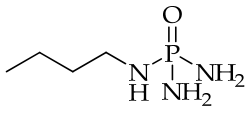

N-(*n*-butyl)phosphoric triamide
(Oxygen analogue)

(5.1.1)

Chadwick et al., 2005; Meneer et al., 2008; Sanz-Cobena et al., 2008; Singh et al., 2008; Zaman et al., 2008a & 2009; Zaman & Blennerhassett., 2010). Ammonia itself is not a greenhouse gas, but it can act as a secondary source of N_2O production after its deposition on land (Martikainen, 1985) and thus contributes indirectly to climate change. To our knowledge, New Zealand is the only country that has included NH_3 reduction from Agrotain treated urea in its national inventory on N_2O. Sherlock et al. (2008) after a literature search on NH_3 emission, recommended to the New Zealand Ministry of Agriculture and Forestry (MAF) that a specific value of 0.1 for $Frac_{GASM}$ and $Frac_{GASF}$ be considered for adoption. In New Zealand, studies where nBTPT (0.025% w/w) was applied reduced NH_3 emissions by 43% from urea and by 48% from urine (Singh et al., 2008; Meneer et al., 2008; Zaman et al., 2008a & 2009; Zaman & Blennerhassett 2010). Based on these estimates of reductions in NH_3 emission from nBTPT treated urea applications, a New Zealand specific value of 0.06 for $Frac_{GASF}$ is recommended for adoption where fertilizers containing the urease inhibitor, nBTPT are applied. Saggar et al. (2010) recommended to MAF that where NBTPT is applied with urea, $Frac_{GASF}$ should be calculated as follows,

$$FracGASF = [(FN_{UI}) \times 0.06] + [(FN - FN_{UI}) \times 0.10]$$

Where $\mathbf{Frac_{GASF}}$ is the fraction of total fertilizer N emitted as NH_3, **FN** is the total amount of applied fertilizer N, $\mathbf{FN_{UI}}$ is the amount of applied fertilizer N treated with the urease inhibitor, nBTPT. Changing the $Frac_{GASF}$ from 0.1 to 0.06 for the current use of 18.4 Gg N of Agrotain treated urea reduces indirect N_2O emissions by 0.012 Gg, which equates to 3.6 Gg $CO_{2\text{-equiv.}}$ However, assuming all urea is applied with nBTPT in New Zealand, changing the $Frac_{GASF}$ from 0.1 to 0.06 will reduce the indirect N_2O emissions by 0.14 Gg, which equates to 43.4 Gg $CO_{2\text{-equiv.}}$

Nitrification inhibitors are compounds (both natural and synthetic) that delay bacterial oxidation of NH_4^+ either by temporarily suppressing the activities of nitrifiers or killing them in the soil, thus maintaining the applied N in more stable form (i.e. NH_4^+-N). Slowing down nitrification in soils lowers N_2O production associated with nitrifier-denitrification (Webster & Hopkins, 1996; Wrage et al., 2001; Ma et al., 2007), or indirectly by reducing the amount of NO_3^- substrate available for denitrification. Among the many synthetic NIs, only nitrapyrin or N-Serve (NP) (2-chloro-6-(tri-chloromethyl) pyridine), dicyandiamide (DCD) and 3,4-Dimethylpyrazol-phosphate (DMPP) have gained substantial practical and commercial importance in agricultural and horticultural crop production.

Nitrapyrin because of its high volatility needs to be injected into the soil. Therefore nitrapyrin may be a preferred NI where injecting chemical fertilizers or farm dairy effluent (FDE) into the soil is a common practice. Unlike nitrapyrin, DCD is relatively soluble in

water, non-volatile, cheap and can be easily treated/coated onto solid ammonium based N fertilizers such as urea, diammonium phosphate (DAP); ammonium nitrate (NH_4NO_3) and ammonium sulfate $(NH_4)_2SO_4$ or directly added into FDE to improve their N use efficiency and minimize N losses. However after application, separation of DCD from applied NH_4^+, DCD leaching, and its rapid decomposition with increasing soil temperature are reported to lower its efficacy. Contrary to this, DMPP has several advantages over DCD and nitrapyrin. Lower application rates (0.5 to 1.0 kg of the active compound ha^{-1}) are needed to achieve optimal nitrification inhibition to reduce N_2O emissions and NO_3^- leaching. After application, DMPP is less prone to leaching and remains effective much longer than that of DCD (Weiske et al., 2001; Zerulla et al., 2001).

In intensive agricultural system like grazed pastures, other mitigation options including feeding dairy cows with low N feed such as palm kernel and maize silage instead of high N pastures to reduce the amount of N in animal excreta, using winter feed pads and restricted grazing to avoid soil compaction and to minimize urine depositions during critical times (winter) (de Klein et al., 2006), natural and constructed riparian wetlands to intercept N entering from adjacent pasture soils and to process it before entering water bodies (Zaman et al., 2008b), applying lime or zeolite as soil amendments to reduce N_2O emissions and shift the balance between harmful N_2O and non-greenhouse N_2 (Zaman et al., 2007, 2008c; Zaman & Nguyen, 2010), adding salts to animal feed to increase urine volume and spread (Ledgard et al., 2007), increasing the hippuric acid concentration in urine by manipulating animal feed (Bertram et al., 2009) have been suggested as additional mitigation tools.

5.2 Soil available organic C concentration

Soil organic C is another important controller of N_2O and N_2 production in soils and sediments as denitrifiers are strictly heterotrophs and use available organic C as electron donor and indirectly affects O_2 concentrations of aerobic soils (Groffman et al., 1987). However the effect of available C on the amounts of N_2O and N_2 produced in and emitted from the soils, as well as on the ratio between the two gases, is reported to vary with soil NO_3^- concentration and WFPS (Zaman et al., 2007, 2008b,c). In anaerobic zones of non-fertilized soils, NO_3^- availability may control the denitrification rates as discussed above in section 5.1, while in soils with high NO_3^- inputs (i.e. after application of chemical fertilizers and FDE or urine patches after grazing), available soil organic C would be the main driver of N_2O and N_2 production via denitrification (Tiedje, 1988). Applying urea fertilizer with C source (wheat straw and green manure) was reported to substantially reduce N_2O emission compared to urea fertilizer alone (Aulakh et al., 2001) possibly due to the microbial immobilization (Tiedje, 1988) or DNRA (Matheson et al., 2002). Zaman et al., (2008b) during an incubation study observed that wetland soils treated with KNO_3 emitted more N_2 emissions than those of the pasture soils which they attributed to the availability of highly enriched organic C and high WFPS in wetland soils. Weier et al. (1993) also measured N_2O and N_2 emissions from 4 soils treated with a range of available C (0, 180 and 360 kg ha^{-1}), NO_3^--N (0, 50 and 100 kg ha^{-1}) and WFPS (60, 75 and 90%). They reported that N_2 emission was favored at the highest available C rate of 360 kg C ha^{-1} and 90%WFPS, while the higher NO_3^- concentration inhibited the conversion of N_2O to N_2, resulting in higher N_2O:N_2 ratios. Similarly Yao et al. (2002) observed a negative correlation between N_2O emission and soil organic C from N fertilized wheat crop. The N_2O:N_2 ratio could be explained by an

interaction of C availability, NO_3^- concentration and enzyme status (Swerts et al., 1996). There are reports that the N_2O:N_2 ratios are lower in the rhizosphere, which provides more available organic C in the form of root exudates and root debris, and is characterized by low partial pressure of O_2 (due to O_2 consumption by plant roots) (Casella et al., 1984).

Depending on the management practices, agricultural soils can act as a source or sink for atmospheric CO_2. Improved land management practices in croplands and grasslands can store up to 1 Gt C in the soil on an annual basis (IPCC, 2000). It is therefore possible to store between 100 to 1000 kg SOC ha^{-1} $year^{-1}$ depending on the climate, soil and vegetation types, and site-specific soil management practices. Improved land management practices like zero or minimum tillage, retention of crop residues via crop rotation and mulching, application of FDE, organic residues and manure, following crop rotation especially with N fixing crops and avoiding burning crop residues after harvest may offer potential mitigation tool to sequester more C in the soils to offset the increase in atmospheric CO_2 as well as to improve soil fertility, soil structure, aggregate stability, pore size geometry and distribution, water and nutrients holding capacity and soil quality (increased microbial and enzymatic activities). Such improvement in soil physical and chemical fertility and health will minimize conducive conditions like anaerobicity and soil compaction which stimulate denitrification. Increased soil C may also help to shift the balance between harmful N_2O and non-greenhouse gas N_2 during denitrification as the activity of nitrous oxide reductase enzymes is stimulated by available soil C.

5.3 Soil pH

Soil pH is among the key regulators of the microbiological processes that affect N_2O and N_2 production and their ratios. Nitrification activity is generally higher with higher soil pH (> 6) (Bremner & Blackmer, 1981; Bramley & White, 1989). The critical soil pH threshold for nitrification is 5; however, nitrification can occur even at a soil pH of 4.5 due to acid-adapted nitrifier strains (Bouwman, 1990). Denitrification has been reported to occur over a wide range of soil pH values (5 to 8) (Weier & Gilliam, 1986; Ramos, 1996; Flessa et al, 1998); however, laboratory experiments with artificially adjusted soil pH suggest, that under optimized conditions (very low pO_2, NO_3^- and glucose amendments), denitrification can proceed even at pHs below 4 or above 10 (Šimek & Hopkins, 1999, Šimek et al., 2002). Numerous laboratory and field studies have shown that soil pH affects N_2O and N_2 and the ratio of these gases (e.g. Weier & Gilliam, 1986; Stevens & Laughlin, 1998). Under controlled environment experiments, we found that raising soil pH to 7 through lime application significantly increased N_2 emission from pasture and wetland soils treated with urine, urea and KNO_3 at 200 kg N ha^{-1} rate (Zaman et al., 2007 & 2008c). More recently in a field experiment, a similar trend of enhanced N_2 after raising soil pH to 7 was observed in pasture soils treated with urea/urine (Zaman & Nguyen, 2010). This idea is further supported by our studies on cattle pasture soil (Hynšt et al., 2007). At the site with the greatest animal impact, the ratio of N_2 to N_2O produced during denitrifying enzyme activity (DEA) measurements was five-fold higher, and the pH was 2 units higher, compared to the site with the least animal impact, which indicated that soil conditions were favourable for production of N_2 rather than N_2O in the area where excretal returns and treading was intense.

Types of chemical N fertilizers are also likely to regulate N_2O:N_2 ratios, as NH_4^+ based fertilizers (i.e. ammonium sulphate, ammonium nitrate, and mono-ammonium phosphate)

are reported to lower soil pH after their application (Thornton et al., 1996; Mulvaney et al., 1997; Nobre, 2001; Cai et al., 2002). For example, Mulvaney et al. (1997) have reported that ammonium-based fertilizers with soil acidifying effects produce a higher N_2O:N_2 ratio compared to alkaline forming fertilizers (anhydrous ammonia, urea or di-ammonium phosphate). Most researchers attribute high N_2O and low N_2 emissions in acidic conditions to the suppression of nitrous oxide-reductase at low soil pH (inhibition at soil pH 4.5) (Kostina et al., 1996; Daum & Schenk 1998; Flessa et al., 1998; Stevens and Laughlin, 1998; Zaman et al., 2007). It is also likely that all denitrifying enzymes are susceptible at low soil pH and produce N_2O from intermediate products (Nagele & Conrad, 1990). However, the extensive review conducted by Šimek and Cooper (2002) reported that the lower rates of N_2 and high N_2O:N_2 ratio at low soil pH could be due to lower amounts of soil organic C and mineral N available to the denitrifying population under acid conditions rather than a direct effect of low pH on denitrification enzymes. Regardless of the biochemical reasons for changes in soil pH on N_2 emission, raising soil pH through application of soil amendment like lime appears to offer a mechanism for mitigation of N_2O (Šimek et al., 2002; Zaman et al., 2007, 2008b, Zaman & Nguyen, 2010).

5.4 Soil aeration and water status

Soil aeration, namely O_2 concentration and gas exchange between soil and atmosphere, affects all microbial N transformation processes including nitrification, denitrification, and DNRA. Control of the denitrification enzymes, especially nitrous oxide reductase, represents the key mitigation option for the rate of N_2O production and can therefore shift the balance between harmful N_2O and non-greenhouse N_2 production across the agricultural landscape (Smith & Tiedje, 1979; Mosier et al., 1986; Robertson & Tiedje, 1987; Henrich & Haselwandter, 1997; Bollmann & Conrad, 1998; Mosier et al., 2002).). In soil, O_2 concentration changes with soil moisture content and organic matter decomposition by soil microorganisms. After rainfall or applying irrigation water, soils become temporarily anaerobic; the extent and duration of anaerobiosis differs with soil types (drainage class). Fine-textured soils with a higher clay content are reported to remain anaerobic for a longer period of time at low WFPS than coarse-textured soils because of the greater number of micro pores in the former (Barton et al., 1999). Therefore fine-textured soils with poorly drained conditions are likely to emit more N_2O for a longer period than those of coarse-textured soils with well-drained conditions (Groffman & Tiedje, 1989; Aulakh et al., 1991; Clayton et al., 1997; Dobbie & Smith, 2001; Saggar et al., 2004a). At higher O_2, partial pressure (>0.5 vol. %), nitrification is expected to proceed, provided there is sufficient water for optimum activity of nitrifiers (Linn & Doran, 1984; Bollmann & Conrad, 1998); if the soil WFPS increases (and pO_2 decreases), the rate of N_2O production and the proportion of N_2O to NO_3^- produced also increases (Smith et al., 2003). Under such specific conditions at WFPS>60%, nitrification is considered to be the predominant source of N_2O as opposed to denitrification or DNRA (Inubushi et al., 1996). Although DNRA is understood to be an anaerobic process, information about the critical levels of WFPS or O_2 for DNRA is lacking in the literature. Denitrification becomes a major source of N_2O and N_2 production at lower O_2 partial pressure (<0.5 vol. %) and higher WFPS (>60%) (Davidson, 1993; Scholefield et al., 1997; Bronson & Fillery, 1998; Khalil et al., 2002). In such scenarios, more aerobic soils are likely to produce mainly N_2O because denitrification reductases (Eq. 3.2.1) especially nitrous oxide reductase is reported to be sensitive to soil O_2 level, while anaerobic soils and

sediments will generate both N_2O and N_2. A number of studies have reported higher amounts of N_2 than N_2O at lower O_2 partial pressure and WFPS above 70% (Eriksen & Hartwig, 1993; Dendooven et al., 1999; Kwong et al 1999, Khalil et al., 2002). Aulakh et al. (2001) reported that gaseous N losses as N_2O after application of urea (120 kg ha^{-1}) to flooded rice were 8 to 10 times higher than those of upland wheat because of the anaerobic conditions in the former. Recently we found that riparian wetland soils treated with NO_3^--N (200 kg N ha^{-1} rate) emitted 4 and 8 times more N_2O and N_2 respectively than pasture soils during 28-day incubation (Zaman et al., 2008 c). However, the relative production of N_2O and N_2 in anaerobic or aerobic soil conditions is not that simple since O_2 level or WFPS is only one of the many known soil and management factors which affect this relationship (Fillery, 1983; Scholefield et al., 1997; Stevens & Laughlin, 1998; Zaman et al., 2008b). In their comprehensive review on emissions of N_2O and NO from fertilized fields published, Bouwman et al. (2002) concluded that restricted drainage and fine texture favors N_2O emissions. Thus our current understanding of the processes of N_2O and N_2 production in anaerobic and aerobic soil conditions is limited. At this stage we can only suggest that improving soil drainage conditions and avoiding soil compaction through use of the heavy farm machinery and grazing animals (pugging) in wet soil conditions (especially in winter) could help to maintain aerobicity in soils, which in turn may reduce N_2O emission rates through nitrification, denitrification and DNRA (Bhandral et al., 2003, 2007b. Luo et al., 2008b).

Apart from the above mentioned factors, temperature is also known to affect N_2O production and the N_2O:N_2 ratio (Cho et al., 1997; Daum et al (1997, Muller et al., 2002). However, controlling soil temperature is mostly beyond the ability of farmers. Manipulation of the interaction between mineral N supply (NH_4^+ and NO_3^-), organic C, soil aeration and pH offers the best hope for minimizing N_2O emission from soils. Similarly the export of N via surface and sub-surface runoff from upland to water bodies can be minimized by using riparian zones (both natural and constructed) along river and stream banks. Since denitrification is considered to be the major NO_3^- removal process in wetland, proper management of wetlands include, regular application of lime to keep the pH above 6.5, sequestering C to build C reserves, and exclusion of grazing animals to minimize N inputs are essential. All these management practices are known to stimulate the activity of nitrous oxide reductase, which will help to result in emissions of more N_2 than N_2O as discussed above.

6. Conclusions

Nitrogen is the most dynamic plant, microbial and animal nutrient which affects the diversity, dynamics, and functioning of many terrestrial, freshwater and marine ecosystems. Gaseous N losses in the form of N_2O are undesirable because N_2O is an important greenhouse gas and is also involved in the depletion of stratospheric ozone. Nitrification, denitrification and DNRA are the main microbial processes for N_2O production across the agricultural landscape which can sometimes operate concurrently in a given soil system. N losses as N_2O across the agricultural landscape are extremely variable and range from about 1% to more than 20 % of the applied N. Such losses are generally higher from wetland soils than those from pasture or arable soils. The critical soil and management factors affecting the rates of N_2O and N_2 production and their ratios are concentration of mineral N, soil

organic C, soil pH, and soil aeration status. N_2 production dominates over that of N_2O at lower mineral NO_3^- content, increasing organic C contents, increasing soil pH (above 6.5), lowering O_2 partial pressure or increasing WFPS; above 70%. Manipulation of these factors offers potential tools for mitigation of N_2O.

7. Acknowledgments

The senior author acknowledges the financial assistance for page charges by Ballance Agri-Nutrients Ltd. We also acknowledge Sharon Long for her assistance in proof reading this chapter and the unknown reviewers for their positive comments.

8. References

Addy, K. Kellogg, D.O. Gold, A.J. Groffman, P.M. Ferendo, G. & Sawyer, C. (2002). In situ pushpull method to determine ground water denitrification in riparian zones. *Journal of Environmental Quality,* 31, pp. 1017-1024.

Alef, K. Kleiner, D. (1986). Arginine ammonification, a simple method to estimate microbial activity potential in soils. *Soil Biology and Biochemistry,* 18, pp. 233-235.

Arah, J.R.M. Smith, K.A. Crichton, L.J. & Li, H.S. (1991). Nitrous oxide production and denitrification in Scottish soils. *Journal of Soil Science,* 42, pp. 351-367.

Armstrong, W. (1964). Oxygen diffusion from the roots of some British bog plants. *Nature,* 264, pp.801-802.

Aulakh, M.S. Doran, J.W. & Mosier, A.R. (1991). In-field evaluation of four methods for measuring denitrification. *Soil Science Society of America Journal,* 55, pp. 1332-1338.

Aulakh, M.S. Khera, T.S. Doran, J.W. & Bronson, K.F. (2001). Denitrification, N_2O and CO_2 fluxes in rice, wheat cropping system as affected by crop residues, fertilizer N and legume green manure. *Biology and Fertility of Soils,* 34, pp. 375-389.

Azam, F. Malik, K.A. & Hussain, F. (1986). Microbial biomass and mineralization-immobilization of nitrogen in some agricultural soils. *Biology and Fertility of Soils,* 2, pp. 157-163.

Barak, P. Molina, J.A.E. Hadas, A. & Clapp, C.E. (1990). Mineralization of amino acids and evidence of direct assimilation of organic nitrogen. *Soil Science Society of America Journal,* 54, pp. 769-774.

Barraclough, D. (1997). The direct or MIT route for nitrogen immobilization, An 15N mirror image study with leucine and glycine. *Soil Biology and Biochemistry,* 29, pp. 101-108.

Barton, L. McLay, C.D.A. Schipper, L.A. & Smith, C.T. (1999). Annual denitrfication rates in agricultural and forest soils, a review. *Australian Jurnal of Soil Research,* 37, pp. 1073-1093.

Bertram, J.E. Clough, T.J. Sherlock, R.R. Condron, L.M. O'Callaghan, M. Wells, N.S. & Ray, J.L. (2009). Hippuric acid and benzoic acid inhibition of urine derived N_2O emissions from soil. *Global Change Biology,* 15, pp. 2067-2077.

Bhandral, R. Saggar, S. Bolan, N.S. & Hedley, M.J. (2003). Nitrous oxide fluxes in soil as influenced by compaction. *Proceedings of the New Zealand Grassland Association,* 65, pp. 265-271.

Bhandral, R. Saggar, S. Bolan, N.S. & Hedley, M.J. (2007). Transformation of nitrogen and nitrous oxide emission from grassland soils as affected by compaction. *Soil and Tillage Research,* 94, pp. 482-492.

Bolan, N.S. Saggar, S. Luo, J. Bhandral, R. & Singh, J. (2004). Gaseous emissions of nitrogen from grazed pastures, processes, measurements and modelling, environmental implications, and mitigation. *Advances in Agronomy,* 84, pp. 37-120.

Bollmann, A. & Conrad, R. (1998). Influence of O_2 availability on NO and N_2O release by nitrification and denitrification in soils. *Global Change Biology,* 4, pp. 387-396.

Bouwman, A.F. (1990). Soils and the greenhouse effect, Proceedings of the International Conference Soils and the greenhouse effect, International Soil Reference and Information Centre ISRIC. John Wiley and Sons, New York, pp. 575.

Bouwman, A.F. Boumas, L.J.M. & Batjes, N.H. (2002). Emissions of N_2O and NO from fertilized fields, Summary of available measurement data. *Global Biogeochemical Cycles,* 16, pp. 1-13.

Bramley, R.G.V. & White, R.E. (1989). The effect of pH, liming, moisture and temperature on the activity of nitrifiers in a soil under pasture. *Australian Journal of Soil Research,* 27, pp. 711-724.

Bremner, J.M. & Blackmer, A.M. (1981). Terestrial nitrification as a source of atmospheric nitrous oxide, In: Delwiche, C.C. (Ed.), Denitrification, Nitrification and Atmospheric Nitrous Oxide. Willey and Sons, New York, pp. 151-170.

Bronson, K.F. & Fillery, I.R.P. (1998). Fate of nitrogen-15-labelled urea applied to wheat on a waterlogged texture-contrast soil. *Nutrient Cycling in Agroecosystems,* 51, pp. 175-183.

Cai, G. White, R.E. Chen, D. Fan, X.H. Pacholski, A. Zhu, Z.L. & Ding, H. (2002). Gaseous nitrogen losses from urea applied to maize on a calcareous fluvo-aquic soil in the North China Plain. *Australian Journal of Soil Research,* 40, pp. 737-748.

Casella, S. Leporini, C. & Nuti, M.P. (1984). Nitrous oxide production by nitrogen-fixing fast growing rhizobia. *Microbial Ecology,* 10, pp. 107-114.

Cavigelli, M.A. & Robertson, G.P. (2001). Role of denitrifier diversity in rates of nitrous oxide consumption in a terrestrial ecosystem. *Soil Biology and Biochemistry,* 33, pp. 297-310.

Cho, C.M. Burton, D.L. & Chang, C. (1997). Denitrification and fluxes of nitrogenous gases from soil under steady oxygen distribution. *Canadian Journal of Soil Science,* 77, pp. 261-269.

Christianson, C.B. & Howard, R.G. (1994). Use of soil thin-layer chromatography to assess the mobility of the phosphoric triamide urease inhibitors and urea in soil. *Soil Biology and Biochemistry,* 26, pp. 1161-1164.

Clark, M. Jarvis, S. & Maltby, E. (2001). An improved technique for measuring concentration of soil gases at depth in situ. *Communications in Soil Science and Plant Analysis,* 32, pp. 369-377.

Clayton, H. McTaggart, I.P. Parker, J. Swan, L. & Smith, K.A. (1997). Nitrous oxide emission from fertilised grassland, A 2-year study of the effects of N fertilizer form and environmental conditions. *Biology and Fertility of Soils,* 25, pp. 252-260.

Corre, M.D. Van Kessel, C. & Pennock, D.J. (1996). Landscape and seasonal patterns of nitrous oxide emissions in a semiarid region. *Soil Science Society of America Journal,* 60, pp. 1806-1815.

Creason, G.L. Byrnes, B.H. & Carmona, G. (1990). Urease inhibitory activity associated with N-butyl thiophosphoric triamide is due to formation of its oxon analog. *Soil Biology and Biochemistry,* 22, pp. 209-211.

Crutzen, P.J. (1981). Atmospheric chemical processes of the oxides of nitrogen including nitrous oxide, In: Delwidche, C.C. (Ed.), Denitrification, Nitrification and Atmospheric Nitrous Oxide. John Wiley, New York, pp. 17-44.

Crutzen, P.J. Mosier, A.R. Smith, K.A. & Winiwarter, W. (2007). N_2O release from agro-biofuel production negates global warming reduction by replacing fossil fuels. *Atmospheric Chemistry and Physics Discussions,* 7, pp. 11191-11205.

Dalal, R. C. W. Wang, G. P. Robertson, & Parton, W. J. (2003). Nitrous Oxide Emission from Australian Agricultural Lands and Mitigation Options: A Review. *Australian Journal of Soil Research*, 41, pp. 165-195.

Daum, D. & Schenk, M.K. (1998). Influence of nutrient solution pH on N_2O and N_2 emissions from a soilless culture system. *Plant and Soil,* 203, pp. 279-287.

Daum, D. Schenk, M.K. & Roeber, R.U. (1997). Extent and N_2O/N_2 ratio of gaseous nitrogen losses from a soilless culture system. *Acta Horticulture,* 450, pp. 519-526.

Davidson, E.A. (1993). Soil water content and the ratio of nitrous oxide to nitric oxide emitted from soil, In: Oremland, R.S. (Ed.), *The Biogeochemistry of Global Change, Radiatively Active Trace Gases*. Chapman and Hall, New York, pp. 369-386.

De Boer, W. Klein Gunnewiek, P.J.A. Veenhuis, M. Bock, E. & Laanbroek, H.J. (1991). Nitrification at low pH by aggregated chemolithotrophic bacteria. *Applied and Environmental Mikrobiology,* 57, pp. 3600-3604.

de Klein, C.A.M. Barton, L. Sherlock, R.R. Li, Z. & Littlejohn, R.P. (2003). Estimating a nitrous oxide emission factor for animal urine from some New Zealand pastoral soils. *Australian Journal of Soil Research,* 41, pp. 381-399.

de Klein, C.A.M. & Eckard, R.J. (2008). Targetted technologies for nitrous oxide abatement from animal agriculture. *Australian Journal of Experimental Agriculture,* 48, pp. 14-20.

de Klein, C.A.M. Smith, L.C. & Monaghan, R.M. (2006). Restricted autumn grazing to reduce nitrous oxide emissions from dairy pastures in Southland, New Zealand. *Agriculture Ecosystems and Environment,* 112, pp. 192-199.

Dendooven, L. Murphy, M.E. & Catt, J.A. (1999). Dynamics of the denitrification process in soil from the Brimstone farm experiment, UK. *Soil Biology and Biochemistry,* 31, pp. 727-734.

Denman, K.L. (2007). Climate change: the physical science basis, In: Solomon, S. Qin, D. Manning, M. Marquis, M. Averyt, K. Tignor, M.M.B. Miller, H.L.J. (Eds.), Contribution of Working Group I to the Fourth Assessment Report of the Intergovernmental Panel on Climate Change. Cambridge University Press, Cambridge, pp. 499-587.

Dobbie, K.E. & Smith, K.A. (2003). Impact of different forms of N fertilizers on N_2O emission from intensive grassland. *Nutrient Cycling in Agroecosytems,* 67, pp. 37-46.

Duxbury, J.M. Harper, L.A. & Mosier, A.R. (1993). Contributions of agroecosystems to global climate change, Agricultural Ecosystem Effects on Trace Gases and Global Climate Change. *American Society of Agronomy*, pp. 1-18.

Eriksen, A.B. & Holtan-Hartwig, L. (1993). Emission spectrometry for direct measurement of nitrous oxide and dinitrogen from soil. *Soil Science Society of America Journal,* 57, pp. 738-742.

Esterman, E.F. & McLaren, A.D. (1961). Contribution of rhyzosplane organisms to total capacity of plants to utilize organic nutrients. *Plant and Soil,* 15, pp. 243-260.

Fillery, I.R.P. (1983). Biological denitrification, In: Freney, J.R. Simpson, J.R. (Eds.), Gaseous Loss of Nitrogen from Plant-Soil Systems. Martinus Nijhoff/Dr. W.Junk Publishers, The Hague, pp. 33-64.

Firestone, M.K. (1982). Biological denitrification, In: Stevenson, F.J. (Ed.), Nitrogen in Agricultural Soils. American Society of Agronomy Inc., Crop Science Society of America, Inc., Soil Science Society of America, Inc.Publisher Madison, Wisconsin, USA, pp. 289-326.

Firestone, M.K. & Davidson, E.A. (1989). Microbiological basis of NO and N_2O production and consumption in soil, In: Andreae, M.O. Schimel, D.S. (Eds.), Report for the Dahlem Workshop on Exchange of the Trace Gases between Terrestrial Ecosystems and the Atmosphere. John Wiley and Sons, Berlin pp. 7-22.

Flessa, H. Wild, U. Klemisch, M. & Pfadenhauer, J. (1998). Nitrous oxide and methane fluxes from organic soils under agriculture. *European Journal of Soil Science,* 49, pp. 327-335.

Frankenberger, W.T. & Tabatabai, M.A. (1982). Amidase and urease activities in plants. *Plant and Soil,* 64, pp. 153-166.

Freney, J.R. & Black, A.S. (1988). Importance of ammonia volatilization as a loss process, In: Wilson, J.R. (Ed.), Advances in Nitrogen Cycling in Agricultural Ecosystems. CAB International, Wallingford, UK, pp. 156-173.

Garcia-Ruiz, R. Pattinson, S.N. & Whitton, B.A. (1998). Denitrification and nitrous oxide production in sediments of the Wiske, a lowland eutrophic river. *Science of the Total Environment*, 210-211, pp. 307-320.

García-Ruiz, R. Pattinson,S.N. Whitton, B.A. 1999. Nitrous oxide production in the river Swale–Ouse, North–East England, *Water Research*, 33 (5), pp. 1231-1237.

Godde, M. & Conrad, R. (2000). Influence of soil properties on the turnover of nitric oxide and nitrous oxide by nitrification and denitrification at constant temperature and moisture. *Biology and Fertility of Soils,* 32, pp. 120-128.

Goodroad, L.L. & Keeney, D.R. (1984). Nitrous oxide production in aerobic soils under varying pH, temperature and water content. *Soil Biology and Biochemistry,* 16, pp. 39-43.

Goossens, A. de Visscher, A. Boeckx, P. & van Cleemput, O. (2001). Two year field study on the emission of N_2O from coarse and middle, textured Belgian soils with different land use. *Nutrient Cycling in Agroecosystems,* 60, pp. 23-34.

Groffman, P.M. (1987). Nitrification and denitrification in soil, a comparison of incubation, enzyme assay and enumeration techniques. *Plant and Soil,* 97, pp. 445-450.

Groffman, P.M. (2002). Non-CO_2 greenhouse gases, Scientific understanding, control options and policy aspects, In: Van Ham, J. Baede, A.P.M. Guicherit, R. Williams-Jacobes, J.G.F.M. (Eds.), Proceedings of the Third International Symposium, Mechanisms,

Rates and Assessment of N_2O in Groundwater, Riparian Zones and Rivers Maastricht, The Netherlands, pp. 159-166.

Groffman, P.M. Gold, A.J. Kellog, D.Q. & Addy, K. (2002). Mechanisms, rates and assessment of N_2O in groundwater, riparian zones and rivers, In: Van Ham, J. Baede, A.P.M. Guicherit, R. Williams-Jacobse, J.G.F.M. (Eds.), Proceedings of the Third International Symposium on Non-CO_2 Greenhouse Gases, Scientific Understanding, Control Options and Policy Aspects. Millpress, Rotterdam, Maastricht, The Netherlands, pp. 159-166.

Groffman, P.M. & Tiedje, J.M. (1989). Denitrification in north temperate forest soils, spatial and temporal patterns at the landscape and seasonal scale. *Soil Biology and Biochemistry,* 21, pp. 613-620.

Gross, P.J. & Bremner, J.M. (1992). Acetone problems in use of the acetylene blockage method for assessment of denitrifying activity in soil. *Communications in Soil Science and Plant Analysis,* 23, pp. 1345-1358.

Grundmann, G.L. Renault, P. Rosso, L. & Bardin, R. (1995). Differential effects of soil water content and temperature on nitrification and aeration. *Soil Science Society of America Journal,* 59, pp. 1342-1348.

Gut, A. Blatter, A. Fahrni, M. Lehmann, B.E. Neftel, A. & Staffelbach, T. (1998). A new membrane tube technique METT for continuous gas measurements in soils. *Plant and Soil,* 198, pp. 79-88.

Henrich, M. & Haselwandter, K. (1997). Denitrification and gaseous nitrogen losses from an acid spruce forest soil. *Soil Biology and Biochemistry,* 29, pp. 9-10.

Hynšt, J. Brůček, P. & Šimek , M. (2007). Nitrous oxide emissions from cattle-impacted pasture soil amended with nitrate and glucose. *Biology and Fertility of Soils,* 43, pp. 853-859.

IFA. (2010). International Fertiliser Association statistics, Nitrogen Fertilizer Consumption by Region, In: Wilson, J.R. (Ed.), Advances in Nitrogen Cycling in Agricultural Ecosystems.

Inubushi, K. Naganuma, H. & Kitahara, S. (1996). Contribution of denitrification and autotrophic and heterotrophic nitrification to nitrous oxide production in andosols. *Biology and Fertility of Soils* 23, pp. 292-298.

IPCC. (2007). Climate Change, Mitigation of Climate Change, Contribution of Working Group III to the Intergovernmental Panel on Climate Change, Fourth Assessment Report, Cambridge.

Jambert, C. Serca, D. & Delmas, R. (1997). Quantification of N, losses as NH_3, NO, and N_2O and N_2 from fertilized maize fields in southwestern France. *Nutrient Cycling in Agroecosystems,* 48, pp. 91-104.

Jenkinson, D.S. & Ladd, J.N. (1981). Microbial biomass in soils, measurement and turn over, In: Paul, E.A. Ladd, J.N. (Eds.), Soil Biochemistry. Marcel Dekker, New York, pp. 415-471.

Kanakidou, M. Keller, M. Melillo, J.M. & Zavaria, G.A. (1989). Trace gas exchange and the chemical and physical climate, critical interactions, In: Andreae, M.O. Schimel, D.S. (Eds.), Exchange of Trace Gases between Terrestrial Ecosystems and the Atmosphere. John Wiley & Sons Ltd. Chichester, pp. 303-320.

Khalil, M.I. Rosenani, A.B. van Cleemput, O. Fauziah, C.I. & Shamshuddin, J. (2002). Nitrous oxide emissions from an ultisol of the humid tropics under maize, groundnut rotation. *Journal of Environmental Quality,* 31, pp. 1071-1078.

Kostina, N.V. Stepanov, A.L. & Umarov, M.M. (1996). Impact of environmental factors of nitrous oxide reduction in some soil types. *Eurasian Soil Science,* 28, pp. 175-184.

Kwong, K.F.N.K. Bholah, A. Veerapen, S. & Singh, V. (1999). Gaseous nitrogen losses from soils under sugar cane in Mauritius, In: Kumar, V. (Ed.), Proceedings of the XXIII ISSCT Congress, New Delhi, India, pp. 70-79.

Ladd, J.N. & Jackson, R.B. (1982). Biochemistry of ammonification, In: Stevenson, F.G.S. (Ed.), Nitrogen in Agricultural Soil. American Society of Agronomy Madison Wisconsin, pp. 173-228.

Ledgard, S.F. & Luo, J. (2008). Nitrogen cycling in intensively grazed pastures and practices to reduce whole-farm nitrogen losses, Multifunctional Grasslands in a Changing World, Organizing Committee of 2008 IGC/IRC Conference. Guangdong People's Publishing House, pp. 292-297.

Ledgard, S.F. Menneer, J.C. Welten, B. Kear, M.J. Dexter, M.M. Lindsey, S.B. Betteridge, K. Crush, J.R. & Pacheco, D. (2007). New nitrogen mitigation technologies for evaluation in the lake Taupo catchment, In: L.D. C. L.J. Y. (Eds.), Proceedings of the Workshop "Design Sustainable Farms, Critical Aspects of Soil and Water Management. Fertilizer and Lime Research Centre, Massey University, Palmerston North, New Zealand, pp. 19-24.

Ledgard, S.F. Penno, J.W. & Sprosen, M.S. (1999). Nitrogen inputs and losses from clover/grass pastures grazed by dairy cows, as affected by nitrogen fertilizer application. *Journal Agricultural Science Cambridge,* 132, pp. 215-225.

Linn, D.M. & Doran, J.W. (1984). Effect of water-filled pore space on carbon dioxide and nitrous oxide production in tilled and nontilled soils. *Soil Science Society of America Journal,* 48, pp. 1267-1272.

Lloyd, A.B. & Sheaffe, M.J. (1973). Urease activity in soils. *Plant and Soil,* 39, pp. 71-80.

Luo, J. & Ledgard, S.F. (2008). A test of a winter farm management option for mitigating nitrous oxide emissions from a dairy farm. *Soil Use and Management,* 24, pp. 121-130.

Ma, W.K. Schautz, A. Fishback, L.A.E. Bedard-Haughn, A. Farrell, R.E. & Siciliano, S.D. (2007). Assessing the potential of ammonia oxidizing bacteria to produce nitrous oxide in soils of a high arctic lowland ecosystem on Devon Island, Canada. *Soil Biology and Biochemistry,* 39, pp. 2001-2013.

Manunza, B. Deiana, S. Pintore, M. & Gessa, C. (1999). The binding mechanism of urea, hydroxamic acid and N-(N-butyl)-phosphoric triamide to the urease active site. A comparative molecular dynamics study. *Soil Biology and Biochemistry,* 31, pp. 789-796.

Martikainen, P.J. (1985). Nitrous oxide emission associated with autotrophic ammonium oxidation in acid coniferous forest soil. *Applied and Environmental Microbiology,* 50, pp. 1519-1525.

Matheson, F.E. Nguyen, M.L. Cooper, A.B. & Burt, T.P. (2003). Short-term nitrogen transformation rates in riparian wetland soil determined with nitrogen-15. *Biology and Fertility of Soils,* 38, pp. 129-136.

Matheson, F.E. Nguyen, M.L. Cooper, A.B. Burt, T.P. & Bull, D.C. (2002). Fate of 15N-nitrate in unplanted, planted and harvested riparian wetland soil microcosms. *Ecological Engineering,* 19, pp. 249-264.

McMahon, P. Dennehy, K. & Sandstrom, M. (1999). Hydraulic and geochemical performance of a permeable reactive barrier containing zero-valent Iron, Denver Federal Center. *Ground Water* 37, pp. 396-404.

Mengel, K. (1996). Turnover of organic nitrogen in soils and its availability to crops. *Plant and Soil*, 181, pp. 83–93.

Mondini, C. Sinicco, T. Cayuela, M.L. Sanchez-Monedero, M.A. 2010.A simple automated system for measuring soil respiration by gas chromatography. *Talanta*, 81, pp. 849–855

Mosier, A.R. Doran, J.W. & Freney, J.R. (2002). Managing soil denitrification. *Journal of Soil and Water Conservation,* 57, pp. 505-513.

Mosier, A.R. Guenzi, W.D. & Schweizer, E.E. (1986). Soil losses of dinitrogen and nitrous oxide from irrigated crops in Northeastern Colorado. *Soil Science Society of America Journal,* 50, pp. 344-348.

Mosier, A.R. & Klemedtsson, L. (1994). Measuring denitrification in the field, In: Weaver, R.W. (Ed.), *Methods of Soil Analysis Part 2 SSSA Book Series, Madison*, WI, pp. 1047-1065.

Muller, C. Martin, M. Stevens, R.J. Laughlin, R.J. Kammann, C. Ottow, J.C.G. & Jager, H.J. (2002). Processes leading to N_2O emissions in grassland soil during freezing and thawing. *Soil Biology and Biochemistry,* 34, 1325-1331.

Mulvaney, R.L. Khan, S.A. & Mulvaney, C.S. (1997). Nitrogen fertilizers promote denitrification. *Biology and Fertility of Soils,* 24, pp. 211-220.

Nägele, W. & Conrad, R. (1990). Influence of soil- pH on the nitrate-reducing microbial populations and their potential to reduce nitrate to NO and N_2O. *FEMS Microbial Ecology,* 74, pp. 49-57.

Nguyen, M.L. Rutherford, J.C. & Burns, D. (1999). Denitrification and nitrate removal in two contrasting riparian wetlands, In: Tomer, M. Robinson, M. Gielen, G. (Eds.), Modelling of Land Treatment Systems. Proceedings of the 20th New Zealand Land Treatment Collective Technical Session. New Zealand Forest Research Institute, Rotorua, NZ New Plymouth, NZ, pp. 127-131.

Nobre, A.D. Keller, M. Crill, P.M. & Harriss, R.C. (2001). Short-term nitrous oxide profile dynamics and emissions response to water, nitrogen and carbon additions in two tropical soils. *Biology and Fertility of Soils,* 34, 363-373.

Parkin, T.B. (1987. Soil microsites as a source of denitrification variability. *Soil Science Society of America Journal,* 51, pp. 1194-1199.

Paul, E.A. & Clark, E. (1996). Ammonification and nitrification, In: Paul, E.A. Clark, E. (Eds.), *Soil Microbiology and Biochemistry*. Academic Press, Inc. , USA, pp. 182-196.

Paul, J.W. & Beauchamp, E.G. (1989). Effect of carbon constituents in manure on denitrification in soil. *Canadian Journal of Soil Science,* 69, pp. 49-61.

Pinay, G. & Decamps, H. (1988). The role of riparian woods in regulating nitrogen fluxes between the alluvial aquifer and surface waters, A conceptual model. *Regulated Rivers Research and Management* 2, pp. 507-516.

Poth, M. & Focht, D.D. (1985). 15N kinetic-analysis of N_2O production by Nitrosomonas europaea, an examination of nitrifier denitrification. *Applied and Environmental Microbiology,* 49, pp. 1134-1141.

Ramos, C. (1996). Effect of agricultural practices on the nitrogen losses to the environment. *Fertilizer Research,* 43, pp. 183-189.

Robertson, G.P. Andreae, M.O. Bingemer, H.G. Crutzen, P.J. Delmas, R.A. Duyzer, J.H. Fung, I. Harriss, R.C. Kanakidou, M. Keller, M. Melillo, J.M. & Zavaria, G.A. (1989). Group report ?race gas exchange and the chemical and physical climate: critical interactions. In: Andreae, M.O. and Schimel, D.S. (eds), Exchange of trace gases between terrestrial ecosystems and the atmosphere. pp. 303 – 320. John Wiley & Sons Ltd. Chichester.

Roberge, M.R. & Knowels, R. (1967). The ureolytic microflora in a black spruce (*Picea mariana* Mill) humus. *Soil Science Society of America Proceedings,* 31, pp. 76-79.

Robertson, G.P. & Tiedje, J.M. (1987). Nitrous oxide sources in aerobic soils, nitrification, denitrification and other biological processes. *Soil Biology and Biochemistry,* 19, pp. 187-193.

Robinson D. (2001). Delta N-15 as an integrator of the nitrogen cycle. *Trends in Ecology and Evolution,* 16, pp. 153–162.

Rochester, I.J. (2003). Estimating nitrous oxide emissions from flood-irrigated alkaline grey claysna. *Australian Journal of Soil Research,* 41, pp. 197-206.

Ryden, J.C. (1983). Denitrification loss from a grassland soil in the field receiving different rates of nitrogen as ammonium. *Journal of Soil Science,* 34, pp. 355-365.

Ryden, J.C. & Lund, L.J. (1980). Nature and extent of directly measured denitrification losses from some irrigated vegetable crop production units. *Soil Science Society of America Journal,* 44, pp. 505-511.

Saggar, S. Andrew, R.M. Tate, K.R. Hedley, C.B. Rodda, N.J. & Townsend, J.A. (2004a). Modelling nitrous oxide emissions from New Zealand dairy grazed pastures. *Nutrient Cycling in Agroecosystems,* 68, 243-255.

Saggar, S. Bolan, N.S. Bhandral, R. Hedley, C. & Luo, J. (2004b). Emissions of methane, ammonia and nitrous oxide from animal excreta deposition and farm effluent application in grazed pastures. *New Zealand Journal of Agricultural Research,* 47, pp. 513-544.

Saggar, S. Bolan, N.S. Singh, J. & Blard, A. (2005). Economic and environmental impacts of increased nitrogen use in grazed pastures and the role of inhibitors in mitigating nitrogen losses. *New Zealand Science Review,* 62, pp. 62-67.

Saggar, S. Hedley, C.B. Giltrap, D.L. & Lambie, S.M. (2007). Measured and modelled estimates of nitrous oxide emission and methane consumption from sheep-grazed pasture. *Agriculture Ecosystems and Environment,* 122, pp. 357-362.

Saggar, S. Luo, J. Giltrap, D.L. & Maddena, M. (2009). Nitrous oxide emissions from temperate grasslands, processes, measurements, modelling and mitigation, In: Adam, I.S. Barnhart, E.P. (Eds.), Nitrous Oxide Emissions Research Progress. Nova Science Publishers, Inc. , pp. 1-66.

Sanz-Cobena, A. Misselbrook, T.H. Arce, A. Mingot, J.I. Diez, J.A. & Vallejo, A. (2008). An inhibitor of urease activity effectively reduces ammonia emissions from soil treated

with urea under Mediterranean conditions. *Agriculture Ecosystem and Environment,* 126, pp. 243-249.

Scholefield, D. Hawkins, J.M.B. & Jackson, S.M. (1997). Use of a flowing helium atmosphere incubation technique to measure the effects of denitrification controls applied to intact cores of a clay soil. *Soil Biology and Biochemistry,* 29, pp. 1337-1344.

Sherlock, R.R. Goh, K.M. Jewell, P. & Clough, T.J. (2009). Review of New Zealand specific FracGASM and FracGASF emission factors, Reports for Ministry of Agriculture and Forestry, pp. 52.

Silver, W.L. Herman, D.J. & Firestone, M.K. (2001). Dissimilatory nitrate reduction to ammonium in upland tropical forest soils. *Ecology,* 82, pp. 2410-2416.

Šimek, M. (2000). Nitrification in soil - terminology and methodology review. *Rostlinna-Vyroba,* 46, pp. 385-395.

Šimek, M. & Cooper, J.E. (2002). The influence of soil pH on denitrification, progress towards the understanding of this interaction over the last 50 years. *European Journal of Soil Science,* 53, pp. 345-354.

Šimek, M. & Hopkins, D.W. (1999). Regulation of potential denitrification by soil pH in long-term fertilized arable soil. *Biology and Fertility of Soils,* 30, pp. 41-47.

Šimek, M. Jíšová, L. & Hopkins, D.W. (2002). What is the so-called optimum pH for denitrification in soil? *Soil Biology and Biochemistry,* 34, pp. 1227-1234.

Singh, J. Saggar, S. Giltrap, D.L. & Bolan, N.S. (2008). Degradation kinetics of dicyandiamide in three soils and its effect on nitrous oxide emission and microbial biomass, An incubation study. *Australian Journal of Soil Research,* 46, pp. 517-525.

Skujins, J.J. (1976). Extracellular enzymes in soils. CRC. *Critical Review of Microbiology,* 4, pp. 383-421.

Smith, K.A. Ball, T. Conen, F. Dobbie, K.E. & Rey, A. (2003). Exchange of greenhouse gases between soil and atmosphere, interactions of soil physical factors and biological processes. *European Journal of Soil Science,* 54, pp. 779-791.

Smith, M.S. & Tiedje, J.M. (1979). Phases of denitrification following oxygen depletion in soil. *Soil Biology and Biochemistry,* 11, pp. 261-267.

Stevens, R.J. Laughlin, R.J. Burns, L.C. Arah, J.R.M. & Hood, R.C. (1997). Measuring the contributions of nitrification and denitrification to the flux of nitrous oxide from soil. *Soil Biology and Biochemistry*, 29, pp.139-151.

Stevens, R.J. & Laughlin, R.J. (1998). Measurement of nitrous oxide and di-nitrogen emissions from agricultural soils. *Nutrient Cycling in Agroecosystems,* 52, pp. 131-139.

Sutka, R.L. Ostrom, N.E. Ostrom, P.H. Breznak, J.A. Gandhi, H. Pitt, A.J. & Li, F. (2006). Distinguishing nitrous oxide production from nitrification and denitrification on the basis of isotopomer abundances. *Applied and Environmental Microbiology*, 72, pp. 638–644.

Swerts, M. Merckx, R. & Vlassak, K. (1996). Influence of carbon availability on the production of NO, N_2O, N_2 and CO_2 by soil cores during anaerobic incubation. *Plant and Soil,* 181, pp. 145-151.

Swerts, M. Merckx, R. & Vlassak, K. (1997). Denitrification, N_2,fixation and fermentation during anaerobic incubation of soils amended with glucose and nitrate. *Biology and Fertility of Soils,* 23, pp. 229-235.

Thornton, F.C. Bock, B.R. & Tyler, D.D. (1996). Soil emissions of nitric oxide and nitrous oxide from injected anhydrous ammonium and urea. *Journal of Environmental Quality,* 25, pp. 1378-1384.

Tiedje, J.M. (1988). Ecology of denitrification and dissimilatory nitrate reduction to ammonium, In: Zehnder, J.B. (Ed.), Biology of Anaerobic Microorganisms. Wiley, New York, pp. 179-244.

Tilsner, J. Wrage, N. Lauf, J. & Gebauer, G. (2003). Emission of gaseous nitrogen oxides from an extensively managed grassland in NE Bavaria, Germany. *Biogeochemistry*, 63 (3), pp. 249-267.

Walker, J.T. Geron, C.D. Vose, J.M. & Swank, W.T. (2002). Nitrogen trace gas emissions from a riparian ecosystem in southern Appalachia. *Chemosphere,* 49, pp. 1389-1398.

Watson, C.J. (2000). Urease activity and inhibition principles and practice, Proceedings International Fertiliser-Society No. 454. International Fertiliser Society, UK, pp. 1-40.

Watson, C.J. Akhonzada, N.A. Hamilton, J.T.G. & Matthews, D.I. (2008). Rate and mode of application of the urease inhibitor N-n-butyl thiophosphoric triamide on ammonia volatilization from surface-applied urea. *Soil Use Management,* 24, pp. 246-253.

Watson, C.J. Miller, H. Poland, P. Kilpatrick, D.J. Allen, M. Garrett, M.K. & Christianson, C.B. (1994a). Soil properties and the ability of the urease inhibitor N-n-butyl thiophosphoric triamide NBTPT to reduce ammonia volatilization from surface-applied urea. *Soil Biology and Biochemistry,* 26, pp. 1165-1171.

Watson, C.J. Miller, H. Poland, P. Kilpatrick, D.J. Allen, M.D.B. Garrett, M.K. & Christianson, C.B. (1994b). Soil properties and the ability of the urease inhibitor N-N-butyl thiophosphoric triamide Nbtpt to reduce ammonia volatilization from surface-applied urea. *Soil Biology and Biochemistry,* 26, pp. 1165-1171.

Watson, C.J. Stevens, R.J. & Laughlin, R.J. (1990). Effectiveness of the urease inhibitor Nbpt N-normal-butyl thiophosphoric triamide for improving the efficiency of urea for ryegrass production. *Fertilizer Research,* 24, pp. 11-15.

Watson, S.W. Valos, F.W. & Waterbury, J.B. (1981). The family nitrobacteraceae, In: Starr, M.P. Stolp, H. Trupe, H.G. Below, A.P. Shlegel, H.G. (Eds.), The Prokaryotes, A handbook on Habits, Isolation, and Identification of Bacteria. Springer-Verlag, Berlin.

Weier, K.L. Doran, J.W. Power, J.F. & Walters, D.T. (1993). Denitrification and the dinitrogen/nitrous oxide ratio as affected by soil water, available carbon, and nitrate. *Soil Science Society of America Journal,* 57, pp. 66-72.

Weier, K.L. & Gilliam, J.W. (1986). Effect of acidity on denitrification and nitrous oxide evolution from Atlantic Coastal Plain soils. *Soil Science Society of America Journal,* 50, pp. 1202-1205.

Weiske, A. Benckiser, G. Herbert, T. & Ottow, J.C.G. (2001). Influence of nitrification inhibitor 3,4-dimethylpyrazole phosphate DMPP in comparison to dicyandiamide DCD on nitrous oxide emissions, carbon dioxide fluxes and methane oxidation during 3 years of repeated application in field experiments. *Biology and Fertility of Soils,* 34, pp. 109-117.

Whitehead, D.C. (1995). Grassland Nitrogen. CAB International, Wallingford, UK.

Wood, P.M. (1990). Autotrophic and heterotrophic mechanisms for ammonia oxidation. *Soil Use and Management,* 6, pp. 78-79.

World Resources Institute (2000). World Resources 2000–2001. World Resources Institute, Washington D.C.

Wrage, N. Velthof, G.L. Beusichem, M.L. & van Oenema, O. (2001. Role of nitrifier denitrification in the production of nitrous oxide. *Soil Biology and Biochemistry,* 33, pp. 1723-1732.

Wrage, N. Velthof, G.L. Laanbroek, H.J. & Oenema, O. (2004). Nitrous oxide production in grassland soils, assessing the contribution of denitrification. *Soil Biology and Biochemistry,* 36, pp. 229-236.

Xu, X. Zhou, L. Cleemput, O.V. & Wang, Z. (2000). Fate of urea-15N in a soil-wheat system as influenced by urease inhibitor hydroquinone and nitrification inhibitor dicyandiamide. *Plant and Soil,* 220, pp. 261-270.

Zaman, M. & Blennerhassett, J.D. (2010). Effects of the different rates of urease and nitrification inhibitors on gaseous emissions of ammonia and nitrous oxide, nitrate leaching and pasture production from urine patches in an intensive grazed pasture system. *Agriculture Ecosystems and Environment,* 136, pp. 236-246.

Zaman, M. & Chang, S.X. (2004). Substrate type, temperature, and moisture content affect gross and net soil N mineralization and nitrification rates in agroforestry systems. *Biology and Fertility of Soils,* 39, pp. 269-279.

Zaman, M. Di, H.J. & Cameron, K.C. (1999a). Gross N-mineralization and nitrification rates and their relationships to enzyme activities and soil microbial biomass in soils treated with dairy shed effluent and ammonium fertilizer in the field. *Soil Use and Management,* 15, pp. 188-194.

Zaman, M. Di, H.J. Cameron, K.C. & Frampton, C.M. (1999b). Gross N mineralization and nitrification rates and their relationships to enzyme activities and soil microbial biomass in soils treated with dairy shed effluent and ammonium fertilizer at different water potentials. *Biology and Fertility of Soils,* 29 (2), pp. 178–186.

Zaman, M. & Nguyen, M.L. (2010). Effect of lime or zeolite on N_2O and N_2 emissions from a pastoral soil treated with urine or nitrate-N fertiliser under field conditions. *Agriculture Ecosystems and Environment,* 136, pp. 254-261.

Zaman, M. Nguyen, M.L. Blennerhassett, J.D. & Quin, B.F. (2008a). Reducing NH_3, N_2O and NO_3-N losses from a pasture soil with urease or nitrification inhibitors and elemental S-amended nitrogenous fertilizers. *Biology and Fertility of Soils,* 44, pp. 693-705.

Zaman, M. Nguyen, M.L. Gold, A.J. Groffman, P.M. Kellogg, D.Q. & Wilcock, R.J. (2008b). Nitrous oxide generation, denitrification and nitrate removal in a seepage wetland intercepting surface and subsurface flows from a grazed dairy catchment. *Australian Journal of Soil Research,* 46, pp. 565-577.

Zaman, M. Nguyen, M.L. Matheson, F. Blennerhassett, J.D. Quin, B.F. (2007). Can soil amendments zeolite or lime shift the balance between nitrous oxide and dinitrogen emissions from pasture and wetland soils receiving urine or urea-N? *Australian Journal of Soil Research,* 45, pp. 543-553.

Zaman, M. Nguyen, M.L. & Saggar, S. (2008c). N_2O and N_2 emissions from pasture and wetland soils with and without amendments of nitrate, lime and zeolite under laboratory condition. *Australian Journal of Soil Research,* 46, pp. 526-534.

Zaman, M. Saggar, S. Blennerhassett, J.D. & Singh, J. (2009). Effect of urease and nitrification inhibitors on N transformation, gaseous emissions of ammonia and nitrous oxide, pasture yield and N uptake in grazed pasture system. *Soil Biology and Biochemistry,* 41, pp. 1270-1280.

Zart, D. & Bock, E. (1998). High rate of aerobic nitrification and denitrification by Nitrosomonas eutropha grown in a fermentor with complete biomass retention in the presence of gaseous N_2O or NO. *Archives of Microbiology,* 169, pp. 282-286.

Zerulla, W. Barth, T. Dressel, J. Erhardt, K. Locquenghien, K.H.V. Pasda, G. Radle, M. & Wissemeier, A.H. (2001). 3,4-Dimethylpyrazole phosphate DMPP-a new nitrification inhibitor for agriculture and horticulture, an introduction. *Biology and Fertility of Soils*, 34, pp. 79-84.

2

The Blend Ethanol/Gasoline and Emission of Gases

Antonio Carlos Santos
Empresa de Pesquisa Energética
Brazil

1. Introduction

By simulation, the sparkling ignition internal combustion engine, mechanic Otto cycle, four strokes, can be approximated to a thermodynamic cycle made of four different phases such as intake, compression (combustion), expansion and exhaustion.

According to Heywood (1988), the combustion reactions from those engines are characterized by a very rapid detonation, with the following characteristics: high pressure, due to the compression phase; a reaction zone extremely thin; the lack of chemical balance because of a very short residence time; a drop in temperature next to the gas valves outlets, due to expansion in the exhaust and then to the environment.

In a stoichiometry, the relative amount of the resulting products to the atmosphere depends on the chemical composition of the fuel, engine design, conditions of operation, the intermediate species that are formed during the process and the presence of a catalyst in the exhaust.

The blended ethanol gasoline has major effects on reducing emissions of greenhouse gases, while the engine design, as well as the operation conditions, and the presence of a catalyst in the exhaust, decrease pollutants and greenhouse gases.

The preliminary combustion processes are explained by reactions mechanisms and chemical kinetics, and are important to show how these gases are formed and to determine the emission levels.

The engine has a decisive role in the efficient burning; in this case, the physical and chemical properties of the fuel must be specified in accordance with the requirements of your project.

On the other hand, in Otto cycle engines, adding ethanol to gasoline, it reduces emissions of greenhouse gases like carbon dioxide (CO_2), methane (CH_4), and nitrous oxide (N_2O), and pollutants like carbon monoxide (CO), volatile organic compounds (VOC). Though, there is an increase in nitrogen oxides (NOx), and aldehydes (RCHO).

The purpose of this study is to compare the emissions of pollutant and greenhouse gases, when using the blend gasoline/ethanol or hydrated ethanol; understanding the differences between the combustion of two types of vehicles, and reviewing mechanisms that allow the increments and reduction of pollutant and the greenhouse gases.

2. Combustion in Otto cycle engines

The amount of the fuel components oxidation depends on temperature, oxygen concentration and how they mix with the gases. For these conditions occur, it is necessary that: the air/fuel ratio to obey stoichiometry; fuel spray be made and, the devices that perform this operation, the carburetor (older system) and electronic fuel injection, are in perfect conditions of operation.

The air / fuel ratio should be closer to stoichiometric. Inadequate concentration of oxygen promotes the partial oxidation of hydrocarbons during the preliminary process of combustion, the expansion and the exhaustion, with the CO, VOC and particulates.

The unfinished spray of fuel provides the accumulation of fuel in the cylinder walls. This occurs either from non calibrated equipments or at the start moment, when the engine is cold. In both cases, the fuel not burned, or partially burned, can form a thin layer on the wall. There is flame extinction and, as a result, we get an incomplete combustion and CO, VOC and particulates emissions. This problem is avoided by the adoption of multipoint injection system, because it is more efficient than the previous one.

Incomplete combustion can occur during startup when the engine is cold, or the spark timing in relation to air / fuel mixture cannot be adequately controlled. In both cases, there may have misfire or partial burning.

The formation of gaps between the cylinder and piston engines, as they get older, allows its filling, due to the flame at the entrance slit, and the mixture escapes from the preliminary process of combustion. The gas coming out of these cracks during the expansion process is a source of CO, VOC and particulates.

The engine oil can form a thin film on the cylinder wall, piston and cylinder head. The layers of oil can absorb hydrocarbons during the compression process and, during the expansion, it could release these substances to the gases formed. This mechanism allows a fraction of the fuel to exhaust of the preliminary process of combustion.

2.1 Mechanisms of chemical reactions in the engines

The detailed chemical mechanisms of pollutant formation and kinetics of these processes is important to determine the emission levels. The breakdown of molecules (pyrolysis) predominates during the preliminary process of combustion while the oxidation of hydrocarbons (which escape the process) occurs during the expansion and exhaust.

For nitrogen oxides, the formation and destruction of intermediate chemical species are not part of the combustion process; but the reactions that produce them occur in this environment.

The combustion reaction mechanisms of several hydrocarbons, including heptane and iso-octane were studied by Curran et al (1997-98) and the pure ethanol by Marinov (1998), both at Lawrence Livermore National laboratory in California.

Westbrook et al (1999) studied in the chemical kinetics model, the number of chemical species involved in combustion reactions. (Table 1)

Fuel	H_2	CH_4	C_3H_8	C_6H_{14}	$C_{16}H_{34}$
Species number	7	30	100	450	1200
Reactions Number	25	200	400	1500	7000

Table 1. Chemical species formed in combustion.

The flue gas analysis carried out shows that many organic compounds found in the exhaust are not originally in the fuel, indicating that significant changes occur during the process.

The observations made in these studies concluded that the reactions of decomposition (pyrolysis) are predominant at high temperatures, above 900K, and the reactions at low temperatures, below 900 K, dominate the oxygen addition reactions.

In a stoichiometric reaction, the relative amount of the resulting products into the atmosphere depends on the chemical composition of fuel, engine design, conditions of operation, the intermediate species that formed during the process and the presence of a catalyst in the exhaust.

The surveys reveal that at high temperatures occur decomposition on fuel molecules, extraction of hydrogen atoms, oxidation, isomerization and addition to double bond.

At this stage, there is a predominance of decomposition reactions and extraction of hydrogen which, according to Curran et al, responds for 50% of fuel consumption, as the example below:

$$RH + O_2 \rightarrow R_1H + OH^{\cdot} \quad (1)$$

$$RH + O \rightarrow R_1H + OH^{\cdot} \quad (2)$$

At temperatures below 900 C occur the following reactions keys: extraction of the H atom of alkanes, cyclic ether, aldehyde or ketone, addition of radicals to oxygen, split hemolytic CC and OO and decomposition of several radicals, radical reaction of the peroxide alkyl with HO_2 and H_2O_2 isomerization of the radical peroxide and hydroperoxide alkyl, scission of hydroperoxy alkyl radical, alkyl hydroperoxide radical oxidation and formation of cyclic ether hydroperoxido alkyl radical and hydroperoxide radical. Many reactions have the product OH and HO_2.

$$RO_2^{\cdot} + H_2O_2 \rightarrow ROOH + HO_2^{\cdot} \quad (3)$$

$$ROOH^{\cdot} \rightarrow alceno + HO_2^{\cdot} \quad (4)$$

$$ROOH^{\cdot} \rightarrow RO^{\cdot} + HO_2^{\cdot} \quad (5)$$

Marinov (1998), citing Borison and Norton and Dryer et al, modeling studies shows that the pyrolysis of ethanol forms the three major isomers radicals.

$$C_2H_5OH + X \rightarrow CH_2CH_2OH + XH \quad (6)$$

$$C_2H_5OH + X \rightarrow CH_3CHOH + XH \quad (7)$$

$$C_2H_5OH + X \rightarrow CH_3CH_2O + XH \quad (8)$$

X are OH, OH_2, CH_3 radicals or O and H atoms.

The addition of ethanol to gasoline increases the concentration of HO and OH_2 throughout the course of combustion and consequent increases the concentration of oxygenated compounds. The presence of theses radicals at high temperatures reduces emissions of HC (equations 1 and 2) and CO, as the following reaction:

$$CO + OH^{\cdot} \rightarrow CO_2 + H^{\cdot} \tag{9}$$

California Environmental Protection Agency (1999) in the article "Air Quality Impacts of the Use of Ethanol in California Reformulated Gasoline", citing a study by Koshland et al (1988), shows that mixing gasoline and ethanol 10% by volume (3.7% oxygen by weight) significantly reduces CO (13%), VOC (6%), benzene (11%), and increases NOx (5%), acetaldehyde (159%) as well as evaporative emissions.

Heywood (1988) estimated the emissions for gasoline without catalytic converted on the following values: NOx, from 500 to 1000 ppm; CO, 1 to 2% and unburned hydrocarbons (expressed as methane) at 3000 ppm.

2.2 Formation of carbon compounds

2.2.1 Carbon Monoxide

According to Muharam (2005), the formation of CO to 1250 K starts from the thermal decomposition of formyl and acetyl radicals, as follows:

$$CHO \rightarrow CO + H \tag{10}$$

$$CH_3CO \rightarrow CO + H \tag{11}$$

At low temperatures, around 600 K, the chain reaction for the formation begins with the decomposition of three isomers of carbonyl radicals and, after the formation of several intermediates, CO is produced through the decomposition and oxidation of small amounts of light cetyl radicals, as follows:

$$CH_3CO \rightarrow CH_3 + CO \tag{12}$$

$$C_2H_5CO \rightarrow C_2H_5 + CO \tag{13}$$

$$CHO + O_2 \rightarrow CO + HO_2^{\cdot} \tag{14}$$

$$C_3H_7CO \rightarrow CO + nC_3H_7 \tag{15}$$

2.2.2 Carbon dioxide

Formation occurs by the reaction of carbon monoxide with the radicals hydroxyl (OH) and hydroperoxide (HO_2); both at high and low temperature, according to the equations:

$$CO + HO_2^{\cdot} \rightarrow CO_2 + OH^{\cdot} \tag{16}$$

$$CO + OH^{\cdot} \leftrightarrow CO_2 + H^{\cdot} \tag{17}$$

Nevertheless, there is an increase of CO_2 emissions. However, this is the best option from environmental point of view, because the removal of CO from the atmosphere is made trough the mentioned reaction, which is preferred, because it is more reactive. This alternative, however, reduces the levels of OH, which is the route for the removal of methane. Consequence, there is an increased concentration of this gas in the atmosphere.

At temperatures of 600 and 700 K, it begins with the decomposition of carbonyl radicals to form the cetyl radical, after the formation of intermediate compounds. The formation of CO_2 also occurs through the reaction between OH radicals and ketones:

$$OH^{\cdot} + CH_2CO \rightarrow CO_2 + CH_3^{\cdot} \quad (18)$$

2.2.3 Methane

In conformity to Muharan (2005), the formation of methane occurs primarily through decomposition of cetyl radicals, with the addition of the oxygen atom to ethylene and decomposition of n-propyl radical which forms an intermediate, the methyl radical. This one reacts with the formaldehyde, ethylene and hydrogen atoms to form methane:

$$CH_2O + CH_3^{\cdot} \rightarrow CH_4 + CHO \quad (19)$$

$$C_2H_4 + CH_3^{\cdot} \rightarrow CH_4 + CHO \quad (20)$$

$$CH_3^{\cdot} + H \rightarrow CH_4 \quad (21)$$

The mechanisms of destruction of the formed methane are shown below:

$$CH_4 + O \rightarrow CH_3^{\cdot} + OH^{\cdot} \quad (22)$$

$$CH_4 + H^{\cdot} \rightarrow CH_3^{\cdot} + H_2 \quad (23)$$

$$CH_4 + OH^{\cdot} \rightarrow CH_3^{\cdot} + H_2O \quad (24)$$

It should be noticed that the formation of methane occurs in conjunction with the emissions of methane occurs in conjunction with hydrocarbons (HC). Heywood (1988) described the formation of these emissions and concluded that the contribution of the occurred processes in the gas cylinder is small.

2.3 Nitrogen compounds

The nitrogen that forms nitric oxide in the combustion, which will route for the formation of nitrous oxide comes from two sources: atmosphere nitrogen (N_2) and organic (in the fuel). The N_2 from the air is the most important source in the reactions that occur in internal combustion engines. Heywood (1988) estimated that if the fuel contains a significant amount of organic nitrogen – over 1% in weight (an example is biomass), the final NO emission can increase between 10 and 30%. In light petroleum distillates (gasoline, for example), this is low, around 0,07 – in this case, the organic nitrogen slightly affects the concentration of NO in the flue gas.

The processes of formation of nitrogen oxides have a different mechanism. It should be noticed, however, that the combustion reactions produce an increase in temperature that

allows the formation of NO which is a NO_2 and N_2O precursor; the interactions with compounds from combustion processes explain their processes of destruction. Thus, the two processes are linked.

There are four proposed mechanisms to explain the formation of NO: the Zeldovich, or thermal NO, Fenimore, or "prompt", NO, from the formation of N_2O, and the decomposition, of organic compounds of nitrogen.

In internal combustion engines, using gasoline, the typical temperatures lie around 2000 K. In this case, the prompt Zeldovich mechanism explains the formation of approximately 95% NO. The contribution due to the prompt NO is estimated in less than 5% and the rest are very small.

Breaking the triple bond of nitrogen from the air requires an extremely hugh activation energy, around 220 Kcal/mol. An oxygen molecule (O_2) is not able to direct reaction between molecular nitrogen and molecular oxygen is too slow. To explain the formation of NO, Zeldovich proposed the following mechanism:

$$O + N_2 \rightarrow NO + N \tag{25}$$

$$O_2 + N \rightarrow NO + O \tag{26}$$

Later, another reaction was added:

$$OH^{\cdot} + N \rightarrow NO + H^{\cdot} \tag{27}$$

This proposed mechanism consisted of three reactions mentioned above is known as the extended Zeldovich mechanism. NO concentrations correspond to equilibrium at temperature conditions at the exit of the cylinders.

Due to the characteristics of combustion reactions, the formation of NO does not reach chemical equilibrium. As the temperature of exhaust gases falls during the course of expansion, the reactions that involve NO stuck and its concentration remains at levels that correspond to equilibrium under conditions of exhaustion.

The combustion reactions under the conditions prevailing in the cylinder at adiabatic flame temperature, in an internal combustion engine, are decisive in the formation of NO and by extension of NOx and N_2O.

The NO formation rate, according to the Zeldovich mechanism, is strongly accelerated above 2000 K and negligible if the temperature is below 1700 K. It is concluded that the exhaust gases to the atmosphere there is no more formation of NO, only reactions with the other gases.

Another factor that may increase the concentration of NO is the contribution from the pyrolysis of ethanol to the concentration of OH and HO_2 radicals. Preferably they react with CO, reducing its emissions, but an increase in concentration should also contribute to the increase of NO (Zeldovich equation of 3).

The residence time of combustion gases in the engine is another variable to be observed. Below 10 seconds, the formation of NO is small; above this value, it is accelerated.

According to Heywood, in the conditions prevailing in the exhaust, the following secondary reactions occur:

$$N_2O \xrightarrow{+O} NO \tag{28}$$

$$N_2O \xleftrightarrow{+H,+OH,+O,+M} N_2 \tag{29}$$

It is observed that an increase in the concentration of OH, due to addition of anhydrous ethanol, reduces the concentration of CO (equation 13) and prevents that:

$$CO + NO \rightarrow N_2O + CO_2 \tag{30}$$

In this case, there is an increase in emissions of NOx and N_2O reduction.

Due to a certain amount of NO formed at high temperature, it can be concluded that at low temperatures the concentrations of N_2O in the output gas into the atmosphere are in an inverse relation with the NOx formed (equation 30).

3. Main variants in the formations of greenhouse gases

Reducing emissions of greenhouse gases and pollutants gases is closely correlated to fuel consumption, so that the vehicle efficiency is reflected in the amount of emitted gases.

The efficiencies and emissions measured in laboratory depend on two factors only: characteristics of manufactured vehicles and used fuel. On the other hand, when the vehicle is in use, the actual emissions vary depending on a number of factors, including the driving cycle, maintenance, age and environmental conditions (temperature, humidity).

Good conditions of public roads, no traffic jams in the city, and conscious motorists improve the driving cycle and then reduce vehicle gases emissions. In addition to these, regular maintenance and old vehicles removing is necessary. These actions depend on investments to keep roads in good conditions, also depend on public policies to encourage the exchange of old cars and supervise drivers.

The lower emissions can be achieved by using low pollution potential fuels. The engine design must be compatible with the physicochemical properties of the fuel, so that the performance can be improved by reducing consumption and mechanical maintenance.

3.1 Characteristics of manufactured vehicles

The characteristics of manufactures vehicles depend on consumer preference for one type of vehicle and automotive technology applied.

In developed countries, like United States, during the economic boom time, consumers prefer bigger and more powerful engines, increasing fuel consumption and emission of greenhouse gases. On countries with less power of purchase, such as Brazil, they have a fleet of more compact vehicles and powerless engines. Thus, they don't pollute that much.

Considering, however, the average age of fleet vehicles in countries with higher power of purchase, they have lower emissions, due to their lower age (older vehicle emit more pollutants than newer ones).

De Cicco and Ross (1993) apud Azuaga (2000) bring together the technical approaches in the manufacture of the vehicle in order to increase the efficiency of vehicles, in three parts: the engine, transmission and load (vehicle weight, size and aerodynamics). In addition, one can cite the final control systems.

The use of advanced technologies in motor improves combustion efficiency, because the incomplete reactions are related to the emissions of some greenhouse gases. Three aspects are discussed: improving the fuel air mixture, for a better dispersion of fuel in the air; the closer this ratio to the stoichiometric equations provided in the reaction, and a shorter residence time of gases in the cylinder.

The most notable improvements regarding to this were the exchange of electronic carburetors by fuel injection, electronic ignition mapped and the adopting of more than one valve per cylinder. The first two technologies, as observed by DeCicco and Ross (1993) apud Azuaga (2000), improved the dosage to be introduced into the combustion chamber through load sensors, speed, temperature and pressure, and the third dispersion of fuel in the air that feeds the engine.

Important to note that improvements have been made to the engine to reduce friction between parts, with the introduction of variable valve timing, a mechanism that allows control of the position according to the vehicle operating conditions and thus, efficiently manage the processes of induction and exhaust (De Cicco and Ross 1993 cited in IPCC 1999).

Combustion gases leaving the exhaust of a vehicle, despite the technological efforts, contain certain amount of greenhouse gases. To eliminate them the auto industry has implemented a converter in the exhaust in order to promote a catalytic chemical reaction between them.

To reduce the loss of the mechanical efficiency of the transmission, which occurs when there is no efficient synchrony between it and the engine, new technologies have been produced, including front-wheel drive, automatic transmission and variable torque control.

This control allows the engine to operate at a lower speed under a given load condition and increases the speed when more power is required, as noticed by De Cicco and Ross (1993), cited Azuaga (2000).

The adoption of front wheel drive cars eliminates the heavy steering shaft providing energy savings by reducing the vehicle weight although it is not suitable for most models of light commercial vehicles.

The load reducing, by reducing the size of the compartments (truck, rear seats etc.) and components weight (through a careful redesign of its parts), and the use of new materials such as plastic, aluminum and mild steel, permit lighter vehicles been manufactured and then, there is a decrease in fuel consumption.

A technologically advanced aerodynamics reduces the consumption because it allows less air resistance. This is possible with the elimination of acute angles in the side panels, between the hood and windshield.

The use of this technology, however, is restricted to passenger cars. It does not apply to light commercial vehicles, which requires open and load spaces, and specific height from the ground to run off the road.

3.2 Characteristics of fuels and emissions

There are limitations in efforts to completely eliminate emissions gases from oil products responsible for global warm. The existence of fossil carbon in its chemical composition will necessarily have compounds like HC, CO_2, CH_4 and CO, reducing of emissions can be done by the use of biofuels and catalysts in the exhaust.

3.2.1 Gasoline

Gasoline, without the addition of ethanol, is primarily made of branched and unbranched aliphatics, cyclic (naphthenic), and aromatics, besides substances that contain atoms of sulfur, nitrogen, metals and oxygen. Table 7 shows the origin and properties of the main substances and blends used in the formulation of gasoline and the processes to obtain it, site Petrobras (2011).

Currently, the refinery gasoline is made of carefully balanced mixtures of hydrocarbons, to meet the performance requirements on engines, and to avoid the emissions of pollutants.

The gasoline chemical composition control is made from their physicochemical properties, such as: ASTM distillation; octane index; volatility; calorific value; and Reid vapor pressure. When analyzing the properties of gasoline manufactured in Brazil, one has to consider that it currently contains 25% of anhydrous ethanol (according to applicable law it may vary between 18 and 25).

The ASTM distillation of petroleum products at atmospheric pressure is one of the tests that evaluate the range and boiling oil and its derivatives to ensure the correct specification of the final product and the refining processes control.

	Process	Boiler point range (°C)	Motor octane number.
Butane. Isopentane	Crude oil distillation and transformation processes	Zero 27	101 75
Alkylate	Alkylation	40 - 150	90 – 100
Light naphtha	Crude oil distillation.	30 - 120	50 – 65
Heavy naptha	Crude oil distillation.	90 - 220	40 – 50
Hydrocracking naphtha	Hydrocracking Process Technology	40 - 220	80 – 85
Cracker naphtha	Fluid catalytic cracking process.	40 - 220	78 – 80
Naphtha polymer	Olefin polymerization.	60 - 220	80 – 100
Coker naphtha	Delayed Coking Process Technology.	30 - 150	70 – 76
Naphtha reform	Catalytic reforming	40 - 220	80 – 85

Table 2. Gasoline.

In Brazil, the application of ASTM distillation (in gasoline) gets ranges from 30 to 215 ° C. The content of 10% gasoline evaporated in the ASTM distillation is related to the minimum amount required for initial ignition to occur; the 50% of the distillate is related to the heating

and engine performance, while the remaining 90% is intended to minimize deposits formation, which is a source of emissions.

Volatility is the fuel agility to turn from liquid to vapor and this property is related to the 10% evaporated ASTM distillation. A fuel with high volatility promotes HC emissions, both in cold start and in the tank.

Currently there is a strong trend in reducing the volatility parameters, without compromising the ignition of the fuel. The way we can reduce this property is decreasing the amount of butane in gasoline in Brazil (see Table 1).

The Reid vapor pressure is the absolute pressure practiced by a mixture at 37.8 ° C with a rate of vapor/liquid of 4 to 1. The parameter is often used to characterize the volatility of gasoline and crude oils.

This test is mainly used to indicate the requirements that must be met for the products transportation and storage, including vehicles, preventing accidents and minimizing the losses.

It is observed that the higher the temperature, the greater is the evaporative emissions, and then the need to specify the volatility according to the region where it will be used and the season of the year.

A fuel with a low heat of vaporization and vapor pressure allows more complete combustion; the opposite can cause incomplete vaporization and a lack of control in the air/fuel relation making the burning process very difficult.

The aromatics have a high heat of vaporization and boiling point, then the difficulty of evaporation. These properties limit their use because they difficult the formation of homogeneous mixture air/fuel. As a result, there is a partial burning with the formation of CO and VOCs, especially during cold start.

Anhydrous ethanol also has a high heat of vaporization, but this property is compensated by its low boiling temperature, 10 ° C. In this case there is no difficulty of forming an air / fuel mixture as occurs with the aromatic.

The octane index measures the ability of a chemical compound to withstand high pressures without detonating. In the event of this fact, there will be a partial burning of fuel.

Engine designers take the octane into account to determine compression ratio, ignition advance curves and injection time.

The linear hydrocarbons have little resistance to compression and, for this reason, its concentration in gasoline should be controlled; the n-heptane, for example, has an octane rating of zero.

Branched hydrocarbons resist high pressures inside the cylinders, without detonation and consequent win of power; iso-octane, for example, has an octane rating of 100.

Hydrocarbons containing double bonds are desirable because they generally have high octane, but there are some restrictions on its use in engines, because they can easily bond with hydrogen to form paraffin. Besides, it is revealed that the decrease of its content decreases the formation of volatile organic compounds.

The aromatics (benzene and toluene are the most used) have the advantage of being chemically more stable than other unsaturated compounds; thus they are more resistant to auto ignition than iso-octane, during compression stroke. Benzene, for example, that has an index equal to 120 octanes, can be used as an agent to raise this ratio in fuels.

Ethanol has high octane without problems enthalpy and the boiling point presented by the aromatics compounds. You can reduce the volume of aromatics, replacing the oxygen, without prejudice to the octane number of gasoline without increasing emissions.

The hydrocarbons have the advantage of having a high calorific value by reducing fuel consumption due to energy availability increase.

Ethanol has a low calorific value compared to hydrocarbons. Consequently, the mixture ethanol/gasoline has a lower calorific value than pure gasoline.

A fuel of higher calorific value, however, has the disadvantage of forming NO, NO_2 and N_2O by extension, due to a higher adiabatic flame temperature.

3.2.2 Ethanol hydrated

The carbon removed from the atmosphere by photosynthesis, and stored in biomass will serve as row material for bioethanol production, which will be burned in engines that emit CO_2 engines.

The process is closed, which net income is zero in terms of CO_2 emissions, while fossil fuel burning releases into the atmosphere carbon stored over millions of years. The addition of ethanol brings the following advantages and disadvantages:

- The fact of having 11% oxygen by mass results in better combustion, reducing emissions of gases such as CO, CH_4 and HC.
- The ethanol carbon is produced by photosynthesis; so it does not contributes to the global warming.
- The presence of oxygen increases compounds like NOx and RCHO. The combination of these agents leads to an increased formation of 'photochemical smog' and tropospheric ozone.
- The calorific value of ethanol is about 30% lower than gasoline.
- The ethanol has high octane index, which allows a higher compression ratio and more powerful engine.

4. Emissions of gases

The reasons why emissions of internal combustion engines varied in the period 1980-2002 were described in “Main variants in the formations of greenhouse gases”.

The emissions, in kg/vehicle, depend on the variables: the fleet, driving cycle, maintenance, fleet age, environmental conditions and traffic. The emission factors depend more on the technology used to improve the characteristics of manufactured vehicles and fuels. The engines did not have significant technological developments in 1980-1985. During this period, the increase in the percentage of ethanol in gasoline and the production of hydrated ethanol engines were responsible for the variations.

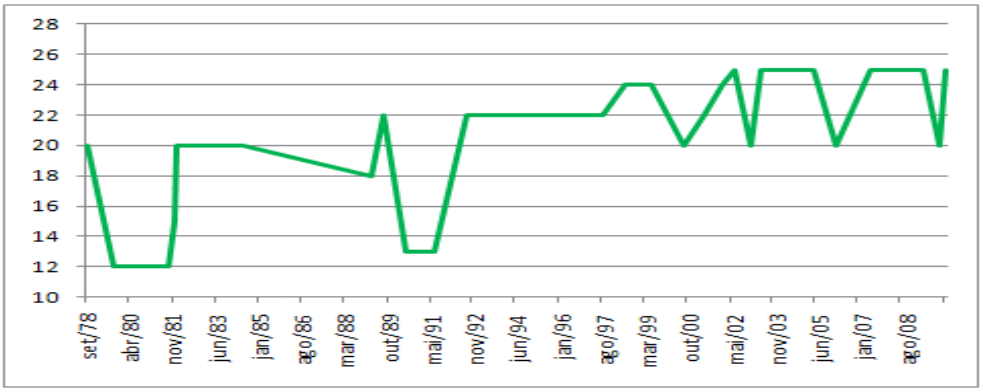

Note: the percentage increase data of ethanol in gasoline were obtained from the ordinances of Ministério de Agriculture, Pecuária e Abastecimento.

Fig. 1. Percentage of Ethanol in Gasoline 1978-2009.

The fall in oil prices and the ethanol supply crisis in 1986 completely changed the automotive scenery in Brazil. Gasoline vehicles, which in the past have had their production reduced, increased its share of the fleet and dominated the market at the expense of hydrated ethanol.

With a fleet reduction of hydrous ethanol in 1987, initially there was an increase in greenhouse gas emissions. They, however, began to decline because of the incentives given by the government for the manufacture of vehicles of 1.000 cc; the conversion of engines to use natural gas; and the use of ethanol vehicles for taxis. After 1992, to accomplish CONAMA Resolution Nº 010/1989, the companies have been introducing new technologies in vehicle manufacturing and fuels formulas (Main variants in the formations of greenhouse gases). These applications allow the reduction of emissions.

In this decade, there has been a considerable increase in metropolis fleet, generating large traffic congestion. In these conditions, there is an increase of emissions.

4.1 Emission factors

The determination of emission factors of Brazilian vehicles must be adapted to the characteristics of the fuels used in Brazil, hydrated ethanol and the blend gasoline/anhydrous ethanol.

The Conselho Nacional de Meio Ambiente (CONAMA) does not require the measurement of CH_4 and N_2O, but includes (HC) and RCHO a corresponding part of the volatile organic compound without methane. Both are not included in international data.

The emission factors of CO, HC, NOx and RCHO for the period 1980 to 2009, used in this work, are from Motor Vehicle Air Pollution Control Program (PROCONVE), while CO_2 and CH_4 are from the First National Atmospheric Emissions Inventory for Road Motor Vehicles of the Ministério do Meio Ambiente.

N_2O emissions will not be calculated due to the lack of emission factors for blend gasoline/ethanol and hydrated ethanol. Some authors use the emission factors of pure

gasoline, but the final figures may be overestimated. For this reason it is not possible to evaluate the effect of the blend.

To understand the role of ethanol in reducing the emission factor of CO, see equations 16 and 17, HC and CH_4 according to equations 1 and 2. For NOx, see equations 25, 26, 27 and 30. RCHO has the precursor products in equations 6 e 7.

CO, NOx emissions factors (left axis of the graphs) and HC (right axis) of the blend ethanol/gasoline are higher than hydrous ethanol in the period between 1980-1985 (Figures 2 and 3).

The ethanol emissions factors of CO, HC, considering the reaction mechanisms, are lower than gasoline and RCHO (right axis of the graphs) higher. However, the lowest values for NOx, can only be understood assuming that the engine of ethanol has better technology than that of gasoline in the period studied (Figures 2 and 3).

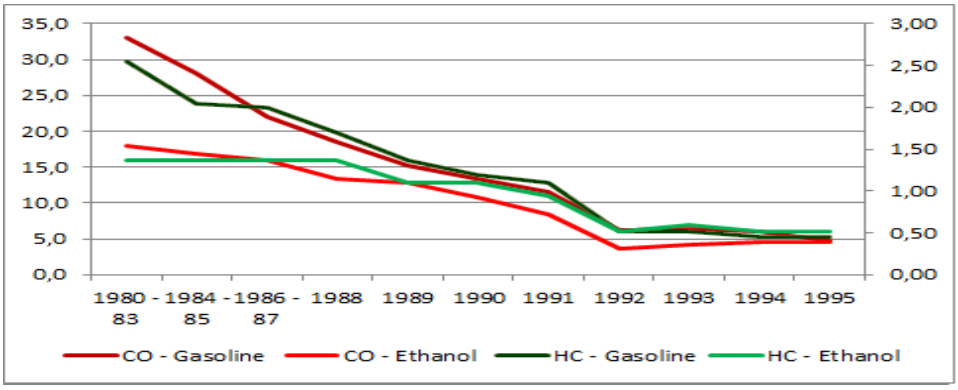

Fig. 2. Emission factors of CO and HC 1980-1995.

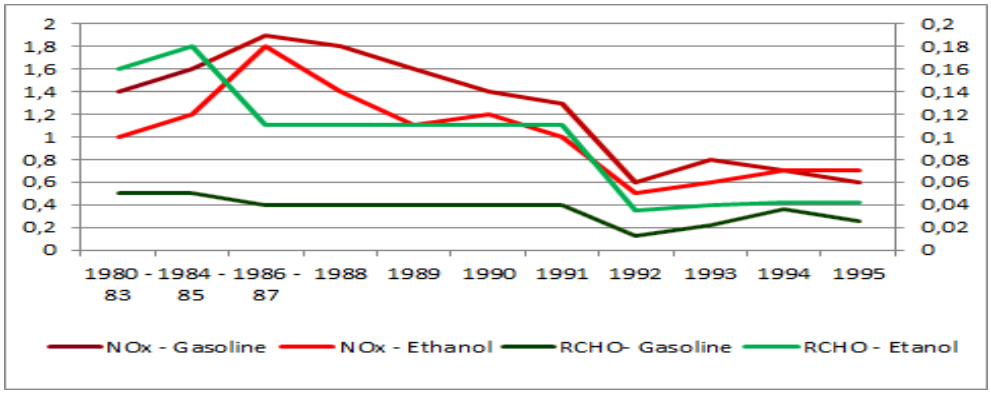

Fig. 3. Emission factors of NOx and RCHO 1980-1995.

The gasoline forms a smaller amount of oxygen. For this reason, their emissions of aldehydes (right axis) are smaller than ethanol (Figure 3), as expected in the mechanisms of combustion reactions.

After 1992, to meet the Resolution CONAMA 010/1989, Automakers and Refineries have introduced new technologies in engines that use a blend of ethanol/gasoline, and formulate new kinds of fuels (see Main variants in the formations of greenhouse gases).

Encouraged by the government, the of 1.000 cc engines manufacturers have participated with 71% of sales in 2001 (dropping to 52,7% in 2009) also contributed to the emissions reducing.

For ethanol engines, the reductions are much smaller, due to their manufacture gradual reduction, as in this case, there were no new technologies incorporated.

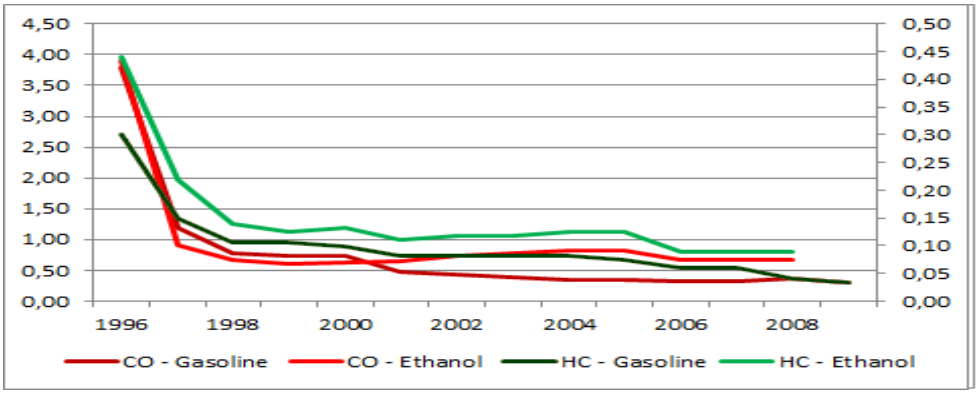

Fig. 4. Emission factors of CO and HC 1996-2009.

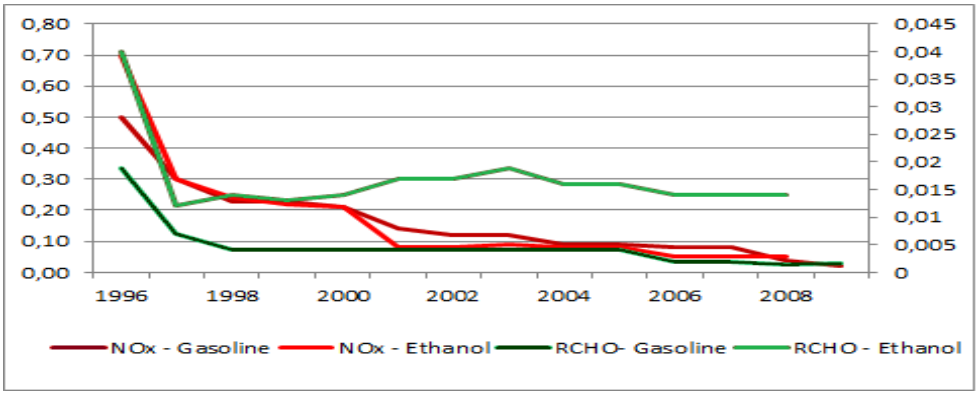

Fig. 5. Emission factors of NOx and RCHO 1996-2009.

The manufacture of flex-fuel engines since 2003 has changed the pattern of emissions of the Brazilian fleet. The engine flex-fuel interrupted the downward trend of emission factors.

For CO and HC there is a wide variation (figure 6). Then, you cannot establish a pattern of behavior.

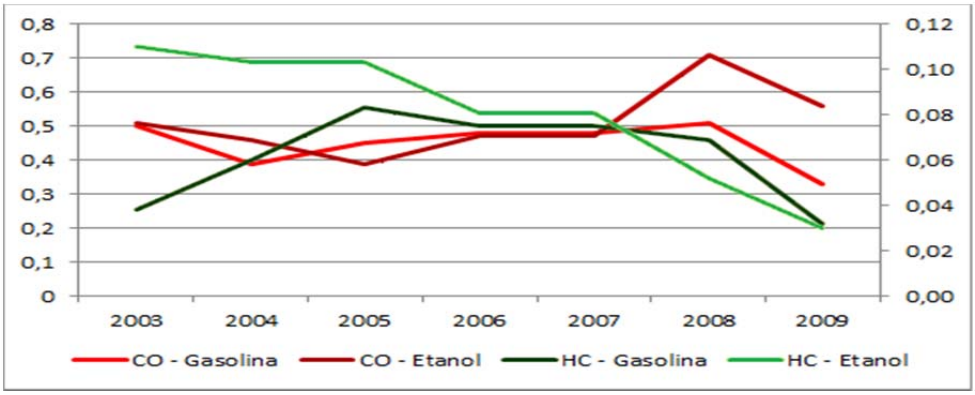

Fig. 6. Emission factors of CO and HC for fuel-flex.

You can see, however, that NOx and RCHO ethanol is higher than gasoline, as expected in the mechanisms of combustion reactions (Figure 7).

The problem with the new technology is the compression ratio, which is not adjusted for the octane best value of both fuels.

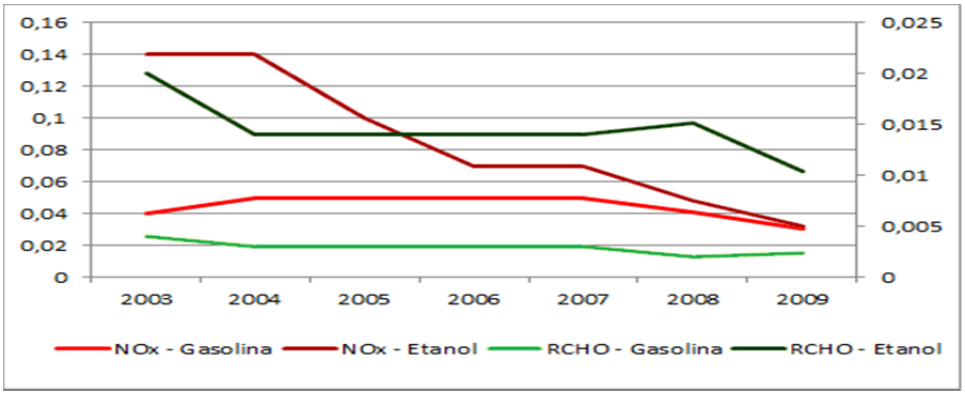

Fig. 7. Emission factors of NOx and RCHO for fuel-flex.

4.2 Gases emissions by Otto cycle vehicles

The variables that influence the emissions of pollutant and greenhouse gases were analyzed in Chapter 3.To analyze the impact of these action variables, first were used data from the National Atmospheric Emissions Inventory for Road Motor Vehicles of the Ministério do Meio Ambiente.

4.2.1 Pollutant gases emissions by Otto cycle vehicles

During the period of 1980-1995, gasoline engines have their emissions of CO, NOx (left axis), and HC, RCHO (right axis), influenced by the reduction of the fleet and the emission factors. Unlike the factors, the emissions follow the expected by the mechanisms of combustion reactions, ie, CO and HC are higher for gasoline, while NOx and RCHO are higher for ethanol.

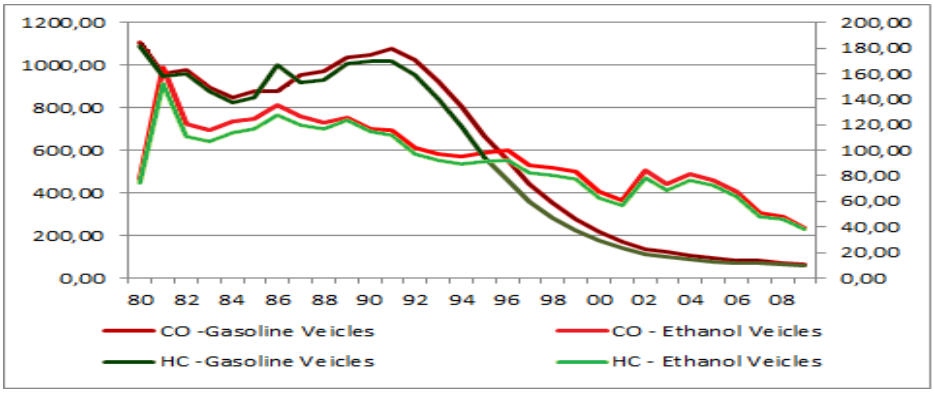

Fig. 8. Emission of CO and HC.

After this period, the fleet reduction of ethanol, and the technological developments of the engines, driven by the demands of Resolution CONAMA 010/1989, started making a difference. Emissions of CO and HC are also higher for ethanol.

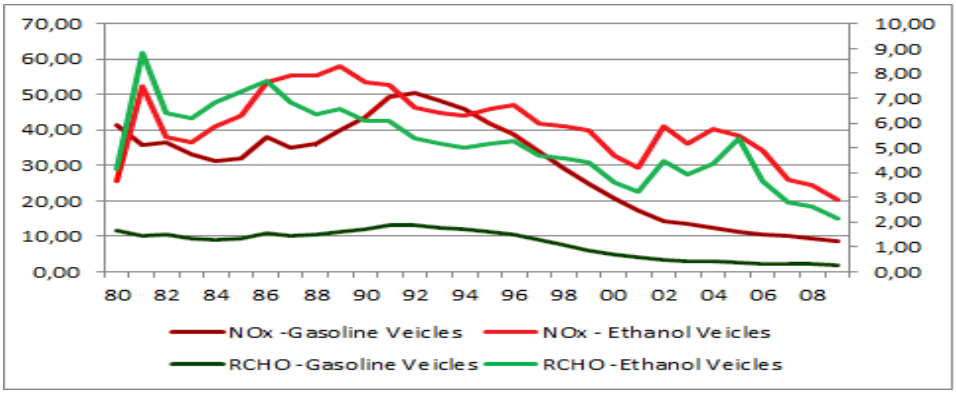

Fig. 9. Emission of NOx and RCHO.

In 2003, a new technology was introduced in Brazil, the engine "flex-fuel", becoming a best-seller. For this reason, hydrated ethanol and gasoline cars gradually ceased to be manufactured in the country and they had to start being imported.

The manufacture of flex-fuel engine has changed the pattern of emissions in the country. The gasoline engines have smaller greenhouse gases emissions, CO, HC and NOx RCHO, compared with ethanol. The reason is the compression ratio, which is not adjusted for the best value of the fuel octane.

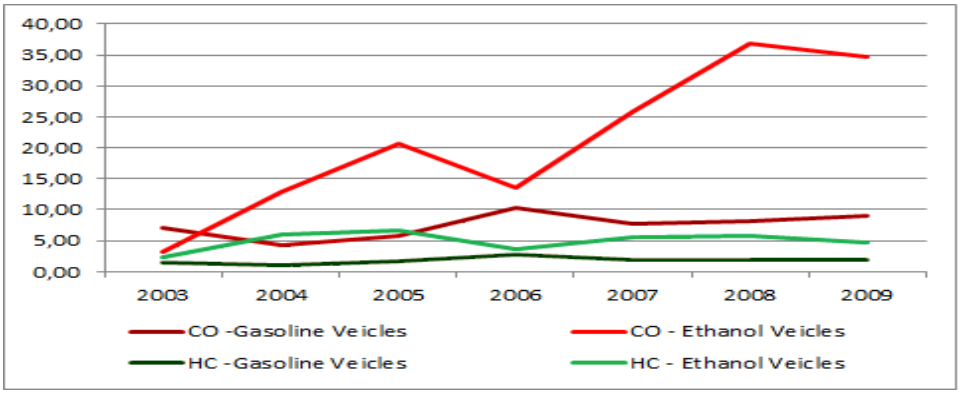

Fig. 10. Emission of CO and HC for fuel-flex.

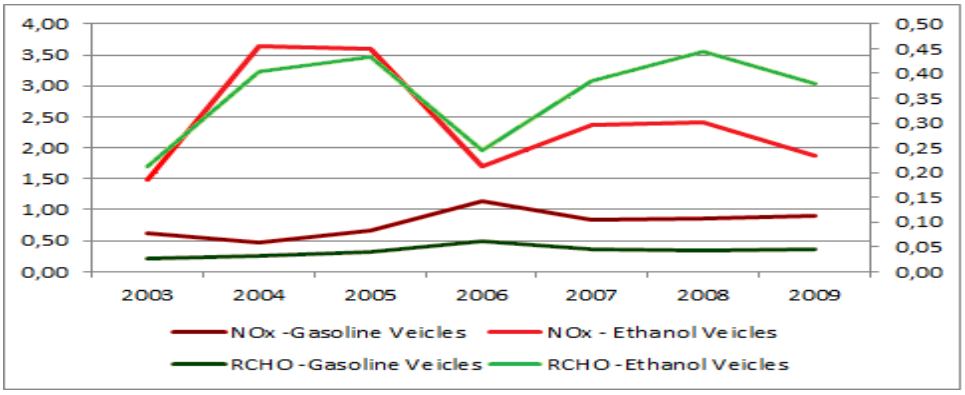

Fig. 11. Emission of NOx and RCHO for fuel-flex.

4.2.2 Greenhouse gas emissions vehicle Otto cycle

Ethanol consumption by the national fleet allows emissions of greenhouse gases in the transportation sector are substantially below those that could be achieved if the only fuel used was pure gasoline.

In the period 1980/87 the decline in fossil CO_2 emissions was due to the use of ethanol, while the increase occurred between 1988/97 was due to the reduction of its use. The decline from 1998/07 is due in part to a fleet of predominantly motor 1000 cc, the technological evolution of engines and from 2003, with the price drop and a greater supply, the market returned to using ethanol, figure 12.

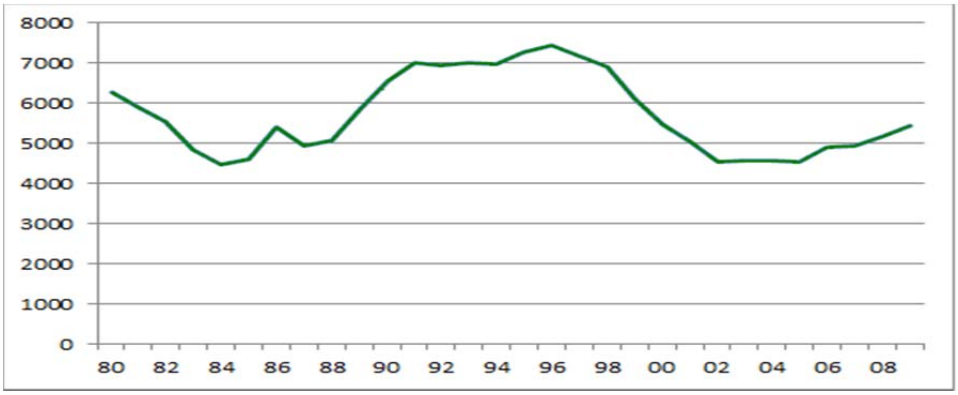

Fig. 12. Emissions of CO_2.

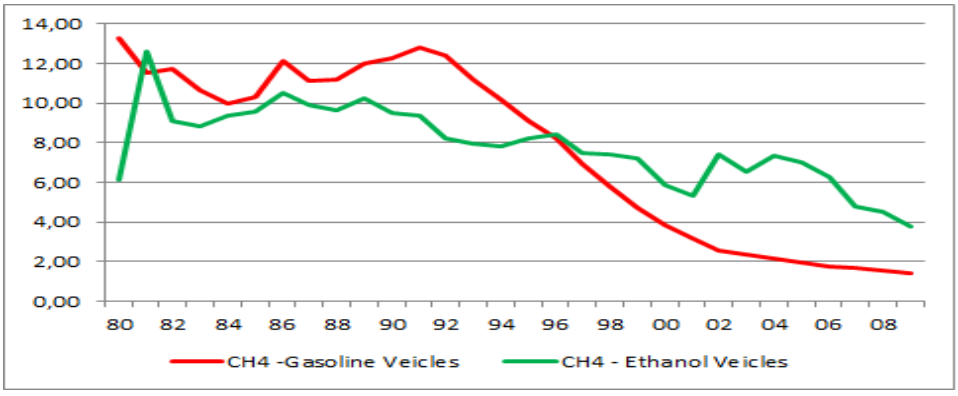

Fig. 13. Emissions of CH_4.

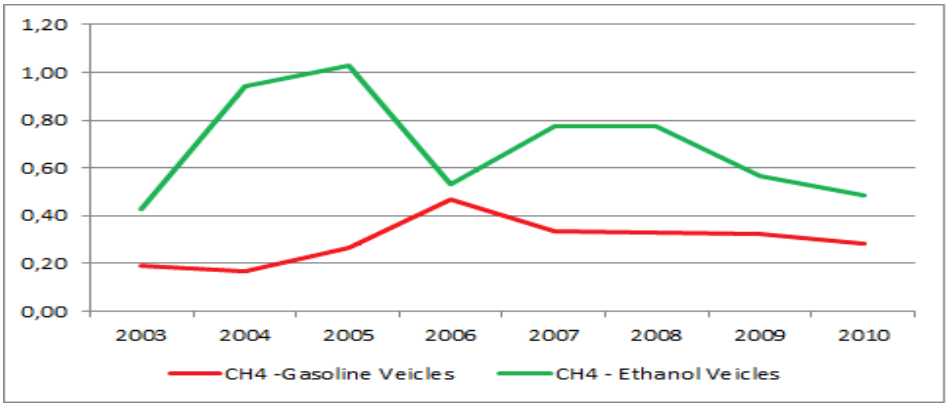

Fig. 14. Emissions of CH4 for fuel-flex

It should be noted that the CO_2 from burning of hydrous ethanol, is not counted in the emissions of greenhouse gases. The carbon removed from the atmosphere through photosynthesis and stored in biomass will serve as a feedstock for biofuel production, which in turn will be burned in engines. The process is closed, whose net income is zero in terms of CO_2 emissions, without considering the contributions of land use disputes whose values are not resolved.

Dedicated gasoline engines, in the period 1980-1995, have its emission of CH_4 affected by the reduction of the fleet and the emission factor. After this period, the fleet reduction of ethanol, the technological developments of the engines, driven by the demands of Resolution CONAMA 010/1989, start making a difference.

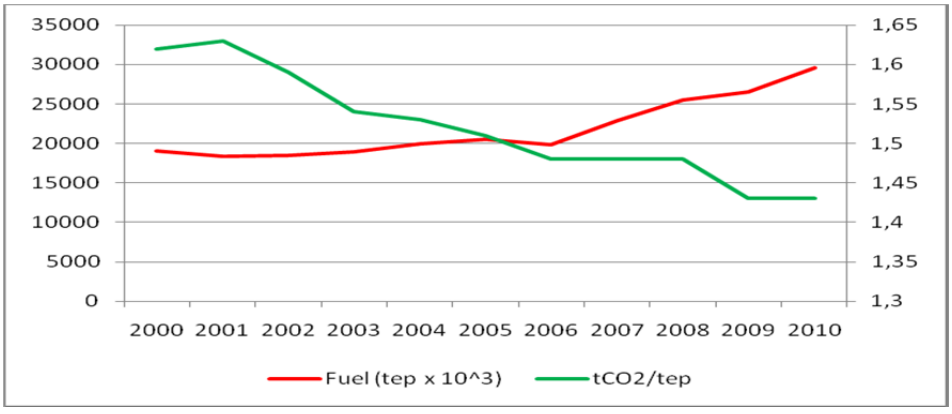

Fig. 15. Avoided Emissions.

4.2.3 Avoided emissions

The replacement of fossil carbon by the one that comes from biofuels reduces CO_2 emissions. We can estimate the difference between those from a hypothetical situation where the fleet of vehicles consumes only pure gasoline and the related to a real situation, where the fleet consists of vehicles that consume a mixture of gasoline/anhydrous ethanol and vehicles that require ethanol hydrated.

The Energy Research Company has estimated the avoided emissions (tCO_2/toe) in the period of 2000 to 2010. For comparison the same figure plotted in fuel consumption (gasoline more ethanol), in the period.

5. Conclusions

The changing profile of the Brazilian fleet allows you to compare the factors that contributed to the amount of emissions of pollutant and greenhouse gases, establishing a connection between the mechanisms of chemical reactions, the fuel composition, the evolution in technology of the vehicle and composition of gases coming out from the exhaust.

The values of the factors and emissions of CO, HC and NOx blend gasoline/ethanol and ethanol are influenced: by the presence of OH, HO_2 radicals and the introduction of new technologies in vehicles manufacturing and fuel formulation.

The addition of ethanol, increasing the OH and HO_2 concentrations, can be noted between 1980 and 1990, when vehicles did not have more advanced technologies. In this case, there was a reduction of the factors and emissions of CO and HC, while the factors for NOx decreased, and the emissions increased.

To meet the CONAMA Resolution No. 010/1989, which was enforced in 1992, vehicles manufacturers have introduced new technologies, including: more efficient engines with less power; catalyzers in the exhaust, reduction in fuel consumption due to an improved aerodynamics, reduction in vehicles weight and the petroleum refiners introduced new formulations.

After 1996, this set of measures began to influence, reducing the factors and the emissions of all gases. The hydrated ethanol vehicle had lower earnings due to lower technology incorporation and to a reduction in manufacturing.

The RCHO factors and emissions are much higher for hydrated ethanol than gasoline / ethanol mix throughout the entire period, including “flex-fuel" engines, showing that the formation of oxygenated hydrocarbons is strongly influenced by the OH and HO_2 radicals.

With the success of "flex-fuel" sales, hydrated ethanol vehicles are no longer manufactured and gasoline is focusing on more power and deluxe segment.

Due to a unique compression ratio for fuels with different octane ratings, "flex-fuel" engines, using blend ethanol and ethanol/gasoline, had a reduction in efficiency and thus higher emissions.

The values of CO and NOx emissions for blend gasoline/ethanol and hydrous ethanol reveal the need of an evolution in technology of the engines "flex-fuel".

The advantage of adding ethanol to gasoline and the manufacturing of engines that use hydrated ethanol are in the emission of greenhouse gases.

Looking at CO_2 emissions of a car that runs on a blend ethanol and gasoline compared to pure gasoline, there is a 22% reduction on average. This decrease reaches 100% when it comes to cars that use ethanol only, without considering the life cycle analysis.

Further studies are needed to understand the influence of adding ethanol to gasoline and the use of hydrous ethanol, such as "Determination of emission factor of N_2O", "Emissions of N_2O by mixing gasoline / ethanol and hydrous ethanol", and "Comparison emissions between pure gasoline and blend gasoline/ethanol".

Considering that in the next year cellulosic ethanol could be a reality, these studies provide a basis for developing policies and technologies that reduce environmental impact.

6. References

Azuaga, Denise. Danos Ambientais Causados por Veículos Leves no Brasil. Dissertação de Mestrado. Universidade Federal do Rio de Janeiro, COPPE. Rio de Janeiro 2000. Availabel at:
http://www.ppe.ufrj.br/ppe/ production/tesis/dazuaga.pdf .

Empresa de Pesquisa Energética. Balanço Energético Nacional, 2010. /MME.

California Environmental Protection Agency. Air Quality Impacts of the Use of Ethanol in California Reformulated Gasoline. AIR RESOURCES BOARD Planning and Technical Support Division. State of Califórnia Allen, Paul (Org.). Novembro 1999. Availabel at:
http://www.arb.ca.gov/cbg/ regact/ethanol/ethfate.htm.

CONAMA. Resolução nº 010/1989. Availabel at:
http://www.areaseg.com/conama/ 1989/010-1989.pdf.

Heywood, John B. Internal Combustion Engine Fundamentals. Singapore: McGraw Hill Book Co. 1988.

Curran, H. J.; Chen J.-S.; Litzinger, T. A. The Lean Oxidation of Iso-Octane at Elevated Pressures. Lawrence Livermore National Laboratory, Livermore, CA 94551. Availabel at:
https://e-reports-ext.llnl.gov/pdf/235217.pdf.

Curran,, H.J.ET AL. A Comprehensive Modeling Study of n-Heptane Oxidation. Lawrence Livermore National Laboratory. Availabel at:
https://www-pls.llnl.gov/data/
docs/science_and_technology/chemistry/combustion/nc7.pdf .

Curran, H. J.et al. Comprehensive Oxidation of Automotive Primary Reference Fuels at Elevated Pressures. Lawrence Livermore National Laboratory, CA 94551. United States of America. Availabel at:
https://wwwpls.llnl.gov/data/docs/science_and_
technology/chemistry/combustion/prf_paper.pdf

Intergovernmental Panel on Climate Change. 2006 IPCC Guidelines for National Greenhouse Gas Inventories, Prepared by the National Greenhouse Gas Inventories Programme. Published: IGES, Japan.

Kilpinen, Pia. NOx Emission Formation in Marine Diesel Engines – towards a quantitative understanding. Availabel at:
http://www.umweltdaten.de/verkehr/downloads/ seeschifffahrt/mn2-03.pdf 1.

Marinov, Nick M. A Detailed Chemical Kinetic Model for High Temperature Ethanol Oxidation. Availabel at:
http://www..cmls.llnl.gov/data/docs/science_and _technology/chemistry/ combustion/ethanol_paper.pdf.

Ministério do Meio Ambiente. – Relatório de Referência – Emissões de Gases de Efeito Estufa no Setor Energético por Fontes Móveis. Brasília. Availabel at:
http://www.mma.gov.br/estruturas/182/_arquivos/emissoes_ veiculares_182.pdf.

Muharam, Yuswan. Modelling of the Oxidation and Combustion of Large Hydrocarbons Using an Automatic Generation of Mechanisms. Dissertação de Mestrado, Universidade de Heidelberg, 18 november 2005. Availabel at:
http://www.itcp.
kit.edu/deutschmann/img/content/05_YMuharam_PhD_UniHD.pdf

PROCONVE/CETESB. Fatores de Emissão. Departamento de Tecnologia de Emissões de Veículos. Availabel at:
http://www.cetesb.sp.gov.br/Ar/emissoes/proconve3.asp.

Westbrook, Charles K. al al. The Internal Combustion at Work. Lawrence Livermore National Laboratory, Livermore United States of America. Availabel at:
https://www.llnl.gov/str/Westbrook.html.

3

Greenhouse Gas Emissions from Hydroelectric Reservoirs: What Knowledge Do We Have and What is Lacking?

Raquel Mendonça[1,2], Nathan Barros[1], Luciana O. Vidal[1],
Felipe Pacheco[1], Sarian Kosten[2] and Fábio Roland[1]
[1]*Federal University of Juiz de Fora, Federal University of Rio de Janeiro*
[2]*Wageningen University*
[1]*Brazil*
[2]*The Netherlands*

1. Introduction

The question that motivated us to write this chapter was "How does hydroelectricity production contribute to the global emissions of greenhouse gases?". Here, we present an overview of (i) scientific advances on the topic and (ii) aspects of hydroelectric reservoir ecology in the context of greenhouse gas production, consumption and emission.

Electricity production is a challenging issue when it comes to mitigating greenhouse gases (GHG) emissions without risking development goals. Non-renewable energy sources, as fossil fuel burning, account for most of the global energy production (68% in 2007) and are responsible for most of the anthropogenic GHG emissions to the atmosphere (40%, International Panel on Climate Change - IPCC, 2007). Compared to fossil fuels, hydropower has been considered an attractive renewable energy source with the advantage of being less harmful in terms of GHG emissions (International Energy Agency - IEA, 2008). Hydropower currently provides about 16% of the world's electricity supply (IEA, 2008) with many countries depending on it for more than 90% of their supply. Indeed, hydropower is a proven, mature, predictable and typically price-competitive technology. Moreover, it has among the best conversion efficiencies of all known energy sources: 90% efficiency as opposed to up to 50% efficiency of e.g. fossil fuel burning. The historical perception of hydroelectricity as being GHG neutral (Hoffert et al., 1998), however, is now known to be flawed. The concern regarding the GHG emissions by hydroelectric reservoirs has steeply increased since the early 90's, even though it remains unclear what their actual emission is.

Although inland water systems naturally produce and emit carbon to the atmosphere (Cole et al., 2007) different characteristics of hydroelectric reservoirs cause that they often produce and emit more than natural systems, especially in the first twenty years after flooding (Barros et al., 2011). This is mainly due to the usually excessive availability of decomposable organic matter in hydroelectric reservoirs. Not only large amounts of soil and terrestrial vegetation are flooded by damming rivers, but terrestrial organic matter derived from land erosion is continuously flushed into reservoirs as well. The usually high water residence

time in reservoirs as compared to rivers, combined with high inorganic nutrient inputs, favors organic matter decomposition and, thus, the production of two major GHGs – carbon dioxide (CO_2) and methane (CH_4). The amount of CO_2 and CH_4 emitted varies (a) among reservoirs (as function of drainage basin characteristics, reservoir morphology, climate, etc.); (b) within reservoirs (along longitudinal gradients from the tributaries to the dam, before and after the dam, etc.); and (c) over time (with reservoir aging, seasonally, daily, with changes in anthropogenic activities in the drainage basin, and with dam operation depending on energy needs and precipitation regime). Attempts to estimate the amounts of CO_2 and CH_4 emitted to the atmosphere should consider such variability which makes it a complex task.

Despite the complexity of the GHG issue, the effect of damming rivers on the atmospheric GHG concentrations cannot be disregarded. The concern about the impacts of hydroelectric reservoirs on the global GHG budgets has been increasing in the same pace as the construction of new dams. Nowadays, there are at least 45,000 large hydroelectric reservoirs in operation worldwide (World Commission on Dams –WCD, 2000). Moreover, recent inventories estimate the total surface area of world's hydroelectric reservoirs at about 350,000 km² (Barros et al., 2011). The substantial size of some hydroelectric projects and the extensive total surface area globally covered by reservoirs require that research determining the impacts of these systems be done at ever-increasing spatial and temporal scales.

This chapter focuses on the GHG emissions that are due to the landscape transformation (damming a river to form a reservoir) and to reservoir operation to produce electricity. First, the scientific advances towards understanding the role of hydroelectric reservoirs and their environmental effects as sources of GHG are delineated. Then, the metabolic processes involved in GHG production and consumption are described with focus on the two major interacting compartments: the water column and the sediment. Next, the external factors influencing the emission rates from reservoirs are discussed. Finally, an overlook of future perspectives in terms of GHG emissions from hydroelectric reservoirs is presented.

2. Important scientific advances

The ever increasing global energy demand and the concern about the changes in environment have lead to an urge to assess the hydropower 'footprint' in terms of GHG emissions to the atmosphere. Since the early 90's the role of hydroelectric reservoirs as sources or, as the opposite, sinks of GHG has rapidly become a global topic of investigation (**Figure 1**). At least 85 globally distributed hydroelectric reservoirs have so far been studied with focus on GHG fluxes (Barros et al., 2011). The first scientific papers focused on reservoirs located in Canada (e.g. Rudd et al., 1993; Duchemin et al., 1995), Brazil (e.g. Rosa & Schaeffer, 1994; Fearnside, 1995, 1997), Panama (Keller & Stallard, 1994) and French Guiana (e.g. Galy-Lacaux et al., 1997; Galy-Lacaux et al., 1999). Later, reservoirs in Finland (e.g. Huttunen et al., 2002), USA (e.g. Soumis et al., 2004), Sweden (e.g. Aberg et al., 2004; Bergstrom et al., 2004) and Switzerland (e.g. Diem et al., 2007) were studied. Only very recently, GHG emissions from reservoirs located in China, the country with the largest installed capacity in the world, became focus of investigation (e.g. Chen et al., 2009; Wang et al., 2011; Zheng et al., 2011) (**Figure 2**).

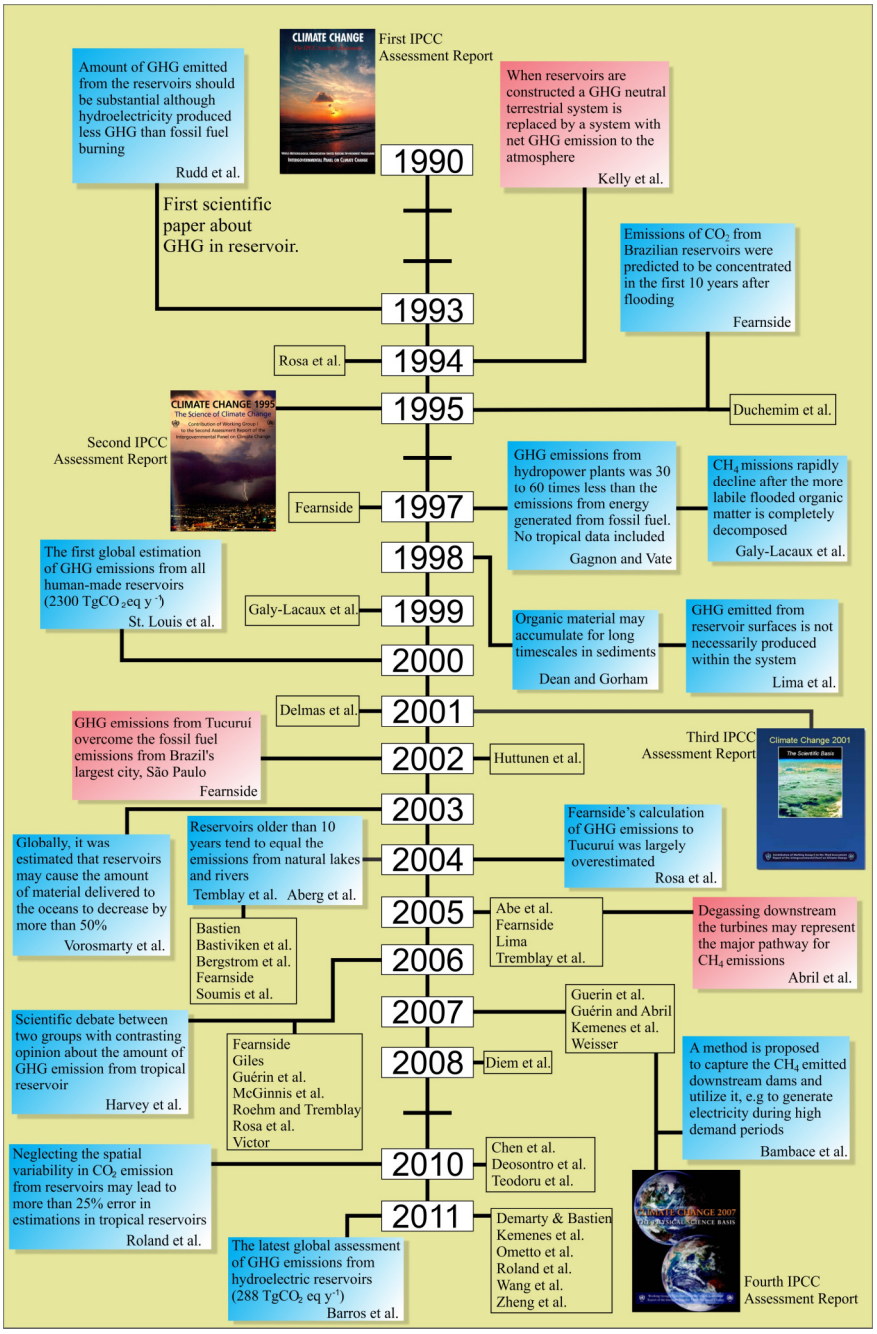

Fig. 1. Timeline of scientific advances regarding the role of hydroelectric reservoirs as sources of GHG to the atmosphere.

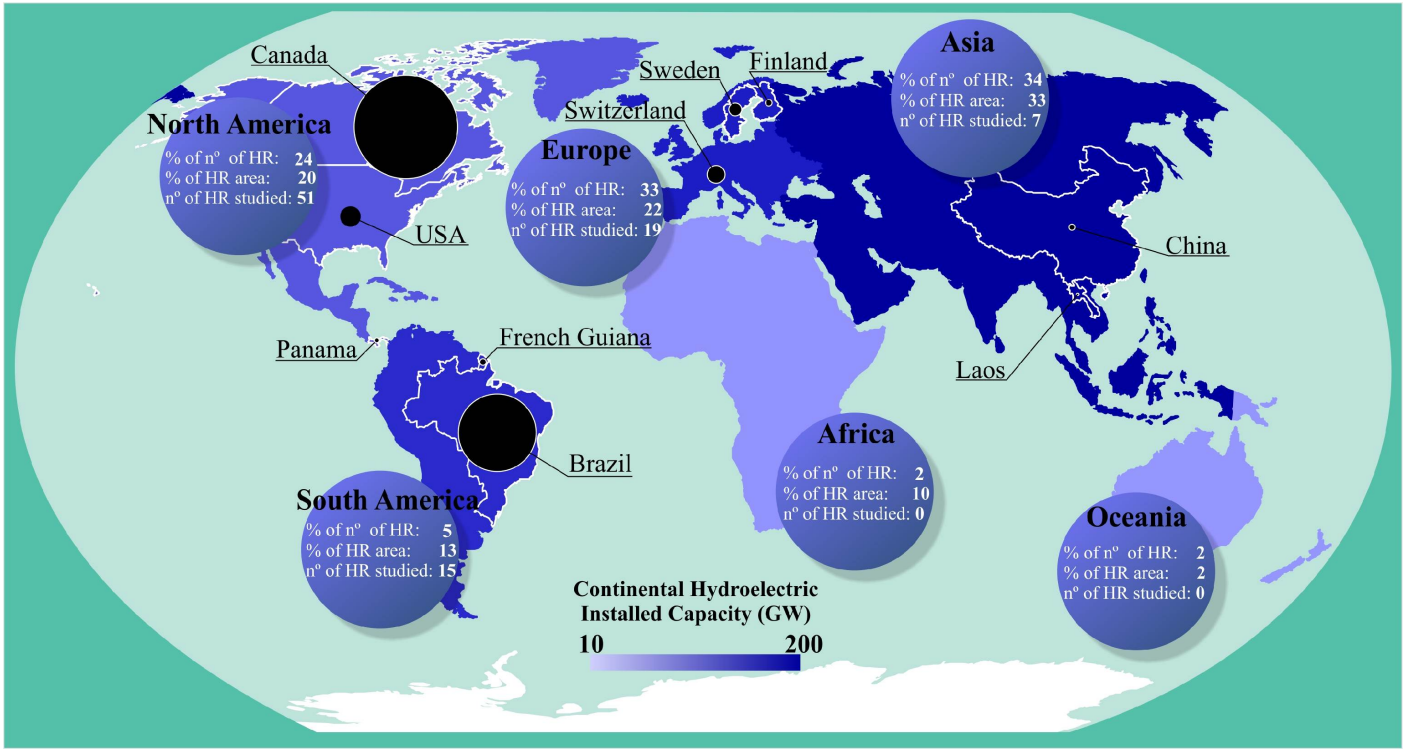

Fig. 2. Global distribution of hydroelectric reservoirs (HR), expressed as the proportion of the total number of reservoirs globally constructed on each continent, the proportion of the global HR area on each continent and the number of HR studied on each continent. The blue gradient indicates the hydroelectric installed capacity per continent. The black circle sizes are proportional to the number of papers published dealing with GHG emissions from reservoirs located in each country. The percentages of total number and total area of hydroelectric reservoirs were calculated based on ICOLD (2007). The numbers of papers published approaching GHG emissions from hydroelectric reservoirs were extracted from Barros et al., 2011, Chanudet et al., 2011, Wang et al., 2011, and Zheng et al., 2011.

2.1 GHG emissions – hydropower versus other electricity sources

Historically, the question to which extent hydropower is a GHG-friendly source of energy has been an important one. A first study focusing on reservoirs in northern Canada suggested that the amount of GHG emitted from reservoirs was substantial when compared to emissions from fossil fuel burning (Rudd et al., 1993). A subsequent assessment estimated that GHG emissions from hydropower plants (considering their full lifecycle) was 30 to 60 times less than the emissions from energy generated from fossil fuel (Gagnon & Van de Vate, 1997). This assessment, however, did not include data from hydroelectric reservoirs in tropical climates which were later found to have relatively high emissions. Yearly GHG emissions from a large reservoir located in the Brazilian Amazon (Tucuruí reservoir), for example, was argued to overcome the fossil fuel emissions from Brazil's largest city, São Paulo (Fearnside, 2002). Others criticized this finding and considered the reservoir GHG emissions to be largely overestimated (Rosa et al., 2004). This critic triggered a scientific debate between two groups with contrasting opinions (Fearnside, 2004; Rosa et al., 2004; Cullenward & Victor, 2006; Fearnside, 2006; Giles, 2006). Although the groups disagree on the amount of GHG emitted from hydropower in relation to other energy sources, they do agree that GHG emissions from tropical reservoirs are large. Emissions from the Brazilian Curuá-Una reservoir, for instance, were argued to overcome the emissions from oil generated electricity (Fearnside, 2005). Later, Brazilian hydroelectric reservoirs were shown to emit less carbon per energy production than thermonuclear power plants, with the exception of some cases of low power density, i.e. low energy production/flooded area ratio (Dos Santos et al., 2006). Finally, a recent inventory including several Brazilian reservoirs located both in the Amazon and in other biomes showed that the GHG emissions per energy produced (GHG/MWh) are lower in most reservoirs, regardless of their age (Ometto et al., submitted). This inventory showed that the highest GHG/MWh rates occur in large Amazonian reservoirs with low energy production rates.

Overall, hydropower may thus produce electricity with one of the lowest life-cycle GHG emissions (Weisser, 2007), especially in non-tropical regions (Barros et al., 2011). Nevertheless, the important role of hydroelectric reservoirs in the global GHG dynamics is unquestionable.

2.2 Organic matter and GHG

The high GHG emissions from hydroelectric reservoirs were originally argued to be due to the decomposition of flooded organic soil and vegetation (Rudd et al., 1993; Abril et al., 2005). This understanding of the role of reservoirs needs to take into account the balance between GHG emissions and consumption prior to and after the impoundment of a certain area (Teodoru et al., 2010). Net GHG emission was considered close to zero prior to impoundment, as emissions from rivers would be compensated by the sink of terrestrial photosynthesis. After flooding, the GHG neutral terrestrial system is replaced by a system with net GHG emissions to the atmosphere (Kelly et al., 1994).

This focus on the flooded organic matter further lead to the understanding that with reservoir aging, the amount of decomposable flooded organic matter would be gradually reduced and, thus, GHG emissions from reservoir surfaces would decline. Indeed, a long-term assessment of GHG emissions from the tropical Petit Saut reservoir showed that CO_2 and CH_4 emissions are high in the first two years after impoundment after which emissions

rapidly decline when the more labile flooded organic matter is decomposed (Galy-Lacaux et al., 1997; Galy-Lacaux et al., 1999). Emissions of CO_2 from Brazilian reservoirs were predicted to be concentrated in the first 10 years after flooding (Fearnside, 1995, 1997). Later, evidence from Canadian systems showed a similar trend and suggested that CO_2 emissions from reservoirs older than 10 years tend to equal the emissions from natural lakes and rivers (Tremblay et al., 2004). Similar results were also reported for a Swedish reservoir which was compared with a natural lake (Aberg et al., 2004). Moreover, a significant negative relationship between age and GHG emissions was registered for temperate reservoirs (St Louis et al., 2000) and for reservoirs located all over the globe (Barros et al., 2011).

Nevertheless, other sources of carbon to reservoirs besides flooded organic matter should be taken into consideration. During their complete lifetime, organic matter and nutrients from the drainage basin are continuously flushed into the systems through tributary rivers (Fearnside, 1995; Roland et al., 2010) and aquatic primary production rates tend to increase (Bayne et al., 1983). Once in the reservoirs, organic matter derived from the drainage basin and from aquatic primary production mineralizes at different rates, the latest being usually more labile (Kritzberg et al., 2005; Vidal et al., 2011). Most of the organic matter mineralization and, thus, most of the GHG production in reservoirs occurs in the sediment (Aberg et al., 2004; Abe et al., 2005). Furthermore, it has become clear that GHG emitted from reservoir surfaces is not necessarily produced within the system, as tributary rivers may export large amounts of GHG to reservoirs (e.g. Lima et al., 1998).

2.3 Global emission estimates

From 2004 on, the studies were marked by a more holistic approach incorporating emissions from water passing through the turbines and downstream of dams, as has been done earlier in the tropical Petit Saut reservoir (Galy-Lacaux et al., 1997). Continuous measurements from Petit Saut reservoir lead to a 10-year assessment of GHG emissions which showed that degassing downstream the turbines may represent the major pathway for CH_4 emissions (Abril et al., 2005). High emissions downstream of dams were registered in other tropical (e.g. Guerin et al., 2006; Kemenes et al., 2007, 2011) and in temperate reservoirs as well (e.g. Soumis et al., 2004; Abril et al., 2005; Roehm & Tremblay, 2006). Motivated by the idea of mitigating CH_4 emissions from reservoirs, a method was proposed to capture the CH_4 emitted downstream dams and utilize it, for instance, to generate electricity during high demand periods (Bambace et al., 2007).

More recently, attention has turned to the spatial variability on GHG emissions within reservoirs. Measurements in tropical reservoirs suggested that neglecting the spatial variability in CO_2 emission from reservoirs may lead to more than 25% error in estimations (Roland et al., 2010). In the same year, spatial variability in CO_2 fluxes from temperate reservoirs was shown to decline with time after impounding (Teodoru et al., 2010). The importance of considering the spatial variability in CH_4 emissions was also addressed based on data from Chinese reservoirs (Zheng et al., 2011).

The first global estimation of GHG emissions from reservoirs was published in 2000 (St Louis et al., 2000). This assessment considered emissions from reservoirs of all uses, including irrigation, water supply, energy generation and others. Based on 21 systems located in temperate climate (i.e. Canada, United States, and Finland), the authors calculated

average emissions of 1400 mg m^{-2} d^{-1} of CO_2 and 20 mg m^{-2} d^{-1} of CH_4. Their estimated emissions from tropical reservoirs (3500 mg m^{-2} d^{-1} of CO_2 and 300 mg m^{-2} d^{-1} of CH_4), though, were based on data from a very small number of systems (four) and might have been overestimated due to the inclusion of young reservoirs (1-2 year old) which have high emissions. After estimating the global area occupied by all reservoirs types, the authors calculated the global emissions of GHG to be 273 Tg of CO_2 and 48 Tg of CH_4 per year. Considering that CH_4 global warming potential is 25 times higher than that of CO_2 (IPCC, 2007), these emissions corresponded to 2,600 Tg of CO_2-equivalents per year.

After 2000, there was an important increase in the amount of data on GHG emissions from reservoirs located in both temperate (e.g. Huttunen et al., 2002; Aberg et al., 2004; Bergstrom et al., 2004; Soumis et al., 2004; Tremblay et al., 2004; Duchemin et al., 2006) and tropical regions (e.g. Delmas et al., 2001; Fearnside, 2002; Rosa et al., 2004; Abril et al., 2005; Guerin et al., 2006 ; Guerin et al., 2007). Comparisons between emissions in different regions were applied as tools to understand the factors controlling emissions from reservoirs. For example, CO_2 emissions from Swedish reservoirs were lower than those reported for other boreal regions, which was attributed to the fact that in Sweden often comparatively small areas with thin layers of organic soil are flooded for reservoir construction (Bergstrom et al., 2004). In 2011 a review of the achievements in 20 years of measurements of CH_4 emission from tropical and equatorial reservoirs came out (Demarty & Bastien, 2011). The document claims that GHG emissions might have been underestimated in the tropics due to the neglect of CH_4 emissions.

Finally, the latest global assessment of GHG emissions from hydroelectric reservoirs compiled data from 85 globally distributed systems which account for about 20% of the global area occupied by hydroelectric reservoirs (Barros et al., 2011). The authors estimated that hydroelectric reservoirs globally emit about 51 Tg of carbon per year (48 Tg per year as CO_2 and 3 Tg per year as CH_4 or 288 Tg of CO_2-equivalents per year) which is low compared to the first global estimation (321 Tg of carbon per year, St Louis et al., 2000). This difference is argued to be caused (i) by the greater amount of data currently available and (ii) by the smaller area occupied by hydroelectric reservoirs (350.000 km^2, Barros et al., 2011) when compared to the area occupied by all types of reservoirs (1.500.000 km^2, St Louis et al., 2000). Furthermore, this latest assessment showed that GHG emissions are correlated to reservoirs age and latitude, with the highest emission rates occurring in the Amazon region.

3. Environmental effects of hydroelectric reservoirs and the consequences for GHG emissions

By definition, hydropower is a renewable source of electricity in which power is derived from the energy of water moving from higher to lower elevations. The amount of energy generated depends both on the accumulated water volume and on the difference in height between the water inlet and the outflow. While dams perform an important function, their effect on landscapes is remarkable: a fragment of river and its adjacent terrestrial environment are transformed in a new freshwater system, the reservoir. According to recent global inventories, 10,800 km^3 of water were impounded in reservoirs (all kinds of reservoirs, e.g. irrigation, water supply, flood control, and aquaculture) in the last half century, causing the sea level to reduce by approximately 30 millimeters (Chao et al., 2008). The construction of reservoirs clearly represents, thus, one of the major human impacts on the hydrological cycle. The effects of such transformation, however, surpass the hydrological level. Impounded areas undergo a cascade of changes which influence, directly or indirectly, the local GHG fluxes (**Figure 3**).

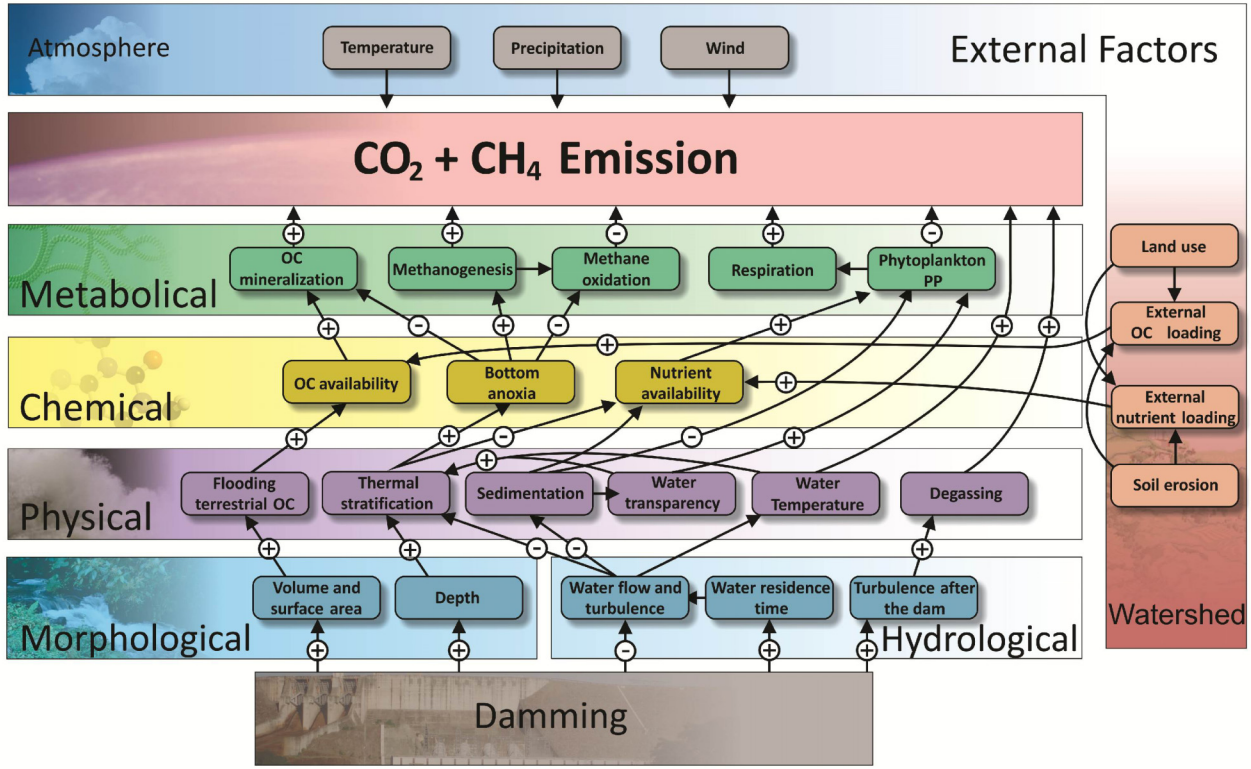

Fig. 3. Diagram illustrating some of the major impacts of damming rivers and their effects on GHG emissions. Direct hydrological impacts of damming rivers trigger a cascade of shifts in the physical and chemical environment, leading to indirect (through changes in metabolism) and direct changes in GHG fluxes. External factors affecting GHG emissions are mainly related to atmospheric conditions and drainage basin characteristics. OC = organic carbon; PP = primary production. Arrows with the (+) symbol represent positive effect; arrows with the (-) symbol represent negative effect.

Prior to dam construction, rivers generally have rapid water flow rates which vary with drainage basin size and topography and respond to the seasonality in the upstream precipitation regime. Precipitation regimes also control variations in river water level, which usually varies within a predictable range. Rivers naturally emit large amounts of CO_2 due to terrestrial organic matter decomposition (Cole et al., 2007; Tranvik et al., 2009). Because the turbulent flow keeps oxygen concentrations high, CH_4 emissions hardly occur (Abril et al., 2005) except in highly organic matter-rich rivers (e.g. Lima et al., 1998). In compensation, terrestrial vegetation surrounding a river course usually functions as a CO_2 sink, since photosynthesis tends to exceed respiration. Furthermore, rivers play a crucial role in removing carbon from the global cycle by carrying large amounts of terrestrial material to the ocean (Schlesinger & Melack, 1981) where it is partially permanently buried (Hedges & Keil, 1995; Hedges et al., 1997).

The construction of dams implies the extension of flooded area. This implies that flooded terrestrial vegetation no longer performs photosynthesis. Instead, the organic matter stored in vegetation, as well as in flooded soil, becomes available for bacterial decomposition (with subsequent release of CO_2 and CH_4). It means that the flooded terrestrial area shifts from being a net sink to a net source of carbon to the atmosphere. The amount of GHG emitted from decomposition of flooded vegetation depends on the size of the flooded area, as well as on the quantity and quality of organic matter.

Moreover, the enlargement of flooded area with reservoirs formation comes with an increase in water volume and causes water residence time (or turnover time) at individual impoundments to increase from less than one day to several years in the case of large dams. The reduction of river water velocity in the headwater of reservoirs results in a decreased sediment-carrying capacity and in the retention of particulate matter transported by rivers. Reservoirs are usually constructed at the lower end of large drainage basins, where rivers usually carry terrestrial material derived from the entire upstream drainage basin. Despite being energetically favourable – it guarantees maximal water inflow and, thus, enhances the potential for energy generation – this strategy implies that high amounts of terrestrial material constantly flow into and accumulate in the reservoirs. Globally, it has been estimated that reservoirs may cause the amount of material delivered to the oceans to decrease by more than 50% (Vorosmarty et al., 2003). Organic matter settled at the bottom of the reservoir has a higher chance to be mineralized than when it would have settled at the ocean bottom (see section 4 for details). As a consequence the net global emission of GHG is enlarged. Nevertheless, it should also be remarked that part of the organic material deposited in the sediment of reservoirs is not mineralized and may accumulate for long timescales (Dean & Gorham, 1998).

Due to the transition from a turbulent-shallow river to a relatively static-deep system, reservoirs tend to undergo thermal stratification, especially in warm regions. The process of thermal stratification is triggered by differences in water density and leads to the formation of water layers: epilimnion (top), metalimnion (intermediate) and hypolimnion (bottom). Once these layers are formed, there is no mixture between top and bottom layers unless some stress (e.g. wind, shift in temperature or increase in water inflow from rivers) breaks water column stability. The establishment of stratification has important effects on oxygen dynamics and, thus, on GHG emissions from reservoirs (see section 4 for details).

4. GHG dynamics in reservoirs – an ecological assessment

The potential of any aquatic system as source or sink of GHG to the atmosphere is ultimately determined by (i) the concentration of GHG dissolved in the water as related to the atmospheric GHG concentration and (ii) the solubility of the gases in the water. The processes of production, consumption and emission of GHG in hydroelectric reservoirs are dependent on their hydrological characteristics, which make of them especial sites in terms of GHG dynamics when compared to other aquatic systems.

4.1 Water column and sediment

Most of the routes of production and consumption of CO_2 and CH_4 are controlled by the aquatic biota metabolism (**Figure 4**). In a nutshell: aerobic respiration produces CO_2 which is consumed through photosynthesis; methanogenic bacteria produce CH_4 which is consumed by methanotrophic bacteria. An exception to the general pattern of biota mediating CO_2 production is the process of photo-oxidation, i.e. the break-down of dissolved organic molecules by solar radiation with the production of several compounds among which CO_2 is the more abundant (Soumis et al., 2007; Bastien, 2005). Production and consumption of GHG within reservoirs, however, are not the only processes controlling GHG stocks in the water column. Tributary rivers flowing into reservoirs may carry variable amounts of GHG

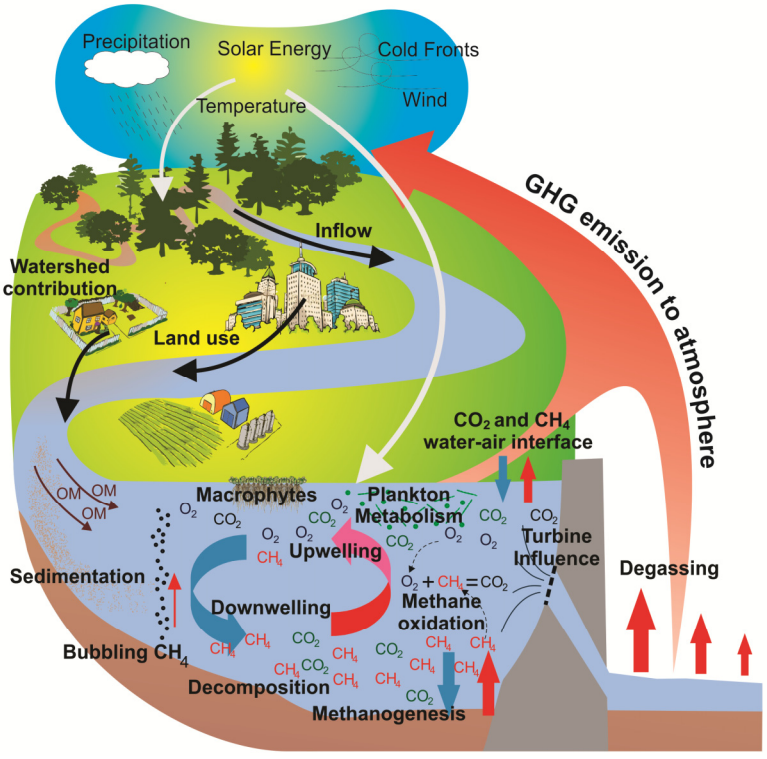

Fig. 4. Main pathways of GHG production, consumption and emission to the atmosphere.

(mostly CO_2 but also CH_4). Moreover, dissolved CO_2 can flow into reservoirs from both surface and groundwater runoff.

A global assessment of lakes with a worldwide distribution showed that most of the lakes in the world are net sources of CO_2 to the atmosphere (Cole et al., 1994; Sobek et al., 2005). The frequently high CO_2 concentrations are argued to rely on the high influx of organic matter and the consequent excess respiration by heterotrophic bacteria. The high availability of terrestrial organic matter in hydroelectric reservoirs causes particularly high heterotrophic respiration in these systems. Especially in young reservoirs where the availability of decomposable organic matter is high, the respiration by aerobic planktonic bacteria is elevated (Roland et al., 2011).

Mineralization may also occur anaerobically in the water column of stratified reservoirs (Abril et al., 2005). With the establishment of stratification, the oxygen consumption due to organic matter mineralization in the bottom layers of reservoirs is no longer offset by water exchange with top oxygenated water layers (see section 3 for details). Thus, bottom water layers become gradually anoxic. Under anoxic conditions, methanogenic bacteria metabolize organic compounds, hydrogen and CO_2 into CH_4 (methanogenesis), leading to high CH_4 concentrations in the bottom layer of reservoirs (Abril et al., 2005). Due to the persistent stratification of reservoirs located in warmer regions, methanogenesis is usually an important pathway of GHG production in those systems (Demarty & Bastien, 2011). However, most of the CH_4 produced in the water column of reservoirs tend to be emitted to the atmosphere as CO_2 due to the oxidation by metanotrophic bacteria at the top oxygenated water layer (Guerin & Abril, 2007).

The overall GHG production in the water column of reservoirs is small compared to the production in the sediments. Great amounts of particulate organic matter transported through rivers tend to sedimentate in reservoirs. Sedimentation is also the fate of organic matter produced by algal photosynthesis in the water column. Once in the sediment, organic matter (i) is mineralized by aerobic or anaerobic bacteria and released as CO_2 and CH_4 (among other compounds) to the water column, (ii) is re-suspended, or (iii) remains buried. The relative importance of each of these processes is system-specific and influences the overall role of a reservoir as net sink or source of GHG to the atmosphere.

Mineralization leads to a general chemical-metabolic gradient within undisturbed sediment profiles. Aerobic mineralization is restricted to the top sediment layer, which may have variable thicknesses depending (i) on the hypolimnetic oxygen concentration, (ii) on the oxygen diffusion coefficient, which is a function of sediment density, sediment porosity, temperature and turbulence at the sediment-water interface and (iii) on the rate of oxygen consumption during organic matter mineralization. Below this top oxygenated sediment layer, anaerobic processes dominate sediment metabolism. While CO_2 is the only GHG gas produced as a result of aerobic decomposition, anaerobic processes produce CH_4 in addition to CO_2. These gases accumulate in sediment pore-water and tend to be released in the water column as a consequence of the difference between concentrations in these two compartments.

Diffusive CH_4 tends to be oxidized into CO_2 by metanotrophic bacteria at the oxygenated top sediment layer or in the water column. The extent of CH_4 oxidation in the water column depends on oxygen availability and, thus, may be higher in deeper reservoirs (Lima, 2005).

It has been shown, e.g., that oxidation in the water column of Petit Saut reservoir can reduce CH_4 emissions at more than 85% (Guerin & Abril, 2007). However, in very organic-rich sediments, the high rates of mineralization combined with the hydrophobic characteristic of CH_4 molecule, can cause CH_4 to form bubbles which tend to be quickly emitted to the atmosphere (Bastviken et al., 2004; McGinnis et al., 2006). Even though the formation of CH_4 bubbles is favoured by high temperatures, temperate reservoirs may also emit significant amounts of CH_4 through bubbling (e.g. Delsontro et al., 2010).

Both aerobic and anaerobic mineralization of organic matter release large amounts of inorganic nutrients, in addition to CO_2 and CH_4, in the water column of reservoirs. The availability of inorganic nutrients, especially phosphorus, combined to the usually high light penetration depth in reservoirs (due to sedimentation of suspended material) favours CO_2 uptake by photosynthesis. Photosynthesis in reservoirs, as in any other aquatic system, is performed by phytoplankton in the water column, attached algae (periphyton) and aquatic plants (macrophytes). However, due to the usually high depth (and high 'total volume/littoral volume' ratio) of reservoirs, the relative importance of periphyton and macrophyte tends to be low compared to the importance of phytoplankton. In eutrophic reservoirs (i.e. high nutrient concentrations and high phytoplankton production) photosynthesis can cause a strong reduction in CO_2 concentrations turning the reservoirs into a sink of atmospheric CO_2. This occurs in reservoirs worldwide, regardless of age or latitude (Barros et al., 2011). The number of reservoirs acting as carbon sinks is, however, low as compared to CO_2 emitting reservoirs.

4.2 GHG flux through the water-atmosphere interface

The excess GHG in the water column of reservoirs tend to be emitted to the atmosphere. Emissions can occur through (i) molecular diffusion at the water-air interface (e.g. Roland et al., 2010; Teodoru et al., 2010), (ii) bubbling from the sediment (e.g. Abe et al., 2005; Lima, 2005) (iii) degassing from water passing at the turbines (e.g. Kemenes et al., 2007, 2011) or (iv) turbulent degassing in downstream rivers (e.g. Guerin et al., 2006) (**Figure 4**).

Diffusive fluxes of CO_2 and CH_4 at the water-atmosphere interface are dependent on the existence of a concentration gradient between these two compartments. If the water at the surface of a reservoir is supersaturated with CO_2 or CH_4 in relation to the atmosphere, gas fluxes occur towards the atmosphere. If, on the other side, surface water is under-saturated in relation to the atmosphere, gas fluxes are from the atmosphere to the water. In the latter case, the reservoir surface represents a sink of atmospheric carbon. The amount of GHG flowing through water-atmosphere interfaces depends on gas solubility in water. Gas solubility is negatively related to temperature and positively related to pressure, according to Le Chatalier's principle. Thus, GHG emissions through diffusion tend to be higher in reservoirs located in warmer regions and at lower altitudes. The surfaces of reservoirs are usually dominated by diffusive fluxes of CO_2, even in cases in which bottom anoxia leads to high CH_4 production (Barros et al., 2011). This is due to the intense oxidation of diffusive CH_4 by methanotrophic bacteria above the interface between anoxic and oxygenated water layers.

On the other hand, GHG emissions through bubbling are dominated by CH_4. This is due to the very low CH_4 solubility in water, which permits the formation of bubbles varying in size

from 2 to 8 millimetres (Delsontro et al., 2010). The bubbles are usually formed in the sediment of reservoirs, under anoxic conditions. Most of the CH_4 emissions in shallow reservoirs occur through bubbling whereas CH_4 bubbles are usually dissolved in the water before reaching the surface in deep reservoirs.

The process of energy generation by the turbines of hydroelectric reservoirs leads to two pathways of GHG emission that do not occur in artificial reservoirs built for other purposes (e.g. irrigation, water supply, flood control, and aquaculture): turbulent degassing of water passing through turbines (energy generation unities) and degassing downstream of dams. The water inlet to generate energy is frequently located in medium or lower parts of the dam which means that water from deep layers of the reservoirs passes through the turbines. These deep water layers are usually CO_2 and CH_4-rich due to both high mineralization rates and high water pressure (i.e. high gas solubility). By passing through the turbines, the gases are exposed to a low pressure and high temperature condition which favors rapid emissions to the atmosphere (Kemenes et al., 2007). Despite the usually high GHG emissions at the turbines, high amounts of both CO_2 and CH_4 remain dissolved in the water downstream the dams. GHG produced in reservoirs may be encountered at sites as far as 40 km downstream of the dam (Guerin et al., 2006).

5. External factors affecting the processes driving GHG emissions to the atmosphere

The great variation in GHG emissions from hydroelectric reservoirs in different parts of the globe is explained by the effect of climate and drainage basin characteristics on GHG dynamics. Climate affects the inputs of carbon from land to the aquatic environment and the rates of GHG production and consumption. Moreover, wind, precipitation and temperature may have important effects on the rates of gas exchange in the water-atmosphere interface. This section brings an overview of some important processes and external factors influencing GHG emissions from freshwater systems with focus on the dynamics of hydroelectric reservoirs.

5.1 Wind

Wind is the major source of energy for water movement in lakes and reservoir. The wind stress at the water surface can results in small turbulence, horizontal currents, vertical currents, surface waves and internal waves (seiches). Where and how those processes will emerge and behave depends on a series of factors such as the size and the shape of water surface, fetch, wind direction, temperature, and surrounding terrain. The response of reservoirs to wind stress depends mainly on the morphometric characteristics of the basin and its location. Reservoirs are typically built in valleys, after confluence of several tributaries. It usually results in long and dendritic water bodies (Ford, 1990), contrasting to the generally circular- or bowl-shaped natural lakes. Therefore, depending on the surrounding terrain, wind can blow aligned with the main-long fetch, increasing its effect over water surfaces. This effect, however, is limited by the dendritic geometry or reservoir, resulting in more complex circulation patterns in certain parts of reservoirs.

Wind effect strongly impacts on GHG emissions. Turbulence, for example, influences the velocity of gas transfer at the water-atmosphere interface (Wanninkhof, 1992). The role of

wind on GHG emissions, however, is not restricted to causing surface turbulence. Wind can also cause deep water circulation and transport of dissolved compounds.

The overall picture that emerges is that reservoirs are highly temperature stratified in summer and only weakly forced by wind, while in spring/winter the mixing process is enhanced by high wind velocity. During high velocity wind events surface water moves toward the shore, where the water piles up and sinks in the process known as downwelling. At the same time at the opposite side, surface water is replaced by water that wells up from below (upwelling) (Monismith, 1985; Stevens & Imberger, 1996; Macintyre et al., 2002; Farrow & Stevens, 2003). However, wind direction and persistency are of great importance as well. Persistent wind aligned with the main reservoir body – resulting in a large fetch – is able to promote downwelling/upwelling (d/u) even at low velocities (Assireu et al., 2011). At the downwelling side of a reservoir, CH_4 oxidation plays an important role, changing CH_4 into CO_2 during the downward dissolved oxygen transport and reducing the CH_4 emission to the atmosphere. At the upwelling side of reservoir, the GHG flux to the atmosphere is enhanced due to the high CO_2 and CH_4 concentrations of emerging water. This clearly influences the spatial variability of GHG emissions within reservoirs (Roland et al., 2010). It was suggested that frequent d/u events in the tropical Manso reservoir could enhance CO_2 emissions with approximately 12% (Assireu et al., 2005; Ometto et al., 2011).

5.2 Precipitation

Precipitation can vary markedly in intensity and frequency from one year to another. Such variability can generate different kinds of seasonal patterns, modifying water turnover time and changing the intensity of environmental processes occurring in the water column of aquatic systems (Armengol et al. 1999). Furthermore, the external loading of organic matter and other compounds to the system often increases with intensive precipitation events. The intensity of these loadings depends on land use, vegetation cover and landscape patchiness (Rybak, 2001). Rain-induced high primary productivity has been observed in some African lakes (Lemoalle, 1975; Melack, 1979; Thomas et al., 2000). In tropical regions, the first rains after the start of the rainy season are expected to a lot of carbon into the reservoir that can be assimilated by bacterioplankton or be buried in the sediment. However, if the residence time of the water is very short, with high flushing rate, most of this carbon and nutrients will not remain long in the system (Amarasinghe & Vijverberg, 2002).

Precipitation also affects CO_2 transfer at the air-water interface. Impinging raindrops causes turbulence, enhancing CO_2 flux across the air-water interface (Takagaki & Komori, 2007). This means that, depending on the difference of gas concentrations between water and atmosphere, the emission/absorption of GHG in aquatic systems can be enhanced by increasing precipitation rates. The rainfall effects can be significant to the local CO_2 budget between water and atmosphere during the rainy season but are not as important to the whole system budget as the wind share effect.

5.3 Temperature

Changes in temperature may affect, directly and indirectly, all processes involved in the production, consumption and emission of GHG in reservoirs. For example, respiration

(Sand-Jensen et al., 2007), primary production in the water column (Flanagan et al., 2003) are strongly influenced by temperature. Although both processes tend increase with warming, it has been argued that respiration has usually a stronger response (Rivkin & Legendre, 2001; Biddanda & Cotner, 2002; Lopez-Urrutia et al., 2006; Sand-Jensen et al., 2007), leading to a net increase in CO_2 production under warmer conditions (Kosten et al 2010). Moreover, evidences from lakes located in different climate regions have shown that more mineralization occurs (with further CO_2 and CH_4 production) and less carbon is buried in the sediment of warmer systems (Gudasz et al., 2010).

Indeed, GHG emissions are higher in reservoirs located in warmer latitudes (Barros et al., 2011). The positive relationship between GHG emissions and temperature implies that environmental changes causing temperature to vary affects the role of hydroelectric reservoirs as GHG sources. Based on the predicted scenarios of global change in temperature (IPCC, 2007) GHG emissions from reservoir will increase, especially in cold regions.

5.4 Drainage basin and river input

Large impoundments may show different zones in terms of CO_2 emission because those fluxes are dependent on flooded biomass and watershed input of organic matter. Compared to natural lakes, reservoirs tend to have shorter water residence times and more complex heterogeneity due to the presence of one or more major water inlets, instead of multiple diffuse water sources characteristic for most natural lakes (Kennedy et al., 1985; Kennedy & Walker, 1990). Reservoirs are intrinsically linked to the rivers that feed them (Baxter, 1977), creating a river–reservoir continuum, in which water and sediment inputs are functions of the land use in the watershed (Kelly, 2001). Watershed land use is often highly correlated with algal cell and nutrients concentrations as has been shown for seven subtropical reservoirs (Burford et al., 2007). This clearly indicates that in order to understand and predict GHG emissions from reservoirs, features of the drainage basin have to be taken into account.

Another important factor to be considered is the difference between the densities of river and reservoir water. When a river reaches a reservoir the water plunges and can flow along the surface (overflow), intermediate (interflow) or deep (underflow) layer, depending on the difference between the water temperature and physical characteristics (e.g. total dissolved solids and suspended solids) (Martin & McCutcheon, 1999). The fate of organic matter influx largely depends on the way the incoming water flows into the reservoirs. If incorporated into deeper layers, anoxic conditions facilitate degradation of organic matter into CH_4. The picture becomes more complicates when, due to the complexity of the system and hydrodynamic factors of the river entrance, waves arise in the interface between river/reservoir water. These waves cause transport of water from the nutrient-rich and GHG-rich deep layer to the surface layer (Assireu et al., 2011).

6. Future perspectives

It is now clear that hydroelectric reservoirs represent a renewable but not a carbon-free source of electricity. Attempts to determine the carbon footprint of hydropower production have lead to significant scientific advances (see section 2 for details). However, it is still a

long way towards a full assessment of the role of hydroelectric reservoirs as sources of GHG to the atmosphere. The major gaps to be filled by future research are related to the quality of current carbon budget estimations. However, other issues need attention, e.g. the outcomes of removal of dams and the development of mitigation strategies.

The assessment of the net role of reservoirs as sinks or sources of GHG to the atmosphere requires more than measurements of carbon fluxes at the water-atmosphere interface of reservoirs. For example, the net change in the carbon cycle due to reservoir construction should consider pre-impoundment carbon sinks and sources from the original river course and the adjacent terrestrial landscape (Teodoru et al., 2010). Scenarios of pre- and post-impoundment fluxes, however, are neglected by most estimates of emissions. Even more importantly, there is a need to evaluate the net effect of reservoir as sink of atmospheric carbon (St Louis et al., 2000; Barros et al., 2011), by comparing carbon burial in reservoirs with carbon burial prior to impoundment (i.e. in the ocean).

The role of reservoirs sediment in the global carbon cycle is still poorly understood. Despite the importance of sediment as the main site for organic matter mineralization and GHG production (especially CH_4) sediment carbon fluxes in reservoirs are restricted to few measurements (e.g. Aberg et al., 2004; Abe et al., 2005). Additionally, reservoirs accumulate large amounts of carbon in the sediment, which compensates at least part of the emissions. It has been estimated that approximately 400 gC m^{-2} y^{1} is buried in reservoirs (Dean & Gorham, 1998; Mulholland et al., 2001). This estimation, however, is based on non-standardized methods which consider, e.g. loss in water storage capacity of reservoirs in the USA and constant values for carbon content and sediment density. There is an urgent need, thus, for research focusing on this potential carbon sink pathway.

Another important source of errors in carbon budgets relies on neglecting variability. Both the neglected variability among and within reservoirs as well as variability over time impacts the precision of carbon flux estimates. The persistent increase in the amount of data, by itself, may contribute to equal out the errors of local and global estimations. Nevertheless, addressing all possible sources of variability is an important task for future research on GHG emissions from reservoirs.

Regarding the variability among reservoirs, the limited amount of data from reservoirs located in the tropics was, until recently, severely limiting the precision of GHG emission estimations from reservoirs (e.g. St Louis et al., 2000). Within the last decade, many tropical reservoirs have become focus of study, permitting a better evaluation of the latitudinal effect on emissions (Barros et al., 2011). Nevertheless, there is still a great need for research in the tropics, since this is where most of the potential for new dams remains (Figure 2). Future research on tropical reservoirs should seek for better estimations of CH_4 emissions, which seems to have been seriously underestimated in the last two decades (Demarty & Bastien, 2011; Wehrli, 2011) in spite of its greater warming potential (more than 20 times more) when compared to CO_2.

Neglecting variability in GHG emissions over time may equally cause great errors in estimations. Especially because GHG emissions reduce as reservoirs age (Barros et al., 2011). Furthermore, fluctuations in carbon cycling may occur on a seasonal (Wang et al., 2011) and even on a daily basis (Roland et al., 2010). The changes in GHG emission rates with time makes the full assessment of the carbon budget in a reservoir is a difficult task. Future studies

of GHG emissions from reservoirs should, thus, seek for a better understanding of the patterns of variation on GHG dynamics with time. Both long-term measurements (including several years) and intensive measurements (in a more frequent basis, e.g. hours) are needed.

Overcoming the issues related to variability of GHG emission in space and time becomes even more challenging due to extreme events (e.g. upwelling). Such events which are very hard to 'catch' may account to a major portion of the GHG emissions from a reservoir (Roland et al., 2010).

Most of the GHG assessments in hydroelectric reservoirs have looked at emissions from decaying biomass after impoundment, as related to the previous emissions (see section 2 for details). Some studies have used a full life-cycle assessment, which considers the emissions during the construction phase of dams (e.g. Chamberland & Levesque, 1996; Gagnon & Van de Vate, 1997; Pacca & Horvath, 2002). However, little attention has been given to the fact that every hydropower plant has an intrinsic operation life-time after which its dam should be deactivated (Pacca, 2007). Moreover, dams may be deactivated and removed due to failures (e.g. error during construction, geological instability, poor maintenance, excess internal erosion etc.). It has been estimated that about 600 dams were removed in the last 100 years in the USA alone (Gleick et al., 2009). The removal of dams was the subject of a special issue published by Bioscience in 2002 which did not mention the effects on GHG emission.

With dam removal, part of the sediment accumulated at the reservoirs will be flushed down river if not otherwise controlled (e.g. dredged). Sediment fate is an important factor determining the amount of carbon returning to the atmosphere – a greater fraction of dredged sediment becomes available for mineralization whereas organic carbon flushing downstream rivers may ultimately accumulate the ocean (Pacca, 2007). Despite the many uncertainties regarding the effects of dam removal, it is now clear that this issue should not be disregarded by future assessments. Answering questions as "how permanent is carbon accumulation in the sediment of reservoirs?" is mandatory to a better understanding of reservoirs' role in the global carbon cycle.

With the continuous and integrated research focusing on revealing the actual role of hydroelectric reservoirs in the global carbon cycle, the gaps in knowledge tend to be reduced at a rapid pace. Recent advances have resulted in important tools for reducing GHG emissions from reservoirs through changes in reservoir management and, even more importantly, through the GHG-intelligent design and location of new hydropower plants. It is now known, for example, that future hydropower projects should seek for better GHG emission/MWh ratios by reducing flooded area to the maximum extent, removing terrestrial vegetation prior to impounding and preserving the vegetation in the drainage basin to avoid soil erosion. The research about hydroelectric projects has been promoting a new generation of scientist that are able to apply fundamental environment sciences – ecology, biology, chemistry, physics and mathematics – to issues representing global concerns. We believe that the scientific community is strongly prepared to discuss the needs for energy and environmental wellness in the future.

7. References

Abe, D.S.; Donald D. Adams; Galli, C.V.S.; Sikar, E. & Tundisi, J.G. (2005). Sediment greenhouse gases (methane and carbon dioxide) in the Lobo-Broa Reservoir, São

Paulo State, Brazil: Concentrations and diffuse emission fluxes for carbon budget considerations. *Lakes & Reservoirs: Research and Management*, Vol.10. No.4, pp. 201-209, 1440-1770

Aberg, J.; Bergstrom, A.K.; Algesten, G.; Soderback, K. & Jansson, M. (2004). A comparison of the carbon balances of a natural lake (L. Ortrasket) and a hydroelectric reservoir (L. Skinnmuddselet) in northern Sweden. *Water Research*, Vol.38. No.3, Feb, pp. 531-538, 0043-1354

Abril, G.; Guerin, F.; Richard, S.; Delmas, R.; Galy-Lacaux, C.; Gosse, P.; Tremblay, A.; Varfalvy, L.; Dos Santos, M.A. & Matvienko, B. (2005). Carbon dioxide and methane emissions and the carbon budget of a 10-year old tropical reservoir (Petit Saut, French Guiana). *Global Biogeochemical Cycles*, Vol.19. No.4, Oct, 0886-6236

Amarasinghe, P.B. & Vijverberg, J. (2002). Primary production in a tropical reservoir in Sri Lanka. *Hydrobiologia*, Vol.487. No.1, Nov, pp. 85-93, 0018-8158

Armengol, J.; Garcia, J.C.; Comerma, M.; Romero, M.; Dolz, J.; Roura, M.; Han, B.H.; Vidal, A. & Simek, K. (1999). Longitudinal processes in canyon type reservoir: the case of Sau (N.E. SPAIN), pp. 313-345. In: *Theoretical reservoir ecology and its applications*, Tundisi, J.G. & Straskraba, M. (eds.), Brazilian Academy of Sciences and Backhuys Publishers, 585p. ISBN 85-87418-02-5, Barcelona

Assireu, A.T.; Alcântara, E.; Novo, E.M.L.M.; Roland, F.; Pacheco, F.S.; Stech, J.L. & Lorenzzetti, J.A. (2011). Inside the hydro-physics processes at the plunge point location: an analysis by satellite and in situ data. *Hydrol. Earth Syst. Sci. Discuss.*, Vol.8. pp. 1-31

Assireu, A.T.; Stech, J.L.; Marinho, M.M.; Cesar, D.E.; Lorenzzentti, J.A.; Ferreira, R.M.; Pacheco, F.S. & Roland, F. (2005). Princípios Físicos e Químicos a Serviço da Limnologia - Um Exercício. In: *Liçoes de Limnologia.*, Rima Editora, ISBN: 8576560593, São Carlos

Bambace, L.A.W.; Ramos, F.M.; Lima, I.B.T. & Rosa, R.R. (2007). Mitigation and recovery of methane emissions from tropical hydroelectric dams. *Energy*, Vol.32. No.6, Jun, pp. 1038-1046, 0360-5442

Barros, N.; Cole, J.J.; Tranvik, L.J.; Prairie, Y.T.; Bastviken, D.; Huszar, V.L.M.; Del Giorgio, P. & Roland, F. (2011). Carbon emission from hydroelectric reservoirs linked to reservoir age and latitude. *Nature Geoscience*, Vol.4. No.9, Sep, pp. 593-596, 1752-0894

Bastien, J. (2005). Impacts of ultraviolet radiation on aquatic ecosystems: greenhouse gas emissions and implications for hydroeletric reservoirs. In: *Greenhouse Gas Emissions - Fluxes and Process. Hydroelectric Reservoirs and Natural Environments*, Tremblay, A., Varfalvy, L., Roehm, C. & Garneau, M., 509-527, Springer-Verlag, ISBN 978-3-540-23455-5, New York

Bastviken, D.; Cole, J.; Pace, M. & Tranvik, L. (2004). Methane emissions from lakes: Dependence of lake characteristics, two regional assessments, and a global estimate. *Global Biogeochemical Cycles*, Vol.18. No.4, Oct 20, 0886-6236

Baxter, R.M. (1977). Environmental Effects of Dams and Impoundments. *Annual Review of Ecology and Systematics*, Vol.8. pp. 255-283, 0066-4162

Bayne, D.R.; Lawrence, J.M. & McGuire, J.A. (1983). Primary productivity studies during early years of West-Point reservoir, Alabama Georgia. *Freshwater Biology*, Vol.13. No.5, pp. 477-489, 0046-5070

Bergstrom, A.K.; Algesten, G.; Sobek, S.; Tranvik, L. & Jansson, M. (2004). Emission of CO_2 from hydroelectric reservoirs in northern Sweden. *Archiv Fur Hydrobiologie*, Vol.159. No.1, Jan, pp. 25-42, 0003-9136

Biddanda, B.A. & Cotner, J.B. (2002). Love handles in aquatic ecosystems: The role of dissolved organic carbon drawdown, resuspended sediments, and terrigenous inputs in the carbon balance of Lake Michigan. *Ecosystems*, Vol.5. No.5, Aug, pp. 431-445, 1432-9840

Burford, M.A.; Johnson, S.A.; Cook, A.J.; Packer, T.V.; Taylor, B.M. & Townsley, E.R. (2007). Correlations between watershed and reservoir characteristics, and algal blooms in subtropical reservoirs. *Water Research*, Vol.41. No.18, Oct, pp. 4105-4114, 0043-1354

Chamberland, A. & Levesque, S. (1996). Hydroelectricity, an option to reduce greenhouse gas emissions from thermal power plants. *Energy Conversion and Management*, Vol.37. No.6-8, Jun-Aug, pp. 885-890, 0196-8904

Chanudet, V.; Descloux, S.; Harby, A.; Sundt, H.; Hansen, B.H.; Brakstad, O.; Serça, D. & Guerin, F. (2011). Gross CO_2 and CH_4 emissions from the Nam Ngum and Nam Leuk sub-tropical reservoirs in Lao PDR. *Science of The Total Environment*, Vol.in press. No.0, pp. 0048-9697

Chao, B.F.; Wu, Y.H. & Li, Y.S. (2008). Impact of Artificial Reservoir Water Impoundment on Global Sea Level. *Science*, Vol.320. No.5873, April 11, 2008, pp. 212-214,

Chen, H.; Wu, Y.Y.; Yuan, X.Z.; Gao, Y.H.; Wu, N. & Zhu, D. (2009). Methane emissions from newly created marshes in the drawdown area of the Three Gorges Reservoir. *Journal of Geophysical Research-Atmospheres*, Vol.114. Sep, pp. 0148-0227

Cole, J.J.; Caraco, N.F.; Kling, G.W. & Kratz, T.K. (1994). Carbon-Dioxide Supersaturation in the Surface Waters of Lakes. *Science*, Vol.265. No.5178, Sep 9, pp. 1568-1570, 0036-8075

Cole, J.J.; Prairie, Y.T.; Caraco, N.F.; Mcdowell, W.H.; Tranvik, L.J.; Striegl, R.G.; Duarte, C.M.; Kortelainen, P.; Downing, J.A.; Middelburg, J.J. & Melack, J. (2007). Plumbing the global carbon cycle: Integrating inland waters into the terrestrial carbon budget. *Ecosystems*, Vol.10. No.1, Feb, pp. 171-184, 1432-9840

Cullenward, D. & Victor, D.G. (2006). The dam debate and its discontents. *Climatic Change*, Vol.75. No.1-2, Mar, pp. 81-86, 0165-0009

Dean, W.E. & Gorham, E. (1998). Magnitude and significance of carbon burial in lakes, reservoirs, and peatlands. *Geology*, Vol.26. No.6, Jun, pp. 535-538, 0091-7613

Delmas, R.; Galy-Lacaux, C. & Richard, S. (2001). Emissions of greenhouse gases from the tropical hydroelectric reservoir of Petit Saut (French Guiana) compared with emissions from thermal alternatives. *Global Biogeochemical Cycles*, Vol.15. No.4, Dec, pp. 993-1003, 0886-6236

Delsontro, T.; McGinnis, D.F.; Sobek, S.; Ostrovsky, I. & Wehrli, B. (2010). Extreme Methane Emissions from a Swiss Hydropower Reservoir: Contribution from Bubbling Sediments. *Environmental Science & Technology*, Vol.44. No.7, Apr 1, pp. 2419-2425, 0013-936X

Demarty, M. & Bastien, J. (2011). GHG emissions from hydroelectric reservoirs in tropical and equatorial regions: Review of 20 years of CH_4 emission measurements. *Energy Policy*, Vol.39. No.7, Jul, pp. 4197-4206, 0301-4215

Diem, T.; Koch, S.; Schwarzenbach, S.; Wehrli, B. & Schubert, C.J. (2007). Greenhouse-gas (CH_4, N_2O and CO_2) emissions from hydroelectric reservoirs in Switzerland.

Dos Santos, M.A.; Rosa, L.P.; Sikar, B.; Sikar, E. & Dos Santos, E.O. (2006). Gross greenhouse gas fluxes from hydro-power reservoir compared to thermo-power plants. *Energy Policy*, Vol.34. No.4, Mar, pp. 481-488, 0301-4215

Duchemin, E.; Lucotte, M.; Canuel, R. & Chamberland, A. (1995). Production of the greenhouse gases CH_4 and CO_2 by hydroelectric reservoirs of the boreal region. *Global Biogeochem. Cycles*, Vol.9. No.4, pp. 529-540,

Duchemin, E.; Lucotte, M.; Canuel, R. & Soumis, N. (2006). First assessment of methane and carbon dioxide emissions from shallow and deep zones of boreal reservoirs upon ice break-up. *Lakes & Reservoirs: Research & Management*, Vol.11. No.1, pp. 9-19, 1440-1770

Farrow, D.E. & Stevens, C.L. (2003). Numerical modelling of a surface-stress driven density-stratified fluid. *Journal of Engineering Mathematics*, Vol.47. No.1, Sep, pp. 1-16, 0022-0833

Fearnside, P.M. (1995). Hydroelectric dams in the Brazilian amazon as sources of greenhouse gases. *Environmental Conservation*, Vol.22. No.1, Spr, pp. 7-19, 0376-8929

Fearnside, P.M. (1997). Greenhouse-gas emissions from Amazonian hydroelectric reservoirs: the example of Brazil's Tucurui Dam as compared to fossil fuel alternatives. *Environmental Conservation*, Vol.24. No.1, Mar, pp. 64-75, 0376-8929

Fearnside, P.M. (2002). Greenhouse gas emissions from a hydroelectric reservoir (Brazil's Tucurui Dam) and the energy policy implications. *Water Air and Soil Pollution*, Vol.133. No.1-4, Jan, pp. 69-96, 0049-6979

Fearnside, P.M. (2004). Greenhouse gas emissions from hydroelectric dams: Controversies provide a springboard for rethinking a supposedly 'clean' energy source - An editorial comment. *Climatic Change*, Vol.66. No.1-2, Sep, pp. 1-8, 0165-0009

Fearnside, P.M. (2005). Do hydroelectric dams mitigate global warming? The case of Brazil's Curuá-Una dam. *Mitigation and Adaptation Strategies for Global Change*, Vol.10. No.5, pp. 675-691,

Fearnside, P.M. (2006). Greenhouse gas emissions from hydroelectric dams: Reply to Rosa et al. *Climatic Change*, Vol.75. No.1-2, Mar, pp. 103-109, 0165-0009

Flanagan, K.M.; McCauley, E.; Wrona, F. & Prowse, T. (2003). Climate change: The potential for latitudinal effects on algal biomass in aquatic ecosystems, Canadian. Journal of Fisheries and Aquatic Sciences, Vol.60. No.6, Oct 20, pp. 635-639, 0706-652X

Ford, D.E. (1990). Reservoir transport processes. In: *Reservoir limnology: ecological perspectives*, Thornton, K.W., Kimmel, B.L. & Payne, F.E., 256, JohnWiley & Sons, New York

Gagnon, L. & Van de Vate, J.F. (1997). Greenhouse gas emissions from hydropower - The state of research in 1996. *Energy Policy*, Vol.25. No.1, Jan, pp. 7-13, 0301-4215

Galy-Lacaux, C.; Delmas, R.; Jambert, C.; Dumestre, J.F.; Labroue, L.; Richard, S. & Gosse, P. (1997). Gaseous emissions and oxygen consumption in hydroelectric dams: A case study in French Guyana. *Global Biogeochemical Cycles*, Vol.11. No.4, Dec, pp. 471-483, 0886-6236

Galy-Lacaux, C.; Delmas, R.; Kouadio, G.; Richard, S. & Gosse, P. (1999). Long-term greenhouse gas emissions from hydroelectric reservoirs in tropical forest regions. *Global Biogeochemical Cycles*, Vol.13. No.2, Jun, pp. 503-517, 0886-6236

Giles, J. (2006). Methane quashes green credentials of hydropower. *Nature*, Vol.444. No.7119, Nov, pp. 524-525, 0028-0836

Gleick, P.H.; Cooley, H.; Cohen, M.J.; Marikawa, M.; Morrison, J. & Palanappn, M. (2009). Dams Removed or Decommissioned in the United States, 1912 to Present. In: *The World's Water 2008-2009*, Gleick, P.H., 239-264, Pacific Institute for Studies in Development, Environment, and Security, Island Press, Washington, D.C.

Gudasz, C.; Bastviken, D.; Steger, K.; Premke, K.; Sobek, S. & Tranvik, L.J. (2010). Temperature-controlled organic carbon mineralization in lake sediments. *Nature*, Vol.466. No.7305, Jul, pp. 478-U3, 0028-0836

Guerin, F. & Abril, G. (2007). Significance of pelagic aerobic methane oxidation in the methane and carbon budget of a tropical reservoir. *Journal of Geophysical Research-Biogeosciences*, Vol.112. No.G3, pp.

Guerin, F.; Abril, G.; Richard, S.; Burban, B.; Reynouard, C.; Seyler, P. & Delmas, R. (2006). Methane and carbon dioxide emissions from tropical reservoirs: Significance of downstream rivers. *Geophysical Research Letters*, Vol.33. No.21, Nov, pp. 0094-8276

Guerin, F.; Abril, G.; Richard, S.; Burban, B.; Reynouard, C.; Seyler, P. & Delmas, R. (2006). Methane and carbon dioxide emissions from tropical reservoirs: Significance of downstream rivers. *Geophysical Research Letters*, Vol.33: L21407. Nov 14, pp. 0094-8276

Guerin, F.; Abril, G.; Serca, D.; Delon, C.; Richard, S.; Delmas, R.; Tremblay, A. & Varfalvy, L. (2007). Gas transfer velocities of CO_2 and CH_4 in a tropical reservoir and its river downstream. *Journal of Marine Systems*, Vol.66. No.1-4, Jun, pp. 161-172, 0924-7963

Hedges, J.I. & Keil, R.G. (1995). Sedimentary organic-matter preservation - an assessment and speculative synthesis. *Marine Chemistry*, Vol.49. No.2-3, Apr, pp. 81-115, 0304-4203

Hedges, J.I.; Keil, R.G. & Benner, R. (1997). What happens to terrestrial organic matter in the ocean? *Organic Geochemistry*, Vol.27. No.5-6, Oct-Nov, pp. 195-212, 0146-6380

Hoffert, M.I.; Caldeira, K.; Jain, A.K.; Haites, E.F.; Harvey, L.D.D.; Potter, S.D.; Schlesinger, M.E.; Schneider, S.H.; Watts, R.G.; Wigley, T.M.L. & Wuebbles, D.J. (1998). Energy implications of future stabilization of atmospheric CO_2 content. *Nature*, Vol.395. No.6705, Oct, pp. 881-884, 0028-0836

Huttunen, J.T.; Vaisanen, T.S.; Hellsten, S.K.; Heikkinen, M.; Nykanen, H.; Jungner, H.; Niskanen, A.; Virtanen, M.O.; Lindqvist, O.V.; Nenonen, O.S. & Martikainen, P.J. (2002). Fluxes of CH_4 ,CO_2, and N_2O in hydroelectric reservoirs Lokka and Porttipahta in the northern boreal zone in Finland. *Global Biogeochemical Cycles*, Vol.16. No.1, Mar, pp. -, 0886-6236

IEA (2008). International Energy Agency. Electricity/Heat in World in 2008. available via http://go.nature.com/6mAAWK

IPCC (2007). Intergovernmental Panel on Climate Change's Fourth Assessment Report

Keller, M. & Stallard, R.F. (1994). Methane Emission by Bubbling from Gatun Lake, Panama. *Journal of Geophysical Research-Atmospheres*, Vol.99. No.D4, Apr 20, pp. 8307-8319, 0148-0227

Kelly, C.; Rudd, J.W.M.; St. Louis, V.L. & Moore, T. (1994). Turning attention to reservoir surfaces, a neglected area in greenhouse studies. *Eos Trans. AGU*, Vol.75. No.29, pp. 332,

Kelly, V.J. (2001). Influence of reservoirs on solute transport: a regional-scale approach. *Hydrological Processes*, Vol.15. No.7, May, pp. 1227-1249, 0885-6087

Kemenes, A.; Forsberg, B.R. & Melack, J.M. (2007). Methane release below a tropical hydroelectric dam. *Geophysical Research Letters*, Vol.34. No.12, Jun, pp. 0094-8276

Kemenes, A.; Forsberg, B.R. & Melack, J.M. (2007). Methane release below a tropical hydroelectric dam. *Geophysical Research Letters*, Vol.34: L1 2809. Jun 23, pp. 0094-8276

Kemenes, A.; Forsberg, B.R. & Melack, J.M. (2011). CO_2 emissions from a tropical hydroelectric reservoir (Balbina, Brazil). *Journal of Geophysical Research-Biogeosciences*, Vol.116. Jul, pp. 0148-0227

Kennedy, R.H.; Thorton, K.W. & D.E., F. (1985). Characterization of the reservoir ecosystem. In: *Microbial Processes in Reservoirs.*, Gunnisson, D., Dr. W. Junk Publishers, Dordrecht

Kennedy, R.H. & Walker, W.W. (1990). Reservoir nutrient dynamics. In: *Reservoir Limnology: Ecological Perspectives*, Thornton, K.W., B.L., K. & F.E., P., John Wiley and Sons, New York

Kosten, K.; Roland, F.; Motta Marques, D.M.L.; Van Nes, E.H.; Mazzeo, N.; Sternberg, L.S.L.; Scheffer, M. & Cole, J.J. (2010). Climate-dependent CO2 emissions from lakes. Global Biogeochemical Cycles, Vol.24. May 8, 0886-6236

Kritzberg, E.S.; Cole, J.J.; Pace, M.M. & Graneli, W. (2005). Does autochthonous primary production drive variability in bacterial metabolism and growth efficiency in lakes dominated by terrestrial C inputs? *Aquatic Microbial Ecology*, Vol.38. No.2, Feb, pp. 103-111, 0948-3055

Lemoalle, J. (1975). L'activité photosynthetic du phytoplankton en relation avec le niveau des eaux du Lac Tchad (Afrique). *Verh. int. Ver. Limnol.*, Vol.19. pp. 5,

Lima, I.B.T. (2005). Blogeochemical distinction of methane releases from two Amazon hydroreservoirs. *Chemosphere*, Vol.59. No.11, Jun, pp. 1697-1702, 0045-6535

Lima, I.B.T.; Novo, E.M.L.M.; Ballester, M.V.R. & Ometto, J.P.H.B. (1998). Methane Production, Transport and Emission in Amazon Hydroelectric Plants. *Veranlundgen der Internationalen Vereinigung für Theoretische und Angewandte Limnologie.*, pp.

Lopez-Urrutia, A.; San Martin, E.; Harris, R.P. & Irigoien, X. (2006). Scaling the metabolic balance of the oceans. *Proceedings of the National Academy of Sciences of the United States of America*, Vol.103. No.23, Jun, pp. 8739-8744, 0027-8424

Macintyre, S.; Romero, J.R. & Kling, G.W. (2002). Spatial-temporal variability in surface layer deepening and lateral advection in an embayment of Lake Victoria, East Africa. *Limnology and Oceanography*, Vol.47. No.3, May, pp. 656-671, 0024-3590

Martin, J.L. & Mccutcheon, S.C. (1999). Hydrodynamics and transport for water quality modeling. Boca Raton

McGinnis, D.F.; Greinert, J.; Artemov, Y.; Beaubien, S.E. & Wuest, A. (2006). Fate of rising methane bubbles in stratified waters: How much methane reaches the atmosphere? *Journal of Geophysical Research-Oceans*, Vol.111. No.C9, Sep, pp. 0148-0227

Melack, J.M. (1979). Photosynthetic Rates in 4 Tropical African Fresh Waters. *Freshwater Biology*, Vol.9. No.6, pp. 555-571, 0046-5070

Monismith, S.G. (1985). Wind-Forced Motions in Stratified Lakes and Their Effect on Mixed-Layer Shear. *Limnology and Oceanography*, Vol.30. No.4, pp. 771-783, 0024-3590

Mulholland, P.J.; Fellows, C.S.; Tank, J.L.; Grimm, N.B.; Webster, J.R.; Hamilton, S.K.; Marti, E.; Ashkenas, L.; Bowden, W.B.; Dodds, W.K.; Mcdowell, W.H.; Paul, M.J. & Peterson, B.J. (2001). Inter-biome comparison of factors controlling stream metabolism. *Freshwater Biology*, Vol.46. No.11, Nov, pp. 1503-1517, 0046-5070

Ometto, J.P.; Cimbleris, A.C.P.; Santos, M.A.; Rosa, L.P.; Abe, D.S.; Tundisi, J.G.; Stech, J.L.; Barros, N.O. & Roland, F. Patterns of carbon emission as a function of energy generation in hydroelectric reservoirs. . *Submitted to Climatic Changes (2011)*, pp.

Ometto, J.P.; Pacheco, F.S.; Cimbleris, A.C.P.; Stech, J.L.; Lorenzzetti, J.A.; Assireu, A.; Santos, M.A.; Matvienko, B.; Rosa, L.P.; Galli, C.S.; Abe, D.S.; Tundisi, J.G.; Barros, N.; Mendonça, R.F. & Roland, F. (2011). Carbon dynamic and emissions in Brazilian hydropower reservoirs. In: *Energy Resources: Development, Distribution, and Exploitation*, Alcântara, E., Nova Science Publishers, New York

Pacca, S. (2007). Impacts from decommissioning of hydroelectric dams: a life cycle perspective. *Climatic Change*, Vol.84. No.3-4, Oct, pp. 281-294, 0165-0009

Pacca, S. & Horvath, A. (2002). Greenhouse gas emissions from building and operating electric power plants in the upper Colorado River Basin. *Environmental Science & Technology*, Vol.36. No.14, Jul, pp. 3194-3200, 0013-936X

Rivkin, R.B. & Legendre, L. (2001). Biogenic carbon cycling in the upper ocean: Effects of microbial respiration. *Science*, Vol.291. No.5512, Mar, pp. 2398-2400, 0036-8075

Roehm, C. & Tremblay, A. (2006). Role of turbines in the carbon dioxide emissions from two boreal reservoirs, Quebec, Canada. *Journal of Geophysical Research-Atmospheres*, Vol.111. No.D24, Dec, pp. 0148-0227

Roland, F.; Cimbleris, A.C.P.; Lobão, L.M. & Vidal, L.O. (2011). Bacterioplankton Metabolism in Hydroelectric Reservoirs. *Oecologia Australis*, Vol.15. pp. 605-617,

Roland, F.; Vidal, L.O.; Pacheco, F.S.; Barros, N.O.; Assireu, A.; Ometto, J.; Cimbleris, A.C.P. & Cole, J.J. (2010). Variability of carbon dioxide flux from tropical (Cerrado) hydroelectric reservoirs. *Aquatic Sciences*, Vol.72. No.3, Jun, pp. 283-293, 1015-1621

Rosa, L.P.; Dos Santos, M.A.; Matvienko, B.; Dos Santos, E.O. & Sikar, E. (2004). Greenhouse gas emissions from hydroelectric reservoirs in tropical regions. *Climatic Change*, Vol.66. No.1-2, Sep, pp. 9-21, 0165-0009

Rosa, L.P. & Schaeffer, R. (1994). Greenhouse-Gas Emissions from Hydroelectric Reservoirs. *Ambio*, Vol.23. No.2, Mar, pp. 164-165, 0044-7447

Rudd, J.W.M.; Harris, R.; Kelly, C.A. & Hecky, R.E. (1993). Are hydroelectric reservoirs significant sources of greenhouse gases. *Ambio*, Vol.22. No.4, Jun, pp. 246-248, 0044-7447

Rybak, J. (2001). Long-term and seasonal dynamics of nutrient export rates from lake watersheds of diversified land cover pattern. *International Association of Theoretical and Applied Limnology, Vol 27, Pt 5, Proceedings*, Vol.27. pp. 3132-3136, 0368-0770

Sand-Jensen, K.; Pedersen, N.L. & Sondergaard, M. (2007). Bacterial metabolism in small temperate streams under contemporary and future climates. *Freshwater Biology*, Vol.52. No.12, Dec, pp. 2340-2353, 0046-5070

Schlesinger, W.H. & Melack, J.M. (1981). Transport of organic-carbon in the worlds rivers. *Tellus*, Vol.33. No.2, pp. 172-187, 0040-2826

Sobek, S.; Tranvik, L.J. & Cole, J.J. (2005). Temperature independence of carbon dioxide supersaturation in global lakes. *Global Biogeochemical Cycles*, Vol.19. No.2, Apr 5, pp. -, 0886-6236

Soumis, N.; Duchemin, E.; Canuel, R. & Lucotte, M. (2004). Greenhouse gas emissions from reservoirs of the western United States. *Global Biogeochemical Cycles*, Vol.18. No.3, Sep, pp. 0886-6236

Soumis, N.; Lucotte, M.; Larose, C.; Veillette, F. & Canuel, R. (2007). Photomineralization in a boreal hydroelectric reservoir: a comparison with natural aquatic ecosystems. *Biogeochemistry*, Vol.86. pp. 123-135, s10533-007

St Louis, V.L.; Kelly, C.A.; Duchemin, E.; Rudd, J.W.M. & Rosenberg, D.M. (2000). Reservoir surfaces as sources of greenhouse gases to the atmosphere: A global estimate. *Bioscience*, Vol.50. No.9, Sep, pp. 766-775, 0006-3568

Stevens, C. & Imberger, J. (1996). The initial response of a stratified lake to a surface shear stress. *Journal of Fluid Mechanics*, Vol.312. Apr 10, pp. 39-66, 0022-1120

Takagaki, N. & Komori, S. (2007). Effects of rainfall on mass transfer across the air-water interface. *Journal of Geophysical Research-Oceans*, Vol.112. No.C6, Jun 8, pp. 0148-0227

Teodoru, C.R.; Prairie, Y.T. & Del Giorgio, P.A. (2010). Spatial Heterogeneity of Surface CO_2 Fluxes in a Newly Created Eastmain-1 Reservoir in Northern Quebec, Canada. *Ecosystems*, Vol.14. No.1, Jan, pp. 28-46, 1432-9840

Thomas, S.; Cecchi, P.; Corbin, D. & Lemoalle, J. (2000). The different primary producers in a small African tropical reservoir during a drought: temporal changes and interactions. *Freshwater Biology*, Vol.45. No.1, Sep, pp. 43-56, 0046-5070

Tranvik, L.J.; Downing, J.A.; Cotner, J.B.; Loiselle, S.A.; Striegl, R.G.; Ballatore, T.J.; Dillon, P.; Finlay, K.; Fortino, K.; Knoll, L.B.; Kortelainen, P.L.; Kutser, T.; Larsen, S.; Laurion, I.; Leech, D.M.; McCallister, S.L.; McKnight, D.M.; Melack, J.M.; Overholt,

E.; Porter, J.A.; Prairie, Y.; Renwick, W.H.; Roland, F.; Sherman, B.S.; Schindler, D.W.; Sobek, S.; Tremblay, A.; Vanni, M.J.; Verschoor, A.M.; von Wachenfeldt, E.; Weyhenmeyer, G.A. (2009). Lakes and reservoirs as regulators of carbon cycling and climate. *Limnology and Oceanography*. Vol. 54. No.6, Nov 09, pp. 2298-2314, 0024-3590

Tremblay, A.; Lambert, M. & Gagnon, L. (2004). Do hydroelectric reservoirs emit greenhouse gases? *Environmental Management*, Vol.33. Jul, pp. S509-S517, 0364-152X

Vidal, L.O.; Graneli, W.; Daniel, C.B.; Heiberg, L. & Roland, F. (2011). Carbon and phosphorus regulating bacterial metabolism in oligotrophic boreal lakes. *Journal of Plankton Research*, Vol.33. No.11, pp. 1747-1756,

Vorosmarty, C.J.; Meybeck, M.; Fekete, B.; Sharma, K.; Green, P. & Syvitski, J.P.M. (2003). Anthropogenic sediment retention: major global impact from registered river impoundments. *Global and Planetary Change*, Vol.39. No.1-2, Oct, pp. 169-190, 0921-8181

Wang, F.; Wang, B.; Liu, C.Q.; Wang, Y.; Guan, J.; Liu, X. & Yu, Y. (2011). Carbon dioxide emission from surface water in cascade reservoirs-river system on the Maotiao River, southwest of China. *Atmospheric Environment*, Vol.45. No.23, Jul, pp. 3827-3834, 1352-2310

Wanninkhof, R. (1992). Relationship between Wind-Speed and Gas-Exchange over the Ocean. *Journal of Geophysical Research-Oceans*, Vol.97. No.C5, May 15, pp. 7373-7382, 0148-0227

WCD (2000). World Commission on Dams. Dams and Development: A New Framework for Decision-Making. Earthscan Publications. Available via http://go.nature.com/rnFEBI

Wehrli, B. (2011). Renewable but not carbon-free. *Nature Geoscience*, Vol.4. No.9, pp. 585-586, 1752-0894

Weisser, D. (2007). A guide to life-cycle greenhouse gas (GHG) emissions from electric supply technologies. *Energy*, Vol.32. No.9, Sep, pp. 1543-1559, 0360-5442

Zheng, H.; Zhao, X.J.; Zhao, T.Q.; Chen, F.L.; Xu, W.H.; Duan, X.N.; Wang, X.K. & Ouyang, Z.Y. (2011). Spatial-temporal variations of methane emissions from the Ertan hydroelectric reservoir in southwest China. *Hydrological Processes*, Vol.25. No.9, Apr, pp. 1391-1396, 0885-6087

4

GHG Emissions Reduction Via Energy Efficiency Optimization

Faisal F. Al Musa, Ali H. Qahtani, Mana M. Owaidh,
Meshabab S. Qahtani and Mahmoud Bahy Noureldin
Saudi Aramco, Dhahran
Saudi Arabia

1. Introduction

There are three major sources of GHG; carbon dioxide (CO2), methane (CH4), and nitrous oxide (N2O). The world's CO2 emissions into the air have been increasing drastically over the past century. The industrial revolution and exploitation of natural resources such as coal and oil have greatly contributed to CO2 emissions. The world's CO2 emissions due to fuel utilization such as natural gas, liquid fuels such as oil, and coal has resulted in CO2 emissions due to energy usage of about 45 billion metric tons by the year 2030. In Japan, for instance, more than 80 % of its GHG emissions are due to energy-based sources resulted from fossil fuel consumption and a boost to the energy efficiency of a single refinery in Japan can result in a reduction of at least 50,000 ton CO2/year.

It is not a matter of indifference or/and skepticism any more, the majority in the world scientific communities do subscribe now to the fact that, the world's environment has been negatively affected by the global warming phenomenon which has caused the average temperature of the earth's surface to increase during the last century due to the irresponsible release of greenhouse gases (GHG) into the atmosphere. From GHG perspective, energy efficiency optimization is not only a fast track approach to reduce energy-based GHG/CO2 emissions but also a cost-effective option towards such endeavor. It does not need behavioral change, which is sometimes difficult to achieve on the short run. It does not also play on the people's level of romance regarding the health of our beloved universe. It touches the heart of mankind's old and new motivations and aspirations for better life. It is industrial people's own benefit. Energy efficiency optimization solution approach as a quick answer to energy-based GHG emissions reduction simply enables us attaining the "water-oil-impossible-mix" via mixing the useful, exhibited in saving money, with the beautiful of saving more than the money, the environment.

At the equipment level, process equipment becomes inefficient when it uses higher energy than the designated one at the same feed and production rates. Extra energy consumption by equipment can be related to aging, part deterioration, process related causes, fouling and so on. Such reasons need to be scrutinized on timely basis in any industrial facility to avoid excessive energy consumption and consequently more GHG emissions. Equipment normally has its standard causes and characteristics for energy efficiency degradations and it can be captured through detailed analysis of its parameters change along the historical

sequence of events during its operation. The relation between GHG emissions and energy efficiency is subject to some factors, such as equipment and drivers types. Gas compressors are driven by electrical motors; steam turbines; and gas turbine drivers. Compressor's driver selection is a major contributor to gas emissions. Electric motors are the least emitters and gas turbines are the most among other drivers.

Industrial community is systematically practicing online equipment-based performance monitoring and diagnosis functions to measure, analyze, improve and control equipment's energy usage to keep its energy consumption under tight control. Although the motivator to steer the equipment energy consumption towards the design figure is to reduce the energy operating cost; that result is also contributing to the reduction of GHG emission. It is the industry practice to identify energy savings opportunities in equipment operation by taking proactive maintenance steps, applying advanced control strategies and real-time optimization. For example oil and gas equipment/units operation load management make reductions in energy usage and greenhouse emissions. Constantly invented/developed new materials, technologies, hardware and design software are also improving equipment's energy efficiency. For instance, materials scientists have helped steam power plant designers to design steam boilers for subcritical and super critical steam generation levels, which were not possible decades ago. Many successful efforts in capital allocation in many industrial facilities are also preventing energy inefficient equipment of being introduced to new industrial sites and/or phasing out inefficient ones in existing facilities before its designated retiring date, is also getting steam every day.

However, for decades ago energy efficiency optimization was merely addressing the energy efficiency of standalone process equipment. Since late seventies in the last century, the landscape has changed. It is not only energy efficiency for the standalone equipment/unit but also for subsystems, systems, complexes and even mega sites as well as industrial cities. This chapter is presenting the impact of adapting the state-of-art in energy efficiency optimization on the GHG emissions reduction. The chapter starts with intra-process integration and clean development mechanism application in refinery Hydrocracking unit (HCU), followed by a method and case study for inter-processes integration in oil refining and then is closed with brief industrial utility system retrofit case study in an oil plant using combined heat and power concept.

2. Intra-process integration and clean development mechanism (CDM)

Oil refineries market is currently undergoing a significant reorientation, with demand moving away from the traditional strongholds of Europe and North America to other regions of the world. This transformation, which began before the recent economic recession, but was accelerated by its effects, both creates a number of opportunities and poses many number of threats to companies involved in the industry and to the environment. Refining operations are a vital aspect of any modern, industrialized economy, and hence much is being invested in trying to produce products that do not rely on refined fuels, we are a little away from a point at which these developments will significantly reduce the market for refined products. Refineries are as usual going to be influenced by environmental regulations, technological innovations, and other important factors and trends which are changing the dynamics of the industry. Oil refining business is likely to see significant investment over the next ten years, where growth will be unevenly spread

throughout the world and consequently generating GHG. The impact of oil refining industry on the environment is becoming more and more apparent nowadays. Industrial emissions contribute to the climate change by emitting green house gases (GHG) into atmosphere. Pollution prevention measures must take place in industrial sector to lower emissions especially in oil refineries which consume huge energy derived from fossil fuels. Pollution prevention is an adequate method for managing the environmental impact associated with industrial facilities. The right pollution prevention strategy aims to eliminate potential pollution from the process at the source before it is being emitted into the environment. Pollution prevention can be in form of energy demand reduction inside process plants. The reduction in energy demand will eventually lead to lower fuel consumption that will result in lower GHG emissions. Such reduction in energy-based GHG emissions will ultimately reduce the environmental impact of industrial facilities. The application of clean development mechanism (CDM) to an oil refinery presented here is confined to only one major unit in the oil refineries called Hydrocracking unit (HCU). The aim is to reduce energy generation-based CO2 emissions at the source via reducing the energy consumption of the HCU. The reduction in fuel usage can be achieved by better integration of the heat exchanger network of the unit to reduce fuel demand in the process by increasing the process-to-process heat exchange duties. Pinch technology is used in this context due to its applicability and practicality to process plants energy reduction. The reduction in energy demand, of a major oil refinery unit presented in this chapter, is an application that has potential implementation as a small scale CDM project. The CDM application/project introduced quantifies the potential CO2 emissions reduction resulted from energy consumption reduction in the HCU.

The oil refinery used in this study is a medium size one, processes 120 000 bbl/d of crude oil. As usual the feed to the refinery is first stabilized by stripping off acid gases and other volatile compounds and then introduced to the atmospheric distillation column followed by vacuum distillation column. The distilled products are then introduced to different process units to produce a variety of petroleum products. The refinery is divided into several process areas. Those process areas are the stabilizer, the atmospheric crude distillation Unit, the vacuum distillation unit, the asphalt recovery, the amine gas treating, the gas concentration unit, the naphtha and kerosene Hydrotreating, demex, Platformer, hydrogen plant, hydrocracker and finally the utilities. The HCU is a major process unit in any refinery. It receives heavy oils and produces more valuable products such as diesel and fuel oil. The purpose of the HCU, presented in this chapter, is to process vacuum gas oil (VGO) from the Vacuum distillation unit (VDU) and De-metalized oil (DMO) from the asphalt oxidization unit. These two low value feed streams are converted into useful products such as liquefied petroleum gas (LPG), light naphtha, heavy naphtha, kerosene, light diesel oil (LDO), and heavy diesel oil (HDO) products. The HCU is divided into two main sections; the first section is the reaction section and the second is the fractionation section.

HCU consists of several process streams and not all of them are used in our case study calculation using pinch technology. The problem's streams data included in our study have, the stream supply temperature (Ts), target temperature (Tt), the heat transfer in term of thermal kW gained or released by the stream, and the heat transfer coefficient (HTC) for the heat transfer equipment. The process streams have been segregated into hot streams (any process stream that needs to be cooled) and cold streams (any process stream that need to be heated). Each stream has been assigned a name based on the content and direction into the

process. Streams are identified based on their composition, if the stream passes through another heat transfer equipment and changes in temperature, then it will be another segment of the same stream; however, if the stream changes in composition in the case of new production from the separation column it becomes different stream.

					DH	CP	HTC
No	Stream	Name	Ts, C	Tt, C	kW	kW/C	kW/m^2.C
1	COLD	VGO/DMO Feed	105.00	393.30	20196	70.05	3.41
1	COLD		393.33	437.78	14200	319.49	56.76
2	COLD	De-C4 col feed	56.67	170.56	18197	159.78	2.27
3	COLD	De-4 Reb Duty	226.11	281.11	17589	319.81	56.76
4	COLD	Frac Feed	266.11	377.22	27644	248.80	56.76
5	COLD	HN Strip reb duty	160.00	171.11	1804	162.35	5.68
6	COLD	Kero Strip Reb duty	226.67	235.00	732	87.85	5.68
7	COLD	LN feed to Frac	60.00	109.44	1092	22.09	3.41
7	COLD		109.44	265.56	929	5.95	0.57
8	HOT	DHC rxn outlet from V-1/2	468.33	385.00	16710	200.52	0.45
9	HOT	HC rxn outlet from V-3/4	426.67	180.00	20196	81.87	1.70
10	HOT	V6 overhead vapor (to V8)	165.00	60.00	37727	359.31	0.40
10	HOT		60.00	43.33	2115	126.88	1.70
11	HOT	V-14 oh vapor	71.11	48.89	1172	52.74	4.55
12	HOT	Fract OH Vapor	81.11	60.00	16353	774.62	5.68
13	HOT	De-4 OH vapor	83.89	57.22	8246	309.22	5.68
14	HOT	LiN product draw	60.00	37.78	375	16.87	2.84
15	HOT	HN product draw	160.00	60.00	3262	32.62	2.27
15	HOT		60.00	37.78	719	32.35	1.70
16	HOT	HN p/a loop	137.78	77.22	7918	130.76	1.70
17	HOT	Kero Product to Storage	227.22	60.00	2580	15.43	2.27
17	HOT		60.00	48.89	129	11.60	1.70
18	HOT	Kero p/a loop	210.00	77.22	5915	44.55	2.27
19	HOT	LDO draw	298.89	252.22	929	19.90	2.27
19	HOT		252.22	196.11	1092	19.47	2.27
19	HOT		196.11	60.00	4310	31.67	2.27
20	HOT	HDO p/a (combined)	321.11	170.56	4100	27.23	2.27
21	HOT	HDO product draw	321.11	60.00	10442	39.99	2.27
22	HOT	Frac btms recycle	362.78	121.11	18197	75.30	2.56
23	HOT	Frac btms FO draw	362.78	79.44	3951	13.95	2.56

Table 1. Problem Data for Hydrocracking Plant

The optimum ΔTmin for HCU is calculated to estimate the minimum temperature difference in the heat exchanger network that will lead to the lowest possible utility demand in the process. The total annualized capital and energy cost is plotted vs. several, ΔTmin values to estimate such optimum at the minimum annualized cost.

The optimum ΔTmin for HCU was calculated to be 13 °C where the total annualized cost reaches the minimum. The total annualized cost consists of the annual energy cost and the annual heat exchanger capital cost. The annual energy cost is obtained simply by multiplying the utility cost by the expected operating hours in the year which is assumed to be 8,400 hours per year to incorporate maintenance and plant shut down. The annualized capital cost incorporates the capital cost multiplied by the money borrowing annualized factor.

The energy reduction as a result of applying the minimum ΔT in the HCU can be compared to the current HCU process energy demand and current GHG emissions. The potential savings in both energy consumption and CO2 emission are then identified. Using pinch techniques, the potential reduction in energy is about 20.1 MWh annually which is equivalent to fuel gas consumption of 631 000 GJ. The potential emission reduction in the

HCU is estimated to be 38 kt of CO2 annually. The potential reduction of the other utilities demand such as cooling water and air cooing utilities is not identified here due to its low value. This potential reduction in CO2 emission as a result of the fuel gas reduction in the HCU due to energy efficiency enhancement can be adopted as a clean development mechanism (CDM) project.

The HCU emission reduction potential can be adopted as a small-scale CDM project. Adopting the small-scale CDM project framework has several advantages such as; ability to combine identical project as one group of project; the project design document and methodologies are simplified for a small scale project and the baseline and monitoring procedures are reduced.

The establishment of the baseline emission is an important step in any CDM project evaluation. Therefore, we need to estimate the as is CO2 emissions without implementing the project. Fortunately, a real parameter data of fuel gas flow can be obtained because it is measured and the emission quantity is related to the fuel consumption. The fuel consumption rate can be measured for the past three years to evaluate the baseline emission situation. The current energy consumed by the HCU process heaters is 71 MWh which is equivalent to 256 GJ of fuel gas. As per given or sampled fuel composition, the CO2 emission factor in the fuel gas is calculated to be 0.217 kg CO2 per kWh.

The current baseline emission can be simply identified as follows:

$PEFC_{j,y} = \sum_i FC_{i,j,y} \times COEF_{i,y}$

Where:

$PEFC_{j,y}$ = CO2 emission from fossil fuel combustion in process j during the year y (tCO2/yr)

$FC_{i,j,y}$ = Quantity of fuel type I combusted in process j during the year y (mass or volume unit / year)

$COEF_{i,y}$ = CO2 emission coefficient of fuel type I in year y (t CO2 /mass or volume unit)

i = fuel types combusted in process j during year y.

For our HCU fuel gas reduction project, the above formula is used to calculate the baseline emission value.

PEFC,j,y = 71.1 MW x 0.217 kg CO2 /kWh x 8400 h = 12967 t CO2/y

The i value is assumed to be 1 because there is one fuel type (fuel gas) and the CO2 content per energy unit has been used instead of CO2 content per mass unit.

HCU exhibits, using pinch technology, an energy efficiency enhancement potential of 21 MWh in fuel. Such reduction in energy consumption can reduce GHG emissions in the HCU to 91,635 t CO2/y from the baseline calculated above if the project is implemented. Using the emission baseline figure, the potential reduction in GHG emissions after implementing the CDM project is estimated to be 38 035 t CO2/y.

It is important to note here that beside the benefit obtained from $ energy saving another $ benefit can be attained due to carbon credit concept. The price of CO2 emission trading

nowadays can play role in determining the feasibility of HCU energy efficiency/emission reduction project. For instance, the annual potential revenue of the CDM project can be estimated to be $ 950,000 per year using an average price of $25 carbon credit per ton [1:3].

3. Inter-processes integration for enhanced energy efficiency and energy-based GHG emissions reduction

Pinch analysis is the technology that provides a systematic methodology for energy saving in processes and total sites. The methodology is based upon thermodynamic principles. Pinch Analysis/technology was first developed in the late 1970s as a technique for optimization of thermal heat recovery, and rapidly gained wide acceptance as a practical approach to the design of Heat Exchanger Networks (HENs). Since then, it has evolved into a general methodology for optimization, based on the principles of process integration.

The technique calculates thermodynamically attainable energy targets for a given process and identifies how to achieve them. A key insight is the pinch temperature, which is the most constrained point in the process. The most detailed explanation of the techniques is by Linnhoff et al. Other pinch analyses were developed for several applications such as mass-exchange networks (El-Halwagi and Manousiouthakis, 1989), water minimization (Wang and Smith, 1994), and material recycle (El-Halwagi et al., 2003).

Pinch analysis has been applied successfully not only to energy systems (heat recovery, pressure drop recovery, power generation), but also to fresh water conservation, wastewater minimization, production capacity de-bottlenecking, and management of chemical species in complex processes.

Applying Pinch technology in heat exchangers networks (HEN) synthesis and retrofit, enable the engineer to calculate the energy requirement for any process, and produce thermally efficient and practical designs. Energy savings are significant compared to previous best designs. Pinch technology is also applied to the optimization/integration of the supply-side, consisting of on-site utilities, such as boilers, furnaces, steam and gas turbines, cogeneration, heat pumps, and refrigeration systems [4:6].

Generally speaking, the objective of the heat exchangers network synthesis for waste heat recovery problem is to design a network that meets an economic criterion such as minimum total annualized cost. Sometimes minimum number of units and minimum energy consumption and GHG emissions in special applications become very legitimate objectives too.

The heat exchangers network synthesis is a multi-variable multi-dimensional optimization problem in which the total network driving distribution depends on each stream conditions and each hot stream minimum approach temperature for heat recovery. Such variables can contribute to number of units, shells, and both the heating and cooling utilities requirements as well as its mix. In pinch technology this multi-variable optimization problem has been reduced to a single variable optimization problem which is the global ΔT_min of the problem that in pinch technology needs to be optimized.

Recent advances in the field of energy efficiency optimization advocate the need to conduct the waste heat recovery targeting phase using several ΔT_min (minimum temperature approach between hot and cold composite curves) and/or using problem process conditions

soft constraints in a systematic way to find better energy targets. New method uses for each hot stream specific ΔT_min and allows minor possible combinations of process conditions to be modified (e.g. 5 F ± in the supply and target temperatures) to customizing the waste heat recovery problem in a way that renders better reductions in energy consumption cost(energy quantity and/or quality/work optimization). The waste energy recovery problem using such new targeting method can now has several degrees of freedom for the waste energy recovery problem optimization, instead of the one parameter problem optimization currently used [7:9].

The above mentioned energy integration targeting methods while can be used at any scale is nowadays focused only on industrial facility via direct integration between the hot and cold streams of its process units. It is usually applied at the process level; and known as intra-process integration. It has proved to be very successful to reducing both energy consumption and energy-based GHG emissions. Integration among many processes, in adjacent geographical locations, can bring in more degrees of freedom to optimize the waste energy recovery problem and consequently presents new horizon to the energy-based GHG emissions reduction to levels never thought of before. For many reasons, direct inter-processes integration is not widely practiced in industry. Many of the reasons hindering the application of inter-process integration among several processes for better energy consumption cost reduction and less energy-based GHG emissions are very valid and need to be addressed in a novel way to enable wider adaptation of direct inter-process integration in existing industrial facilities and naturally for mega facilities, zones and even cities in the future plants.

Since the emanation of the pinch technology and its evolution to pinch analysis technique for process synthesis, the direct inter-processes integration has been considered impractical. Many arguments, such as the processes are normally have different start up and shut down times; the processes can work at partial loads; the processes can have seasonal changes in its conditions; utility systems, heaters and HEN capital will not be reduced due to changes in processes schedule and operation philosophy; the disturbance in one process can propagate to another one if they are integrated; the distance-time/velocity lags affect the controllability of processes; the geographical distances among processes will cost us energy in pumping or compression and capital in piping, pumping and compression; safety might be impacted due to the travel of a fluid from one hazardous area to another; the fear of leakage and so on, are certainly valid. Therefore, direct inter-processes integration while is beneficial to energy conservation and the GHG emissions reduction, is still to date almost ignored in industrial community.

Due to those concerns most of the current methods for inter-process integration are indirect and conducted using buffer systems. Buffer systems are either steam system or hot oil system or sometimes both. However, the industrial community does agree that, direct integration approach in inter-process integration (between several plants) is more efficient and can render more saving in energy consumption and energy-based greenhouse gas emissions [10:16]. In this chapter we demonstrate, that huge potential for energy consumption and GHG emissions reduction in oil refining (more than 5 % in-house) can be attained through smart integration among processes.

It is instructive to note here that, while we agree with the validity of those arguments we believe that we can still find a room for improvement in energy efficiency enhancement and

energy-based GHG emissions reduction via identifying at the energy integration targeting phase best possible scenarios for inter-processes integration and then trying to find cost effective solutions to the above mentioned concerns via smart plants "matching".

The general intuition regarding the integration among several processes that assumes, the more you integrate among the processes, the better you save in energy consumption and consequently in the energy-based GHG emissions sometimes are not always fully true.

3.1 Direct inter-processes integration case study data

For N plants, there will be a cretin number of possible inter-process integration combinations. Starting from 1 for a single plant, 2 combinations for two plants, 5 combinations for three plants, 15 combinations for four plants (our example) up to 4.6386x10^18 possible combinations for 25 plants only. These possible combinations are identified through Bell's numbers. The Bell numbers (1, 1, 2, 5, 15, 52, 203, 877, 4140, 21147, 115975, 678570, 4213597, ...) describe the number of ways a set with n elements can be partitioned into disjoint, non-empty subsets [17].

For example, the set {1, 2, 3} can be partitioned in the following ways:

- {{1}, {2}, {3}}
- {{1, 2}, {3}}
- {{1, 3}, {2}}
- {{1}, {2, 3}}
- {{1, 2, 3}}.

In this chapter, the data used for the demonstration of the possible energy consumption and GHG emissions reduction due to inter-processes integration method is a four existing plants in a typical oil refinery. It is used to illustrate the useful impact of inter- process integration between different plants on both energy consumption and energy-based GHG emissions reduction. These data extracted from literature are presented below. We selected the heat recovery approach temperature for the whole problem to be 15 C [18]. Our intention for such selection is to use reasonable value for our method testing and not to compare with results of other methods. For the purpose of exhibiting the method of selecting which units to integrate inside a whole facility and the potential impact of the optimal selection on both energy consumption and GHG emissions reduction we considered from the whole refinery, the big energy consumers (the elephants in energy consumption) such as Fluid Catalytic Cracking Unit (FCCU), Crude/Vacuum Distillation Unit (CDU/VDU), Visbreaker/thermal cracking Unit (VBU) and Platformer/reformer Unit (PLAT). The four plants selected for the inter-processes direct integration targeting study presented in this chapter are numbered as per the table below.

Plant	FCCU	CDU/VDU	VBU	PLAT
Reference Number	1	2	3	4

Table 2. The four plants and their referenced numbers

The details of each stream data as presented by Fraser and Gillespie [18], are shown in tables 3, 4, 5 & 6.below.

1- FCCU				
Type	No	Ts (°C)	Tt (°C)	Heat Capacity (KW/°C)
H	1	165.5	90.0	22.616
H	2	282.0	796.5	54.389
H	3	274.0	37.5	9.163
H	4	164.0	27.0	36.141
H	5	327.0	261.0	44.321
H	6	363.0	246.0	26.76
H	7	327.0	165.0	16.772
H	8	201.0	104.0	5.405
H	9	140.9	38.0	162.055
H	10	144.5	51.0	15.252
C	11	74.0	295.0	62.462
C	12	143.0	164.0	129.383
C	13	94.0	125.0	126.44

Table 3. Stream data for the FCCU

2- CDU/VDU				
Type	No	Ts (°C)	Tt (°C)	Heat Capacity (KW/°C)
H	1	172.5	67.6	116.951
H	2	260.0	189.8	75.104
H	3	309.0	269.5	95.138
H	4	333.4	189.4	14.91
H	5	116.8	49.7	72.242
H	6	272.0	210.0	303.711
H	7	210.0	79.8	58.8
H	8	146.0	18.2	144.92
H	9	50.5	18.2	152.687
H	10	189.0	26.1	69.661
H	11	198.9	171.1	13.477
C	12	26.0	261.7	221.887
C	13	261.7	356.5	430.191
C	14	338.2	409.8	257.147
C	15	26.7	96.1	136.283

Table 4. Stream data for the CDU/VDU

3- VBU				
Type	No	Ts (°C)	Tt (°C)	Heat Capacity (KW/°C)
H	1	135.6	30.0	19.506
H	2	255.0	176.1	9.887
H	3	353.3	198.9	43.165
H	4	198.9	171.1	14.477
H	5	171.1	75.0	19.279
C	6	327.8	457.8	54.685
C	7	158.3	160.0	221.49
C	8	126.7	176.7	15.599
C	9	126.7	176.7	133.329
C	10	126.7	146.7	21.364

Table 5. Stream data for the VBU

4- PLAT				
Type	No	Ts (°C)	Tt (°C)	Heat Capacity (KW/°C)
H	1	503.9	366.1	67.382
H	2	366.1	178.9	3.807
H	3	366.1	253.9	26.094
H	4	303.3	36.7	63.175
H	5	76.7	26.7	24.568
H	6	232.2	112.2	15.107
H	7	79.4	32.2	39.78
H	8	112.0	23.9	0.738
H	9	67.2	27.2	75.556
H	10	157.2	32.2	7.905
H	11	43.3	26.3	4.773
H	12	92.0	65.0	1.773
H	13	107.0	32.2	7.671
C	14	66.1	370.6	76.121
C	15	232.2	247.2	195.269
C	16	36.7	125.6	20.378
C	17	112.0	112.8	2506.929
C	18	157.2	163.9	106.929
C	19	92.0	97.2	38.98
C	20	370.6	495.6	94.091
C	21	452.8	497.2	106.519
C	22	480.6	496.1	114.065

Table 6. Stream data for the PLAT

3.2 Direct inter-processes integration case study results and discussion

As mentioned earlier, the four plants that were considered are FCCU (1), CDU/VDU (2), VBU (3) & PLAT(4). The 15 possible combinations which include 14 possible inter-process integration schemes (A to N) are listed in table 7 below. Combination labeled O is the no inter-process integration case where each plant is in a standalone intra-process integration status.

Sets	Combination Name
{1,2,3,4}	A
{1,2,3}{4}	B
{1,2,4}{3}	C
{1,2}{3,4}	D
{1,2}{3}{4}	E
{1,3,4}{2}	F
{1,3}{2,4}	G
{1,3}{2}{4}	H
{1,4}{2,3}	I
{1}{2,3,4}	J
{1}{2,3}{4}	K
{1,4}{2}{3}	L
{1}{2,4}{3}	M
{1}{2}{3,4}	N
{1}{2}{3}{4}	O

Table 7. The 15 possible combinations for 4 plants

Before we calculate the energy targets for each combination above using pinch technology/process integration technique presented earlier in this chapter, let us try to test our intuition regarding the expected output regarding the combination that render best energy consumptions and the rank of each combination.

Our first hypothesis/intuition is that, the energy consumption values due to inter-process integration among the four units, all as one unit, is going to be better than the intra-process integration/ standalone unit integration. If there is no benefit from inter-process integration, than standalone intra-process integration. Then, there is no point to spend capital for integration among processes; complicating the plant start-up and its abnormal situations management without saving in energy consumption and reduction in GHG emissions. This correct hypothesis means that set A in the table above, where all four units are treated as one unit is going to be the best set and set O in the same table above, where each unit is handled independently, is going to be the worst set from energy consumption point of view and naturally from energy-based GHG emissions too. In other words from energy consumption and energy-based GHG emissions, combination A is the upper limit of possible energy saving and GHG emissions reduction. The same logic that advocate the integration of all units to get best energy consumption saving, will lead us to a general crude intuition thinking that always, the more we integrate plants; the better reduction in both energy requirements and Greenhouse Gases emissions as well we get. This untested second

hypothesis, is deciding the next best combination after the A combination (in which the four plants/units were all together integrated from energy consumption point of view). This hypothesis says, if you cannot integrate the four plants, rendering best energy saving, all together at least try to integrate three of them, and if you cannot integrate the three plants all together try to integrate two of them in pairs to get the best possible energy saving and energy-based GHG emissions reduction. That is the intuition obtained from combination A that shown the superiority of inter-processes integration on the standalone intra-process integration and can lead us to false conclusion, if we do not test this hypothesis.

To test this hypothesis we suggest two possible schemes. Our hypothesis is that, the next best integration among the processes may be either the one that has the highest number of integrated processes in a set or the one that has the highest number of integrations/pairings in the set. For example we need to test and find an answer to the following questions: Which combination is better, is it the B combination? where we have three units integrated together and one unit is in standalone intra-process integration status (i.e. one integration in the set) or is it the G combination? Where in this combination we have two integrations in the set (where unit 1 and unit 3 are integrated and unit 2 and unit 4 are integrated). The test procedure to the above second hypothesis will lead us to either one of the two schemes A and B shown in the table 8 below.

Scheme A			Scheme B		
#	Combinations	Mix	#	Combinations	Mix
1	{1,2,3,4}	All	1	{1,2,3,4}	All
2	{1}{2,3,4}	1-3 or 3-1	2	{1,2}{3,4}	2-2 only
3	{1,3,4}{2}		3	{1,3}{2,4}	
4	{1,2,4}{3}		4	{1,4}{2,3}	
5	{1,2,3}{4}		5	{1}{2,3,4}	1-3 or 3-1
6	{1,2}{3,4}	2-2 only	6	{1,3,4}{2}	
7	{1,3}{2,4}		7	{1,2,4}{3}	
8	{1,4}{2,3}		8	{1,2,3}{4}	
9	{1,2}{3}{4}	2-1-1 only	9	{1,2}{3}{4}	2-1-1 only
10	{1,3}{2}{4}		10	{1,3}{2}{4}	
11	{1,4}{2}{3}		11	{1,4}{2}{3}	
12	{1}{2,3}{4}		12	{1}{2,3}{4}	
13	{1}{2,4}{3}		13	{1}{2,4}{3}	
14	{1}{2}{3,4}		14	{1}{2}{3,4}	
15	{1}{2}{3}{4}	1-1-1-1	15	{1}{2}{3}{4}	1-1-1-1

Table 8. The 15 possible combinations for 4 plants

The above two schemes says that the best combinations for the inter-processes integration is naturally the 4 plants all together. The next best (2, 3, 4, 5) are either the integration of three plants all together and the fourth is a standalone one as per scheme A or the two plants integrations in pairs as per scheme B, where for instance process plant/unit 1 and process plant/unit 2 are integrated together and process plant/unit 3 and process plant/unit 4 are

also integrated together. The following next best scenarios (6, 7, 8) are the reverse of this assumption. It is important to note here that the testing of the above hypothesis based upon the two suggested schemes A and B is going to be proved unsatisfactory even though the hypothesis looks logical and we cannot use this hypothesis as a rule for inter-process integration scenario selection. We will shortly see such conclusion after calculating the energy targets for each case, in the suggested schemes A and B, and discussing the findings from these calculations. As shown in table 9, the heating (Qh) and cooling (Qc) utilities targets, (at $\Delta T_{\_min}$=15 C) were calculated for each set of the 15 possible combinations identified for the four plants. Then, the minimum heating and cooling requirements for each set are calculated followed by the ranking of each set based on the total minimum energy requirements. The table below shows in the first column the sets list of all possible plants integration combinations, the second column is the combination label, the third column and the fourth column are the minimum heating and minimum cooling utilities requirement Qh1 & Qc1 respectively of the whole 4 plants together. It is useful to note that, the Qh1 & Qc1, Qh2 & Qc2, Qh3 & Qc3, and Qh4 & Qc4 are the minimum heating and minimum cooling requirements for the plants between brackets {}. For instance, in combination G, the Qh1 &Qc1 are the minimum heating and minimum cooling utilities requirements of plants {1,3} and the Qh2 &Qc2 are the minimum heating and minimum cooling utilities requirements of plants {2,4}. Qh total and Qc total required in G combination are the summation of Qh1 & Qh2 and Qc1& Qc2, respectively.

Sets	Combination Name	Qh1	Qc1	Qh2	Qc2	Qh3	Qc3	Qh4	Qc4	Qh Total required	Qc Total required	Rank
{1,2,3,4}	A	99,760	43,318							99,760	43,318	1
{1,2,3}{4}	B	83,945	37,143	18,885	9,245					102,830	46,388	4
{1,2,4}{3}	C	93,993	41,151	6,944	3,344					100,937	44,495	2
{1,2}{3,4}	D	80,345	37,143	24,474	11,234					104,819	48,377	5
{1,2}{3}{4}	E	80,345	37,143	6,944	3,344	18,885	9,245			106,175	49,733	9
{1,3,4}{2}	F	53,008	27,567	55,801	24,800					108,809	52,367	11
{1,3}{2,4}	G	36,473	20,672	68,631	27,990					105,104	48,662	6
{1,3}{2}{4}	H	36,473	20,672	55,801	24,800	18,885	9,245			111,160	54,718	14
{1,4}{2,3}	I	46,514	24,673	59,401	24,800					105,916	49,474	8
{1}{2,3,4}	J	29,751	17,550	72,231	27,990					101,982	45,540	3
{1}{2,3}{4}	K	29,751	17,550	59,401	24,800	18,885	9,245			108,037	51,595	10
{1,4}{2}{3}	L	46,514	24,673	55,801	24,800	6,944	3,344			109,260	52,818	12
{1}{2,4}{3}	M	29,751	17,550	68,631	27,990	6,944	3,344			105,326	48,884	7
{1}{2}{3,4}	N	29,751	17,550	55,801	24,800	24,474	11,234			110,026	53,584	13
{1}{2}{3}{4}	O	29,751	17,550	55,801	24,800	6,944	3,344	18,885	9,245	111,382	54,940	15

Table 9. The 15 possible combinations for 4 plants

Let us now have a deep look to table 9, "Rank" column. The table gives us the answer to our hypothesis test/question regarding what is the second best inter-process integration after the all together four plant inter-processes integration?. This question is important to us since full integration among all plants might be costly and impractical. Our hypothesis suggested adapting either one of two schemes (scheme A or scheme B) depicted in table 8. It is clear now that table 9 gives us a negative answer to such hypothesis.

Based on the calculations and numbers in the rank column in table 9, we generated table 10, to definitely answer the question of, What is the next best inter-process integration scenario? that comes after the four plants all-together inter-process integration. Table 10 shows few ranks different than our expectation. It is a fact that the optimum solution (ranked 1) happens when there is a full integration between all the four plants and the worst from energy saving point of view (rank 15) occurs when there is no integration between any of the four plants. In between these two scenarios, the sequence continues with the logic that says that better solutions are reached with the scenario that has higher number of integrated plants combinations (the ones that has three plants all together and one standalone plant) such as ({1,2,4} rank 2, {2,3,4} rank 3, and finally {1,2,3}) rank 4. However, this is not always true since rank 11 ({1, 3, 4}, {2}) broke the expected priority/sequence and half of the six 2-1-1 mix (ranks 7, 9 and 10) which contain one combination only(least possible inter-process integration), provides better energy consumption and less energy-based GHG emissions solution than it. These better combinations are as follows respectively: ({1}, {2, 4}, {3}) and ({1, 2}, {3}, {4}) and ({1}, {2, 3} , {4}). It says that for the specific refinery application data used in this chapter and the ΔT_{min}=15 C used if you only integrate the CDU/VDU with the reformer/PLAT or the FCCU or the VBU you will have less process design complication and better energy consumption saving than integrating all the plants together without the ADU/VDU, left as a standalone. Another finding from table 10 calculations ranking is that, the 2-2 inter-processes integration scenarios in which every two plants are integrated together most of the 2-2 scenarios, two out of three possible combinations, are better than the 2-1-1 scenarios of integration (six possible combinations in which only two plants are integrated and the rest are standalone plants). This one combination which is not following the hypothesis now is the 2-2 mix (rank 8) that contains the combination ({1, 4} {2, 3}). Rank 7 combination which is only one process-to process matching is better not much but it is less complication in the process design and better energy consumption saving and consequently better reduction in energy-based GHG emissions. It means that complexity in process design is not always mandatory to save energy. In our refining application here the above finding tell us that integrating the ADU/VDU with PLAT is the best scenario (when we are only allowed one process to process integration to do). integration/matching ADU/VDU with the "wrong process" such as VBU can bring in negative impact. In summary, it is clear that all 3-1 mix sets are better than all the 2-1-1 mix sets and all the 2-2 mix sets except one 3-1 mix set (rank 11) where it has higher energy requirements than three 2-1-1 mix sets (rank 7, 9 and 10) and all 2-2 mix sets (rank 5, 6 and 8). The second best sets are all the 2-2 mix sets but the rank 8 set.

In order to evaluate the concept of inter-processes integration on the energy-based GHG emissions, we calculated the energy consumption of the standalone plants at different ΔT_min and listed the results in tables 11, 12 and 13 as shown below. The minimum heating and cooling requirements are shown for each plant as a standalone assuming perfect intra-process integration and with no inter-process integration between plants at several minimum approach temperatures (ΔT_{min}) using ΔT_{min}=15 , 5 and 1 C respectively. It is well known to the experienced in the field of energy efficiency optimization that when the ΔT_{min} is reduced both the minimum heating and minimum cooling utilities requirement are reduced and the energy-based GHG emissions will be decreasing as well. It is also accepted to the experienced in the field that the heat exchangers network capital cost that achieves such saving in energy consumption, most of the time, will be increasing. For the sake of simplicity in calculating the GHG emissions reduction associated with energy saving, we are using for the energy-based

GHG emissions calculation the relationship suggested by Smith [5]. For each MW of heat saved in a furnace using fuel gas and has about 90 % firing efficiency, the fuel gas saved is going to reduce the amount of CO2 emissions from that furnace by 300 kg. We are also ignoring the GHG emissions saving due to the reduction in plant cooling utility.

Ranking of Best Scenarios		
Rank	**Mix**	**Combinations**
1	All	{1,2,3,4}
2	1-3 or 3-1	{1,2,4}{3}
3	1-3 or 3-1	{1}{2,3,4}
4	1-3 or 3-1	{1,2,3}{4}
5	2-2 only	{1,2}{3,4}
6	2-2 only	{1,3}{2,4}
7	2-1-1 only	{1}{2,4}{3}
8	2-2 only	{1,4}{2,3}
9	2-1-1 only	{1,2}{3}{4}
10	2-1-1 only	{1}{2,3}{4}
11	1-3 or 3-1	{1,3,4}{2}
12	2-1-1 only	{1,4}{2}{3}
13	2-1-1 only	{1}{2}{3,4}
14	2-1-1 only	{1,3}{2}{4}
15	1-1-1-1	{1}{2}{3}{4}

Table 10. The proposed best scenario for the 4 plants problem inter-process integration

	1	**2**	**3**	**4**	$\Delta T_{\_min}$=15 C	
	FCCU	CDU/VDU	VBU	PLAT		
Qh (KW)	29,751	55,801	6,944	18,885	**Qh total=**	**111,382**
Qc (KW)	17,550	24,800	3,344	9,245	**Qc total=**	**54,940**
Pinch Temp.	158	272	141.7	81.1		

Table 11. Minimum Heating/Cooling requirements at $\Delta T_{\_min}$=15 C

	1	**2**	**3**	**4**	$\Delta T_{\_min}$=5 C	
	FCCU	CDU/VDU	VBU	PLAT		
Qh (KW)	29,016	52,832	6,676	17,946	**Qh total=**	**106,470**
Qc (KW)	16,815	21,831	3,076	8,306	**Qc total=**	**50,028**
Pinch Temp.	148	266.7	131.7	79.4		

Table 12. Minimum Heating/Cooling requirements at $\Delta T_{\_min}$= 5 C

	1	2	3	4	$\Delta T_{\_min}$=1 C (impossible)	
	FCCU	CDU/VDU	VBU	PLAT		
Qh (KW)	28,715	51,557	6,521	17,560	**Qh total=**	**104,353**
Qc (KW)	16,514	20,556	2,921	7,920	**Qc total=**	**47,911**
Pinch Temp.	144	262.7	137.7	79.4		

Table 13. Minimum Heating/Cooling requirements at $\Delta T_{\_min}$=1 C (impossible)

Comparing the total heating, cooling requirements and consequently the associate energy-based GHG emissions is our next task. First we will do the comparison for the standalone intra- process integration at descending ΔT_min to target for best GHG emission attainable using intra-process integration. Then we will compare the best possible target with the one that can be attained using inter- processes integration at ΔT_min, equal to 15 C.

Using previously mentioned simple relationship between MW of heat saved and amount of CO2 reduction obtained, we can easily calculate the reduction in CO2 emissions from the refinery biggest energy consumers due to intra-process integration at descending ΔT_min to be 31202 tone CO2/year and 62196 tone CO2/year respectively. It is 3 to 6 % maximum. Practically we can reach the 3 % but to get better than that we need extremely expensive HEN and the 6 %, at ΔT_min equal to 1 C, is unattainable/impractical. To reach such 3% reduction in the GHG emissions using ΔT_min equal 5 C will also need costly HEN design too. The results of direct inter-processes integration at ΔT_min equal 15 C can render the same amount of GHG emission reduction of %3 and even better through 9 possible scenarios/combinations. Such combinations are listed and ranked from 1 to 9 in table 9. The unattainable 6 % reduction in the energy-based GHG emissions using intra-process integration can be reached and even a little better (up to 10 %) using direct inter-processes integration techniques. Four scenarios/combinations can exhibit such fact, taking the rank from 1 to 4 in table 9. These combinations are as follows: direct inter-process integration of ADU/VDU, FCCU, VBU and PLAT processes all together, FCCU, CDU/VDU and VBU together and PLAT as a standalone, FCCU, CDU/VDU and PLAT together and VBU as a standalone, CDU/VDU, VBU , and PLAT together and FCCU as standalone.

It can be noticed from this discussion that in order to attain more aggressive GHG emissions reduction targets using intra-process integration techniques, even if we tried to use ΔT_min equal to 1 C which is currently impractical using the available state-of-art heat exchanger technology, we have no way but to use inter-process integration. There are 4 sets/combinations in the inter-process integration application at reasonable ΔT_min equal to 15 C, which can defeat the minimum heating and cooling requirements and consequently the energy-based GHG emissions of the almost impossible ΔT_min equal to 1 C in the intra-process integration application. That means, for an oil refinery with excellent intra-process integration applications; to obtain in-house GHG emissions reduction target of 6 % or more, as per the case study presented in this chapter, we have to resort to inter-processes integration application. Nowadays, the industrial community perception is that the only way to do such inter-process integration is to make it indirectly via buffer system (steam or hot oil). Such approach is currently adapted in industry but it has its limitations. Such limitations combined with the need to push the envelope and reduce the refining business GHG emissions will lead towards using more of the direct inter-processes integration.

4. Combined heat and power plant (CHP) retrofit

One of the famous options in industrial facilities to cut energy consumption cost and reduce emissions is the adaptation of the cogeneration technology. Co-generation or "CHP" is simply known as the production of two forms of useful energy from the same fuel source. Cogeneration systems are used to produce electricity, and use the excess (waste) heat for process steam generation, hot water heating, space heating, and other thermal needs.

There are several types of co-generation plants. One is the steam turbine- based cogeneration plant consisting of a steam turbine with the usual controlled steam extraction(s) for process steam supply. The other type is a gas-turbine- based cogeneration plant consisting of one or more gas turbines exhausting products of combustion through one or more heat-recovery steam generators (HRSGs), which produce steam for the heat supply [19:21]. The thermodynamic efficiency of a cogeneration plant is simply, (P + H)/Q1; where; P and H are the power and heat outputs of the cogeneration plant, respectively and Q1, is heat input .

The oil plant, presented here, is responsible for stabilizing and shipping crude oil and this normally needs large amount of energy mainly in form of steam and power. The plant receives crude oil from different wells and then separates the gas from the oil. The crude oil is stabilized, where light components are separated, and then pumped for shipment to users. The separated gas goes to natural gas liquid process (NGL) plants. Fuel is used by boilers and gas turbine generators. The steam generated from boilers goes to high pressure steam header at 625 psig. High pressure steam is used by back pressure steam turbines throughout the plant to drive oil shipper pumps. The steam coming out from the back pressure steam turbines is sent to the 60 psig header. The 60 psig steam is used to pre-heat the crude oil stream before entering crude stabilization column.

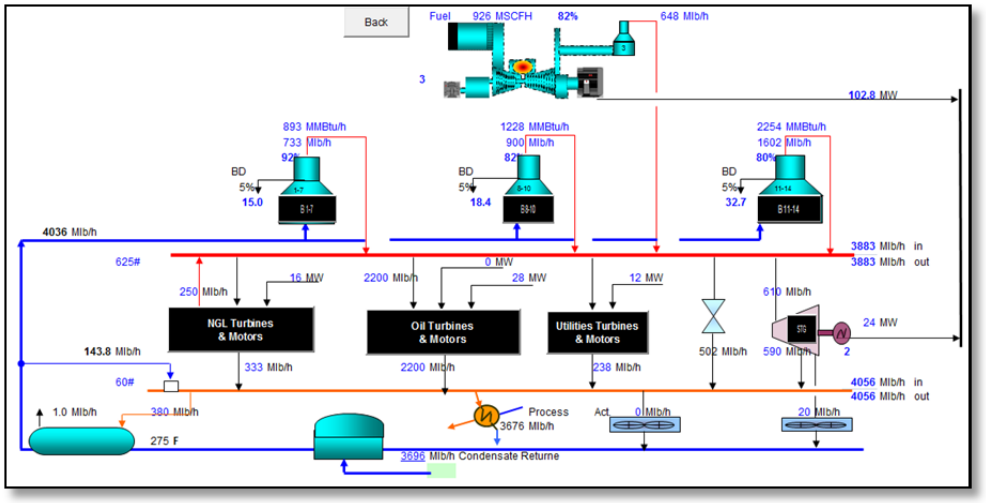

Fig. 1. Oil Stabilization Plant CHP Model

Fig.1 above gives an overview on the oil plants' utilities model. The oil plant has 10 boilers with total steam production of 4.5 Million bounds per hour (Mlb/h). The maximum steam demand can be found in winter interval where the plant is in need of almost the full boilers capacity. Oil plant historical data shows that the maximum steam demand, at winter time, is equal to 4.4 Mlb/h, and the minimum steam demand, at summer, is equal to 3.2 Mlb/h. The oil plant has two simple cycle gas turbine generators, each capable of generating 40 MW at 38 C. The plant power demand varies between 75 MW in summer and 53 MW in winter and the average power consumption per year is about 60 MW. The oil plant is tied up to the nation-wide electricity grid. Usually the plant internal power generation units are reliable but that is made to avoid any failure that can result in any disruption to the oil plant production.

Retrofitting the existing two simple cycle gas turbines with two heat recovery steam generators (HRSGs) can result in less energy consumption and less GHG emission. The steam generated from the two HRSGs would be equivalent to a production of two old small boilers producing 340 Klb/h of steam. Thus, the fuel used in the two old boilers will be saved in addition to eliminating their emissions.

In order to calculate the fuel saving, it is necessary to have a relation between the fuel consumption and the steam generation of the two old boilers. Such relation can be developed from plant's historical real time data via curve fitting techniques.

Boiler #	Fuel VS. Steam
B-1	Fuel (MSCFh) = 1.0917 * Stm (klb/h) + 6.4138
B-2	Fuel (MSCFh) = 1.3983 * Stm (klb/h) – 15.38

Table 14. Two small boilers fuel vs. steam equations

From plant's historical data, the average steam produced from the two small boilers is 340 (thousand bounds per hour) Klb/h; i.e. each producing 170 klb/h.

Fuel savings (avoided) = Boilers Fuel consumption

$$= (170 \times 1.0917 + 6.4138) + (170 \times 1.3983 - 15.38)$$

$$= 414.3338 \text{ KSCF/h (thousand standard cubic feet per hour)}$$

Energy saving (MMBtu/h) = Fuel Btu Content * Boilers fuel consumption

$$= 1.090 \text{ KBtu/SCF} \times 414.3338 \text{ KSCF/h} = 451.6 \text{ MMBtu/h}$$

Note: Assuming HHV of fuel is 1090 Btu/SCF

Now, let's compare the efficiency of simple cycle with the expected co-generation efficiency, for simple cycle system:

$$\text{Simple cycle } (\mu) = \frac{Output}{Fuel} = \frac{Powr}{Fuel}$$

Where,

Power = electrical power output in Btu/h

Fuel = Fuel energy input in Btu/h

Consider a power demand of 53 MW; the corresponding fuel input to simple cycle gas turbines is 532.86 KSCF/hr.

Power (MMBtu/hr) = 53,000 KW * 3412.14 Btu/KWh = 180.8 MMBtu/hr.

Fuel Input (MMBtu/hr) = 532,860 SCF/hr * 1090 Btu/SCF = 580.8 MMBtu/hr.

Simple cycle (μ) = 31.13 %.

For the case of cogeneration system:

$$\text{Co-generation cycle } (\mu) = \frac{Output}{Fuel} = \frac{Powr+Steam}{Fuel}$$

At winter time the units have to operate at full load (40 MW each) and generate steam (340 Klb/h) of steam. The plant power need only 53 MW, so there will be an access power of 27 MW; let's assume that the excess power has no value. Calculating the efficiency:

Power (MMBtu/hr) = 53,000 KW * 3412.14 Btu/KWh = 180.8 MMBtu/hr.

For calculating the useful heat energy, assuming 100% utilization. The steam Internal energy (Enthalpy) for 625 psig, 380 F steam header is 1370 Btu/lb and BFW enthalpy is about 270 Btu/lb.

Steam heat energy = ΔH (Btu/lb) * Steam Flow (Lb/hr)

$$= (1370 - 270) * 340{,}000 = 374 \text{ MMBtu/hr}$$

Fuel Input (Btu/hr) = 773,075 SCF/hr * 1090 Btu/SCF = 842.6 MMBtu/hr.

Co-generation cycle (μ) = 66%

Having the two co-generation units installed, and the two old boilers demolished. Let's see the impact on the total emissions:

NOx & CO2 Emissions calculation:

$$\text{NOx (g/s)} = 0.32 * 0.126 * (\text{Fuel Gas Consumption}) \quad (1)$$

$$\text{SO2 (g/s)} = [0.126*(16*32*2)/(0.7302*527)/1000] * (\text{Fuel Gas Consumption}) \quad (2)$$

Knowing, the average availability of the two boilers per year and their consumption and using the above formulas (1) & (2) gives a reduction on total emissions of 1.25 metric ton per day. Other benefit appears when converting to co-generation cycle is that the heat going to the ambient will be significantly reduced from 1000 F to about 300 F.

In summary, the adaptation of co-generation technology in the oil plant exhibits economical and environmental benefits over the simple cycle power generation and stand alone steam boilers. Well designed and operated cogeneration plant will always improve energy efficiency for systems requiring steam and power in oil and gas facilities. The typical energy

efficiency of a co-generation system, normally between 70-90%, simply means significant reduction in CO2, SO2, NOx emissions compared to other stand alone generation of power and heat in oil and gas industry.

5. Concluding remarks

GHG emission reduction can be addressed successfully using energy efficiency optimization techniques in design and operation of industrial facilities. Energy efficiency optimization in process plants, on the equipment level (compressors, boilers, furnaces and so on), sub-system level (combined heating and power CHP), complete process level (crude oil fluid catalytic cracking) and site-wide level (refinery and refinery-chemical integrated facility and even mega industrial complex) is a fast and cost effective way to reduce GHG emissions at the source.

While the industry's already adapted intra-process integration and indirect inter-processes integration bring value to the task of energy consumption and energy-based GHG emissions reduction, aggressive direct inter-processes integration can also be adapted on large scale in industrial community to boost the efforts for energy conservation and GHG emissions reduction. It can enable us stretch the envelope beyond GHG emissions targets and reach better ones in many industrial sites such as in-house oil refining GHG emissions reduction target.

It is instructive to mention that direct inter-process integration that can render us better results beyond the attainable from perfect intra process integration and indirect inter-processes integration do not necessarily have to be done using excessive connections among the plants to reach the desired targets for GHG emissions. From our industrial experience we can surly tell that in many cases two or three connections at most between plants are enough to reach reasonable level of the best desired energy consumption and GHG emissions reduction targets. The details of such finding will be presented in future work.

While we are addressing in this chapter the role of energy efficiency optimization in GHG emissions reduction, we also believe that increasing the use of renewable non-hydrocarbon based energy sources are very efficient way to tackle the GHG emissions problem even on the process plant level. Solar energy in industrial applications especially in remote areas for oil, water pumping and gas compression, and administration areas lighting and cooling can be a very viable. The utilization of solar power for water heating, steam generation and large scale air-conditioning, as solar cooling, is very valid greenhouse gas emissions reduction option. We believe that adapting both energy efficiency optimization and flexible customization of renewable as a clean source of energy at plant's level will be fast and cost-effective approach to attain desired GHG emissions reduction targets.

6. References

[1] Birkeland, H & Energi, N 2007, 'Provisions of Small Scale Projects', paper presented to CDM Capacity Building in Servian Institutions, Belgrade, 26 September 2007.

[2] Hayashi, D & Michaelowa, A 2007, 'Lessons from Submission and Approval Process of Large-Scale Energy Efficiency CDM Methodologies', paper presented to UNIDO/CTI/UK Trade and Investment Seminar on Energy Efficiency, Vienna, Austria, 19-22 March 2007.

[3] UNFCCC 2009a, *Efficient Utilization of Waster Energy in Industrial Facility*, New York, USA

[4] Linnhoff,B.(1993). Pinch analysis-state of the art overview. *Trans.Inst.Chem.Eng.* ,Part A5, 503-522.

[5] Smith, R (2005), *Chemical Process Design and Integration*, 2nd edition, Manchester: Wiley

[6] El-Halwagi, M..M.,(1997),Pollution prevention through process integration, Academic Press, San Diego

[7] Noureldin, M.B., and A. Hasan,(2006), Global energy targets and optimal operating conditions for waste-energy recovery in Bisphenol-A plant, Applied Thermal Engineering, 26, 374-381.

[8] Noureldin, M.B and Aseeri, A.S.(2010), System, method and program product for targeting and optimal driving force distribution in energy recovery systems" US Patent 7,698,002

[9] Noureldin, M.B and Aseeri, A.S.,(2011), Advanced method and software for targeting and optimal driving force distribution in energy recovery systems", US Patent 7,873,443

[10] Ahmad, S., and Hui, C.W. (1991), Heat recovery between areas of integrity, Computers and Chemical engineering, 12, 809-832

[11] Hui, C.W. and Ahmad, S.,(1994), Total site heat integration using the utility system, Computers and Chemical engineering, 18, 729

[12] Dhole, V.R.; Linhoff B. (1992), Total site targets for fuel, cogeneration, emissions and cooling, computers and Chemical engineering, 17, S101-S109

[13] Amidpour, M., and Polley, G.T. (1997), Application of problem decomposition in process integration. Transactions of the Institute of Chemical engineering, 75, 53-63

[14] Rodera, H., and M.J. Bagajewicz,(1999a), Targeting procedures for energy savings by heat integration across plants", *AIChE* Journal, 45, 1721

[15] Rodera, H., and M.J. Bagajewicz,(2001), Multipurpose Heat exchanger networks for heat integration across plants"Ind. Eng.Chem.Res., 40, 5585

[16] Bagajewicz, M.I and Rodera, H..,(2002), Multiple plant heat integration in a total site", *AIChE* Journal, 48,(10), 2255-2270

[17] http://mathforum.org/advanced/robertd/bell.html

[18] Fraser, D.M., and Gillespie, N.E , (1992), The application of pinch technology to retrofit energy integration of an entire oil refinery , Transactions of Institute of Chemical Engineering, 70, 395-406

[19] Mavromatis, S.P. and Kokossis, A.C., (1998), Conceptual optimization of utility networks for operational variations-I. Targets and level optimization, Che.Eng. Sci, 53(8), 1585-1608

[20] Varbanov, P.,S., Doyle, S., and Smith, R. (2004), modeling and optimization of utility systems, Trans IChemE, Part A, chem. Eng Res Des, 82(A5), 561-578

[21] Varbanov, P.,S., Perry, S., Makwana, Y., Zhu, X., and Smith, R. (2004), Top-level analysis of site utility system, Transactions of Institute of Chemical Engineering, 82(A6), 784-795

5

Greenhouse Gas Emissions from Non-Cattle Confinement Buildings: Monitoring, Emission Factors and Mitigation

S. Godbout[1,2], F. Pelletier[1], J.P. Larouche[1], M. Belzile[1], J.J.R. Feddes[1,3], S. Fournel[1,2], S.P. Lemay[1,2] and J.H. Palacios[1]

[1]*Research and Development Institute for the Agri-Environment, Québec City, QC,*
[2]*Department of Soil Science and Agri-Food Engineering, Université Laval, Québec City, QC,*
[3]*Department of Agricultural, Food and Nutritional Science, University of Alberta, Edmonton, Canada*

1. Introduction

Worldwide environmental issues are dominated by climate change, especially by the increase in greenhouse gas (GHG) emissions (UNDP, 2007). The rise in of GHG concentrations in the atmosphere has become a major environmental concern as revealed in the Kyoto Protocol (AAFC, 2000). Besides contributing to global warming by absorbing infrared radiation, carbon dioxide (CO_2), methane (CH_4) and nitrous oxide (N_2O) have been declared the most harmful gases for ecosystems, apart from ammonia (NH_3) (Pain, 1998; Copeland, 2009).

Agricultural practices account for 10 to 12% of world total GHG emissions, however, it could reach between 17 and 32% (8,5-16,5 Pg CO_2-eq) by including all agriculture-related emission sources (Bellarby et al., 2008). Agricultural GHG emissions can be divided into three main groups: a) CH_4 emissions from cattle enteric fermentation; b) CH_4 and N_2O emissions due to manure management practices; and c) N_2O emissions from cultivated fields, including direct emissions from crop land and pasture and indirect emissions resulting from the use of nitrogen fertilizer in agriculture.

Manure management alone is responsible for 13% of GHG emissions from the agricultural sector with CH_4 and N_2O accounting for 33 and 67% of CO_2-eq, respectively (Steinfield et al., 2006). Current trends suggest that this level will substantially increase over the coming decades as the intensification of livestock activities continues. On the other hand, CH_4 and N_2O have a global warming potential of 21 and 310 times over hundred years greater than CO_2, respectively, based on their ability to contribute to climate change (Houghton et al. 1995). Hence, the environmental impact of livestock operations can not be considered negligible.

Currently, many countries have to use internationally agreed values to evaluate their GHG emissions. By describing the GHG emission sources and presenting the emission factors from non-cattle production, this chapter will improve the knowledge of scientists and

politicians about the contribution of agriculture to global warming. Moreover, this chapter provides quick information on monitoring and mitigation of GHG emissions.

2. Gas emissions from animal confinement buildings

2.1 The source of contaminants

Contaminants exhausted from animal confinement buildings include various gases, dust particles, micro-organisms and odours. The most important gases are CO_2, NH_3, hydrogen sulphide (H_2S), CH_4, N_2O and some trace gases (aldehydes, amines, aromatics, organic acids, sulphur compounds, etc.). NH_3, CH_4 and N_2O are produced from manure decomposition while CO_2 is primarily a product of animal metabolism (Hartung & Phillips, 1994).

In most confinement buildings, manure is stored as a liquid or semi-solid beneath the animals for a short or long period of time. Both the manure attached to the flooring material and the manure stored under the animals produce these gases.

Manure decomposition begins in the stomach of the animal where the consumed feed undergoes early anaerobic decomposition by the intestinal flora at a temperature between 38 and 40 °C. Once the manure is excreted and exposed to air, a new type of bacteria grows according to the manure management method practiced. Depending on ambient temperature, this change takes 12 to 24 h (Barrington, 1999).

In the case of solid manure to which straw is added, animal manure is decomposed by aerobic bacteria. These bacteria break down organic matter and stabilize the manure. Once stabilized, almost no gas or odorous compounds will be produced (Barrington, 1999).

In liquid manure, a population of facultative bacteria (aerobic or anaerobic) grows rapidly. These bacteria decompose organic matter and produce gases and odorous compounds. The emission of these contaminants is thus carried throughout storage (Barrington, 1999). Figure 1 presents a schematic view of the emission mechanisms from anaerobic decomposition of liquid manure.

The production of N_2O during storage and treatment of animal manure occurs during nitrification and denitrification of nitrogen contained in the manure. Nitrification is the oxidation of ammonium (NH_4^+) to nitrate (NO_3^-), and denitrification is the reduction of NO_3^- to N_2O or atmospheric nitrogen (N_2). Generally, as the degree of aeration of the waste increases, so does the amount of N_2O produced (Olsen et al., 2003).

2.2 Emission calculation

Two parameters are very important in determining gas emission rates, namely the gas concentration (inlet and outlet) and the air exchange rate (Fig. 2). Gas emissions are calculated by multiplying the difference in concentration by the mass flow of gas, which is calculated from the mass flow of air. The GHG emissions can be calculated for each sampling period using Equation 1. In this equation, the specific volume of air ($v = (P_{atm} - P_v)/(287 \times T)$; ASABE, 2010) is used to obtain the mass flow of air from the volumetric flow rate.

$$E_{GHG} = (C_{out} - C_{in}) \times \frac{Q}{N_{animals}} \times \frac{P_{atm} - P_v}{287 \times T} \times \frac{M_{GHG}}{M_{air}} \times 525,6 \quad (1)$$

where E_{GHG} represents CO_2, CH_4 or N_2O emissions for one animal space during one sampling event (g yr^{-1} $animal^{-1}$), C_{out} is the GHG exhaust concentration from the animal space (ppmv), C_{in} is the incoming GHG concentration to the animal space (ppmv), Q is the average room air exchange rate during the sampling event (m^3_{air} min^{-1}), $N_{animals}$ is the number of animals in the room, P_{atm} and P_v are respectively the atmospheric pressure at sea level and the vapour pressure (Pa), T corresponds to the temperature (K), M_{GHG} characterize the molar masses of CO_2 (44 g mol^{-1}), CH_4 (16 g mol^{-1}), or N_2O (44 g mol^{-1}), M_{air} signifies the molar mass of air (29 g mol^{-1}), 287 is the thermodynamic constant of air (J kg^{-1} K^{-1}) and 525,6 is a conversion factor (mg min^{-1} to g yr^{-1}).

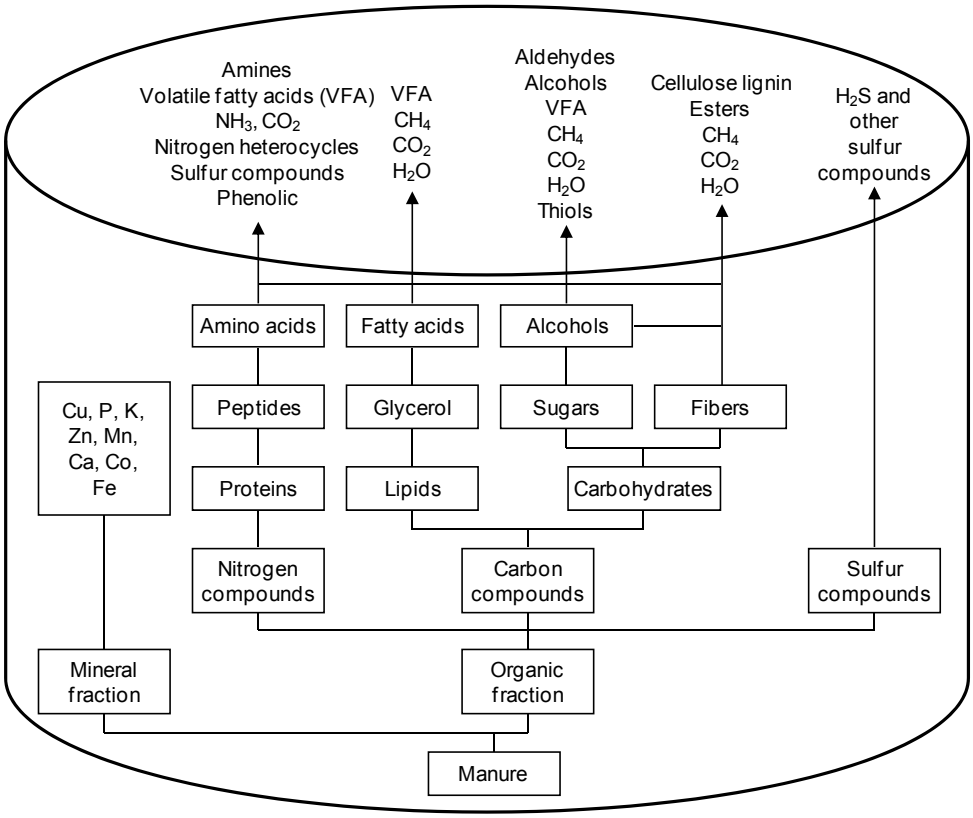

Fig. 1. Emissions from anaerobic decomposition of liquid manure (adapted from de la Farge, 1978; IPT, 1998; Taiganides, 1987; UGPVB, 1996; O'Neill & Phillips, 1992)

The majority of the pig and poultry operations are mechanically ventilated whereas confined cattle facilities are primarily naturally ventilated. The methodology to estimate gas emissions depends on wind speed, direction, building opening orientation and outside-inside temperature differential.

The inlet and outlet gas concentrations play an important role. Monitoring methodologies differ among countries. The air exchange rate of an animal housing facility must be

measured accurately. This would apply to both mechanically ventilated (MV) buildings and naturally ventilated (NV) facilities or a combination of the two ventilation systems. Buildings with combined systems are commonly referred to as hybrid ventilation systems (HV). Many methods have been developed to measure ventilation rates from animal housing facilities.

The following sections will address these topics with a complete description of an experimental setup used by the authors for sampling and analysis of GHG emitted by a number of non-cattle confinement buildings. Also best methods for measuring the air flow rate in both MV and NV barns are suggested.

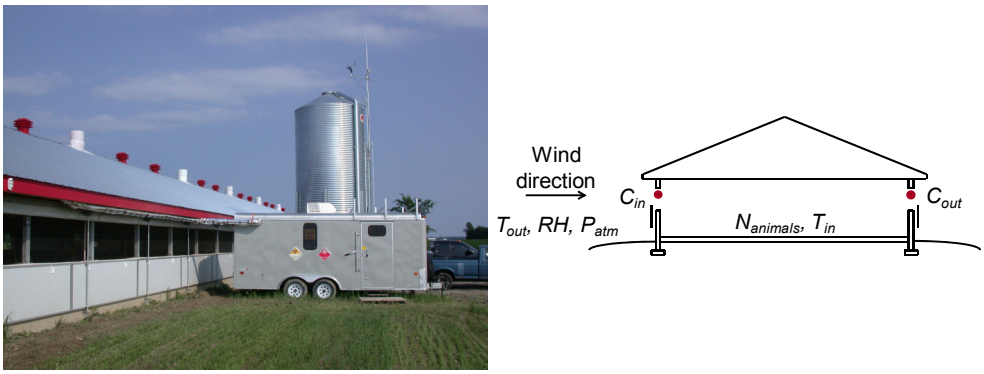

Fig. 2. View of an emission measurement set up on a naturally ventilated barn.

3. Concentration measurements: gas sampling and analysis

3.1 Atmospheric concentration gas analysis

Since the ambient air is used for ventilation of animal buildings, the determination of gas emissions from agricultural activities initially requires a measurement of the ambient air concentration. The contribution of farming systems under study may affect the GHG ambient concentrations near the facility. The measurement of atmospheric concentration need to use equipment having great sensitivity and selectivity like those utilizing optical properties of gas such as Fourier transform infrared spectroscopy (FTIR), photoacoustic spectroscopy (PAS) and non dispersive infrared analyser (NDIR) or separation techniques like chromatography with selective detectors (Neftel et al., 2006).

Since agricultural and forest soils are involved in gas exchange with the atmosphere and many agricultural activities like animal husbandry are significant sources of CH_4 and N_2O, several studies were conducted to quantify emissions from soils and livestock buildings. In those projects, a number of researchers primarily interested in the characterization of emissions from livestock buildings often work with PAS in the infrared (Blanes-Vidal et al., 2008; Cabaraux et al., 2008; Philippe et al., 2007). While for other authors interested in analytical development or atmospheric flux measurements from soils, separation by chromatography seems to be the preferred means of detection and quantification of trace gases in ambient air (Loftfield et al., 1997; Sitaula et al., 1992; Weiss, 1981; Blackmer & Bremner, 1977).

The air is mainly composed of N_2, oxygen (O_2) and argon (Ar) with several others gases in trace concentrations like CO_2, CH_4 and N_2O. These components can be separated by chromatography and detected by different detectors more or less specific to the target gas. The technique is simple, proven and allows the simultaneous quantification of CO_2, CH_4 and N_2O in the gaseous effluents discharged to the atmosphere. Compared to other techniques having the required sensitivity, like most modern spectroscopic techniques, the chromatography is known to produce reliable results and can be envisaged as a moderate to low cost technique with easy apparatus implementation.

These three GHG are easily separated at low temperature on a column filled with porous polymers Porapak Q or Chromosorb 102 (Cowper & DeRose, 1983). However, the analysis strategy depends on the detectors used and additional gases to be separated and quantified in the sample. Methane can be precisely measured by a flame ionization detector (FID) on a wide range of concentrations ranging from parts per million to volume percent (Cowper & DeRose, 1983) which is suitable for measuring emissions from a livestock building where CH_4 concentrations will range from atmospheric pressure of 1,7 ppmv (Brasseur et al., 1999) to less than 5 000 ppmv for most of the time. To measure atmospheric concentrations of CO_2, a particular approach should be implemented. The approach involves the reduction of CO_2 to CH_4 with hydrogen over a nickel catalyst and detection by the FID (Cowper & DeRose, 1983).

In order to obtain the required sensitivity for the quantification of N_2O at concentrations found in ambient air, the electron capture detector (ECD) is commonly used to measure atmospheric concentrations. Some work has been done with N_2 alone as a carrier gas (Jiang et al., 2007; Arnold et al., 2001; Loftfield et al., 1997) while others were performed with an Ar/CH_4 mix (95/5) as carrier gas or as make-up gas to the detector (Jiang et al., 2007; Heinemeyer & Kaiser, 1996; Sitaula et al., 1992; Weiss, 1981; Mosier & Mack, 1980). It was also noted that impurities in a carrier gas can strongly influence the response of the ECD (Phillips et al., 1979) and that the addition of O_2 in the carrier gas increases the sensitivity of ECD to allow the determination of atmospheric concentrations of CO_2 (Cowper & DeRose, 1983). Even if the dynamic range of the ECD is limited, the range of concentration for CO_2 and N_2O encountered for most confinement buildings are limited. The typical measured concentrations range from atmospheric concentration (360 ppmv for CO_2 and 0,31 ppmv for N_2O; Brasseur et al., 1999) up to 5 000 ppmv for CO_2 and up to 10 ppmv for N_2O.

3.2 Sampling and management of gas samples

The system developed for the quantification of gas emissions from the agricultural sector has two main functions, first the collection and management of the sample and second the analysis of the sample. Samples are taken sequentially from several sampling points and continuously transported to the analysis system. CO_2, CH_4 and N_2O are analyzed with a gas chromatograph (GC). An example of the gas sample collection system is shown in Fig. 3.

For each sample location, gases are pumped through a membrane filter made of polytetrafluoroethylene (50 mm diameter, 0,2 µm pore size) and routed in a Teflon tube (6,4 mm OD, 0.8 mm wall) of variable length depending on the distance between the sampling location and the analysis system. The Teflon tubes are connected to a rotary valve allowing the sequential sampling and analysis of up to 16 locations. A purge diaphragm pump allows

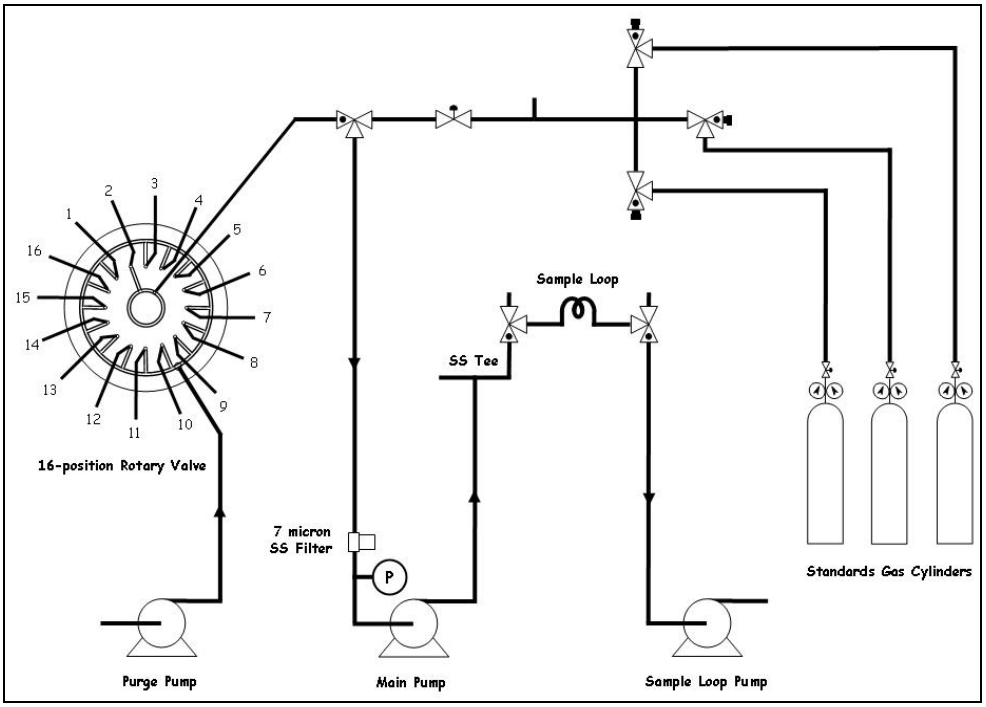

Fig. 3. Gas sample collection system

for back flowing of ambient air through the Teflon gas lines that are not under analysis to minimize stagnation of sample in the tubes.

The gas flow from the source to the analyser is provided by the main diaphragm pump which delivers the gas to a stainless steel tee fitting. A small filtering sleeve made of sintered stainless steel (7 µm pore size) placed upstream of the main pump provides extra equipment protection against fine dust. The stainless steel tee allows the diaphragm pump to draw a fraction of the sample to flow continuously through the 1 000 µL sample loop of the GC. Two solenoid valves are used to isolate the sample loop in order to balance the pressure of the sample with atmospheric pressure before injection. The sample excess is exhausted to the atmosphere.

The solenoid valve placed between the 16-position rotary valve and the main pump allow for selecting the sample gas analysed from the rotary valve or a selection of calibration gases including ambient air and pressurized gas cylinders controlled by solenoid valves.

All components of the sample collection system that are in contact with the sample gas are either Teflon (ex.: sample tubes), Teflon coated (ex. : pump diaphragms) or stainless steel 316 (ex.: rotary valve, fittings, etc.).

The Teflon sampling tubes from the sampling locations to the analyzer are placed inside a series of ducts maintained by circulating air at approximately 35 °C. The complete system including the 16-position rotary valve, the GC and the pumps are installed in a temperature

controlled mobile laboratory. T-type thermocouples are used to monitor the temperature in the heated ducts and the temperature inside and outside the mobile lab. A data logger controlled by the computer of the GC can acquire and archive various parameters measured during periods of analysis. It also controls the electric actuator of the 16-position rotary valve and the various solenoid activated valves of the gas collection system of the samples.

3.3 Chromatographic analysis of greenhouse gases

The strategy for the chromatographic analysis is the separation of the three gases on packed columns filled with the porous polymer Porapak Q 80/100 mesh. A pre-column (3,2 mm OD, 1 m long) connected in series before the analytical column (3,2 mm OD, 3 m long) removes some substances that may be present in the gas samples. These substances, which are retained longer than N_2O in the pre-column, can include water, NH_3 and some sulphur compounds that may have adverse effects on the detectors or on the columns.

CH_4 is quantified with a FID, while CO_2 and N_2O are measured with an ECD. However following the initial set-up of the chromatographic analysis, CO_2 was quantified with the FID after reduction with hydrogen over a nickel catalyst. Subsequently, following the chance observation of the detection of CO_2 by the ECD, the quantification of CO_2 is transferred to the ECD. This minimises the gradual loss of the effectiveness of the nickel catalyst and also allows a better separation of CO_2 and N_2O which is not affected by the disruption of the baseline caused by the actuation of the detector valve.

Figure 4 shows a schematic of the tubing configuration of the GC used for the separation and quantification of the greenhouse gases and Fig. 5 shows a picture of the column arrangement inside the GC oven and a picture of the outside of the GC.

The oven of the GC is maintained at 60 °C for the duration of the analysis. The 10-port injection valve and the 6-port detector valve are mounted on top of the GC. The zero grade nitrogen is used as carrier gas and is introduced at the three entry points of the pneumatic system of the GC at an equal flow rate of 25 ml min^{-1}. The two detectors are maintained at 325 °C and the FID is supplied with 30 ml $min^{-1}$of hydrogen UHP and with 300 ml $min^{-1}$of zero grade air produced by a commercial generator. All the necessary tubing, fittings and valves installed in the GC are made of stainless steel.

The sequence of the analysis begins when the injection valve is actuated to allow the carrier gas to flow through the sample loop and thus transfer the sample gas into the pre-column and the analytical column. After elution of the N_2O from the pre-column, the injection valve returns to its original position to allow the back flush of the pre-column and further elution of the analytical column. After detection of CH_4 on the FID, the detector valve is actuated to allow quantification of the CO_2 and N_2O on the ECD. The retention times are 2,9 min for CO_2, 1,6 min for CH_4 and 3,8 min for N_2O. Examples of chromatograms obtained for analysis of standard calibration gases and ambient air are presented in Figs. 6 and 7, respectively. With an analysis time of 5 min for the chromatographic analysis and a turnover of less than 7 min between analyses, the chromatographic system allows continuous acquisition of sufficient data to adequately describe agricultural process.

Normal operation of the GC is provided in part by the control software for the electrical parameters and also by periodic checks of the pressure on low pressure gauges on the

cylinder gas regulators and on the pressure gauges mounted on three controls of the carrier gas admission in the GC which operate near 234 kPa.

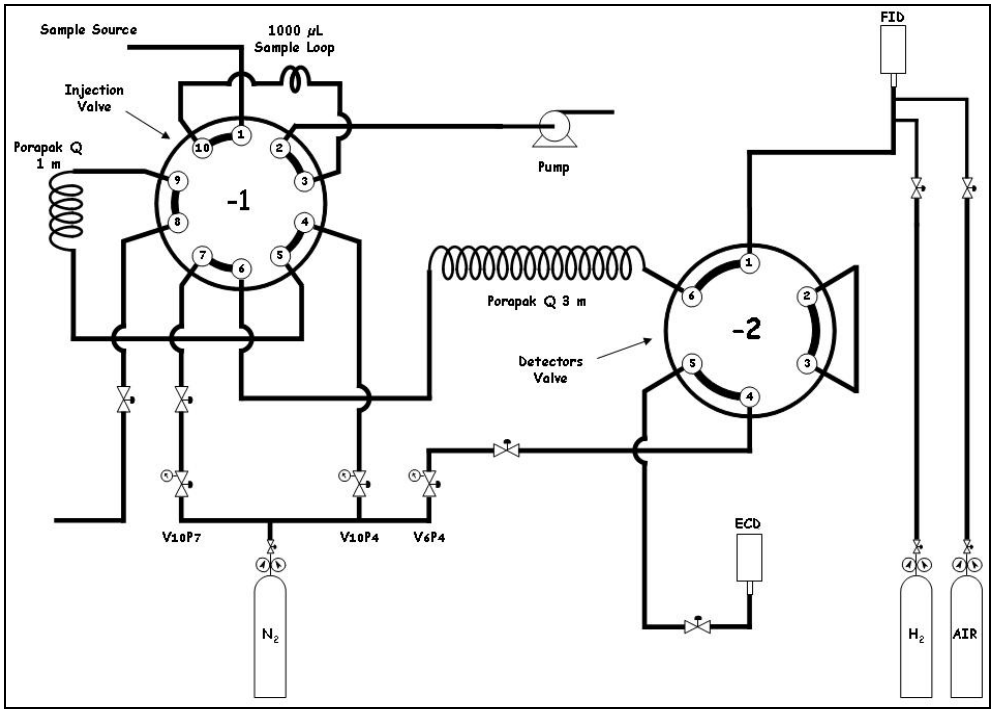

Fig. 4. Tubing configuration of the chromatograph

Fig. 5. Standard gas chromatograph and oven

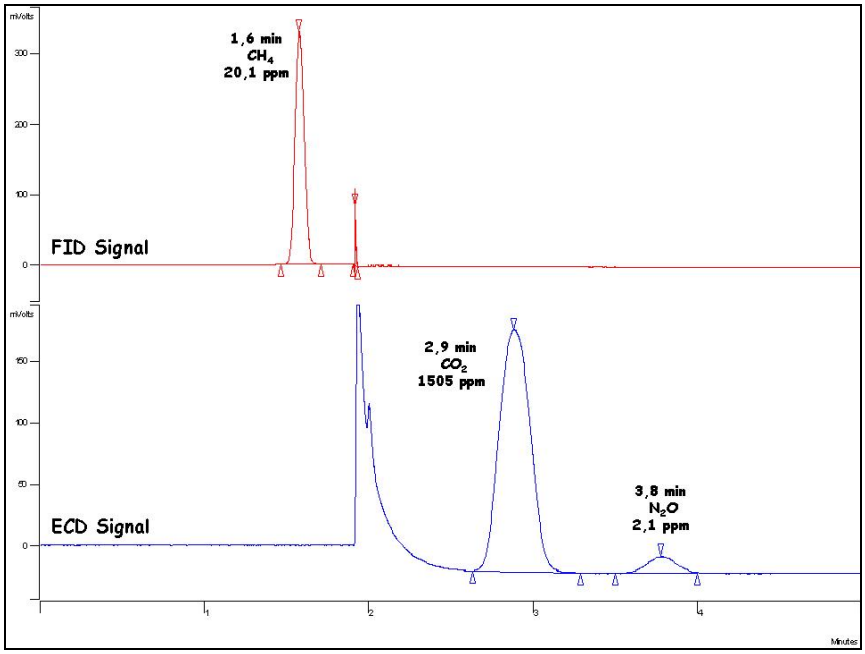

Fig. 6. Chromatograms of the greenhouse standard calibration gases

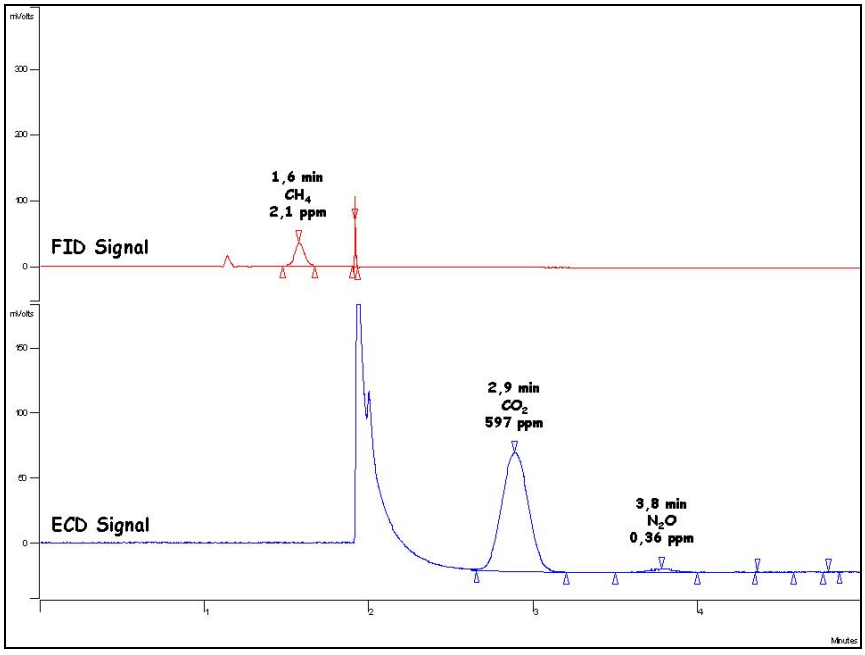

Fig. 7. Chromatograms of an ambient air sample

3.4 Quality control of the analyses

Chromatographic instrumentation analysis is usually calibrated at the beginning of each period of analysis using standard calibration gases qualified as "Certified Standards". The three GHG are available mixed and diluted with N_2 in a single cylinder and at concentrations similar to those expected in real samples. The response factors of the chromatographic analysis are calculated with a single point calibration for each analyzed gas since the response of the detectors used are linear over the concentration ranges encountered.

To document the long-term performance of the overall system and to control the quality of the data obtained, standard analysis are performed automatically at a specified frequency. The samples used are the ambient air in the mobile laboratory and the standard gases from cylinders used for calibration of the GC. The curves showing the responses of the system over time are used to observe and confirm the periods of normal operation of the system and other statistical calculations on the results are used to estimate the overall accuracy of analysis including management and quantification of the sample. Table 1 shows typical examples of results for standard analysis.

	Ambient air			Standard calibration gases		
	CH_4	CO_2	N_2O	CH_4	CO_2	N_2O
Mean value (ppmv)	2,0	595	0,32	20,5	1 510	2,1
Precision (%)	5,8	4,6	16,0	1,0	3,8	5,8
Maximum value (ppmv)	2,4	638	0,41	20,7	1 589	2,3
Minimum value (ppmv)	1,9	541	0,21	20,1	1 403	1,9

Table 1. Typical concentrations measured for standard analysis

4. Ventilation rate measurement

4.1 Basic principle

To determine the gas emission rates of an animal housing facility, the air exchange rate of the facility must be measured accurately. In northern climates, HV buildings have become more common since buildings relying on NV during cold weather conditions develop numerous problems. These problems include poor inlet air distribution into the building, poor control of the exchange air within the building, uneven temperature and air velocity distribution throughout the building. Therefore, HV buildings rely on MV during cold weather conditions and on NV during spring, summer and fall weather conditions.

4.2 Mechanically ventilated barn

Many methods have been developed to measure ventilation rates from animal housing facilities. These have included airborne tracer techniques (Leonard et al., 1984), diffusion of animal-produced CO_2 (Feddes et al., 1984) or heat (Barber et al., 1994), vane anemometers (Heber et al., 2000), orifice plates (Godbout et al., 2005), multi-port averaging pitot tubes (Clark et al., 2008) and thermal (e.g., hot-wire) anemometers (Feddes & McQuitty, 1980). Each of these methods, however, has limitations.

Fan airflow rates can be evaluated using a standardized ventilation conduit developed using the standard ANSI/ASHRAE 41.2-1987 (RA 92) (ASHRAE, 1992). The static pressure

difference between the interior of the room and the outside of the building as well as the fan rotational speed of each ventilation stage should be continuously measured during the trials. During measurements within the duct, conditions occurring during each trial are recreated (static pressure and rotation speeds of each stage of ventilation). Collected data make it possible to calculate regression equations for each fan predicting air flow rate based on room static pressure and fan rotation speed. Regression equations are calculated from the supplier information (Belzile et al., 2006).

For MV buildings, the ventilation related data collected are: daily number of animals and their mass, hourly mean exhaust fan rotational speeds, building static pressures and hourly temperatures inside and outside the building.

Ventilation rates can be predicted using a CO_2 balance. Using data monitored in that barn, the animal CO_2 production values can be calculated from published data like, e.g., values suggested by CIGR (2002).

4.3 Natural and hybrid ventilated barn

Determining the ventilation rate of NV or HV buildings remains challenging. With ventilation controls becoming more sophisticated, side curtain and ridge vent openings can be controlled more precisely based on anticipatory logic used to determine upcoming temperatures and wind conditions. Traditionally, NV buildings have only been used for larger animals where changes in the thermal environment are not as critical. With improved controller logic, NV buildings will soon be used more extensively for housing smaller animals. Consequently, the ability to predict airflow in these facilities is very important in controlling the thermal and non-thermal well-being of the confined animals.

A number of researchers have proposed methods to calculate the air exchange rates in NV buildings. These airflow rates are dependent on wind speed at the opening and effectiveness of the opening. Morsing et al. (2002) and Choinière et al. (1988) reported coefficients to be used for agricultural buildings to calculate the wind speed at the opening. Nääs et al. (1998) and Choinière et al. (1988) described an algorithm to determine an opening effectiveness relative to the wind direction. This methodology is described as the ventilation rate due to wind and thermal buoyancy.

For HV buildings, the ventilation related data collected included: daily number of animals and their mass, hourly wind speed and direction, curtain opening areas, operating status of the exhaust fans and hourly temperatures inside and outside the building. As for MV buildings, ventilation rates from NV and HV barns can be predicted by establishing a CO_2 balance. In order to be representative, the CO_2 concentrations should be measured at least at three locations: on each side of the barn close to the curtains and in the center of the barn at the animal level. For HV barns, the CO_2 concentrations should also be measured close to the fans.

5. Emission factors from swine and poultry confined buildings

5.1 Swine production

The literature identifies emission factors from the three types of swine confinement buildings (Table 2). The swine production system begins with the maternity stage

comprising both of gestating sows and farrowing sows with their piglets. Gestating sows are usually reared either in individual stalls or in group pens. Farrowing sows and their piglets are mainly kept in farrowing crates. The swine nursery or post-weaning building rears the weaning piglets brought from the maternity. Piglets remain there until they reach a certain weight, generally between 20 and 25 kg. Feed and ambient conditions are adjusted with pig growth. Then, pigs are transferred to grower/finisher facilities until they leave for slaughter.

Growing phase	Gas	Units	Mean emissions**	Minimum value	Maximum value	Standard deviation
Maternity	CO_2	kg d^{-1} sow^{-1}	5,29	1,83	9,35	2,26
	CH_4	g d^{-1} sow^{-1}	30,1	13,3	119,7	25,3
	N_2O	g d^{-1} sow^{-1}	0,00	0,00	0,00	0,00
	GHG *	g CO_2-eq. d^{-1} sow^{-1}	632	-	-	-
Nursery	CO_2	kg d^{-1} $piglet^{-1}$	0,55	0,49	0,59	0,04
	CH_4	g d^{-1} $piglet^{-1}$	2,77	0,32	10,7	4,11
	N_2O	g d^{-1} $piglet^{-1}$	0,007	0,000	0,010	0,005
	GHG *	g CO_2-eq. d^{-1} $piglet^{-1}$	60,3	-	-	-
Grower/ finisher	CO_2	kg d^{-1} pig^{-1}	1,92	0,30	5,00	1,05
	CH_4	g d^{-1} pig^{-1}	5,54	1,16	17,5	4,72
	N_2O	g d^{-1} pig^{-1}	0,66	0,00	3,50	1,39
	GHG *	g CO_2-eq. d^{-1} pig^{-1}	321	-	-	-

* Total greenhouse gas emissions calculated on a CO_2-equivalent basis considering the mean emissions and the global warming potential of CH_4 (21) and N_2O (310).
** References: Gallman et al., 2003; Gallmann & Hartung, 2000; Godbout et al., 2003, 2006; Groot Koerkamp & Uenk, 1997; Guarino et al., 2003; Guimont et al., 2007; Hinz & Linke, 1998; Lemay et al., 2007; Sharpe et al., 2001; Zhang et al., 2007.

Table 2. GHG emission factors for swine confined buildings (adapted from Hamelin et al., 2009)

Overall, sows produce more CO_2 on an animal basis (5,29 kg d^{-1} $animal^{-1}$) than weanling piglets (0,55 kg d^{-1} $animal^{-1}$) or grower/finisher pigs (1,92 kg d^{-1} $animal^{-1}$) since the CO_2 production increases as the animal weight grows. In fact, the emission ratios between two growing stages correspond approximately to the animal unit ratios.

In the same way, the greater amount of urine and feces excreted by sows favours the establishment of anaerobic conditions and the CH_4 emission (30,1 g d^{-1} $animal^{-1}$) in comparison with the offspring (2,77 and 5,54 g d^{-1} $animal^{-1}$, respectively for weanling piglets and grower/finisher pigs).

N_2O emissions from maternity and nursery were relatively close to zero as found in several studies. Grower/finisher pigs emit 0,66 g N_2O d^{-1} $animal^{-1}$. The non frequent change in protein requirements during the growth stage leads to more N being excreted.

5.2 Poultry production

Broilers are mainly reared on a floor surface covered with bedding. Laying hens can be reared in multiple-deck battery cages, aviary systems, high-rise systems or percheries. In the first case, there is a possibility to dry manure directly under the cages with different manure drying systems. Table 3 presents emission factors from these two types of poultry production confinement buildings.

Production type	Gas	Units	Mean emissions **	Minimum value	Maximum value	Standard deviation
Broiler	CO_2	kg yr^{-1} $bird^{-1}$	31,5	31,5	31,5	-
	CH_4	g yr^{-1} $bird^{-1}$	12,3	8,3	20,0	6,7
	N_2O	g yr^{-1} $bird^{-1}$	17,6	4,0	34,2	12,6
	GHG *	kg CO_2-eq. yr^{-1} $bird^{-1}$	5,71	-	-	-
Layer	CO_2	kg yr^{-1} hen^{-1}	28,2	12,6	37,8	2,87
	CH_4	g yr^{-1} hen^{-1}	44,7	4,0	80,0	18,7
	N_2O	g yr^{-1} hen^{-1}	10,9	0,63	30,0	11,3
	GHG *	kg CO_2-eq. yr^{-1} hen^{-1}	4,32	-	-	-

* Total greenhouse gas emissions calculated on a CO_2-equivalent basis considering the mean emissions and the global warming potential of CH_4 (21) and N_2O (310).
** References: Chadwick et al., 1999; EPA, 2001; Fabbri et al., 2007; Fournel, 2011; Groot Koerkamp & Uenk, 1997; Hörnig et al., 2001; Monteny et al., 2001; Neser et al., 1997, as cited in Jungbluth et al., 2001; Sneath et al., 1996, as cited in Jungbluth et al., 2001; Wathes et al., 1997; Wu-Haan et al., 2007.

Table 3. GHG emission factors for broiler and layer confinement buildings

Broiler and layer productions emit similar quantities of CO_2 to the atmosphere (31,5 and 28,2 kg yr^{-1} $head^{-1}$, respectively). However, the different layer systems using liquid manure management generate a greater emission factor for CH_4 (44,7 g yr^{-1} $head^{-1}$) comparatively to broiler systems with litter (12,3 g yr^{-1} $head^{-1}$). On the other hand, litter increases the succession of nitrification and denitrification phases which result in greater N_2O emissions (17,6 g yr^{-1} $head^{-1}$ vs. 10,9 g yr^{-1} $head^{-1}$).

6. Mitigation techniques

6.1 In animal production

Several technologies have been developed to reduce gas and odour emissions from livestock housing. Several of these techniques, including reduction efficiencies for each technology, were inventoried by Godbout et al. (2010) from an exhaustive literature review. The inventory revealed that progress has been made in reducing odour and ammonia emissions, while less concern has been placed on GHG emissions. Three distinct techniques have been recognized, namely under slat separation, air cleaning and nutrient management.

6.2 In-barn manure management: under-slat separation

Separating urine and feces beneath the slats and removing both the solid and liquid fractions frequently is a reliable manure management technique to reduce gas and odour

emissions from buildings (Andersson, 1995; Arogo et al., 2001; Bernard et al., 2003; Jongebreur, 1981). The aim of this technique is to separate solid and liquid phases of the manure immediately after it falls through the slats to reduce the contact time between both phases. Three major under-slat manure separation systems have been studied over the years: the conveyor net, the V-shape scraper and the conveyor belt.

The conveyor net is composed of a mesh, tensioned under the slats, through which urine can flow while feces are collected. When this separation system is mechanized, the conveyor scrapes the feces to the end of the building while the urine stays in a gutter that is sloped toward a conventional storage pit (Fig. 8a).

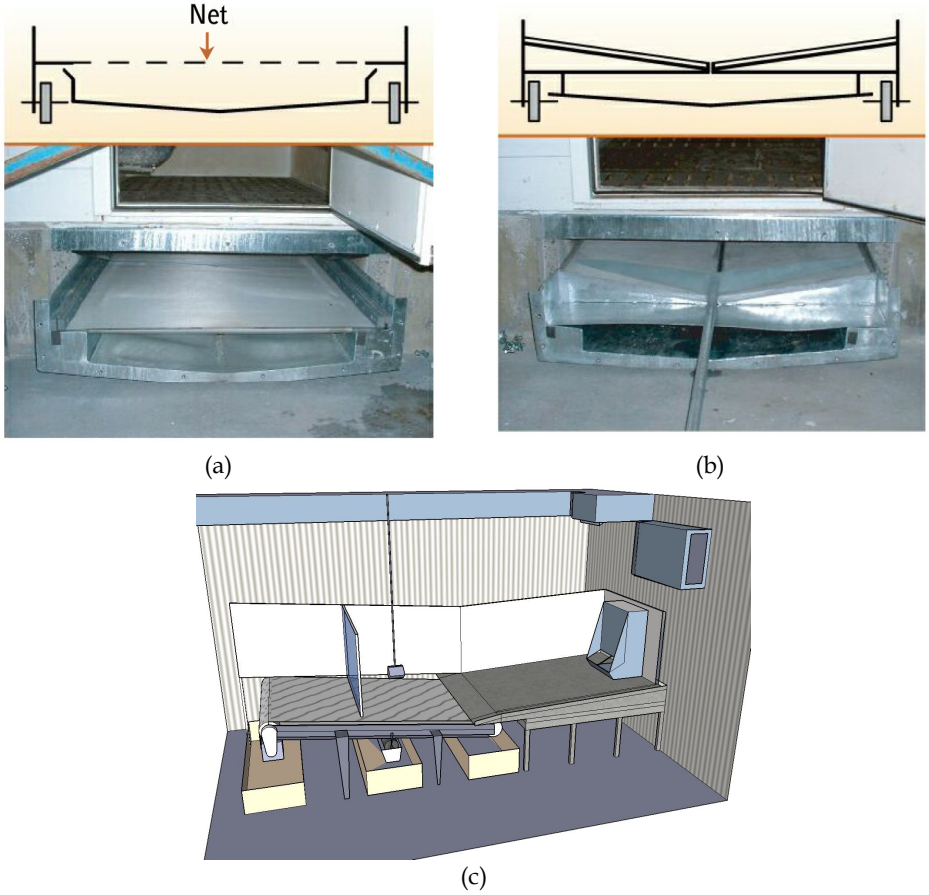

Fig. 8. a) Conveyor net (Lemay et al., 2007); b) V-shape scraper (Lemay et al., 2007); c) Diagram of the conveyor belt (adapted from Lemay et al., 2007)

In V-shaped scrapers (Fig. 8b), the feces stay on inclined gutter walls while urine is gathered into the bottom of the gutter and continuously drains out of the room by gravity. The solid fraction remaining on the inclined walls is scraped at a certain frequency using mechanically driven scrapers. Godbout et al. (2010) measured CO_2 and CH_4 emissions from a V-shaped scraper and compared these to a pull-plug system (emptied every week). However, even if emission reductions were observed, there were no statistical differences.

Conveyor belts (Fig. 8c) were adapted from poultry to swine production, placing the belt at an angle under the slatted portion of the pens. Its lower edge feeds into a pipe that collects the urine and transports it to the end of the building, thus allowing the separate collection of urine and feces within the hog house (van Kempen et al., 2003). Koger et al. (2003) founded that CH_4 emission from a belt-based housing were reduced between 52 and 83% throughout the grower period studied comparatively to conventional pig houses.

Most of studies evaluating these techniques have been mainly conducted in order to measure the reduction of NH_3 emissions (Voermans and van Asseldonk, 1990; Voermans and van Poppel, 1993; Hendriks and van de Weerdhof, 1999). The study carried out by Belzile et al. (2006) found 13% and 19% CO_2 and CH_4 emission reduction, respectively, from a conveyor net compared to a drainage system without separation (emptied once a week). The same gas reduction values could be expected from the other separation techniques since they use the same principle.

6.3 Air cleaning

Air cleaning techniques for livestock buildings have the potential to improve air quality. However, efforts have been focused for improving performances on the reduction of dust and the abatement of NH_3 and H_2S. The air cleaning techniques are classified into two broad categories, physicochemical treatment and biological treatment (Godbout et al., 2010).

The physical - chemical absorption (scrubbing) is the physicochemical method most widely used for the treatment of air. This is a technology developed for many industrial applications. Gases are absorbed when the air from the barn is in contact with a liquid in which gas become soluble within the solution. The mass transfer from gas to the liquid is achieved by using a filter material within the filter unit (Devinny et al., 1999). The filter material usually has a large porosity, or void volume, and a large specific area (Melse & Ogink, 2005). Water is often used as the liquid solvent and its pH can be adjusted (basic or acid) depending on the pollutant to increase the solubility of gases. Contaminated air is introduced, either horizontally (crosscurrent) or upwards (counter-current), resulting in good contact between air and water, and enabling mass transfer from gas to liquid phase. A fraction of the trickling water is continuously recirculated; another fraction is discharged and replaced by fresh water (Fig. 9) (Melse & Ogink, 2005).

On the other hand, a biological treatment of air is based on the capacity of microorganisms to transform organic and inorganic pollutants into non-toxic compounds and odour free (Devinny et al., 1999; Hartung et al., 2001; Revah & Morgan-Segastume, 2005). Three main types of bioreactors are currently used: biofilters, biotrickling filters and bioscrubbers (Fig. 10). The basic mechanism is the same for all biological treatment systems; the difference is

due to the equipment configuration to carry out the transfer between the gas and the liquid, and on the pollutant biodegradation process (Table 4) (Devinny et al. 1999; Revah & Morgan-Segastume, 2005). Removal efficiency for NH_3 and H_2S emissions with a biological treatment can range from 6 to 100% and 3 to 99%, respectively (Nicolai & Janni 2001; Armeen, 2008; Iranpour et al., 2005). The reduction of odour emission is also widely variable, going from 29 to 100% depending of the operation conditions (Luo, 2001). A first bioreactor prototype developed by Belzile et al. (2010) found that NH_3 emissions from small-scale swine chambers were reduced by 62 to 91% and H_2S emissions were decreased by 24 to 66% by the biological treatment compared to a drainage system without separation (emptied once a week). However no significant reduction was obtained for CO_2 and CH_4 emissions at this first stage.

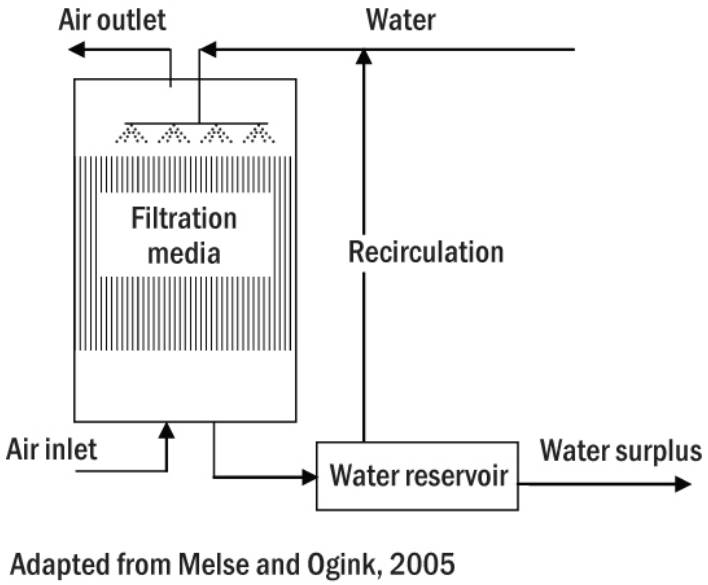

Fig. 9. A counter-current air scrubber (adapted from Melse & Ogink, 2005)

The discharged water from a scrubber might be used as nitrogen fertilizer for crops; sometimes the water is added to the liquid manure storage (Melse et al., 2009). The discharge water from a biotrickling filter might be treated in a denitrification process in order to decrease the nitrogen content (Melse et al., 2009; Sakuma et al., 2008).

Reactor	Microorganisms	Liquid phase
Biofilter	Fixed	Stationary
Biotrickling filter	Fixed	Flowing
Bioscrubber	Suspended	Flowing

Table 4. Classification of biological reactors for air treatment

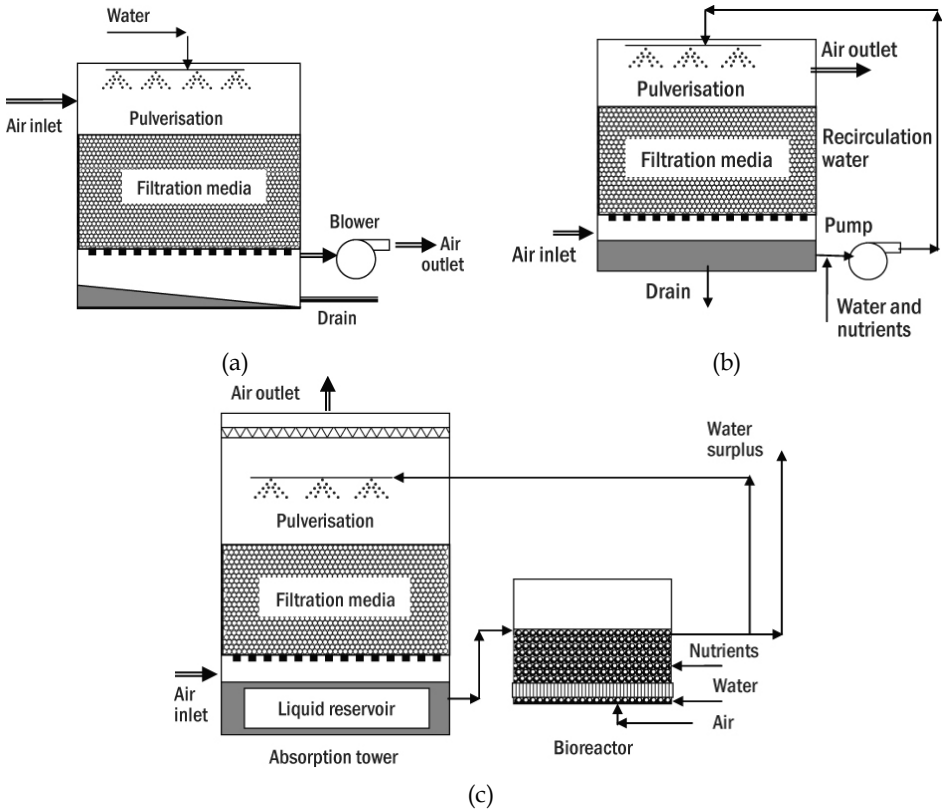

Fig. 10. a) Diagram of a closed biofilter system (adapted from Devinny et al., 1999);
b) Diagram of a biotrickling filter (adapted from Revah & Morgan-Segastume, 2005);
c) Diagram of a bioscrubber (adapted from Revah & Morgan-Segastume, 2005).

6.4 Nutrient management

An additional method to reduce emissions caused by excess nitrogen is the alteration of the ratio of nitrogen excretion in urine versus feces by nutrient management (Mroz et al., 1993). Reduction of dietary protein combined with supplementation of synthetic amino acids in pig diets might reduce total nitrogen excretion by 25 to 40% (Hartung & Phillips, 1994; Kay & Lee, 1997). Additionally, the inclusion of fermentable carbohydrates or non-starch polysaccharides into diets stimulates bacterial fermentation in the hindgut and reduced urinary versus fecal nitrogen ratio by 68% (Canh et al., 1997a).

However, GHG emission reduction is generally not measured or documented when using nutrient management. Principally, studies target reducing NH_3 and other odorant compound emissions (Garry et al., 2007; Le et al., 2006; Lyngbye et al., 2006). GHG emissions measurements (CO_2, CH_4 and N_2O) were carried out by Godbout et al. (2010) when protein content is reduced and lysine is increased in the diet. As a result, such diet treatment presented no impact on CO_2 and N_2O emissions while CH_4 emissions increased by 58% compared to a commercial diet. Therefore, a more thorough analysis should be carried out for a better understanding of dietary management in GHG emission reduction.

7. Summary and conclusions

Contaminants exhausted from confined animal buildings include various gases, dust particles, micro-organisms and odours. The most important gases are CO_2, NH_3, H_2S, CH_4, N_2O and some trace gases (aldehydes, amines, aromatics, organic acids, sulphur compounds, etc.). The main GHG emitted from livestock building are CH_4, N_2O (from manure decomposition) and CO_2 (from animal metabolism). Generally, CH_4 emissions are more present in liquid manure management while N_2O is produced under solid manure management.

The emission is the product of the gas concentration and the air exchange rate. An accurate measurement of these values is very important and is still a challenge today for emissions from agricultural sources. Since the agricultural emissions are very low, the concentration measurement requires equipment having great sensitivity and selectivity like those utilizing optical properties of gas such as FTIR, PAS and NDIR or separation techniques like chromatography with selective detectors. Most of the gases in air which are mainly composed of N_2, O_2 and Ar with several others gases in trace concentrations like CO_2, CH_4 and N_2O can be separated by chromatography and detected by different detectors more or less specific to the target gas. The technique is simple, proven and allows the simultaneous quantification of CO_2, CH_4 and N_2O. Compared to other techniques having the required sensitivity, like modern spectroscopic techniques, gas chromatography is known to produce reliable results and can be envisaged as moderate to low cost techniques with easy apparatus implementation.

The air flow measurement is very important and often, a lot of uncertainty is related to this value bringing an error in the emission determination. The measurement techniques are function of the ventilation system. Three main systems exist: MV, NV and HV buildings. Various methods have been developed to measure ventilation rate from animal housing facilities including airborne tracer techniques, diffusion of animal-produced CO_2 or heat, vane anemometers and orifice plates. Each of these methods, however, has limitations.

In the case where is not possible to measure emissions, values from literature can be used for swine, broiler and layer productions. The typical CO_2 emissions for sows, weanling piglets and grower/finisher pigs are 5,29, 0,55 and 1,92 kg d^{-1} $animal^{-1}$, respectively. The greater amount of urine and faeces excreted by sows favours the establishment of anaerobic conditions and the CH_4 emissions (30,1 g d^{-1} $animal^{-1}$) in comparison with the offspring (2,77 and 5,54 g d^{-1} $animal^{-1}$, respectively for weanling piglets and grower/finisher pigs). N_2O emissions from maternity and nursery were relatively close to zero as found in several studies. Grower / finisher pigs emit 0,66 g N_2O d^{-1} $animal^{-1}$. Broiler and layer productions emit similar quantities of CO_2 to the atmosphere (31,5 and 28,2 kg yr^{-1} $animal^{-1}$, respectively). However, the different layer systems using liquid manure management generate a greater emission factor for CH_4 (44,7 g yr^{-1} $animal^{-1}$) comparatively to broiler systems with litter (12,3 g yr^{-1} $animal^{-1}$). The N_2O emissions range from 10,9 to 17,6 g yr^{-1} $head^{-1}$. However, since the gas emissions are influenced by many factors, on-site measurement should be privileged instead of typical values from literature to determine the typical emissions from building.

Several technologies have been developed to reduce odour and gas emissions from swine housing. Two in-barn approaches are encouraging: the under slat separation system and diet manipulation while air cleaning systems have been developed for the exhaust air outlet. In agreement with the literature, the under slat separation system can reduce around 13% and 19% of CO_2 and CH_4 emissions, respectively. No studies have reported GHG emission reductions using diet manipulation. Many types of air cleaning systems already exist and they have been developed mainly for odour and ammonia emission reductions and the effect on GHG is not clearly shown.

8. Acknowledgments

The authors wish to acknowledge P. Brassard and M. Girard for their contributions to this chapter.

9. References

Andersson, M. (1995). *The Effect of Different Manuring Systems on Ammonia Emissions in Pig Buildings. A Comparing Study between Scrapers Under Slatted Floors and Rubber Mats Under Slatted Floors*, Report 100, Lund, Swedish University of Agricultural Sciences, Department of Agricultural Biosystems and technology

Armeen, A.; Feddes, J. J. R.; Leonard, J. J., & Coleman, R. N. (2008). Biofilters to Treat Swine Facility Air: Part 1. Nitrogen Mass Balance. *Canadian Biosystems Engineering*, Vol.50, No.6, pp. 21-28

Arnold, S. L.; Parkin, T. B.; Doran, J. W.; Eghball, B. & Mosier, A. R. (2001). Automated Gas Sampling System for Laboratory Analysis of CH_4 and N_2O. *Communications in Soil Science and Plant Analysis*, Vol.32, No.17&18, pp. 2795–2807

Arogo, J.; Westerman, P.W.; Heber, A.J.; Robarge, W.P. & Classen, J.J. (2001). Ammonia in Animal Production –A Review, *ASAE Annual International Meeting*, Paper No 01-4089, Sacramento, California, USA, July 30-August 1, 2001

ASABE. (2010). *Psychrometric Data*, American Society of Agricultural and Biological Engineers,ASAE Standard D271.2 APR1976 (R2010)

ASHRAE. (1992). *Standard Methods for Laboratory Airflow Measurement*, American Society of Heating, Refrigerating and Air-Conditioning Engineers, inc., ANSI/ASHRAE 41.2-1987 (RA 92), ISSN 1041-2336, Atlanta, Georgia, USA

Barrington, S. (1999). Comment se fait-il que les gaz des fumiers liquides soient tellement nauséabonds? [Why Do Gases from Liquid Manure Stink So Much?]. *Le producteur de lait québécois*, Vol.20, No.3, pp. 41-45

Barber, E.M. ; Strom, J.S.; Bantle, M.R.L.; Morsing, S. & Feddes, J.J.R. (1994). Ventilation Performance Standards – Applying Danish Experience in Canada. *Applied Engineering in Agriculture*, Vol.10, No.3, pp. 395-401

Belzile, M.; Lemay, S.P.; Zegan, D.; Feddes, J.J.R.; Godbout, S.; Larouche, J.-P.; & Martel, M. (2010). Reduction of Gas and Odour Emissions from a Swine Building Using a Biotrickling Filter, *XVIIth World Congress of the International Commission of Agricultural Engineering*, Québec City, Québec, Canada, June 13-17, 2010

Belzile, M.; Godbout, S. ; Lemay, S.P. ; Lavoie, J. ; Lachance, I. & Pouliot, F. (2006). Impact de la séparation fèces-urine sous caillebotis sur la qualité de l'air ambiant en porcherie [Impact of the Separation of Feces and Urine Under the Slats on the Quality of Ambient Air in Swine Buildings]. *Journées Recherche Porcine*, Vol.38, pp. 21-26.

Belzile, M.; Lemay, S.P.; Godbout, S.; Côté, C. & Lavoie, J. (2006). Gas Concentrations and Emissions in Milk-Fed Calf Buildings, *CSBE/SCGAB 2006 Annual Conference*, July 16-19, 2006

Bernard, C. ; Côté, D. ; Giroux, M. ; Grégoire, R. ; Joncas, R. & Martin, D.-Y. (2003). Mémoire de l'Institut de recherche et de développement en agroenvironnement inc. [Report of the Research and Development Institute for the Agri-Environment inc.]. In: *Commission sur le développement durable de la production porcine au Québec*, April 16, 2003

Blackmer, A.M. & Bremner, J.M. (1977). Gas Chromatographic Analysis of Soil Atmospheres. *Soil Science Society of American Journal*, Vol.41, pp. 908-912

Blanes-Vidal, V.; Hansen, M.N.; Pedersen, S. & Rom, H.B. (2008). Emissions of Ammonia, Methane and Nitrous Oxide from Pig Houses and Slurry: Effects of Rooting Material, Animal Activity and Ventilation Flow. *Agriculture, Ecosystems and Environment*, Vol.124, pp. 237-244

Brasseur, G.P.; Orlando, J.J. & Tyndall, G.S., (Ed.). (1999). *Atmospheric Chemistry and Global Change*. Oxford University Press, New York. In: Cabaraux, J.F.; Philippe, F.X.; Laitat, M.; Canart, B.; Vandenheede, M. & Nicks, B. (2008). Gaseous Emissions from Weaned Pigs Raised on Different Floor Systems. *Agriculture, Ecosystems and Environment*, Vol.130, pp. 86-92

Canh, T.T.; Verstegen, M.W.A.; Aarnink, A.J.A. & Schrama, J.W. (1997). Influence of Dietary Factors on Nitrogen Partitioning and Compositions of Urine and Feces of Fattening Pigs. *Journal of Animal Science*, Vol.75, pp. 700-706

Chadwick, D.R.; Sneath, R.W., Phillips, V.R. & Pain, B.F. (1999). A UK Inventory of Nitrous Oxide Emissions from Farmed Livestock. *Atmospheric Environment*, Vol.33, No.20, pp. 3345-3354

Choiniere, Y.; Blais, F. & Munroe, J.A. (1988). A Wind Tunnel Study of Airflow Patterns in a Naturally Ventilated Building. *Canadian Agricultural Engineering*, Vol.30, No.2, pp. 293-297

CIGR. (2002). *4th Report of Working Group on Climatization of Animal Houses – Heat and Moisture Production at Animal and House Levels,* International Commission of Agricultural Engineering, Section II, Horsens, Denmark

Clark, O.G.; Segura, J.C.; Feddes, J.J.R. & Ouellette, C. (2008). Multiport Averaging Pitot Tube to Measure Airflow Rates from Exhaust Fans. *Canadian Biosystems Engineering*, Vol.50, pp. 5.1-5.7

Cowper, C.J. & DeRose, A.J. (1983). The Analysis of Gases by Chromatography. Pergamon Series in Analytical Chemistry, Volume 7, Pergamon Press Ltd., United Kingdom

de la Farge, B. (1978). Les déchets de l'élevage porcin : traitement – valorisation [Swine Production Wastes: Treatment – Valorization]. Ph.D thesis, Université Paul Sabatier, Toulouse, France

Devinny, J. S.; Deshusses, M. A. & Webster, T. S. (1999). *Biofiltration for Air Pollution Control*, Lewis Publishers, Washington, DC, USA

EPA. (2001). *Emissions from Animal Feeding Operations*. Environmental Protection Agency, Draft Report No. 68-D6-0011. Research Triangle Park, North Carolina: Emission Standards Division, Office of air quality planning and standards

Fabbri, C.; Valli, L., Guarino, M., Costa, A. & Mazzotta, V. (2007). Ammonia, Methane, Nitrous Oxide and Particulate Matter Emissions from Two Different Buildings for Laying Hens. *Biosystems Engineering*, Vol.97, pp. 441-455

Feddes, J.J.R. & J.B. McQuitty. (1980). Design of an Air-Speed Sensor System. *Canadian Agricultural Engineering*, Vol.22, No.1, pp. 97-99

Feddes, J.J.R.; Leonard, J.J. & McQuitty, J.B. (1984). Carbon Dioxide Concentration As a Measure of Air Exchange in Animal Housing. *Canadian Agricultural Engineering*, Vol.26, No.1, p. 53-56

Fournel, S. (2011). *Étude comparative des émissions de gaz et d'odeurs issues de différents systèmes de gestion des déjections en production d'œufs de consommation* [Comparative Study of Gas and Odour Emissions from Different Manure Management Systems in Egg Production], M.Sc. thesis, Université Laval, Québec City, Québec, Canada

Gallmann, E. & Hartung, E. (2000). Evaluation of the Emission Rates of Ammonia and Greenhouse Gases from Swine Housings, *Proceedings of the 2nd International Conference on Air Pollution from Agricultural Operations*, pp. 92-99, Des Moines, Iowa, USA

Gallmann, E.; Hartung, E. & Jungbluth, T. (2003). Long-Term Study Regarding the Emission Rates of Ammonia and Greenhouse Gases from Different Housing Systems for Fattening Pigs – Final Results, *Proceedings of the International Symposium on Gaseous and odour emissions from animal production facilities*, pp. 122-130, Horsens, Denmark, June 1-4, 2003

Garry, B.P.; Fogarty, M.; Curran, T.P. & O'Doherty, J.V. (2007). The Effect of Cereal Type and Exogenous Enzyme Supplementation in Pig Diets on Performance, Odour and Ammonia Emissions from Finisher Pigs. *Livestock Science*, Vol.109, pp. 212–215

Guarino, M.; Fabbri, C., Navarotto, P., Valli, L., Moscatelli, G., Rossetti, M. & Mazotta, V. (2003). Ammonia, Methane and Nitrous Oxide Emissions and Particulate Matter Concentrations in Two Different Buildings for Fattening Pigs, *Proceedings of the International Symposium on Gaseous and odour emissions from animal production facilities*, pp. 140-149, Horsens, Denmark, June 1-4, 2003

Godbout, S.; Lemay, S.P.; Pelletier, F.; Belzile, M.; Larouche, J.P.; Tamini, L.D.; Palacios, J. H. & Zegan, D. (2010). *Réduction des émissions gazeuses et odorantes aux bâtiments porcins : techniques simples et efficaces applicables à la ferme* [Gas and Odour Emission Reductions in Swine Barns: Simple and Effective Techniques Applicable at the Farm], Final Report, Québec City, Québec, Canada: Research and Development Institute for the Agri-Environment inc.

Godbout, S.; Belzile, M., Lachance, I., Lemay, S.P., Turgeon, M.J., Dufour, V., Pouliot, F. & Marquis, A. (2006). *Évaluation technico-économique d'un système de séparation solide/liquide des déjections à la source dans un bâtiment porcin et les impacts sur l'environnement – Volet II* [Technico-Economical Assessment of an In-Barn Solid/Liquid Separation System for Pig Slurry and Impacts on the Environment – Phase II], Final Report, Québec City, Québec, Canada: Research and Development Institute for the Agri-Environment inc.

Godbout, S.; Lavoie, J.; Lemay, S.P.; Lachance, I.; Pouliot, F. & Belzile, M. (2005). Impact of In-Barn Manure Separation on the Biological Air Quality of Swine Buildings, *ASAE Annual International Meeting*, Paper No. 055018, Tampa, Florida, USA

Godbout, S.; Laguë, C., Lemay, S.P., Marquis, A. & Fonstad, T.A. (2003). Greenhouse Gas and Odour from Swine Operations Under Liquid Manure Management in Canada, *Proceedings of the International Symposium on Gaseous and odour emissions from animal production facilities*, pp. 426-443, Horsens, Denmark, June 1-4, 2003

Groot Koerkamp, P.W.G. & Uenk, G.H. (1997). Climatic Conditions and Aerial Pollutants in and Emissions from Commercial Animal Production Systems in the Netherlands, *Proceedings of the International Symposium of Ammonia and Odour Control from Animal Production Facilities*, pp. 139-144, AB Rosmalen : Netherlands

Guimont, H.; Dufour, V. ; Pelletier, F. ; Coulibaly, A. ; Giguère, C. ; Godbout, S. ; Lemay, S.P. ; Massé, D.I. ; Pouliot, F. & Fortin, N. (2007). Évaluation technique et économique d'un système d'isolement des fèces avec grattes en « V » dans un engraissement commercial. [Technical and Economical Assessment of a « V » Scraper System for Isolation of Feaces in a Commercial Fattening Barn], Rapport final [Final Report], Québec City, Québec, Canada : CDPQ, IRDA, La Coop fédérée & AAC

Hamelin, L.; Pelletier, F. & Godbout, S. (2007). Impacts environnementaux, économiques et sociaux des différentes chaînes de gestion des déjections des poules pondeuses [Environmental, Economical and Social Impacts of Different Manure Management Systems in Layer Production], Final Report, Québec City, Québec, Canada: Research and Development Institute for the Agri-Environment inc.

Hartung, J. & Phillips, V.R. (1994). Control of Gaseous Emissions from Livestock Buildings and Manure Stores. *Journal of Agricultural Engineering Research*, Vol.57, No.3, pp. 173-189

Heber, A.; Lim, T.; Ni, J.; Grant, R. & Sutton, A. (2000). *Development of a Site-Specific Odor Impact Distance Guideline for Swine Production Systems*, Report No. 98-131. Washington, DC: National Pork Producers Council

Heinemeyer, O. & Kaiser, E.A. (1996). Automated Gas Injector System for Gas Chromatography: Atmospheric Nitrous Oxide Analysis. *Soil Science Society of American Journal*, Vol.60, pp. 808-811

Hendriks, H.J.M & van de Weerdhof, A.M. (1999). *Dutch Notes on Bat for Pig- and Poultry Intensive Livestock Farming*. Draft published by Ministery of Housing, Spatial Planning and the Environment et Ministery of Agriculture, Nature Management and Fisheries, The Netherlands

Hinz, T. & Linke, S. (1998). A Comprehensive Experimental Study of Aerial Pollutants in and Emissions from Livestock Buildings – Part 2: Results. *Journal of Agricultural Engineering Research*, Vol.70, pp. 119-129

Hörnig, G.; Brunsch, R., Stollberg, U., Jelínek, A., Plíva, P. & Češpiva, M. (2001). Ammonia, Methane and Carbon Dioxide Emissions from Laying Hens Kept in Battery Cages and Aviary Systems, *Proceedings of the 2nd Agricultural Engineering Conference of Central and East European Countries*, pp. 37-43, Prague, Czech Republic, 23-24 October, 2001

Houghton, J.T.; Meira Filho, L.G.; Callander, B.A.; Harris, N.; Kattenberg, A. & Maskel, K., (Ed). (1995). *IPCC Second Assessment Report: Climate Change 1995*, 572 pp., Cambridge University Press

Iranpour, R.; Cox, H.H.J.; Deshusses M.A. & Schroeder, E.D. (2005). Literature Review of Air Pollution Control Biofilters and Biotrickling Filters for Odor and Volatile Organic Compound Removal. *Environmental Progress*, Vol.24, No.3, pp. 254-267

ITP. (1998). Odeurs et environnement – Cas de la production porcine [Odours and Environment – Swine Production Case]. Institut technique du porc, Paris, France

Jiang, X.; Ku, W.L.; Shia, R.L.; Li, Q.; Elkins, J.W.; Prinn, R.G. & Yung, Y.L. (2007). Seasonal Cycle of N_2O: Analysis of Data. *Global Biogeochemical Cycles*, Vol.21, doi:10.1029/2006GB002691

Jongebreur, A.A. (1981). *Housing System and Their Influence on the Environment. Environmental Aspects of Housing for Animal Production*, pp. 431-436, Butterworths, London, UK

Jungbluth, T.; Hartung, E. & Brose, G. (2001). Greenhouse Gas Emissions from Animal Houses and Manure Stores. *Nutrient Cycling in Agroecosystems*, Vol.60, pp. 133-145

Kay, R.M. & Lee, P.A. (1997). Ammonia Emission from Pig Buildings and Characteristics of Slurry Produced by Pigs Offered Low Crude Protein Diets, *Proceedings of the International Symposium on Ammonia and Odour Control from Animal Production Facilities*, pp. 253-260, CIGR and EurAgEng publication, Rosmalen, The Netherlands

Koger, J.B.; Kaspers, B.A.; Burnette, R.P.; van Kempen, M.H.J.G. & van Kempen, T.A.T.G. (2003). *Manure Belts for Harvesting Urine and Feces Separately and Improving Air Quality in Swine Facilities*. Report to the Smithfield Panel, Raleigh, North Carolina, USA, 21 May, 2003

Le, P.D.; Aarnink, A.J.A.; Jongbloed, A.W.; van der Peet Schwering, C.M.C.; Ogink, N.W.M. & Verstegen, M.W.A. (2006). Effects of Crystalline Amino Acid Supplementation to the Diet on Odor from Pig Manure. *Journal Animal Science*, Vol.85, pp. 791–801

Lemay, S.P.; Godbout, S., Bergeron, R., Belzile, M., Predicala, B., Laguë,C., Marquis, A., Pouliot, F. & Rondeau, F. (2007). *Développement d'un nouveau concept d'enclos pour élevages porcins "sans lattes" permettant de séparer les déjections et de réduire les émissions gazeuses et odorants* [Development of a New Pen Concept Without Slats Allowing to Separate Slurry Phases and Reduce Gaseous and Odorant Emissions for Pig Production], Final Report, Québec City, Québec, Canada: Research and Development Institute for the Agri-Environment inc.

Leonard, J.J.; Feddes, J.J.R. & McQuitty, J.B. (1984). Measurement of VR Using a Tracer Gas. *Canadian Agricultural Engineering*, Vol.26, No.1, pp. 49-51

Loftfield, N.; Flessa, H.; Augustin, J. & Beese, F. (1997). Automated Gas Chromatographic System for Rapid Analysis of the Atmospheric Trace Gases Methane, Carbon Dioxide, and Nitrous Oxide. *Journal of Environmental Quality*, Vol.26 pp. 560-564

Luo, J. (2001). A Pilot-Scale Study on Biofilters for Controlling Animal Rendering Process Odours. *Water Science and Technology*, Vol.44, No.9, pp. 277-285

Lyngbye, M.; Hansen, M.J.; Riis, A.L.; Jensen, T.L. & Sørensen, G. (2006). 1000 Olfactometry Analyses and 100 TD-GC/MS Analyses to Evaluate Methods for Reducing Odour from Finishing Units in Denmark, *Workshop on Agricultural Air Quality*, Washington, D.C., USA

Melse, R.W.; Ogink, N.W.M. & Rulkens, W.H. (2009). Air Treatment Techniques for Abatement of Emissions from Intensive Livestock Production. *The Open Agriculture Journal*, Vol.3, pp. 6-12

Monteny, G.J.; Groenestein, C.M. & Hilhorst, M.A. (2001). Interactions and Coupling between Emissions of Methane and Nitrous Oxide from Animal Husbandry. *Nutrient Cycling in Agroecosystems*, Vol.60, pp. 123–132

Morsing, S.; Ikeguchi, A.; Bennetsen, J.C.;. Strøm, J.S; Ravn, P. & Okushima, L. (2002). Wind Induced Isothermal Airflow Patterns in a Scale Model of a Naturally Ventilated Swine Barn with Cathedral Ceiling. *Applied Engineering in Agriculture*, Vol.18, No.1, pp. 97-101

Mosier, A. R. & Mack, L. (1980). Gas Chromatographic System for Precise, Rapid Analysis of Nitrous Oxide. *Soil Science Society of American Journal*, Vol.44, pp. 1121-1123

Mroz, Z.; Jongbloed, A.W.; Beers, S.; Kemme, P.A.; de Jonge, L.; van Berkum, A.K. & van der Lee, R.A. (1993). Preliminary Studies on Excretory Patterns of Nitrogen and Anaerobic Deterioration of Faecal Protein from Pigs Fed Various Carbohydrates. In: *Nitrogen Flow in Pig Production and Environmental Consequences*, Verstegen, M.W.A.; den Hartog, L.A.; van Kempen, G.J.M. & Metz, J.H.M., (Ed.), 247-252, Pudoc Scientific Publishers, Wageningen, The Netherlands

Nääs, I.A.; Moura, D.J.; Bucklin, R.A. & Fialho, F.B. (1998). An Algortithm for Determining Opening Effectiveness in Natural Ventilation by Wind. *Transactions of the ASAE*, Vol.41, No.3, pp. 767-771

Neftel, A.; Fischer, C. & Flechard, C. (2006). Measurements of Greenhouse Gas Fluxes from Agriculture. *International Congress Series*, vol.1293, pp. 3-12

Nicolai, R.E. & Janni, K.A. (2001). Biofilter Media Mixture Ratio of Wood Chips and Compost Treating Swine Odors, Department of Biosystems and Agricultural Engineering, University of Minnesota, USA

Olsen, K.; Wellisch, M.; Boileau, P.; Blain, D.; Ha, C.; Henderson, L.; Liang, C.; McCarthy, J. & McKibbon, S. (2003). *Canada's Greenhouse Gas Inventory: 1999-2001*, Greenhouse Gas Division, Environment Canada, 205 pp.

O'Neill, D.H. & Phillips, V.R. (1992). A Review of the Control of Odour Nuisance from Livestock Buildings. Part 3. Properties of the Odorous Substances, Which Have Been Identified in Livestock Wastes or in the Air Around Them. *Journal of Agricultural Engineering Research*, Vol.53, No.1, pp. 23-50

Philippe, F.X.; Laitat, M.; Canart, B.; Vandenheede, M. & Nicks, B. (2007). Comparison of Ammonia and Greenhouse Gas Emissions Furing the Fattening of Pigs, Kept Either on Fully Slatted Floor or on Deep Litter. *Livestock Science*, Vol.111, pp. 144-152

Phillips, M.P.; Sievers, R.E.; Goldan, P.D.; Kuster, W.C. & Fehsenfeld, F.C. (1979). Enhancement of Electron Capture Detector Sensitivity to Nonelectron Attaching Compounds by Addition of Nitrous Oxide to the Carrier Gas. *Analytical Chemistry*, Vol.51, pp. 1819-1825

Revah, S. & Morgan-Sagastume, J.M. (2005). Methods of Odor and VOC Control. In: *Biotechnology for Odour and Air Pollution Control*, Shareefdeen, Z. & Singh, A., (Ed.), Springer, Verlag, Berlin, Heidelberg

Sakuma, T.; Jinsiriwanit, S.; Hattori, T. & Deshusses, M.A. (2008). Removal of Ammonia from Contaminated Air in a Biotrickling Flter – Denitrifying Bioreactor Combination System. *Water research*, Vol.42, pp. 4507–4513

Sharpe, R.R.; Harper, L.A. & Simmons, J.D. (2001). Methane Emissions from Swine Houses in North Carolina. *Chemosphere – Global change science*, Vol.3, pp. 1-6

Sitaula, B.K.; Luo, J. & Bakken, L.R. (1992). Rapid Analysis of Climate Gases by Wide Bore Capillary Gas Chromatography. *Journal of Environmental Quality*, Vol.21, pp. 493-496

Taiganides, E. P. (1987). Animal Waste Management and Wastewater Treatment. In: *World Animal Science B6, Animal Production and Environmental Health*, Strauch (Ed.), Elsevier, Amsterdam, 324 pp.

UGPVB. (1996). Les gaz en élevage porcin: une problématique à dominance ammoniac [Gases in Swine Production: Ammonia Is a Major Case], Union des groupements des producteurs de viande de Bretagne, 67 pp.

van Kempen, T.; Kaspers, B.; Burnette, P.; van Kempen, M. & Koger, J.B. (2003). Swine Housing With A Belt For Separating Urine And Feces; Key To Flexibility. *Swine Housings II Proceedings Conference*, pp. 159-165, Research Triangle Park, North Carolina, USA, 12-15 October, 2003. ASAE Publication Number 701P1303, ed. L.D. Jacobson.

Voermans, J.A.M. & van Asseldonk, M.M.L. (1990). Separation of Pig Manure Under a Slatted Floor. *Proefverslag-Proefstation-voor-de-Varkenshouderij*, No P1.151, 32 pp.

Voermans, J.A.M. & van Poppel, F. (1993). Scraper Systems in Pig Houses. *Proceedings of Livestock environment IV*, pp. 650-656, Coventry, UK, July 6-9, 1993

Wathes, C.M.; Holden, M.R., Sneath, R.W., White, R.P. & Phillips, V.R. (1997). Concentrations and Emissions Rates of Aerial Ammonia, Nitrous Oxide, Methane, Carbon Dioxide, Dust, and Endotoxin in U.K. Broiler and Layer Houses. *British Poultry Science*, Vol.38, No.1, pp. 14-28

Weiss, R.F. (1981). Determinations of Carbon Dioxide and Methane by Dual Catalyst Flame Ionization Chromatography and Nitrous Oxide by Electron Capture Chromatography. *Journal of Chromatographic Science*, Vol.19, p. 611-616

Wu-Haan, W.; Powers, W.J., Angel, C.R., Hale III, C.E. & Applegate, T.J. (2007). Effect of an Acidifying Diet Combined with Zeolite and Slight Protein Reduction on Air Emissions from Laying Hens of Different Ages. *Poultry Science*, Vol.86, pp. 182-190

Zhang, Q.; Zhou, X.J., Cicek, N. & Tenuta, M. (2007). Measurement of Odour and Greenhouse Gas Emissions in Two Swine Farrowing Operations. *Canadian Biosystems Engineering*, Vol.49, pp. 6.13-6.20

6

The Effect of Organic Farms on Global Greenhouse Gas Emissions

Risa Kumazawa
Duquesne University
USA

1. Introduction

The emission of greenhouse gases (GHGs) is a great concern for mankind as it believed that when GHGs such as carbon dioxide (CO_2), nitrous oxide (N_2O), and methane (CH_4), trap energy from the sun, they contribute to global warming. Even though greenhouse gases occur naturally in the atmosphere, there are noteworthy man-made contributions through agricultural and industrial production. Agricultural land itself contributes to 12% of global GHG emissions while emissions from all sectors related to agricultural production contribute to an estimated 25-30% of all GHG emissions (International Trade Centre, 2007). The Kyoto Protocol was established in Kyoto, Japan in December, 1997 as an amendment to the United Nations Framework Convention on Climate Change (UNFCCC) to regulate global GHG emissions. It remains the most comprehensive international agreement to date through the setting of target reductions by industrialized nations in North America, Europe, Asia and Australia, commonly known as "Annex I" countries, shown in Table A-1 of the Appendix.

The emissions of methane, projected to have approximately 20 times the global warming potential of carbon dioxide in trapping heat in the atmosphere (Morgenstern, 1991; Shih et al., 2006; International Trade Centre, 2007; EPA, 2011a) are caused by enteric fermentation and manure management, both of which are strongly correlated with livestock numbers (Vermont & De Cara, 2010), in addition to rice cultivation (McCarl & Schneider, 2000; Nalley et al., 2011). Enteric fermentation is a digestive process where microbes in ruminant animals such as cows, goat and sheep break down food, producing methane as a byproduct. Anaerobic decomposition (without oxygen) of organic matter in livestock manure leads to methane emissions. The U.S. Environmental Protection Agency's website also mentions natural sources of methane such as wetlands, oceans, wildfires as well as man-made sources including landfills (EPA, 2011a).

The emissions of nitrous oxide, projected to be far more potent at about 300 times the global warming potential of carbon dioxide (International Trade Centre, 2007; EPA, 2011b), stem from livestock management (nitrogen content from animal feeds), soil disturbance (both soil loss and degradation), fertilizer/ other chemical use and the burning of agricultural residues (Ruttan, 2002; Flugge & Schilizzi, 2005). The combustion of fossil fuels and microbes in tropical forests are also discussed as sources on the EPA's website (EPA, 2011b).

Carbon dioxide emissions, the least potent GHG in agriculture stem from fuel use (diesel and petrol) to operate heavy machinery and equipment (Flugge & Schilizzi, 2005) and soils

from changes in land use, including deforestation (International Trade Centre, 2007). However, the amount of CO_2 emissions from agriculture alone is trivial (McCarl & Schneider, 2000)[1] even though the total emission of this GHG is the largest compared to the five others (Grunewald & Martinez-Zarozos, 2009).

Table 1 shows the most recent GHG emissions by Annex I status and sector for 2005. These numbers are compiled using World Resources Institute's Climate Analysis Indicators Tool (CAIT, version 8.0) for 39 Annex I countries (including the European Union) and 146 non-Annex I countries. In furnished tables, Malta is erroneously labeled as an Annex I country. It is not certain whether Malta is also counted as an Annex I country in the tool that was used to generate this table. It became a European Union member (with Cyprus) after the protocol was signed but has not changed its non-Annex I status (UNFCCC, 2008).

Sources of GHG Emissions	**All Countries**	**Annex I Countries**	**Non-Annex I Countries**
1) Carbon Dioxide (CO_2) Emissions:			
Energy:			
Electricity & Heat	44.9%	45.1%	44.2%
Manufacturing & Construction	18.9%	14.5%	24.0%
Transportation	19.5%	24.7%	13.5%
Fugitive Emissions	0.7%	0.2%	1.2%
Industrial Processes	4.3%	1.9%	7.0%
2) Methane (CH_4) Emissions:			
Other Fuel Combustion	3.9%	2.4%	4.6%
Fugitive Emissions	24.2%	38.7%	19.5%
Industrial Processes	0.1%	0.3%	0.0%
Agriculture	51.4%	36.6%	57.7%
Waste	20.4%	22.1%	18.2%
3) Nitrous Oxide (N_2O) Emissions:			
Other Fuel Combustion	7.1%	13.6%	4.3%
Industrial Processes	4.8%	9.3%	3.2%
Agriculture	84.7%	72.4%	89.5%
Waste	3.4%	4.7%	3.0%

Table 1. Sources of 2005 GHG Emissions by Sector

While data is available for methane and nitrous oxide emissions solely in agriculture, there is no comparable carbon dioxide emission data specific to the industry. As expected, agricultural CH_4 and N_2O emissions contribute more for non-Annex I countries, those that

[1] The EPA's estimate of agricultural CO_2 emissions for the United States in 1996 was less than 1% of the U.S. total emissions of this GHG.

are not subject to the country-specific reductions outlined in the Kyoto Protocol. The pattern is not clear for agricultural CO_2 emissions which may appear in several of the existing categories shown in Table 1. In addition, the total CO_2 emissions exclude the supplementary data on CO_2 emissions from land-use change and forestry which is only available for 14% of the countries (4 Annex I countries and 22 non-Annex I countries). As a result, I do not analyze agricultural carbon dioxide emissions in this chapter and focus on just agricultural methane and nitrous oxide emissions.

Figure 1 and Figure 2 show agricultural emissions of both methane and nitrous oxide (the left panels are for the total levels and the right panels are for the per capita levels) averaged across Annex I and non-Annex I countries. They are measured in thousand metric tons CO_2 equivalent ($MtCO_2e$) and $MtCO_2e$ respectively. This data is compiled from World Bank's World Development Indicators (WDI) from 1990, available every five years until 2005.

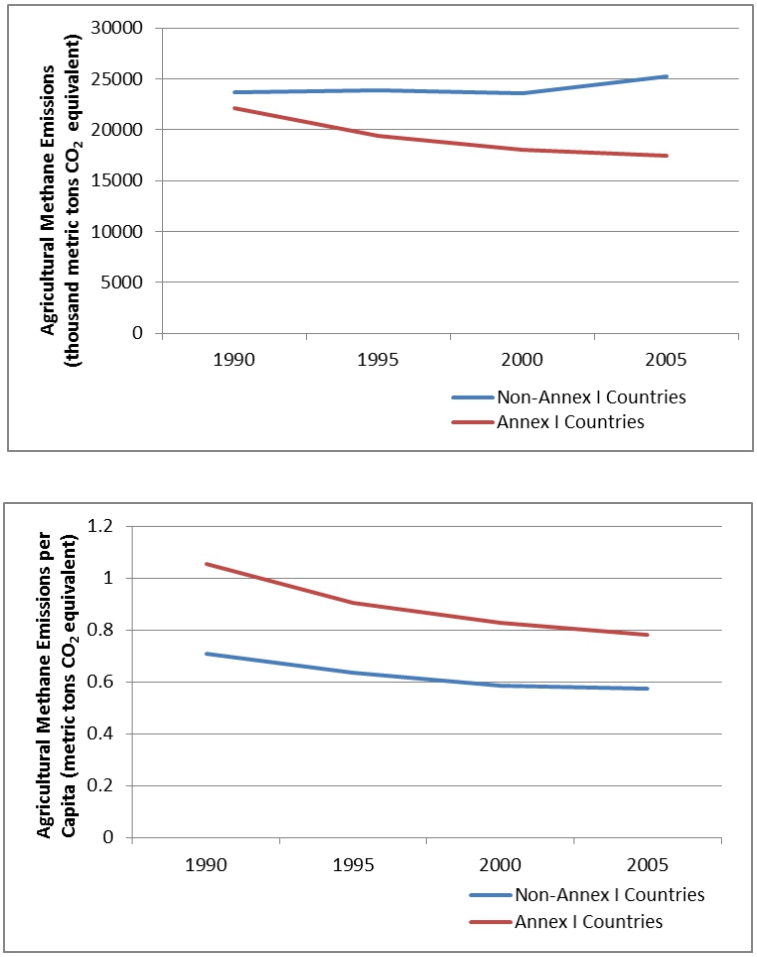

Fig. 1. (a) Agricultural CH_4 Emissions and (b) Agricultural CH_4 Emissions per Capita

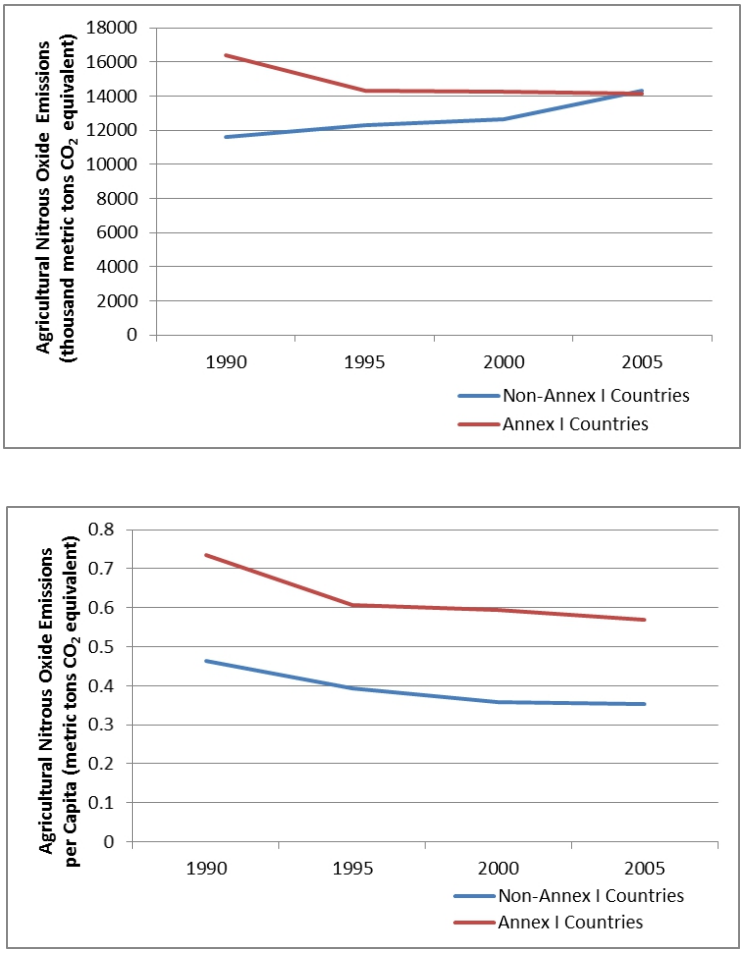

Fig. 2. (a) Agricultural N_2O Emissions and (b) Agricultural N_2O Emissions per Capita

Without controlling for population, both agricultural CH_4 and N_2O emissions increased for just non-Annex I countries. This is not surprising given that one of the world's most heavily populated countries with substantial emissions, China, is in this category. Since the signing of the Kyoto Protocol, Annex I countries have been experiencing declines in the total levels. On a per capita basis, both GHG emissions declined at about the same rate after 1995 even though non-Annex I countries are not subject to target reductions. Roca et al. (2001) argue that the environmental pressure to assimilate is an important consideration for countries.

In recent years, there has been a shift toward organic farm production in Western societies, primarily for promoting better health and for implementing sustainable business practices (Ruiz de Maya et al., 2011). It has been argued that organic farms provide an unintended side benefit of reducing the greenhouse gas emissions (International Trade Centre, 2007). Organic products are defined as, "goods that respect the environment and that are manufactured

without the use of synthetic pesticides, herbicides, chemical fertilizers, growth hormones, antibiotics or gene manipulation" (Chen, 2009). As the Kyoto Protocol is not aimed at reducing the emissions of developing countries, I argue that organic farming practices may have accounted for the reduction of GHGs in only Annex I countries. These are also countries that can afford organic production as such farms tend to operate on a smaller scale and may not employ the least-cost production techniques due to the tradeoffs between quality and quantity. Furthermore, agriculture in developing countries tends to be large-scale and more likely non-organic since it serves as the primary export industry that has the competitive edge in low-cost production in the world. With frequent use of fertilizers, pesticides and herbicides to maximize agricultural output, such practices are predicted to have increased the greenhouse gas emissions in non-Annex I countries relative to Annex I countries.

This research makes a contribution to the literature that explores a direct link between organic farming practices and the emissions of nitrous oxide and methane across countries. The chapter continues as follows. After a cross-disciplinary and detailed literature review in various areas, I provide the economic model to be estimated. The chapter concludes after a discussion of the empirical results and conclusions.

2. Review of the literature

Below, a review of the literature is provided in three key areas: (1) the Kyoto Protocol and its effectiveness; (2) previous models of GHG emissions using the Environmental Kuznets Curve (EKC) model and (3) the mitigating effects of organic farms on GHG emissions.

2.1 The Kyoto protocol and Its pros and cons

The effectiveness of the Kyoto Protocol has continued to be contemplated by researchers across disciplines. The international agreement calls for the reduction in combined emissions of six of the main greenhouse gases, carbon dioxide, nitrous oxide, methane, hydrofluorocarbons, perfluorocarbons and sulfur hexafluoride (McCarl & Schneider, 2000; UNFCCC, 2008). There are specific emission targets listed for each of the 38 industrialized nations plus the European Union ("Annex I countries"), outlined in a section called "Annex B" in the protocol. These reduction targets in GHG emissions which are listed in Table A-1 of the Appendix will account for a 5.3 percent collective reduction of the 1990 emission levels by the first commitment period of 2008-2012 (Sathiendrakumar, 2003; Finus, 2008; Grunewald & Martinez-Zarzoso, 2009). Belarus and Turkey were not parties to the UNFCCC and so they are Annex I countries that have no target reductions. The United States remains the sole Annex I country that has not ratified the Kyoto Protocol despite being an integral member (Kumazawa & Callaghan, 2010). Most countries use the 1990 baseline emissions but Japan and the former members of the Soviet Union have argued for flexible baselines.

While setting rigid country-specific target reductions, the protocol allows for flexibility in meeting these targets through emissions trading, clean development mechanism (CDM) or joint implementation between countries as long as eligibility requirements are met (Rollings-Magnusson & Magnusson, 2000; McKibbon & Wilcoxen, 2002; Finus, 2008). The Kyoto Protocol recognizes the uniqueness of the agricultural industry in the emissions reduction process. In another section of the protocol called "Annex A," the agricultural sources of emissions listed include enteric fermentation, manure management and deforestation while sinks to offset the emissions include afforestation and reforestation (McCarl & Schneider, 2000; UNFCCC, 2008).

One of the shortcomings of the Kyoto Protocol is that it did not go into force until 2005, eight years after it was adopted in 1997. It was only after Russia's ratification that 55 countries which had emitted at least 55% of the greenhouse gases had ratified the protocol (Finus, 2008; Grunewald & Martinez-Zarzoso, 2009). The UNFCCC's principle of "common but differentiated responsibilities" means that the responsibilities for reduction efforts fall disproportionately on the industrialized nations because they had contributed more toward GHG emissions than others. Another criticism of the protocol is that it does not address each GHG and sector individually as separate but linked agreements (Barrett, 2008).

The most problematic areas in the international agreement have been compliance and participation (Bohringer, 2003). The United States is still the only Annex I country which has yet to ratify the protocol and its target reduction of 7 percent is not binding even though a substantial 25% of the world's emissions originate in the US (Sathiendrakumar, 2003). The cost of compliance is not cheap and is estimated to be as much as 2.6 percent of the US GDP (Jaffe et al., 1995), a costly price to pay for a country which is in a chronic trade deficit. Australia and Russia initially followed in the footsteps of the United States but they ratified the protocol in 2007 and 2004, respectively, with provisions.

2.2 Previous research using the EKC Model

Agricultural production has long been considered to be an essential condition for a country's overall economic growth (Ruttan, 2002) in the development phase. However, few paid attention to how this growth was achieved until recent decades when it became evident from scientific data that global warming should be a cause for major concern. As countries experience economic development, they typically transition away from traditional and labor-intensive small-scale farming toward capital-intensive and even chemically-intensive large-scale farming (Ruttan, 2002; Goodstein, 2008). The economies of scale from the latter farms contribute to lower prices, creating comparative advantages in the global market. It is only when countries become richer that people can afford to demand more control over pollution and environmental degradation (Goodstein, 2008; Dasgupta et al., 2002), a reason why more regulations for pollutants exist in the environmentally-conscious and affluent Western societies.

The Environmental Kuznets Curve (EKC) hypothesis states that there is an inverted U-shaped relationship between economic development and environmental damages. Figure 3 shows that until a country reaches a turning point, there is continuous environmental degradation, at which point the country reverses the path and starts to experience an environmental improvement (Grossman and Krueger, 1995).

Past empirical research that uses the EKC model analyzes the impact of carbon dioxide (Shafik, 1994; Schmalensee et al., 1998; Dijkgraaf & Vollebergh, 2005; Aldy, 2007; Grunewald & Martinez-Zarzoso, 2009; Kumazawa & Callaghan, 2010) and common air pollutants including sulfur dioxide (Grossman & Krueger, 1995; Roca et al., 2001; Harbaugh et al., 2002). One of the few studies which investigated the EKC model for nitrous oxide and methane is the research by Roca et al. (2001).

Empirically, the Environmental Kuznets Curve is shown by the effect of the GDP per capita (Y) and GDP per capita squared on the emissions per capita (E), all in logged form for a panel data regression analysis. The square of the logged income per capita is included to allow for nonlinearity in the parameter. The log transformation of the variables Y and E

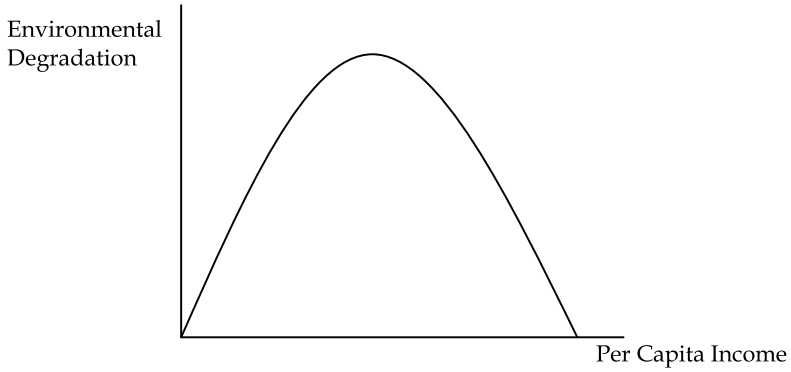

Fig. 3. Environmental Kuznets Curve (EKC)

the conventional EKC model where the subscript i denotes country and the subscript t denotes year in a cross-sectional time series data set. τ stands for a matrix of year dummy variables that control for the time trend. The time-invariant heterogeneity (α_i) and the idiosyncratic time-varying error term (ε_{it}) make up the composite error term. Past research indicates that political institutions play a role (Congleton, 1992). This may be an example of the unobservable heterogeneity, in addition to country land mass and country temperature/ climate which stay relatively constant over time. The betas are the regression coefficients, β_0 the intercept and β_1 and $\beta_2$the slopes.

$$\ln(E)_{it}=\beta_0+\beta_1\ln(Y_{it})+\beta_2[\ln(Y_{it})^2]+\tau_t+\alpha_i+\varepsilon_{it} \quad (1)$$

Grossman & Krueger (1995) and Schmalensee et al. (1998) find empirical evidence for the EKC model that developed countries experience the "inverted-U" EKC in their environmental emissions. Grossman and Krueger (1995) find the turning point to be before a country reaches a per capita income of $8,000. Notable exceptions are Shafik (1994) and Dijkgraaf & Vollebergh (2005) who do not find the same shape for their EKC. The role of industrial production has been incorporated in recent studies of CO_2 emissions. Aldy (2007) finds that emission-intensive industrial production grows faster when there are fewer regulations. Kumazawa & Callaghan (2010) estimate an "augmented EKC model" (the conventional EKC model with additional independent variables) controlling for industrial production and test for structural breaks in the pre- and post- agreement years of the Kyoto Protocol. The authors find that carbon dioxide emissions, especially for industrialized nations (Annex I countries) show a decline since the signing. The model used in this chapter will be a variation of this augmented EKC model, specifically for agricultural production. Roca et al. (2001) find that only sulfur dioxide emissions exhibits the classic inverted U-shape of the EKC for Spain. Both methane and nitrous oxide emissions have increased but not decreased with economic growth for the country.

2.3 The mitigating effects of GHG emissions through organic farming

Mitigating the effects of non-CO_2 greenhouse gases is not an entire new idea in agriculture. Collecting methane from livestock manure through anaerobic digesters and using the captured gas, known as "biogas" to generate electricity reduces overall GHG emissions on farms (Shih et al., 2006; Lazarus et al., 2011). McCarl & Schneider (2000) advocate the

reduction in the use of nitrogen fertilizers and animal feed with nitrogen content to reduce nitrous oxide emissions.

Mitigating the effects of N_2O and CH_4 through organic farm practices follow along similar lines. The only study to date on this topic is the one conducted by the International Trade Centre (2007). In it, the following arguments are made. Organic farms engage in ley-farming where the field is left fallow after a few years of growing cash crops. The grasses and other plants grown on these fields during the fallow phase increase the nitrogen content of soils naturally without relying on nitrogen fertilizers which is seen as a direct cause of nitrous oxide emissions. In 2005 alone, global consumption of nitrogen fertilizers amounted to a staggering 91 million tons (International Trade Centre, 2007). Manure from livestock can also be recycled as a natural fertilizer, instead of being treated as waste material which, if not treated properly also contributes to emissions.

Organic agriculture also reduces the number of livestock per hectare, which is directly proportional to the emissions of both nitrous oxide and methane. The concentration of nitrous oxide can be more manageable with fewer livestock. In addition, the effects of methane from enteric fermentation and anaerobic decomposition can be reduced by having fewer livestock. Anaerobic digestion of manure and the production of biogas, while not a completely organic production method, have been at the forefront especially on organic farms. These are methods used on organic farms that directly reduce both methane and nitrous oxide emissions in addition to providing chemical and fertilizer-free products for the health-conscious consumers.

3. Data

Even though the idea of investigating the relationship between greenhouse gases and agriculture specifically to do with organic farming practices is very simple, compiling the data set proved to be extremely difficult. While carbon dioxide emission data is readily available for most countries annually over several decades, the same cannot be said of nitrous oxide and methane emission data.

At first glance, the World Resources Institute's Climate Analysis Indicators Tool (CAIT, version 8.0) seems to provide the most comprehensive data for 185 countries in 1990, 1995, 2000 and 2005 for both GHGs. However, upon careful analysis, there seem to be errors in reporting. Sometimes, countries that have small but positive total emissions per capita of either N_20 or CH_4 (in units of $MtCO_2e$) have zero emissions due to rounding to only one decimal place (for instance, 0.04 rounded to one decimal place becomes 0.0). This makes the distinction between a very small number and an actual zero to be indistinguishable. The agricultural emissions of both of these gases also suffer from the same problem.

The World Bank's World Development Indicators (WDI) also reports agricultural emissions of both N_2O and CH_4 for 133 countries (excluding Hong Kong, Taiwan and other island nations) in the same four years. These numbers do not always match those from the World Resources Institute but are measured in thousands of $MtCO_2e$, with several decimal places. I obtain these numbers so that the emissions per capita can be calculated with ease by multiplying the emissions by a thousand and dividing by the population. The population, real GDP per capita (in 2000 $US) and fertilizer consumption information are also extracted from WDI for the same countries that have the two GHG emission data. The size of the

arable land in hectares is obtained for all countries using FAOSTAT, a data extraction tool for the Food and Agriculture Organization of the United Nations.

There are further problems in obtaining additional control variables for the estimation of the augmented EKC model for CH_4 and N_2O emissions. The most problematic is the key information on organic farming. Both the WDI and FAOSTAT have variables on organic land relative to agricultural or arable land but there are more missing values than observations for most countries until the late 2000s. Euromonitor International's World Environment Factbook (2008) has comprehensive data on the number of organic farms, average size of organic farms (in hectares), land used in organic farming (in hectares) and the share of organic land relative to total land for 2001 to 2007 for 71 countries of the world. Even though the use of these variables would reduce the sample size to less than 50%, as there are no alternatives, I do so without much hesitation.

I obtained data on consumption of pesticides (thousand tons), herbicides (thousand tons), livestock numbers (in 1000 heads) and production of cereals (all grains including rice in thousand tons) from the World Environment Factbook (2008) as well. Each of these variables can also be obtained using FAOSTAT in finer detail (for example, gross production value of rice and consumption of nitrogen from fertilizers) but again, there were substantial missing values for most countries which made the data unusable. Table A-3 in the Appendix outlines all variables collected, the data sources and availability of countries and years.

The final sample of 55 countries for the augmented EKC model consists disproportionately of industrialized nations due to the availability of data. Annex I countries are overrepresented (there is 87% of them) while non-Annex I countries are underrepresented (there is only 14% of them). These countries make up approximately 60% of the world's agricultural emissions of methane and 50% of the world's agricultural emissions of nitrous oxide. China which emits 15% of the world's emission of agricultural methane and 22% of the world's agricultural nitrous oxide is excluded in the analysis because it does not have the key organic farming information. Japan, Philippines, Singapore and South Korea are excluded due to the same reason, for the lack of organic farm data.

4. Empirical estimation

Since the data for emissions of agricultural methane and nitrous oxide are available in 1990, 1995, 2000 and 2005, the country data is stacked for the four years in panel format, allowing for an unbalanced panel. In the conventional EKC model, a panel regression is run for the logged per capita emissions on logged per capita income and the squared logged per capita income, with three dummy variables for the years. This is done for each GHG separately for all 131 countries and then by Annex I status. A positive sign on ln (GDP per capita) and a negative sign on ln $(GDP)^2$ presence of an inverted U-shaped EKC. The results are presented in Table 2 and Table 3. The Hausman Specification Test is used to test between the fixed-effect model and the random-effect model, where α_i is randomly distributed.

The EKC model, augmented with organic farm practices and other sources of the GHGs, has some data constraints. The additional variables are collected for 2001 to 2007 and 2005 is the only where all variables are available at the same time. For livestock, pesticide, herbicide and cereal data, I approximate the 2000 data with 2001 data, as there is not enough data in the time series to be extrapolating the missing values reliably for each country. The resulting panel data is for two years, for a subset of 55 countries.

For agricultural emissions of CH_4, the conventional EKC model is augmented with arable land size, the number of organic farms and livestock, consumption of pesticides and production of cereals. These independent variables are chosen based on the literature. They are converted to logs so that elasticities are estimated. Methane stems from both enteric fermentation and anaerobic decomposition, manure management of livestock and rice cultivation. All variable, except the number of organic farms, are expected to increase methane emissions. The number of organic farms is expected to reduce methane emissions through organic practices used in agricultural production. The results are presented in Table 4.

For agricultural emissions of N_2O, the conventional EKC model is augmented with arable land size, the number of organic farms and livestock and consumption of fertilizers, pesticides and herbicides, all in logged form. These variables are also chosen based on the literature. Nitrous oxide stems from chemical usage on farms and livestock management. All variables, except the number of organic farms, are expected to increase nitrous oxide emissions. The results are presented in Table 5.

5. Results

The conventional EKC models for agricultural methane and nitrous oxide emissions are presented in Tables 2 and 3. A full list of countries used is provided in Table A-2 of the Appendix.

Variable	All Countries	Annex I Countries	Non-Annex I Countries
ln (GDP per capita)	0.411* (0.219)	-2.114*** (0.582)	1.057*** (0.277)
ln (GDP per capita)^2	-0.013 (0.015)	0.169*** (0.035)	-0.066*** (0.020)
Dummy Variable for 1990	0.330*** (0.025)	0.670*** (0.049)	0.249*** (0.027)
Dummy Variable for 1995	0.184*** (0.024)	0.454*** (0.049)	0.138*** (0.026)
Dummy Variable for 2000	0.072*** (0.021)	0.185*** (0.036)	0.049** (0.024)
Constant	-3.360 (0.787)	4.110 (2.443)	-5.146 (0.942)
R^2	0.410	0.682	0.360
Number of Observations	513	152	357
Number of Countries	131	38	92
Average Number of Years	3.9	4.0	3.9
Hausman Specification Test (χ^2)	16.52**	33.07***	30.25***

Notes: (1) Standard errors in parentheses below coefficients.

(2) Statistical significance at 1% (***) , 5% (**) and 10% (*).

Table 2. Conventional EKC Model for Agricultural Methane Emissions

In Table 2, the coefficients on ln (GDP per capita) and ln (GDP per Capita)^2 indicate that Annex I countries face an unexpected U-shaped EKC while non-Annex I countries face the expected inverted U-shaped EKC. However, the result for Annex I countries may be due to the relative short span of emission data which is only available every five years. Most developed countries would have already achieved economic growth by 1990. For Annex I countries, on average, a one percent increase in income per capita decreases per capita emissions of methane by 2 percent. For non-Annex I countries, on average, a one percent increase in income per capita raises emission per capita by 1 percent. All year dummy variables have positive and statistically significant coefficients. The Hausman Specification Tests across all three columns indicate that the fixed-effect model is the appropriate model which takes into consideration the time-invariant characteristics of each country.

In Table 3, the EKC has the expected inverted-U shape for non-Annex I countries and the unexpected U-shape for Annex I countries again. This time, the coefficient on ln (GDP per capita) is not statistically significant, meaning that income per capita has no effect on emissions per capita of nitrous oxide. The coefficient for non-Annex I countries is slightly higher compared to the previous table. All year dummy variables, while unreported in the table, have positive and statistically significant coefficients. The Hausman Specification Tests across all three columns indicate that the fixed-effect model is the appropriate model again.

Variable	**All Countries**	**Annex I Countries**	**Non-Annex I Countries**
ln (GDP per capita)	0.714***	-0.347	1.214***
	(0.223)	(0.516)	(0.304)
ln (GDP per capita)^2	-0.024	0.068**	-0.066***
	(0.016)	(0.031)	(0.022)
Dummy Variable for 1990	0.307***	0.564***	0.244***
	(0.025)	(0.043)	(0.030)
Dummy Variable for 1995	0.168***	0.355***	0.145***
	(0.025)	(0.044)	(0.029)
Dummy Variable for 2000	0.080***	0.166***	0.066**
	(0.021)	(0.032)	(0.026)
Constant	-5.381	-3.668	-6.705
	(0.801)	(2.164)	(1.033)
R^2	0.375	0.681	0.313
Number of Observations	513	152	357
Number of Countries	131	38	92
Average Number of Years	3.9	4.0	3.9
Hausman Specification Test (χ^2)	36.50***	53.31***	108.19***

Notes: (1) Standard errors in parentheses below coefficients.

(2) Statistical significance at 1% (***) , 5% (**) and 10% (*).

Table 3. Conventional EKC Model for Agricultural Nitrous Oxide Emissions

The augmented EKC model for methane is presented in Table 4. Compared to the conventional EKC model, the results are dissimilar for the different groups of countries due to the smaller cross-sections of countries and fewer years used. First, the inclusion of additional independent variables makes the EKC seemingly less robust, an observation made by Harbaugh et al. (2002) as both income variables are no longer statistically significant. For Annex I countries, livestock plays a significant role in increasing methane emissions. On average, a one percent increase in livestock numbers increases the agricultural methane emissions per capita by 0.8 percent, ceteris paribus. However, for non-Annex I countries, it is the consumption of fertilizers that matters. On average, a one percent increase in fertilizer consumption increases the agricultural methane emissions per capita by 0.3 percent, ceteris paribus. The production of cereal shows no significant impact on methane. This may be due to the fact that this variable measures the production of other grains, too.

Variable	**All Countries**	**Annex I Countries**	**Non-Annex I Countries**
ln (GDP per capita)	0.053 (0.382)	-0.083 (0.414)	0.122 (0.970)
ln (GDP per capita)^2	0.008 (0.024)	0.012 (0.027)	0.0002 (0.064)
ln (Arable Land in Hectares)	-0.155** (0.072)	-0.027 (0.083)	0.017 (0.138)
ln (Number of Organic Farms)	-0.004 (0.021)	0.055*** (0.019)	-0.051 (0.038)
ln (Number of Livestock)	0.405*** (0.072)	0.783*** (0.088)	0.171 (0.144)
ln (Consumption of Pesticides)	0.059 (0.050)	0.036 (0.044)	0.306*** (0.097)
ln (Production of Cereals)	-0.012 (0.058)	0.021 (0.054)	0.037 (0.107)
Dummy Variable for 2000	0.065*** (0.015)	0.062*** (0.017)	0.036 (0.042)
Constant	-6.404 (1.799)	-14.302 (3.063)	-8.003 (3.822)
R^2	0.545	0.901	0.505
Number of Observations	97	62	35
Number of Countries	54	33	21
Average Number of Years	1.8	1.9	1.7
Hausman Specification Test (χ^2)	6.27	40.41***	6.50

Notes: (1) Standard errors in parentheses below coefficients.

(2) Statistical significance at 1% (***) , 5% (**) and 10% (*).

Table 4. Augmented EKC Model for Agricultural Methane Emissions

The result that stands out is the effect of the number of organic farms for Annex I countries. It has an unexpected positive sign and is statistically significant. While not reported, other variables for organic farm production (average size of organic farms, land used in organic farming and the share of organic land relative to total land) also exhibit positive but smaller

effects on methane emissions. Perhaps, it signifies the shortcoming of what these variables actually measure. There is no distinction on whether the organic farms are dairy farms or not. If there are disproportionate shares of dairy farms among organic farms, it is entirely possible to expect the sign on the variable to be positive through enteric fermentation and anaerobic decomposition.

It is noteworthy that for all columns except Annex I countries, the Hausman Specification Test could not reject the random-effect model. A shortcoming of this model may be that the natural sources of methane such as the number of landfills and wetlands were not controlled for due to the lack of available data.

The augmented EKC model for nitrous oxide is presented in Table 5. Again, the results differ from those of the conventional EKC model. The income variables are not statistically significant except for the case where all countries are considered together and show the inverted-U shape.

Variable	**All Countries**	**Annex I Countries**	**Non-Annex I Countries**
ln (GDP per capita)	1.536***	0.444	-0.623
	(0.551)	(0.674)	(0.822)
ln (GDP per capita)^2	-0.086**	-0.016	0.072
	(0.038)	(0.042)	(0.059)
ln (Arable Land in Hectares)	0.233*	0.100	0.586***
	(0.131)	(0.126)	(0.145)
ln (Number of Organic Farms)	0.022	0.081**	-0.051
	(0.029)	(0.035)	(0.034)
ln (Number of Livestock)	0.213*	0.038	-0.045
	(0.123)	(0.160)	(0.150)
ln (Consumption of Pesticides)	0.367**	-0.181	1.045***
	(0.155)	(0.202)	(0.201)
ln (Consumption of Herbicides)	-0.250	0.122	-0.877**
	(0.153)	(0.180)	(0.238)
ln (Fertilizer Consumption)	0.155**	0.099	0.460***
	(0.061)	(0.062)	(0.108)
Dummy Variable for 2000	0.031	0.090***	0.004
	(0.026)	(0.026)	(0.058)
Constant	-16.996	-6.195	-13.755
	(3.384)	(5.110)	(4.946)
R^2	0.506	0.725	0.936
Number of Observations	94	60	34
Number of Countries	52	32	20
Average Number of Years	1.8	1.9	1.7
Hausman Specification Test (χ^2)	40.6***	53.18***	63.48***

Notes: (1) Standard errors in parentheses below coefficients.

(2) Statistical significance at 1% (***) , 5% (**) and 10% (*).

Table 5. Augmented EKC Model for Agricultural Nitrous Oxide Emissions

Across all columns, the Hausman Specification Tests show the rejection of the random-effect model in favor of the fixed-effect model. Furthermore, the natural sources of N_2O are not controlled for in the regressions due to the lack of available data.

For Annex I countries, only the number of organic farms matter and it is again, statistically significant with the wrong sign. For non-Annex I countries, the use of chemicals in agricultural production increase N_2O emissions. On average, a one percent increase in pesticide consumption increases agricultural emissions of nitrous oxide per capita by one percent, all else equal. Similarly, a one percent increase in fertilizer consumption increases the same GHG emission per capita by 0.5 percent, all else equal. Curiously, the consumption of herbicides decreases emissions per capita. Perhaps, this is indicative of how the combination of chemicals used in agricultural production affects nitrous oxide emissions.

6. Conclusions

This chapter is one of the first kinds to investigate the Environmental Kuznets Curve hypothesis for nitrous oxide and methane, specifically in agriculture. Using a sample of 131 countries, the conventional EKC model shows the classic inverted-U EKC for non-Annex I countries of the Kyoto Protocol for both GHGs. These are countries which are not subject to the target emission reductions in Annex B of the international agreement. As these countries experienced economic development, per capita agricultural emissions of both methane and income per capita increased until the turning points were reached and started to decline. Controlling for income, the dummy variables for years indicate higher emissions.

On the other hand, the Annex I countries, those that have committed to reductions in emissions of the six greenhouse gases by ratifying the Kyoto Protocol, exhibit a U-shaped EKC for both GHGs. This means that emissions have been decreasing with income but have increased again after a critical point. However, most Annex I countries had already experienced much of their economic development before 1990. Without additional data, it is difficult to ascertain what the shape of this EKC implies for Annex I countries. While the cross-section of countries used was large, the time series only spanned four years as the emission data is only collected every 5 years in 1990, 1995, 2000 and 2005. Even though the protocol went into force, the true test of the effectiveness lies in comparing the numbers in 2010 which reflects the first commitment period of 2008-2012.

The estimation of the augmented EKC model proved to be rather difficult. While the inclusion of additional independent variables makes the EKC seemingly less robust (Harbaugh et al., 2002), it is not reasonable to claim that the income variables pick up all variations in environmental emissions using the conventional EKC model. Omitted variable bias is a serious problem that cannot be ignored. In light of the study by Kumazawa & Callaghan (2010) which focused on augmenting the conventional EKC to show the impact of industrial production on the emissions of carbon dioxide, I estimated the augmented EKC for agricultural production on the emissions of methane and nitrous oxide in the industry.

Additional variables included in the augmented EKC model are the number of livestock, chemicals (fertilizers, pesticides, herbicides) used and the number of organic farms, along with a few others. However, these variables are not available for numerous countries and in the same years as the emission data. The resulting sub-sample used was for 55 countries of the original 131 countries, which are disproportionately Annex I countries and excludes a high emission non-Annex I country, China. This is one of the shortcomings of this research,

that data is not readily available for all countries for various aspects of agricultural production and for all known sources of methane and nitrous oxide.

The results of the augmented EKC model are mixed. For example, livestock numbers only contribute to methane emissions in Annex I countries. The number of organic farms has a positive and statistically significant impact on emissions of both CH_4 and N_2O, only in industrialized nations. This variable may not be measuring the organic practices of such farms and needs further analysis. Nitrous oxide emissions are contributed primarily through fertilizer and pesticide use of non-Annex I countries.

The implication of this research is that there is hope for organic agricultural practices which will help to mitigate the emissions of methane and nitrous oxide, which are more harmful and prevalent in agriculture compared to carbon dioxide. Engaging in sustainable agricultural practices will not only be healthy for consumers but will be more productive for farmers if they creatively choose methods that reduce greenhouse emissions and are environmentally friendly. The Kyoto Protocol's effectiveness in the future also lies in incorporating the role of developing nations in the reduction process. Finding the balance between these will help reduce the emissions of both methane and nitrous oxide in agriculture.

7. Appendix

Country	2008-2012 Target (% of 1990 baseline emission levels)	Ratification Date
Australia	+8%	2007
Austria	-8%	2002
Belarus	--	2004
Belgium	-8%	2002
Bulgaria	-8%	2002
Canada	-6%	2002
Croatia	-5%	2007
Czech Republic	-8%	2001
Denmark	-8%	2002
Estonia	-8%	2002
European Union	-8%	2002
Finland	-8%	2002
France	-8%	2002
Germany	-8%	2002
Greece	-8%	2002
Hungary	-6%	2002
Iceland	+10%	2002
Ireland	-8%	2002
Italy	-8%	2002
Japan	-6%	2002
Latvia	-8%	2002
Liechtenstein	-8%	2004
Lithuania	-8%	2003

Luxembourg	-8%	2002
Monaco	-8%	2006
Netherlands	-8%	2002
New Zealand	0%	2002
Norway	+1%	2002
Portugal	-8%	2002
Romania	-8%	2001
Russian Federation	0%	2004
Slovakia	-8%	2002
Slovenia	-8%	2002
Spain	-8%	2002
Switzerland	-8%	2003
Turkey	--	2009
Ukraine	0%	2004
United Kingdom	-8%	2002
United States	-7%	Not Yet Ratified

Table A-1. Annex I Countries with Emission Targets in Annex B of the Kyoto Protocol

Albania	Gabon	*Pakistan*
Algeria	Georgia	Panama
Angola	*Germany*	Paraguay
Argentina	Ghana	*Peru*
Armenia	*Greece*	Philippines
Australia	Guatemala	*Poland*
Austria	Haiti	*Portugal*
Azerbaijan	Honduras	Qatar
Bahrain	*Hungary*	Republic of Korea
Bangladesh	Iceland	Republic of Macedonia
Belarus	*India*	Republic of Moldova
Belgium	*Indonesia*	*Romania*
Benin	Iran	*Russian Federation*
Bolivia	Iraq	*Saudi Arabia*
Bosnia & Herzegovina	*Ireland*	Senegal
Botswana	*Israel*	Singapore
Brazil	*Italy*	*Slovakia*
Brunei Darussalam	Jamaica	*Slovenia*
Bulgaria	Luxembourg	*South Africa*
Cambodia	Japan	*Spain*
Cameroon	*Jordan*	Sri Lanka
Canada	*Kazakhstan*	Sudan
Chile	Kenya	*Sweden*
China	Kuwait	*Switzerland*
Colombia	Kyrgyzstan	Syrian Arab Republic
Congo	*Latvia*	Tajikistan
Costa Rica	Lebanon	Tanzania
Côte d'Ivoire	Libya	*Thailand*
Croatia	*Lithuania*	Togo
Cuba	*Malaysia*	Trinidad & Tobago
Cyprus	Malta	*Tunisia*

Czech Republic	Mexico	*Turkey*
Democratic People's Republic of Korea	Mongolia	Turkmenistan
Democratic Republic of Congo	*Morocco*	*Ukraine*
Denmark	Mozambique	United Arab Emirates
Dominican Republic	Myanmar	*United Kingdom*
Ecuador	Namibia	*United States of America*
Egypt	Nepal	Uruguay
El Salvatore	*Netherlands*	Uzbekistan
Eritrea	*New Zealand*	*Venezuela*
Estonia	Nicaragua	*Vietnam*
Ethiopia	Nigeria	Yemen
Finland	*Norway*	Zambia
France	Oman	Zimbabwe

Table A-2. Countries with Emissions Data (Used in EKC Model in Tables 2 and 3) and Subset of Italicized Countries (Used in Augmented EKC Model in Tables 4 and 5)

Variable	**Data Source**	**Year(s) Available**	**Countries Available**
Agricultural Methane Emissions per Capita (thousand $MtCO_2e$)	World Development Indicator (Word Bank)	1990, 1995, 2000, 2005	133
Agricultural Nitrous Oxide Emissions Per Capita (thousand $MtCO_2e$)	World Development Indicator (Word Bank)	1990, 1995, 2000, 2005	133
Population	World Development Indicator (Word Bank)	1960-2009	215
Gross Domestic Product per Capita (constant 2000 $US)	World Development Indicator (Word Bank)	1960-2009	215
Fertilizer Consumption (kg per hectare of Arable Land)	World Development Indicator (Word Bank)	1990-2009	215
Dummy Variable for Annex I Status	Kumazawa & Callaghan (2010)	1980-2009	210
Arable Land (Hectares)	FAOSTAT (Food and Agriculture Organization of the United Nations)	1961-2009	234
Livestock (1000 Heads)	World Environmental Factbook (Euromonitor International)	2001-2007	71
Number of Organic Farms	World Environmental Factbook (Euromonitor International)	2001-2007	71
Pesticide Consumption (1000 tons)	World Environmental Factbook (Euromonitor International)	2001-2007	71
Herbicide Consumption (1000 tons)	World Environmental Factbook (Euromonitor International)	2001-2007	71
Production of Cereals (1000 tons)	World Environmental Factbook (Euromonitor International)	2001-2001	71

Table A-3. Variables and their Sources

8. References

Aldy, J.E. (2007). Divergence in State-Level per Capita Carbon Dioxide Emissions. *Land Economics,* 83, 3, pp. 353-369.

Barrett, S. (2008). Climate Treaties and the Imperative Enforcement. *Oxford Review of Economic Policy* , 24, 2, pp. 239-258.

Bohringer, C. (2003). The Kyoto Protocol: A Review and Perspectives. *Oxford Review of Economic Policy*, 19, 3, pp. 451-466.

Chen, M.F. (2009). Attitude toward Organic Foods among Taiwanese as Related to Health Consciousness, Environmental Attitudes, and the Mediating Effects of a Healthy Lifestyle. *British Food Journal*, 111, 2, pp.165-178.

Congleton, R.D. (1992). Political Institutions and Pollution Control. *Review of Economics and Statistics*, 74, 3, pp. 412 – 421.

Dasgupta, S., Laplanta, B., Wang, H. & Wheeler, D. (2002). Confronting the Environmental Kuznets Curve. *Journal of Economic Perspectives*, 16, 1, pp. 147-168.

Dijkgraaf, E. & Vollebergh, H.R. (2005). A Test for Parameter Homogeneity in CO_2 Panel EKC Estimations. *Environment & Resource Economics* 32, 2, pp. 229-239.

Environmental Protection Agency (2011) Sources and Emissions (Methane). Retrieved from http://www.epa.gov/methane/sources.html.

Environmental Protection Agency (2011) Sources and Emissions (Nitrous Oxide). Retrieved from http://www.epa.gov/nitrousoxide/sources.html.

Euromonitor International (2008). *World Environmental Databook 2008/2009* (2e), Euromonitor International Plc, ISBN: 978-1-84264-471-3, London, UK.

Finus, M. (2008). The Enforcement Mechanism of the Kyoto Protocol: Flawed or Promising Concepts? *Letters in Spatial and Resource Sciences*, 1, 1, pp. 13-25.

Flugge, F. & Schilizzi, S. (2005). Greenhouse Gas Abatement Policies and the Value of Carbon Sinks: Do Grazing and Cropping Systems Have Different Destinies? *Ecological Economics*, 55, 4, pp. 584-598.

Food and Agriculture Organization of the United Nations (2011). FAOSTAT. Data compiled from http://faostat.fao.org/site/291/default.aspx.

Goodstein, E.S. (2008). *Economics and the Environment* (5e), John Wiley and Sons, Inc., ISBN 978-0-471-76309-3, Hoboken, NJ, USA .

Grossman, G.M. & Krueger, A.B. (1995). Economic Growth and the Environment. *Quarterly Journal of Economics*, 110, 2: pp. 353-377.

Grunewald, N. & Martinez-Zarzoso, I. (2009). Driving Factors of Carbon Dioxide Emissions and the Impact from Kyoto Protocol. CESifo Working Paper No. 2758. Retrieved from http://www.cesifo-group.de/portal/pls/portal/docs/1/1186086.PDF.

Harbaugh, W.T., Levinson, A. & Wilson, D.M. (2002). Reexamining the Empirical Evidence for an Environmental Kuznets Curve. *Review of Economics and Statistics*, 84, 3, pp. 541-551.

Helm, D. (2003). The Assessment: Climate Change Policy. *Oxford Review of Economic Policy* 19, 3, pp. 349-361.

Jaffe, A., S.R. Peterson, Portney, P.R. & Stavins, R.N. (1995) Environmental Regulation and the Competitiveness of U.S. Manufacturing: What Does the Evidence Tell Us? *Journal of Economic Literature* 33, 1, pp. 132-163.

Jorgenson, A.K. (2007). Does Foreign Investment Harm the Air We Breathe and the Water We Drink? A Cross-National Study of Carbon Dioxide Emissions and Organic

Water Pollution in Less-Developed Countries, 1975 to 2000. *Organization and Environment*, 20, 2, pp. 138-149.

International Trade Centre [UNCTAD/WTO] (2007). Organic Farming and Climate Change, *Doc.No. MDS-08-152.E*. Research Institute for Organic Agriculture (FiBL). Retrieved from https://www.fibl-shop.org/shop/pdf/mb-1500-climate-change.pdf

Kumazawa, R. & Callaghan, M.S. (2010). The Effect of the Kyoto Protocol on Carbon Dioxide Emissions. *Journal of Economics and Finance*, online edition from Springer, DOI: 10.1007/s12197-010-9164-5.

Lazarus, W.F., Goodkind, A., Gallagher, P. & Conway, R. (2011). Carbon Prices Required to Make Digesters Profitable on U.S. Dairy Farms of Different Sizes. *Department of Applied Economics Staff Paper P11-1*, University of Minnesota. Retrieved from http://ageconsearch.umn.edu/bitstream/98628/2/p11-01revised.pdf.

McCarl, B.A. & Schneider, U.A. (2000). U.S. Agriculture's Role in a Greenhouse Gas Emission Mitigation World: An Economic Perspective. *Review of Agricultural Economics*, 22, 1, pp. 134-159.

McKibbin, W.J. & Wilcoxen, P.J. (2002). The Role of Economics in Climate Change Policy. *Journal of Economic Perspectives*, 16, 2, pp. 107-129.

Morgenstern, R.D. (1991). Comprehensive Approach to Global Climate Change. *Papers and Proceedings of the American Economic Association*, 81, 2, pp. 140-145.

Nalley, L., Popp, M. & Fortin, C. (2011). The Impact of Reducing Greenhouse Gas Emissions in Crop Agriculture: A Spatial- and Production-Level Analysis. *Agricultural and Resource Economic Review*, 40, 1, pp.63-80.

Roca, J., Padilla, E., Farre´, M. & Galletto, V. (2001). Economic Growth and Atmospheric Pollution in Spain: Discussing the Environmental Kuznets Curve Hypothesis. *Ecological Economics*, 39, 3, pp.85-99.

Rollings-Magnusson, S. & Magnusson, R.C. (2000). The Kyoto Protocol: Implications of a Flawed but Important Environmental Policy. *Canadian Public Policy*, 26, 3, pp. 347-359.

Ruiz de Maya, S., Lopez-Lopez, I. & Munuera, J.L. (2011). Organic Food Consumption in Europe: International Segmentation Based on Value System Differences. *Ecological Economics*, 70, 10, pp.1767-1775.

Ruttan, V.W. (2002). Productivity Growth in Agriculture: Sources and Constraints. *The Journal of Economic Perspectives*, 16, 4, pp. 161-184.

Sathiendrakumar, R. (2003). Greenhouse Emission Reduction and Sustainable Development. *International Journal of Social Economics*, 30, 12, pp. 1233-1248.

Schmalensee, R., Stoker, T.M. & Judson, R.A. (1998). World Carbon Dioxide Emissions. *Review of Economics and Statistics*, 80, 1, pp. 15-27.

Shafik, N. (1994). Economic Development and Environmental Quality: An Econometric Analysis. *Oxford Economic Papers* 46, October, pp. 757-773.

Shih, J.S., Burtraw, D., Palmer, K. & Siikamaki, J. (2006). Air Emissions of Ammonia and Methane from Livestock Operations, *RFF DP 06-11*, Resources for the Future. Retrieved from http://www.rff.org/documents/RFF-DP-06-11.pdf.

United Nations Framework Convention on Climate Change (2008). Kyoto Protocol reference Manual on Accounting of Emissions and Assigned Amounts. Retrieved from http://unfccc.int/resource/docs/publications/08_unfccc_kp_ref_manual.pdf.

Vermont, B. & De Cara, S. (2010). How Costly is Mitigation of Non-CO_2 Greenhouse Gases from Agriculture? A Meta-Analysis. *Ecological Economics*, 69, 7, pp.1373-1386.

Winkler, H. (2008). Measurable, Reportable and Verifiable: the Keys to Mitigation in the Copenhagen Deal. *Climate Policy*, 8, pp. 534-547.

World Resources Institute (2011). Climate Analysis Indicators Tool (CAIT) Version 8.0., Washington, DC. Data compiled from http://cait.wri.org/cait.php?page=yearly.

7

Exploitation of Unconventional Fossil Fuels: Enhanced Greenhouse Gas Emissions

Judith Patterson
Concordia University
Canada

1. Introduction

Carbon dioxide (CO_2), methane (CH_4), nitrous oxide (N_2O), and ozone (O_3) are the principal naturally occurring radiatively active gases in the earth's atmosphere (Ruddiman, 2001). These gases are responsible for trapping outgoing infrared radiation in the earth's atmosphere, heating it, and thus keeping the earth's average temperature at approximately 15°C. These gases act as the panes of glass in a greenhouse, trapping in heat from sunlight, and consequently are also referred to as greenhouse gases (GHG).

The concentration of greenhouse gases throughout earth's history has fluctuated naturally, with plate tectonics being the primary, first order control. However, since the Industrial Revolution rapid rises in combustion-related GHG's, principally CO_2, have resulted from related increases in the extraction and burning of the fossil fuels oil, natural gas, and coal. Concern has existed over rising GHG levels and potential climate change since the early 1970's (reviewed in Patterson and Perl, 2007). It is now the consensus of the majority of the scientific community that increases in atmospheric GHG are responsible for measured increases in global average air and sea surface temperature.

The onset of industrialization in the 18th Century was enabled by the widespread use of coal, followed by oil and natural gas in the 19th and 20th centuries. The first resources of all three fossil fuels used were those easily accessible on land. With depletion of these sources, exploration and development has expanded to offshore fields and also to those fossil carbon accumulations inaccessible by conventional means.

The increase in the annual amounts of fossil fuel combustion in terms of barrels of oil, cubic metres of natural gas, and tonnes of coal is estimated to account for an increasingly larger component of the annual flux of CO_2 to the atmosphere. While there are natural sources of CO_2 emissions to the atmosphere (e.g. volcanic eruptions, decay of vegetation), the global increase in CO_2 concentration is attributable primarily to fossil fuel burning (Intergovernmental Panel on Climate Change [IPCC], 2007). Similarly, extraction and distribution related CH_4 emissions and combustion related N_2O are increasing as well. Following the 2008-09 recession, world primary energy consumption increased 5.6% (British Petroleum [BP], 2011). In the 21st century, fossil fuels now account for 81% of the global primary energy mix (Table 1; International Energy Agency [IEA], 2011a).

Added to this now is a new component. The initially accessed oil and gas reservoirs were shallow, and of high quality (National Energy Technology Laboratory, [NETL], 2011). With the depletion of easily accessed conventional deposits of oil and natural gas, the unconventional deposits of these fuels are increasingly being exploited. However with these resources a large energy commitment, which often involves carbon combustion, is required to extract the fuel and render it viable for refining and ultimately consumable in existing equipment. Therefore, there is not just the conventional input of energy and materials to produce fuel, but there are also additional combustion and extra resources involved in the extraction and/or upgrading of the unconventional fuel before it can be treated as a conventional product. This gives the final refined product from an unconventional source a higher carbon intensity (amount of carbon per unit of fuel burned). This creates an additive greenhouse effect to every unit of unconventional oil or gas consumed.

Fuel	**Global Use %**
Oil	33
Coal	27
Natural gas	21
Nuclear	6
Renewables	
Biomass burning	10
Hydro electricity	2
Others	1

Table 1. Global Primary Energy Mix, 2008. Oil and gas values include fuel from both conventional and unconventional sources. Data from IEA (2011a).

The purpose of this paper is to review the role of extraction and processing of unconventional oil and natural gas and the impact on greenhouse gas production. The peak of production of conventional oil has not resulted in diminished use of oil; rather, it has resulted in increased production of oil from unconventional sources. Similarly, natural gas from unconventional sources is assuming an increasing role in the global gas market (IEA, 2011b). Production of fossil fuels from unconventional sources creates more greenhouse gases than from conventional sources. Previous work by Brandt and Ferrell (2007), using IPCC scenarios, found significant potential impacts on GHG's from the substitution of unconventional oil products for conventional oil. This work examines the increased reliance on unconventional oil and natural gas to meet growing energy demands, and the impact on GHG emissions if increasing demand for fuel is met by unconventional sources with higher carbon intensity.

2. Greenhouse gases in the atmosphere

Radiatively active gases are produced by many different means in the earth system. The carbon cycle is governed by complex mechanisms involving plate tectonics, the biosphere, and solid earth-atmosphere interactions (Press and Siever, 1986). Carbon dioxide (CO_2) is introduced to the atmosphere by several processes, including volcanism, combustion, decay of organic material, and respiration. CO_2 is also removed from the atmosphere by several processes, including photosynthesis, dissolution in the oceans, geological burial of organic material, and ultimately plate subduction at tectonic boundaries (Press and Siever, 1986).

The concentration of CO_2 in the atmosphere has varied throughout geologic history. For ancient sequences, millions of years old, atmospheric concentrations are inferred by the use of proxies. However, using ice cores drilled into continental glaciers, measured gas values from air trapped in the ice have yielded the values of atmospheric CO_2 concentrations for the past 800,000 years of the Pleistocene and Holocene periods. This research on ice cores has been one of the most significant and valuable contributions made to the understanding of greenhouse gases and climate in the recent geological record. In 1958, a continuous monitoring programme of atmospheric CO_2 values was undertaken on the island of Mauna Loa in Hawaii (Keeling et al, 2001; Keeling et al, 2011).

Variations in the concentration of atmospheric CO_2 through the past 800,000 years are illustrated in Figure 1. CO_2 concentrations changed, as did temperature throughout the past eight glacial cycles, with low levels of CO_2 during globally cold intervals with ice sheet expansion and high amounts of CO_2 in warm, interglacial periods. As seen in Figure 1, CO_2 values fluctuated between fairly fixed boundaries, ranging from 170 to 290 ppmv, until the beginning of the Industrial Revolution. Minimum CO_2 values were recorded during glacial maximums, and maximum CO_2 values in interglacial periods. The last 10,000 years, known as the Holocene epoch, have been remarkably stable in temperature and CO_2 values. However, beginning with the Industrial Revolution, CO_2 levels began to increase and at the present value of 390 ppmv are now higher than at anytime in the last 800,000 years. This increase is

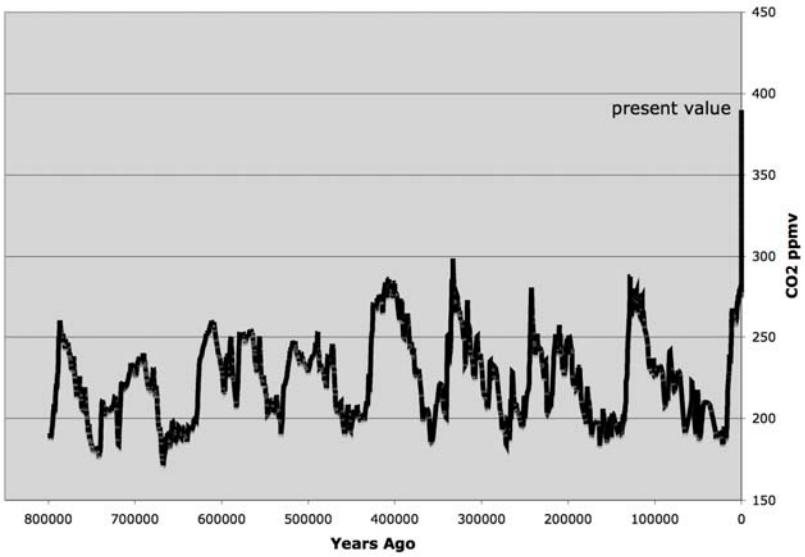

Fig. 1. Record of atmospheric CO_2 in ppmv 800,000 years ago to the present. Ice core data from Supplementary materials in Luthi et al, 2008, including Monnin et al, 2001; Pepin et al, 2001; Petit et al, 1999; Raynaud et al, 2005; Siegenthaler et al, 2005. Data from 1958 CE onwards, Keeling et al, 2001, and Keeling et al, 2011

attributed to the intensified use of fossil fuels with the onset of industrialization and, to a lesser degree, land use changes (IPCC, 2007). The earth's geological systems are unable to remove CO_2 at the same rate as it is input, and thus excess CO_2 is accumulating in the atmosphere.

Methane (CH_4) is produced due to anaerobic decay of organic material. Methane is also the principal constituent of natural gas. The cycling of methane (CH_4) is complexly tied to geological and biological activity. Research has shown that large-scale releases of methane to the atmosphere have occurred due to geological activity, including bursts from methane clathrates (e.g. Nisbet, 2002) and degassing of methane-rich sedimentary rocks following intrusion of magmas (e.g. Storey et al, 2007). Atmospheric concentrations of CH_4 in the last 800,000 years are shown in Figure 2. Ice core records show the same pattern of CH_4 as that seen with CO_2 through the glacial cycles, with low levels of CH_4 when it is cold and high levels during warm interglacial intervals. Throughout the past 800,000 years, methane also fluctuated between upper and lower boundary conditions, as measured from ice cores, and since the Industrial Revolution has increased dramatically to the present value of 1800 ppbv.

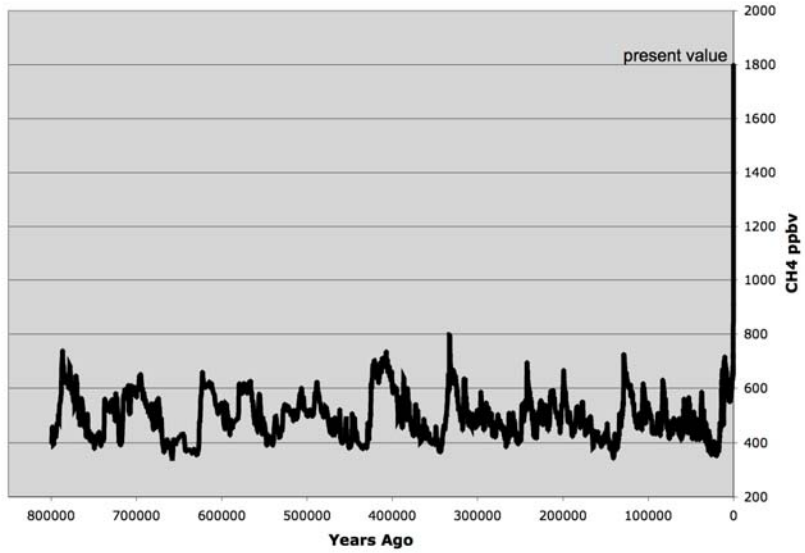

Fig. 2. Record of atmospheric CH_4 in ppbv over the past 800,000 years to the present. Ice Core data from online Supplementary materials in Loulergue et al, 2008, including Delmotte et al, 2004; Spahni et al, 2005; Lisiecki and Raymo, 2005; recent data from Dlugokencky, E., et al, 2009.

The increase of atmospheric methane since the Industrial Revolution is attributed to increased anthropogenic activities including land use changes, increased rice cultivation, and growth in the number of ruminant livestock. Fugitive emissions of methane from coal,

oil, and natural gas extraction and transportation are also a factor in the increase in atmospheric methane. Presently, agriculture and fossil fuel exploitation account for two-thirds of annual anthropogenically derived CH_4 emissions (Montzka et al, 2011). The main contributor is agriculture (dominated by ruminant emissions and rice cultivation). Extraction and transportation of natural gas and oil, followed by coal, are the dominant energy related emission sources of CH_4 (Montzka et al, 2011), and contribute 18% of anthropogenic CH_4 emissions globally (U.S. Environmental Protection Agency [EPA], 2011). It should be noted however, that the United Nations Framework on Climate Change (UNFCC) data on gas production and emissions are only reported for Annex-I parties (IEA, 2011a) and thus actual emissions may be higher.

The distribution of anthropogenically produced greenhouse gas emissions, expressed in CO_2 equivalents, is shown in Table 2 below. This does not include greenhouse gas emissions from natural sources (e.g. volcanoes, wetlands). The unit of measure, CO_2 eq, is defined as "the amount of CO_2 emission that would cause the same time-integrated radiative forcing, over a given time horizon, as an emitted amount of a long-lived GHG or a mixture of GHGs" (IPCC, 2007, p. 14). This value is obtained by multiplying the amount of a GHG by its Global Warming Potential (GWP) over a given time horizon (IPCC, 2007). The GWP is a means of comparing the relative climatic impacts of the different gases (Montzka et al, 2011).

Greenhouse Gas	Source	Percentage of Annual Anthropogenic Global Emissions in CO_2 eq
CO_2	Fossil fuel use	56.6
CO_2	Deforestation, decay of biomass	17.3
CO_2	Cement production and natural gas flaring	2.8
CH_4	Agriculture and fossil fuel production	14.3
N_2O	Combustion, agriculture	7.9
F	Hydrofluorocarbons (HFC's), perfluorocarbons (PFC's) and sulphur hexafluoride (SF_6)	1.1

Table 2. Distribution of anthropogenically generated GHG by sector in CO_2eq. From IPCC (2007)

Fugitive emissions are all GHG emissions from the oil and gas industry except for emissions from fossil fuel combustion (IPCC, 2006). The sources of fugitive emissions include leaks, evaporation, venting, flaring, pipeline breaks or dig-ins, and well blowouts. Some are well characterized, e.g. tank evaporation, process vents, and flare systems (IPCC, 2006), but others are accidental and unpredictable.

3. Oil

The industrial use of fossil fuels began in the 18th C with coal, and oil followed in the late 19th C. Oil is now the dominant fuel in the global primary energy mix, accounting for 33% of energy used in 2008 (IEA, 2010). In 2010 there was a 3.1% increase in global oil consumption from 2009 (British Petroleum [BP], 2011). This was in part driven by the emerging economies

of China and India, which will increasingly shape global energy demand (IEA, 2010). "China is currently the most important country in shaping future energy markets" (IEA, 2011a, p. 15), and it has surpassed the U.S. as the world's largest energy consumer (BP, 2011). Transportation is expected to continue to be the main driver for the increased demand for oil (IEA, 2010).

Oil resources are classified as conventional and unconventional. Conventional oil consists of crude, natural gas liquids (NGL), and condensates (IEA, 2010; Sorrel et al, 2010). Crude oil is a mixture of hydrocarbons that exists as a liquid under surface conditions (IEA, 2010). It initially flows easily from a well and is one of the least expensive and easiest to process of the petroleum products. The bulk of the oil that has been used to date on the planet was the easily accessible crude oil. NGL's are light hydrocarbons that are produced within a natural gas stream in a hydrocarbon reservoir (IEA, 2010). Condensates are light liquid hydrocarbons recovered from gas reservoirs, and are classed as NGL's (IEA, 2010).

Unconventional oil is derived from sources that include extra-heavy oil, bitumen[1] (tar/oil sands), oil shale, coal (coal-to-liquid CTL), and natural gas (gas-to-liquid GTL); (IEA, 2010; Sorrel et al, 2010). Primary fields of unconventional oil are the bitumen deposits in Alberta, Canada and the heavy oil in the Orinoco Belt of Venezuela. Unconventional oil requires the addition of resources – natural gas, energy and water – to extract and transform the material into oil that can then be processed at conventional refineries. Biofuels and coal-to-liquid (CTL) are not included in this paper.

The variation between conventional and unconventional oil is illustrated by API values (Table 3). API gravity is a measure of the density of a petroleum liquid relative to water. An API >10 means lighter than water, <10 is heavier than water (Stratton et al, 2010).

Oil	API°
Light crude	>35
Medium	26-35
Heavy	<20
Extra-heavy and Bitumen	<10

Table 3. API gravity values for the different oils (IEA, 2010; Martinez-Palou et al, 2011).

3.1 The peak of conventional and the rise of unconventional oil

The annual global production and consumption of oil, from all sources (crude, bitumen, shale oil, and NGL's), is shown in Figure 3[2]. Production has risen from 31.8 mb/d in 1965 to 82.1 mb/d (million barrels a day) in 2010 (BP, 2011). There have been dips, due to the oil

[1] In this paper, the term bitumen is used. It is an objective descriptor of the extra-heavy petroleum found in Northern Alberta, Canada, and avoids "taking sides" in the oil vs. tar sands debate.
[2] "Differences between these world consumption figures and world production statistics are accounted for by stock changes, consumption of non-petroleum additives and substitute fuels, and unavoidable disparities in the definition, measurement or conversion of oil supply and demand data." BP, 2011, p. 9.

embargo in the early 1970's, the Iranian Revolution of 1979 and ensuing global economic downturn (Patterson and Perl, 2007), and most recently the 2008-09 recession, but overall the trend has grown inexorably upwards.

Oil is a finite resource. M. King Hubbert forecast the peak in production in U.S. oil, based on his observations in Texas oil fields (Hubbert, 1949). Production from an individual well and aggregates of wells that make up a field, rises steadily at first and then, when approximately half the reserve has been extracted, the yield peaks and declines in the form of a normal distribution. Based on these observations, Hubbert (1971) went on to predict an estimate for the peak in production of global oil. This concept was revisited in the now-classic Campbell and Laherrère paper "The End of Cheap Oil" (1998).

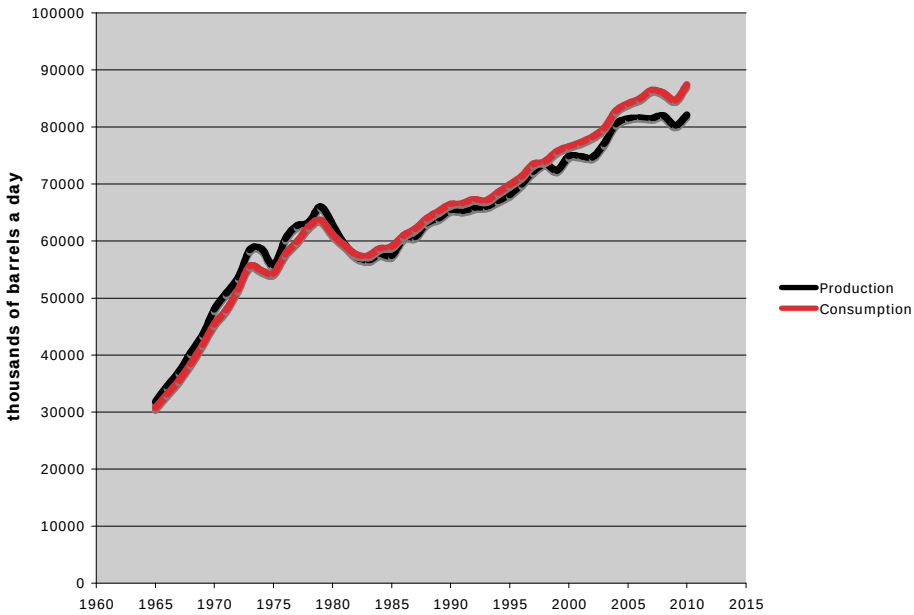

Fig. 3. Global oil production and consumption 1965-2010. Data from BP (2011).

Currently, production of conventional crude is at 68-69 mb/d, with unconventional oil, NGL's, and condensates making up the balance. In 2009, world production of oil was 81.0 mb/d (IEA, 2010). Of this, 67.9 mb/d of crude were produced; natural gas liquids (10.8 mb/d) and unconventional oil (2.3 mb/d) made up the balance (IEA, 2010). It appears that the peak of production of conventional crude oil was at 70 mb/d in 2006 (IEA, 2010). The International Energy Agency believes that if governments put in place the energy and climate policies that they have currently committed to, then the peak of conventional crude oil has indeed probably passed (IEA, 2010).

There is tremendous debate about the size of remaining conventional reserves (Sorrel et al, 2010). For example, with the decline of Arctic sea ice in the summer months, new fields are available for exploration. Offshore discoveries, including deepwater, have contributed

significantly to conventional reserves since the 1990's. Since 2000, more than half the oil discovered is in deep water (IEA, 2010). However, the average size of new fields has continued to fall (IEA, 2010), and it is thought unlikely that new giant fields of conventional oil will be found (Sorrel et al, 2010). Rather than a peak of production of conventional oil, Sorrel et al (2010) suggest that the production values from conventional fields may form a "bumpy plateau".

Patterson and Perl (2007) discussed the possibility of two paths for world energy consumption, with the peak of production of conventional crude oil. Replacements for conventional crude are all more costly, hence it was postulated that the increased price in oil could have the effect of reducing oil consumption that CO_2 climate mitigation policies (e.g. Kyoto Protocol) had failed to achieve. The other path was increased utilization of unconventional resources and rising global oil combustion, with concomitant emissions, regardless of price.

The record of global average oil prices is shown in Figure 4. Although there have been significant fluctuations, the average annual price has remained above US$60 for six years now (BP, 2011). Given the apparent unresponsiveness of consumption to high prices, there seems to be no monetary throttle on the continued rise in oil production and consumption.

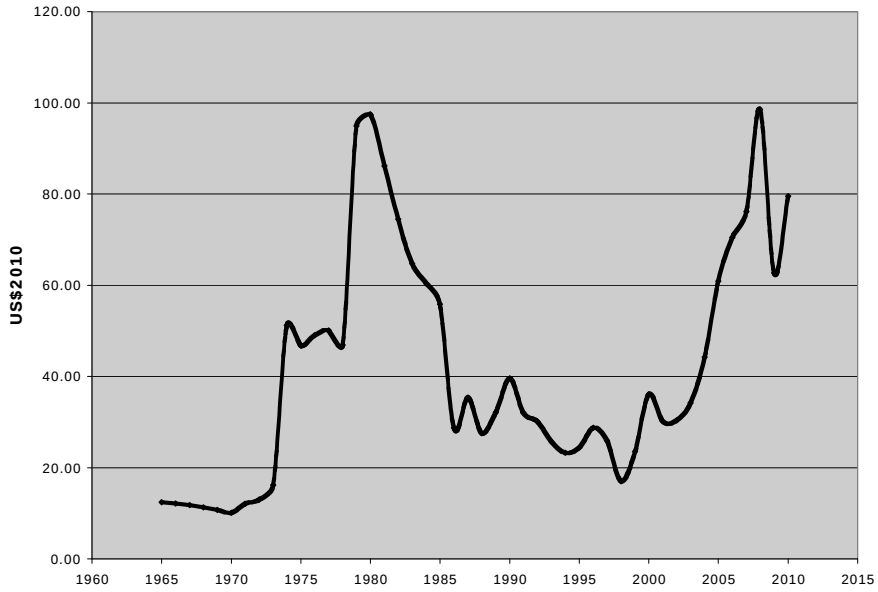

Fig. 4. Oil Prices 1965-2010 adjusted to US$2010. Data from BP (2011).

The decline in production from producing conventional fields means that new production must come from other sources if demand is to be met. In 2010, this means an extra 3 mb/d must be added each year either from enhanced recovery of existing conventional fields, discovery of new conventional fields, or through the exploitation of unconventional resources (Sorrel et al, 2010).

Oil from unconventional sources is predicted to play an increasing role in the world oil supply (IEA, 2010). Over 50% of the world's petroleum reserves (Head et al, 2003) consist of degraded oil, preserved either as heavy oil or bitumen. Heavy oil and extra heavy oil production is currently rising around the world (Martinez-Palou et al, 2010), and Venezuela is expected to increase output from the Orinoco belt (Watkins, 2010). Some estimates, reported in Baynard (2011), suggest that oil exploration and production activities in the Venezuelan heavy oil belt may increase by 600% in the next two decades.

The Canadian bitumen deposits of Alberta will also play a significant role. Estimates for future production from the Canadian bitumen sand are varied and conflicting. Rates of production of 3.7 mb/d are forecast for 2025, (Canadian Association of Petroleum Producers [CAPP], 2011), while predictions for production in 2030 range from 5 mb/d (Soderburgh et al, 2007) to 6 mb/d (Cambrian Energy Research Associates [CERA], 2009).

Evidence for the predicted growth in production from Alberta bitumen deposits can also be seen in plans for pipeline development. As of this writing the contentious Keystone XL pipeline, from northern Alberta to Texas, has passed Canadian and U.S. Environmental Protection Agency (EPA) approval and is contingent upon approval by the White House. In Canada, the Northern Gateway Pipeline has been proposed to run from northern Alberta to the deep-water port of Kitimat B.C. for export overseas, presumably to the Chinese market. These plans are meeting fierce opposition (see http://www.huffingtonpost.ca/2011/09/02/keystone-xl-protest-naomi-klein_n_947117.html; http://www.tankersnothankers.ca). Also, Enbridge Pipelines Inc. has requested permission from the National Energy Board of Canada to proceed with the Trailbreaker project. This would initially change flow in a portion of the pipeline in Ontario. Ultimately, a reversal in pipeline flow between Portland, Maine, (U.S.A.) and Montreal, Canada would allow Alberta bitumen products to travel to the east coast of the U.S., for export overseas and to southern U.S. ports and refineries (Vanderklippe, 2011a). Finally, both Canadian railways, Canadian National, and Canadian Pacific, are exploring increased oil movement by rail as business options (Vanderklippe, 2011b).

3.2 Production of unconventional oil; energy and resources required

The production of conventional oil involves exploration, drilling, establishment of the wellhead, and construction of pipelines to move the oil to refineries. In later stages, as the well becomes depleted, secondary recovery with pumping, or water or CO_2 injection, is used to extract the oil. The enhanced recovery techniques add to the energy costs of the production of conventional crude oil. Greenhouse gas emissions associated with the production of conventional crude oil are combustion related CO_2 from construction, operation, and transportation. Methane emissions from field operations include venting, oil storage tanks, and well venting and flaring (IPCC, 2006; EPA, 2011). Natural gas in remote locations is often disposed of by flaring (Martinez-Palou et al, 2011).

In the case of conventional crude oil, the product that flows out of the well needs little modification before entering the pipeline. However, this is not the case with the unconventional oil. Any existing technology for the conversion of unconventional fossil fuel

to liquid hydrocarbon suitable for refining as conventional petroleum carries significant environmental burdens. The unconventional resource must be extracted, separated from the host rock and, depending upon the composition, upgraded before being sent to a refinery. All of this requires energy, water, and feedstock for upgrading. In the section below the processes used to produce oil from bitumen are used as an outline to illustrate the energy and resources required.

Bitumen is a complex hydrocarbon that requires enhanced extraction techniques and upgrading before the liquid product can be sent to a conventional liquid petroleum refinery. Bitumen has a high viscosity and will not flow unaltered. There are two methods by which the bitumen is produced; surface mining followed by extraction of the bitumen from the sand, and in-situ separation of the bitumen and removal from the ground. In both cases, upgrading of the bitumen to a lighter hydrocarbon fluid resembling conventional petroleum is required before refining of the product can take place. Currently most of the bitumen that is removed by surface mining is upgraded as part of the overall on-site process, and these are known as integrated operations (CAPP, 2009). Only some of the in situ operations upgrade the product before transportation to refineries; the bitumen from other in situ plants is blended with a diluent to enable the non-upgraded material to flow in pipelines to southern upgrading and refining facilities (CAPP, 2009).

In the open-pit mining sites, truck and shovel operations are the main method of extracting and transporting the oil sand from the ground (Isaacs, 2007). Ore is transported to crushers by heavy truck (Alberta Chamber of Resources, 2004) with energy supplied by diesel fuel. At the crushers, the ore is broken down (Alberta Chamber of Resources, 2004) and then the crushed ore undergoes slurrying and hydrotransport in pipelines (Isaacs, 2007) to the separation facility (Alberta Chamber of Resources, 2004). In this process, called conditioning, the crushed oil sand is mixed with steam and water. In the dynamic movement, the separation of oil from sand begins (Isaacs, 2007; Chow et al, 2008). Most separation of mined bitumen is done by using the Clark method (Hyndman and Luhning, 1991), involving hot water, NaOH, and steam (Holowenko et al, 2000); first developed by Dr. Karl Clark in 1929 (Chow et al, 2008). The separation of the bitumen from the sand is an iterative process in which as much bitumen as possible is extracted from the sand slurry before being sent to the tailings pond (Alberta Chamber of Resources, 2004; Chow et al, 2008).

Following extraction of the bitumen it is sent for upgrading, the process whereby the extracted bitumen is transformed into a synthetic crude oil that can be sent by conventional pipeline to refineries where it can be used as a feedstock, similar to conventional petroleum (Hyndman and Luhning, 1991). The upgrading step is a complex petrochemical engineering process that reduces the viscosity of the hydrocarbon product and decreases the sulphur, nitrogen, and metals content (Hyndman and Luhning, 1991; Isaacs, 2007; Humphries, 2008). Natural gas is the principle feedstock for hydrogen in the upgrading process (Soderburgh et al, 2007; Humphries, 2008).

Extraction of bitumen from the host sandstone at depths too great for economically viable surface mining is accomplished by the use of techniques that reduce the viscosity of the bitumen and allow it to be pumped to the surface (Chow et al, 2008). In the development of

an in situ operation, seismic lines are cleared, drilling sites are constructed, roads are built, and pipelines are constructed (Johnson and Miyanishi, 2008; Schneider et al, 2003).

Steam assisted gravity drainage (SAGD) is a forefront technology for in situ extraction, and is the most economically attractive method for the deep deposits of the Athabasca field (Chow et al, 2008). Advances in horizontal drilling have aided the development of this technology. Two horizontal wells are drilled, one above the other; steam at 250°C is injected into the top well, and the loosened bitumen is collected in the bottom production well (Isaacs, 2007). A new technology involves the use of expanding solvents. In this technique, expanding solvent steam assisted gravity drainage (ES-SAGD) combines steam and solvent in the injection process (Chow et al, 2008).

The Cyclic Steam Stimulation (CSS) process involves the injection of high temperature steam at high pressure into the bitumen deposit underground (Chow et al, 2008). The high-pressure steam fractures the sediment, allowing the steam to spread and heat the bitumen, reducing its viscosity and allowing it to flow (Chow et al, 2008).

Once the bitumen is extracted from underground, the majority of the product is treated with diluent so that it will flow and goes by pipeline to refineries, while the remainder is upgraded in northern Alberta (Alberta Chamber of Commerce, 2004). The main source of the diluent is natural gas. Blending with traditional condensate diluent requires a 70:30 ratio of bitumen to condensate (CAPP, 2009). Upgraded light crude can also be used and is blended in a 50:50 ratio with the bitumen for pipeline transport to refineries (CAPP, 2009). The production of heavy and extra-heavy oils face similar production challenges.

The transportation of bitumen, heavy or extra-heavy oils that have not yet been upgraded from the fields to the energy markets, pose technological challenges because of high density, viscosity, low API gravity, and salt and heavy metal content (Martinez-Palou et al, 2011). While sending oil by pipeline is the most efficient and convenient method of transportation, the low mobility of these oils, and wax and ashphaltene deposits on pipeline walls, create technical problems (Martinez-Palou et al, 2011).

To overcome these problems, pipeline transportation of heavy oil can be effected by reducing the viscosity of the oil, minimizing wall drag in the pipe, and in-situ upgrading of the oil prior to transport (Martinez-Palou et al, 2011). Viscosity can be reduced by dilution with natural gas condensates, partial upgrading, formation of oil/water emulsions, reconfiguration of internal shear, and heating the oil and pipelines. Adding heat to the oil and pipeline and re-heating through directed fire heaters at pumping stations is the second most common method for reducing the viscosity of the heavy oil. (Martinez-Palou et al, 2011). In offshore settings, subsea pipelines must be heated when transporting heavy or extra heavy oil. All these techniques have added energy costs, and consequently greenhouse gas implications, particularly the direct heating of the heavy oil along the length of the pipeline.

3.3 Quantification of Life cycle Greenhouse gas emissions associated with conventional and unconventional petroleum

The greenhouse gas emissions associated with both conventional and non-conventional liquid petroleum fuels have been investigated as these industries have grown, and concern

over greenhouse gas emissions from these sectors has increased (e.g., (S&T)² Consultants Inc., 2008; Skone and Gerdes, 2008; Charpentier et al, 2009; Stratton et al, 2010). These are the emissions associated with fuel production, from extraction out of the ground to transportation to the refinery, including flaring of associated natural gas. These emissions include fugitive greenhouse gases from the wells and venting. In the case of the Canadian bitumen this includes all emissions associated with extraction and upgrading, including fugitive methane emissions from open-pit mining operations.

Generally speaking, the ratio of energy used to the energy in the final product (energy produced) is about 6% for conventional crude oil, approximately 20-25% for extra-heavy oil and nearly 30% for bitumen in sandstone (IEA, Energy Technology Systems Analysis Programme [ETSAP], 2010). Comparison of the emissions produced through the production of conventional and unconventional oil, produced from bitumen, are shown in Table 4, below. The values for conventional crude include recovery and transportation emissions, and exclude oil from Angola and Nigeria. The values for the unconventional oil are for Alberta bitumen, extracted either by open pit mining or by in situ processes (SAGD), and then upgraded to synthetic crude oil. The values are taken from the review by Charpentier et al (2009) and Stratton et al (2010).

Fuel Product	gCO_2eq/MJ
Conventional crude	4.5 – 9.6 (Charpentier et al, 2009)
	5 – 10 (Stratton et al, 2010)
Synthetic crude oil	
Mining	9.2 - 26.5 (Charpentier et al, 2009)
SAGD	16.2 - 28.7 (Charpentier et al, 2009)

Table 4. Upstream CO_2eq energy by feedstock.

Life cycle analysis can be undertaken for bitumen that ultimately is used in transport vehicles. These GHG life cycle emissions are divided based upon the extraction method; open-pit mining, SAGD, or CCS. For example, the emissions associated with the life cycle of fuel that is ultimately burned in a light duty vehicle (conventional automobile) are referred to as "well-to-wheels"; that is, from the drilled well or mining pit to the fuel tank of the vehicle and subsequent combustion. Similarly, aviation kerosene emissions are referred to as "well-to-wake" (Stratton et al, 2010).

Examples of conventional versus unconventional liquid petroleum life cycle greenhouse gas emissions are presented in Table 5, below. The greenhouse gases considered are combustion and non-combustion related products, CO_2, CH_4, and N_2O, and are reported in total as CO_2 equivalents (CO_2eq), based on the GWP of each gas (IPCC, 2007). The "well-to-wheels" values are presented as gCO_2eq/km for the production and combustion of the final refined product (gasoline) in vehicles ((S&T)² Consultants Inc., 2008). Values are presented gCO_2eq /MJ of energy in the "well-to-wake" aviation fuel (Stratton et al, 2010).

	Conventional crude gCO_2e/km	Unconventional (bitumen) gCO_2e/km	Ratio Unconventional/ conventional
Light Duty vehicle "well-to-wheels"[3]	316.3	354 (surface mining)	1.12
		390 (SAGD)	1.23
		384 (CSS)	1.21
	Conventional crude gCO_2e/MJ	Unconventional (bitumen) gCO_2e/MJ	Ratio Unconventional/ conventional
Aviation Kerosene[4] Jet A "Well-to-Wake"	87.5	99.8 (surface mining)	1.14
		108.2 (SAGD)	1.24

Table 5. Comparative life cycle GHG emissions for gasoline for light duty vehicles and aviation kerosene for conventional and unconventional oil feedstocks.

4. Natural gas

Natural gas is the third most abundant fuel in the global energy mix (Table 1), and is projected to overtake coal in projections of energy use to 2035 (IEA, 2011). Power generation is the main sector for gas demand, where gas has been replacing coal (IEA, 2011). In 2007, 33% of the global natural gas production was consumed for electrical generation (EIA, 2010). Figure 5 shows production and consumption of natural gas since 1970[5]. Natural gas production has tripled in the past 35 years and is tightly followed by consumption. The influence of China is seen also in the development of the natural gas market. For example, China is installing liquefied natural gas (LNG) re-gasification terminals and buying shale gas resources in North America (IEA, 2011a).

Conventional natural gas reservoirs may be found with or without oil. Gas that accumulates with oil is referred to as associated gas, while non-associated gas does not accumulate with oil (Energy Information Agency [EIA], 2010). Conventional gas reservoirs are sandstone or carbonate formations that have both porosity and permeability (interconnected pores so that the gas can flow) (Holditch, 2006). With conventional gas reservoirs, once the well is drilled the gas is easily extracted. Gas production involves drilling to the reservoir and setting up the wellhead and pipelines for gas to flow from the reservoir to market. Processing involves stripping out impurities (e.g. H_2S). Pipeline quality natural gas is 95-98% methane (EPA, 2011). The gas is transmitted along high-pressure pipelines with pumping stations distributed along the length of the pipeline, with final distribution to end-users.

[3] Data from (S&T)[2] Consultants Inc., 2008.

[4] Data from Stratton et al, 2010. The values presented are the baseline scenario; the value for conventional crude is the weighted average of all crude oil fed into U.S. refineries except for Canadian oil sands.

[5] "The difference between these world consumption figures and the world production statistics is due to variations in stocks at storage facilities and liquefaction plants, together with unavoidable disparities in the definition, measurement or conversion of gas supply and demand data." BP, 2011, p. 23.

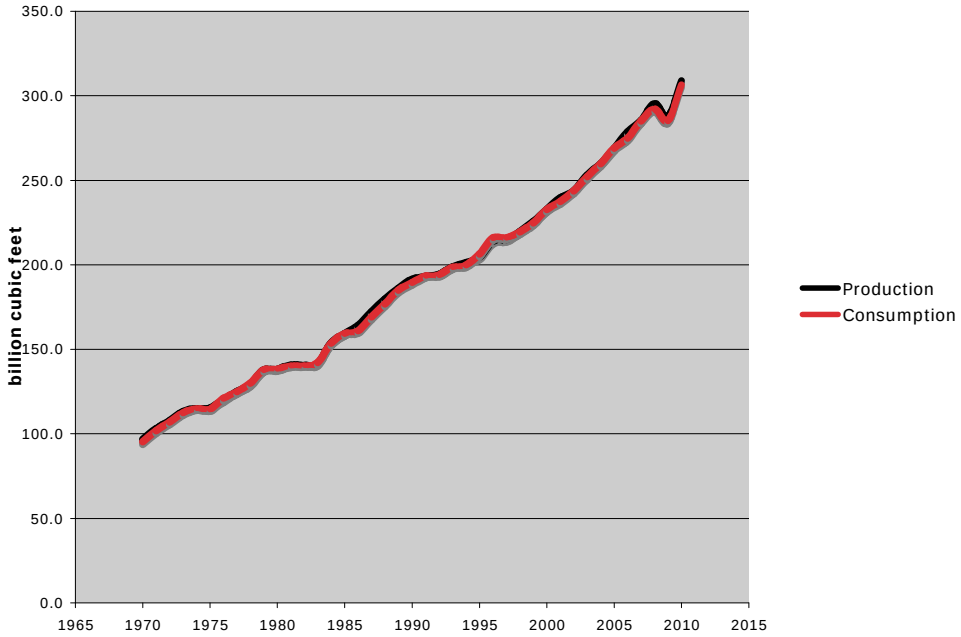

Fig. 5. Global Natural Gas Production and Consumption 1970-2010. Data from BP (2011).

4.1 Unconventional gas

The principal sources of unconventional gas are tight gas, coal-bed methane, and shale gas (Bourdaire, 2011; Holditch and AdDeenMadani, 2011; IEA, 2011a). Tight gas and coalbed methane (CBM) have been produced economically for four decades now, with shale gas production being relatively recent (Bourdaire, 2011; IEA, 2011a). In the U.S., the production of unconventional gas up to 2008 was distributed approximately as 70% from tight gas, 20% CBM, and 10% from shale gas (Bourdaire, 2011).

Globally, approximately 13% of marketed gas is from unconventional sources (IEA, 2010). Presently, unconventional gas is principally being produced in Canada and the U.S. In 2009, the production of unconventional gas exceeded conventional in the U.S., and it now makes up ~60% of marketed production in that country (IEA, 2011a). The peak of production of conventional gas was shown to have been reached in 2008 (IEA, 2011a, Figure 1.13, p. 36), and consequently, unconventional gas is increasingly meeting global demand. The production of unconventional gas doubled in the last eight years to 350 bcm in 2010 (IEA, 2010).

Deposits of unconventional gas are predicted to increasingly meet the growing demand for natural gas, and there are large quantities of this resource. In China, India, and Australia, unconventional gas development is focused on coal-bed methane, while tight gas is of interest in North Africa and shale gas in Poland (IEA, 2011b). Globally, the share of unconventional gas is predicted to rise from 13% of total natural gas production to 25% in 2035. Total global annual production is predicted to rise from 3.3 trillion cubic metres (tcm) in 2010, to 5.1 tcm in that time period (IEA, 2011a).

Unconventional gas reservoirs have low permeability and cannot produce at economic flow rates or economic volumes unless the reservoir is pumped or stimulated by hydraulic fracture treatment, horizontal wellbores, and/or multiple wellbores (Holditch, 2006). Recovery factors for unconventional gas tend to be much lower than for conventional gas, only about 15-30% of gas initially in place (GIIP) versus 80% recovery of GIIP for conventional deposits (Massachusetts Institute of Technology [MIT], 2010).

4.1.1 Tight gas

Tight gas development started in the 1970's (American Association of Petroleum Geologists [AAPG], 2011). Global tight gas production has risen from 6 billion cubic metres (bcm) in 1993 to 93 bcm in 2009 (Shell, 2011). It is estimated that at least 6000 trillion cubic feet (tcf) are in place in the US alone (NETL, 2011). Tight gas is trapped in impermeable, low-permeability, or non-porous sedimentary rock (Holditch, 2006; NETL, 2011). The extraction of tight gas requires fracturing and chemical alteration, which makes it costly. To get economic flow rates and/or to recover economic volumes the formation must be stimulated using hydraulic fracturing and/or horizontal well bores (AAPG, 2011).

4.1.2 Coalbed methane

Methane has historically always been a problem in coalmines, due to the risk of explosion during mining operations (EPA, 2004). In the formation of coal from organic material, methane gas is produced and is adsorbed onto the sides of small pores of the coal (EPA, 2004). Coal is structurally weak and consequently fractures easily so coal beds are typically characterized by networks of connected fractures (EPA, 2004). Water in coal beds contributes to the hydrostatic pressure that keeps methane gas adsorbed to the surface of the coal (United States Geological Survey, 2000; NETL, 2011).

As a natural gas, coalbed methane is difficult to produce, although it is relatively pure and does not contain H_2S (Government of Alberta, 2011). Coalbed methane is produced by reducing pressure in the coalbed (National Energy Board [NEB], 2007). When pressure is reduced the methane desorbs, diffuses through the coal, and then flows through the fractures (NETL, 2011). This reduction in pressure may be achieved by drilling and pumping out the groundwater in the coal bed, which brings water to the surface (Berquist et al, 2007; USGS, 2010; NEB, 2007; NETL, 2011). The initial pumping-out of groundwater may need additional flow enhancement and generally is followed by more drilling and hydraulic fracturing to enlarge pre-existing natural fractures in the coal seams (EPA, 2004; NEB, 2007; NETL, 2011). Fracturing fluids containing proppants (usually fine sand) are injected into the coal bed and then pumped back out, leaving the proppants to keep the fractures open, and thus increasing the permeability and allowing the methane to flow (EPA, 2004).

4.1.3 Shale gas

Shales are dense, fine-grained rocks, with very limited porosity (Kargbo et al, 2010). Shales hosting natural gas are rich in organic material (Kargbo et al, 2010; Kerr, 2010; Osborn et al, 2011), with natural gas in the pores of these rocks (Kargbo et al, 2010). Shales are so impermeable that they often act as cap seals on reservoirs of conventional oil and gas.

Therefore, extraction of the gas is very difficult. It is the last unconventional gas to be developed (Bourdaire, 2011).

Shale gas is extracted utilizing directional drilling and hydraulic fracturing techniques, the same as those used for tight-gas and coalbed methane recovery (Osborn et al, 2011). Multiple wellheads are required (Osborn et al, 2011). Multi-stage fracturing techniques are used with horizontally drilled wells (Kargbo et al, 2010). The drilling "fracking" fluid contains gels, acid, biocides, surfactants, and scale inhibitors to prevent precipitation of sulphate and carbonate (Kargbo et al, 2010). With development of the Marcellus Shale in Pennsylvania and New York, the wells are fractured laterally for just under a kilometer (954m) from the wellbore (Kargbo et al, 2010).

With each well, the hydraulic fluid mix is pumped in with millions of gallons of water mixed with chemicals and sand. Sand grains are proppants, keeping the fractures open and artificially creating permeability so the gas can flow (Kerr, 2010). The multistage fracturing techniques use large amounts of water, which must be managed (Kargbo et al, 2010). In the Marcellus Shale, the fracturing of each horizontal well requires 2-10 million gallons of water (7.7-38 ML) (Kargbo et al, 2010), with other estimates of 3-4 million gallons per well (Kerr, 2010). As much as 80% of the fluid may not be recovered (Kargbo et al, 2010). After drilling the wastewater must be treated onsite or trucked to a wastewater treatment facility. Flow from a new well can decline 60-80% in the first year of production (Kerr, 2010) and may have to be repeatedly fractured in order to continue producing.

4.2 Greenhouse gases from conventional and unconventional gas production and transportation

Greenhouse gases from both conventional and unconventional natural gas include direct and indirect combustion related CO_2 emissions and fugitive methane emissions. Direct CO_2 emissions are related to end-use combustion (Howarth et al, 2011; Wood et al, 2011). Indirect emissions of CO_2 are those produced by extraction, development, and transportation of the natural gas to market (Howarth et al, 2011). This includes combustion of fossil fuels, usually diesel, to drive pumps, drills, compressors, and to transport equipment and resources to and from the well site (Wood et al, 2011).

The energy used as a percentage of the energy produced for conventional gas is about 6% (IEA ETSAP, 2010). When comparing conventional natural gas to unconventional shale gas, the additional direct and indirect "well-to-burner" CO_2 emissions are only marginally higher for shale gas (Howarth et al, 2011; IEA, 2011a; Wood et al, 2011). The ratio between energy used to energy produced between conventional natural gas and that from unconventional tight gas, CBM, and shale gas is relatively small (IEA ETSAP, 2010). Indirect emissions from shale gas in the U.S. are estimated to be 1.2 – 1.7 gC/MJ (Marcellus shale; Santoro et al, 2011), compared to 15 gC/MJ for direct end-use combustion (Hayhoe et al, 2002). Wood et al (2011) estimate that additional direct emissions of CO_2 from shale gas are only 0.14 to 1.63 tonnes of CO_2e/TJ greater than those from combustion of conventional natural gas (57 tonnes of CO_2e/TJ). Therefore, for conventional and shale gas, the GHG emissions are dominated by CO_2 from direct end-use burner combustion and also by fugitive methane emissions, discussed below (Howarth et al, 2011; Wood et al, 2011).

A significant amount of gas is also flared at the wellhead, releasing CO_2. In 2010 an estimated 134 bcm of natural gas was flared (IEA, 2011a). The World Bank has initiated the Global Gas Flaring Reduction programme to attempt to reduce this waste from flaring. Given total annual global production of 3193 bcm of natural gas (BP, 2011), losses of 95bcm due to venting and leakages, and flaring of 134 bcm, approximately 7% of annually produced natural gas is lost to the atmosphere as greenhouse gases.

For both conventional and unconventional gas production, methane emissions result from drilling, wellhead establishment, normal operations, routine maintenance, and fugitive emissions. A significant amount of raw methane is released to the atmosphere by pressure venting, leakages, or due to accidents (IEA, 2011a). Fugitive methane emissions occur during transportation, storage, distribution, from connections between pipes and vessels, valves, leaks from wellheads, and along transmission lines (Howarth et al, 2011; Wood et al, 2011). Fugitive emissions also include gas that migrates to the surface around the outside of the wellhead casing (IPCC, 2006). The U.S. EPA in 2006 estimated annual releases of 95 bcm of gas due to leaking and venting, with a greater loss due to leakage rather than venting. The gas industry is now using enhanced sensing equipment to locate and seal leaking wells and pipelines (Kargbo et al, 2010).

The amount of fugitive methane produced is much higher for unconventional natural gas than for conventional. Hydraulic fracturing (fracking) fluids used in tight gas and shale gas beds come back up the well as "flow back" fluids, with large quantities of methane in the fluid (Howarth et al, 2011). It is estimated that in conventional well completion, fugitive emissions account for only 0.01% of methane emissions over the lifetime of the well, versus an estimated 0.6-1.3% in tight sandstones, and 1.9% for shale gas (Howarth et al, 2011).

Fugitive methane emissions can continue after well completion from shale gas deposits. Cement casing of wells becomes more challenging with depth and may cause aquifer contamination (Kargbo et al, 2010; Wood et al, 2011). There is documentation of systemic contamination by methane of aquifers overlying the Marcellus and Utica shales where they have been exploited in northeast Pennsylvania and upper New York State (Osborn et al, 2011). Measured methane concentrations increased in drinking water wells when a gas well was within 1 km (Osborn et al, 2011). Isotopic $\delta 13C - CH_4$ data was consistent with the methane being of deep, thermogenic origin, and not biogenic (Osborn et al, 2011). Methane in wells, close to the surface of the earth, can easily migrate and escape to the atmosphere. Wood et al (2011) contains a review of numerous examples of wellbore failure and migration of methane from the fractured rock to the surface, with explosions in some cases. In Quebec, of 31 shale gas exploration sites, 19 leaked methane. All have now been shut and a moratorium placed on any shale gas activity (Marsden, 2011).

5. Conclusions

Since the Industrial Revolution in the mid-18th Century, fossil fuel use has become the dominant energy source for humans on the planet. Fossil fuels now supply 81% of the global energy mix (IEA, 2011a). The primary use of oil is in transportation, and the greatest demand for natural gas is in electrical power generation. Global production of oil has doubled since 1970, and production of natural gas has tripled in the same interval (BP, 2011).

Oil and natural gas are both present in conventional and non-conventional forms. Conventional oil and natural gas deposits located on continents and nearshore marine shelves - at shallow depths - made them easily, and therefore cheaply, accessible. The late portions of the first decade of the 21st Century saw the peak of production of conventional crude oil (IEA, 2010) and also conventional natural gas (IEA, 2011a). Easily accessed deposits of conventional oil and gas have been largely depleted, and enhanced recovery techniques need to be used on these diminished reserves. Extraction is now focused on deepwater offshore oil and unconventional deposits of oil and gas.

With increased extraction and use of fossil fuels have come amplifications in the atmospheric abundance of carbon dioxide and methane, the two most abundant greenhouse gases. Concentrations of both gases are now at higher levels than at any time in the past 800,000 years (Luthi et al, 2008; Loulergue et al, 2008). Enhanced levels of greenhouse gases in the atmosphere are believed by the majority of scientists to be responsible for warming of the planet, and concomitant climate change. Policy efforts (e.g. the Kyoto Protocol) and price increases in oil have failed to rein-in usage of fossil fuels and the production of combustion related greenhouse gases. The peak of production of conventional oil has not resulted in diminished use of oil; rather it has resulted in increased production of oil from unconventional sources. Similarly, natural gas from unconventional sources is assuming an increasing role in the global gas market (IEA, 2011b). Demand continues to grow, even though prices remain near historical highs for oil.

To meet the demand for these fuels, rates of exploitation of both unconventional oil and natural gas are growing each year. Both unconventional oil and natural gas share common denominators in that they require extra energy and resources, and are more expensive to produce. They both have higher carbon intensity, producing more greenhouse gases per unit of energy delivered as a final product than conventional oil and natural gas products. There is an increased use of unconventional fuels in order to fill the shortfall left by the peak of production of conventional oil and natural gas. Given that each unit of unconventional oil and natural gas has up to 20% more associated greenhouse gas emissions than a conventional equivalent, there is an enhancement of greenhouse gas in the atmosphere as consumption of unconventional fossil fuels increases.

It is difficult to envisage what will stop the juggernaut of fossil fuel consumption and related GHG increases, barring a global economic collapse. Infrastructure exists, and continues to be built, for both established and developing societies dependent upon oil and natural gas. The large potential reserves of unconventional oil and natural gas can fuel industrialized economies well into the future. It is increasingly difficult to be optimistic of any mitigation of atmospheric GHG growth and climate change in light of the ongoing exploitation of unconventional oil and natural gas.

6. Acknowledgements

This chapter is dedicated to my late husband, Jamie Tiller. I thank Andy Jacobson, NOAA Earth System Research Laboratory, for CO_2 ice core data references, Robert W. Howarth for shale gas references, Rushdia Mehreen for help with figures, and Myke Wilder for invaluable technical editing.

7. References

Alberta Chamber of Resources, 2004. Oil Sands Technology Roadmap: Unlocking the Potential. 92pp. http://www.acr-alberta.com/Portals/0/projects/OSTR_report.pdf

AAPG (American Association of Petroleum Geologists), 2011. Tight Gas Sands. http://emd.aapg.org/technical_areas/tightGas.cfm

Baynard, C.W., 2011. The landscape infrastructure footprint of oil development: Venezuela's heavy oil belt. Ecological Indicators, vol. 11, p. 789-810.

Bergquist, E., P. Evangelista, T.J. Stohlgren, and N. Alley, 2007. Invasive species and coal bed methane development in the Powder River Basin, Wyoming. Environmental Monitoring and Assessment, vol. 128, p. 381-394.

Bourdair, J-M, 2011. Unconventional Gas. Presented at the 9th International Association for the Study of Peak Oil and Gas Conference, April 27-29, 2011. http://www.aspo9.be/assets/ASPO9_Wed_27_April_Bourdaire.pdf

Brandt, A., and Ferrell, A, 2007. Scraping the bottom of the bararel: greenhouse gas emissions consequences of a transition to low-quality and synthetic petroleum resources. Climatic Change, vol. 84, p. 241-263.

BP, 2011. British Petroleum Statistical Review of World Energy June 2011. 49pp. http://www.bp.com/statisticalreview

CERA (Cambridge Energy Research Associates), 2009. Growth in the Canadian Oil Sands: Finding the new balance. An IHS CERA Special Report, Cambridge, Massachusetts, U.S., 12pp.

Campbell, C., and Laherrère, J. H. 1998. The end of cheap oil. *Scientific American* 278:78–83.

CAPP, 2009. Crude Oil: Forecast, Markets, and Pipeline Expansions. Canadian Association of Petroleum Producers, June 2009, 48pp. 2009-2025 Canadian Crude Oil Forecast and Market Outlook

CAPP (Canadian Association of Petroleum Producers), 2011. Crude Oil: Forecast, Markets, and Pipelines, 40pp. http://www.capp.ca/getdoc.aspx?DocId=190838. Accessed September 22, 2011.

Charpentier, A.D., J.A. Bergerson, and H.L. MacLean, 2009. Understanding the Canadian oil sands industry's greenhouse gas emissions. Environmental Research Letters, vol. 4, 11pp.

Chow, D.L., T.N. Nasr, R.S. Chow, and R.P. Sawatzky, 2008. Recovery Techniques for Canada's Heavy Oil and Bitumen Resources. Journal of Canadian Petroleum Technology, vol. 47, no. 5, p. 12-17.

Delmotte, M., Chappellaz, J., Brook, E., Yiou, P., Barnola, J.M., Goujon, C., Raynaud, D., and Lipenkov, V., 2004. Atmospheric methane during the last four glacial–interglacial cycles: Rapid changes and their link with Antarctic temperature. J. Geophys. Res. 109, 12104, 13 pp..

Dlugokencky, E., L. Bruhwiler, J. W. C. White, L. K. Emmons, P. C. Novelli, S. A. Montzka, K. A. Masarie, P. M. Lang, A. M. Crotwell, J. B. Miller, and L. V. Gatti, 2009. Observational constraints on recent increases in the atmospheric CH_4 burden. Geophysical Research Letters, vol. 36, L18803, 5 pp.

Energy Information Agency, EIA, 2010. International Energy Outlook 2010.

http://205.254.135.24/oiaf/ieo/nat_gas.html

Energy Information Agency, EIA, 2011. The geology of natural gas resources. http://www.eia.gov/todayinenergy/detail.cfm?id=110

EPA (U.S. Environmental Protection Agency), 2011. Natural Gas STAR program, 2011. http://www.epa.gov/gasstar/basic-information/index.html

EPA (U.S. Environmental Protection Agency), 2004. Characteristics of Coalbed Methane Production and Associated Hydraulic Fracturing Practices. Chapter3 In Evaluation of Impacts to Underground Sources June 2004 of Drinking Water by Hydraulic Fracturing of Coalbed Methane Reservoirs. 32pp. http://www.epa.gov/ogwdw/uic/pdfs/cbmstudy_attach_uic_ch03_cbm_practices.pdf

Government of Alberta, 2011. Alberta Energy: Coalbed Methane. http:/www.energy.alberta.ca/NaturalGas/754.asp

Hayhoe K, Kheshgi HS, Jain AK, Wuebbles DJ (2002) Substitution of natural gas for coal: climatic effects of utility sector emissions. Climatic Change 54:107–139.

Holditch, S.A. 2006. *Tight Gas Sands.* SPE Paper 103356. Distinguished Author Series, J Pet Tech.

Holditch, S.A., and H. AdDeen Madani, 2011. Global Unconventional Gas—It Is There, But Is It Profitable? http://www.jptonline.org/index.php?id=533

Howarth, R.W., Renee Santoro, and Anthony Ingraffea, 2011. Methane and the greenhouse-gas footprint of natural gas from shale formations. Climatic Change, 12pp.

Head, I.M., D.M. Jones, and S.R. Larter, 2003. Biological activity in the deep subsurface and the origin of heavy oil. Nature, vol. 426, p. 344-352.

Holowenko, F.M., M.D. MacKinnon, and P.M. Fedorak, 2000. Methanogens and sulfate-reducing bacteria in oil sands fine tailing water. Canadian Journal of Microbiology, vol. 46, p. 927-937.

Hubbert, M. K. 1949. Energy from fossil fuels. *Science* 109:103–109.

Hubbert, M. K. 1971. The energy resources of the Earth. *Scientific American* 225:66–70.

Humphries, M., 2008. North American Oil Sands: History of Development, Prospects for the Future. CRS Report for Congress. Order Code RL34258, 30pp. Marc Humphries Report to Congress 2008

Hyndman, A.W., and Luhning, 1991. Recovery and upgrading of bitumen and heavy oil in Canada. Journal of Canadian Petroleum Technology, vol. 30, no. 2, p. 61-71.

IEA (International Energy Agency), 2010. World Energy Outlook 2010. International Energy Agency,Paris, France, 738 pp.

IEA (International Energy Agency), 2011a. Are we entering a Golden Age of Gas? World Energy Outlook 2011, 131 pp.

IEA (International Energy Agency), 2011b. Global surge of activity follows successful production of 'unconventional' gas in U.S. http://www.iea.org/index_info.asp?id=1762

IEA ETSAP (Energy Technology Systems Analysis Programme), 2010. Unconventional Oil and Gas Production. IEA ETSAP Technology Brief P02 – May 2010, 8 pp. http://www.iea-etsap.org/web/E-TechDS.asp

IPCC (Intergovernmental Panel on Climate Change) 2006. 2006 IPCC Guidelines for National Greenhouse Gas Inventories, Chapter 4, Fugitive Emissions, 78 pp.

IPCC (Intergovernmental Panel on Climate Change) 2007. Climate Change 2007: Synthesis Report. An Assessment of the Intergovernmental Panel on Climate Change, 52 pp.

Isaacs, E., 2007. The Canadian Oil Sands in the Context of the Global Energy Demand. Extended Abstract for the 17th Convocation of the International Council of Academies of engineering and Technological Sciences (CAETS), Tokyo, Japan, October, 200

Johnson, E., and Miyanishi, K., 2008. Creating new landscapes and ecosystems: The Alberta Oil Sands. Annals of the New York Academy of Sciences, vol. 1134, p. 120-145.

Kargbo, D. M., R.G. Wilhelm, and D.J. Campbell, 2010. Natural Gas Plays in the Marcellus Shale: Challenges and Potential Opportunities. Environmental Science and Technology, vol. 44, p. 5679-5684.

Keeling, C. D., S. C. Piper, R. B. Bacastow, M. Wahlen, T. P. Whorf, M. Heimann, and H. A. Meijer, 2001. Exchanges of atmospheric CO_2 and $^{13}CO_2$ with the terrestrial biosphere and oceans from 1978 to 2000. I. Global aspects, SIO Reference Series, No. 01-06, Scripps Institution of Oceanography, San Diego, 88 pages, 2001. http://scrippsco2.ucsd.edu

Keeling, R. F., S. C. Piper, A. F. Bollenbacher and S. J. Walker, 2011. Atmospheric CO_2 concentrations (ppm) derived from in situ air measurements at Mauna Loa, Observatory, Hawaii: Latitude 19.5°N Longitude 155.6°W Elevation 3397m. Scripps CO2 Program (http://scrippsco2.ucsd.edu) Scripps Institution of Oceanography (SIO), University of California, La Jolla, California USA 92093-0244
http://scrippsco2.ucsd.edu/data/in_situ_co2/monthly_mlo.csv

Kerr, R.A., 2010. Natural Gas from Shale Bursts Onto the Scene. Science, vol. 328, no. 5986, p. 1624-1626.

Lisiecki, L. E., and Raymo, M. E., 2005. A Pliocene-Pleistocene stack of 57 globally distributed benthic $d^{18}O$ records. Paleoceanography 20, PA2007.

Loulergue, L., A. Schilt, R. Spahni, V. Masson-Delmotte, T. Blunier, B. Lemieux, J.-M. Barnola, D. Raynaud, T.F. Stocker, and J. Chappellaz, 2008. Orbital and millennial-scale features of atmospheric CH_4 over the past 800,000 years. Nature, vol. 453, p. 383-386.

Luthi, Dieter, Martine Le Floch, Bernhard Bereiter, Thomas Blunier, Jean-Marc Barnola, Urs Siegenthaler, Dominique Raynaud, Jean Jouzel, Hubertus Fischer, Kenji Kawamura & Thomas F. Stocker, 2008. High-resolution carbon dioxide concentration record 650,000–800,000 years before present. Nature, vol. 453, p. 379-382.

Marsden, Wm., 2011. "Quebec outlines shale gas rules". Montreal Gazette, May 6, 2011, p. A11.

Martinez-Palou, R., M. de Lourdes Mosqueira, B. Zapata-Rendon, E. Mar-Juarez, C. Bernal-Huicochea, J. de la Cruz Clavel-Lopez, and J. Aburto, 2011. Transportation of heavy

and extra-heavy crude oil by pipeline: A Review. Journal of Petroleum Science and Engineering, vol. 75, p. 274-282.

Monnin, E., Indermuhle, A., Dallenback, A., Fluckiger, J., Stauffer, B., Stocker, T., Raynaud, D., and Barnola, J.-M., 2001. Atmospheric CO_2 concentrations over the last glacial termination. Science 291, 112–114.

Montzka, S.A., E.J. Dlugokencky, and J.H. Butler, 2011. Non-CO_2 greenhouse gases and climate change. Nature, vol. 476, p. 43-50.

MIT (Massachussets Institute of Technology), 2010. MIT (2010) *The future of natural gas,* an interdisciplinary study the Massachussets Institute of Technology's Energy Initiative ISBN (978-0-9828008-0-5 Copyright MIT 2010. http://web.mit.edu/mitei/research/studies/report-natural-gas.pdf

NEB (National Energy Board), 2007. Coalbed Methane Fact Sheet. http://www.neb.gc.ca/clf-nsi/rnrgynfmtn/nrgyrprt/ntrlgs/hrsshcnynclbdmthn2007/clbdmthnfctsht-eng.html

NETL (National Energy Technology Laboratory), 2011. Future Supply and Emerging Resources: Coal Bed Natural Gas. http://www.netl.doe.gov/technologies/oil-gas/futuresupply/coalbedng/coalbed_ng.html

Nisbet, E.G., 2002. Have sudden large releases of methane from geological reservoirs occurred since the last Glacial Maximum, and could such releases occur again? Philosophical Transactions of the Royal Society London A, vol. 360, no. 1793, p. 581-607.

Osborn, S. G., A. Vengosh, N.R. Warner, and R.B. Jackson, 2011. Methane contamination of drinking water accompanying gas-well drilling and hydraulic fracturing. Proceedings of the National Academy of Sciences, vol. 108, no. 20, p. 8172-8176.

Patterson, J., and Perl, A., 2007. The End of Cheap Oil: Crossroads for Kyoto. Energy Sources, Part B, vol. 2, p. 105-111.

Pepin, L., Raynaud, D., Barnola, J. M. & Loutre, M. F., 2001. Hemispheric roles of climate forcings during glacial–interglacial transitions as deduced from the Vostok record and LLN-2D model experiments. J. Geophys. Res. 106, 31885–31892.

Petit, J. R., Jouzel, J., Raynaud, d., Barkov, N., Barnola, J.-M., Basile, I., Beders, M., Chappellaz, J., Davis, M., Delaygue, G., Delmotte, M., Kotlyadov, V., Legrand, M., Lipendov, V., Lorius, C., Pepin, L., Ritz, C., Saltzman, E., and Stievenard, M., 1999. Climate and atmospheric history of the past 420,000 years from the Vostok ice core, Antarctica. Nature 399, 429–436.

Press, F., and Siever, R., 1986. Earth, 4th Edition. W.H. Freeman, New York, 656 pp.

Raynaud, D., Barnola, J.-M., Souchex, R., Lorrain, R., Petit, J.-R., Duval, P., and Lipendov, V., 2005. Palaeolclimatology: The record for marine isotopic stage 11. Nature vol. 436, p. 39–40.

Ruddiman, W., 2001. Earth's climate: Past and Future. W.H. Freeman, New York, 465 pp.

(S&T)² Consultants Inc., 2008. 2008 GHGENIUS UPDATE, prepared for Natural Resources Canada, Office of Energy Efficiency, Ottawa, Ontario, 86pp.

Santoro, R., R.W. Howarth, and A. R. Ingraffea, 2011. Indirect Emissions of Carbon Dioxide from Marcellus Shale Gas Development. A Technical Report from the Agriculture, Energy, and Environment Program at Cornell University, 28pp. http://www.eeb.cornell.edu/howarth/IndirectEmissionsofCarbonDioxidefromMarcellusShaleGasDevelopment_June302011 .pdf

Schneider, R.R., J.B. Stelfox, S.Bouton, and S. Wassel, 2003. Managing the Cumulative impacts of land-uses in the Western Canadian Sedimentary Basin: A modeling Approach. Conservation Ecology, vol. 7, issue 1, article 8, 15pp.

Shell, 2011. Unlocking natural gas from unconventional sources. http://www.shell.co.uk/home/content/gbr/aboutshell/media_centre/annual_reports_and_publications/swuk/summer_2011/shale_tight_gas.html

Siegenthaler, U., Stocker, T., Monnin, E., Luthi, D., Schwander, J., Stauffer, B., Raynaud, D., Barnola, J.-M., Fischer, H., Masson-Delmotte, V., and Jouzel, J., 2005. Stable carbon cycle–climate relationship during the Late Pleistocene. Science 310, 1313–1317.

Skone, T and Gerdes, K, *Development of Baseline Data and Analysis of Life Cycle Greenhouse Gas Emissions of Petroleum-Based Fuels*, DOE/NETL-2009/1346, National Energy and Technology Laboratory: Pittsburgh, Pennsylvania, 2008; http://www.netl.doe.gov/energyanalyses/pubs/NETL%20LCA%20Petroleum-Based%20Fuels%20Nov%202008.pdf (accessed September 20, 2011).

Soderburgh, B., Robelius, F., and K. Aleklett, 2007. A crash programme scenario for the Canadian oil sands industry. Energy Policy, vol. 35, p. 1931-1947.

Sorrell, S., Speirs, J., Bentley, R., Brandt, A., and Miller, R., 2010. Global Oil depletion: A review of the evidence. Energy Policy, vol. 38, no. 9, p. 5290-5295.

Spahni, R., Chappellaz, J., Stocker, T., Loulergue, L., Hausammann, G., Kawamura, K., Fluckiger, J., Schwander, J.., Raynaud, D., Masson-Delmotte, V., and Jouzel, J., 2005. Atmospheric methane and nitrous oxide of the Late Pleistocene from Antarctic ice cores. Science, vol. 310, p. 1317–1321.

Stearns, M., J.A. Tindall, G. Cronin, M.J. Friedel and E. Bergquist, 2005. Effects of coal-bed methane discharge waters on the vegetation an soil econsystem in Powder River Basin, Wyoming. Water, Air, and Soil Pollution, vol. 168, p. 33–57.

Storey, M., R.A. Duncan, and C.C. Swisher, 2007. Paleocene-Eocene Thermal Maximum and the Opening of the Northeast Atlantic. Science, vol. 316, p. 587-589.

Stratton, R.W., H.M. Wong, and J.I. Hileman, 2010. PARTNER Project 28 Report: Life cycle greenhouse gas emissions from alternative jet fuels, 153 pp. Partnership for AiR Transportation Noise and Emissions Reduction Report No. PARTNER-COE-2010-001http://web.mit.edu/aeroastro/partner/reports/proj28/partner-proj28-2010-001.pdf (accessed September 20, 2011).

United States Geological Survey (USGS), 2000. Water Produced with Coal-Bed Methane. USGS Fact Sheet FS-156-00.

Vanderklippe,N. 2011a. Enbridge pipeline plan sparks opposition. http://www.theglobeandmail.com/report-on-business/enbridge-pipeline-plan-sparks-opposition/article2175079/

Vanderklippe, N. 2011b. CN, CP push for a 'pipeline on rails'.

http://www.theglobeandmail.com/globe-investor/cn-cp-push-for-a-pipeline-on-rails/article1898062/

Watkins, E., 2010. Venezuelan oil output set for rise. Oil and Gas Journal, vol. 108, n. 20, p 39-40.

Wood R, Gilbert P, Sharmina M, Anderson K, Fottitt A, Glynn S, Nicholls F (2011) Shale gas: a provisional assessment of climate change and environmental impacts. Tyndall Center, University of Manchester, Manchester, England. http://www.tyndall.ac.uk/sites/default/files/tyndall-coop_shale_gas_report_final.pdf

8

The Role of US Households in Global Carbon Emissions

Md Rumi Shammin
Oberlin College
USA

1. Introduction

United States (US) is currently responsible for about 20% of global carbon emissions. The residential sector is responsible for a little over 20% of this emission. From this perspective, US households account for about 4% of global carbon emissions. Such sector-based approach is commonly used in energy analysis and energy policy. However, this is not necessarily a complete representation of the reality of household carbon emissions. The residential sector includes all energy directly used by homes and related carbon emissions. Two important elements are missing in this approach: energy used for transportation by people living in these homes and the embodied energy in all non-energy goods and services consumed by them. Another approach for reporting household emissions, based on the various end uses of energy in US homes, provides a more detailed understanding of the use of energy for heating, cooling, cooking, appliances, consumer electronics and automobiles. This approach also falls short of identifying emissions beyond the residential sector and personal transportation sub-sector. There is, however, another way of estimating total household carbon emissions. The industrial sector produces products that are transported by the transportation sector and marketed by the commercial sector and eventually consumed by people. Therefore, people in the US consume energy directly in the form of electricity, natural gas, and other fuels for their homes and automobiles. They also consume energy indirectly through the consumptions of various products and services. Combining the emissions related to the direct and indirect consumption of energy, people are accountable for about 71% of US carbon emissions (Shammin & Bullard, 2009) – which is significantly higher than the 20% represented by the residential sector. According to this approach, US households account for about 14% of global carbon dioxide (CO_2) emissions – roughly equal to the total emissions of the 27 member states of the European Union. People in the US thus have a significant opportunity to contribute to the reduction of global carbon emission[1].

This chapter presents a new, more comprehensive, more interesting and above all, more empowering approach to household carbon emissions in the US. It focuses on how US households contribute to greenhouse gas emissions, how they can play an important role in

[1] In this chapter *carbon emissions* and *CO_2 emissions* are used interchangeably. All data are reported for CO_2.

reducing global carbon emissions, and also how such efforts will potentially make them more resilient in the long run.

2. Carbon emissions by US households

There are multiple ways of estimating household carbon emissions. In fact, currently there is no established system of calculating and reporting total household carbon emissions for US households that includes a comprehensive accounting of the various ways households are directly and indirectly responsible for carbon emissions. US Environmental Protection Agency (EPA) and Energy Information Agency (EIA) both publish yearly reports on US greenhouse gas (GHG) emissions. These reports are organized around the major sectors of the economy (henceforth referred to as the *Sectoral* approach) and provide a macro-level overview of US GHG emissions. Another way household GHG emissions are often reported is based on various energy end uses – such as appliances, HVAC (heating, ventilation and air conditioning) systems, lights, cars, etc. (henceforth referred to as the *End Use* Approach). The sections below investigate the current methods of estimating carbon emissions under both of these approaches. Some boundary conditions need to be established prior to that. About 83% of US GHG emissions are carbon based of which more than 98% is energy-related (see figure 1). Hence the specific analysis of this paper will focus mainly on energy related carbon emissions. It should, however, be noted that GHG emissions from non-carbon sources also play a significant role in global climate change particularly on a global scale, but they are kept outside of the scope of this analysis.

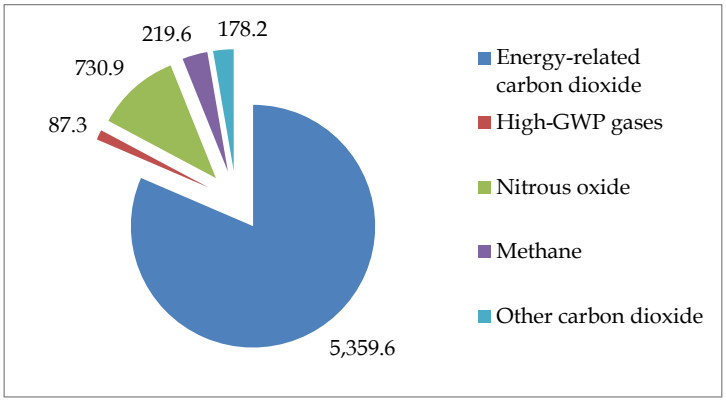

Fig. 1. 2009 US greenhouse gas emissions by gas in million metric tons (EIA, 2011)

2.1 The sectoral approach

The *sectoral* approach looks at the four major sectors of the US economy: residential, commercial, industrial and transportation. Emissions from electricity generation are distributed between these sectors, but are also sometimes reported separately. This picture is technically sound and the accounting method is time-tested - resulting in fairly accurate estimation of total carbon emissions for the economy as a whole by adding up the parts (see figure 2). This approach is consistent with government planning, budgeting and other fiscal activities. The *sectoral* approach also helps in the development of appropriate policies for

managing carbon emissions for the different sectors. Still, the *sectoral* approach provides a limited understanding of the total carbon emissions and ways of reducing emissions at the household level. It implies that households are responsible for primarily residential emissions and part of the transportation related emissions. Perhaps this is because the *sectoral* approach is not organized around people, their behavior, and their lives; rather it is categorized on the basis of macro-economic activities. Hence, the *sectoral* analysis is limited in its ability to explicitly represent the different ways people interact with the various economic sectors.

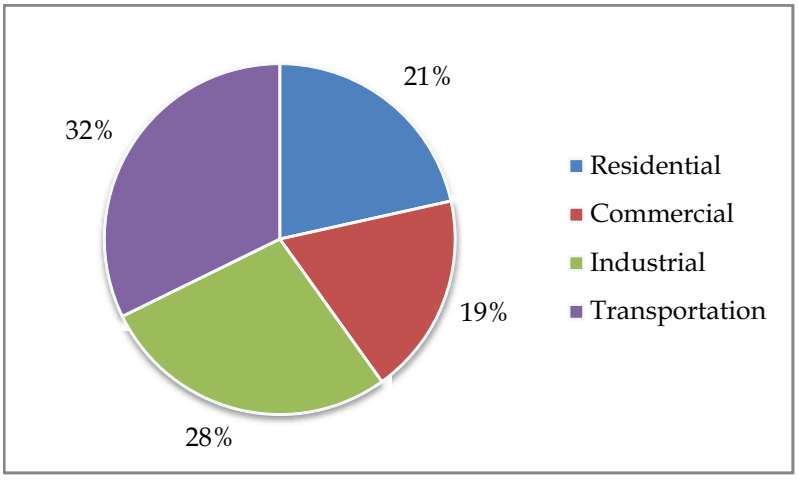

Fig. 2. US CO_2 emissions by economic sectors (EIA, 2011)

It is possible to link people's lives with the economic sectors included in *sectoral* analysis. First, the residential sector emissions are directly attributable to individuals in US households. These are emissions resulting from electricity, natural gas (or propane), fuel oil, wood, and other fuels used as a source of energy by residential consumers. People have a reasonable level of control over their use of these resources – within the constraints of existing infrastructure and resource availability. Second, a large part of emissions from the transportation sector are from personal automobiles. This part of the transportation sector emission is also directly attributable to people. Similar to the first case, people have a lot of control over their transportation emissions: choice of transportation mode, fuel efficiency of automobiles, place of residence relative to workplace and other daily destinations, etc. Together, the two above cases account for about 39% of carbon emissions that can be linked directly to people (based on data for 2009 from EIA, 2011). The remaining 61% is more complicated and requires deeper understanding of the life cycle of products and services. As mentioned earlier, the industrial sector produces products that are transported by the transportation sector and marketed by the commercial sector and eventually consumed by people. Sometimes there are multiple layers in the supply chain of products. Some industrial outputs are transported as parts or input materials for other industries before eventually making it to the marketplace. People are not always direct consumers either. Industries themselves consume various products or services and so do various commercial enterprises and non-governmental organizations. Another big consumer is the government itself – for

its various organizations including defense (military, air force, navy and various intelligence agencies). Ultimately all these different consumptive activities and related carbon emissions can be linked back to people. They are all intended to provide people with essential and non-essential products (including public infrastructure) and services (including social services and national security). These linkages are not clearly identifiable in the current representation of the *sectoral* analysis of carbon emissions.

2.2 The end use approach

In contrast to the *sectoral* approach, the *end use* approach provides a more detailed overview of micro-level energy use and carbon emissions by US households. Under this approach, the various energy end uses in households are documented and related carbon emissions are quantified. This includes energy used by HVAC systems, cooking, water heating, appliances, lighting, and other devices such as televisions, computers, and other household electronics. EIA routinely conducts the Residential Energy Consumption Survey (RECS) to generate data for *end use* analysis. The results of the *end use* approach is important for understanding the relative magnitudes of energy consumption by different systems within households and identifying opportunities for conservation and efficiency improvements to reduce household GHG emissions. While this approach is crucial for the purposes stated above, it is still limited to direct consumption of energy and related emissions. It provides a more in-depth understanding of residential sector emissions, but does not shed any additional light on the linkages between households and the other economic sectors listed under the *sectoral* approach.

2.3 Towards a more complete accounting of household emissions

Over the past four decades development of input-out analysis using methods developed by Nobel Laureate Wassily Leontief (Leontief, 1970) has made it possible to use economic input-out analysis to carry out more complete estimates of household energy consumption and carbon emissions. This is based on two related concepts: a) life cycle analysis: a method of estimating the impact of any resources use over its life cycle - from the point of raw material extraction to ultimate disposal of postconsumer wastes; and b) embodied energy (or embodied carbon): energy use or carbon emissions that occur at various stages over the life cycle of products and services that people eventually consume. This is applicable to both direct energy resources (electricity, natural gas, gasoline and other fuel) and non-energy goods and services (food, clothing, entertainment, insurance etc.). The following two examples illustrate this. A life cycle perspective of gasoline demonstrates that it is not just the emissions resulting from burning gasoline in automobiles, but energy is used and carbon emissions occur for finding, drilling, transporting, refining, and marketing gasoline. These add about 25% carbon emissions that are indirectly attributable to gasoline use. Therefore, the embodied CO_2 emissions for gasoline is 2.3 kg/liter from direct burning and an additional 0.6 kg/liter from indirect sources – resulting in a total embodied CO_2 of 2.9 kg/liter. While this example explains life cycle analysis and embodied emissions for an energy resource, all non-energy goods and services also have similar embodied life cycle emissions. For example, energy related emissions take place throughout the life cycle of the clothes people buy. If all these emissions are added up and normalized for every dollar spent on clothing in the US, the embodied CO_2 emissions for clothing amount to 0.43 kg/$.

Life cycle analysis – particularly for all products and services in an economy - appears to be a daunting task. This is where Leontief's work on input-output analysis came in handy. Originally developed for macro-economic analysis, Leontief formulated a mathematical process of inverting the complex matrix of all inter-sector transactions in an economy to derive the total final consumption of individual sectors (Leontief, 1970). This allowed for tracking the flow of money through and between sectors in any given year. Robert Herendeen, Bruce Hannon, Clark Bullard, and others associated with the Energy Resources Group at the University of Illinois carried out the seminal work of using Leontief's method to track the flow of money spent on energy resources (or in some cases the physical flows of energy) within the US economy and then converting the results into the physical quantities of energy used by various industries and enterprises. When this data is combined with national consumer expenditure data, one can actually estimate both the energy intensities of products and services and of households of different income groups (Bullard & Herendeen, 1975; Herendeen & Tanaka, 1976; Herendeen, 1978; Herendeen et al., 1981). Notable follow-up work that builds on this approach has been done by Manfred Lenzen of University of Sydney, Rutger Hoekstra of Statistics Nederlands, and many others who used this approach to not only estimate energy intensities but also carbon emissions and other environmental impacts. Hoekstra (2010) compiled a database of the development of environmental analysis based on Leontief's input-out method. More recent estimates of energy and carbon intensities are reported in Shammin et al (2010), Shammin & Bullard (2009), and Bin & Dowlatabadi (2005). These papers primarily used the Economic Input Output Life Cycle Analysis (EIOLCA) database developed at Carnegie Melon University[2]. This method now allows for a much more complete and in-depth understanding of household energy use and carbon emissions that can directly be linked to people's behavior and choices. While details on the methods can be found in the papers cited above, figure 3 provides a generic outline of the process of using economic input-output analysis to estimate carbon intensities for goods and services and combining that with consumer expenditure data to derive total household carbon emissions.

3. Consumption based household CO_2 emissions

An analysis of the US economy on the basis of personal consumption and other expenditures presents a very different perspective than the *sectoral* and *end use* approaches. In this view, based on data from the Bureau of Economic Analysis, personal consumption expenditures in 2003 accounted for about 70% of the gross domestic product (GDP) while the remaining 30% was shared by government expenditure, investment, and net exports[3]. Here, US households contributed about 4.17 billion metric tons of CO_2 emissions through their consumption of various goods and services – about 71% of the national total emissions of 5.86 billion metric tons[4]. Based on numbers reported in figure 4, a few key indicators can be calculated for 2003: the energy and CO_2 intensities of the economy were 10,058 kJ/$ and

[2] Carnegie Mellon University Green Design Institute. Economic Input-Output Life Cycle Assessment (EIO-LCA), Available from: http://www.eiolca.net

[3] For consumption based household emissions, all numbers are for the year 2003 for consistency with the results of economic input-output analysis of embodied energy and carbon reported in Shammin et al (2010) and Shammin & Bullard (2009).

[4] These calculations are based on data from Table 1.5 of the Annual Energy Outlook 2007 published by the EIA and results reported in Shammin & Bullard (2009).

0.55 kg/$ respectively; annual per-capita emission was 20 metric tons/person; and annual per-household emission was 51 metric tons/household.

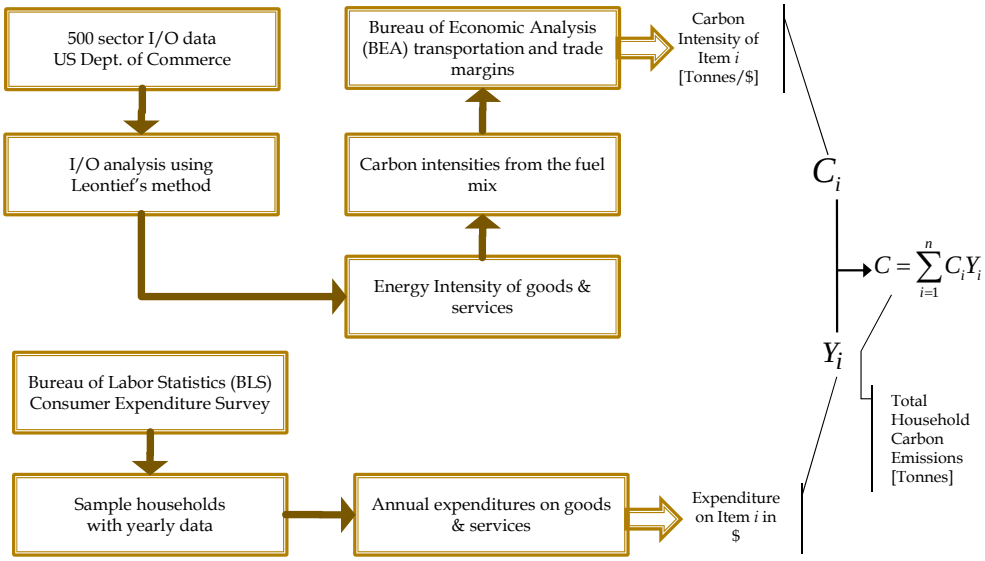

Fig. 3. Process of calculating carbon intensities using economic input-output analysis and total household carbon emissions by summing the product of carbon intensity and consumer expenditure data for individual sectors across all *n* consumer items. (Shammin, 2009)

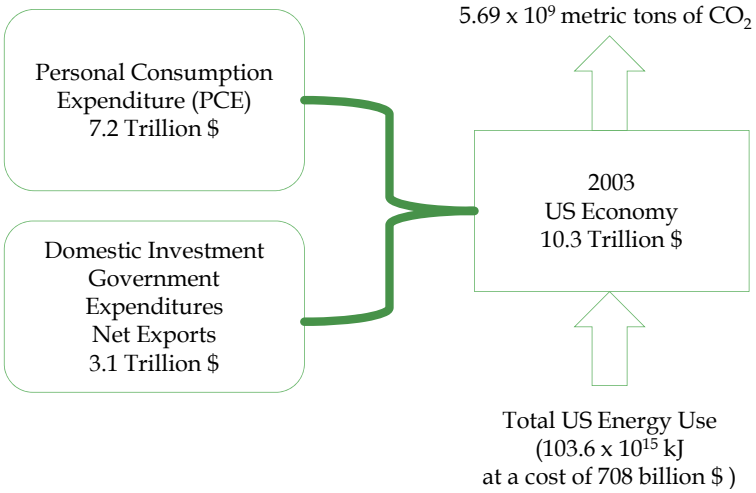

Fig. 4. GDP components, energy use and CO_2 emissions for the US economy, 2003. (Based on data from EIA and BEA)

The consumption based perspective on household emissions communicates a very different message to people. It shows that people have the power to directly and indirectly affect a large component of the nations' carbon emissions through behavior and lifestyle changes that would affect their consumption patterns and preferences. People also have the power to affect the remaining 29% of emissions; however, that would require engagement beyond personal choices. Through political activism and voting patterns, people in a democracy have the power to communicate how the government should spend their tax dollars. Regarding domestic investment, increasingly there are options being available to make investment choices on the basis of environmental performance. Finally, export-import policies can be reformed to trade with partners that are more environmentally responsible. None of this is easy; but at least this way of relating people and their behavior with national carbon emissions and mitigation opportunities provides a perspective that is either missing or inadequately addressed in the *sectoral* and *end use* approaches.

3.1 CO_2 emissions by the average US household

The most recent results to date for consumption-based carbon emissions for US households are reported in Shammin & Bullard (2009). The methods are based on calculations of energy intensities using input-output analysis described in Shammin et al (2010). These two papers also discuss the assumptions, nuances, and uncertainties associated with this approach. In 2003, the average household in the US spent about $49,000 of which only 6.5% was spent on direct energy. The total embodied CO_2 emission per household was about 37 metric tons of which about 65% was from direct energy. Thus, a small percent of household expenditure is actually responsible for the bulk of its carbon emissions. However, it is also interesting to see that the remainder of household expenditures made on non-energy goods and services were responsible for about 35% of the total embodied carbon emissions by the average household. This is a significant part of household emissions that is associated with life cycle emissions and the linkages between people and the sectors of the economy beyond residential and personal automobiles. The breakdown of total expenditure and total embodied carbon emissions are shown in figure 5a and 5b.

3.2 CO_2 Intensities of consumption categories

Shammin & Bullard (2009) reports detailed carbon intensities for all personal consumption categories based on standard classification of the Bureau of Labor Statistics. A list of carbon intensities for major consumption categories is given in table 1. The distribution of carbon emissions between expenditure categories shown in figure 5b and the intensities in table 1 together provide valuable insights into household energy consumption and related conservation opportunities.

It is important to understand the different implications of the magnitude of CO_2 emissions attributable to households (~37 metric tons/household-yr), the percentage share of specific consumption categories (~38% for residential energy), and the above carbon intensities. The total annual carbon emission, which is the grand total derived by summing the products of the carbon intensities and expenditures for individual items as shown earlier in figure 3, is actually the ultimate measure for the carbon footprint of a given household. Energy efficiency and conservation measures are intended to reduce this total emission. It is now a common consensus among most proposals for climate legislation that US needs to reduce

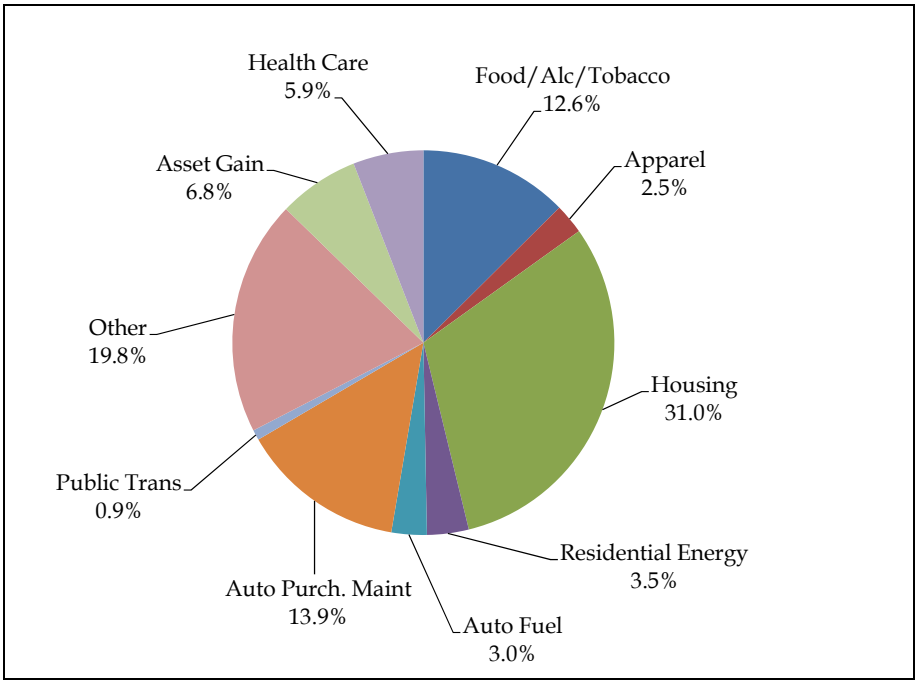

Fig. 5a. Breakdown of annual expenditures for the average US household in 2003

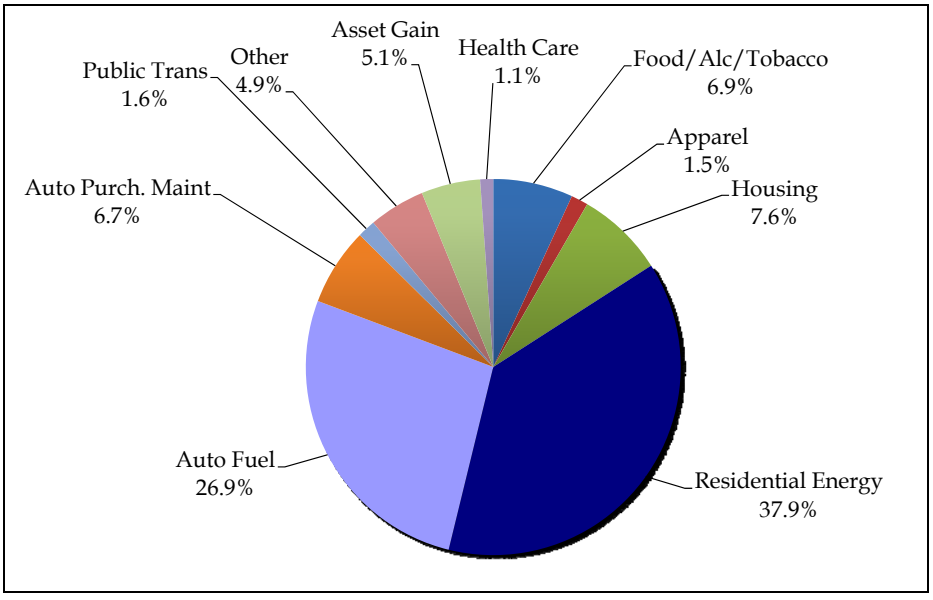

Fig. 5b. Breakdown of annual CO_2 emissions for the average US household in 2003

CO_2 emissions by 80% or more. This cannot be achieved without significant reductions at the household level. Share of emissions by specific consumption categories is also important because small percent reductions in large categories can result in a bigger difference than large percent reductions in small categories. Finally, carbon intensities indicate how carbon efficient different consumption categories are and provide an explicit basis for comparisons across categories.

	CO_2 Intensity (kg/$)
Average CO_2 Intensity (all categories)	0.80
Average CO_2 Intensity of Direct Energy	7.53
Natural gas	6.25
Electricity	8.02
Fuel oil and other fuels	8.07
Gasoline and motor oil	6.87
Average CO_2 Intensity of Indirect Energy	0.32
Housing	0.34
Owned dwellings	0.24
Telephone services	0.17
Water and other public services	0.59
Household operations	0.16
Housekeeping supplies	0.34
Household furnishings and equipment	0.33
Housing structure	0.80
Cars and trucks, new	0.46
Cars and trucks, used	0.50
Other vehicles	0.66
Vehicle finance charges	0.14
Maintenance and repairs	0.29
Vehicle insurance	0.07
Vehicle rental, leases, licenses, other charges	0.19
Public transportation	1.38
Food	0.41
Alcoholic beverages	0.33
Tobacco products and smoking supplies	0.13
Apparel, footwear and related services	0.43
Health care	0.14
Personal care products and services	0.27
Entertainment	0.22
Reading/education	0.21
Cash contributions	0.27
Personal insurance and pensions	0.11
Miscellaneous	0.28

Table 1. CO_2 intensities of major household consumption categories.

3.3 Predictors of household CO_2 emissions

Energy consumption and related carbon emissions vary across households depending on several key demographic and lifestyle related factors. Household income is the most influential predictor of total household emissions and how those emissions are distributed across various consumption categories. In general, the relationship between income and carbon emissions is non-linear (figure 6) – resulting in regressive impacts on low income households (Shammin & Bullard, 2009).

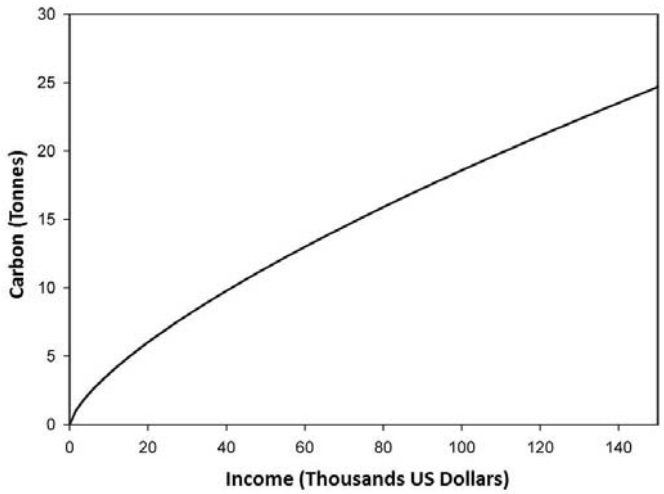

Fig. 6. Relationship between annual household income and carbon emissions. (Shammin & Bullard, 2009)

There is a large difference in the total annual carbon emissions and the share of indirect carbon emissions between households belonging to the lowest and highest income quintiles. In 2003, the total CO_2 emission of the highest quintile (~68 metric tons) was four times higher than that of the lowest quintile (~17 metric tons). At the same time, the share of indirect emission was close to 50% for the highest quintile as opposed to less than 20% for the lowest quintile. The latter has important implications: if price of direct energy resources go up as a result of climate change legislations, the effect on low income households will be disproportionately higher than high income households. Figure 6 shows that if a new cap-and-trade or carbon tax policy puts a price on carbon emissions at $100/metric ton, the impact on low income households can be more than 4% of their income as opposed to less than 2% for high income households (Shammin & Bullard, 2009).

Another important predictor of household emissions is the location of residence. Households in rural areas consumed about 17% higher total energy compared to households of the same income level residing in urban locations. Bigger homes, longer commutes, greater use of outdoor power equipment, etc. are typically responsible for this difference. Other predictors that affect total household energy consumption include: family size (about 28% more for a family of 4 compared to single-occupant households), number of cars (about 27% more for a household with two cars compared to households with no cars),

and housing type (about 44% more for single-family homes compared to apartments). These differences, reported in Shammin et al (2010), are estimated for households with the same income having different demographic and lifestyle configurations. While these differences are for total energy consumption, they would yield very similar differences in total household carbon emissions as well.

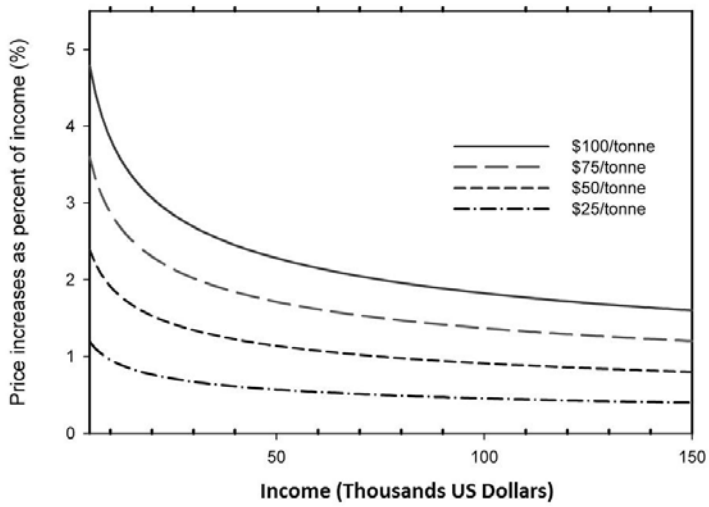

Fig. 7. Price increases for goods and services consumed by households as percent of annual household income due to different prices of carbon emissions. Here, emission data is for carbon and not CO_2 and tonne = metric tons. (Shammin & Bullard, 2009)

4. The role of households in reducing CO_2 emissions

Consumption based approach to household carbon emissions puts households and the people living in them front and center in exploring ways of reducing national carbon emissions. This requires households to develop a comprehensive strategy for carbon emission reductions that involves specific actions to address the various sources of emissions: direct emissions, indirect emissions, and emissions related to government expenditure, investment, and net exports. A pre-requisite for this is the motivation and willingness by members of any given household to undertake the solutions that apply to them. Literature in environmental psychology has several studies that investigate ways of motivating people to change behavior and adopt conservation and efficiency measures to reduce their carbon footprint (Nolan et al, 2008; Parnell & Larsen, 2005). Examples of successful interventions from some recent research include: innovative ways of providing real time feedback on energy and resource use (Petersen et al 2007; Petersen & Frantz, 2009) and offering financial incentives for reducing resource consumption (Suter & Shammin, 2010). Once households are committed to reduce emissions, they have to balance several

different approaches to address their total emissions. Throughout this process, households need to monitor their carbon footprint and track their progress in order to achieve most effective results. People are used to budget their income and expenses on a regular basis. Current challenges of climate change require people to go beyond financial budgeting and begin to develop methods to monitor their energy use and carbon emissions. The paradigm shift and associated challenges required for this to become mainstream involve discussions that are beyond the scope of this chapter.

The *end use* approach mentioned earlier provides the basis for reductions of direct emissions for households within the scope of the residential sector and personal transportation sub-sector. These mostly include direct conservation and efficiency measures that households can take.

Conservation measures: these involve reducing carbon intensive behaviors or replacing carbon intensive behaviors with emission-free options. Examples include:

a. walking/biking instead of using automobiles
b. reducing number of daily trips using motorized transportation
c. using clotheslines instead of dryers
d. making weather appropriate clothing choices indoors and airflow/shade management instead of using air conditioning
e. lowering thermostat setting in winter and raising it in summer
f. lowering water heater temperature
g. choosing to live in a smaller home
h. choosing to drive a smaller automobile

Efficiency measures: these involve replacing less efficient equipment with more efficient ones to achieve the same task. Examples include:

a. upgrading inefficient HVAC systems and appliances
b. improving insulation and reducing leakage in homes
c. using more efficient water heaters
d. replacing incandescent light bulbs with compact fluorescent or light emitting diode light bulbs
e. taking inventory of household electronics, eliminate unnecessary ones, and using power strips and on/off switches to avoid phantom loads
f. using public transportation instead of personal automobile
g. replacing fuel-inefficient vehicles with more fuel-efficient vehicles
h. regular maintenance of home appliances, HVAC equipment, and automobiles
i. installing renewable energy systems in homes such as solar, wind, geothermal, etc.
j. building homes that are designed to maximize the use of passive solar energy

The interplay between conservation and efficiency measures is also important to understand. Here, the ultimate goal is to reduce carbon emissions. However, overemphasis on efficiency measures may lead to *Jevon's Paradox* (people replacing inefficient cars with efficient ones and then driving more miles than before to offset or overshoot energy/carbon savings). On the contrary, when conservation and efficiency measures are coupled, households will be able to maximize their emission reductions. Dietz et al (2009) shows that

reasonably achievable household emissions reduction in the US can be approximately 20% within 10 years if the most effective non-regulatory interventions are used.

In addition to the direct emissions, consumption based approach also allows for households to understand, estimate, monitor and reduce indirect carbon emissions. US society has been on a treadmill of consumption for several decades where more consumption is considered a desirable goal. The core message in this approach is that consumption of non-energy goods and services has associated life cycle carbon emissions and thus reducing consumption would help reduce carbon emissions. As shown in table 1, there is very little difference in the carbon intensity of the various consumption categories responsible for indirect carbon emissions. Any reduction in consumption, irrespective of which items are avoided, would yield similar reductions in a household's carbon footprint. Notable exceptions are water and public transportation. Another related issue is rebound effects. If money saved from the reduction of direct energy is re-spent on other goods and services, part of the conservation savings would be offset. For example, if a household saves $1,500 by conserving direct energy consumption, they would reduce their CO_2 emissions by about 11 metric tons. If that money is re-spent on other goods and services, that would generate about 0.5 metric tons of additional CO_2 – resulting in a net savings of 10.5 metric tons. For a single household this may appear to be a small effect, but added across the economy this addition amounts to more than 50 million metric tons. This effect can become much larger if this money is re-spent on more carbon intensive choices such as flying to far-away places for family vacations.

Influencing the components of GDP beyond personal consumption (see figure 4) requires a different approach – since these involve decision making entities that are exogenous to individual households. A democratic society has avenues for people to influence decisions made by the government about how public tax dollars should be spent – through voting patterns, writing letters to representatives, and other types of civic engagement and political activism. If government expenditure on building roads is shifted towards the development of high speed rail or government subsidy to fossil fuels is shifted towards new incentives for renewable energy projects, significant reductions in carbon emissions can be achieved in the government expenditure component. It is also important to note that reductions of direct and indirect carbon emissions by households would not change the carbon intensity of the underlying infrastructure such as the source mix of power generation or transportation driven by internal combustion engines. Reduction in household electricity use would only go so far if more than 80% of the electricity is generated from coal (which is the case in many US states such as Ohio). Through activism and engagement, people have the opportunity to influence a shift from carbon intensive fossil fuel based sources to carbon-neutral or carbon-free renewable sources. This will have a large impact on economy-wide reductions in carbon emissions.

In terms of the investment component of GDP, many investment portfolios now make information on environmental performance or carbon offsets available to investors. If more and more people invest in these green stocks, the carbon footprint of investment can go down. Perhaps the most complicated component of GDP for people to influence is net exports – as this involves carbon emissions associated with industries and commercial ventures in other countries. Reforms in trade policies can allow more partnerships with countries, industries and multi-national companies that promote climate friendly operations. If policy is ultimately reflective of the will of the people, then households can

play a role in paving the way for such transitions from carbon intensive to a low carbon or carbon-free economy.

Finally, reducing carbon emissions is not necessarily about compromises and sacrifices. There are multiple benefits of low carbon lifestyle in a low carbon economy for households. First, humanity is currently threatened by the grim prospect of catastrophic consequences unless human-induced climate change is slowed, halted or reversed. While there are theories about winners and losers in a post climate change world, in reality everyone is at risk as the global economy is now more interconnected than ever before. We have already seen how crisis in East Asian markets had ripple effects throughout the world and how economic downturn in the US is affecting other countries. Locally, households, communities and regions with low carbon footprint will be more resilient against increased prices of carbon intensive energy resources and consequent increases in the price of goods and services. Thus, a more comprehensive and aggressive strategy for reducing carbon emissions by households, particularly in a carbon intensive nation such as the US, makes sense on many levels: for the sustainability of human race, for a healthy environment for future generations, for economic stability, for social security, and for the development of more engaged and resilient communities.

5. Conclusion

The daunting task of combating climate change is a defining challenge of the present generation. Reducing global carbon emissions is the most important aspect of that challenge. The US is a major player in global climate mitigation initiatives – since it is responsible for more than 20% of global carbon emissions. While the residential sector in the US accounts for about 20% of US emissions, this chapter demonstrates that households can directly and indirectly play a very important role in reducing all of the nations' carbon emissions. They have direct control over about 46% of embodied carbon emissions in the US by managing their consumption of energy resources and indirect control over another 25% of emissions by managing their consumption patterns. They can also play a role in influencing the remaining 29% by promoting and/or supporting initiatives to reduce the carbon footprint of energy systems, government expenditures, investment portfolios, and even businesses and industries beyond US borders. They can do this by becoming more engaged citizens and exercising their democratic privileges. The *sectoral* and *end use* approaches used to represent household emissions in the US are important, but limited in terms of helping people fully understand how their lives are connected to all sectors of the economy. The consumption based approach presented in this chapter constitute a more comprehensive accounting of household emissions as it includes embodied carbon over the life cycle of products and services that people consume to support their lifestyle. Most importantly, this approach offers people much more direct ways of relating personal choices with large scale reductions of national carbon emissions. This is a perspective that has the potential to empower people to become proactive agents of change and provide more explicit tools to make a difference in the battle against climate change.

6. Acknowledgment

I would like to acknowledge my co-authors of the two papers (Shammin & Bullard, 2009; Shammin et al, 2010) that formulate the conceptual and analytical basis for the main

arguments presented in this paper. Special thanks go to Robert A. Herendeen at the University of Vermont and Clark W. Bullard at the University of Illinois for their mentorship and collaboration on the research that has made this chapter possible.

7. References

Bin, S. & Dowlatabadi, H. (2005). Consumer lifestyle approach to U.S. energy use and the related CO_2 emissions. *Energy Policy,* Vol. 33, pp. 197–208

Bullard, C.W. & Herendeen, R.A. (1975). The energy cost of goods and services. *Energy Policy,* Vol. 3, pp. 268–278

Dietz, T., Gardner, G., Gilligan,, J., Stern, P. & Vandenbergh, M. (2009). Household actions can provide a behavioral wedge to rapidly reduce US carbon emissions. *Proceedings of the National Academy of Sciences*, Vol. 44, pp. 18452–18456

EIA (2011). Annual Energy Outlook 2011. *US Energy Information Agency*. Washington D.C.

Herendeen, R.A. (1978). Total energy cost of household consumption in Norway, 1973. *Energy*, Vol. 4, pp. 615–630

Herendeen, R.A. & Tanaka, J. (1976). Energy cost of living. *Energy*, Vol. 1, pp. 163–178.

Herendeen, R.A., Ford, C., & Hannon, B. (1981). Energy cost of living, 1972–73. *Energy*, Vol. 6, pp. 1433–1450

Hoekstra, R. (2010). Towards a complete database of peer reviewed articles on environmentally extended input-out analysis. Paper presented at the 18th *International Input-output Conference*, June 20 – 25, Sydney, Australia

Leontief, W. (1970). Environmental Repercussions and the Economic Structure: An Input-Output Approach. *Review of Economic Statistics*, Vol. 52, pp. 262-277

Nolan, J., Schultz, P., Cialdini, R., Goldstein, N. & Griskevicius, V. (2008). Normative social influence is underdetected. *Personality and Social Psychology*, Bulletin 34, pp. 913 – 923.

Parnell, R. & Larsen, O. P. (2005). Informing the Development of Domestic Energy Efficiency Initiatives: An Everyday Householder-Centered Framework. *Environment and Behavior,* Vol. 37, No. 6, pp. 787-807

Petersen, J.E. & Frantz, C. (2009). Employing multiple modes and scales of real-time feedback to engage, educate, motivate and empower electricity and water conservation. Paper presented at the *Behavior, Energy and Climate Change (BECC)* meeting, November 15-18, Washington D.C.

Petersen, J. E., Shunturov, V., Janda, K., Platt, G. & Weinberger, K. (2007). Dormitory residents reduce electricity consumption when exposed to real-time visual feedback and incentives. *International Journal of Sustainability in Higher Education,* Vol. 8, No. 1, pp. 16-33

Shammin, M., 2009. Embodied Carbon Emissions by US Households: Missing emissions and equity impacts of calculators used in carbon offsets. Paper presented at the 5th Bi-Annual Meeting of the US Society for Ecological Economics: Science and Policy for a Sustainable Future, May 31 – June 3, Washington DC.

Shammin, M., Herendeen, R. A., Hanson, M. & Wilson, E. (2010). A Multivariate Analysis of the Energy Intensity of Sprawl versus Compact Living in the US for 2003. *Ecological Economics*, Vol. 69, Issue 12, pp.2363–2373

Shammin, M. & Bullard, C. (2009). Impact of Cap-and-trade Policies for Reducing Greenhouse Gas Emissions on U.S. Households. *Ecological Economics*, Vol. 68, pp. 2432–2438.

Suter, J and Shammin, M. 2010. Estimating Payback to Residential Energy Efficiency Measures: A Field Experiment. Selected paper prepared for presentation at the Agricultural & Applied Economics Association 2010 AAEA, CAES, & WAEA Joint Annual Meeting, Denver, Colorado, July 25-27, 2010.

9

The Uncertainty Estimation and Use of Measurement Units in National Inventories of Anthropogenic Emission of Greenhouse Gas

Oleh Velychko[1] and Tetyana Gordiyenko[2]
[1]*State Enterprise "All-Ukrainian State Scientific and Production Centre for Standardization, Metrology, Certification and Protection of Consumer" (SE "Ukrmetrteststandard")*
[2]*State Enterprise "Ukrainian Scientific-Research and Educational Centre of Standardization, Certification and Problems of Quality" (SE "UkrSREC")*
Ukraine

1. Introduction

A global policy for environmental protection is needed and is under discussion. One of the effects of modern global policy for environmental protection includes the multitude of measurements that are part of the process of environment protection, including the estimation of greenhouse gas (GHG) emission. Global climate studies bring together an enormous range of sciences and for a sound model to be developed it is necessary that the data from all these areas be comparable. The only way for this to be assured is for measurements in all areas of science to be made in terms of a well-defined system of units, namely the International System of Units (SI).

Human activities to have major impacts on the global climate change which caused by an increase of GHG in the atmosphere. In general, there is now a demand for people to have confidence in the credibility of the results of measurements because in so many ways decisions based on the data that come from measurements are increasingly seen to have a direct influence on the economy, human health and safety, and welfare. The United Nations (UN) and its member states adopted the UN Framework Convention on Climate Change (UNFCCC). Parties of the UNFCCC must estimate GHG anthropogenic emissions and to develop annual national GHG inventories.

The governing bodies of the World Meteorological Organization (WMO) and of the UN Environment Programme (UNEP) created a body, the Intergovernmental Panel on Climate Change (IPCC), to marshal and assess scientific information on the subject. For monitoring of global climate change and providing reliable data for climate modelling, a Global Atmospheric Watch (GAW) programme has started by the WMO. The UNFCCC is also starting probably the largest environmental monitoring programme in the world. Parties of UNFCCC can estimate GHG emissions in using two general approaches: direct measurement or proxy data (Velychko O. & Gordiyenko T., 2007a, 2011).

Today's global economy depends on reliable measurements and tests, which are trusted and accepted internationally. Metrology is the scientific study of measurement. Measurements have always been essential in supporting international trade and regulation. Metrology delivers the basis for the comparability of test results, e. g. by defining the units of the measurement and by providing traceability and associated uncertainty of the measurement results. Measurement results may be used provided that the corresponding characteristics of measurement uncertainty are known.

The tasks of the Joint Committee for Guides in Metrology (JCGM) are to maintain and promote the use of the Guide to the Expression of Uncertainty in Measurement (known as the GUM) and the International Vocabulary of Metrology (known as the VIM). The JCGM has taken over responsibility for these two documents, who originally published them under the auspices of the International Bureau of Weights and Measures (BIPM), the International Organization of Legal Metrology (OIML), the International Organization for Standardization (ISO), the International Electrotechnical Commission (IEC), the International Federation of Clinical Chemistry and Laboratory Medicine (IFCC), the International Union of Pure and Applied Chemistry (IUPAC), the International Union of Pure and Applied Physics (IUPAP), the International Laboratory Accreditation Cooperation (ILAC).

The General Conference on Weights and Measures (CGPM) adopted SI, for the recommended practical system of units of measurement. The nearly universal use of the SI has brought coherence to all scientific and technological measurements, a worldwide consensus on the evaluation and expression of uncertainty in measurement would permit the significance of a vast spectrum of measurement results in science, engineering, commerce, industry, and regulation to be readily understood and properly interpreted. Many of the quantities, their recommended names and symbols, and the equations relating them, are listed in the international standards ISO/IEC 80000, in which it is proposed that the quantities and equations used with the SI. The IUPAP recognizes the SI for expressing the quantitative results of measurements in physics. The IUPAC serves to advance the worldwide aspects of the chemical sciences and to contribute to the application of chemistry in the service of Mankind (Velychko O. & Gordiyenko T., 2007a, 2010).

Some metrological terms are used in special guides of the IPCC, which to use for preparation of national inventories of GHG. Therefore it is important to compare uncertainty estimation with international ecological and metrological guides, and to consider peculiarities of their using also. It is also important to consider peculiarities of SI units used in those ecological guides.

2. The use metrological terms in international environmental guides

All branches of science and technology need to choose their vocabulary with care. Each term must have the same meaning for all of its users. In order to try and resolve this problem in field of metrology at an international level, eight international organizations developed VIM. The IPCC and the UNFCCC resolved this problem in environmental field.

Throughout the review process, it is asked to assess the quality of the each Party's UNFCCC national inventory submission, with quality being determined by criteria (TACCC – Fig. 1):

transparency (disclosing sufficient and appropriate GHG-related information to allow intended users to make decisions with reasonable confidence); *accuracy* (reducing bias and uncertainties as far as is practical); *completeness* (including all relevant GHG emissions and removals); *consistency* (enabling meaningful comparisons in GHG-related information) and *comparability* (estimates of emissions and removals reported by countries in inventories should be comparable among countries) (ISO 14064-1…3, IPCC 2006). For this purpose, countries should use agreed methodologies and formats for estimating and reporting national inventories.

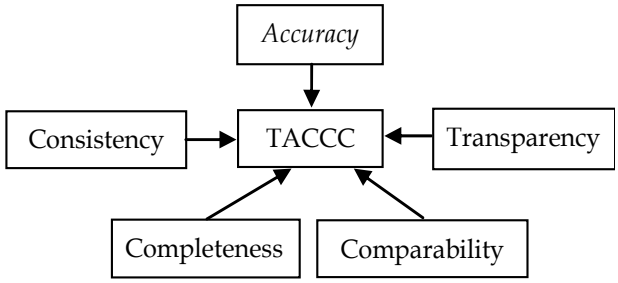

Fig. 1. The TACCC criteria

Definitions associated with conducting an uncertainty analysis include *accuracy*, *precision*, *uncertainty*, and *error* are described in GPG 2000, IPCC 2006, ISO 14064-1…3, VIM 2007, ISO 5725-1, ISO 3534-1 (Velychko O. & Gordiyenko T., 2005, 2007a, 2007b). Comparison of same metrological (and some statistical) and environmental guides and international standards terms are provided in Table 1.

Metrological terms	**Environmental terms**
A*ccuracy*: closeness of agreement between a measured quantity value and a true quantity value of a measurand (VIM 2007); closeness of agreement between a test result and the accepted reference value (ISO 5725-1, ISO 3534-1).	*Accuracy*: a general term which describes the degree to which an estimate of a quantity is unaffected by bias due to systematic error (GPG 2000); a relative measure of the exactness of an emission or removal estimate (IPCC 2006); reducing bias and uncertainties as far as is practical (ISO 14064-1…3).
Precision: closeness of agreement between indications or measured quantity values obtained by replicate measurements on the same or similar objects under specified conditions (VIM 2007); the closeness of agreement between independent test results obtained under stipulated conditions (ISO 5725-1, ISO 3534-1)	*Precision*: the inverse of uncertainty in the sense that the more precise something is, the less uncertain it is (GPG 2000); closeness of agreement between independent results of measurements obtained under stipulated conditions (IPCC 2006).

Metrological terms	**Environmental terms**
Uncertainty: non-negative parameter characterizing the dispersion of the quantity values being attributed to a measurand, based on the information used (VIM 2007); an estimate attached to a test result which characterizes the range of values within which the true value is asserted to lie (ISO 5725-1, ISO 3534-1).	*Uncertainty*: an uncertainty is a parameter, associated with the result of measurement that characterises the dispersion of the values that could be reasonably attributed to the measured quantity (GPG 2000); lack of knowledge of the true value of a variable that can be described as a probability density function characterizing the range and likelihood of possible values (IPCC 2006); parameter associated with the result of quantification which characterizes the dispersion of the values that could be reasonably attributed to the quantified amount (ISO 14064-1…3).
Error: measured quantity value minus a reference quantity value (VIM 2007); the test result minus the accepted reference value (of the characteristic), which is the sum of random errors and systematic errors (ISO 5725-1, ISO 3534-1).	*Error*: a general term referring to the difference between an observed (measured) value of a quantity and its "true" (but usually unknown) value and does not carry the pejorative sense of a mistake or blunder (GPG 2000).
Systematic error: component of measurement error that in replicate measurements remains constant or varies in a predictable manner (VIM 2007); a component of the error which, in the course of a number of test results for the same characteristic, remains constant or varies in a predictable way (ISO 5725-1, ISO 3534-1).	*Systematic error*: the difference between the true, but usually unknown, value of a quantity being estimated, and the mean observed value as would be estimated by the sample mean of an infinite set of observations (GPG 2000, IPCC 2006).
Random error: component of measurement error that in replicate measurements varies in an unpredictable manner (VIM 2007); a component of the error which, in the course of a number of test results for the same characteristic, varies in an unpredictable way (ISO 5725-1, ISO 3534-1).	*Random error*: the random error of an individual measurement is the difference between an individual measurement and the above limiting value of the sample mean (GPG 2000, IPCC 2006).

Metrological terms	Environmental terms
Coverage interval: interval containing the set of true quantity values of a measurand with a stated probability, based on the information available (VIM 2007).	*Confidence interval*: the range in which it is believed that the true value of a quantity lies (GPG 2000); the true value of the quantity for which the interval is to be estimated is a fixed but unknown constant, such as the annual total emissions in a given year for a given country (IPCC 2006).
Covariance: means of the mutual dependence of two random variables (GUM 1993).	*Covariance*: a measure of the mutual dependence between two variables (GPG 2000).
Correlation: the relationship between two or several random variables within a distribution of two or more random variables (ISO 3534-1).	*Correlation*: mutual dependence between two quantities (GPG 2000, IPCC 2006).
Correlation coefficient: measure of the relative mutual dependence of two variables, equal to the ratio of their covariances to the positive square root of the product of their variances (GUM 1993).	*Correlation coefficient*: a number laying between –1 and +1 which measures the mutual dependence between two variables which are observed together (GPG 2000, IPCC 2006).

Table 1. Metrological and environmental guides and international standard terms

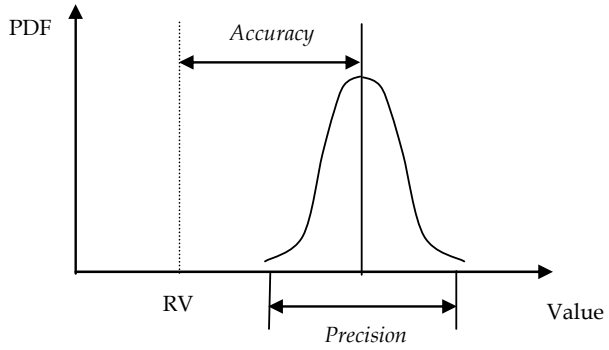

Fig. 2. Relationship between accuracy and precision

The *accuracy* and *precision* of individual measurements will depend upon the equipment and protocols used to make the measurements. A measurement system (equipment) is designated valid if it is both *accurate* and *precise*. The relationship between accuracy and precision is shown in Fig. 2 (PDF is probability density function; RV is reference value).

The concept "*measurement accuracy*" is not a quantity and is not given a numerical quantity value (VIM 2007). The term *accuracy*, when applied to a set of test results, involves a

combination of random components and a common systematic error or bias component (ISO 5725-1, ISO 3534-1). Estimates should be accurate in the sense that they are systematically neither over nor under true emissions or removals, so far as can be judged, and that uncertainties are reduced so far as is practicable (IPCC 2006).

Accepted reference value is a value that serves as an agreed-upon reference for comparison, and which is derived as: a theoretical or established value, based on scientific principles; an assigned or certified value, based on experimental work of some national or international organization; a consensus or certified value, based on collaborative experimental work under the auspices of a scientific or engineering group; when the first three are not available, the expectation of the (measurable) quantity, i.e. the mean of a specified population of measurements.

Measurement precision is usually expressed numerically by measures of imprecision, such as standard deviation, variance, or coefficient of variation under the specified conditions of measurement (VIM 2007). *Precision* is the inverse of uncertainty in the sense that the more precise something is, the less uncertain it is (IPCC 2006).

Precision depends only on the distribution of random errors and does not relate to the true value or the specified value. The measure of precision usually is expressed in terms of imprecision and computed as a standard deviation of the test results. Less precision is reflected by a larger standard deviation. "Independent results" means results obtained in a manner not influenced by any previous result on the same or similar test object. Quantitative measures of precision depend critically on the stipulated conditions (ISO 3534-1). The relationship between small or large accuracy and precision is shown in Fig. 3.

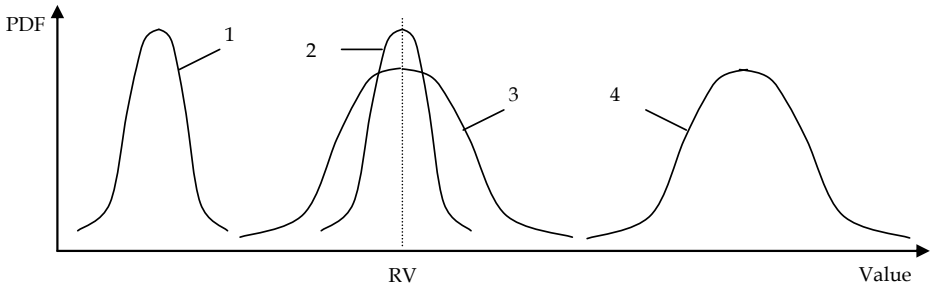

Fig. 3. Small or large accuracy and precision (1-small accuracy and large precision; 2-large accuracy and large precision; 3-large accuracy and small precision; 4-small accuracy and small precision)

The parameter (for uncertainty) may be, for example, a standard deviation called standard measurement uncertainty (or a specified multiple of it), or the half-width of an interval, having a stated coverage probability. In general, for a given set of information, it is understood that the measurement uncertainty is associated with a stated quantity value attributed to the measurand (VIM 2007).

Uncertainty of measurement comprises, in general, many components. Some of these components may be estimated on the basis of the statistical distribution of the results of a

series of measurements and can be characterized by *standard deviations*. Estimates of other components can only be based on experience or other information (ISO 3534-1).

Uncertainty depends on the analyst's state of knowledge, which in turn depends on the quality and quantity of applicable data as well as knowledge of underlying processes and inference methods (IPCC 2006). Uncertainty information typically specifies quantitative estimates of the likely dispersion of values and a qualitative description of the likely causes of the dispersion (ISO 14064-1…3).

Uncertainty should be distinguished from an estimate attached to a test result which characterizes the range of values within which the expectation is asserted to lie. This latter estimate is a measure of precision rather than of accuracy and should be used only when the true value is not defined. When the expectation is used instead of the true value the expression "random component of uncertainty" should be used.

Systematic measurement error, and its causes, can be known or unknown. A correction can be applied to compensate for a known systematic measurement error. *Random measurement errors* of a set of replicate measurements form a distribution that can be summarized by its expectation, which is generally assumed to be zero, and its variance (VIM 2007).

Error of result is the test result minus the accepted RV (of the characteristic). Error is the sum of systematic and random errors. *Systematic error* may be known or unknown; *random error* it is not possible to correct (ISO 3534-1).

The relationship between error and uncertainty is shown in Fig. 4 (GUM 1993).

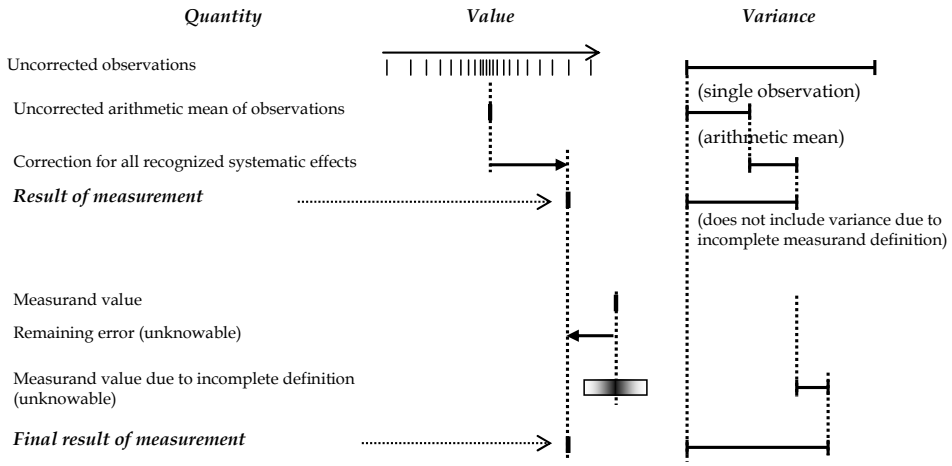

Fig. 4. Relationship between error and uncertainty

To express of the measurement result is used the expanded measurement uncertainty with a specified coverage interval which does not need to be centred on the chosen measured quantity value. This interval should not be termed "confidence interval" to avoid confusion with the statistical concept and can be derived from an expanded measurement uncertainty (GUM 1993, VIM 2007).

The level of belief is expressed by the probability, whose value is related to the size of the interval. It is one of the ways in which uncertainty can be expressed. In practice a confidence interval is defined by a probability value, say 95%, and confidence limits on either side of the mean value x. In this case the confidence limits would be calculated from the PDF such that there was a 95% chance of the true value of the quantity being estimated by x lying between those limits. Commonly limits are the 2.5 percentile and 97.5 percentile respectively (GPG 2000).

The *confidence interval* is a range that encloses the true value of this unknown fixed quantity with a specified confidence (probability). Typically, a 95 % confidence interval is used in greenhouse gas inventories. From a traditional statistical perspective, the 95 % confidence interval has a 95 % probability of enclosing the true but unknown value of the quantity. An alternative interpretation is that the confidence interval is a range that may safely be declared to be consistent with observed data or information. The 95 %confidence interval is enclosed by the 2.5^{th} and 97.5^{th} percentiles of the PDF (IPCC 2006).

Dependencies among input sources will matter only if the dependencies exist between two sources to which the uncertainty in the GHG national inventory is sensitive and if the dependencies are sufficiently strong. For the quantities evaluation of dependence of two or more input sources used the correlation coefficient.

A value of +1 of *correlation coefficient* means that the variables have a perfect linear relationship; a value of –1 of correlation coefficient means that there is a perfect inverse linear relation; and a value of 0 of correlation coefficient means that there is no straight line relation. It is defined as the covariance of the two variables divided by the product of their *standard deviations* (σ). The population standard deviation is the positive square root of the variance. It is estimated by the sample standard deviation that is the positive square root of the sample variance (GPG 2000, IPCC 2006).

For the preparation of GHG national inventories used the activity data (AD) and emission factor (EF). *Activity data* is data on the magnitude of a human activity resulting in emissions or removals taking place during a given period of time. Data on energy use, metal production, land areas, management systems, lime and fertilizer use and waste arisings are examples of AD. *Emission factor* is a coefficient that quantifies the emissions or removals of a gas per unit activity. EF is often based on a sample of measurement data, averaged to develop a representative rate of emission for a given activity level under a given set of operating conditions (IPCC 2006).

3. Uncertainty estimation in international environmental and metrological guides

Parties of UNFCCC can estimate GHG emissions in using two general approaches: direct measurement or proxy data. The concept of uncertainty in direct measurements is more consistent with a statistical concept of uncertainty. The statistical issues include precision and calibration of measurement equipment, fraction of population captured, frequency of sampling, etc. In contrast, proxy data is more typically in the form of AD and EF. The proxy data approach requires assumptions as to the relationship between some activity and actual emissions (IPCC 2006).

GHG emissions can be measured either directly or indirectly. The indirect approach usually involves the use of an estimation model (e.g., AD and an EF), while the direct approach requires that emissions to the atmosphere be measured directly by some form of instrumentation (e.g., continuous emissions monitor). As the data used in the direct or indirect measurement of GHG emissions are subject to random variation there is always statistical uncertainty associated with the resulting emission estimates.

The uncertainty in this relationship must be considered as well as the accuracy and precision in measurements in the proxy data itself. An uncertainty is a parameter, associated with the result of measurement that characterizes the dispersion of the values that could be reasonably attributed to the measured quantity (GPG 2000). An *uncertainty analysis* of a model aims to provide quantitative measures of the uncertainty of output values caused by uncertainties in the model itself and in its input values, and to examine the relatively importance of these factors.

The IPCC guides (GPG 2000, IPCC 2006) use two main statistical concepts: the PDF and *confidence limits*. On Fig. 5 show PDF and cumulative distribution function (CDF) graphs. The PDF describes the range and relative likelihood of possible values; confidence limits give the range within which the underlying value of an uncertain quantity is thought to lie (confidence interval). The IPCC Guides suggest the use of a 95 % confidence interval, which is the interval that has a 95 % probability of containing the unknown true value.

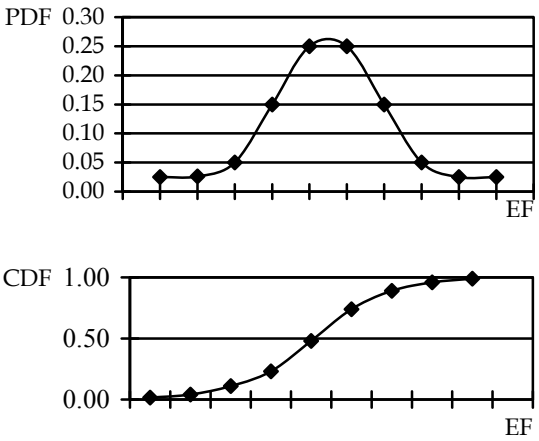

Fig. 5. PDF (a) and CDF (b) graphs

PDF is a mathematical function which characterizes the probability behaviour of population. It is a function $f(x)$ which specifies the relative likelihood of a continuous random variable X taking a value near x, and is defined as the probability that X takes a value between x and $x+dx$, divided by dx, where dx is an infinitesimally small number. Most PDFs require one or more parameters to specify them fully.

The probability that a continuous random variable X lies in between the values a and b is given by the interval of the PDF, $f(x)$, over the range between a and b:

$$\Pr(a \le x < b) = \int_{b}^{a} f(x)dx \,.$$

The PDF is the derivative (when it exists) of the distribution function ($F(x)$ for a random variable X specifies the probability $\Pr(X \le x)$ that X is less than or equal to x):

$$f(x) = \frac{dF(x)}{dx} \,.$$

In practical situations, the PDF used is chosen from a relatively small number of standard PDFs and the main statistical task is to estimate its parameters. Thus, for inventory applications, a knowledge of which PDF has been used is a necessary item in the documentation of an uncertainty assessment (GPG 2000).

Uncertainty information on the EF, AD and other parameters used for the uncertainty analysis must be collected to create PDF (for the Monte Carlo method) or mean and standard deviation of the data (for the error propagation method). As this uncertainty data is collected, the correlations between parameters should also be considered.

The measurement error is one of the first types of uncertainty of GHG emission inventories, which may be: results from errors in measuring, recording and transmitting information; finite instrument resolution; inexact values of measurement standards and reference materials; inexact values of constants and other parameters obtained from external sources and used in the data-reduction algorithm; approximations and assumptions incorporated in the measurement method and estimation procedure; and/or variations in repeated observations of the emission or uptake or associated quantity under apparently identical conditions. Measurement error can be reduced using more precise measurement methods, avoiding simplifying assumptions and ensuring, that measurement technologies are appropriately used and calibrated.

Uncertainties also may be a result of: measurements were attempted but no value was available (missing data); and measurement data are not available either because the process is not yet recognized or a measurement method does not yet exist (lack of completeness). Where a PDF can be identified, sources of uncertainty can be addressed by statistical means (*type A of uncertainty* for GUM 1993). There can be structural uncertainties that are not easily incorporated into a quantitative uncertainty analysis in the form of a PDF. These types of situations are typically outside the scope of statistics (*type B of uncertainty* for GUM 1993).

Comparison of uncertainty estimation in metrological and environmental guides are provided in Table 2 (Velychko O. & Gordiyenko T., 2005; Gordiyenko T. & Velychko O., 2006; Velychko O. & Gordiyenko T., 2007a; Velichko O. N. & Gordienko T. B., 2007c, 2009; Velychko O. M. & Gordiyenko T. B., 2008; Velychko O. & Gordiyenko T., 2009).

The pragmatic approach for producing quantitative uncertainty estimation is using the best available estimates, which are often a combination of measured data, published information, model outputs, and expert judgement. Although uncertainties determined from measured data are often perceived to be mote rigorous than uncertainty estimates based on models, and similarly.

Metrological guides	**Environmental guides**
Type A of GUM 1993 regulated using assessment of uncertainty (components evaluated by statistical methods to a series of repeated determinations) and use equation: $u_A = \frac{s}{\sqrt{n}}$, where: *s* is the standard deviation; *n* is the number of measurements.	Rule A of GPG 2000 regulated using assessment of uncertainty and use equation: $U_{total} = \frac{\sqrt{(U_1 \cdot x_1)^2 + (U_2 \cdot x_2)^2 + \ldots + (U_n \cdot x_n)^2}}{x_1 + x_2 + \ldots + x_n}$, where: U_{total} is percentage of uncertainty in the sum of the quantities*; x_i and U_i are the uncertain quantities and percentage of uncertainties associated with them, respectively.
Type B of GUM 1993 regulated using assessment of uncertainty (components evaluated by other means) and use equation: $u_B = \frac{U}{k}$, where: *U* is the expanded uncertainty given in Certificate; *k* is the coverage factor (typically *k* = 2).	Rule B of GPG 2000 regulated using assessment of uncertainty (if impossible use statistical processing) and use equation: $U_{total} = \sqrt{U_1^2 + U_2^2 + \ldots + U_n^2}$, where: U_{total} is percentage of uncertainty in the product of the quantities*; U_i are percentage of uncertainties associated with each of the quantities.
In GUM 1993 the overall uncertainty arising from the combination of type A and type B uncertainties calculated used equation: $u_c = \sqrt{\sum_{i=1}^{m} u_i^2}$ or $\hat{u}_c = \sqrt{\hat{u}_A^2 + \hat{u}_B^2}$, and $U_p = k \cdot u_c$ where: u_c is the total uncertainty; u_i is the components of uncertainty; U_p is the expanded uncertainty.	In IPCC 2006 the overall uncertainty arising from the combination of EF and AD uncertainty calculated used equation: $U_T = \pm\sqrt{(U_E^2 + U_A^2)}$, where: U_E is percentage of uncertainties associated with the EF; U_A is percentage of uncertainties associated with the AD, so long as $\lvert U_E \rvert$, $\lvert U_A \rvert$ < 60 %**.
* half the 95 % confidence interval divided by the total and expressed as a percentage; ** the 60 % limit is imposed because the rule suggested for U_T requires σ to be less than about 30 % of the central estimate, and we are interpreting the quoted range as ± 2σ.	

Table 2. Uncertainty estimation in metrological and environmental guides

Probability distribution is a function giving the probability that a random variable takes any given value or belongs to a given set of values. The probability on the whole set of values of the random variable equals 1. Many commonly used PDF distributions of practical important are: uniform; triangular, normal; lognormal; and fractile (Fig. 6).

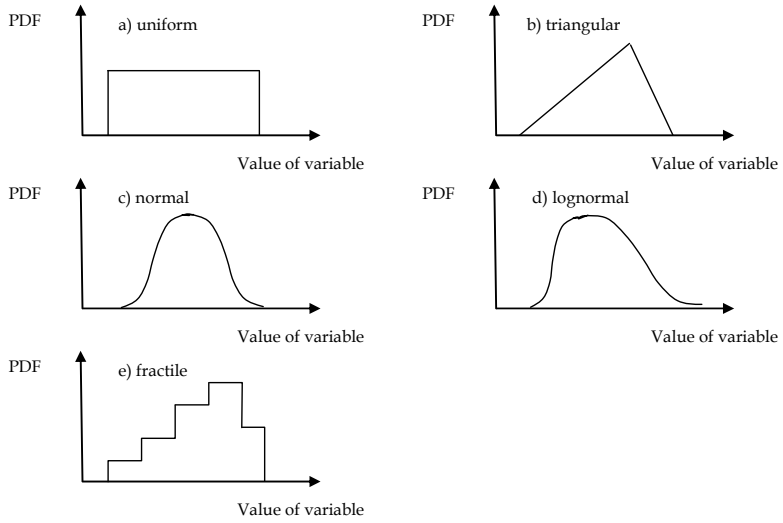

Fig. 6. Some commonly used PDF models

Uniform distribution describes an equal likelihood of obtaining any value within a range. Sometimes the uniform distribution is useful for representing physically-bounded quantities. The PDF of the uniform distribution is given by:

$$f(x) = \begin{cases} 1/(b-a), \text{ for } a \le x \le b, \\ 0 \quad \text{elsewhere}, \end{cases}$$

where:

$\mu = (a+b)/2$ is a mean and;

$\sigma^2 = (a+b)^2/12$ is the variance.

The *triangular distribution* is appropriate where upper and lower limits and a preferred value are provided by experts but there is no other information about the PDF. The triangular distribution can be asymmetrical. The PDF of the triangular distribution is given by:

$$f(x) = \begin{cases} 2(x-a)/\{(b-a)(m-a)\}, \text{ when } a \le x \le m \text{ and } a < m \le b, \\ 2(b-x)/\{(b-a)(b-m)\}, \text{ when } m \le x \le b \text{ and } a \le m < b, \\ 0 \qquad \text{elsewhere}, \end{cases}$$

where:

a, b are minimum and maximum value respectively;

m is mode (most likely position), subject to $a \le m \le b$.

The *normal* (*or Gaussian*) *distribution* is most appropriate when the range of uncertainty is small, and symmetric relative to the mean. This distribution arises in situations where many individual inputs contribute to an overall uncertainty, and in which none of the individual uncertainties dominates the total uncertainty. The PDF of the normal distribution is given by:

$$f(x) = \frac{1}{\sigma\sqrt{2\pi}} e^{-\frac{(x-\mu)^2}{2\sigma^2}}, \text{ for } -\infty \le x \le \infty.$$

The *lognormal distribution* may be appropriate when uncertainties are large for a non-negative variable and known to be positively skewed. If many uncertain variables are multiplied, the product asymptotically approaches lognormality. The PDF of the lognormal distribution is given by:

$$f(x) = \frac{1}{\sigma_l x\sqrt{2\pi}} e^{-\frac{(\ln x-\mu_l)^2}{2\sigma_l^2}}, \text{ for } 0 \le x \le \infty.$$

The parameters required to specify the function are: μ_l the mean of the natural log transform of the data; and σ_l^2 the variance of the natural log transform of the data. The data and information that the inventory compiler can use to determine the input parameters are: μ_l is mean; σ^2 variance; and the relationships:

$$\mu_l = \ln\frac{\mu^2}{\sqrt{(\sigma^2+\mu^2)}} \quad \text{and} \quad \sigma_l = \sqrt{\ln\left(\frac{\sigma^2}{\mu^2}+1\right)} \quad .$$

Fractile distribution is a type of empirical distribution in which judgements are made regarding the relative likelihood of different ranges of values for a variable (GPG 2000).

The rules for *uncertainties propagation* specify how to algebraically combine the quantitative measures of uncertainty associated with the input values to the mathematical formulae used in GHG national inventory compilation, so as to obtain corresponding measures of uncertainty for the output values. The *Monte Carlo analysis* is suitable for detailed category-by-category assessment of uncertainty, particularly where uncertainties are large, distribution is non-normal (non-Gaussian), the algorithms are complex functions and/or there are correlations between some of the activity sets, EF, or both (GPG 2000).

Simplified estimation of expanded measurement uncertainty for Type A is shown on Fig. 7.

Measurement uncertainty of the values equation is used:

$$Y = f(X_1, X_2, ..., X_m),$$

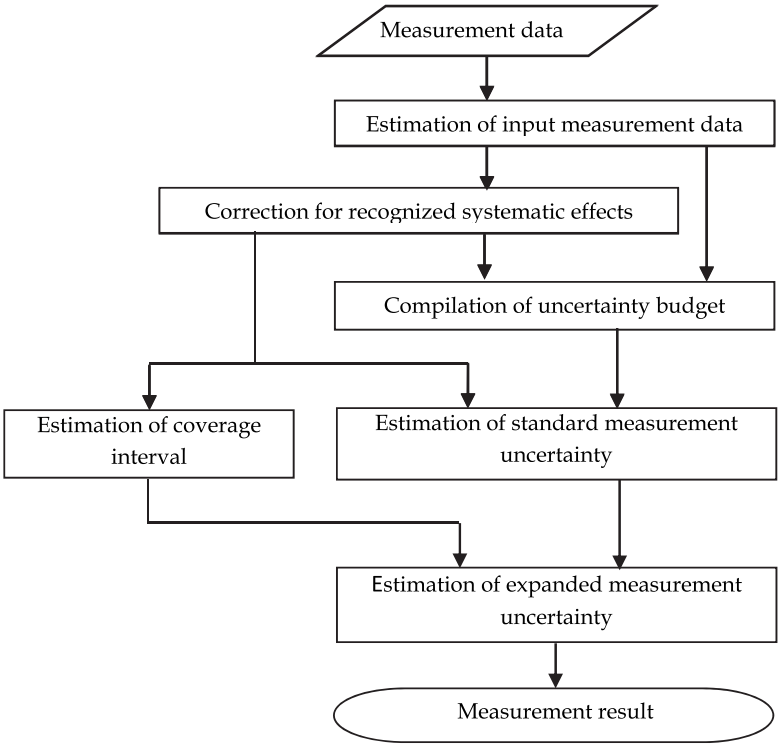

Fig. 7. Simplified estimation of expanded measurement uncertainty

where:

$X_1, \ldots, X_m$ are entrance value (direct measured value or other value which have an influence on measurement results);
m is quantity values;
f is functional dependence type.

Estimation of the standard measurement uncertainty $u_A(x_i)$ of measurement i-th input values without correlation input values may be calculated by means of the following equation:

$$u_A(x_i) = \sqrt{\frac{1}{n_i(n_i-1)} \sum_{q=1}^{n_i} \left(x_{iq} - \overline{x}_i\right)^2},$$

where:

x_{iq} is the measurement results of i-th input values;

$\overline{x}_i = \frac{1}{n} \sum_{q=1}^{n_i} x_{iq}$ is the arithmetic median of measurement results of i-th input values.

The overall standard uncertainty u_c (Table 2) determined by a combination of uncertainties components; estimation of the expanded measurement uncertainty U_p may be calculated by means of the equation from Table 2 (GUM 1993).

Statistical uncertainty in the context of GHG inventories is usually presented by giving an uncertainty range expressed in a percentage of the expected mean value of the emission. This range can be determined by calculating the "confidence limits", within which the underlying value of an uncertain quantity is thought to lie for a specified probability. The "confidence level" determines the probability, that the true value of emission is situated within the identified uncertainty range.

Determining the *t*-factor *t* (standard error that is to be estimated follows a *t*-distribution) can be done by using the Table 3.

Number of measurements (*n*)	***t*-factor (*t*) for confidence level 95 %**
3	4,30
5	2,78
8	2,37
10	2,26
50	2,01
100	1,98
∞	1,96

Table 3. *t*-factors for the 95% confidence level

4. Uncertainty estimation with correlation values

Necessity in the analysis of covariance and autocorrelation for the uncertainty estimates of emission foul and greenhouse gases exists. It is importantly to investigate the correlations of the estimated values relevant to emissions as in the context one estimation and the various estimations of emission foul and GHG.

If correlation exists between input values then this correlation is essential and can not be ignored. Covariance of input values may be estimated experimentally, on condition of possible the change of input correlated values (the estimation of type A covariance), or with the using of necessary data on the correlation changeability of values which relate to this measurement (the evaluation of type B covariance).

In practical cases input values often appear to be correlated, as far as the evaluation of their values is used by the same standards, measuring instruments, standard data and even method of measurement which possess peculiar uncertainty. If direct measurement results are not correlated then calculated value of covariance is expected to be close to zero.

Covariance with the estimations of two input values may be equal to zero or selected as negligible, if: these values are not correlated (values measurement are run repeatedly in various independent experiments, or they present the various estimations of values which made independently); any values may be is accepted as an constant; there is negligible data for calculation of covariance related with the estimations of these values.

Comparison of the uncertainties estimations of input values with correlation in metrological and environmental guides are driven in Table 4 (Velychko O. & Gordiyenko T., 2007b).

Metrological guides	**Environmental guides**
Entrance value is non correlated	
Using estimation of uncertainty in accordance with the law of propagation of uncertainty and use equation (GUM 1993): $u_c(y)=\sqrt{\sum_{i=1}^{m}(\partial f/\partial x_i)^2}$, $u^2(x_i)=\sqrt{\sum_{i=1}^{m}u_i^2(y)}$ or $u_c(y)=\sqrt{c_1^2u^2(x_1)+c_2^2u^2(x_2)+...+c_m^2u^2(x_m)}$, where: $u(x_i)$, $u_i(y)$ are standard uncertainty input ($i=1,m$) and output value respectively; y, x_i are estimations of measurable value Y and input value X_i respectively.	Using estimation of uncertainty Rule A and use equation (GPG 2000, IPCC 2006): $U_{total}=\frac{\sqrt{(U_1\cdot x_1)^2+(U_2\cdot x_2)^2+...+(U_n\cdot x_n)^2}}{x_1+x_2+...+x_n}$, where: U_{total} is percentage of uncertainty in the sum of the quantities; x_i, U_i are uncertain quantities and percentage of uncertainties associated with them, respectively.
Entrance value is correlated	
Using estimation of uncertainty in accordance with the law of propagation of uncertainty and use equation (GUM 1993): $u_c(y)=\sqrt{\sum_{i=1}^{m}(\partial f/\partial x_i)u^2(x_i)+2\sum_{i=1}^{m-1}\sum_{j=i+1}^{m}u(x_i,x_j)}$ or $u_c(y)=\sqrt{\sum_{i=1}^{m}u_i^2(y)+2\sum_{i=1}^{m-1}\sum_{j=i+1}^{m}c_ic_ku(x_i,x_j)}$ where: $u(x_i,x_j)$ is estimation covariance with two input estimations x_i and x_j; y is estimation of measurable value Y; x_i, x_j are estimation input values X_i and X_j respectively.	Not numerical estimated in GPG 2000 and IPCC 2006.
The degree of correlation between x_i and x_j is characterized by the estimated correlation coefficient (GUM 1993): $r(x_i,x_j)=r(x_j,x_i)=u(x_i,x_j)/[u(x_i)u(x_j)]$, where: $r(x_i,x_j)=r(x_j,x_i)$; $-1\le r(x_i,x_j)\le 1$.	A value of correlation coefficient of +1 means that the variables have a perfect direct straight line relation; a value of –1 means that there is a perfect inverse straight line relation; and a value of 0 means that there is no straight line relation (GPG 2000). It is defined as the covariance of the two variables divided by the product of their standard deviations.

Table 4. Uncertainty estimation with correlation in metrological and environmental guides

For correlation coefficient $r(x_i, x_j) = \pm 1$ uncertainties contribution is:

$$u_{i,j}(y) = \left| u_i(y) \pm u_j(y) \right| = \left| c_i u(x_i) \pm c_j u(x_j) \right| ;$$

if the estimates x_i and x_j are independent, $r(x_i, x_j) = 0$, and a change in one does not imply an expected change in the other.

Uncertainties aggregation arises of two various processes: aggregation of emissions one gas which complies with the law of propagation of uncertainty; aggregation of emissions bound with several gases. Into second case emission must be result in common scale, and been used for this process consists in the application of Global Warming Potentials (GWP).

Comparison of the emission sources with allowance for correlation and covariance of input values in metrological and environmental guides are driven in Table 5.

Metrological guides	**Environmental guides**
Correlation and covariance for entrance value	
For correlation and covariance with type *A* using the following equation: $u(\bar{x}_i, \bar{x}_k) = [1/n(n-1)] \sum_{j=1}^{n} (x_{ij} - \bar{x}_i)(x_{kj} - \bar{x}_k)$.	The sample covariance of paired sample of random variables *X* and *Y* is calculated using the following equation (GPG 2000, IPCC 2006): $s_{xy}^2 = \frac{1}{n} \sum_{i}^{n} (x_i - \bar{x})(y_i - \bar{y})$, where: x_i, y_i, $i = 1,\ldots,n$ are items in the sample; $\bar{x}$ and $\bar{y}$ are sample means respectively.
For correlation and covariance with type *B* using the following equation: $u(x_i, x_k) = \sum_{l=1}^{L} c_{il} \cdot c_{kl} \cdot u^2(Q_l)$, where: c_{il} , c_{kl} are sensitivity coefficients respectively; $u(Q_l)$ is standard uncertainty of variables Q_l .	
Uncertainties contribution every input values and sensitivity coefficient	
Uncertainties contribution $u_i(y)$ every input values X_i to uncertainty $u(y)$ using the following equations (GUM 1993): $u_i(y) = \lvert c_i \rvert u(x_i)$; $c_i = \partial y / \partial x_i = \partial Y / \partial X_i \big\vert_{x_1, x_2, \ldots, x_m}$ where: c_i are sensitivity coefficients; y is estimation of measurable value *Y*; $x_1, \ldots, x_m$ are input values ($i = 1, m$). For direct measurement all sensitivity coefficients are equal 1.	Sensitivity coefficient λ calculated using the following equation (GPG 2000): $\lambda = \partial E_T / \partial a$, where: E_T is the aggregated emissions; a is input quantity (or parameter). Dispersion of tendency for emission two different time $E(t)$ and $E(t + \Delta t)$ with Δt using the following equation: $\sigma^2(\Delta E) = 2\sigma^2{}_E (1 - r(\Delta t))$. where: $r(\Delta t)$ is correlation coefficient

Table 5. Comparison of uncertainty contributions in metrological and environmental guides

Some variables which are necessary aggregation, do not are Gauss, large dispersion and correlated with other variables are have. In this case the application of Monte-Carlo method

for uncertainties aggregation is presented the most preferable. The Monte Carlo analysis can be performed at the source category level, for aggregations of source categories, or for the inventory as a whole. It analysis can deal with PDF of any physically possible shape and width, can handle varying degrees of correlation (both in time and between source categories) and can deal with more complex models.

Algorithm of uncertainty estimation with correlation according to GUM 1993 is present on Fig. 8.

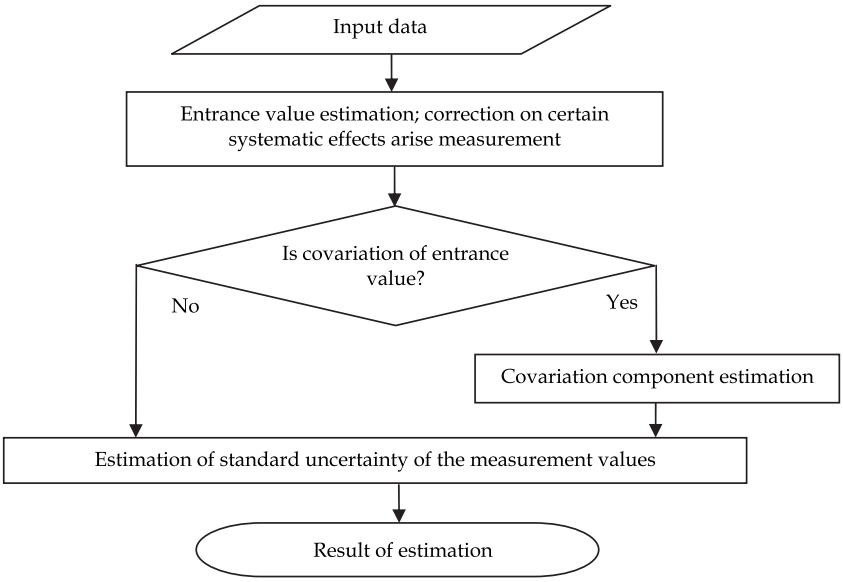

Fig. 8. Uncertainty estimation algorithm with correlation according to GUM 1993

Uncertainty results in compliance with GUM 1993 can be calculated with use a few well known commercially available software. Special software can be a useful tool for uncertainty estimation (Velychko O., 2008).

Overall uncertainty in total national GHG emissions in the current year, calculated using Rule A (corresponding Type A in accordance with GUM) and use equation

$$U_T = E_i \cdot U_{\sum B} / \sum E_T ,$$

where:

$U_{\sum B}$ is estimation of overall uncertainty Rule B;

E_i is GHG emissions from certain source category in CO_2-equivalent, Gg;

E_T is total GHG emissions from all source categories in CO_2-equivalent, Gg.

If overall uncertainty is correlated across years using estimation of overall uncertainty Rule B with uncertainty of EF only (assume AD to be equal 0 %).

For uncertainty of tendency of the GHG emission with EF uncertainty U_{EFt} (percentage) use equation:

$$U_{EF_t} = c_A \cdot U_{EF} ,$$

where: c_A is Type A sensitivity coefficient.

If between EF have not correlation necessary use Type B sensitivity and to multiply by $\sqrt{2}$.

For uncertainty of tendency of the GHG emission with AD uncertainty U_{ADt} (percentage) use equation:

$$U_{AD_t} = \sqrt{2} c_B \cdot U_{AD} ,$$

where: c_B is Type B sensitivity coefficient.

If between AD have correlation necessary use Type A sensitivity and not necessary to multiply by $\sqrt{2}$.

For estimation of uncertainty contribution U_{tdi} (percentage) which to make one's on tendency of overall GHG emission for each emission categories for Rule B use equation:

$$U_{tdi} = \sqrt{U_{EF_t}^2 + U_{AD_t}^2} .$$

For estimation of overall uncertainty contribution U_{td} (percentage) which to make one's on tendency of overall GHG emission use equation (GPG 2000):

$$U_{td} = \sqrt{\sum_i U^2{}_{tdi}} .$$

On Fig. 9 gives developed an uncertainty estimation algorithm with tendency, correlation and covariance according to GPG 2000 and IPCC 2006 which taking into consideration main requirements of GUM 1993.

5. Greenhouse Gas Protocol Uncertainty Tool

The IPCC 2006 for assessment GHG emissions used statistical AD of fuel combustion activities for different sectors and sources category and take account of direct and indirect GHG: CO_2, CH_4, N_2O, CO, NO_x, NMVOCs. Important element used IPCC 2006 is determination and/or selection EF which is take from IPCC 2006 ("default") or calculated as local for country, sectors, sources category or process. Accounts data submit in Common Reporting Format (CRF) which is standard data tables. IPCC 2006 contain chapter of key conceptions uncertainties, describe being types uncertainties, methods assessment (estimation) of uncertainties in GHG emission inventory.

The GHG Protocol Uncertainty Tool is based on the IPCC 2006 and should be considered as an addition to the calculation tools provided by the GHG Protocol Initiative. The GHG Protocol is to describe the functionality of the tool and to give user a better understanding of how to prepare, interpret, and utilize inventory uncertainty estimation (Velychko O. & Gordiyenko T., 2005, 2007a).

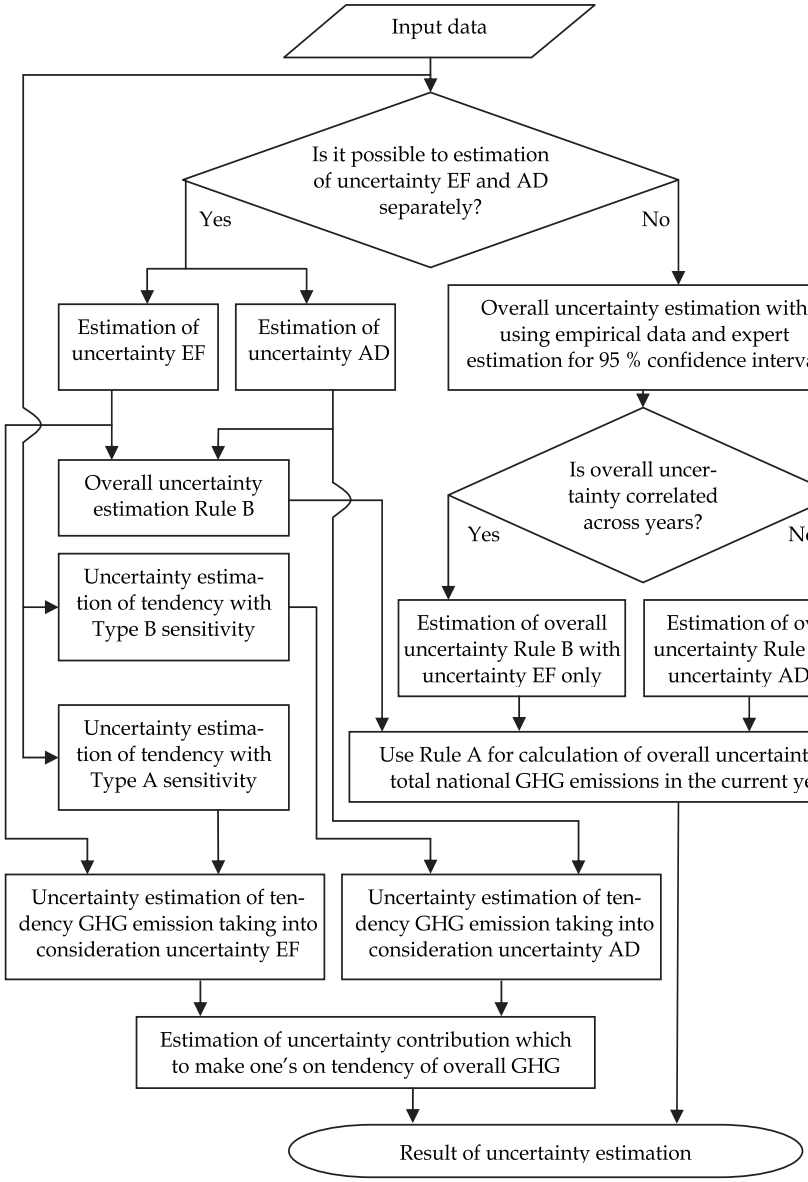

Fig. 9. Developed uncertainty estimation algorithm according to GPG 2000 and IPCC 2006

All IPCC guides use elements and reference to GUM 1993. GPG 2000 is the response to the request from the UNFCCC for the IPCC to complete its work on uncertainty and prepare a report on good practice in inventory management. Most of the statistical definitions given GPG 2000 lie within the context of "classical" frequency-based statistical inference, although it is acknowledged that this is not the only theory of statistical inference.

GPG 2000 describes two tiers of uncertainty estimation for GHG emission inventories for provided for combining source category uncertainties into uncertainty estimation for total national emissions and for emission trends: *Tier 1* – estimation of uncertainties by source category using the error propagation equation via Rules A and B and simple combination of uncertainties by source category to estimate overall uncertainty for one year and the uncertainty in the trend; *Tier 2* – estimation of uncertainties by source category using the Monte Carlo analysis, followed by the use of the Monte Carlo techniques to estimate overall uncertainty for one year and the uncertainty in the trend.

IPCC 2006 describes two tiers: *Tier 1* – for combining uncertainties in inventory data is to use the error propagation method. This method has limitations, in that it assumes normality in the input PDF (it cannot easily deal with correlations between datasets or across time and dependency between source categories that may occur because the same AD or EF may be used for multiple estimates); *Tier 2* – to use the Monte Carlo analysis which avoids all the limitations of the error propagation method (the principle of the Monte Carlo analysis is to select random values of each parameter, e.g., EF and AD, from within their individual PDF, and to calculate the corresponding values, e.g., emissions).

The GHG Protocol Uncertainty Tool is based on the IPCC 2006 and should be considered as an addition to the calculation tools provided by the GHG Protocol Initiative. The GHG Protocol Initiative has developed this guidance along with a calculation tool based on Excel spreadsheets. This calculation tool automates the aggregation steps involved in developing basic uncertainty estimation for GHG inventory data.

The GHG Protocol display uncertainties associated with GHG inventories: scientific uncertainty and uncertainty estimation last can be further classified into two types: model uncertainty and parameter uncertainty. *Scientific uncertainty* arises when the science of the actual emission and/or removal process is not sufficiently understood. *Uncertainty estimation* arises any time GHG emissions are quantified. Therefore all emission or removal estimates are associated with uncertainty estimation.

Model uncertainty refers to the uncertainty associated with the mathematical equations (i.e., models) used to characterize the relationships between various parameters and emission processes. Emission estimation models that consist of only AD times an EF only involve parameter uncertainties, assuming that emissions are perfectly linearly correlated with the AD parameter.

Parameter uncertainty refers to the uncertainty associated with quantifying the parameters used as inputs (e.g., AD and EF) into estimation models. This uncertainty can be evaluated through statistical analysis, measurement equipment precision determinations, and expert judgment. Emission estimated from direct emissions monitoring will generally involve only parameter uncertainty (e.g., equipment measurement error). The type of uncertainty most amenable to assessment of inventory is the uncertainties associated with parameters (e.g. AD, EF, and other parameters) used as inputs in an emission estimation model. GHG Protocol identified two types of parameter uncertainties in this context: *systematic* and *statistical* uncertainties (GHG Protocol).

Systematic uncertainty occurs if data are systematically biased (the average of the measured or estimated value is always less or greater than the true value). Biases can arise, because EF

are constructed from non-representative samples, all relevant source activities or categories have not been identified, or incorrect or incomplete estimation methods or faulty measurement equipment have been used.

Statistical uncertainty results from natural variations (e.g. random human errors in the measurement process and fluctuations in measurement equipment). This uncertainty can be detected through repeated experiments or sampling of data. Complete and robust sample data will not always be available to assess the statistical uncertainty in every parameter. For most parameters only a single data point may be available. Random uncertainty can be detected through repeated experiments or sampling of data.

The different uncertainties associated with GHG inventories according GHG Protocol shown on Fig. 10.

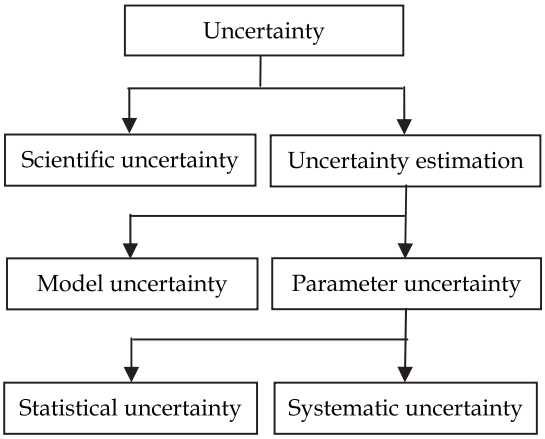

Fig. 10. Uncertainties associated with GHG inventories

The GHG Protocol is designed to aggregate statistical uncertainty assuming a *normal distribution* of the relevant variables and uses the first order error propagation method (Gaussian method), which corresponds to Tier 1 of the GPG 2000. This method should only be applied if the following assumptions are fulfilled: the errors in each parameter must be normally distributed (i.e. Gaussian); there must be no biases in the estimator function (i.e. that the estimated value is the mean value); the estimated parameters must be uncorrelated (i.e. all parameters are fully independent); individual uncertainties in each parameter must be less than 60 % of the mean. This procedure is repeated many times, using a computer, and the results of each calculation run build up the overall emission PDF.

A second approach is to use a technique based on a Monte Carlo simulation that allows uncertainties with any probability distribution, range, and correlation structure to be combined, provided they have been suitably quantified. This method, which corresponds to Tier 2 of the GPG 2000, can be used to estimate the uncertainty of single sources as well as to aggregate uncertainties for a site.

Calculation and ranking of uncertainties of indirectly measured emissions are shown in Table 6.

AD (e.g. quantity of fuel used)	Unit used to measure AD	Uncertainty of AD*, ± %	GHG EF	Unit of GHG EF (for kg CO_2)	Uncertainty of AD*, ± %	CO_2 emissions, kg	CO_2 emissions in metric tones	Uncertainty of calculated emissions, %	Certainty ranking	Auxiliary variable 1	Auxiliary variable 2
A	B	C	D	E	F	G	H	I	J	K	L
						A·D	G/1000	$I = \sqrt{C^2 + F^2}$		(H·I)	K^2
1000.00	GJ	± 5.0	56.10	$kgCO_2$/ GJ	± 10.0	56100.00	56.10	± 11.2	Good	6.27	39.34
10.00	GJ	± 10.0	54.33	$kgCO_2$/ GJ	± 10.0	543.30	0.54	± 14.1	Good	0.08	0.01
…	…	…	…	…	…	…	…	…	…	…	…
* confidence interval expressed											

Table 6. The GHG Protocol Uncertainty Tool

Calculating aggregation of uncertainties uses equation:

$$\pm U = \pm \sqrt{\sum_{i=1}^{n} (H_i \cdot I_i)^2} \Big/ M ,$$

where:

H_i is CO_2 emissions from *i*-th source, tones;

I_i is percentage of uncertainty of calculated emissions from *i*-th source;

M is total CO_2 emissions, tones.

According GUM 1993 the symbol "±" should be avoided whenever possible because it has traditionally been used to indicate an interval corresponding with expanded uncertainty.

In GHG Protocol *measurement uncertainty* is usually presented as an uncertainty range, i.e. an interval expressed in ± percent of the mean value reported (e.g. 100 t ± 5 %). The likely causes of *uncertainty with direct measurement* are generally related to the measurement techniques used. Methods with a high degree of variability will typically lead to a high degree of statistical uncertainty in the final estimates. In the case of *indirect measurement* the uncertainties are related to the AD, and the EF.

The aggregation of uncertainties using this approach is facilitated by the GHG Protocol, which provides automated worksheets for directly and indirectly measured emissions.

For user that characterizes uncertainty numerically, a sum of squares approach may be used to calculate the confidence interval for the product of two or more factors. This approach is only valid if the uncertainties follow a normal distribution and if the individual uncertainties are less than 60%. The relative confidence interval (the ± percent) of the product is the square root of the sum of the squares of the relative (percent) confidence intervals of each factor.

6. The use of measurement units in environmental guides

SI units are recommended for use throughout science, technology and commerce. Each physical quantity has only one SI unit, even if this unit can be expressed in different forms. In some case the same SI unit can be used to express the values of several different quantities. The SI adopted series of prefixes for use in forming the decimal multiples and submultiples of SI units.

The International Committee of Weights and Measures (CIPM), recognizing that users would wish to employ the SI with units which are not part of it but are important and widely used, listed three categories of non-SI units: units to be maintained; to be tolerated temporarily; and to be avoided.

In reviewing this categorization the CIPM agreed a new classification of non-SI units: units accepted for use with the SI (for environmental guides – tonne or "metric ton"); units accepted for use with the SI whose values are obtained experimentally (-); and other units currently accepted for use with the SI to satisfy the needs of special interests (hectare). Non-SI unit tonne is accepted for use with the SI. It includes units, which are in continuous

everyday use, in particular the traditional units of time and of angle, together with a few other units, which have assumed increasing technical importance (Tailor B. N., 1995).

The series of international standards on air quality includes the standardization of methods for the measurement of gases, vapours and particles (for example, ISO 4226). In order to enable results to be compared either between countries, it is essential to use agreed of measurement units to report the results and other relevant information. It is also desirable to keep the number of measurement units to a minimum. Those international standards lay down the units and symbols to be used when reporting results of air quality measurements.

Used in environmental guides and international standards (GPG 2000, IPCC 2006, ISO 4226) SI units, and also non-SI units and their conversion factors are shown in Table 7 (Velychko O. & Gordiyenko T., 2005; Velychko O. & Gordiyenko T., 2007a).

Units for quantity	**SI units**	**Non-SI units**	**Conversion factor**
Units for weight	Gram (g): Mg, Gg, Tg, Pg	Pound (lb)	1 lb = 454 g 1 g = 0.002205 lb 1 mg = 10^{-3} g 1 µg = 10^{-6} g 1 ng = 10^{-9} g 1 pg = 10^{-12} g 1 Mg = 10^{6} g 1 Gg = 10^{9} g 1 Tg = 10^{12} g 1 Pg = 10^{15} g
	Kilogram (kg)	Tonne (t): kt, Mt, Gt	1 t = 10^{3} kg = 1 Mg 1 kg = 2.2046 lb 1 kt = 10^{3} t = 1 Gg 1 Mt = 10^{6} t = 1 Tg 1 Gt = 10^{9} t = 1 Pg
		Short ton (sh t)	1 sh t = 0.9072 t 1 t = 1.1023 sh t
Units for length	Metre (m): µm	–	1 µm = 10^{-6} m
Units for substances*	Percent (% by volume)	–	–
	Percent (% by mass)	–	–
	Milligram per cubic metre (mg/m^3) Microgram per cubic metre (µg/m^3) Nanogram per cubic metre (ng/m^3) Picogram per cubic metre (pg/m^3)	Milligram per litre (mg/l)	1 mg/l = 10^{3} mg/m^3

Units for quantity	SI units	Non-SI units	Conversion factor
Units for energy	Joule (J): GJ, TJ	Calorie$_{IT}$ (cal$_{IT}$)	1 cal$_{IT}$ = 4.1868 J
		British thermal unit (Btu)	1 Btu = 1055.056 J 1 GJ = 10^9 J 1 Tj = 10^{12} J
		Tonne of oil equivalent (toe)	1 toe = $1 \cdot 10^{10}$ cal$_{IT}$ = 41.868 GJ 1 ktoe = 41.868 TJ
		Kilowatt-hour (kWh)	1 kWh = $3{,}6 \cdot 10^6$ J 1 TJ = $2.78 \cdot 10^5$ kWh
Units for power	Watt (W): kW, MW, GW	Horse power (HP)	1 kW = 10^3 W 1 MW = 10^6 W 1 GW = 10^9 W 1 HP = 735.499 W
Units for square	Square metre (m^2)	Hectare (ha)	1 ha = 10^4 m^2
Units for volume	Cubic metre (m^3)	Dry gallon US (gal)	1 dm^3 = 10^{-3} m^3 1 gal dry(US) = 4.405 dm^3
Units for time	Second (s)	Minute (min)	1 min = 60 s
		Hour (h)	1 h = 60 min = 3600 s
		Day (d)	1 d = 24 h = 1440 min
		Year (yr)	–
Units for temperature	Kelvin (K)	Degree Celsius (°C)	1 °C = 1 K
Units for pressure	Pascal (Pa): kPa	Atmosphere (atm)	1 kPa = 10^3 Pa 1 atm = 101.325 kPa
* if concentrations are expressed in terms of mass per unit volume, temperature and pressure (as well as humidity) are required.			

Table 7. Used units for quantities and their conversion factors in environmental guides and international standards

7. Conclusion

Metrological and environmental international guides and standards comparison has shown peculiarities of used terms and uncertainty analysis with correlation and covariance of input values. Metrological and environmental guides use two types of uncertainty, and also used the Monte Carlo analysis of uncertainty. Environmental guides use more simplified approaches of the uncertainty analysis and also specifically use of data, which based on many models. Specific approaches to the uncertainty estimation in trend of GHG emissions imply realization of long-term observation and also environmental guide's consideration correlation of data across years.

It is necessary to apply international metrological guide to the expression of uncertainty in measurement – GUM 1993 and international vocabulary of metrology – VIM 2007, which are developed by eight international organizations in the field metrology, standardization, physicists and chemistry, during the preparation of environmental guides concerning the

analysis of uncertainty. Also need to use approaches international metrological guide GUM 1993 for uncertainty assessment for GHG inventory with correlation or covariance of input values in the development of new and reconsideration of old international environmental guides is recommended.

SI units as well as traditional non-SI units are used in environmental guides. It considerably complicates the preparation of national experts of ecological information and its comparative analysis. Environmental guides that are used on international level must be prepared with preferably employment of SI units.

8. References

2006 IPCC Guidelines for National Greenhouse Gas Inventories (IPCC 2006). *IGES,* Japan, 2006.

IPCC Good Practice Guidance and Uncertainty Management in National Greenhouse Gas Inventories (GPG 2000). *IPCC*, Switzerland, 2000.

ISO3534-1:1993. Statistics. – Vocabulary and symbols. – Part 1: Probability and general statistical terms. *ISO*, 1993.

ISO 4226:1993. Air quality. – General aspects. – Units of measurement. *ISO*, 1993.

ISO 5725-1:1994. Accuracy (trueness and precision) of measurement methods and results. – Part 1: General principles and definitions. *ISO*, 1994.

ISO 14064-1:2006. Greenhouse gas emissions. Part 1: Specification with guidance at the organization level for quantification and reporting of greenhouse gas emissions and removals. *ISO*, 2006.

ISO 14064-2:2006. Greenhouse gas emissions. Part 2: Specification with guidance at the project level for quantification, monitoring and reporting of greenhouse gas emission reductions or removal enhancements. *ISO*, 2006.

ISO 14064-3:2006. Greenhouse gases. Part 3: Specification with guidance for the validation and verification of greenhouse gas assertions. *ISO*, 2006.

ISO/IEC Guide 98-3:2008 Uncertainty of measurement. – Part 3: Guide to the expression of uncertainty in measurement (GUM 1993). *ISO*, 2008.

ISO/IEC Guide 99:2007 International vocabulary of metrology. – Basic and general concepts and associated terms (VIM 2007). *ISO*, 2007.

Gordiyenko T. & Velychko O. (2006) Peculiarities of Using Uncertainty in Environmental Guides, *International Workshop on Advanced Methods for Uncertainty Estimation in Measurement* (AMUEM 2006), Sardagna-Trento, Italy, 5 p.

Greenhouse Gas Protocol Guidance on uncertainty assessment in GHG inventories and calculating statistical parameter uncertainty (GHG Protocol). Business Council for Sustainable Development, *World Resources Institute*, 2003.

Tailor B. N. (1995) Guide for the Use of the International System of Units (SI), *NIST* Special Publication 811, 1995 Edition, 84 p.

The International Systems of Units (SI): 8th Edition. *BIPM*, 2006, 180 p.

Velychko O. & Gordiyenko T. (2005) Peculiarities of using metrological terms and SI units in environmental guides. *Joint International IMEKO TC1+TC7 Symposium "Metrology and Measurement Education in the Internet Era"*. Ilmenau, Germany, pp. 124–127.

Velychko O. & Gordiyenko T. (2007a) The use of metrological terms and SI units in environmental guides and international standards. *Measurement*. Vol.40, Issue2 (February 2007), pp. 202–212.

Velychko O. & Gordiyenko T. (2007b) Estimation of uncertainty with correlation values in international metrological and environmental guides, *1st IMEKO TC19 Intern. Symp. on Measurements and Instrumentation for Environmental Monitoring*. Proceeding. Iasi, Romania, pp. 8–12.

Velichko O. N. & Gordienko T. B. (2007c) Comparisons of uncertainty assessment in international metrological and environmental guides, *Measurement Techniques*, Vol.50, No 5 (2007), pp. 490–495.

Velychko O. M. & Gordiyenko T. B. (2008) Uncertainty estimation at determination of pollutant emission, *7th Intern. Symp. "Metrology 2008"*. Havana, Cuba, 12 p.

Velychko O. (2008) Using of Validated Software for Uncertainty Analyses Tools in Accredited Laboratories, *Key Engineering Materials*, Vols. 381–382, pp. 599–602.

Velychko O. & Gordiyenko T. (2009) The use of guide to the expression of uncertainty in measurement for uncertainty management in National Greenhouse Gas Inventories, *International Journal of Greenhouse Gas Control*, Vol.3, Issue4, pp. 514-517.

Velichko O. N. & Gordienko T. B. (2009) Methodologies of calculating of pollutants emission in atmosphere and their uncertainty assessment, *Measurement Techniques*. Vol.52, No2 (February 2009), pp. 193–199.

Velychko O. & Gordiyenko T. (2010) The implementation of general guides and standards on regional level in the field of metrology. Journal of Physics: Conf. Series, Vol. 238., Numb. 1, 012044, 6 p.

Velychko O. & Gordiyenko T. (2011) Greenhouse Gases Global Monitoring Systems: Ecological and Metrological Aspects. Proceedings Joint IMEKO TC 11–TC 19–TC 20 Intern. Symp. "*Metrological Infrastructure, Environmental and Energy Measurement*" (IMEKO-MI2011), Cavtat, Dubrovnik Riviera, Croatia, p. 125–130.

10

Detection of Greenhouse Gases Using the Photoacoustic Spectroscopy

Marcelo Sthel et al.*
State University of the Northern Fluminense Darcy Ribeiro (UENF)
Brazil

1. Introduction

Global warming is one of the main environmental problems of the XXI Century. It is generated by the intensive use of fossil fuels that leads to the so-called greenhouse effect (Meinshausen et al.,2009; Allen et al., 2009; Sthel et al., 2010; Hansen et al., 2008; Hansen & Makiko, 2004; Rosenzweig et al, 2008). It causes climate changes (Steffen et al., 2004; Solomon et al.,2009; Kevin et al., 2006; Kurz et al.,2008; Greene et al., 2009; Nathan P et al., 2008; Siddall et al., 2009; Sander et al, 2006; Emanuel, 2005; Peza & Simmonds, 2005; Janssen, 1998; Mann et al., 1998) and produces significant damages to the human society and biodiversity, such as the melting of the poles with the consequent increasing of oceans level, the intensity increasing of hurricanes, extreme events, changes in the rainfall patterns (floods, desertification), oceans acidification and biodiversity decreasing. Recently, the Intergovernmental Panel on Climate Change (IPCC) report (IPCC, 2007), published in February 2007, indicated based on meteorological studies, that the earth's global average temperature rose about 0.8ºC in the last 150 years, mainly due to human activities. The global atmospheric concentrations of carbon dioxide(CO_2), methane (CH_4) and nitrous oxide (N_2O)have risen considerably as a result of human activities since 1750. Increases in global carbon dioxide concentration are primarily due to the use of fossil fuels and changes in the use of the soil through practices such as deforestation, biomass burning and biomass decomposition. Practices such as logging, peat decomposition and burning and other techniques employed in the modern agriculture are resulting in an increased concentration of methane and nitrous oxide. While the global atmospheric concentration of carbon dioxide has increased from a pre-industrial value of about 280 ppmv to 379 ppmv in 2005, the global atmospheric concentration of methane (CH_4) has increased from a pre-industrial value of about 715 ppbv to 1774 ppbv in 2005 and the global atmospheric concentration of nitrous oxide has risen from pre-industrial value of about 270 ppbv to 319 ppbv in 2005.

Therefore, it is necessary to use suitable analytical techniques to identify the atmospheric components and to determinate their trace concentrations. A trace sensor of atmospheric pollutants must meet a set of fundamental requisites. High selectivity is necessary to

* Marcelo Gomes[1], Guilherme Lima[1], Mila Vieira[1], Juliana Rocha[1], Delson Schramm[1], Maria Priscila Castro[1], Andras Miklos[2], Helion Vargas[1]
[1]*State University of the Northern Fluminense Darcy Ribeiro (UENF), Brazil*
[2]*Fraunhofer Institute for Building Physics, Germany*

distinguish the gas species present in a multicomponent gas mixture, such as air, and high sensitivity is essential to detect very low concentrations of substances. A large dynamic range is important to monitor the gas components at high and low concentrations using a unique instrument. In addition, a good time resolution ensures the possibility of on-line analyses controlled by a computer. Photoacoustic spectroscopy meets these requirements that enable this technique to offer important advantages in pollutant gas monitoring.

In conventional spectroscopy, the absorption of radiation is measured from the power transmitted through the sample. On the contrary, in photoacoustic spectroscopy, the absorbed radiation power is determined directly via its heat and hence the sound produced in the sample. This methodology is based on the so called photoacoustic effect which consists on the generation and detection of pressure waves (sound) inside a resonant cell, where the gas samples are placed. These samples are exposed to the incidence of modulated radiation, absorbing it at determined wavelengths. The resonant absorption of radiation generates a modulated heating in the sample and, therefore, a sound signal is produced (photoacoustic effect) and detected by highly sensitive microphones coupled, inside the cell. These microphones convert the sound signal into an electric signal, which is filtered and detected by a lock-in amplifier. Photoacoustic spectroscopy is widely used for the detection of several gases in the concentration range of ppbv and sub-ppbv(Mothé et al., 2010; Berrou et al., 2010; Sthel et al.,2011; Harren et al.,2008; Thomas, 2006; Rocha et al., 2010; Elia et al., 2009; Sorvajärvi et al., 2009; Sigrist et al., 2008; Angelmahr et al.,2006; Filho et al., 2006; Schramm et al., 2003; Harren et al., 2000; Miklos et al., 2001; Gondal, 1997; Repond & Sigrist, 1996; Sigrist, 1994a, 1994b). There are some types of trace gas detection systems based on continuous wave (CW) CO_2 laser, optical parametric oscillator (OPO) in combination with photoacoustic spectroscopy and quantum cascade laser (QCL). These experimental arrangements are efficient in the detection of greenhouse gases and their precursors.

2. Photoacoustic spectroscopy

Currently, photoacoustic spectroscopy has been consolidated as an effective option for trace gases analysis for high sensitivity trace gases analysis (detection limits in the range of sub-ppbv and ppbv), good selectivity, possibility of in situ measurements and continuous flow systems associated with the possibility of non-destructive analysis are attributes that allow photoacoustic to be a powerful analytical tool for gases monitoring. The photoacoustic effect consists on the generation of sound waves from the absorption of a pulsed modulated radiation. It was discovered in 1880 by Alexander Graham Bell (Bell, 1880). This discovery raised the interests of other researchers, such as John Tyndall (Tyndall, 1881), Wilhelm Röntgen (Röntgen, 1881) and Lord Rayleigh (Rayleigh,1881). However, the lack of equipment (radiation sources, microphones, amplifiers, etc.) prevented the immediate development of this new research field, and soon the photoacoustic effect has become a mere scientific curiosity, remained virtually forgotten for over half a century.

In the late 1930s, Viengerov (Viengerov et al., 1938) introduced an infrared absorption photoacoustic system to analyze gases infrared absorption. Then, Luft (Luft,1943) improved the sensitivity of this technique, allowing absorption measurements of gaseous species in the concentration range of ppmV (10^{-6}). Since the 1960s, the development of

Lasers, sensitive microphones and lock-in amplifiers permitted this technique to have a great technical development. In 1968, L. B. Kerr and J. G. Atwood conducted the first photoacoustic experiments using Laser as the radiation source (Kerr & Atwood, 1968). Using a continuous wave CO_2 laser as excitation source, they achieved a minimum absorption coefficient of 1.2 x 10^{-7} cm^{-1} of CO_2 diluted in nitrogen. In 1971, L. B. Kreuzer, using a HeNe laser operating on 3.39 μm, attained a detection limit of 10ppbv of methane diluted in nitrogen (Kreuzer, 1971). Kreuzer, N. D. Kenyon and C. N. K. Patel used CO_2 and CO lasers as radiation sources to perform photoacoustic measurements of many trace gases (Kreuzer et al., 1972). The use of a photoacoustic cell operating at in resonant mode, associated with the modulation of the excitation beam in the acoustic resonance frequencies of the cell, was introduced in 1973 by CF Dewey Jr., RD Kahn and CE Hackett (Dewey et al., 1973). The success achieved by these pioneering studies provided a great interest in the application of photoacoustic spectroscopy in trace gases analysis in many scientific areas, especially in pollutant gas studies.

Advances in laser technology allowed the development of new infrared radiation sources continuously operating in a wide range of wavelengths, especially in the mid-infrared region. Among these new Lasers, the most promising for gas sensing are the optical parametric oscillator (OPO) and the quantum cascade laser (QCL). The combination of these new radiation sources with photoacoustic cell optimized settings (differential photoacoustic cell, intra-cavity arrangements or multi-pass) enabled major advances in trace gases photoacoustic detection.

2.1 Photoacoustic effect in gases

The photoacoustic signal generated and detection in gases been studied mainly by Kreuzer (Kreuzer, 1971) and revised and expanded by several authors(Harren & Reuss, 1997; Miklos & Hess, 2001; Hess, 1992; West, 1983; Meyer & Sigrist, 1990). Molecular absorption of photons results in the excitation of molecular energy levels (rotational, vibrational and electronic) degrees freedom. The excited state loses its energy by radiative processes, such as spontaneous or stimulated emission, and/or by collisional relaxation, in which the state energy is transformed into translational one.

In the case of vibrational excitation, radiative emission and chemical reactions do not play an important role, because the radiative lifetimes of vibrational levels are long compared with the time needed for collisional deactivation at pressures used in photoacoustic. Furthermore, the photon energy is too small to induce chemical reactions. For 1 atm pressure, the vibrational-translational non-radiative decay time is typically around 10^{-6}-10^{-9}s, whereas the radiative lifetime is between 10^{-1} and 10^{-3} s (Hess, 1983). Thus, in practice, the absorbed energy is completely released as heat, appearing as translational (kinetic) energy of the gas molecules.

By modulating the intensity or the wavelength of the incident radiation, the sample local heating and expansion become periodic. If radiation intensity is modulated (without optical saturation), the heat density in the sample (H) is directly proportional to the volumetric density of molecules (N), to the absorption cross section of the absorbing molecule (σ) and to the incident laser radiation intensity (I_0). Therefore, the gas heat production is given by:

$$H(\mathbf{r},t) = N\sigma I_0 e^{i\omega t} \tag{1}$$

The sample pressure oscillations (p) are related to the heat production by the following equation:

$$\nabla^2 p - \frac{1}{v^2}\frac{\partial^2 p}{\partial t^2} = -\frac{\gamma - 1}{v^2}\frac{\partial H}{\partial t} \tag{2}$$

where v, γ, and H are the sound velocity, the adiabatic co- efficient of the gas, and the heat density deposited in the gas by light absorption, respectively. All dissipative terms of heat diffusion to the cell walls and viscosity were despised.

For many applications, this simplified approach is sufficient, although in some cases, more stringent treatment that takes into account relaxation effects is necessary. Since the amplitude of the acoustic waves produced depends on both the nature of the absorbing gases and their concentrations, the photoacoustic detection allows qualitative and quantitative analysis of gas mixtures.

The acoustic wave is generated in places where light is absorbed by the monitored species. The photoacoustic signal S(λ) produced by a single absorbing gaseous species diluted in a non absorbing gas can be expressed as:

$$S(\lambda) = CP(\lambda)N_{tot}c\sigma(\lambda) = CP(\lambda)\alpha(\lambda)c \tag{3}$$

Where C is the cell constant, which depends on the cell geometry, the microphone responsivity and on the nature of the acoustic mode, P(λ) is the laser power at the wavelength λ, N_{tot} is the total density of molecules, considering a pressure of 1013hPa and a temperature of 20°C, $N_{tot} \approx 2.5 \times 10^{19}$ molecules/cm^3, c and σ (λ) are, respectively, the concentration (mole fraction) and the absorption cross section of the absorbing molecule and $\alpha(\lambda)=N_{tot.}c\sigma(\lambda)$ is the so called gas absorption coefficient (cm^{-1}).

Using equation 3, it is possible to determine the minimum detectable gas concentration in the photoacoustic spectrometer, through:

$$c_{\min} = \frac{S_{\min}}{N_{tot}CP\sigma} = \frac{S_{\min}}{CP\alpha} \tag{4}$$

where S_{min} (λ) is the minimum detectable signal, which is usually measured by passing a flow of non-absorbing inert gas (usually nitrogen or synthetic air) in the photoacoustic cell. The minimum signal is produced by the various sources of noise, which are always present in photoacoustic detection, determining its limitations. The most common sources of noise in photoacoustic systems include acoustic signals caused by the windows heating, the absorption and scattering of radiation on the cell resonator walls, by molecules adsorbed on them, the noise caused by the gas flow and electronic noise.

We can notice that the signal is obtained at a given wavelength, which is specific for the molecule we wish to detect. Moreover, the obtained signal is directly proportional to the concentration of the absorbing gas. Thus, it is possible to obtain the concentration as a function of the generated signal.

In order to determine the concentration of various gaseous species in a multicomponent sample, the photoacoustic signal can be obtained for different wavelengths, corresponding to the absorption of each analyzed component. In this case, the signal can be obtained by the relation:

$$S(\lambda_i) = CP(\lambda_i)N\sum_{j=1}^{n} c_j \sigma_{ij} \tag{5}$$

with i = 1, 2, ..., m and j = 1, 2, ..., n e m ≥ n.Here, $P_i = P(\lambda_i)$ represents the laser power at wavelength λ_i and c_j is the concentration of the component $_j$ with absorption cross section σ_{ij} at λ_i. This equation solution for each gas species concentration is given by:

$$c_j = \frac{1}{CN}\sum_{i=1}^{m}(\sigma_{ij})^{-1}\left(\frac{S_i}{P_i}\right) \tag{6}$$

Where $(\sigma_{ij})^{-1}$ is the inverse matrix of the matrix σ_{ij}. The success of this method in multicomponent mixture analysis strongly depends on the nature of the matrix σ_{ij} (Sigrist, 1994a; Meyer et al., 1988). The trivial case is represented by a diagonal matrix (σ_{ij}), where a set of wavelengths λ_i can be selected and the absorption by a single gas component occurs in each λ_i. However, this ideal case without interference between the absorptions due to different gas species in a multicomponent mixture hardly occurs. Instead, considerable effort is needed to discriminate the various components, as well as to identify any unexpected component. Iterative algorithms using least squares regression and based on prior knowledge of the absorption cross sections (σ_{ij}) have been developed to fit the photoacoustic spectrum of multicomponent samples (Moeckli, 1998).

2.2 Lasers as radiation sources

The selectivity required for the identification of the components of a gaseous mixture is achieved in spectroscopy when lasers are employed. Due to its high radiance, narrow linewidth and wide spectral range of emission, lasers are indeed suitable for trace gas monitoring. They allow a selective detection of different gases in trace level concentration (lower limit: parts per trillion by volume) even when there is overlapping of spectrum lines from different molecules. It is known that for molecules, absorption spectra in the near infrared (NIR) and the infrared (IR) ranges work as fingerprints, that is, they are unique for each molecular species. Currently, there are commercially available lasers that emit in these regions, for example, semiconductor lasers (DFB diode lasers) and gas lasers (CO and CO_2), respectively. The great advantage of using these light sources is the resulting high spectral resolution.

Promising new sources of light are the quantum cascade lasers (QCL). These lasers emit in the mid-IR range, where the molecules have higher absorption coefficients, and operate at room temperature. Since the photoacoustic signal intensity is also a function of the molecular absorption coefficients, the low power these lasers emit is hence compensated. Another important feature and advantage of these lasers is the high spectral resolution. Furthermore, the emission wavelength can be selected to match two, or more, absorption lines of a given molecule. Third generations of extremely promising lasers are the Optical Parametric Oscillator lasers (OPO).

2.2.1 CO_2 laser

The use of tunable CO_2 lasers (Patel, 1964), through the scanning of its emission wavelengths (9-11μm) ensures the exploration of the so-called molecular fingerprint, enabling the identification and simultaneous monitoring of several gaseous compounds with a single instrument. Figure 1 shows the absorption spectra of ozone (O_3), ammonia (NH_3) and ethylene (C_2H_4), for the emission range of a CO_2 laser. As gas lasers have high power (> 10 watts) and the signal intensity is directly proportional to the emitted light power, its use results in sensitivities in the range of pptv. Nevertheless, these lasers have two disadvantages, they are large and expensive and thus its use is limited to laboratories.

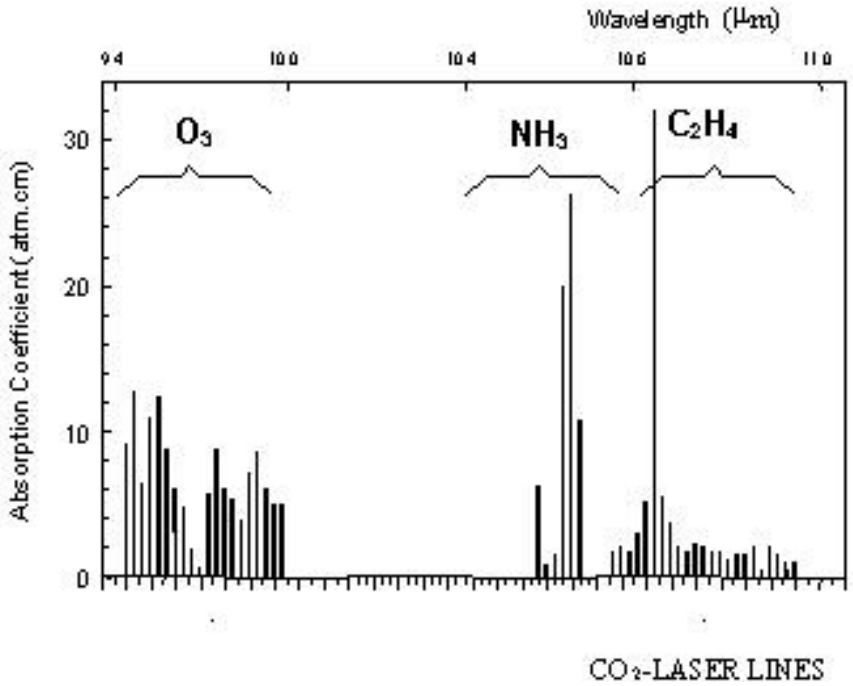

Fig. 1. Fingerprints of ozone (O_3), ammonia (NH_3) and ethylene (C_2H_4) corresponding to the emission lines of a CO_2 laser.

2.2.2 Quantum Cascade Laser (QCL)

The quantum cascade laser (QCL), introduced by Faist (Faist, et al., 1994,1997), represents an excellent source of radiation for trace gas monitoring. Although providing output power well below the CO_2 laser (a few mW), this source has some advantages such as compact size, continuous emission, high spectral resolution and the possibility of being operated near room temperatures.

In addition, they can be manufactured to operate in a wide range of wavelengths, from 3 to 24 μm. Among its applications, we highlight the environmental monitoring, industrial process control, besides chemical and biomedical applications. (Beck et al., 2002)

The QCL laser coupled with a photoacoustic detector has been successfully used to measure the concentration of different gases which absorb radiation in the mid- infrared spectral region, such as ozone (Silva et al., 2004), ammonia (Baptista-Filho et al., 2006), and NO_2 and N_2O gases. (Lima et al, 2006; Grossel et al., 2007)

This type of laser is part of the family of semiconductor lasers, with the particularity of using quantum transitions within the same band. A quantum cascade laser comprises a series of alternate thin layers of two different materials. This configuration enables different electrical potentials to be established across the device, so that electrons can get trapped in these sites, called quantum wells. Thus, a series of sub-bands with different energies is created inside the conduction band.

When stimulated, the electrons undergo transitions and quantum tunneling to a lower energy sub-band, and consequently photons are emitted. A single electron can perform several transitions, that is, issue multiple photons. (Gmachl et al., 2001; Beyer et al., 2003)

Another important characteristic of quantum cascade lasers is that the wavelength can be determined by the thickness of the layers, rather than being determined by the energy difference between bands. The thickness and refractive index change by setting different temperatures turning the wavelength (Kosterev et al., 2002; Curl et al., 2010; Kosterev et al., 2002).

2.2.3 The Optical Parametric Oscillator laser (OPO)

An interesting optical process that has been used to produce near- and mid-infrared radiation is the optical parametric generation. In 1962, Armstrong et al and Kroll described the fundamental theory of the optical parametric generator and three years later, Giordmaine and Miller demonstrated the operation of an optic parametric oscillator (Armstrong et al., 1962; Giordmaine & Miller, 1965). When an optically nonlinear crystal is submitted to electromagnetic fields of high density of energy such as those present in pulsed lasers, the electrons respond with significant displacement that gives rise to the contribution of the second-order nonlinear component for the electric polarization of a nonlinear medium. The mixing of two electromagnetic waves under condition of nonlinear polarization produces parametric effects such as second harmonic generation (frequency doubling), sum frequency generation and difference frequency generation. In the latter case (figure 2), when the nonlinear crystal is pumped by two input photons with wavelength at λ_p (pump photon) and λ_s (signal photon, $\lambda_s > \lambda_p$), the signal photon stimulates the conversion of a pump photo into a new signal and an idler photon with wavelength at $\lambda_i^{-1} = \lambda_p^{-1} - \lambda_s^{-1}$ (fulfilling the energy conservation principle). Of course, the efficiency of such conversion is limited to phase match between the pump and signal waves. This process of increasing the number of signal photons is known as optical parametric amplification (OPA) and thus it fundamentally differs from the amplification mechanism in laser since no population inversion and excited states take place. Theoretically, the remarkable advantage of OPA is the infinity possibility of combining two waves that generates a third wave with different wavelength. This fulfills the expected desirable feature of an excitation source for analytical spectroscopy application that is the broad wavelength tunability. Therefore, this makes the optical parametric phenomena of great significance to spectroscopy application in the sense

of allowing selective trace gas detection and thus analysis of multicomponents samples, such as the air. Although the finite width of the emission line may reduce the selectivity, for atmosphere application the broadening of the line width of detected specie due to the atmospheric pressure (Demtröder, 2003; Sigrist a, 1994) for itself reduces the significance of an ultra-narrow line width of an applied source.

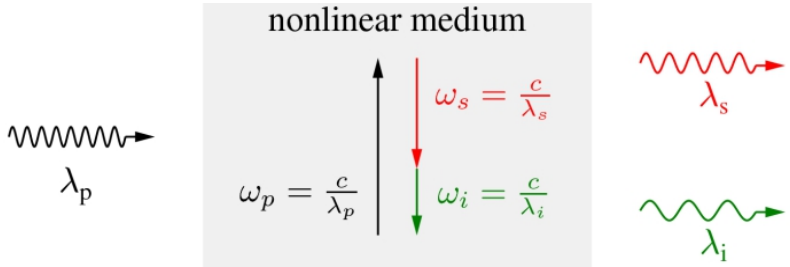

Fig. 2. Optical parametric process. The incident pump radiation with wavelength λ_p and circular frequency at ω_p is converted into signal and idler radiations with wavelength λ_s and λ_i and circular frequency at ω_s and ω_i, respectively. c is the velocity of the light in the medium.

The efficiency of the nonlinear conversion depends on the phase matching of the pump and signal waves. The dispersion of electromagnetic wave propagating through a crystal is directly related to the refractive index of the media that is different for each wavelength. Therefore the pump and signal wave move in and out of phase relatively to each other, limiting the quantity of generated signal photons. Consequently, initially the first issue was to find materials that provide phase matching for at least two wavelengths. The use of birefrigent crystalline materials was the first key to fix the relative phase of the pump and signal waves. However, the available range of wavelengths that satisfies the phase-matching condition is limited to the variability of birefrigent crystalline materials. More recently, the use of periodically poled lithium niobate (PPLN) has overcome this restriction. PPLN chips display an engineered inverted orientation of lithium niobate crystals that promotes a quasi-phase-matched combination of the pump and signal waves compensating the phase mismatch present in parametric interaction (Fejer et al., 1992;Tang et al., 1992).

For the optic parametric oscillator (OPO), the crystal is initially pumped by photons of only one wavelength λ_p. Based on the fundamental quantum uncertainty in the electric field (quantum noise), a pump photon (λ_p) propagating in a nonlinear optical crystal spontaneously breaks up spontaneously into two lower-energy photons with wavelength at λ_s (signal photon) and λ_i (idler photon) (Zhang et al., 1993; Zhou et al., 1998). This optic parametric process is called optic parametric generation (OPG). Afterwards, the created signal wave mixes with the pump wave under condition of nonlinearity resulting in new signal and idler waves (stimulated generation). To increase the number of signal and idler photons, the crystal is placed within an optic cavity formed by two mirrors (optical resonator). Single resonance is achieved when the signal wave is reflected back and forth in the optic cavity.

3. Detection of greenhouse gases: Experimental setups

3.1 CO_2 laser experimental setup

The methodologies based on photothermal techniques, mainly CO_2 laser photoacoustic spectroscopy, have suitable characteristics to detect trace gas, as high sensitivity and selectivity and possibility of in situ measurements. A CO_2 laser based photoacoustic spectrometer (Figure 3) can be used to detect volatile organic compounds (VOCs) emissions, such as ethylene (Demtröder, 2003; Fejer et al., 1992, Tang et al., 1992, Zhang et al., 1993). Ethylene is a reactive pollutant, since it is an unsaturated organic compound (Zhou et al., 1998). For this reason, this chemical species is a precursor for the generation of the tropospheric ozone (Da Silva et al., 2006), which is present in photochemical smog and directly affects human health. Besides, ozone is a powerful greenhouse gas, whose formation is greatly potentiated by the incidence of sun radiation and the presence of nitrogen oxides (NO_x) (Yu & Kung, 1999; McCulloch et al., 2005; Teodoro et al., 2010). According to the Intergovernmental Panel of Climatic Changes (IPCC), ozone has a positive radiative forcing of about 0.35 W/m², being, therefore, an important source of global warming.

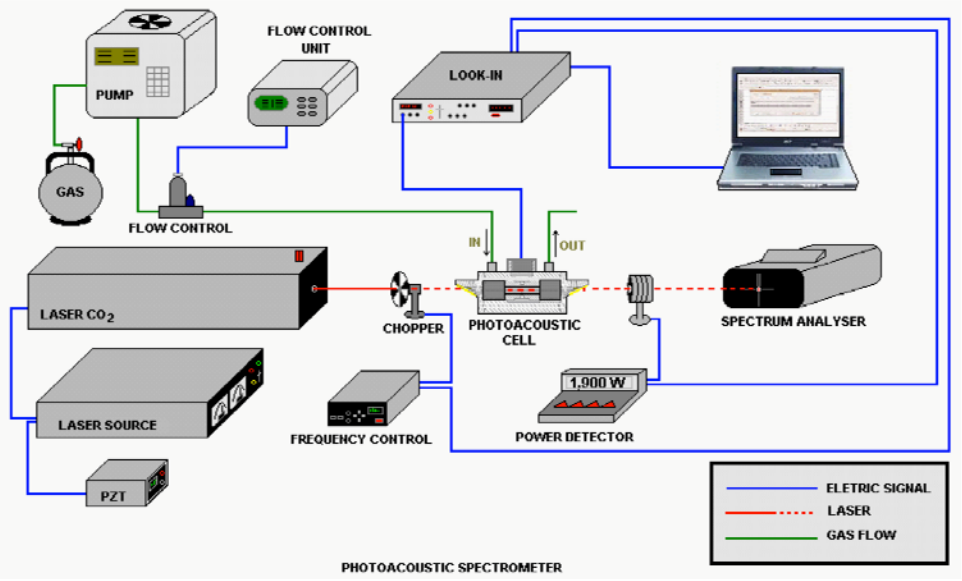

Fig. 3. Scheme of the photoacoustic experimental setup

To guarantee a refined detection of ethylene, the photoacoustic spectrometer is daily calibrated by submitting the cell to a flow of a certified mixture. This measurement was carried out using a certified gas mixture of 1.1 ppmV ethylene in N_2 flowing into the cell at a rate of 83.3 sccm (standard cubic centimeter). The acoustic signal is detected by a microphone that generates an electric signal. This electric signal is pre-amplified and then detected by a lock-in amplifier (Stanford SR850) with a time constant of 300 ms. The lock-in response is registered in a microcomputer. A continuous wave CO_2 infrared laser (LTG, model LTG150 626G), tuneable over about 80 different lines between 9.2 and 10.6 μm, with a

power of 1.9W at the emission line 10P(14) (10.53 μm), by internal PZT (Piezoelectric Transducer), is employed as the excitation source. At this power level, no saturation effects of the photoacoustic signal were observed. These lines can be swept by a step motor controlled by a microcomputer. Within this spectral region, many small molecules show a unique fingerprint. The photoacoustic instrument used has been developed for the detection of small concentrations of gases. All the measurements and the sample collection are made at room temperature. Therefore, the analysis of these samples is made for a number of n different species, rather than just one. This was accomplished by measuring the photoacoustic (PA) signal $S(\lambda_i)$ at a set of wavelengths λ_i (i = 1, 2… m) chosen on the basis of the absorption spectra of the individual components to be detected. These individual absorption spectra were obtained from the HITRAN-PC database, which calculates the absorption cross sections (σ) of a given molecule at different wave numbers $k_i = 1/\lambda_i$ in a given interval. Thus, the expression used to determine the concentrations of a given component in the multicomponent gas mixture is the eq. (5). The absorption cross section σ_{ij} is related to the photoacoustic generation efficiency of each gas component for each CO_2 laser line. The sum is taken over the n components present in the sample.

3.1.1 Photoacoustic cell calibration and sensitivity measurements

The calibration and sensitivity measurements of the photoacoustic cell were performed by obtaining the cell coupling constant C in the eq (5). This was performed by taking a 1.1 ppmV certified mixture of ethylene in N_2 and diluting it in nitrogen until the least concentration achieved (about 16 ppbv) (Mothé et al, 2010). A linear dependence of the photoacoustic signal on the ethylene concentration could be proven and this linearity could be extended to ppmV levels. The absorption cross section σ of ethylene is well known at the 10P(14) (949.51cm^{-1}) CO_2 laser line ($\sigma = 170 \times 10^{-20}$ cm^2). Hence, the C constant value was then obtained from the eq. (3), which yielded 40.2 V.cm/W. The unity of the cell coupling constant was furnished by the manufacturer of our photoacoustic cell (Prof. Markus W. Sigrist). Recent measurements made in greenhouse gas SF_6, indicated that using the CO_2 laser, it was possible to achieve a detection limit of 20 ppbv. (Rocha et al., 2010)

3.2 Quantum Cascade Laser (QCL) experimental setup

With the recent development of quantum-cascade lasers (QCLs), compact, low-cost, solid-state radiation sources are available, covering the important infrared (IR) region with specific molecular absorption lines. In addition, spectral regions can be selected in which water vapor has a very low absorption coefficient, known as atmospheric windows. Another important advantage of QCLs in practical applications is that they work near room temperature, whereas diode lasers such as lead salt lasers, which emit in the fundamental IR region, have to be cryogenically cooled. Recent applications of QCLs clearly indicate their potential as tunable light sources in the mid-infrared, especially between 3 - 13 μm, with strong fundamental absorption bands. Current interest is based on the lack of other convenient coherent laser sources. In fact, it can be expected that QCLs will open new possibilities for real-time diagnostics of various molecular species in the 3-5 μm and 8-13 μm atmospheric windows.(Kosterev et al., 2002) Pulsed quantum-cascade distributed-feedback (QC-DFB) lasers provide quasi room temperature operation, combined with a high spectral selectivity and sensitivity, real time measurement capabilities, robustness, and compactness.

For this reason, QCLs are ideal for the development of compact trace gas analyzers that are also suitable for field measurements. In recent years the detection of a series of important trace gases has been demonstrated with these devices.(Faist, et al., 1994,1997; Beck et al., 2002; Silva et al., 2004; Baptista-Filho et al., 2006; Lima et al, 2006; Grossel et al., 2007; Gmachl et al., 2001; Beyer et al., 2003; Kosterev et al., 2002; Curl et al., 2010; Kosterev et al., 2002). By way of illustration we report on measurements of sulphur hexafluoride and methane with a homemade Laser Photoacoustic Spectrometer equipped with QC lasers and a Differential Photoacoustic Cell. The motivation of our research comes from the need for simple, sensitive, and spectrally selective devices for measuring traces of greenhouse gases in agriculture, automobile exhaust monitoring, power distribution facilities, cattle breeding and chemistry industries. The experimental set up employed in the detection limit determination of the analyzed gases is illustrated in Figure 4.

As radiation source, a pulsed quantum cascade is normally used. In this experiment two quantum cascade lasers were employed separately, each laser emission band matching the absorption lines of one of the specified molecules. The laser used in the detection of CH_4, emits in the range of 7.71 - 7.88 μm and can reach a power of 5.6 mW (at lowest operating temperature of the laser), the one employed in the detection of SF_6, emits in the range of 10.51 - 10.56 μm and can reach a power of 3.7 mW.

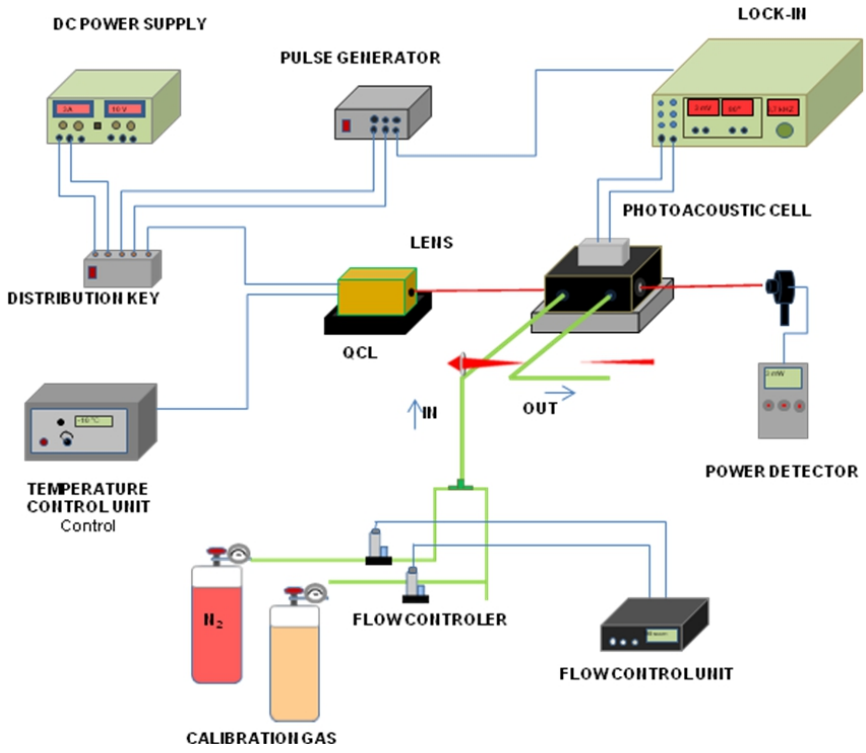

Fig. 4. Experimental set up using quantum cascade laser.

The laser emission lines are given according to the diode temperature, which is determined by a temperature control unit. The pulsed QCL light beam, with a repetition rate of 400kHz and a pulse duration of 50ns (duty cycle of 2%), is gated by an external transistor-to-transistor logic (TTL) signal at 3.8kHz to excite the first longitudinal acoustic mode of the resonant differential photoacoustic cell. A germanium lens (focus ~30.7 mm and diameter ~10.35mm) is employed to focus the QCL radiation through the cell. The cell (Miklos, 2001) has two resonant cylindrical tubes (5.5 mm in diameter and 4 cm in length) on whose edges are arranged acoustic buffers which reduce noise caused by gas turbulence and background signal produced by the heating in the cell windows when these are exposed to the radiation. The gas flow streams through both pipes and noise and background are equally detected by the microphones placed on each of them, but only the microphones placed in the tube crossed by the laser beam detect the pressure change induced by the absorption of modulated radiation in the gaseous sample containing the molecules under consideration. Thus the photoacoustic signal is obtained by simple differentiation of the signal produced by the microphones in the two tubes.

The laser power is monitored by a power detector (OPHIR, 3A-SH-ROHS) and the gases flows are controlled by electronic mass flow controllers (model MKS, 247), one of de 50 sccm and one of 300sccm. The PA data analysis was performed by the lock-in technique using a lock-in amplifier (model Stanford SR_850 DSP) with a set data acquisition time constant of 300ms.

3.2.1 Calibration and sensitivity measurements

The following concentration measurements were performed keeping the temperature of each laser constant. At these emission lines the lasers power was 0.8 mW, feed current of 26.2 mA, for the laser used to measure CH_4, and 1.12 mW, feed current of 25.3 mA, for the laser used to measure SF_6. In such type of measurement, a high stability is observed during the entire experiment. In order to determine the detection boundaries of the gases of interest, a dilution of standard mixtures were carried out. Dilution experiments are depicted in figure 5 and figure 6. Small concentrations of the investigated gases were synthesized by using two electronic mass-flow controllers, one for N_2 (with full scale control of 200 sccm) and another for the investigated gas (CH_4 or SF_6) (with full scale control of 50 sccm). The electronic mass-flow controllers were connected in parallel to the gas inlet of the photoacoustic cell. The initial concentrations of 4.5 ppmv CH_4 and 5 ppmv SF_6 was diluted with pure nitrogen (zero gas) down to the lowest concentrations detected by the system.

The acoustic and electronic noise was determined by blocking the laser light while keeping all other devices running. The value of the noise signal was typically 0.300μV. As expected (Eq.3) , a linear dependence of the photoacoustic signal on the methane and sulphur hexafluoride concentration was found. The fitted straight line are also shown in Figures 5 and 6. The smallest measured concentrations were of 1.5 ppmv for methane and 49 ppbv for sulphur hexafluoride (Rocha et al., 2010 b). Although the smallest concentration of methane detected was of 1.5 ppmv, the strong linear slope of the fitted straight line allows us to estimate that the instrumentation has the sensitivity to detect concentration changes smaller than 1.5 ppmv. In recent measurements made with methane, it was possible to achieve an experimental detection limit of 50 ppbv, for this gas (Rocha et al, 2011). It is possible to estimate a detection limit of 30 ppbv methane, by extending the straight line until the noise limit, at a signal to noise ratio, in single pass (Grossel et al., 2007).

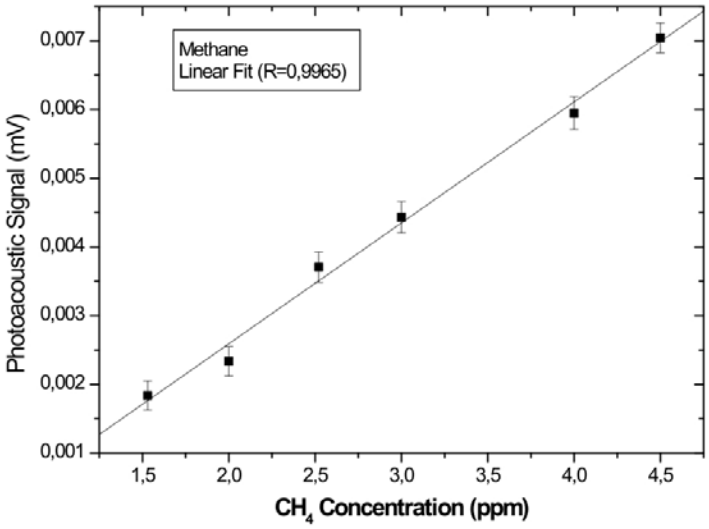

Fig. 5. Calibration curve for methane.

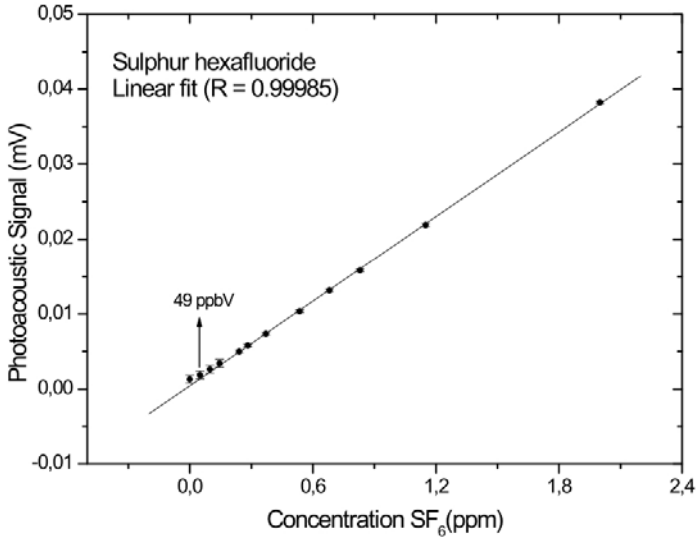

Fig. 6. Calibration curve for sulphur hexafluoride.

The photoacoustic spectroscopy with quantum cascade lasers has proved to be extremely efficient for the detection of greenhouse gases (Atkinson, 2000), being sensible and selective. In the case of the greenhouse gas methane, this methodology allows measurements in anthropogenic sources that emits methane in concentration higher than 1.5 ppmv and also atmospheric measurements, once it is estimated that the current average concentration of this gas in the atmosphere is of 1.7 ppmv. For sulphur hexafluoride the method is suitable

for concentrations greater than 49 ppbv, a concentration already detected by conventional equipments. Another important greenhouse gas is the nitrous oxide (N_2O) which can also be detected by quantum cascade laser (QCL), whose detection limit of 14 ppbv was obtained for this gas (Grossel et al, 2007).

3.3 OPO Laser experimental setup

Figure 7 shows a schematic diagram of an experimental setup for an OPO in a simple grazing-incidence grating configuration (GIOPO) (Yu & Kung, 1999). Two gold mirrors (M1 and M2) are used to produce an optical resonator. The pump light (1064 nm) is put into the resonator by 45º incidence on a third mirror (M3) coated for high reflection at 1064 nm and high transmission for signal and idler waves. A coated highly transmitting at 1064 nm lens (L1) is used to focus the pump beam at the middle of the PPLN crystal (C1) length. In the GIOPO configuration a grating (600/mm groove density) (G1) is placed at grazing incidence relative to the cavity axis. The grating serves as dispersing element. The diffracted first order off the grazing is reflected back into the cavity by M2 and used as injection seed. The zero order is out coupled from the resonator to be used as exciting light for photoacoustic spectroscopy. Before the beam reaches the photoacoustic detector, a highly reflecting mirror at 1064 nm is employed to eliminate the pump wave and a germanium element (Ge) is used to filtering the signal wave from the beam. This OPO configuration results in a typical linewidth of about 0.1 cm^{-1} and the idler wave covers a wavelength range between 2.4 and 4 μm with power average of some hundreds of miliwatts by either tuning the mirror M2 or changing the temperature of the crystal.

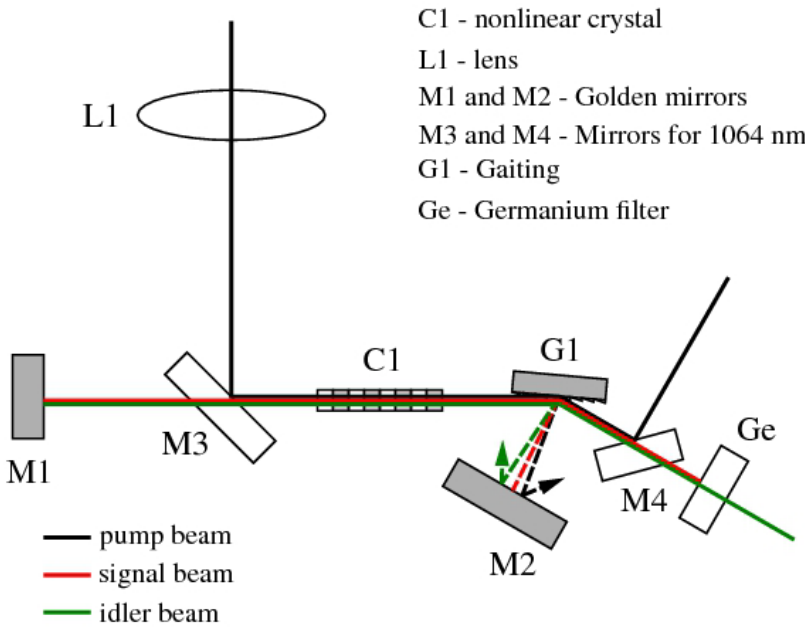

Fig. 7. Schematic setup for OPO with in a grazing-incidence grating configuration.

Owing to the wavelength tunability of the OPO, in recent years it has been shown the feasibility of using optical parametric oscillator as light source for trace gas detection of several chemical species of environmental appeal. Limits of part per billion for greenhouse gases have been demonstrated when OPO is combined with photoacoustic detection methods. Concentration limit of 60 ppbv (part per billion by volume) and 20 ppbv were estimated for nitrous oxides (N_2O) and methane (C_2H_4), respectively, when the OPO radiation is in amplitude modulated (Costopoulos et al., 2002, Liang et al., 2000). The sensitivity of the detection for methane can be improved when the technique of wavelength modulation of the OPO radiation, combined with multipass configuration, is employed. This modulation mode has the advantage of the suppression of the baseline caused by hits of the cell windows and the reflection on the mirrors. According to Nd *et all* , an ultimate sensitivity of 136 parts in 10^{12} for methane was estimated when the technique of wavelength modulation is used (Kung et al., 2004) [92].

Since the increase rate of greenhouse in the atmospheric air is higher than the sensitivity of an OPO setup, it gives rise in this way the possibility of using OPO devices to monitor the annual change of pollutants in atmospheric air. Detection of N_2O in ambient air was already carried out using photoacoustic spectroscopy. Applying the photoacoustic spectroscopy in combination with a pulsed grazing-incident optical parametric oscillator, concentrations of 311 ppbv were found for ambient samples collected at nearby roads (Da Silva et al., 2006).

4. Conclusion

The Photoacoustic Spectroscopy has proved to be extremely sensitive and selective for gas detection. Several experimental arrangements with laser sources have been presented to the detection of greenhouse gases and its precursors in the ppmv and ppbv range. Recent advances in radiation sources for photoacoustic detection of gases has been presented, such as the quantum cascade laser (QCL) and the optical parametric oscillator (OPO) system as well as improvements in the photoacoustic detector, like the differential photoacoustic cell and the simple resonant photoacoustic cell. Such progresses encourage the development of new researches in the field of atmospheric pollution.

5. References

Abeles, F.B. & Heggestad, H.E. (1973) Ethylene: An urban air pollutant. *J. Air Pollut. Cont. Assoc.* , *23*, 517-521. ISSN 0002-2470.

Allen, M. R.; Frame, D. J.; Huntingford, C.; Jones, C. D.; Meinshausen, J. A. L. M. & Meinshausen, N (April 30 2009). Warning Caused by Cumulative Carbon Emissions Towards the Trillionth Tonne, *Nature*, Vol. 458. ISSN 0028-0836.

Angelmahr, M.; Miklos, A. & Hess, P., (2006) Photoacoustic Spectroscopy of formaldehyde with tunable laser radiation at the part per billion level. *Appl. Phys. B* , *85*, 285-288. ISSN: 0946-2171 (print version) ISSN: 1432-0649 (electronic version).

Armstrong, J. A.; Bloembergen, N.; Ducuing, J. & Pershan, P. S.(1962). Phys. Rev. 127, 1918. ISSN 1943-2879.

Atkinson, R. (2000). Atmospheric chemistry of VOCs and NO_x. *Atmosph. Environ. 34*, 2063-2101. ISSN 1352-2310.

Baird, C. (2002). *Environmental Chemistry*, 2nd ed.; Brookman: Porto Alegre, Brazil. ISBN 9788536300023.

Baptista-Filho, M.; Da Silva, M.G.; Sthel, M.S.; Schramm, D.U.; Vargas, H.; Miklos, A. & Hess, P., (2006) Ammonia detection using quantum-cascade laser photoacoustic spectroscopy. Applied Optics, 45: 4966-4971 ISSN: 1559-128X (print) ISSN: 2155-3165 (online).

Beck, M., et al. (2002) Continuous Wave Operation of a Mid-Infrared Semiconductor Laser at Room Temperature. Science Vol. 295. ISSN 0036-8075 (print), 1095-9203 (online).

Bell, A. G., (1880). On the production and reproduction of sound. *Am. J. Sci.* 20, 305-324. ISSN: 1945-452X (online) ISSN: 0002-9599 (print).

Berrou, A.; Raybaut, M.; Godard, A. & Lefebvre, M., (2010). High-resolution photoacoustic and direct absorption spectroscopy of main greenhouse gases by use of a pulsed entangled cavity doubly resonant OPO. *Appl. Phys. B* , *98*, 217-230. ISSN: 0946-2171 (print) ISSN: 1432-0649 (electronic version).

Beyer, T.; Braun, M. ; Lambrecht, & A. Fast (2003) .Gas spectroscopy using pulsed quantum cascade lasers, J. Appl. Phys, 93, 3158–3160 ISSN: 0947-8396 (print) ISSN: 1432-0630 (electronic version).

Costopoulos, D.; Miklos, A. & P. Hess, Appl. Phys. B 75, 385 (2002). ISSN: 0946-2171 (print) ISSN: 1432-0649 (electronic version).

Curl, R. F.; Capasso, F.; Gmachl, C.; Kosterev, A. A.; McManus, B.; Lewicki, R. ; Pusharsky, M.; Wysocki, G. & Tittel, F. K. (2010). Quantum cascade lasers in chemical physics. Chemical Physics Letters, 487, 1–18 ISSN 0003-6951 (print) ISSN 1077-3118 (online).

Da Silva,M.G.Da Silva, M.G.; Miklós, A.; Falkenroth, A. & Hess, P., (2006) Photoacoustic measurement of N_2O concentrations in ambient air with a pulsed optical parametric oscillator, Appl. Phys. B 82, 329–336.). ISSN: 0946-2171 (print) ISSN: 1432-0649 (electronic version).

Demtröder, W. (2003) *Laser Spectroscopy: basic concepts and instrumentation*, pag. 75-81, Third Edition (Springer-Verlag, Berlin. ISBN 3-540-67838-7.

Dewey, C. F., Jr., Kamm, R. D., & Hackett, C. E., (1973). Acoustic amplifier for detection of atmospheric pollutants. *Appl. Phys. Lett.* 23, 633-635. ISSN 0003-6951 (print) ISSN 1077-3118 (online).

Elia, A.; Lugarà, P. M.; Di Franco, C. & Spagnolo, V., (2009). Photoacoustic Techniques for Trace Gas Sensing Based on Semiconductor Laser Sources, *Sensors*, *9*, 9616-9628. ISSN 1424-8220

Emanuel, K.; (2005) Increasing destructiveness of tropical cyclones over the past 30 years. *Nature*, Vol. 436/4. ISSN 0028-0836.

Faist, J et al, (1994). Quantum cascade laser. Science 264, 553. ISSN 0036-8075 (print) 1095-9203 (online)

Faist J. et al, (1997). "Distributed feedback quantum cascade lasers," Appl. Phys. Lett. 70, 2670–2672. ISSN 0003-6951 (print) ISSN 1077-3118 (online).

Fejer, M. M.; Magle, G. A.; Jundt, D. H. & Byer, R. L. (1992) IEEE J. Quantum Electron. 18, 907. ISSN: 0018-9197.

Filho, M.B.; Silva, M.G.; Sthel, M.S.; Schramm, D.U.;Vargas, H.; Miklos, A. & Hess, P., (2006). Ammonia detection by using quantum cascade laser Photoacoustic Spectroscopy. *Appl. Opt.*,*45*, 4966-4971. ISSN: 1559-128X (print) ISSN: 2155-3165 (online).

Giordmaine, J. A. & Miller, R. C. (1965). Phys. Rev. Lett. 14, 973 . ISSN. 0031-9007 (print) 1079-7114 (online).

Gmachl, C.; Capasso, F; Sivco, D.L. & Cho, A., (2001) Recent progress in quantum cascade lasers and applications,. Reports on Progress in Physics, 64: 1533-1601. ISSN 0034-4885(print) ISSN 1361-6633 (electronic version).

Gondal, M.A., (1997). Laser photoacoustic spectrometer for remote monitoring of atmospheric pollutants, Applied Optics, Vol. 36, No. 15ISSN: 1559-128X (print) ISSN: 2155-3165 (online).

Greene, C. H.; Monger, B. C.; McGarry, L. P., (2009*).* Some like it cold, northern shrimp stocks thrive when climatic conditions lead to cold bottom waters. *Science,* Vol. 324. ISSN 0036-8075 (print), 1095-9203 (online).

Grossel, A.; Z´eninari, V.; Parvitte, B.; Joly, L. & D. Courtois (2007). Optimization of a compact photoacoustic quantum cascade laser spectrometer for atmospheric flux measurements: application to the detection of methane and nitrous oxide. Appl. Phys. B 88, 483–492. ISSN: 0946-2171 (print) ISSN: 1432-0649 (electronic version).

Hansen, J. & Makiko, (2004). Greenhouse gas growth rates, *PNAS,* vol.101, no. 46 ISSN: 1091-6490.

Hansen, J. et al. (2008) Target atmosphere CO_2: Where Should Humanity Aim . *The Open Atmospheric Science journal,* 2, 217-231. ISSN: 1874-2823.

Harren, F. & Reuss, J. R., (1997). Photoacoustic spectroscopy 'Encyclopedia of Applied Physics' Vol. 19 (Ed.) G.L. Trigg (VCH, Weinheim, 413-435 . ISBN 3–527–28134–7 .

Harren, F. J.M.; Cotti, G.; Oomens, J. & Hekkert, S. te L., (2000). Photoacoustic Spectroscopy in Trace Gas Monitoring, *Encyclopedia of Analytical Chemistry,* pp. 2203–2226, John Wiley & Sons Ltd, Chichester. ISBN 0471851981.

Harren, F.J. M. et al, (2008). Laser-based systems for trace gas detection in life sciences, Applied Physics B, 92, 343-349. ISSN: 0946-2171 (print) ISSN: 1432-0649 (electronic version).

Hess, P. (1983). Resonant photoacoustic spectroscopy. *Top. Curr. Chem*. 111, 1-32. ISSN 0340-1022(print) ISSN 1436-5049(electronic version).

Hess, P., (1992). Principles of photoacoustic and photothermal detection in gases. In *Principles and Perspectives of Photothermal and Photoacoustic Phenoma* (A. Mandelis, Ed.), Chapter 4. Elsevier, New York. ISSN: 0301-4797

IPCC. (February 2007). *Climate Change: The Physical Science Basis*; Report of Working Group I; IPCC: Paris, France. ISBN 9291691224.

Janssen, M. (1998). Use of complex adaptive systems for modeling global Change, *Ecosystems*, 1, 457-463 ISSN 1432-9840 (print) ISSN 1435-0629 (electronic version).

Kerr, E. L., & Atwood J. G., (1968). The laser illuminated absorptivity spectrophone: A method for measurement of weak absorptivity in gases at laser wavelengths. *Appl. Opt.* 7, 915-92 ISSN: 1559-128X (print) ISSN 2155-3165 (online).

Kosterev, A. A. & Tittel, F. K., (2002). Chemical sensors based on Quantum Cascade Lasers. IEEE Journal of Quantum Eletronics, V.38, N.6, 582-591. ISSN 0018–9197.

Kosterev, A. A.; Curl, R. F.; Tittel, F. K. ; Rochat, M.; Beck, M.; Hofstetter, D. & Faist, J. (2002). Chemical sensing with pulsed QC-DFB lasers operating at 15.6 _m, Appl. Phys. B,75, 351–357 ISSN: 0946-2171 (print) ISSN: 1432-0649 (electronic version).

Kreuzer, L. B., (1971). Ultralow gas concentration infrared absorption spectroscopy *J. App/. Phys*. 42. ISSN 2934-2943. (print) ISSN 0021-8979. (electronic version).

Kreuzer, L. B., Kenyon, N. P., & Patel, C. K. N., (1972). Air pollution: Sensitive detection of ten pollutant gases by carbon monoxide and carbon dioxide lasers. *Science* 177, 347-349. ISSN 0036-8075 (print), 1095-9203 (online).

Kurz, W. A. et al, (2008). Mountain pine beetle and forest carbon feedback to climate change, *Nature,* Vol. 452. ISSN : 0028-0836.

Liang, G.C.; Liu, H.H.; Kung, A.H. ; Mihacsi, A.; Miklos, A. & Hess, P. (2000) J. Phys. Chem. A, 104, 10179 . ISSN 1089-5639.

Lima J.P. et al, (2006). Photoacoustic Detection of NO_2 and N_2O using quantum cascade lasers. Appl. Phys. B, 85, 279-284. ISSN: 0946-2171 (print) ISSN: 1432-0649 (electronic version).

Luft, K. F., (1943). Ueber eine neue Methode der registrierenden Gasanalyse mit Hilfe der Absorption ultraroter Strahlen ohne spektrale Zerlegung. *Z. Tech.. Phys.* 5, 97- 104. ISSN: 1063-7842 (print) ISSN: 1090-6525 (electronic version).

Mann, M. E.; Bradley, R. S. & Hughest, M. K., (1998.) Global temperature patterns and climate forcing over the past six centuries. *Nature,* Vol. 392. ISSN : 0028-0836.

McCulloch, M.T.; Langford, N. & Duxbury, G. (2005) Real- time trace- level detection of carbon dioxide and ethylene in car exhaust gases. *Appl. Opt. 44*, 2887-2884. ISSN: 1559-128X (print) ISSN: 2155-3165 (online).

Meinshausen, M. et al, (2009). Greenhouse – Gas Emission Targets for Limiting Global Warning to 2 ◦ C. *Nature*, 458 ISSN : 0028-0836.

Meyer, P. L., Bernegger, S., & Sigrist, M. W., (1988). On-line monitoring of air pollutants with a mobile computer-controlled CO_2-laser photoacoustic system.*Springer Ser. Opt. Sci.* 58, 127-130 . ISSN: 0342-4111.

Meyer, P. L., & Sigrist, M. W., (1990). Atmospheric pollution monitoring using CO_2-laser photoacoustic spectroscopy and other techniques. *Rev. Sci. Instrum.* 61, ISSN 1779-1807 (print) ISSN 0034-6748. (electronic version).

Miklos, A.; Hess, P. & Bozoki, P., (2001) Application of acoustic resonators in photoacoustic trace gas analysis and metrology. *Rev. Sci. Instrum.*, *72*, ISSN 1937-1955. (print) ISSN 0034-6748. (electronic version).

Moeckli, M.A.; Hilbes C. & Sigrist, M.W. (1998) . Photoacoustic Multicomponent Gas Analysis Using a Levenberg-Marquardt Fit Algorithm *Appl. Phys*. B . 67, 449–458 . . ISSN: 0946-2171 (print) ISSN: 1432-0649 (electronic version).

Mothé, G.; Castro , M.; Sthel,M; Lima, G.; Brasil,L; Campos, L.; Rocha, A& Vargas, H, (2010).Detection of Greenhouse Gas Precursors from Diesel Engines Using Electrochemical and Photoacoustic Sensors, *Sensors* , *10*, 9726-9741. ISSN 1424-8220.

Nathan P, et al, (2008). Attribution of polar warming to human influence Nature *Geoscience, Vol. 1* ISSN : 1752-0894.

Ng, J.; Kung, A.H.; Miklos, A. & Hess, P.(2004). Opt. Lett. 29, 1206 . ISSN: 0146-9592 (print) ISSN: 1539-4794 (online).

Patel, C. K. N. (1964). "Continuous-Wave Laser Action on Vibrational-Rotational Transitions of CO_2". *Physical Review* 136,1187-1193 ISSN 1050-2947 (Print) ISSN 1094-1622 (Online)

Peza, A. B. & Simmonds, I., (2005). The first South Atlantic hurricane: Unprecedented blocking, how shear and climate change, *Geophysical Research Letters,* Vol. 32, Li 5712. ISSN 0094-8276.

Rayleigh,J. W. (Lord), (1881). The photophone. *Nature (London)* 23, 274-275. ISSN 0028-0836.

Repond, P. & Sigrist, M.W., (1996). Photoacoustic Spectroscopy on trace gases with continuously tunable CO_2 laser, Applied Optics, Vol. 35, No 21 .ISSN: 1559-128X (print) ISSN: 2155-3165 (online version).

Rocha, M.; Sthel, M ; Lima, G.; Da Silva, M. , Schramm, D; Miklós, A. & Vargas,H, (2010) a. A Sulfur Hexafluoride Sensor Using Quantum Cascade and CO_2 Laser-Based Photoacoustic Spectroscopy, *Sensors* , *10*, 9359-9368 ISSN 1424-8220.

Rocha M.V.,Sthel M.S., Gomes M.S. ,Schramm, D. U. Vargas, H. (2010) b .Greenhouse gases detection with quantum cascade laser photoacoustic spectroscopy, Air & Waste Management Association's 103 rd ANNUAL CONFERENCE & EXHIBITION",Calgary, Canadá. ISSN: 1052-6102. ISBN: 978-1-617-82093-9.

Rocha, M. V.; Sthel, M. S.; Silva, M. G.; Paiva, L. B.; Pinheiro, F. W. ; Miklòs, A. & Vargas, H. (2011). Quantum Cascade laser photoacoustic detection of methane emitted from natural gas powered engines, accepted for Applied Optics B (in press). ISSN 0946-2171

Rosenzweig, C. et al, (2008). Attributing physical and biological impacts to antropogenic climate change, *Nature,* Vol 453. ISSN 0028-0836.

Röntgen, W. C., (1881). Ueber Toene, welche durch intermittierende Bestrahlung eines Gases entstehen.*Ann. Phys.* (Leipzig) [3] 12, 155-159. ISSN: 0003-4916.

Rothman, L.S.; Gamache, R.R.; Tipping, R.H.; Rinsland, C.P.; Smith, M.A.H.; Benner, D.C.; Devi, V.M.; Flaud, J.M.; Camy-Peyret, C.; Perrin, A.; Goldman, A.; Massie, S.T.; Brown, L.R. & Toth, R.A. (1992)Quantitative Spectroscopy and Radiative Transfer 48, 469–507 ISSN: 0022-4073.

Sander et al, B. D., (2006). Forced and unforced ocean temperature changes in Atlantic and Pacific tropical cyclogenesis regions, *PNAS,* vol. 103, no. 38. ISSN: 1091-6490.

Schramm, D. U.; Sthel, M. S.; da Silva, M. G. ; Carneiro, L. O.; Junior, A. J. S. & H. Vargas, *(2003).* Application of the Laser Photoacoustic Spectroscopy on the Analysis of Gas Samples Emitted by Diesel Engines. *Inf. Phys. Technol* ,44, p 263-269. ISSN 1424-8220.

Seinfeld, J.H. (1986). *Atmospheric Chemistry and Physics of Air Pollution*; John Wiley & Sons: Hoboken, NJ, USA. ISBN: 0-471-65128-1.

Seinfeld, J.H. (1989). Urban air pollution: State of the science. *Science* , *243*, 745-752. ISSN 0036-8075 (print), 1095-9203 (online).

Siddall, M.; Stocker, T. F. & Clark, P. U., *(2009).* Constrains on future sea-level from past sea-level change, *Nature Geoscience,* Vol. 2. ISSN : 1752-0894.

Sigrist, M.W., (1994) a. *Air Monitoring by Spectroscopic Techniques. Chemical Analysis*; John Wiley & Sons, Inc.; New York, NY, USA, Volume 12 ISBN 0-8247-8946-6.

Sigrist, M. W., (1994)b. Laser Photoacoustic Spectrometry for Trace Gas Monitoring, *Analyst,, Vol. 119 ,* 525 ISSN 0003-2654.

Sigrist, M.W.; Bartlome, R.; Marinov, D.; Rey, J.M.; Vogler, D.E.; Wächter, H. (2008) Trace gas monitoring with infrared laser-based detection schemes. *Appl. Phys. B* ,, *90*, 289-300. . ISSN 0946-2171 (print) ISSN 1432-0649 (electronic version).

Silva, M. G.; Vargas, H.; Miklós, A. & Hess, P. (2004) Photoacoustic detection of ozone using quantum cascade laser, Appl. Phys. B , 78, 1513–1516. . ISSN 0946-2171 (print) ISSN 1432-0649 (electronic version).

Solomon, S. et al., *(*2009*)*, Irreversible climate change due to carbon dioxide emissions, *PNAS,* Vol. 106, no. 6, ISSN 1091-6490.

Sorvajärvi, T.; Manninen, A. ; Toivonen, J.; Saarela, J. & Hernberg, R. (2009) Resonant photoacoustic cell for pulsed laser analysis of gases at high temperature *Rev. Sci. Instrum* , 80, 123103. ISSN 0034-6748. (print) ISSN 1089-7623(electronic version).

Steffen, W.; Sanderson, A.; Jäger, J.; Tyson, P.D.; Moore, B., III; Matson, P.A.; Richardson, K.; Oldfield, F.; Schellnhuber, H.-J.; Turner, B.L., II &Wasson, R.J (2004). *Global Change and the Earth System: A Planet under Pressure*; Springer-Verlag: Heidelberg, Germany. ISBN: 3-540-42400-8.

Sthel, M.S.; Tavares, J.R.; Lima, G.R.; Mothé, G.; Schramm, D.U.S.; Da Silva, M.G. & Castro, M.P.P. (2010)Atmospheric pollution: Global warming and a possible use of bio-fuels wide scale. *Int. Rev. Chem. Eng. 1*. 564-570. ISSN: 0020-6318.

Sthel, M.S.; Schramm, D.U.; Lima, G.R., Carneiro, L.; Faria Jr. , R.T.; Castro, M.P.P.;Alexandre, J.; Toledo, R. ; Silva, M.G. & H. Vargas, 2011). CO2 laser photoacoustic detection of ammonia emitted by ceramic industries, *Spectrochimica Acta* Part A 78, 458–462. ISSN 1386-1425.

Tang, C. L. ; Bosenber, W. R.; Ukachi, T. ; Lane, R.J. & Cheng, L.K. (1992). Proc. IEEE, 80, 365. ISSN 0018-9219.

Teodoro, C.G.; Schramm, D.U.; Sthel, M.S.; Lima, G.; Rocha, M.V.; Tavares, J. & Vargas, H. (2010). CO_2 laser photoacoustic detection of ethylene emitted by diesel engines used in urban public transports. *Infr. Phys. Technol. 53*, 151-155. ISSN 1424-8220.

Thomas, S., (2006). Photoacoustic Spectroscopy for process analysis *Anal. Bioanal. Chem*., *384*, 1071-1086. ISSN: 1618-2650.

Trenberth, K. E. & Shea, D. J., (2006). Atlantic hurricanes and natural variability in 2005, *Geophysical Research Letter,* Vol. 33, 1029 ISSN: 0094-8276.

Tyndall,J., (1881). Action of an intermittent beam of radiant heat llpon gaseous matter. *Proc. R. Soc. London* 31, 307-317. ISSN 1364-5021.

Viengerov, M., (1938). *Dokl. Akad. Nauk SSSR* 19,687. ISSN 0002-3264.

Weidmann, D.; Kosterev, A.A.; Roller, C.; Curtel, R.F.; Fraser, M.P.; & Tittel, F.K. (2004). Monitoring of ethylene by a pulsed quantun cascade laser. *Appl. Opt. 43*, 151-155. ISSN 1559-128X (print) ISSN 2155-3165 (online).

West, G. A., (1983). Photoacoustic spectroscopy. *Rev. Sci. Instrum.* 54, 797-817. ISSN (printed): 0034-6748.

Wolf, G.T. & Korsog, P.E. (1992) Ozone control strategies based on the ratio of volatile organic compound to nitrogen oxides. *J. Air Waste Manage. Assoc. 42*, 1173-1177. ISSN: 1047-3289.

Wright, S.; Duxbury, G. & Langford, N. (2006). A compact quantum-cascade laser based spectrometer for monitoring the concentrations of methane and nitrous oxide in the troposphere, Appl. Phys. B 85, 243-249 . ISSN: 0946- 2171 (print) ISSN: 1432-0649 (electronic version).

Yu,C.S. & Kung, A.H. (1999). Grazing-incidence periodically poled $LiNbO_3$ optical parametric oscillator, Optical Society of America, 16, 2233-2238. ISSN 1943-0620.

Zhang, J. Y.; Huang, J. Y. & Shen, J. Y. R. (1993) Opt. Soc. Am. B 10, 1758. ISSN 1520-8532.

Zhou, J. X.; Hou, X.; Yang, K. X.; Tsai, S. J. J. &Michel, R. G. (1998) Appl. Spec. 52, 176 ISSN 0021-9037.

11

Miniaturized Mass Spectrometer in Analysis of Greenhouse Gases: The Performance and Possibilities

Shuichi Shimma and Michisato Toyoda
Osaka University
Japan

1. Introduction

It is no doubt that mass spectrometry (MS) is widely applied to several research fields. In recent years, design and development of novel miniaturized mass spectrometers have been at the forefront of research in MS. A lot of miniaturized mass spectrometers are reported and commercialized from a lot of institutes and industries. The instruments have widespread applications, for example, detection and identification of chemical and biological hazards for the homeland security (Contreras et al., 2008; Smith et al., 2011), the food safety (Garcia-Reyes et al., 2009) and so on. Because of their small size and lightweight, miniaturized mass spectrometers have a potential for field use. These features are absolutely suitable for on-site environmental analyses, especially in greenhouse gases analyses. However, there are few reports on application of miniaturized mass spectrometers in this research field. This chapter describes instrumentation and application feasibility of miniaturized mass spectrometers to the greenhouse gases analysis. This chapter is consists of following four sections.

1. New analytical concept of "On-site mass spectrometry" and field usable mass spectrometers,
2. Introduction of our technology: multi-turn time-of-flight (TOF) mass spectrometer (MULTUM),
3. Miniaturized ultra-high mass resolution multi-turn TOF mass spectrometer "MULTUM-S II",
4. Application of greenhouse gases detection using MULTUM-S II.

2. "On-site mass spectrometry" using miniaturized mass spectrometers

In this section, a novel analytical concept "On-site mass spectrometry", overview of several reported miniaturized mass spectrometers and issues for the field use are mentioned.

2.1 On-site mass spectrometry

The basis of science is to measure phenomena of nature in real-time and with strict accuracy. However, we know that it is the most difficult to perform such measurements using high

performance analyzers. We must often prepare a lot of appropriate instruments to detect each target. In this sense, the features of mass spectrometers, for example variations of detectable targets, sensitivity and throughput, have advantages over other analytical instruments. Based on this point, "On-site mass spectrometry" is to bring high specifications mass spectrometers into field sites and to provide high quality mass spectrometric data in real-time. This concept is challenging, but on-site mass spectrometry attracts rising attention.

Considering conventional analytical methodologies using mass spectrometers, samples are usually taken from field sites. Then, the samples are brought into laboratories and purified before introducing into high performance mass spectrometers. Here, high performance mass spectrometers equipped in the laboratory have generally large size. To bring mass spectrometers into the on-site is required in several research fields, however, can we bring such instruments into the on-site? The answer is probably impossible. It is essential to miniaturize mass spectrometers with keeping performances ideally. Furthermore, we have to require not only simple and high performance miniaturized mass spectrometers to measure poorly purified samples but also simple sampling methods/sample preparations.

2.2 Overview of miniaturized mass spectrometers

Methods to reduce weight and size were attempted by various research groups. According to the reported papers on miniaturized mass spectrometers, a wide variety of instruments type including ion traps, quadrupole mass filters (QMF) (Geear et al., 2005), magnetic sector mass spectrometers (Diaz et al., 2001a; Diaz et al., 2001b), and TOF mass spectrometers (Cornish&Cotter, 1997; Cotter et al., 1999; Berkout et al., 2001; Ecelberger et al., 2004) were described. The main specifications are summarized in Table 1. It is considered that ion traps or QMF are more favourable than other instruments for miniaturization. In fact, almost all commercialized miniature mass spectrometers, for example *Guardion-7* (Lammert et al., 2006) and *Griffin Analytical 600* in Table 1, have adopted ion traps and QMF. In addition, it can be noted that there is a large variety of ion traps: (1) three dimensional hyperbolic ion traps, (2) rectilinear ion traps (Liang et al., 2008; Fico et al., 2009; Li et al., 2009; Ouyang et al., 2009), (3) toroidal ion traps (Lammert et al., 2006), (4) planar electrode ion traps (Austin et al., 2007; Austin et al., 2008; Yang et al., 2008), and (5) cylindrical ion traps (Van Amerom et al., 2008; Wells et al., 2008; Chaudhary et al., 2009).

Why were a lot of miniaturized mass spectrometers developed using ion trap techniques? The main reasons for choosing ion traps for portable instruments are that ion traps provide a relaxed vacuum condition, simple structures for easily miniaturized geometry with weight saving. A portable ion trap mass spectrometer system "Mini 11" was reported in 2009 (Gao et al., 2009), whose total weight with batteries is 5.0 kg, power consumption is 35 W, and dimensions are 22 cm x 12 cm x 18 cm. In addition to the miniaturized characteristics, the instrument has been coupled with wide varieties of ambient ionization sources, for example desorption electrospray ionization, electrospray ionization and paper spray ionization (Li et al., 2011; Soparawalla et al., 2011).

Instrument	Weight (kg)	Power (W)	Size (*H* x *L* x *W* mm)	Analyzer type
Mini 11	4	30	180 x 220 x 120	Rectilinear ion trap
Guardion-7	14.5	120	380 x 390 x 230	Toroidal ion trap
HAPSITE system	19	30	180 x 460 x 430	QMF
Griffin 450	8.6	600	488 x 488 x 536	Cylindrical ion trap
Suitcase TOF	-	-	-	TOF
IonCam	19	150	438 x 432 x 254	Mattauch-Herzog sector
MULTUM-S II	36	600	450 x 640 x 230	TOF

Instrument	Ionization method	Mass (*m/z*) range	Resolution	Vendor/institute
Mini 11	MIMS, direct leak, ESI, DESI	2000	100	Purdue University
Guardion-7	EI	40 – 500	540	Torion Technologies Inc.
HAPSITE system	EI	41 – 300	-	INFICON
Griffin 450	EI	40 – 425	400	FLIR
Suitcase TOF	MALDI	50 000	30	Johns Hopkins Univ.
IonCam	EI	7 – 250	250	O. I. Analytical
MULTUM-S II	EI	1 - 1000	30 000	Osaka University

Table 1. Specifications of miniaturized mass spectrometers. MIMS, membrane inlet MS; EI, electron ionization; DESI, desorption electrospray ionization; ESI, electro spray ionization; MALDI, matrix-assisted laser desorption ionization.

2.3 A few issues for miniaturized mass spectrometers

Miniaturized instruments, especially ion traps or QMF described above, appear to have usable performance in the field use. However, sensitivity and mass resolution in these physically smaller devices are lower compared to laboratory instruments. To overcome the loss of sensitivity due to lower transmission of ions into and out of the analyzer, ion traps using array geometry were proposed. On the other hand, high mass resolution cannot in principal be obtained in QMF or ion traps. The typical mass resolution in miniaturized mass spectrometers is less than a few hundreds as shown in Table 1.

We consider that miniaturized instruments would be more commonly utilized in the future. In particular, high mass resolution is important when it is difficult to perform sufficient sample preparations as described in section 1. In this case, high mass resolution is important to avoid false positive and false negative from contaminant peaks.

How can we realize miniaturized high mass resolution mass spectrometers? In general, mass spectrometers for high mass resolution mass spectrometry are magnetic sector mass analyzers, Fourier transform ion cyclotron resonance (FT-ICR) mass spectrometers (Marshall

et al., 1998; Hu et al., 2005), and TOF mass spectrometers. However, if high mass resolution is to be achieved in these instruments, the size of instruments will become large and heavy. Especially, magnetic sector mass analyzers and FT-ICR mass spectrometers are required large electrical magnets and superconductive magnets. Therefore, it is difficult for simply miniaturized these instruments to improve mass resolution. This point is supported by specifications of IonCam listed in Table 1 (Hadjar et al., 2011).

According to the structural simplicity and weight, TOF mass spectrometers are more favorable for reduction in size. Here, the mass resolution ($m/\Delta m$) of TOF can be written as

$$\frac{m}{\Delta m} = \frac{T}{2\Delta T} \tag{1}$$

T and ΔT are TOF and a peak width (FWHM: full-width at half maximum), respectively. We can easily find that mass resolution is directly proportional to TOF (i. e., the size of the instrument). Therefore, simply shortening of the flight length to miniaturize the instrumentation size decreases mass resolution.

To overcome this fundamental problem, the flight length is extended by various methods. The proposed systems are listed as follows:

1. Electrostatic multi-pass mirror systems (Wollnik&Przewloka, 1990; Casares et al., 2001; Wollnik&Casares, 2003).
2. Helical or jig-saw type systems (Matsuda, 2000; Satoh et al., 2005; Satoh et al., 2007; Yavor et al., 2008; Satoh et al., 2011).
3. Multi-turn ion optical geometries using electrostatic sectors (Poschenrieder, 1972).

In our laboratory, the multi-turn type TOF mass spectrometers, which have a figure of eight flight path, are mainly designed and constructed. The first multi-turn TOF mass spectrometer "MULTUM-Linear plus" was constructed. In the next section, we will introduce the overview and the developing history.

3. History of multi-turn time-of-flight (TOF) mass spectrometers in Osaka University

Detailed discussions about the ion optical conditions which need to be met for operation of the multi-turn TOF mass spectrometer have been given elsewhere (Ishihara et al., 2000). Here, we simply explain the overview of our developed system and features of the ion optical system of the multi-turn TOF mass spectrometer.

3.1 Development history of MULTUM at Osaka University

Figure 1 shows the development history of multi-turn TOF mass spectrometers at Osaka University. We designed and constructed the first multi-turn TOF mass spectrometer "MULTUM Linear plus" as a laboratory model for cometary exploration (Matsuo et al., 1999; Toyoda et al., 2000; Toyoda et al., 2003). The system consists of four discrete units, each comprised of an electrostatic quadrupole lens, a cylindrical electrostatic sector and an electrostatic quadrupole lens. The total path length of one cycle is 1.284 m. The entire system

was fixed on a base plate of 40 cm x 40 cm. Using the electron ionization (EI) for a gas analysis, a maximum mass resolution using this instrument of 350 000 (*m/z* 28 of N_2^+) was achieved after 500 cycles (approximately 645 m in flight length). This system was not simple for operation; 28 electrostatic quadrupole lenses were used. As a next generation multi-turn mass spectrometer, we studied more simplified optical geometries. As a result, a new geometry of "MULTUM II" was designed and constructed (Okumura et al., 2004a; Okumura et al., 2004b). In the MULTUM II geometry, no quadrupole lenses were used. MULTUM II consisted of only four toroidal electrostatic sectors. The components were dramatically reduced. The total path length of one cycle was 1.308 m.

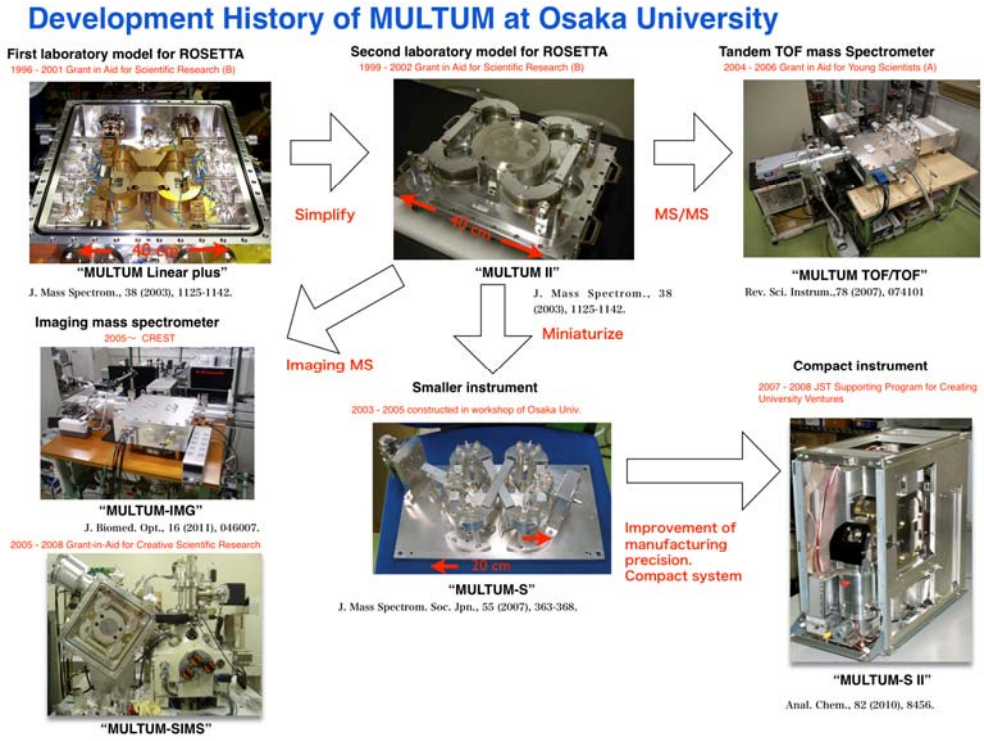

Fig. 1. Development history of MULTUM series.

The maximum mass resolution of 250 000 (*m/z* 28 of N_2^+) was achieved after 1200 cycles (approximately 1500 m in flight length). MULTUM II was equipped with not only the EI ion source but a matrix-assisted laser desorption/ionization (MALDI) ion source for biological applications. Using the MALDI ion source, a mass resolution of 61 000 was achieved for a deca peptide of angiotensin I.

Recently, we have been developing various types of mass spectrometers based on the MULTUM II technology. The first instrument was a tandem TOF mass spectrometer "MULTUM-TOF/TOF" for the structural analysis of biomolecules (Toyoda et al., 2007). The second instruments were used for imaging mass spectrometry. Here, imaging mass

spectrometry is a novel visualization method using mass spectrometry (Amstalden et al., 2010). The stigmatic imaging was performed with "MULTUM-IMG" (Hazama et al., 2008a; Hazama et al., 2008b). Another instrument was equipped with an ionization source for secondary ion mass spectrometry (SIMS), so that the instrument was used for high spatial resolution (approximately sub micrometer) imaging mass spectrometry. The third instruments were miniaturized multi-turn TOF mass spectrometers "MULTUM-S" and "MULTUM-S II" (Shimma et al., 2010). MULTUM-S was the first prototype. This instrument was manufactured using a wide-use lathe and milling machine, resulting in a lack of manufacturing precision and assembly accuracy. The "MULTUM-S II" was optimized the design of ion optics and manufacturing precision. The detailed descriptions of MULTUM-S II are found in section 4.

3.2 Ion optics of MULTUM

There are two conditions that are required for multi-turn systems. The first is the geometrical conditions, namely the necessity to close the ion optical orbit. Multi-turn TOF mass spectrometer geometries with such an orbit have previously been proposed (Poschenrieder, 1972; Sakurai et al., 1999). They did not, however, satisfy the second condition, namely the "perfect focusing" condition (Ishihara et al., 2000). Therefore, in these cases, it is expected that the ion beam will diverge in both time and space. Then, both the mass resolution and the ion transmission (sensitivity) are compromised as the number of cycles around the instrument increases. To avoid this problem, ions should return to the point of origin in the system. In other words, the absolute value of the position and angle at the final position (which is identical with the initial position) should be the same as at the initial position in both the horizontal and vertical directions. Such conditions can be expressed using the transfer matrix method in the first order approximation as

$$\begin{pmatrix} x_f \\ \alpha_f \\ y_f \\ \beta_f \\ \gamma \\ \delta \\ l_f \end{pmatrix} = \begin{pmatrix} \pm 1 & \underline{0} & 0 & 0 & 0 & \underline{0} & 0 \\ \underline{0} & \pm 1 & 0 & 0 & 0 & \underline{0} & 0 \\ 0 & 0 & \pm 1 & \underline{0} & 0 & 0 & 0 \\ 0 & 0 & \underline{0} & \pm 1 & 0 & 0 & 0 \\ 0 & 0 & 0 & 0 & 1 & 0 & 0 \\ 0 & 0 & 0 & 0 & 0 & 1 & 0 \\ \underline{0} & \underline{0} & 0 & 0 & R(l|\gamma) & \underline{0} & 1 \end{pmatrix} \times \begin{pmatrix} x_i \\ \alpha_i \\ y_i \\ \beta_i \\ \gamma \\ \delta \\ l_i \end{pmatrix} \tag{2}$$

Here, the ion optical position vectors (x, α, y, β, γ, δ), where x, y and α, β denote the lateral and angular deviations of the ion under consideration from a reference ion at the object. The mass and energy deviations and pathlength deviation are described as γ, δ and λ. The subscripts i and f represent initial and final position, respectively. It should be noted that the character $\underline{0}$ (zero with underline) means the matrix element which should be forced to be zero. Accordingly, we require the "nine-fold focusing", i.e. the nine $\underline{0}$ elements should be zero. By introducing symmetry in the arrangement of the ion optical components (i. e. the figure of eight geometry), multiple focusing conditions are easily achieved. We found ion optical systems ("MULTUM", "MULTUM II") for a multi-turn TOF mass spectrometer which satisfy perfect focusing.

4. Miniaturized multi-turn TOF mass spectrometer "MULTUM-S II"

In this section, we explain the system and novel characteristics of the recently developed miniaturized TOF mass spectrometer "MULTUM-S II"

4.1 Overview of MULTUM-S II

Photograph of the developed MULTUM-S II system are shown in Fig. 2. The size of the analyzer is less than 20 cm x 20 cm, which is the half size of MULTUM II (Fig. 2a). The photograph of the whole system is shown in Fig. 2b. The developed system consists of the following: the ion source, multi-turn mass analyzer, vacuum system, and high voltage circuit unit. The complete mass spectrometer weighs 35 kg. The total size of the instrument is 45 cm x 25 cm x 64 cm. The equipped ionization source is a two-stage acceleration ion source of EI type introduced by W. C. Wiley and I. H. McLaren (Wiley&McLaren, 1955). The accelerated ions are focused using the Einzel lens. After focusing, the ions are injected into the multi-turn TOF mass spectrometer.

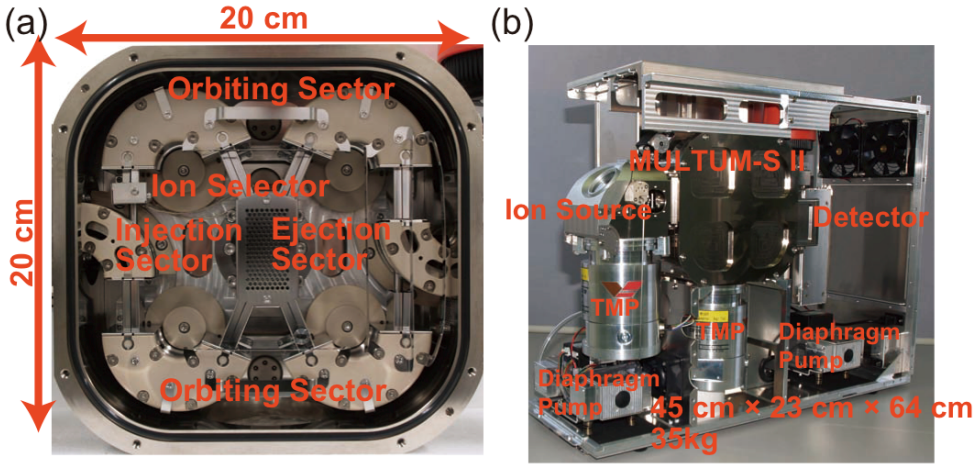

Fig. 2. Desktop high-mass resolution TOF mass spectrometer "MULTUM-S II"; (a) the inside of the analyzer, (b) the outside of the system.

The main geometry of the analyzer was the same as MULTUM II. In the miniaturized instruments, it is an important issue on how ions are introduced with high efficiency into the mass analyzer from the ion source. Additionally, introduced ions need to travel with stability in the closed orbit to obtain high mass resolution. In the previous MULTUM system described in section 3, the ion beam passed through small holes in the outer electrodes of two of the electric sectors. When ions were injected or ejected, the voltages applied to the sector electrodes were switched. To prevent the reduction of resolution due to instability of the power supply for switching, we offer higher stability (< 50 ppm) (Toyoda et al., 2007).

In order to overcome the problem of ion injection/ejection and stable traveling, MULTUM-S II has two additional sectors shown in Fig. 2a. Since these sectors specialized in ion injection/ejection, the static voltage is simply applied to the orbiting sectors. For this reason, the electrical circuits for MULTUM-S II could be simplified and miniaturized.

4.2 Data acquisition methods

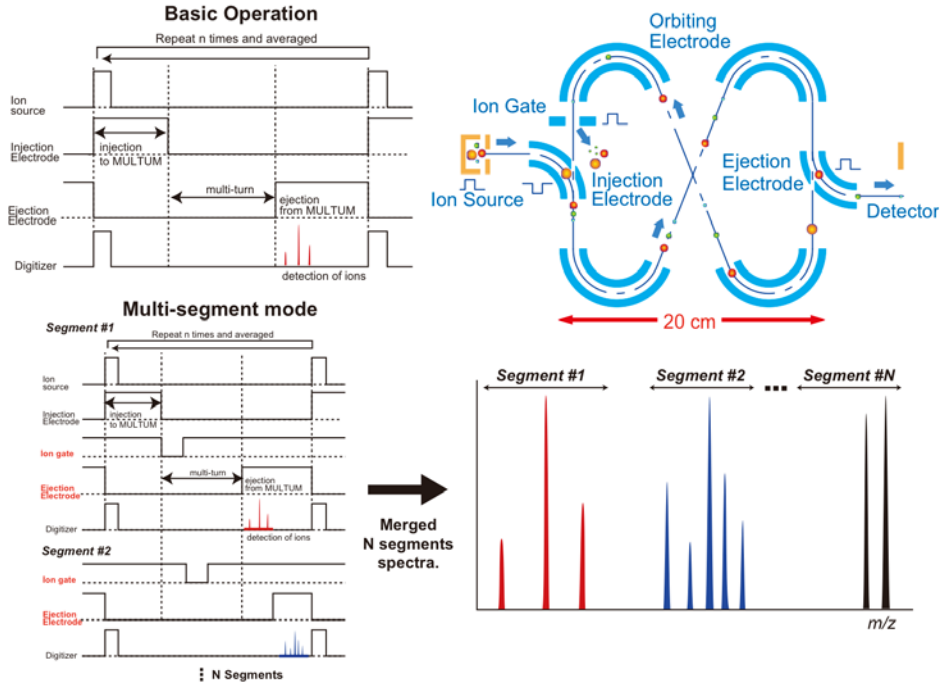

Fig. 3. Operation diagram of MULTUM-S II.

Block diagrams of the timing control are shown in Fig. 3. In the basic operation, the ions were extracted from the EI ion source by applying the pulsed voltage to the push electrode. The voltage applied to Injection Electrode was turned on when ions were injected into the analyzer part. After the ions had been injected into the analyzer, the voltage applied to Injection Electrode was turned off. On the other hand, the voltage applied to Ejection Electrode was initially switched off; thus, the ion packets flew into the closed orbit composed of Orbiting Electrodes. After a preset number of cycles, the voltage applied to Ejection Electrode was switched on, and the ion packets were ejected from the closed orbit. Then, the ions were detected. Therefore, the switching timing of Ejection Electrode controlled the number of cycles. Due to the performance of the digitizer equipped in our system, the repetition time of the cycle in Fig. 3 was 1 kHz. Therefore, acquisition time for one spectrum was 1 millisecond.

This feature becomes powerful tool for specific ion measurement, however "Overtaking problem" will appear in detection of ions over the wide mass range. During orbiting, lighter ions take over the heavier ions, because the ion speed depends on the mass of the ion. To avoid the over taking problem, the measuring mass range is divided into some segments. In this multi-segment mode, Ion Gate equipped in the orbiting trajectory controls the mass range. Therefore, the switching timing of Ion Gate and Ejection Electrode are individually configured as shown in Fig. 3. In this operation mode, our software automatically calculates

the timing of Ion Gate and Ejection Electrode. Users can only input the target mass value and the number of cycles. After spectra acquisition, obtained segment mass spectra are merged in one spectrum as shown in Fig. 3.

4.3 Obtained mass spectra of low mass ions using MULTUM-S II

In the specifications of mass spectrometer, the detectable mass range is important. The wide mass range is obviously preferred. The upper mass is restricted to the ionization methods, so that the upper mass value of MULTUM-S II is approximately *m/z* 1000. The lower limit is also important for the simultaneous gas analysis. However, high resolution MS in the low mass region, which is less than *m/z* 50, is generally difficult due to the electric noise from the instruments. As shown in Table 1, the lower mass limits of almost all instruments are *m/z* 40. In our instrument, the electric circuits are very simple. This feature becomes a strong advantage in detection of low mass molecules. Figure 4 is detection of hydrogen. In this experiment, standard gas of hydrogen was directly introduced into the ionization chamber via a needle valve. The peak at *m/z* 2 derived from hydrogen molecules were clearly detected. The detected peaks around *m/z* 15 were derived from residual gases. This result demonstrated that the detectable mass range in MULTUM-S II was very wide.

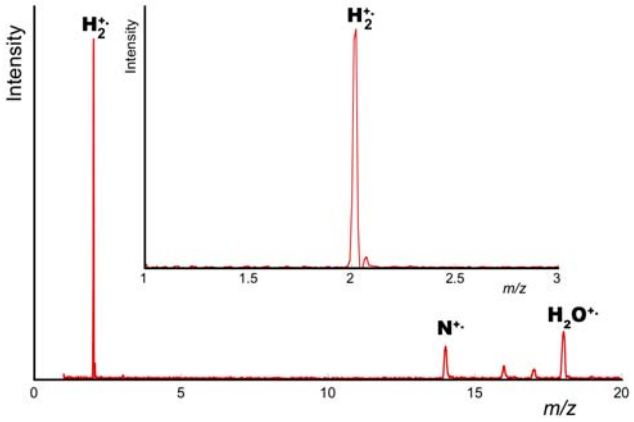

Fig. 4. Detection of molecules in the low mass region. Hydrogen molecule was detected with low electrical noise.

The next result is a separation of helium atom (He) and deuterium molecules (D_2). Since both He and D_2 had the nominal mass of *m/z* 4, He and D_2 were detected as one peak in the low mass resolution mass spectrum (Fig. 5a). To obtain this spectrum, the standard gases of He and D_2 were directly introduced into the ionization chamber via the needle valve. Before the introduction, these two gases were mixed in the gas-sampling bag. Figure 5b is the high mass resolution mass spectrum at 10 cycles. The values of the accurate mass were 4.0026 in He and 4.0282 in D_2. Although the mass difference between He and D_2 was 0.025 u, MULTUM-S II was able to easily separate He and D_2 even in the miniaturized instrument.

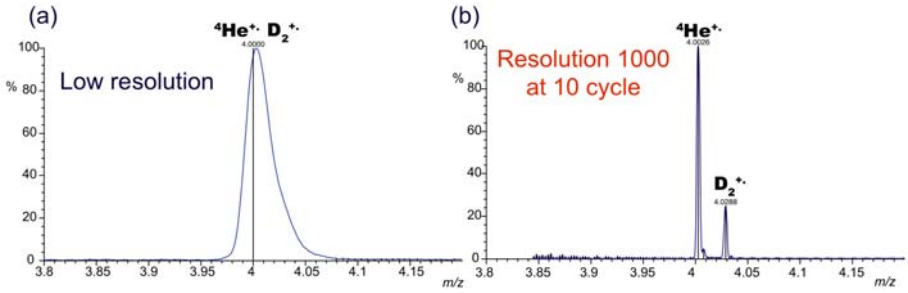

Fig. 5. Separation of ^4He and D_2 doublet; (a) the low mass resolution mass spectrum and (b) high mass resolution mass spectrum. The number of cycles was 10 cycles.

5. Applications for greenhouse gases detection using "MULTUM-S II"

As shown in section 4, MULTUM-S II have a powerful potential especially for the gas detection. The final section describes application of MULTUM-S II for high resolution and simultaneous greenhouse gases detection, especially carbon dioxide (CO_2), nitrous oxide (N_2O) and methane (CH_4). In the conventional methodology in the field study, researchers collect samples in the field, bring them into laboratory, and then analyze using laboratory equipped instruments. As another procedure, researchers prepare and place several detectors to detect each species directly in the field. However, a great variety of detectable species and portability in MULTUM-S II will be the powerful merits for the field study in the future. This high quality gas analyzer will also help the reduction of systematic error attributed to different detectors and measurement conditions.

5.1 High mass resolution mass spectra of greenhouse gases

Figure 6 is a high-mass resolution mass spectrum of CH_4 at 10 cycles. In this spectrum, the peak of CH_4 is separated from the oxygen peak (both nominal mass is *m/z* 16) derived from the fragment ion of the oxygen molecule or di-charged ion of oxygen molecule. The obtained mass resolution was 3200. We consider that this feature is merit for monitoring of CH_4 without oxygen contamination.

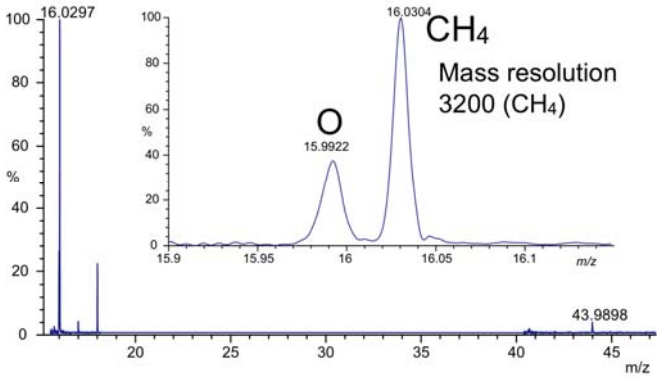

Fig. 6. High-resolution mass spectrum of oxygen and methane.

Real-time monitoring of N_2O is required to elucidate the generating mechanism and investigate its trend of spread. N_2O is known as the greenhouse gas, and the warming effect is about 310 times larger than CO_2. Furthermore, N_2O is one of the ozone-depleting substances (Ravishankara et al., 2009). If we try to carry out real-time monitoring of N_2O and CO_2 simultaneously using mass spectrometry, a mass spectrometer with high mass resolution is required, because the nominal mass of N_2O is the same as that of CO_2. However, the difference of accurate mass between CO_2 and N_2O is 0.0113 u, therefore these two peaks were expected to be separated in MULTUM-S II as shown in Fig. 5 (b) and Fig. 6 . In this experiment, the mixture of ultrapure CO_2 and N_2O (49.4%:50.6%) was purchased from DAIHO SANGYO Inc. (Minato-ku, Tokyo, Japan). This standard gas was introduced into the EI ion source via the needle valve. Figure 7 shows the obtained mass spectra by changing the number of cycles. Figure 7a shows the mass spectrum of the CO_2 and N_2O doublet peak after 10 cycles. In this cycle, the doublet peak did not still separate due to the lack of mass resolution. After 20 cycles (Fig. 7b), the top of the peak began to separate. After 50 cycles (Fig. 7c), these two peaks were

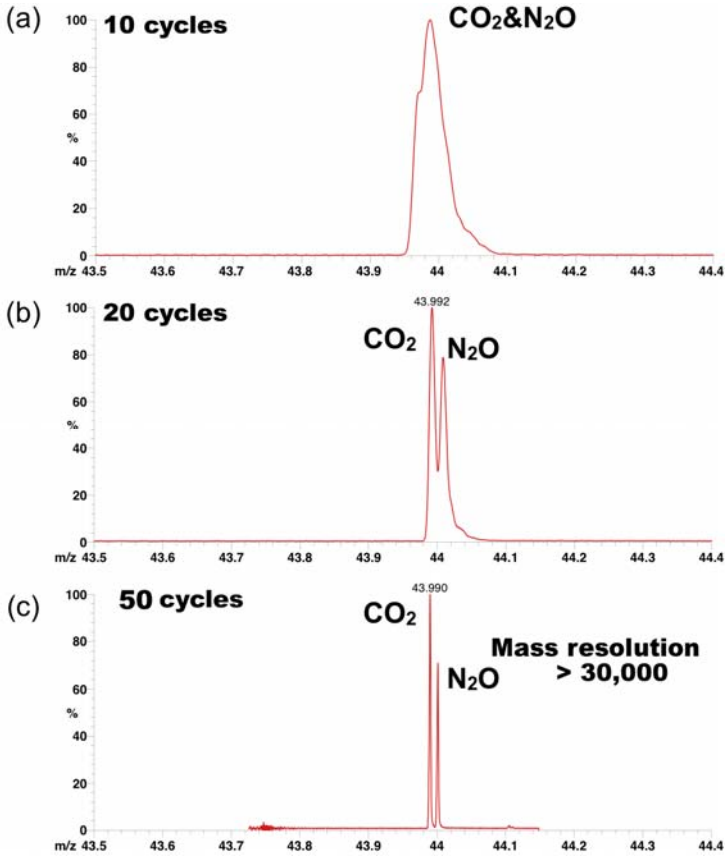

Fig. 7. Separation of CO_2 and N_2O doublet; the spectrum at (a) 10 cycles, (b) 20 cycles and (c) 50 cycles.

completely separated, and consequently, the obtained mass resolution was 30 000. This ultra high mass resolution was firstly achieved in the miniaturized mass spectrometers. This mass resolution was comparable to those of laboratory-equipped instruments. We would like to note that the maximal time to acquire one spectrum was 1 millisecond as described in section 4.2. Therefore, high mass resolution accompanying the fast data acquisition will be helpful for the on-site real-time monitoring.

Achieving high mass resolution is advantageous when trying to determine accurate masses. In the previous study, the mass accuracy of 2.3 ppm was achieved (Shimma et al., 2010). Availability of accurate mass measurement in the miniaturized mass spectrometer is another advantage to MULTUM-S II.

5.2 Direct sample injection method

We could confirm the separation of CO_2 and N_2O doublet using MULTUM-S II. The next experiment was to perform the simultaneous gas detection. In the simultaneous gas detection, there was concern about a dynamic range. To confirm the capability of detection in both low and high concentration species, detection of 30 ppm N_2O in the air was performed. The standard gas of 30 ppm N_2O (N_2 balanced) was purchased from DAIHO SANGYO Inc. In this experiment, the operation mode of multi-segment mode was used. Three segments were configured to detect N_2, O_2, CO_2 and N_2O. The obtained mass spectrum at 50 cycles is shown in Fig. 8.

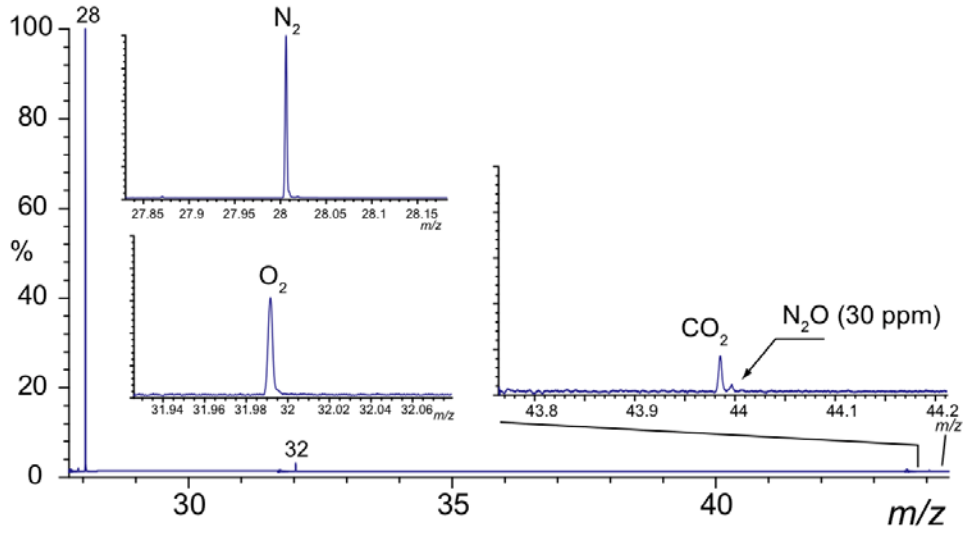

Fig. 8. Simultaneous gas detection of N_2, O_2, CO_2 and N_2O in 50 cycles.

As shown in Fig. 8, the balanced N_2 peak was predominantly detected. The 30 ppm N_2O was detected with complete separation of CO_2, however, the peak intensities of other species were extremely low. Considering the concentration of N_2O in the nature, the concentration is much lower than 30 ppm. Therefore, the dominant species of N_2 and O_2 in the air should be removed to realize the higher sensitive N_2O detection.

5.3 Combination of rough separation and high resolution MS for real-time monitoring

In the conventional gas chromatographic technique, the main contents of air (N_2, O_2, Ar) and (CO_2, N_2O) can be separated using Carbon PLOT column. We firstly performed the gas chromatography of their content using a gas chromatography coupled with MULTUM-S II (Fig. 9a). In this experiment, the GS-CarbonPLOT column (30 m x 0.32 mm i.d.; 3 μm film thickness) was purchased from Agilent Technologies (Santa Clara, CA, USA). The column temperature was kept an isothermal condition of 40°C. The obtained the total ion chromatogram and mass chromatogram of *m/z* 44 are shown in Fig. 9b. In these chromatograms, the non-polar contents of N_2, O_2 and Ar were clearly separated from CO_2 and N_2O. Furthermore, due to the different polarity of CO_2 and N_2O, the enough separation of these peaks was also achieved. However, the duration of analysis was three minutes.

The generation of N_2O via activities of microorganisms is known as a fast process (HAYATSU et al., 2008; Kool et al., 2010). Therefore, higher sampling rate is likely to be required. According to the GC techniques, one of the methodologies to shorten analysis time is truncation of the capillary column. Understandably, the separation capability of the capillary column is reduced.

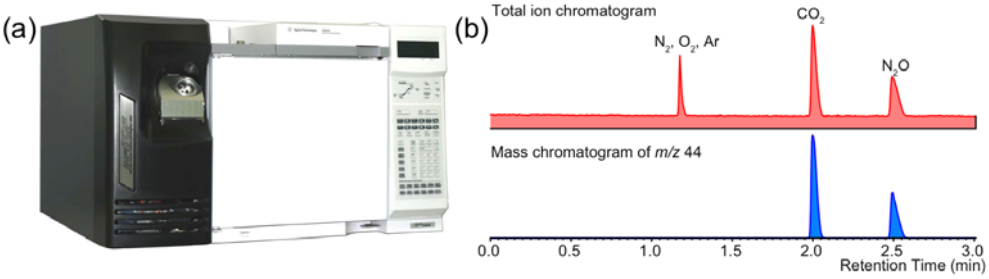

Fig. 9. (a) GC-MULTUM system; (b) the conventional chromatographic separation of (N_2, O_2, Ar) and (CO_2, N_2O)

Here, we consider that higher separation capability for the GC system is unnecessary in this case. As shown in Fig. 7, the complete separation of CO_2 and N_2O can be available in our system. Therefore, we have only to perform the rough GC separation of (N_2, O_2, Ar) and (CO_2, N_2O). To demonstrate this idea, we performed gas chromatography with a 10 m PLOT column.

The obtained chromatograms are shown in Fig. 10. We found that the separation was completed within one minute. In this experiment, the ions of N_2 and O_2 were not detected, because their retention time was too fast. According to the value of the vacuum gauge just after sample injection, the large amount of gases seemed to be injected into the ionization source at a time. Under this condition, electrical discharge could occur. Therefore, we applied the high voltage to the ionization source after five seconds of sample injection.

Due to the short capillary column, the peaks derived from CO_2 and N_2O were not separated in the total ion chromatogram shown in Fig. 10. However, the averaged mass spectra from the retention time 0.3 min to 0.35 min, the high-mass resolution mass

spectrometry was performed (inset of Fig. 10a). The obtained mass chromatograms are also shown in Fig. 10b and Fig. 10c. These results indicate that our idea worked correctly. We could establish the combination of rough gas chromatograph and high mass resolution mass spectrometry.

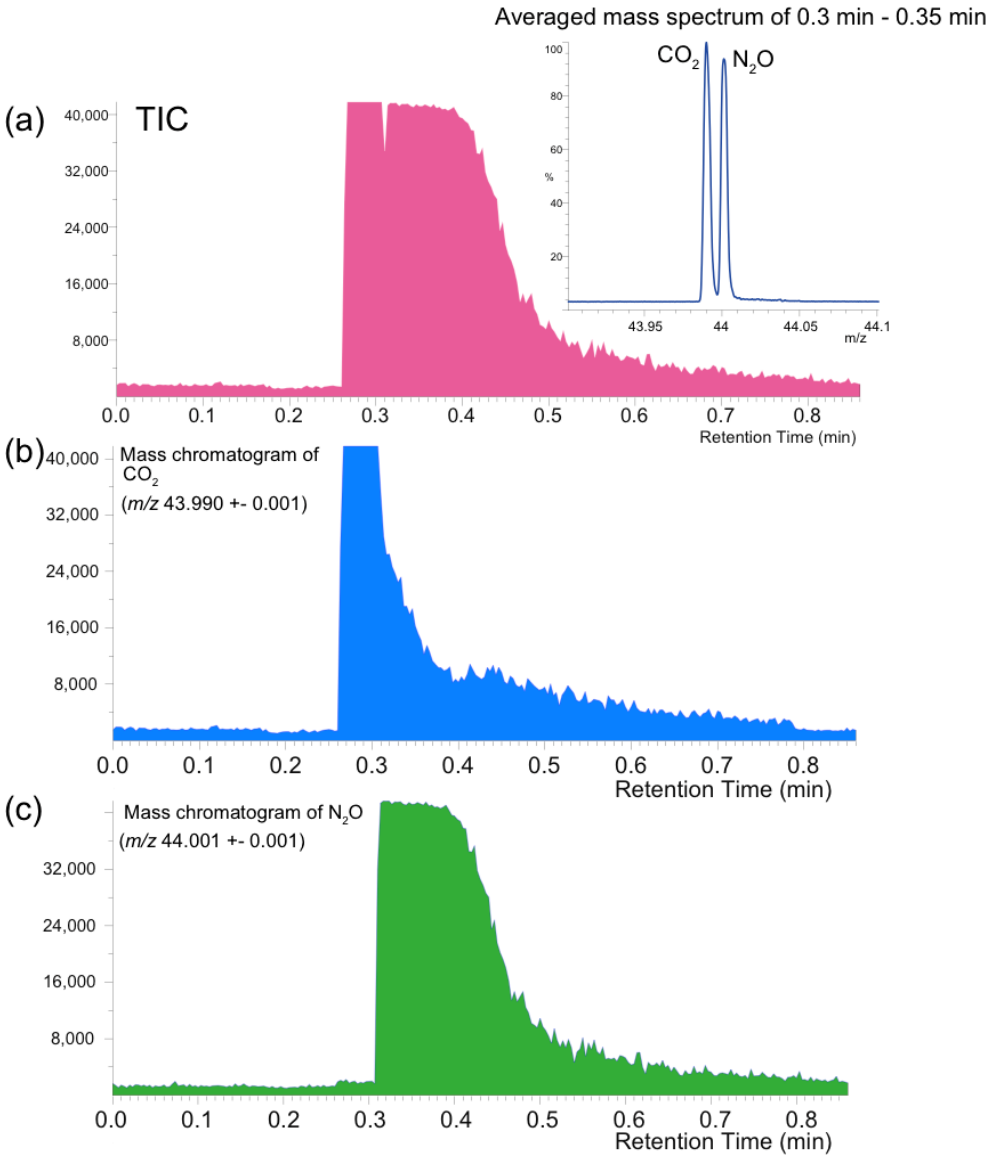

Fig. 10. The rough chromatographic separation of CO_2 and N_2O; (a) total ion chromatogram, (b) the mass chromatogram of CO_2, and (c) the mass chromatogram of N_2O.

5.4 Future tasks for on-site simultaneous greenhouse gas detection

We successfully confirmed the methodology to inject the main components of air and greenhouse gases separately into the ionization source. Considering the field use, to bring GC system to the field is unrealistic for the real-time monitoring. To overcome this problem, we designed and developed a simple automatic gas sampler (Fig. 11). This sampling system is consists of a six port valve, two solenoid valves, a mass flow controller, a sampling loop, a diaphragm pump for the gas sampling, and the short PLOT column. The operation of valves is controlled using a lab-built LabVIEW base software. In our laboratory, the performance evaluation of this sampling system including the optimization of sampling condition is ongoing.

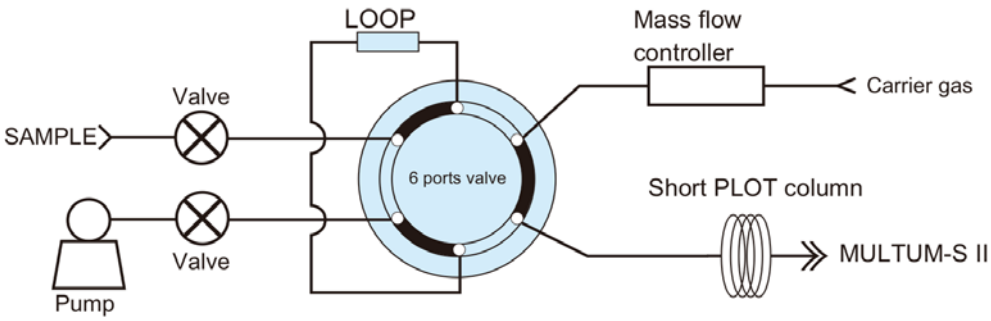

Fig. 11. Proposed automatic gas sampler.

Another task to realize the high sensitive on-site greenhouse gas monitor is reduction of background pressure in the analyzer. The typical pressure value during measurement was between 8 x 10^{-5} Pa and 1 x 10^{-4} Pa. This pressure was insufficient for the sub ppm level N_2O detection. Due to higher background pressure, contamination peaks derived from residual gases in analyzer were detected. Ionization space in the EI source is understandably finite, therefore the total number of ions stored in the ionization source is also finite. This is known as the space charge effect. If the contaminant ions are reduced, the number of ions of interest will be relatively increased. To realize the pressure below 10^{-5} Pa level, we designed a highly sealed ionization chamber specialized for the gas monitoring. The material of the chamber was titanium to reduce outgassing from the inner chamber wall. This chamber will be manufactured in the near future.

6. Conclusion

In this chapter, we described the overview of novel miniaturized mass spectrometers and their applications. Our developed the unique miniaturized TOF mass spectrometer "MULTUM-S II" has comparable mass resolution to lab-equipped mass spectrometers ($m/\Delta m$ > 30 000). At present, we performed proof-of-concept studies for real-time

greenhouse gas monitoring system using MULTUM-S II. Based on issues from this study, MULTUM-S II is under improvement for the high sensitive gas detection.

7. Acknowledgement

The authors thank Prof. Ryusuke Hatano of Hokkaido University for his fruitful discussion. This work was supported by a Supporting Program for Creating University Ventures, from the Japan Science and Technology Agency (JST). One of the authors (M. T.) was supported by Grant in Aid for Young Scientists (A) (21685010) from the Ministry of Education, Culture, Sports, Science and Technology, Japan.

8. References

Amstalden v.H., Smith D.F. & Heeren R.M.A. (2010). A concise review of mass spectrometry imaging. *Journal of Chromatography A,* Vol. 1217, No. 25, pp. 3946-3954, ISSN 0021-9673.

Austin D.E., Peng Y., Hansen B.J., Miller I.W., Rockwood A.L., Hawkins A.R. & Tolley S.E. (2008). Novel ion traps using planar resistive electrodes: Implications for miniaturized mass analyzers. *J. Am. Soc. Mass Spectrom.,* Vol. 19, No. 10, pp. 1435-1441, ISSN 1044-0305.

Austin D.E., Wang M., Tolley S.E., Maas J.D., Hawkins A.R., Rockwood A.L., Tolley H.D., Lee E.D. & Lee M.L. (2007). Halo ion trap mass spectrometer. *Anal. Chem.,* Vol. 79, No. 7, pp. 2927-2932, ISSN 0003-2700.

Berkout V.D., Cotter R.J. & Segers D.P. (2001). Miniaturized EI/Q/oa TOF mass spectrometer. *J. Am. Soc. Mass Spectrom.,* Vol. 12, No. 6, pp. 641-647, ISSN 1044-0305.

Casares A., Kholomeev A. & Wollnik H. (2001). Multipass time-of-flight mass spectrometers with high resolving powers. *Int. J. Mass Spectrom.,* Vol. 206, No. 3, pp. 267-273, ISSN 1387-3806.

Chaudhary A., van Amerom F.H.W. & Short R.T. (2009). Development of microfabricated cylindrical ion trap mass spectrometer arrays. *J. Microelectromech. S.,* Vol. 18, No. 2, pp. 442-448, ISSN 1057-7157.

Contreras J.A., Murray J.A., Tolley S.E., Oliphant J.L., Tolley H.D., Lammert S.A., Lee E.D., Later D.W. & Lee M.L. (2008). Hand-portable gas chromatograph-toroidal ion trap mass spectrometer (GC-TMS) for detection of hazardous compounds. *J. Am. Soc. Mass Spectrom.,* Vol. 19, No. 10, pp. 1425-1434, ISSN 1044-0305.

Cornish T.J. & Cotter R.J. (1997). High-order kinetic energy focusing in an end cap reflectron time-of-flight mass spectrometer. *Anal.Chem.,* Vol. 69, No. 22, pp. 4615-4618, ISSN 0003-2700.

Cotter R.J., Fancher C. & Cornish T.J. (1999). Miniaturized time-of-flight mass spectrometer for peptide and oligonucleotide analysis. *J. Mass Spectrom.,* Vol. 34, No. 12, pp. 1368-1372, ISSN 1076-5174.

Diaz J.A., Giese C.F. & Gentry W.R. (2001a). Portable double-focusing mass-spectrometer system for field gas monitoring. *Field Anal. Chem. Technol.,* Vol. 5, No. 3, pp. 156-167, ISSN 1086-900X.

Diaz J.A., Giese C.F. & Gentry W.R. (2001b). Sub-miniature ExB sector-field mass spectrometer. *J. Am. Soc. Mass Spectrom.,* Vol. 12, No. 6, pp. 619-632, ISSN 1044-0305.

Ecelberger S.A., Cornish T.J., Collins B.F., Lewis D.L. & Bryden W.A. (2004). Suitcase TOF: A man-portable time-of-flight mass spectrometer. *Johns Hopkins APL Tech. Dig.,* Vol. 25, No. 1, pp. 14-19, ISSN 0270-5214.

Fico M., Maas J.D., Smith S.A., Costa A.B., Ouyang Z., Chappell W.J. & Cooks R.G. (2009). Circular arrays of polymer-based miniature rectilinear ion traps. *Analyst,* Vol. 134, No. 7, pp. 1338-1347, ISSN 0003-2654.

Gao L., Li G.T., Nie Z.X., Duncan J., Ouyang Z. & Cooks R.G. (2009). Characterization of a discontinuous atmospheric pressure interface. multiple ion introduction pulses for improved performance. *Int. J. Mass Spectrom.,* Vol. 283, No. 1-3, pp. 30-34, ISSN 1387-3806.

Garcia-Reyes J.F., Jackson A.U., Molina-Diaz A. & Cooks R.G. (2009). Desorption electrospray ionization mass spectrometry for trace analysis of agrochemicals in food. *Anal. Chem.,* Vol. 81, No. 2, pp. 820-829, ISSN 0003-2700.

Geear M., Syms R.R.A., Wright S. & Holmes A.S. (2005). Monolithic MEMS quadrupole mass spectrometers by deep silicon etching. *J. Microelectromech. S.,* Vol. 14, No. 5, pp. 1156-1166, ISSN 1057-7157.

Hadjar O., Johnson G., Laskin J., Kibelka G., Shill S., Kuhn K., Cameron C. & Kassan S. (2011). IonCCD fordirect position-sensitive charged-particle detection: From electrons and keV ions to hyperthermal biomolecular ions. *J. Am. Soc. Mass Spectrom.,* Vol. 22, No. 4, pp. 612-623, ISSN 1044-0305.

Hayatsu M., Tago K. & Saito M. (2008). Various players in the nitrogen cycle: Diversity and functions of the microorganisms involved in nitrification and denitrification. *Soil Science & Plant Nutrition,* Vol. 54, No. 1, pp. 33-45, ISSN 1747-0765.

Hazama H., Aoki J., Nagao H., Suzuki R., Tashima T., Fujii K., Masuda K., Awazu K., Toyoda M. & Naito Y. (2008a). Construction of a novel stigmatic MALDI imaging mass spectrometer. *Appl. Surf. Sci.,* Vol. 255, No. 4, pp. 1257-1263, ISSN 0169-4332.

Hazama H., Nagao H., Suzuki R., Toyoda M., Masuda K., Naito Y. & Awazu K. (2008b). Comparison of mass spectra of peptides in different matrices using matrix-assisted laser desorption/ionization and a multi-turn time-of-flight mass spectrometer, MULTUM-IMG. *Rapid Commun. Mass Spectrom.,* Vol. 22, No. 10, pp. 1461-1466, ISSN 0951-4198.

Hu Q.Z., Noll R.J., Li H.Y., Makarov A., Hardman M. & Cooks R.G. (2005). The orbitrap: A new mass spectrometer *J. Mass Spectrom.,* Vol. 40, No. 4, pp. 430-443, ISSN 1076-5174.

Ishihara M., Toyoda M. & Matsuo T. (2000). Perfect space and time focusing ion optics for multiturn time of flight mass spectrometers. *Int. J. Mass Spectrom.,* Vol. 197, No. 1-3, pp. 179-189, ISSN 1387-3806.

Kool D.M., Wrage N., Zechmeister-Boltenstern S., Pfeffer M., Brus D., Oenema O. & Van Groenigen J.-. (2010). Nitrifier denitrification can be a source of N2O from soil: A revised approach to the dual-isotope labelling method. *Eur. J. Soil Sci.,* Vol. 61, No. 5, pp. 759-772, ISSN 1365-2389.

Lammert S., Rockwood A., Wang M., Lee M., Lee E., Tolley S., Oliphant J., Jones J. & Waite R. (2006). Miniature toroidal radio frequency ion trap mass analyzer. *J. Am. Soc. Mass Spectrom.,* Vol. 17, No. 7, pp. 916-922, ISSN 1044-0305.

Li A., Wang H., Ouyang Z. & Cooks R.G. (2011). Paper spray ionization of polar analytes using non-polar solvents. *Chem. Commun.,* Vol. 47, No. 10, pp. 2811-2813, ISSN 1359-7345.

Li X.X., Jiang G.Y., Luo C., Xu F.X., Wang Y.Y., Ding L. & Ding C.F. (2009). Ion trap array mass analyzer: Structure and performance. *Anal. Chem.,* Vol. 81, No. 12, pp. 4840-4846, ISSN 0003-2700.

Liang G., Sugiarto A., Harper J.D., Cooks R.G. & Zheng O.Y. (2008). Design and characterization of a multisource hand-held tandem mass spectrometer. *Anal. Chem.,* Vol. 80, No. 19, pp. 7198-7205, ISSN 0003-2700.

Marshall A.G., Hendrickson C.L. & Jackson G.S. (1998). Fourier transform ion cyclotron resonance mass spectrometry: A primer. *Mass Spectrom.Rev.,* Vol. 17, No. 1, pp. 1-35, ISSN 0277-7037.

Matsuda H. (2000). Spiral orbit time of flight mass spectrometer. *J. Mass Spectrom. Soc. Jpn,* Vol. 48, No. 5, pp. 303-305, ISSN 1340-8097.

Matsuo T., Ishihara M., Toyoda M., Ito H., Yamaguchi S., Roll R. & Rosenbauer H. (1999). A space time-of-flight mass spectrometer for exobiologically-oriented applications. *Adv. Space Res.,* Vol. 23, No. 2, pp. 341-348, ISSN 0273-1177.

Okumura D., Toyoda M., Ishihara M. & Katakuse I. (2004a). Application of a multi-turn time-of-flight mass spectrometer, MULTUM II, to organic compounds ionized by matrix-assisted laser desorption/ionization. *J. Mass Spectrom.,* Vol. 39, No. 1, pp. 86-90, ISSN 1076-5174.

Okumura D., Toyoda M., Ishihara M. & Katakuse I. (2004b). A compact sector-type multi-turn time-of-flight mass spectrometer 'MULTUM II'. *Nucl. Instr. Meth. A,* Vol. 519, No. 1-2, pp. 331-337, ISSN 0168-9002.

Ouyang Z., Noll R.J. & Cooks R.G. (2009). Handheld miniature ion trap mass spectrometers. *Anal. Chem.,* Vol. 81, No. 7, pp. 2421-2425, ISSN 0003-2700.

Poschenrieder W.P. (1972). Multiple-focusing time-of-flight mass spectrometers part II. TOFMS with equal energy acceleration. *Int. J. Mass Spectom. Ion Phys.,* Vol. 9, No. 4, pp. 357-373, ISSN 0020-7381.

Ravishankara A.R., Daniel J.S. & Portmann R.W. (2009). Nitrous oxide (N2O): The dominant ozone-depleting substance emitted in the 21st century. *Science,* Vol. 326, No. 5949, pp. 123-125, ISSN 0036-8075.

Sakurai T., Nakabushi H., Hiasa T. & Okanishi K. (1999). A new multi-passage time-of-flight mass spectrometer at JAIST. *Nucl. Instr. Meth. A,* Vol. 427, No. 1,2, pp. 182-186, ISSN 0168-9002.

Satoh T., Sato T. & Tamura J. (2007). Development of a high-performance MALDI-TOF mass spectrometer utilizing a spiral ion trajectory. *J. Am. Soc. Mass Spectrom.,* Vol. 18, No. 7, pp. 1318-1323, ISSN 1044-0305.

Satoh T., Tsuno H., Iwanaga M. & Kammei Y. (2005). The design and characteristic features of a new time-of-flight mass spectrometer with a spiral ion trajectory. *J. Am. Soc. Mass Spectrom.,* Vol. 16, No. 12, pp. 1969-1975, ISSN 1044-0305.

Satoh T., Sato T., Kubo A. & Tamura J. (2011). Tandem time-of-flight mass spectrometer with high precursor ion selectivity employing spiral ion trajectory and improved offset parabolic reflectron. *J. Am. Soc. Mass Spectrom.,* Vol. 22, No. 5, pp. 797-803, ISSN 1044-0305.

Shimma S., Nagao H., Aoki J., Takahashi K., Miki S. & Toyoda M. (2010). Miniaturized high-resolution time-of-flight mass spectrometer MULTUM-S II with an infinite flight path. *Anal. Chem.,* Vol. 82, No. 20, pp. 8456-8463, ISSN 0003-2700.

Smith J.N., Noll R.J. & Cooks R.G. (2011). Facility monitoring of chemical warfare agent simulants in air using an automated, field-deployable, miniature mass spectrometer. *Rapid Commun. Mass Spectrom.,* Vol. 25, No. 10, pp. 1437-1444, ISSN 1097-0231.

Soparawalla S., Tadjimukhamedov F.K., Wiley J.S., Ouyang Z. & Cooks R.G. (2011). In situ analysis of agrochemical residues on fruit using ambient ionization on a handheld mass spectrometer. *Analyst,* ISSN 0003-2654.

Toyoda M., Giannakopulos A.E., Colburn A.W. & Derrick P.J. (2007). High-energy collision induced dissociation fragmentation pathways of peptides, probed using a multuitum tandem time-of-flight mass spectrometer "MULUM-TOF/FOF". *Rev. Sci. Instrum.,* Vol. 78, pp. 074101,.

Toyoda M., Ishihara M., Yamaguchi S., Ito H., Matsuo T., Roll R. & Rosenbauer H. (2000). Construction of a new multi-turn time-of-flight mass spectrometer. *J. Mass Spectrom.,* Vol. 35, No. 2, pp. 163-167, ISSN 1076-5174.

Toyoda M., Okumura D., Ishihara M. & Katakuse I. (2003). Multi-turn time-of-flight mass spectrometers with electrostatic sectors. *J. Mass Spectrom.,* Vol. 38, No. 11, pp. 1125-1142, ISSN 1076-5174.

Van Amerom F.H.W., Chaudhary A., Cardenas M., Bumgarner J. & Short R.T. (2008). Microfabrication of cylindrical ion trap mass spectrometer arrays for handheld chemical analyzers. *Chem. Eng. Commun.,* Vol. 195, No. 2, pp. 98-114, ISSN 0098-6445.

Wells J.M., Roth M.J., Keil A.D., Grossenbacher J.W., Justes D.R., Patterson G.E. & Barket D.J. (2008). Implementation of DART and DESI ionization on a fieldable mass spectrometer. *J. Am. Soc. Mass Spectrom.,* Vol. 19, No. 10, pp. 1419-1424, ISSN 1044-0305.

Wiley W.C. & McLaren I.H. (1955). Time-of-flight mass spectrometer with improved resolution. *Rev. Sci. Instrum.,* Vol. 26, No. 12, pp. 1150-1157,.

Wollnik H. & Casares A. (2003). An energy-isochronous multi-pass time-of-flight mass spectrometer consisting of two coaxial electrostatic mirrors. *Int. J. Mass Spectrom.,* Vol. 227, No. 2, pp. 217-222, ISSN 1387-3806.

Wollnik H. & Przewloka M. (1990). Time-of-flight mass spectrometers with multiply reflected ion trajectories. *Int. J. Mass Spectrom. Ion Proc.,* Vol. 96, No. 3, pp. 267-274, ISSN 0168-1176.

Yang M., Kim T.Y., Hwang H.C., Yi S.K. & Kim D.H. (2008). Development of a palm portable mass spectrometer. *J. Am. Soc. Mass Spectrom.,* Vol. 19, No. 10, pp. 1442-1448, ISSN 1044-0305.

Yavor M.I., Verentchikov A.N., Hasin J., Kozlov B., Gavrik M. & Trufanov A. (2008). Planar multi-reflecting time-of-flight mass analyzer with a jig-saw ion path. *Physics Procedia,* Vol. 1, No. 1, pp. 391-400, ISSN 1875-3892.

12

CO_2 and CH_4 Flux Measurements from Landfills – A Case Study: Gualeguaychú Municipal Landfill, Entre Ríos Province, Argentina

Romina Sanci and Héctor O. Panarello
Instituto de Geocronología y Geología Isotópica (UBA-CONICET)
Argentina

1. Introduction

Municipal solid waste (MSW) landfills are used to dispose of household wastes: food and garden waste, paper, metal, glass, wood, textiles, rubber, leather, plastic, ash, dust and electronic waste (Meju 2000). Decomposition of landfilled MSW by long-term physicochemical, chemical and biological processes causes dissolution or decay of landfill materials and production of leachate and gases (Bjerg et al. 2005). In particular, bacterial decomposition of the biodegradable fraction of MSW generates mainly methane (CH_4) and carbon dioxide (CO_2) as well as a wide variety of minor and trace components: hydrogen, water vapor, hydrogen sulfide, ammonia, and volatile organic compounds (Scottish Environment Protection Agency [SEPA], 2004). In spite of efforts being made to control landfill gases (LG) - gas containment, collection and utilisation, flaring and treatment- , these are usually released into the atmosphere directly and indirectly, from the ground or via sub-surface gas migration, respectively.

These LG emissions into the atmosphere represent potential hazards that are of concern locally, regionally and globally (UK Environment Agency, 2010). The trace components of LG pose an odour and toxicity risk (although CO_2 is also toxic if it is present in high enough concentrations). Explosion and asphyxia risk is related to sub-surface migration and accumulations in enclosed spaces. Root zone displacement of oxygen by landfill gas is the most likely cause of local ecotoxicity. In addition, volatile organic compounds (VOC) have detrimental effects on human health and they participate in photochemical pollution as precursors of tropospheric ozone. CO_2 and CH_4 are greenhouse gases and contribute to global warming. Landfills have been implicated as being the largest anthropogenic sources of atmospheric CH_4 in the world, comprising about 11% of the total anthropogenic global CH_4 contribution (Spokas et al., 2003).

Direct measurements of CH_4 and CO_2 emissions from ground to atmosphere are used as an effective tool to estimate the degassing rate of individual sources and to calibrate global Earth degassing estimates (Cardellini et al. 2003). Early studies of diffuse degassing, focus on the flow of CO_2 out of the soil, commonly called CO_2 ''flux'' or ''efflux'' and expressed as [mass] [area] $^{-1}$ [time] $^{-1}$, they were developed in agricultural or ecological areas to measure soil respiration or the flux from soil of other gaseous species (Hanson et al. 1993; Kinzig and

Socolow, 1994; Norman et al. 1992; Parkinson 1981). Later, they were applied in active volcanic-geothermal environments where CO_2 is derived from some geologic source at depth (Bergfeld et al. 2001; Chiodini et al. 1999, 2004; Gerlach et al. 2001) and also in landfills (Borjesson et al., 2000; Georgaki et al. 2008; Hedge et al., 2003; Jha et al., 2008; Mosher et al., 1999; Pier & Kelly, 1997).

In this chapter, we summarize all the steps involved in the process of the quantifying of CO_2 and CH_4 fluxes (background, measurement methods calibration, geostatistical treatment of results, presentation of data) from landfills, and its application in Gualeguaychú Municipal Landfill, Entre Ríos province, Argentina. The method of determining the biodegradation processes of solid wastes by extracting gases with a probe and analyzing carbon isotopes on those gases is also included in the text. In addition, the dissolution of these gases in shallow aquifers is evaluated since in the case study that we present the groundwater acts as a sink for the CO_2 that is developing in the landfill.

2. Gases production during waste decomposition

The composition of LG will vary from one site to another, from one cell of a landfill to another, and will change over time. Because of this, it is possible to find varying amounts CO_2, CH_4 and trace components, plus nitrogen and oxygen derived from air that has been drawn into the landfill. LG production is a function of the composition (organic content), density of and moisture content of wastes, climate variables, particle size and thickness of landfill cover, air-filled porosity, pH, temperature, nutrient availability, methods of land filling (i.e. open dumping or sanitary landfill) and structural features of the site (Barlaz et al. 2004; Kumar et al. 2004).

In addition, LG composition depends on the predominant form of microbial activity (e.g. aerobic/anaerobic) within the landfill environment. Assuming that an anaerobic environment is achieved and maintained after waste placement, a pattern of five sequential stages for LG production or biodegradation stages (Figure 1) is proposed: aerobic, non-methanogenic anaerobic, unsteady methanogenic anaerobic, steady methanogenic anaerobic and mature phases (Farquar and Rovers 1973; (Scottish Environment Protection Agency [SEPA], 2004). During the initial stage of organic degradation within a landfill, CO_2 is produced in molar equivalents to free O_2 consumed. Once O_2 concentration is low enough, anaerobic oxidation, hydrolysis and acidification reactions begin and CO_2 concentration (up to 70%), hydrogen and organic acids such as acetic reach their peak. As anaerobic degradation continues, the concentrations of acetic and other organic acids decreases, associated with an increase in CH_4 generation (methanogenesis). CO_2 concentration declines and methanogenesis begins to prevail, establishing a phase of steady CH_4 production: 50–70% CH_4 (with 30 to 50% CO_2). During the last stage (mature), there is not enough organic substrate required for microbial activity and the composition of interstitial gases becomes more similar to atmospheric air.

3. Landfill gases measurements

3.1 Accumulation chamber methods

To assess the impacts of anomalous emissions to the atmosphere, different accumulation chamber methods to measure CO_2 and CH_4 fluxes from individual sources have been used over recent years. Norman et al. (1997) described these methods as closed static chambers

(non-steady-state non-flow-through chamber), closed dynamic chambers (non-steady-state chamber flow-through) and open dynamic chambers (steady-state flow-through chamber).

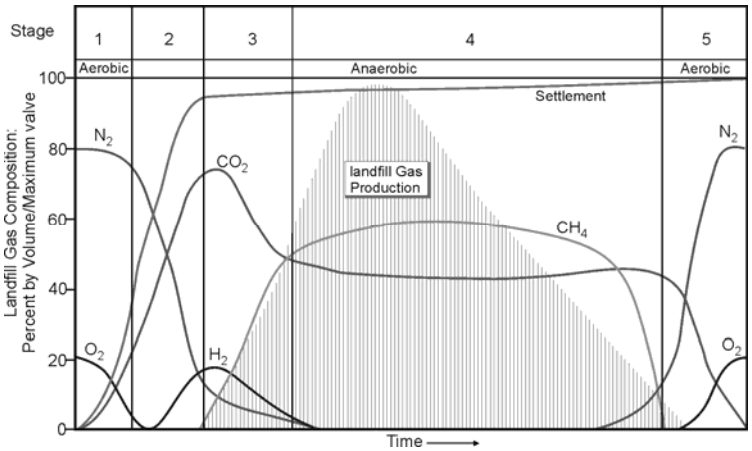

Fig. 1. Biodegradation stages during solid waste decomposition (Scottish Environment Protection Agency [SEPA], 2004): 1. aerobic, 2. non-methanogenic anaerobic, 3. unsteady methanogenic anaerobic, 4. steady methanogenic anaerobic, 5. mature.

In closed chamber methods (static and dynamic), the CO_2 flux is determinated from the rate of concentration increase in a isolated chamber, that has been placed on the soil surface for a known period of time. In static chambers, samples are taken using disposable syringes wich are transported and analized in laboratory. In dynamic chambers, the gas is extracted from the chamber, sent to an external infrared gas analyzer (IRGA), and then injected again into the chamber (Figure 2). In open chamber systems, described by Iritz et al. (1997), Moren and Lindroth (2000) and Rayment and Jarvis (1997), CO_2 flux is calculated from the difference between CO_2 concentration at the inlet and the outlet of the chamber.

None of these methods have yet been recognized as standard because experimental work has indicated differences in estimating fluxes among chamber types (Jensen et al. 1996) and has demonstrated limitations related with the chamber design (Hutchison and Mosier 1981; Welles et al. 2001). Consequently, some researchers have begun to carry out studies to determine the accuracy of measurements in comparison with a true flux through calibration systems to calculate the actual CO_2 flux and thus to estimate the real contribution to the global carbon cycle (Butnor and Johnsen 2004; Martin et al. 2004; Nay et al. 1994; Widen and Lindroth 2003). Likewise, Pumpanen et al. (2004) have determined correction factors for different chambers and specific soil types. The accumulation chamber method has also been tested under controlled laboratory conditions (Chiodini et al. 1998; Evans et al. 2001).

3.2 Other techniques to measure landfill gases

To characterize the biodegradation stages during waste decomposition, soil gas probes at different depths, made of stainless steel, are used to measure soil CO_2, CH_4, N_2 and O_2 levels. Soil gases are brought to the vicinity of the tip of the probe by applying a vacuum and collected in TedlarTM bags (Figure 3). Samples are analysed in the laboratory by gas

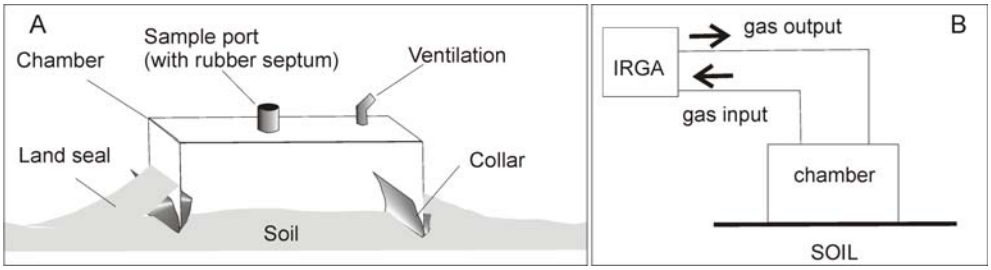

Fig. 2. Sketch of the instrument used to measure fluxes. A. Taken and modified from Kinzig and Socolow (1994). B. Taken and modified from Chiodini *et al.* (1998)

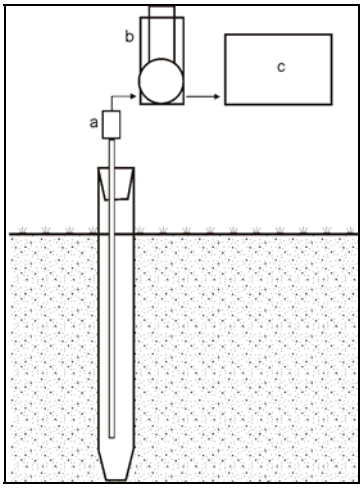

Fig. 3. Diagram of soil probe. A: filter, B: vacuum pump; C: Tedlar bags

chromatography. In addition, the determination of stable isotopes of carbon in CH_4 and CO_2 is an effective way to identify the different phases of biodegradation in a landfill (Coleman et al. 1993; Hackley et al. 1996). According to these authors, CO_2 is isotopically light during the initial aerobic and anaerobic oxidation phases of biodegradation with $\delta^{13}C$ values that range from -35 to -10‰, which covers the range of most terrestrial plants. The initial input of isotopically light CO_2 associated with the earlier biodegradation phases is soon overcome during the methanogenesis phase by the constant input of isotopically heavy CO_2 associated with acetate fermentation and microbial CO_2 reduction (the two primary metabolic pathways by which microbial CH_4 is produced). During methanogenesis, CH_4 is enriched in the lighter carbon isotope (^{12}C) and the CO_2 associated with microbial CH_4 production is enriched in the heavier isotope (^{13}C). Thus, in a semiclosed environment such as a landfill, the $\delta^{13}C$ of CO_2 is strongly affected by methanogenesis reactions with reported values between -10 and +20‰.

4. Data analysis

Flux measurements are distributed over regular grids, following Wang and Qi's (1998) statement that although three sampling patterns (regular grid, simple random and cellular

stratified sampling) are widely used in environmental studies, for a given sampling density, the regular grid provides better estimations than the other two. Histograms are plotted for the fluxes measured in the field and are log-transformed (ln) and fitted on a cumulative probability curve to verify the lognormal distribution and to identify different flux populations through changes in graph slope (Bergfeld et al. 2001; Cardellini et al. 2003; Chiodini and Frondini 2001; Gerlach et al. 2001).

Since geospatial techniques are advisable to estimate the whole landfill surface flux from the spatially distributed chamber sites (Spokas et al. 2003), variograms are used to determine the level of spatial dependence of different sites. In experimental variograms (omnidirectional and directional) the semivariance $\gamma(h)$ is plotted against the lag(h)—i.e. distance between sample sites (Webster & Oliver 1992). Since variograms may take several forms, different theoretical models are fitted to the data using the VARIOWIN software (Eddy & Paninatier 1996). Kriging is applied to generate contour maps, using the parameters of the variogram model that have been derived from the experimental variogram. Kriging is an interpolation method that takes advantage of the spatial dependence of a given variable. A number of papers compare spatial interpolation methods under different conditions, and kriging has proven to give the best estimations in numerous cases (Börjesson et al. 2000; Spokas et al. 2003).

5. Landfill gases effects on groundwater

LG contain a range of components that can dissolve in aqueous media, e.g. CO_2, CH_4 and some traces. In landfills, CO_2 is the most water-soluble constituent of LG. The dissolution of this gas is partially responsible for observed variations in LG emissions to the atmosphere. CO_2 can dissolve in groundwater as described by Henry's law and react with water to form a balance of several ionic and nonionic species, collectively known as dissolved inorganic carbon –DIC- (Stumm & Morgan 1996). These species are free carbon dioxide ($CO_2(aq)$), carbonic acid (H_2CO_3), bicarbonate (HCO_3^-) and carbonate (CO_3^{2-}). The balance of these species, which ultimately affects CO_2 solubility, depends on the pH, amongst other things. CO_2 interacts with water as follows:

$$CO_2\,(aq) + H_2O \leftrightarrow H_2CO_3 \leftrightarrow HCO_3^- + H^+ \leftrightarrow CO_3^{2-} + 2H^+ \quad (1)$$

Moreover, adding CO_2 to groundwater changes the pH in the absence of interaction with aquifer solids. Kerfoot et al. (2004) calculated that landfill CO_2 may cause pH to drop to 4.7 in the absence of buffering reactions. However, carbonic acid can react with carbonate minerals (such as calcite) in the aquifer to buffer pH changes, according to the following reaction:

$$H_2CO_3\,(aq) + CaCO_3\,(s) \leftrightarrow Ca^{2+}\,(aq) + 2HCO_3^-(aq) \quad (2)$$

Although a rise in alkalinity suggests that groundwater is affected by the CO_2 generated in the landfill, it should be noted, that it might also be caused by leachates. Large amounts of CO_2 are produced in the landfill beneath the water table by organic matter decay into groundwater. Some of the CO_2 is retained as bicarbonate, part of it may be converted to CH_4 by microbes and the rest is released by outgassing (Baedecker and Back 1979).

CH_4 in water has the potential to act as a reducing agent, chemically reducing species and thereby potentially dissolving metal ions from aquifer solids (Kerfoot et al., 2004). An

example is the reaction with pyrolusite to produce soluble manganese (II) from insoluble insoluble manganse (IV):

$$4MnO_2\,(s) + CH_4 + 8H^+ \leftrightarrow 4Mn_2^+ + CO_2 + 6H_2O \quad (3)$$

In addition, carbon isotope analysis of DIC in groundwater is a useful tool to determine the sources of CO_2 (soil gas, dissolution of calcareous material, CO_2 produced by solid waste organic decomposition). Values of δ^{13}C-DIC between -15‰ and -12‰ can be explained by isotope fractionation from the fixation of CO_2 from soil respiration in the form of HCO_3^- within a process of calcite dissolution (Mook, 2000). In agreement with the explanation in section 3.2, δ^{13}C-DIC values richer than -12‰ can be explained by the input of enriched CO_2 from solid waste degradation which dissolves calcite (Kerfoot et al., 2003).

6. Isotopic analysis

As has been previously stated, the determination of stable isotopes of carbon in gases and groundwater is an effective way to identify solid waste biodegradation processes in a landfill. Samples of soil gas and groundwater are analyzed to determine the $^{13}C/^{12}C$ ratio on $BaCO_3$ obtained from precipitating CO_2 and HCO_3^- with alkaline $BaCl_2$. In our laboratory experiments, the resulting $BaCO_3$ is collected on an acid-washed glass fibre filter (GF/F) under a nitrogen atmosphere, rinsed with distilled water and dried to 60ºC. Then, samples are reacted with H_3PO_4 (100%) in vacuo, according to MacCrea (1950). The resulting CO_2 is cryogenically purified; transferred with liquid N_2 to a glass vial and measured against a working standard (CO_2 from Carrara marble) in a dual inlet, triple collector mass spectrometer, Finnigan MAT Delta S. Carbon isotope composition is expressed as δ^{13}C, according to:

$$\delta^{13}C = 1000 \left(\frac{\left[{}^{13}C / {}^{12}C\right]_S - \left[{}^{13}C / {}^{12}C\right]_R}{\left[{}^{13}C / {}^{12}C\right]_R} \right) ‰ \quad (4)$$

where $^{13}C/^{12}C$ is the carbon isotope ratio, suffix S corresponds to the sample and suffix R to the reference standard, Pee Dee belemnitella (PDB), redefined in function of the NBS 19, TS-Limestone standard as V-PDB (Gonfiantini et al. 1995). Analytical uncertainty (2σ) was ±0.2%.

7. Case Study: Gualeguaychú Municipal Landfill, Entre Ríos Province, Argentina

7.1 Site description

The Gualeguaychú municipal landfill is located 3 km south of that city, in the southeast of the province of Entre Rios, Argentina (Figure 4). The municipal facility was first exploited for mineral extraction, and waste was later disposed of in the depressions. One part of this facility was used for final disposal of MSW and closed in 2000 when it had filled up. Gas emissions were sampled there. There is no information regarding any environmental protection actions undertaken during the operation of the site, but visual observation of the site revealed that the topsoil cover is permeable and not compacted. So far, according to

geophysical studies (Pomposiello et al. 2009; Prezzi et al. 2005) in the filled-up disposal area, are of household origin and the filling depth does not exceed 2 m. Another part of the facility is currently being landfilled. There are no gas vents or recovery systems.

The Gualeguaychu municipal solid waste final disposal site (MSWDS) is located in the lower section of the Gualeguaychu River basin, which has a subhumid–humid climate (Sanci et al., 2009a). The Punta Gorda Group underlying the MSFDSW is the unit outcropping in the study area (Iriondo, 1980). Most of the sedimentary cover in the province of Entre Rios belongs to this group, which is composed mainly of brown, yellow and greenish silts (loess), clays and calcareous levels called ''tosca'', composed of calcite. It was formed in lacustrine and aeolian environments and was assigned to Middle–Upper Pleistocene age (Iriondo, 1996). In addition, this group is intercalated by fluvial facies and silty levels, with abundant marine fossils from the marine ingression in the upper Pleistocene (Pereyra et al. 2002). The Punta Gorda Group contains a low-productivity phreatic aquifer, whose water is used for livestock farming and agriculture. This unit acts like a semi-confining layer for the underlying aquifer (Salto Chico) that is highly productive and has high quality of water, used for human consumption and irrigation.

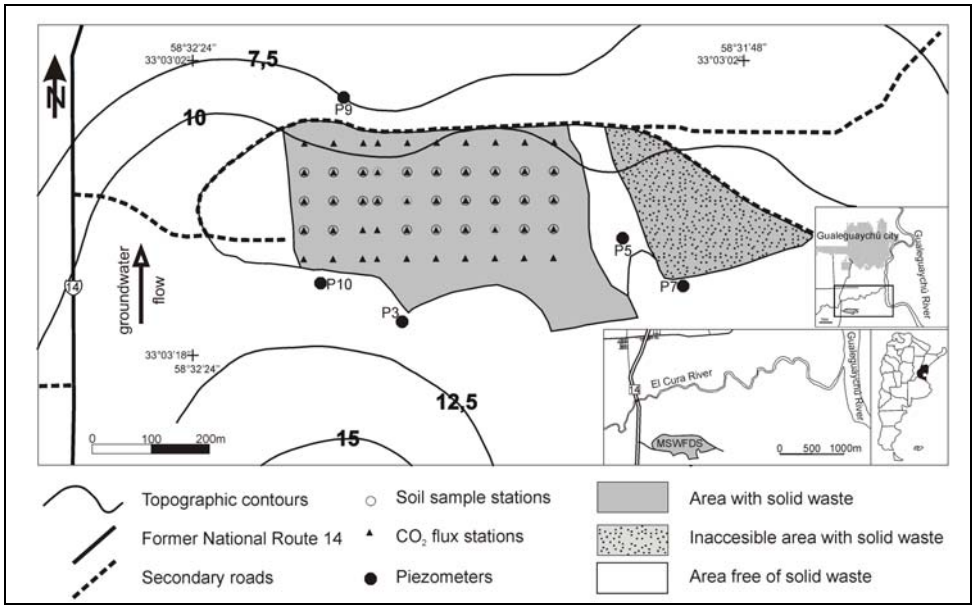

Fig. 4. Localization and description of MWSFDS

7.2 Measurement methods calibration

The accumulation chamber (0.26-m high and 0.30-m diameter) was placed on a collar that had been previously installed on the ground. The chamber also had outlet and inlet manifolds connected to the external pump in order to mix and distribute the air inside. A flow-meter was intercalated in order to regulate the mixing rate. There was also a port to test the temperature within the chamber. A pressure-relief vent was connected at the top of the chamber to

maintain the outside-inside pressure equilibrium. Flux rates were calculated by fitting linear regression to the variation of concentration (C) vs. time and adjusting for chamber volume (0.018 m^3) and covered area (0.070 m^2), according to the following equation:

$$F = \left(\frac{V}{A}\right)\left(\frac{dC}{dt}\right) \quad (5)$$

where F is the surface emission rate (g m^{-2} day^{-1}), V is the chamber volume and A is the soil area under the chamber and dC/dt is the variation of C with t within the chamber.

The dynamic and static closed chamber methods were applied during fieldwork, after calibration in the laboratory (Sanci et al. 2009b). This calibration consisted of a system where known CO_2 concentrations flowed through different porous materials, simulating CO_2 diffusion through the soil. This system allowed the determination of the differences between reference CO_2 flux values and experimental measurements under different sampling conditions. In the closed dynamic chamber method, soil gases are pumped for analysis from the accumulation chamber to a portable IRGA (PP Systems EGM-4) and subsequently returned to the chamber. The best fit (deviation smaller than 10%) was obtained taking short readings every 3 min during 12 min and mixing 25 s prior to CO_2 extraction (R^2 = 0.99). The best mixing rate was 250 ml min^{-1}. The portable IRGA has an internal pump and a scale of (0–20,000) μmol mol^{-1}. It allows the determining of CO_2 concentrations within an analytical uncertainty of ±1% of the reading. In the closed static chamber method, soil gases are extracted with syringes and analysed by gas chromatography (GC-TCD HP 5890 Series II). Although both methods allow measuring CO_2 fluxes directly, the static method allows the detection of another greenhouse gas, CH_4, which proved to be useful in the exploratory surveys. The best fit (deviation <10%) was obtained taking three samples every 10 min during 20 min (R^2 = 0.99) and mixing 35 s prior to CO_2 sampling. The best mixing rate was 250 mL min^{-1}.

7.3 Gas samples

The surveyed area covers about 150,000 m^2. Measurements were distributed over regular grids: spacing was 100 m in the exploratory survey (March 2007, 14 sites), in the detailed surveys spacing was 50 m (50 sites) and 25 m (107 sites) respectively. Detailed surveys were carried out in July and October 2007. No measurements were made in the inaccessible part of the MSWFDS (Figure 4). Fieldwork was undertaken in dry and stable periods to avoid the influence of rainfall, soil humidity and atmospheric pressure on surface emissions. During the exploratory survey, CH_4 and CO_2 fluxes were measured with the static chamber method, whereas the dynamic chamber method was used during the detailed surveys for CO_2 flux measurements. Sampling density was increased taking into consideration the original location of the sites of the exploratory fieldwork.

In the exploratory survey, CO_2 fluxes ranged from 25 g m^{-2} day^{-1} to 194 g m^{-2} day^{-1}. CH_4 fluxes were not detected. In the detailed fieldwork, CO_2 fluxes in 50 and 107 stations ranged from 5 g m^{-2} day^{-1} to 214 g m^{-2} day^{-1} and from 31 g $m^{-2}day^{-1}$ to 331 g m^{-2} day^{-1}, respectively. Irregularly spaced stations upstream of the MSWFDS were added to the study in October to measure the background values of soil respiration, which ranged from 29 g m^{-2} day^{-1} to 59 g m^{-2} day^{-1}. At all surveyed sites, soil temperature ranged from 21°C to 30°C (March), 12°C to 17°C (July) and 20°C to 30°C (October).

CO_2 flux data sets of the three campaigns are plotted in histograms (Figure 5). Distribution of measured CO_2 fluxes in the longest data set (107 sites) is log-normal, as can be seen in the linear cumulative probability plot of ln(CO_2) flux of Figure 6a. Changes in slope indicate the presence of different populations within the data set, as follows: below 62 g m^{-2} day^{-1} (ln < 4.2) coinciding with measured background values beyond the MSWFDS; intermediate, between 67 g m^{-2} day^{-1} and 191 g m^{-2} day^{-1} (4.3 < ln < 5.3); and high values, above 219 g m^{-2} day^{-1} (ln>5.3). Mean CO_2 flux in the first population (23% of the data) at the 95% confidence level is (46 ± 4) g m^{-2} day^{-1} (or 13 g C m^{-2} day^{-1}). Mean CO_2 flux in the intermediate population (63% of the data) is (110 ± 9) g m^{-2} day^{-1} (or 30 g C m^{-2} day^{-1}). Mean flux in the third population (14% of the data) is (270 ± 22) g m^{-2} day^{-1} (or 74 g C m^{-2} day^{-1}). Extreme populations (high and low fluxes) correspond to a smaller number of sampling sites than the intermediate flux population. In addition, an estimation of CO_2 released to the atmosphere in tn day^{-1} (Table 1) from MSWFDS was calculated taking into account the mean of each sub-population and their respective areas (sub-population mean x percentage of total population x total revealed area).

Since variogram reliability increases with the number of sites used in the model, the different regular sampling grids (14, 50 and 107 site surveys) were analysed until the geostatistical analysis indicated that an adequate sampling density had been achieved (Sanci et al. 2009a). Omni-directional and directional variograms were plotted, and spatial dependence was only observed between log-transformed data of CO_2 fluxes in the 107-site

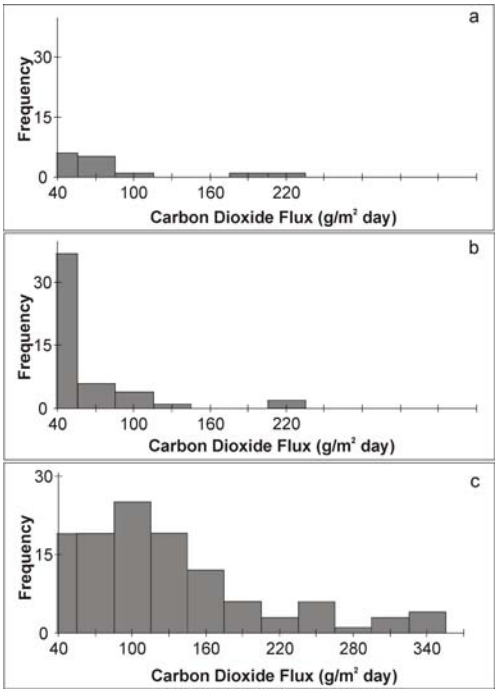

Fig. 5. Histograms of the CO_2 flux data from the three field campaigns: a. 14 stations (March); b. 50 stations (July); c. 107 stations (October).

Subpopulation	Percentage of total population (%)	Number points	Mean CO_2 Flux (g/m² día) with 95% confidence level	CO_2 released to atmosphere (tn day^{-1})
Background	23	25	46 (42-50)	1,59
Intermediate	63	67	110 (101-119)	10,39
High	14	15	270 (248-292)	5,67

Table 1. Statistical parameters of the sub-populations determined for the 107 stations sampled in October 2007.

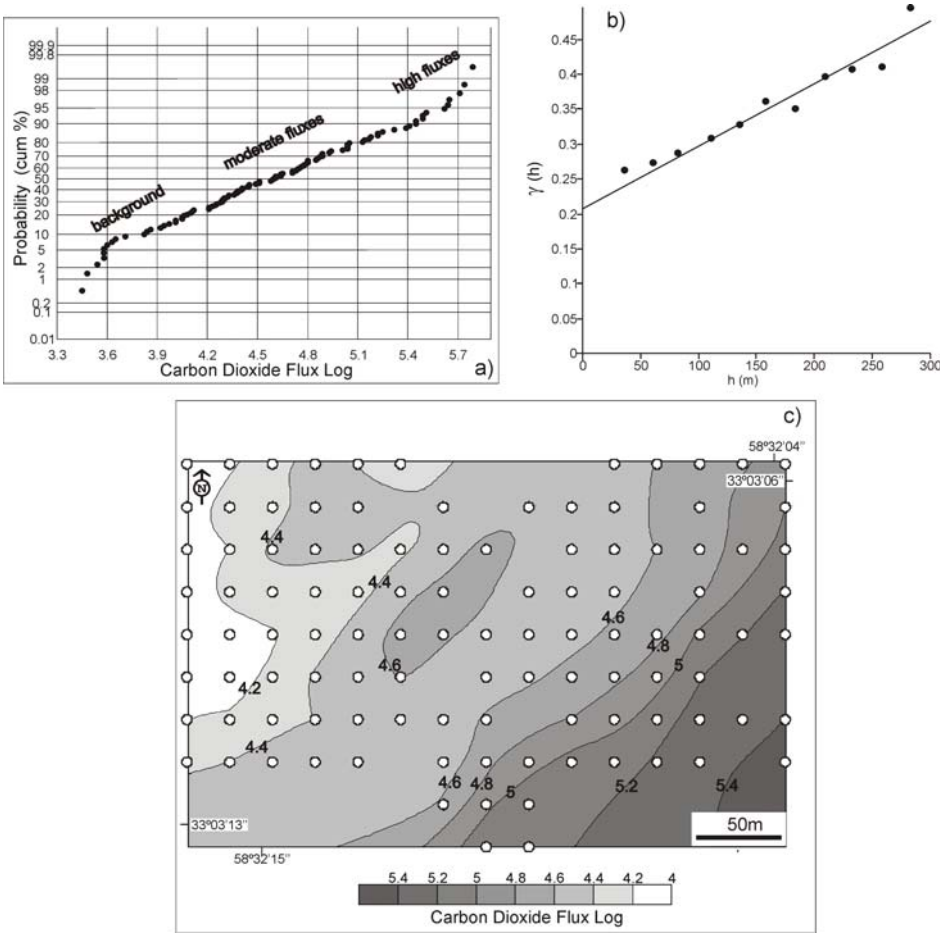

Fig. 6. A. Linear cumulative probability plot of ln(CO_2) flux of 107 stations; B. Omnidirectional variogram; C. Contours map of ln(CO_2) flux (Sanci et al., 2011).

survey (Sanci et al., 2011). The semivariance γ(h) plotted against a 30 m lag (h) between sample points is shown in Figure 6a. This variogram is linear with nugget effect, and its

parameters were used to elaborate the contour map of ln(CO_2) flux by kriging (Figure 6b). The distribution of ln(CO_2) flux indicates that diffuse gas fluxes from the MSWFDS are not spatially homogeneous: values grow towards the southeast.

To characterize the biodegradation stages within MSFDSW, relative concentrations were analysed of CO_2, CH_4, O_2 and N_2, and the isotopic composition of CO_2 ($^{13}C/^{12}C$) was determined. A stainless steel probe was inserted to 20 cm and soil gases brought to the vicinity of the tip of the probe by applying a vacuum. Soil gas samples were taken at 28 locations spaced at 50 m, which coincide with sites where CO_2 fluxes were measured. Samples were collected in TedlarTM bags and analysed in laboratory with a GC-TCD HP 5890 Series II. Volume fraction of CO_2 in soil gas samples ranged from ca. 0.01 to 0.103. In all cases, CH_4 fractions were <0.01, while those of O_2 and N_2 ranged from 0.165 to 0.209 and from 0.701 to 0.780, respectively, close to atmospheric concentrations. Isotope ratio $^{13}C/^{12}C$ for CO_2 was determined by bubbling the sampled CO_2 into an alkaline $BaCl_2$ solution which precipitated as $BaCO_3$. The $\delta^{13}C$–CO_2 ranged from -34.2 to -17.6‰. The plot of CO_2 concentration versus $\delta^{13}C$–CO_2 of Figure 7 (Sanci et al., 2011) shows two areas where different processes take place. One is related to normal soil respiration, about 0.01 of CO_2 (Welles et al. 2001). The second has values above 0.01, which may indicate the presence of anomalous concentrations of CO_2 from the biodegradation of urban solid waste (Pier & Kelly 1997) with a possible contribution of soil respiration. In the first group, $\delta^{13}C$ ranges from -25.4to -17.6‰, and in the second from -34.2 to -17.8‰.

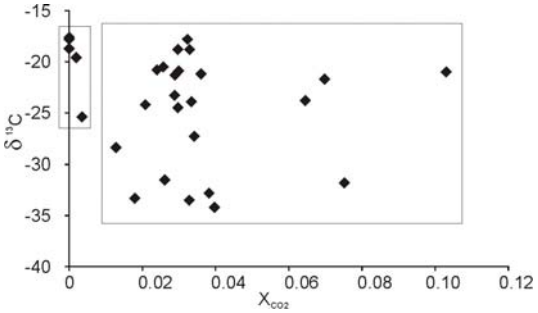

Fig. 7. $\delta^{13}C$–CO_2 versus CO_2 concentrations (Sanci et al., 2011).

7.3 Groundwater samples

Considering that MSW were buried at the same depth as the water table (0.10 to 1.70 m below surface) groundwater samples for hydrochemical and isotopic analyses were taken in October 2007 to check whether the phreatic aquifer was acting as a sink for the CO_2 generated by waste biodegradation. Groundwater samples were filtered and stored in 1000-mL plastic bottles and cooled until analysis. pH, temperature, electrical conductivity and alkalinity were determined in the field. The latter was determined by titration with H_2SO_4. Major ion concentrations were measured in laboratory: Na^+ ,K^+, Ca^{2+} and Mg^{2+} by atomic absorption spectrometry (Buck Scientific 200 A); $SO4^{2-}$, as S, was quantified by inductively coupled plasma-atomic emission spectroscopy (BAIRD-ICP 2070) and Cl^- by titration with $AgNO_3$. Carbon isotopic analyses on groundwater were done according the procedure explained in section 6. Piezometers for groundwater observation were installed before

October 2007 to compare the electric conductivity measured in situ with that estimated by geoelectrical studies (Pomposiello et al. 2009). Wells were drilled to a depth of ≤2.6 m, along the main direction of the local groundwater flow (S–N): upstream (P3–P10), downstream (P9) and within the landfill (P7–P5).

Measured physical and chemical parameters are shown in Table 2 and the chemical classification of water in Figure 8a (sodium chloride and bicarbonate waters). Hydrochemical and isotope values varied in the different flow paths: P3 to P9; P10 to P9; P7 to P5 (Sanci et al., 2011). Alkalinity and δ^{13}C-DIC tended to increase along the flow paths previously mentioned (Figure 8b). Values changed from 2.98 mmol L^{-1}/-12.1‰to 8.29 mmol L^{-1}/4.4‰ (P3–P9), 2.44 mmol L^{-1}/-15.0‰ to 8.29 mmol L^{-1}/4.4‰ (P10–P9) and 8.18 mmol L^{-1}/-8.1‰ to 41.45 mmol L^{-1}/0.8‰ (P7–P5). Considering the results obtained for P3 and P10

Parameter	P3	P10	P9	P7	P5
Temperature (°C)	18.5	19	23.2	21.3	20.4
pH	6.9	6.9	7.1	6.9	7.0
Conductivity (µS/cm)	610	720	2440	1320	5450
Alkalinity (mmol/L)	2.98	2.44	8.29	8.18	41.45
Sulphate (mmol/L)	0.05	0.05	0.08	0.30	5.00
Chloride (mmol/L)	2.20	3.75	13.68	5.42	13.15
Sodium (mmol/L)	4.52	4.65	20.75	14.53	70.90
Potassium (mmol/L)	0.06	1.46	0.16	0.02	0.07
Calcium (mmol/L)	0.67	0.45	0.47	0.39	0.77
Magnesium (mmol/L)	0.23	0.30	1.60	0.33	1.81
δ^{13}C (‰ vs. PDB)	-12.1	-15.0	4.4	-8.1	0.8
Analytical error (%) 100*(Cat-|An|)/(Cat+|An|)	8.86	8.17	6.17	5.97	8.42

Table 2. Groundwater composition of piezometers

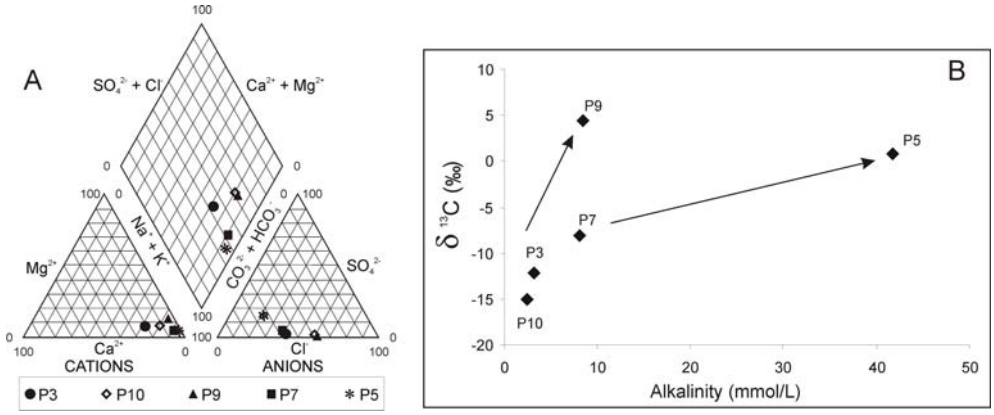

Fig. 8. A. Piper diagram showing the chemical classification of wells. P3, P7, P5: sodium bicarbonate groundwater; P10, P9: sodium chloride groundwaterchemical classification of groundwater; B. Alkalinity versus δ^{13}C-DIC (Sanci et al., 2011).

as background (pristine water), and the evolution of groundwater flow along the MSFDSW, calcium concentrations downstream are similar to background values. On the other hand, concentrations of magnesium, sulphate, chloride and sodium are greater than background concentrations.

7.4 Interpretation of results

The measurement of CO_2 fluxes in the MSWFDS with previous calibration in laboratory made it possible to reliably measure the spatial variability of the emissions in the field. CO_2 fluxes obtained (31–331 g m^{-2} day^{-1}) revealed the skewed distribution of the data (Figure 5c). This type of distribution (log-normal) was also observed in other soil CO_2 flux studies of natural and anthropic emission sources (Bergfeld et al. 2001; Cardellini et al. 2003; Chiodini and Frondini 2001; Gerlach et al. 2001). Logarithmic probability plots (Fig. 6b) show the polymodal distribution of CO_2 fluxes. They are a combination of three log-normal populations, which indicate that different processes of CO_2 generation take place. Low CO_2 fluxes are similar to the background values found around the MSFDSW and derive from soil respiration (Welles et al. 2001). The remaining values can be grouped into moderate and high fluxes. Values for both populations agree with those reported for biodegradation of solid waste in other sanitary landfills (Cardellini et al. 2003; Georgaki et al. 2008; Hedge et al. 2003; Jha et al. 2008; Pier & Kelly 1997). Spatial variations observed in surface CO_2 flux distribution (Figure 6c) are due to MSFDSW inhomogeneities. This variability may indicate that waste was buried in a NW–SE direction. Younger parts of the MSFDSW where biodegradation started later are more likely to have the highest CO_2 flux values.

Quantified anomalous CO_2 fluxes within the MSFDSW show that the site is still undergoing MSW biodegradation. Measured CO_2, CH_4, N_2 and O_2 concentrations are similar to those described for an initial phase of aerobic oxidation or a posthumous stage of biodegradation (mature), and they are different from those described for anaerobic phases. Considering the time since the end of operations at the MSFDSW (about 10 years), the values obtained for these gases may indicate that the MSFDSW is in a mature stage. Moreover, the results obtained for C isotopes in the probe-sampled CO_2 (-34.2 to -17.6‰) suggest that the MSWFDS is in an aerobic phase of biodegradation.

Although concentrations of CO_2, CH_4, N_2 and O_2 and C isotope are indicators of the degree of maturity of sanitary landfills, in practice, the factors affecting gas generation need to be considered. These factors affect the duration of each particular biodegradation stage, as well as the degrees of phase overlap and phase omission. In this case, the shallow burial of waste (2 m), the absence of CH_4 and mainly the permeability of the top cover due to little compaction and inadequate materials, make it possible to assume that anaerobic conditions necessary for methanogenic reactions have not been achieved in the MSFDSW. Therefore, since MSW were first disposed, biodegradation was completely aerobic or the initial phase of aerobic oxidation might have been followed by another phase of anaerobic oxidation with no generation of CH_4, arriving at the current maturation stage.

Data show that groundwater alkalinity grows across the MSFDSW in the direction of underground flow (Fig. 8). This suggests an input of C generated by anomalous CO_2, which dissolves calcite from calcareous levels such as ''tosca'' in the MSFDSW. The interaction between carbonic acid and mineral carbonates might even buffer pH variations through

increased CO_2 (no changes are observed in the pH of the samples). Moreover, the expected effect of the MSWFDS CO_2 gas on groundwater chemistry could be an increase not only in alkalinity, but also in calcium. Calcium concentrations obtained in this study were similar to the background values. The presence of clays promoting the Ca/Na exchange reaction would explain this fact. In addition, the results of applying stable C isotopes on DIC ($\delta^{13}C$ of -15.0 to 4.4 ‰) confirmed the changes observed in water alkalinity due to the anomalous ingression of CO_2. $\delta^{13}C$-DIC values richer than -12‰ can be explained by the input of CO_2 from MSW degradation which dissolves calcite (a geologically feasible process). Another possibility is the decomposition of dissolved organic matter within the phreatic aquifer due to infiltration of leachates, given observable signs, such as previous geophysical studies (Pomposiello et al. 2009), subhumid/humid climate with annual rainfall of 1,077 mm, permeable cover, shallow phreatic aquifer and increased concentration of leachate associated constituents such as chlorides and sodium. Enrichment of $\delta^{13}C$-DIC in groundwater affected by leachates reached +13‰ (van Breukelen et al. 2003) and +20‰ (North et al. 2004). Future studies will examine and compare the hydrogeochemical changes caused by the dissolution of landfill gases with those produced by the presence of leachates.

8. Conclusions

According to the experiences obtained in the process of quantification of CO_2 and CH_4 fluxes, the two most important factors that had to be considered were the sampling methods and the sampling sites. In the first case, none of the accumulation chamber methods are nowadays considered to be standard because of differences in flux estimations between chamber types or chamber-specific limitations. Therefore, laboratory experiments were needed to achieve accurate flux measurements before applying those methods in the field. In addition, to assess a reliable spatial variability of fluxes, it was necessary to test different regular sampling grids until the geostatistical analysis indicated that an adequate sampling density had been achieved. The degree of spatial dependence between chamber sites was analyzed in experimental variograms.

In this way, direct measurements of CO_2 diffuse degassing from surface, with the accumulation chamber methodology tested in laboratory, allowed the detection of the spatial variability of CO_2 fluxes in the MSWFDS and the assessment of CO_2 released to atmosphere from this source. Different subpopulations were identified by the statistical and geostatistical analyses of CO_2 fluxes. Processes giving rise to the subpopulations are background values attributable to plant respiration and different anomalous values related to biodegradation of urban solid waste disposed in the MSWFDS.

Analysis of probe-sampled concentrations of CO_2, CH_4, N_2 and O_2, as well as carbon isotope composition of the CO_2, showed that the current process is an aerobic phase of biodegradation. However, other factors that affect the gas generation were also considered to determine the phase of biodegradation of MSWFDS. They were: the time since the end of operations in the MSWFDS, the characteristics of the environment where MSW were disposed (mainly permeability of capping due to little compaction and inappropriate cover material), the shallow depth of SW burial and the absence of CH_4. All of these factors made it possible to assume that we are in the presence of a mature or posthumous stage of biodegradation, and allowed us to assume that biodegradation in the MSWFDS was

completely aerobic or that it may have gone through a period of anaerobic oxidation, without developing methanogenic processes.

Based on the increase in groundwater alkalinity as it flows across the MSWFDS and the DIC isotope composition, two different situations are possible: either CO_2 derived from MSW biodegradation is dissolving, or dissolved organic matter is decaying within the free aquifer due to the presence of leachates. Future research will be devoted to determining which of these possibilities best explains the process.

9. Acknowledgment

This research was supported by the Instituto de Geocronología y Geología Isotópica (UBA-CONICET) and PICT 2002 Nº 12243. The authors are grateful to Eduardo Llambıas, Anibal Tricarico and Gabriel Giordarengo for their collaboration in the field.

10. References

Baedecker, M. & Back, W. (1979) Hydrogeological processes and chemical reactions at a landfill. *Ground Water* , Vol. 17, Nº 5, pp. 429–437

Barlaz, M.; Green, R.; Chanton, J.; Goldsmith, C. & Hater, G. (2004) Evaluation of a biologically active cover for mitigation of landfill gas emissions. *Environ Sci Technol*, Vol. 38, pp. 4891–4899

Bergfeld, D.; Goff, F. & Janik, C. (2001) Elevated carbon dioxide flux at the Dixie Valley geothermal field, Nevada; relations between surface phenomena and geothermal reservoir. *Chem Geol*, Vol. 177, pp. 43–66

Bjerg, P.; Albrechtsen, H.; Kjeldsen, P. & Christensen, T. (2005) The groundwater geochemistry of waste disposal facilities. In: *Treatise on Geochemistry,* Volume 9, B. Sherwood Lollar (Ed.), pp. 579–612, Elsevier–Pergamon, Oxford

Borjesson, G.; Danielson, A. & Svensson, B. (2000) Methane fluxes from a Swedish landfill determined by geostatistical treatment of static chamber measurements. *Environ Sci Technol* , Vol. 34, pp. 4044–4050

Butnor, J. & Johnsen, K. (2004) Calibrating soil respiration measures with a dynamic flux apparatus using artificial soil media of varying porosity. *Eur J Soil Sci* , Vol. 55, pp. 639–647

Cardellini, C.; Chiodini, G.; Frondini, F.; Granieri, D.; Lewicki, J. & Peruzzi, L. (2003) Accumulation chamber measurement of methane fluxes: application to volcanic-geothermal areas and landfills. *Appl Geochem*, Vol. 18, pp. 45–54

Chiodini, G.; Cioni, R.; Guidi, M.; Raco, B. & Marini, L. (1998) Soil CO_2 flux measurement in volcanic and geothermal areas. *Appl Geochem*, Vol. 13, Nº 5, pp. 543–552

Chiodini, G.; Frondini, F.; Kerrick, D.; Rogie, J.; Parello, F.; Peruzzi, L. & Zanzari, A. (1999) Quantification of deep CO_2 fluxes from Central Italy. Examples of carbon balance for regional aquifers and soil diffuse degassing. *Chem Geol*, Vol. 159, pp. 205–222

Chiodini, G. & Frondini, F. (2001) Carbon dioxide degassing from the Albani Hills volcanic region, Central Italy. *Chem Geol*, Vol 177, pp. 67–83

Chiodini, G. ; Avino, R.; Brombach, T.; Caliro, S.; Cardellini, C. ; De Vita, S.; Frondini, F.; Granieri, D.; Marotta, E. & Ventura, G. (2004) Fumarolic and diffuse soil degassing west of Mount Epomeo, Ischia, Italy. *J Volcanol Geotherm Res*, Vol. 133, pp. 291–309

Coleman, D.; Liu, C.; Hacley, K. & Benson, L. (1993) Identification of landfill methane using carbon and hydrogen isotope analysis, *Proceedings of 16th International Madison Waste Conference, Municipal & Industrial Waste*, pp. 303–314, Department of Engineering Professional Development, University of Wisconsin, Madison.

Eddy, W. & Paninatier, Y. (1996) *Variowin: software for Spatial Data Analysis in 2-D*, Springer, New York

Evans, C.; Sorey, M.; Kennedy, B.; Stonnestrom, D.; Rogie, J. & Shuster, D. (2001) High CO_2 emissions through porous media: transport mechanisms and implications for flux measurement and fractionation. *Chem Geol*, Vol. 177, pp. 15–29

Farquar, G. & Rovers, F. (1973) Gas production during refuse decomposition. *Water Air Soil Pollut*, Vol. 2, pp. 483–495

Georgaki, I.; Soupios, P.; Sacas, N.; Ververidis, F.; Trantas, E.; Vallianatos, F. & Manios, T. (2008) Evaluating the use of electrical resistivity imaging technique for improving CH_4 and CO_2 emission rate estimations in landfills. *Sci Total Environ*, Vol. 389, pp. 522–531

Gerlach, T.; Doukas, M.; McGee, K. & Klesser, R. (2001) Soil efflux and total emission rates of magmatic CO_2 at the Horseshoe Lake tree kill, Mammoth Mountain California, 1995–1999. *Chem Geol*, Vol. 177, pp. 85–99

Gonfiantini, R.; Stichler, W. & Rozanski, K. (1995) Standards and intercomparison materials distributed by the International Atomic Energy Agency for stable isotope measurements, *Proceedings of a consultants meeting of reference and intercomparison materials for stable isotopes of light elements*, pp. 13–29, IAEA, Vienna.

Hackley, K.; Liu, C. & Coleman, D. (1996) Environmental isotope characteristics of landfill leachates and gases. *Ground Water*, Vol. 34, Nº 5, pp. 827–836

Hanson, P.; Wullschleger, S.; Bohlman, S. & Todd, D. (1993) Seasonal and topographic patterns of forest floor CO_2 efflux from an upland oak forest. *Tree Physiol*, Vol. 13, pp. 1–15

Hedge, U.; Chang, T. & Yang, S. (2003) Methane and carbon dioxide emissions from Shan-Chu-Ku landfill site in northern Taiwan. *Chemosphere*, Vol. 52, pp. 1275–1285

Hutchison, J. & Mosier, A. (1981) Improved soil cover method for field measurements of nitrous oxide fluxes. *Soil Sci Soc Am J*, Vol. 45, pp. 311–316

Iriondo, M. (1980) El Cuaternario de Entre Ríos. *Rev Asoc Cienc Nat Litoral*, Vol. 11, pp. 125–141

Iriondo, M. (1996) Estratigrafía del Cuaternario de la cuenca del río Uruguay, *XIII Congreso Geológico Argentino y III Congreso de Exploración de Hidrocarburos*, pp. 15–25, AGAIAPG, Buenos Aires.

Iritz, Z.; Lindroth, A. & Gardenas, A. (1997) Open ventilated chamber for measurements of H_2O and CO_2 fluxes from the soil surface. *Soil Technol*, Vol. 10, pp. 169–184

Jensen, L.; Mueller, T.; Tate, K.; Ross, D.; Magid, J & Nielsen, N. (1996) Soil surface CO_2 flux as an index of soil respiration in situ: a comparison of two chamber methods. *Soil Biol Biochem*, Vol. 28, Nº 10–11, pp. 1297–1306

Jha, A.; Sharma, C.; Singh, N.; Ramesh, R.; Purvaja, R. & Gupta, P. (2008) Greenhouse gas emissions from municipal solid waste management in Indian mega-cities: a case study of Chennai landfill sites. *Chemosphere*, Vol. 71, pp. 750–758

Kerfoot, H.; Baker, J. & Burt, D. (2003) The use of isotopes to identify landfill gas effects on groundwater. *J Environ Monit,* Vol. 5, pp. 896-901

Kerfoot, H.; Baker, J. & Burt, D. (2004) Geochemical changes on ground water due to landfill gas effects. *Ground Water Monit Rem*, Vol. 24, Nº 1, pp. 60–65

Kinzig, A. P. y Socolow, R. H. (1994) Human impacts on nitrogen cycle. *Physics Today,* Vol. 47, Nº 11, pp. 24-31

Kumar, S.; Mondal, A.; Gaikwad, S.; Devotta, S. & Singh, R. (2004) Qualitative assessment of methane emission inventory from municipal solid waste disposal: a case study. *Atmos Environ*, Vol. 38, pp. 4921–4929

MacCrea, J. (1950) On the isotopic chemistry of carbonates and paleotemperature scale. J *Chem Phys*, Vol. 18, Nº 6, pp. 849–857

Martin, J.; Bolstad, P. & Norman, J. (2004) A carbon dioxide flux generator for testing infrared gas analyser based soil respiration systems. *Soil Sci Soc Am J*, Vol. 68, pp. 514–518

Meju, M. (2000) Geoelectrical investigation of old/abandoned, covered landfill sites in urban areas: mode development with a genetic diagnosis approach. *J Appl Geophys*, Vol. 44, pp. 115–150

Mook, W. (2000) Natural abundance of the stable isotopes of C, H and O, In: *Environmental isotopes in the hydrological cycle: principles and applications*, W., Mook (Ed.), pp. 89–120, UNESCO, Paris

Morën, A. & Lindroth, A. (2000) CO_2 exchange at the floor of a boreal forest. *Agric For Meteorol*, Vol. 101, pp. 1–14

Mosher, B.; Czepiel, P. & Harriss, R. (1999) Methane emissions at nine landfill sites in the northeastearn United States. *Environ Sci Technol*, Vol. 33, pp. 2088–2094

Nay, S.; Matsson, K. & Bormann, B. (1994) Biases of chamber methods for measuring soil CO_2 efflux demonstrated with a laboratory apparatus. *Ecology*, Vol. 75, pp. 2460–2463

Norman, J.; Garcia, R. & Verma, S. (1992) Soil surface CO_2 fluxes and the carbon budget of a grassland. *J Geophys Res*, Vol. 97, Nº D17, pp. 18845–18853

Norman, J.; Kucharik, C.; Gower, S.; Baldocchi, D.; Crill, P.; Rayment, M.; Savage, K. & Striegl, R. (1997) A comparison of six methods for measuring soil-surface carbon dioxide fluxes. *J Geophys Res,* Vol. 102, pp. 28771–28777

North, J.; Rusell, D. & Barrie, M. (2004) The use of carbon and nitrogen isotope ratios to identify landfill leachate contamination: Green Island Landfill, Dunedin, New Zealand. *Environ Int*, Vol. 30, pp. 631–637

Parkinson, K. (1981) An improved method for measuring soil respiration in the field. *J Appl Ecol*, Vol. 18, pp. 221–228

Pereyra, F.; Tchilinguirian, P. & Baumann, V. (2002) Hoja Geológica 3360-IV Gualeguaychú. Boletín No 335, Servicio Geológico Minero Argentino, Buenos Aires

Pier, P. & Kelly, J. (1997) Measured and estimated methane and carbon dioxide emissions from sawdust waste in the Tennessee Valley under alternative management strategies. *Bioresour Technol*, Vol. 61, pp. 213–220

Pomposiello, C.; Dapeña, C.; Boujon, P. & Favetto, A. (2009) Tomografías eléctricas en el Basurero Municipal Ciudad de Gualeguaychú, provincia de Entre Ríos. Evidencias de contaminación. *Rev Asoc Geol Arg*, Vol. 64, pp. 603–614

Prezzi, C.; Orgeira, M.; Ostera, H. & Vazquez, C. (2005) Ground magnetic survey of a municipal solid waste landfill: pilot study in Argentina. *Environ Geol*, Vol. 47, Nº 7, pp. 889–897

Pumpanen, J.; Kolari, P.; lvesniemi, H.; Minkkinen, K.; Vesala, N.; Lohila, A.; Larmola, T.; Morero, M.; Pihlatie, M.; Janssens, I.; Yuste, J.; Gru¨nzweig, J.; Reth, S.; Subke, J.; Savage, K.; Kutsch, W.; Østreng, G.; Ziegler, W.; Anthoni, P.; Lindroth, A. & Hari, P. (2004) Comparison of different chamber techniques for measuring soil CO_2 efflux. *Agric For Meteorol*, Vol.123, pp. 159–176

Rayment, M. & Jarvis, P. (1997) An improved open chamber system for measuring soil CO_2 effluxes in the field. *J Geophys Res*, Vol. 102, pp. 28779–28784

Sanci, R.; Ostera, H. & Panarello, H. (2009a) Determinación del flujo de CO_2 en antrópicas: sitio de disposición final municipal, Gualeguaychú, Entre Ríos. *Rev Asoc Geol Arg*, Vol. 65, Nº 3, pp. 533–544

Sanci, R.; Panarello, H. & Ostera, H. (2009b) Assessment of soil moisture influence on CO_2 flux: a laboratory experiment. *Environ Geol*, Vol. 58, pp. 491–497

Sanci, R.; Panarello, H. & Ostera, H. (2011) CO_2 emissions from a municipal site for final disposal of solid waste in Gualeguaychú, Entre Ríos Province, Argentina. *Environ Earth Sci* DOI 10.1007/s12665-011-1260-0

Scottish Environment Protection Agency [SEPA] (2004) Guidance on the management of landfill gas. Avaible from: http://www.sepa.org.uk/waste/waste_regulation/landfill.aspx

Spokas, K.; Graff, C.; Morcet, M. & Aran, C. (2003) Implications of the spatial variability of landfill emission rates on geospatial analyses. *Waste Manage*, Vol. 23, pp. 599–607

Stumm, W. & Morgan, J. (1996) *Aquatic chemistry*, Environmental Science and Technology, New York

UK Environment Agency (2010). Guidance on monitoring landfill gas surface emissions. Avaible from: http://www.environment-agency.gov.uk/business/sectors/108918.aspx

Van Breukelen, B.; Roling, F.; Groen, J.; Griffioen, J. & Van Verseveld, H. (2003) Biogeochemistry and isotope geochemistry of a landfill leachate plume. *J Contam Hydrol*, Vol. 65, pp. 245–268

Wang, X. & Qi, F. (1998) The effects of sampling design on spatial structure analysis of contaminated soil. *Sci Total Environ*, Vol. 224, pp. 29–41

Webster R, Oliver MA (1992) Sample adequately to estimate variograms of soil properties. *J Soil Sci* 43: 177–192

Welles, J.; Demetriades-Shah, T. & McDermitt, D. (2001) Considerations for measuring ground CO_2 effluxes with chambers. *Chem Geol*, Vol. 177, pp. 3–13

Widën, B. & Lindroth, A. (2003) A calibration system for soil carbon dioxide-efflux measurements chambers: description and application. *Soil Sci Soc Am J*, Vol. 67, pp. 327–334

Part 2

Greenhouse Gases Effect and Management

13

Greenhouse Effect

Andrew A. Lacis
NASA Goddard Institute for Space Studies
New York, NY
USA

1. Introduction

The greenhouse effect is the physical warming of the ground surface that arises in semi-transparent planetary atmospheres that are heated by solar radiation. In order for the greenhouse effect to operate, the planet's atmosphere must be sufficiently transparent at visible wavelengths to allow significant amounts of solar radiation to be absorbed by the ground surface. The atmosphere must also be sufficiently opaque at thermal wavelengths to prevent thermal radiation emitted by the ground surface from escaping directly out to space. In such planetary atmospheres, the long-wave opacity for the absorption of radiation at thermal wavelengths is provided by the so-called greenhouse gases (e.g., water vapor, carbon dioxide, methane, nitrous oxide), although absorption by particulate matter such as that due to clouds and aerosols can also make significant contributions to the greenhouse effect. The net effect of the planetary greenhouse effect is to keep the ground surface of the planet at a warmer temperature than it would otherwise be if there were no greenhouse effect. The operation of a greenhouse effect also imparts a temperature gradient in the planet's atmosphere, with the highest temperatures being at the ground, decreasing with height in the atmosphere. This is primarily a radiative effect that is expected to occur in all planetary atmospheres where the ground surface is heated by solar radiation, and there is substantial atmospheric opacity at thermal wavelengths of the spectrum.

2. Planetary comparisons

In our solar system, the greenhouse effect operates on those terrestrial planets that have substantial atmospheres (i.e., Earth, Mars, and Venus), including also on Saturn's moon Titan. Typically, carbon dioxide is the key greenhouse gas that keeps the ground surface temperatures of the terrestrial planets warmer than they would be without the greenhouse effect. The importance of carbon dioxide as a greenhouse gas stems from its very strong absorption bands that cover much of the thermal spectrum, and also because carbon dioxide does not condense and precipitate from the atmosphere at the prevailing temperatures on the terrestrial planets. Being so much farther from the sun, the atmosphere of Titan is much colder than the atmospheres of the terrestrial planets, so much so that carbon dioxide and water vapor cannot be maintained in gaseous form on Titan. Instead, the greenhouse effect on Titan is sustained primarily by pressure-induced

methane, hydrogen, and nitrogen, to keep the surface temperature on Titan some 12°C (22°F) warmer than it would otherwise be if Titan were warmed only by its absorbed solar radiation (McKay et al., 1991). With Saturn being 9.5 times further from the Sun than the Earth, the solar radiation incident on Titan is about 90 times fainter than the solar radiation that is incident on Earth, endowing Titan with a frigid atmosphere and a surface temperature of 82 K (−191°C, −312°F).

Of the terrestrial planets, Venus has by far the strongest greenhouse effect. This is because the atmosphere of Venus is nearly a 100 times more massive and denser than that of Earth, and also because the atmosphere of Venus is composed almost entirely of the prime greenhouse gas, carbon dioxide. The large atmospheric pressure on Venus greatly broadens the carbon dioxide absorption lines to provide strong absorption across the entire thermal spectrum. Only about 1% of the incident solar radiation penetrates to the ground, but the thermal opacity in the atmosphere of Venus is so large as to produce a greenhouse effect that is about 15 times greater than that on Earth. Because of this, the surface temperature on Venus is nearly 460°C (860°F), which is hot enough to melt lead and vaporize mercury. Moreover, this is about 500°C (900°F) hotter than the surface of Venus would be (−40°C, −40°F) if Venus were simply in thermal equilibrium with the global mean solar energy that is absorbed by the Venus atmosphere, without benefit of the greenhouse effect. Interestingly, the non-greenhouse equilibrium temperature of Venus is actually some 12°C (22°F) colder than the corresponding equilibrium temperature of Earth, even though Venus is closer to the Sun and receives twice the terrestrial insolation. This situation arises because the cloud-shrouded atmosphere of Venus is far more reflecting than that of Earth, reflecting more than 70% of the incident sunlight, whereas Earth reflects only about 30%.

On Earth, the strength of the greenhouse warming effect is a more moderate 33°C (60°F). This amount of greenhouse warming makes the global mean surface temperature of the Earth a relatively comfortable 15°C (59°F) instead of an otherwise frigid −18°C (−1°F), which would be the equilibrium temperature for Earth with a planetary albedo of 30% and no greenhouse effect to trap the absorbed solar radiation. Carbon dioxide is also the key greenhouse gas of the terrestrial atmosphere, but with a very important distinction. In the terrestrial atmosphere, most of the greenhouse effect is actually provided by water vapor and by clouds, with only about 20% due to carbon dioxide. This is because Earth is the 'water' planet where water in all of its forms has a central role in defining the properties of the terrestrial climate system. The greenhouse warming provided by carbon dioxide and the other non-condensing greenhouse gases like methane, nitrous oxide, and ozone, allows water vapor to evaporate and remain in the atmosphere. This produces a strong 'feedback effect' which magnifies that part of the greenhouse warming that is uniquely attributable to the non-condensing greenhouse gases. Thus, water vapor with its strong absorption bands in the thermal part of the spectrum, accounts for approximately 50% of the terrestrial greenhouse effect. Long-wave absorption by cloud particles, which absorb radiation at all wavelengths of the thermal spectrum, accounts for about 25% of the total greenhouse effect. The highly interactive atmosphere of Earth serves to produce the uniquely variable climate that exists nowhere else in the solar system.

In contrast to Venus and Earth, the Martian atmosphere is very thin and tenuous, being scarcely 1% of the Earth's atmosphere. Like Venus, the Martian atmosphere is composed

primarily of carbon dioxide. Interestingly, the column amount of carbon dioxide in the Martian atmosphere is actually about fifty times greater than in the atmosphere of Earth. Nevertheless, Mars can only muster a small amount of greenhouse warming (about 5°C, or 9°F). The reason for this is that the atmospheric pressure is a very important factor in determining the efficiency of greenhouse gas performance. Because of the small atmospheric pressure on Mars (less than one hundredth that on Earth), the spectral absorption lines of carbon dioxide on Mars are very narrow, and therefore act like a picket fence that lets most of the thermal radiation emitted by the Martian ground surface to escape directly out to space. This does not happen on Earth because of the atmospheric pressure that is exerted by the radiatively inactive nitrogen and oxygen, causing the spectral absorption lines of carbon dioxide and water vapor to be greatly broadened, making them more effective absorbers of thermal radiation. And, for comparison, it is the extremely high pressure on Venus that makes the carbon dioxide absorption of thermal radiation particularly efficient in the Venus greenhouse effect.

On Mercury, there is no tangible atmosphere, and hence there is no opportunity for the greenhouse effect to operate. Accordingly, the surface temperature on Mercury is determined solely as the result of local thermal equilibrium with the absorbed solar radiation, producing scorching hot temperatures on the sunlit side, and being abysmally cold on the dark side.

The strength of the planetary greenhouse effect is something that can, at least in principle, be determined by direct measurement. Perhaps the most basic measurement of a planet's energy balance is the reflected solar energy. Given the planet's distance from the Sun, it is therefore taken for granted that the incident solar radiation is a known quantity. Upon subtracting the reflected solar radiation from the incident solar energy flux, the energy input to the planet is thus defined. Other potential energy sources such as tidal, geothermal, nuclear, etc. are several orders of magnitude smaller than the absorbed solar radiation, and therefore need not be considered. A very natural and logical assumption that is commonly made is that the planet is in global energy balance, meaning that the thermal radiation emitted by the planet is going to be equal to the absorbed solar energy. Accordingly, this determines the outgoing long-wave energy that the planet radiates out to space. The long-wave energy emitted to space then serves to define the effective radiating temperature of the planet by equating the emitted energy to its equivalent Planck, or blackbody radiation, as summarized in equation form by

$$\pi R^2 S_o (1 - A) = 4\pi R^2 \sigma T_E^4 \quad (1)$$

where πR^2 is the projected geometrical area of the planet, S_o is the solar constant, A is the planet's bond albedo on the solar side of the equation. On the thermal side $4\pi R^2$ is the total surface area of the planet, σ is the Stefan-Boltzmann constant (5.67×10^{-8} W/m^2 K^{-4}), and T_E is the effective radiating temperature of the planet. The outgoing long-wave flux is also a subject for direct measurement, while the effective temperature is defined numerically from the long-wave flux through the Stefan-Boltzmann law.

$$F_{LW} = \sigma T_E^4 \quad (2)$$

and

$$T_E = [S_o (1 - A)/4\sigma]^{1/4} \quad (3)$$

Also needed is the information about the planet's surface temperature and the up-welling thermal flux that is emitted by the ground surface, both of which are measurable quantities. Direct measurements have been made by space probes that landed on the surfaces of Mars and Venus. Space based measurements are also possible by using selected spectral windows in the long-wave spectrum where radiation from the ground surface can escape directly out to space. Such measurements are a topic in remote sensing. They rely on associating the intensity of the measured spectral radiance with the equivalent spectral brightness of Planck radiation. By such means, microwave measurements of Venus were the first indication that the surface temperature of Venus was exceedingly hot, before verification by direct space probe measurements. A summary of planetary greenhouse parameters is listed in Table 1.

Parameter	Mars	Earth	Venus
T_S(K)	215	288	730
T_E(K)	210	255	230
σT_S^4 (W/m^2)	121	390	16,100
σT_E^4 (W/m^2)	111	240	157
G_T(K)	5	33	500
G_F(W/m^2)	10	150	~16,000
P_S(bar)	0.01	1	100

Table 1. Planetary greenhouse parameters. (After Lacis et al., 2011).

The greenhouse parameters listed in Table 1 are all measurable quantities so that, at least in principle, the strength of the greenhouse effect of a planet is empirically determinable. As explained above, the effective temperature, T_E(K), is actually a measure of either the emitted long-wave radiation at the top of the atmosphere, or the absorbed solar radiation by the planet, as given by Equation (3). Direct measurements of the globally averaged radiative fluxes at the top of the atmosphere and at the ground surface are actually quite difficult to obtain, particularly in view of the large variability of the solar and thermal radiative fluxes both geographically and with time, and also as a function of wavelength and viewing geometry. In practice, it is a combination of observational data analyses and theoretical modeling that is required to refine our knowledge of the planetary greenhouse parameters.

Basically, it is the long-wave radiative fluxes at the top of the atmosphere and at the ground surface that define the greenhouse effect. The strength of the planetary greenhouse effect is expressed as the difference between the up-welling long-wave flux emitted by the ground surface, and the outgoing long-wave flux at the top of the atmosphere. Thus,

$$G_F = \sigma T_S^4 - \sigma T_E^4 \quad (4)$$

and

$$G_T = T_S - T_E \quad (5)$$

where the greenhouse strength G_F is expressed in flux (W/m^2) units, and G_T is expressed as a temperature (ΔT_K) difference. The two greenhouse expressions are equivalent. G_F expressed in flux units is more directly comparable to radiative modeling results and

observational data. G_T expresses the strength of the greenhouse effect directly in terms of the temperature difference by which the global mean surface temperature would be increased in comparison to the temperature that would exist if there were no greenhouse effect. The numbers given in Table 1 represent annually-averaged global-mean values. Obviously, the strength of the greenhouse effect varies with geographic location and with season. While the well-mixed non-condensing greenhouse gas contribution to the greenhouse effect may tend to be globally uniform and steady in time, the water vapor and the cloud feedback contribution to the greenhouse effect is strongly variable, geographically, seasonally, and even inter-annually.

It is interesting that of the numbers in Table 1, the outgoing long-wave fluxes of the three planets, as represented by the effective temperature, are so similar. More noteworthy are the factors of a 100 difference in the massiveness of the respective atmospheres, as represented by the surface pressure P_S. In all three atmospheres, carbon dioxide is the key greenhouse gas. But the Earth is unique in that its greenhouse effect includes feedback amplification.

3. Geological perspective

It is the combination of solar radiative heating and the strength of the greenhouse effect that determines the surface temperature of a planet. In the early days of the solar system some 4.5 billion years ago, the Sun had only about 75% of its present luminosity. But, as hydrogen in the interior of the Sun gets transformed into heavier elements, this causes the temperature and luminosity of the Sun increase, which in turn produces a slow and steady rise in the energy input to the terrestrial climate system. This is sometimes called the astrophysical climate forcing, and this type of solar radiative forcing will continue unabated. In several billion years time it will make the Earth too hot to be habitable.

While changes in solar insolation act to regulate the inflow of energy to the atmosphere and ground, it is the strength of the greenhouse effect that exerts its influence on the terrestrial climate system by regulating the energy outflow, and by generating additional heating of the ground surface by down-welling long-wave radiation. Here, carbon dioxide plays the leading role. In the early days of the Earth when the Sun was much less luminous, high concentrations of carbon dioxide where able to keep the temperature habitable for life forms to get established and to take root.

Over million-year time scales, volcanoes are the principal source of atmospheric carbon dioxide, and weathering of rocks is the principal sink (Berner, 2004), with the biosphere of the Earth also participating both as a source and as a sink. Because the principal sources operate independently of each other, the atmospheric level of carbon dioxide can fluctuate unchecked. There is geological evidence that shows glaciation was taking place at tropical latitudes 650 to 750 million years ago (Kirschvink, 1992), suggesting that snowball Earth conditions might have existed at that time. If, over millions of years, rock weathering were to exceed volcanic replenishment, atmospheric carbon dioxide could fall below its critical value, thus sending the Earth to snowball conditions. Eventually, with the ocean covered by ice, and thus prevented from taking up carbon dioxide, sufficient buildup of atmospheric carbon dioxide from volcanic eruptions would gradually bring the Earth out of its snowball state climate.

The Cenozoic era, comprising the past 65.5 million years, marks the Cretaceous extinction of dinosaurs and the auspicious rise of mammals. During this era, the level of atmospheric concentration of carbon dioxide peaked near 3000 parts per million roughly 50 million years ago (Royer, 2006). This coincided with peak global warming when the global mean ocean temperature was some 12°C warmer than present (Hansen et al., 2008). The information on carbon dioxide concentrations comes from carbon isotope analysis obtained from ocean core data (Fletcher, 2008), and temperature information is deduced from oxygen-18 variations in the ocean core data. It so happens that about two tenths of one percent of atmospheric oxygen is oxygen-18, or heavy oxygen with ten neutrons instead of the nominal eight. Since oxygen-18 concentration relative to oxygen-16 is systematically temperature dependent, this ratio can therefore be used as a geological thermometer to estimate global temperature changes in the geological record.

It is generally believed that it was enhanced weathering of rocks associated with the formation of the Himalayas that brought the atmospheric carbon dioxide down to a critical 450 ppm level, at which point the Antarctic polar ice cap began to form about 34 million years ago. The geological record clearly shows the close coupling between the level of atmospheric carbon dioxide and the global temperature of Earth, suggesting a thermostat-type control by atmospheric carbon dioxide in regulating the surface temperature of Earth. All along, the terrestrial biosphere has also played a very critical role in the time evolution of the global carbon cycle by having sequestered most of Earth's carbon in the form of limestone, and not allowed it to accumulate in the atmosphere as was apparently the case on Venus.

On thousand-year time scales, both the Antarctic and Greenland ice core data show that atmospheric carbon dioxide has fluctuated between 180 to 300 ppm over the glacial-interglacial cycles during the past 650,000 years (Jansen et al., 2007), with close coupling between the carbon dioxide concentration, ice volume, sea level, and global temperature. The relevant physical processes that control atmospheric carbon dioxide on thousand-year timescales between the glacial and interglacial extremes are not yet fully under-stood, but appear to involve the biosphere, ocean chemistry, and ocean circulation, with a significant role for Milankovitch variations in the Earth-orbital parameters which alter the seasonal distribution of incident solar radiation in the polar regions. While in the context of current climate, carbon dioxide is clearly an externally imposed radiative forcing on the climate system (as the direct result of fossil fuel burning) in the context of recorded human history, within the longer geological record, carbon dioxide is seen to be a variable quantity, albeit on a very slow time scale.

In some ways Venus is the twin sister of Earth. Both planets have similar mass and size, similar composition, similar amounts of carbon, an a generally similar location within the solar system, Based on this, there is well-grounded speculation, supported by isotope evidence, that originally Venus may have supported an ocean and an atmosphere similar to that of Earth. The suggestion is that for some reason Venus was not able to sequester its store of carbon in the form of limestone as Earth was able to accomplish. In this scenario, carbon dioxide arising from volcanic eruptions continued to accumulate within the Venusian atmosphere, increasing its greenhouse effect to the point where eventually all ocean water was vaporized. Water vapor then was carried high into the atmosphere where

it was photolyzed by the intense sunlight and the liberated hydrogen was lost to space. There is thus the lingering suspicion that the current climate on Venus might well be attributed to the absence of having had appropriate life forms that could have prevented the critical buildup of carbon dioxide and thus prevented the runaway greenhouse effect that has rendered Venus inhospitable to life.

4. Historical understanding

The basic understanding of the greenhouse effect mechanism was first described in 1824 by the French mathematician and physicist Joseph Fourier (Fourier, 1824). This was also that period in time when conservation of energy, the most basic and fundamental concept of physics, was being formulated and quantified. Solar energy from the Sun is absorbed, and warms the Earth. An equal amount of thermal energy must then be radiated to space by the Earth in order to maintain its equilibrium energy balance. Otherwise the temperature of Earth would either keep rising indefinitely, or decrease indefinitely. In this spirit, Fourier performed experiments on atmospheric heat flow and pondered the question of how the Earth stays warm enough for plant and animal life to thrive. Fourier realized that much of the thermal radiation emitted by the Earth's surface was being absorbed within the Earth's atmosphere, and that some of this absorbed radiation was then being re-emitted downward, providing additional warming of the ground surface over and above that attributable just to the direct absorption of solar energy.

In 1863, the Irish physicist John Tyndall (Fleming, 1998) provided experimental support for Fourier's greenhouse idea, demonstrating by means of quantitative spectroscopy that the common atmospheric trace gases, such as water vapor, ozone, and carbon dioxide, are strong absorbers and emitters of thermal radiant energy, but are essentially transparent to visible sunlight. It was clear to Tyndall from his measurements that water vapor was the strongest absorber of thermal radiation, and therefore, the most influential atmospheric gas controlling the Earth's surface temperature. Meanwhile on the other hand, the principal components of the atmosphere, nitrogen and oxygen, were found to be radiatively inactive, providing only the atmospheric framework and temperature structure within which water vapor and carbon dioxide can exert their radiative influence. With this understanding of the radiative properties of the absorbing gases in the atmosphere, Tyndall speculated in 1861 that a reduction in atmospheric carbon dioxide could in fact induce an ice-age climate.

Utilizing the work of Tyndall and the careful measurements of heat transmission through the atmosphere compiled by the American astronomer Samuel Langley, the Swedish chemist and physicist Svante Arrhenius was the first to develop a quantitative mathematical framework of the terrestrial greenhouse effect (Arrhenius, 1896). Arrhenius published his heat-balance calculations of the Earth's sensitivity to carbon dioxide change in 1896. His radiative modeling results were remarkably similar to our current understanding of how the terrestrial greenhouse effect keeps the surface temperature some 33°C (or 60°F) warmer than it otherwise would be. Given that Arrhenius' basic interest was to explain the likely causes of ice-age climate, his greenhouse model was quite successful. He showed that reducing atmospheric carbon dioxide by a third would cool the global surface temperatures by −3°C (−5.5°F), and that doubling carbon dioxide would cause the tropical latitudes to warm by 5°C (9°F), with somewhat larger warming in polar regions, results that are in surprisingly

close agreement with current climate modeling simulations for the expected change in global surface temperature in response to the doubling of carbon dioxide forcing.

In 1905, the American geologist Thomas Chamberlin made the important finding that the greenhouse contribution by atmospheric water vapor behaved as a positive feedback mechanism (Christianson, 1999). In his thinking, Chamberlin noted that surface heating by solar radiation, or surface heating due to other agents such as carbon dioxide, raises the atmospheric temperature and leads to evaporation of more water vapor. This extra amount of water vapor produces additional heating and the further evaporation of additional water vapor. When the added heat source is taken away, any water vapor that is in excess of its equilibrium amount will precipitate from the atmosphere. Clearly, this is not a runaway situation. Rather, the change in the externally applied heating simply results in the establishment of a new equilibrium for the amount of water vapor that the atmosphere can hold. Since water vapor is an efficient greenhouse gas, the net effect of this interaction produces a significantly larger temperature change than would otherwise be the case if the amount of atmospheric water vapor did not change, demonstrating that it is carbon dioxide (and the other non-condensing greenhouse gases) that are the controlling factor of the terrestrial greenhouse effect. As a result, atmospheric water vapor and clouds act as feedback effects that magnify the greenhouse heating that is initially supplied by the non-condensing greenhouse gases, or by other radiative forcings.

5. Terrestrial greenhouse effect

In the terrestrial greenhouse, carbon dioxide accounts for approximately 7°C (13°F) of the total 33°C (60°F) greenhouse effect. The other non-condensing greenhouse gases, i.e., ozone, methane, nitrous oxide, and anthropogenic chlorofluorocarbons, add another 3–4°C (5–7°F) to the overall global greenhouse strength. Because clouds absorb thermal radiation at all wavelengths of the thermal spectrum, this makes clouds into important contributors to the terrestrial greenhouse effect. Even aerosols, in particular the larger sized desert dust particles, with their substantial absorption and scattering at thermal wavelengths, make a small but non-negligible, contribution to the terrestrial greenhouse effect. Also, the cooling efficiency of volcanic aerosols is reduced by about 10% because of their non-negligible greenhouse effect (Lacis and Mishchenko, 1995).

The greenhouse effect is intimately an integral part of the global energy balance within the climate system. Basically, it is the greenhouse effect that determines how the long-wave thermal energy is transformed from its initial emission from the ground surface to its final destination out to space from the top of the atmosphere. In the process, this effectively defines the strength of the terrestrial greenhouse effect and determines the magnitude of the greenhouse warming over and above what the surface temperature would be if the ground surface were determined by simply being in equilibrium with the absorbed sunlight. In general terms, the nominal global mean surface temperature of the Earth is about 288 K (15°C, 59°F). The corresponding thermal radiation emitted by the ground surface is very closely described by the 'black body', or Planck emission, which is proportional to the fourth power of the surface temperature. This yields 390 W/m^2 for the up-welling long-wave flux emitted by the ground surface. However, the long-wave flux to space leaving the top of the atmosphere is about 240 W/m^2, which has been verified by satellite-based long-wave

radiative flux measurements of the Earth's energy balance. The flux difference of 150 W/m² between the up-welling surface flux and the long-wave flux at the top of the atmosphere that is emitted out to space, is a simple measure of the strength of the terrestrial greenhouse effect. As a further point, in terms of black body Planck radiation, the 240 W/m² that is radiated out to space corresponds to a Planck temperature of 255 K (−18°C, −1°F), which is sometimes referred to as the effective temperature of the Earth. Thus, the temperature difference between the surface temperature and the effective temperature (33 K, 33°C, 60°F) provides another equivalent measure of the strength of the terrestrial greenhouse, one that is expressed in terms of temperature.

The relative efficacy of any particular atmospheric greenhouse contributor is determined by how strongly it will absorb thermal radiation, and on how weakly the absorbed thermal radiation is re-emitted to space. According to the principles of radiative physics, the emissivity of a substance must be equal to its absorptivity. It is notable that the absorptivity of most absorbing materials has very little dependence on temperature, while the emission of thermal radiation is very strongly dependent on the temperature of the emitting body (varying approximately as the fourth power of the temperature of the radiating substance). As a result, clouds that are near the ground are poor contributors to the greenhouse effect because they absorb and re-emit thermal radiation at nearly the same temperature. Cirrus clouds, on the other hand, are very strong greenhouse contributors because they absorb the relatively high-temperature radiation emitted from the ground surface, but because they are located at a cold temperature, they emit to space only a small fraction of the radiation they have absorbed. This is the basic principle of efficient radiative operation of the greenhouse effect: absorb the up-welling high-temperature radiation, and emit radiation at a much colder temperature. This kind of radiative interaction makes for efficient trapping of heat within the atmosphere below.

5.1 Modeling realism

The modern approach to the study of Earth's climate and of the human impact on climate began in the 1930s with the work of Guy Callendar (Fleming, 1998), a British engineer who very systematically documented the time trend of anthropogenic fossil fuel use and was able to make the connection between fossil fuel burning and the corresponding increase in atmospheric carbon dioxide. However, realistic modeling of the Earth's climate system did not become feasible until the 1960s and 1970s when the availability of high-speed large-memory computing systems began to be applied to the analysis of what is really a very complex problem in atmospheric physics. At present time, capable climate models are being run at dozens of climate centers worldwide. Their modeling task is to simulate the workings of current climate system in great detail. The model generated climate is represented by the global maps and vertical profiles of evolving atmospheric temperature, wind, water vapor, clouds, aerosols, and greenhouse gases. The objective of the modeling effort is to understand how the climate system works. By demonstrating the ability to model the geographic and seasonal patterns and variability of temperature, winds, cloudiness and precipitation, this will establish confidence to model the changes in global climate that are occurring as the result of global warming due to the increase in atmospheric greenhouse gases produced by human industrial activity.

Since the greenhouse problem is largely radiative in nature, it follows that effective radiative modeling is the key. Unfortunately, the spectral absorption properties of greenhouse gases is very complex, consisting of many thousands of individual spectral lines of widely varying strengths, grouped in different sized often overlapping bunches, spread across the entire long-wave spectrum. Moreover, the width of each line is strongly pressure dependent, and there is a temperature dependence of the absorption strength as well. Before the advent of large computers, it was common practice then to rely on empirical formulas and statistical band models to represent the spectral absorption properties of the different atmospheric gases. The atmospheric temperature profile is the one additional, and absolutely essential factor that is required in order to perform the radiative calculations. Given a multi-layered model of the atmosphere, the radiative calculations yield heating rate profiles of solar radiation and cooling rate profiles of thermal radiation. By means of brute force time marching, the results of the heating and cooling rate calculations are applied over a short time interval to recalculate the atmospheric temperature profile until the radiative heating and cooling rates balance each other. Such atmospheric heat balancing calculation (Manabe and Moller, 1961) produce an atmospheric temperature profile that is in radiative equilibrium.

Radiative equilibrium might be adequate to represent the Martian atmosphere, but not that of Earth. The atmospheric lapse rate, or the rate that the atmospheric temperature decreases with height, has a defining role in determining the strength of the terrestrial greenhouse effect. The temperature structure of the atmosphere becomes established as the direct result of radiative heating and cooling, including also the effects of atmospheric dynamics and thermodynamics. If radiation were the only means of energy transport in the atmosphere, given the large thermal opacity of the atmosphere, the resulting temperature gradient needs to be very steep in order to export all of the energy radiated by the ground surface out to space. The greenhouse effect corresponding to such a 'radiation only' atmosphere would be about 66°C (120°F), or about twice its actual value of 33°C (60°F). But such a purely radiative temperature gradient would be dynamically unstable against convection. Convection would set in, and heat energy would be transported upward by a newly enabled parallel means of energy transport to establish a less-steep temperature gradient that would be stable against further convection. This problem was resolved by including a 'convective adjustment' to the atmospheric temperature gradient (Manabe and Strickler, 1964) to produce a realistic profile for the atmospheric temperature, and thus provide a realistic atmospheric structure for the calculation of the radiative fluxes.

5.2 Temperature lapse rate

In the Earth's atmosphere, water vapor plays a very important role in energy transport by convection. This is because water vapor contains latent heat energy which is released to the atmosphere when water vapor condenses, thus making energy transport by convection that much more energetic than by dry gas alone. The net effect of including water vapor in the convective energy transport establishes what is called the 'moist adiabatic' temperature gradient, a very persistent characteristic of the terrestrial atmosphere. It had been noticed from meteorological observations that as temperatures changed, the moisture content in the atmosphere changed by large amounts, but that the relative humidity profile tended to be more stable. By imposing a condition of 'fixed relative humidity' when calculating the

thermal equilibrium of the atmosphere, more realistic temperature profiles could be obtained (Manabe and Wetherald, 1967).

The need to have a realistic atmospheric structure in order to be able to calculate accurate radiative fluxes is self-evident. It is also clear that the terrestrial atmosphere is very complex in both the radiative properties of the atmospheric constituents as well as the atmospheric dynamics and thermodynamics that are involved in producing the resultant temperature structure. In the early models, improvisation and approximation were the rule, primarily because the computer resources to do better were not available. In current state-of-the-art climate models the problems of determining the atmospheric structure, including as well the vertical distribution of water vapor, clouds, greenhouse gases, and temperature, all of which vary geographically and with time, are gradually beginning to be addressed in realistic fashion.

5.3 Current climate models

A rather full description of our current climate modeling capabilities, including the success in our ability to model the terrestrial climate system, and our ability to address the looming problems of global warming and climate change that confront the future of humanity is contained in the *IPCC AR4 (2007) Report of the Intergovernmental Panel on Climate Change* (Solomon et al, 2007). The overall objective is to be able to simulate the basic behavior of the climate system in terms of fundamental physics principles. This means that the evaporation and condensation of water vapor is computed based on local temperature, pressure, wind speed, relative humidity, and surface conditions. Atmospheric winds are calculated from hydrodynamics principles and include dependence on pressure, temperature, topography, and surface roughness. The incident solar radiation is calculated at each geographic point depending on its latitude and longitude, and also includes the effects of changing Earth-Sun distance and variation in orbital parameters. All this is being done with the highest spatial, vertical and time resolution that is supported by current computer speed and memory. This typically means that current climate models might employ a horizontal resolution of 50-500 km, support 20-100 vertical layers, and employ an 0.5-3 hour time resolution. Such climate models generate a lot of simulated 'climate' data which then can be compared to similarly voluminous observational data of spatial and seasonal maps of temperature, water vapor, cloud, and precipitation variations to critically evaluate the climate modeling performance. If a climate model can reproduce the observational data with reasonable fidelity, there is then reason to believe that such a model might be useful for analyzing past trends of climate change, and also in making prediction for the future.

One example of such a model is the GISS ModelE climate model (Schmidt et al., 2006). This climate model can be operated at different resolutions for the horizontal, vertical, and time dimensions. It is coupled to a fully interacting ocean model to provide an accurate rendering of the temporal response of the climate system to changes in radiative forcing. The model produces realistic simulations of current climate temperature, precipitation, water vapor, and clouds. More specifically, the GISS ModelE produces realistic atmospheric temperature profiles, and realistic horizontal and vertical distributions of water vapor and clouds – all the information that is necessary to calculate accurate radiative fluxes and atmospheric heating and cooling rates.

5.4 Radiative transfer modeling

The GISS ModelE radiative transfer model has been specifically designed to render accurate results for the radiative fluxes and the radiative heating and cooling rates throughout the atmosphere for any specified atmospheric temperature structure and absorbing gas and cloud distribution. The starting point for modeling the absorption by atmospheric gases is the HITRAN line atlas (Rothman et al., 2009) which contains absorption line strengths, line positions, widths, and energy levels for several hundred thousand lines for water vapor, carbon dioxide, ozone, and other atmospheric gases. This information is used in line-by-line models to calculate the spectral transmission and absorption by the different greenhouse gases, including the effects of overlapping absorption, with very high precision. The line-by-line results are time consuming, but they serve as the standard of reference to which much faster methods of calculation can be compared and validated for use in climate modeling applications. The correlated *k*-distribution method (Lacis and Oinas, 1991) is a widely used approach for reproducing the line-by-line accuracy to well within 1% for all the greenhouse gases, including an accurate rendering of the non-linearities due to pressure broadening and the overlapping absorption for widely varying absorber amounts. For thermal radiation the effects of multiple scattering are accounted for as parameterized corrections, but they are modeled explicitly for solar radiation. All in all, the GISS modelE radiative transfer modeling is performed with high accuracy, as verified by a wide range of line-byline calculations.

The ModelE radiation treatment has been designed to be both comprehensive and flexible. At each grid point of ModelE, accurate radiative fluxes are calculated at each model time step in response to ever changing temperature profiles, clouds, aerosols, and greenhouse gases. These calculations are performed globally at thousands of grid points, and thousands of times annually. In this way, accurate values of globally and annually averaged fluxes at the ground surface and at the top of the atmosphere are obtained for a more convenient analysis of the terrestrial greenhouse effect and of the global energy balance, results that include a detailed and realistic rendering of the climate system and its seasonal variability. Moreover, with the current computer speed and memory capabilities, all of this data can be stored and reprocessed over and over again. This is where the radiation model flexibility comes into play. All of the different greenhouse gases, clouds, and aerosols can individually be selected or zeroed out, and the radiative calculations repeated to obtain a quantitative measure of the non-linear effects of overlapping absorption by different combinations of greenhouse gases.

5.5 Greenhouse warming attribution

While it is important to have an accurate measure of the total greenhouse strength for our current-climate atmosphere, it is equally important to have a clear understanding of the relative contribution that each of the atmospheric constituents makes to the total strength of the greenhouse effect. This task was performed with the GISS ModelE (Schmidt, et al., 2010) whereby the radiative effects of the different atmospheric constituents were evaluated individually one by one, so as to determine their relative importance. The results of these calculations are summarized in Table 2.

LW absorber	single-addition		single-subtraction		normalized average	
	W/m²	fraction	W/m²	fraction	W/m²	fraction
H_2O	94.7	.458	59.8	.534	74.7	.490
cloud	56.2	.272	23.2	.207	37.3	.244
CO_2	40.3	.195	24.0	.214	31.0	.203
O_3	4.0	.019	1.7	.015	2.7	.018
N_2O	4.1	.020	1.5	.013	2.6	.017
CH_4	3.5	.017	1.2	.011	2.2	.014
CFCs	1.0	.005	0.2	.002	0.6	.004
aerosol	3.0	.014	0.4	.004	1.5	.010
sum	206.8	1.000	112.0	1.000	152.6	1.000

Table 2. Single-addition & single-subtraction LW flux changes. (After Lacis et al., 2010)

The results in Table 2 were obtained by starting with a one-year's worth of ModelE climate data which had been run to equilibrium for 1980 atmospheric conditions. For this model, the globally averaged annual-mean long-wave up-welling flux at the ground surface was 393.9 W/m² (T_S = 288.7 K), and the long-wave flux at the top of the atmosphere emitted to space was 241.3 W/m² (T_E = 255.4 K), with the total strength of the greenhouse effect G_F = 152.6 W/m² (G_T = 33.3 K). Upon zeroing out all atmospheric absorbers, the outgoing long-wave flux to space was that emitted by the ground surface, 393.9 W/m². The absorbers were then added in individually one at a time, and the reduction in outgoing flux re-evaluated. These are the global annual mean flux changes listed in the left hand single-addition column. Thus, water vapor by itself reduced the outgoing flux by 94.7 W/m², cloud alone by 56.2 W/m², carbon dioxide alone by 40.3 W/m², with smaller amounts for the minor greenhouse gases. The sum of these single-addition contributions adds up to 206.8 W/m², indicative of the substantial effect of non-linear overlapping absorption since the sum total flux reduction with all greenhouse gases acting together is 152.6 W/m². In the second column these fractional single-addition contributions have been normalized to unity.

Similarly, the single-subtraction columns were obtained by subtracting each individual atmospheric absorber one at a time from the full compliment of absorbers. In this case, the reference top of the atmosphere outgoing long-wave flux was 241.3 W/m². By removing water vapor alone, the flux emitted to space increased by 59.8 W/m², 23.2 W/m² for cloud alone, 24.0 W/m² for carbon dioxide alone, with smaller amounts for the minor contributors. Again, because of non-linear overlapping absorption effects, the individual flux changes only sum to 112.0 W/m², instead of 152.6 W/m². The single-subtraction results are similarly normalized to unity.

The single-addition and single-subtraction results are then weighted by their closeness to the equilibrium G_F value. Thus, by taking 0.572 times the group-subtraction values plus 0.428 times the single-addition values, we arrive at the normalized average results for the radiative flux and corresponding fractional contributions to the total greenhouse effect by

the individual greenhouse contributors. In round numbers, of the total greenhouse effect for the current climate atmosphere, about 50% is directly attributable to water vapor, 25% to clouds, 20% to carbon dioxide, and the remaining 5% due to the minor greenhouse gases, i.e., methane, nitrous oxide, ozone, and chlorofluorocarbons.

5.6 Forcing/feedback significance

The most important conclusion to be drawn from this greenhouse attribution is that the individual radiative flux contributions to the total greenhouse effect can be gainfully subdivided into two separate groups: (1) the thermodynamically inactive non-condensing greenhouse gases (carbon dioxide and the other minor trace gases), which basically remain in the atmosphere once they enter there; and (2) the thermodynamically active condensing species (water vapor and clouds), which evaporate, condense, and precipitate, and thus respond quickly to changes in local temperature and other meteorological conditions. To be sure, the non-condensing greenhouse gases do interact chemically, but these chemical reactions are slow acting processes that result in atmospheric life times ranging from a decade to longer than several centuries. Because of this, the non-condensing greenhouse gases effectively behave as permanent fixtures of the atmosphere, and as such, provide a steady amount of radiative heating that is largely independent of varying meteorological conditions. The condensing species, on the other hand, adjust rapidly to changes in meteorological conditions, behaving as feedback effects that seek to establish the maximum allowable equilibrium concentration in accordance with the background atmospheric temperature structure that is provided by the non-condensing greenhouse gases.

Accordingly, the amount of water vapor that the atmosphere can sustain is temperature dependent, as dictated by the Clausius-Clapeyron equation. Basically, this means that a warmer atmosphere can sustain more water vapor, and a colder atmosphere less. Possession of strong long-wave absorption bands by water vapor make water vapor a strong positive feedback in response to radiative forcing produced by the non-condensing greenhouse gases. Since clouds are closely dependent on the amount of available water vapor, clouds are likewise classified as part of the fast feedback processes, with the added complication that clouds also reflect solar radiation, a cooling effect that offsets the cloud greenhouse effect. From these climate modeling analyses it is clear that the non-condensing greenhouse gases provide the sustaining radiative forcing for the terrestrial greenhouse effect, but that water vapor and clouds, in their role as climate feedbacks, act as amplifiers (by about a factor of four) of the radiative forcing provided by the non-condensing gases.

As further evidence to emphasize this very point, recent climate modeling experiments were performed to demonstrate even more clearly the feedback role of water vapor and clouds in the current climate system (Lacis et al., 2010). In these experiments all of the non-condensing greenhouse gases were set to zero. Without the radiative forcing temperature support by the non-condensing greenhouse gases, excess atmospheric water vapor rapidly condensed and precipitated from the atmosphere, plunging the Earth inevitably toward an ice bound state. This was a clear-cut demonstration that the non-condensing greenhouse gases do indeed control the magnitude of the terrestrial greenhouse effect. Since carbon dioxide is by far the

strongest of the non-condensing greenhouse gases in the atmosphere, the argument can be effectively made that carbon dioxide is indeed the principal control knob that governs the temperature of Earth. This has important consequences and bearing on our understanding of current climate change as well as the changes in climate that have taken place over geological time scales.

5.7 Present-day perspective

It is illuminating to examine the historically recent change in atmospheric carbon dioxide in the broader geological context. The ice core record shows that during the last ice age, when the global temperature was roughly 5°C (9°F) colder than current climate, the atmospheric carbon dioxide was at levels near 180 ppm. In fact, the Vostoc ice core data show four major ice-age cycles during the 420,000 year time span with the carbon dioxide level peaking near 280 ppm during the relatively brief interglacial warm interludes when global temperatures were similar to present day conditions. During the coldest extremes of the ice-age cycle, the carbon dioxide level is seen to drop to its lowest levels near 180 ppm. Hansen has used this geological data to establish an empirically based sensitivity to radiative forcings for the fast-feedback processes of the climate system. In his ice-core data analysis, Hansen finds the terrestrial climate sensitivity to be such that the global surface temperature warms about 3°C per 4 W/m² of radiative forcing.

The significance of all this information is becoming ever more clear, pointing to a growing global warming climate crisis. The geological record and climate modeling analyses show that carbon dioxide is indeed the principal control knob, or thermostat, that is instrumental in governing the temperature of Earth through its controlling influence on the terrestrial greenhouse effect.

The inescapable conclusion is that the anthropogenic forcings continue to add onto the growing strength of the terrestrial greenhouse effect. The continuing high rate of increase in atmospheric carbon dioxide is particularly worrisome because the present levels are near 390 ppm, far in excess of the more typical 280 ppm for the interglacial maxima. This raises concern of an approaching a 'tipping point', thought to be about 450 ppm, beyond which the radiative equilibrium of the Earth would no longer be capable of sustaining polar icecaps (Hansen et al., 2007). Moreover, since the atmospheric residence time of carbon dioxide is very long, and measured in centuries, this makes the reduction of atmospheric carbon dioxide a difficult undertaking once a decision is eventually reached to limit or reverse the growth of carbon dioxide emissions.

The present biosphere has not experienced climate under such levels of atmospheric carbon dioxide, so there is cause for concern regarding the survival rate of many species under the impending changes in Earth's climate that are being forced by human industrial activity. Because of the very large heat capacity of the ocean, full impact of these radiative forcings is slow to materialize, raising the false hope that climate change is not serious, and may not even be happening. Such opinions stem from the significant uncertainties in modeling the rate at which the climate is changing. Because of the non-linearities in feedback interactions, there is additional uncertainty in regard to sensitivity of the climate feedbacks that act to determine the magnitude of the eventual change in climate. Still

larger uncertainties abound in modeling the space-time response of the climate system because horizontal energy transports tend to be several orders of magnitude larger than corresponding greenhouse gas radiative forcings that are the ultimate instigators of global climate change.

While there remain legitimate uncertainties regarding the details of time specific, local, and regional global climate change, these uncertainties should not be projected onto the solid evidence that human industrial activity is busy driving Earth's climate into uncharted territory. The atmospheric carbon dioxide control knob is currently being turned at a much faster rate than ever before.

In view of the pivotal role that carbon dioxide plays in governing the global temperature of Earth, a great deal of attention has being focused on obtaining accurate measurements of atmospheric carbon dioxide, and how carbon dioxide has been changing with time. In 1958, Charles Keeling, a research chemist at Scripps Institute in California, began making such high-precision measurements of carbon dioxide and of the other greenhouse gases such as methane and nitrous oxide. These very high precision measurement techniques have been subsequently applied to measuring the gaseous composition of air bubbles trapped in glacial ice, thereby extending knowledge of atmospheric composition over time scales that go back more than 420,000 years, as in the Antarctic Vostoc ice-core data. These ice-core measurements show that the atmospheric concentration of carbon dioxide has increased from its pre-industrial level of 280 parts per million in 1850 to the present value near 390 ppm, and exhibits a steady rate of increase by about 2 ppm per year.

5.8 Future prospects

The problem that we face today, has been described by James Hansen in his book *Storms of my Grandchildren*. The problem is that carbon dioxide is not only the principal thermostat that governs the global temperature of Earth, carbon is also the principal fuel that powers the human civilization. It is expected that at the current rate of fossil fuel use, the critical level of 450 ppm for carbon dioxide will be reached in about thirty years. Clearly, the thermal inertia of the ocean and the polar ice caps is very large, and it would take many centuries for the polar ice to melt. But upon reaching 450 ppm for atmospheric carbon dioxide, the terrestrial climate will be set on a collision course where the Earth will no longer be able to support polar ice caps. And the obvious implication of this is the eventual rise in sea level by some 70 meters, which would inundate most of the land areas where civilization resides.

Fortunately, because of the very large heat capacity of the ocean, there is still some time for humans to react and bring the global warming problem under control. While the radiative forcing attributable to the carbon dioxide that is being added to the atmosphere is felt instantaneously, the surface temperature change associated with this increase in radiative forcing materializes more slowly. Thus, about 40% of the global equilibrium temperature response materializes in about 5 years as the ocean mixed layer warms in response to the applied forcing. As the heat begins to diffuse downward into the deep ocean, about 60% of the total temperature response is reached in about 100 years, with approach to the 100% level taking several thousand years. It should also be noted that the

enhancement of the greenhouse effect by water vapor and cloud feedbacks (the fast feedback processes) is not directly in response to the amount of carbon dioxide in the atmosphere per se, but rather to the change in temperature that is generated by the carbon dioxide increase.

There is also substantial natural variability within the climate system that produces global temperature fluctuations by several tenths of a degree on inter-annual and decadal time scales, including climate system response to the 11-year sunspot cycle. However, all of these temperature fluctuations are relative to a zero reference point, while the steady increase in the strength of the terrestrial greenhouse effect continues unabated. These fluctuations produce random looking changes in global temperature that tend to mask and obscure the steadily increasing global warming signal of carbon dioxide. Perhaps of more immediate concern are the likely prospects for an increase in the weather extremes such as more severe droughts and more severe floods, all fueled by the greater energy that is being added to the hydrological cycle as the global temperature rises and atmospheric water vapor increases. The more menacing future concern is the inevitable rise in sea level.

There is no mistaking the fact that the level of atmospheric carbon dioxide is increasing, and this continued increase causes the strength of the terrestrial greenhouse effect to keep on increasing. Accordingly, there is no viable alternative to counteract the impending effects of global warming except through direct human action to reduce the level of atmospheric carbon dioxide, to control the strength of the terrestrial greenhouse effect which ultimately determines the surface temperature of Earth and the global climate that results therefrom.

5.9 Public perception

Assessing the real cause and the perceived reality of global climate change has become a heated topic in the public discourse, particularly in the United States. Global warming has been denounced as the "greatest hoax ever" by prominent Senators and Congressmen. There are well organized efforts funded by fossil fuel interests to discredit climate science and to promote discord and mistrust in the public mind. The presumed rationale for this anti-climate science crusade by fossil fuel interests is perhaps similar to the reaction of the tobacco industry in response to the linking of deleterious health impacts to smoking. In their thinking, if global warming is determined to be harmful to human interests, the pressure to limit carbon dioxide emissions will be harmful to fossil fuel financial interests. On the other hand, there are environmental groups who already perceive global warming as a brewing environmental disaster that is already happening. They are demanding immediate action to curtail the use of fossil fuels. This brawling has attracted the attention of a broad spectrum of individuals from many different disciplines weighing in with opinions and suggestions as to how best understand what is really happening with global climate.

The terrestrial climate system however is very complex, and is not really amenable to simple analyses and interpretations. So, for example, performing a 'more sophisticated' statistical analysis of the global temperature record will not yield quantitative attribution as the cause of global warming because the existing temperature record is much too short, and there are too many causative factors that are not adequately accounted for that impact the global

temperature. Also, sufficiently precise measurements that would definitively describe what is happening in the climate system are not available. And, there are aspects of the climate system, particularly interactions of the atmosphere with ocean dynamics that give rise to the so-called natural variability that is still not fully understood. All of this provides plenty of room for rampant skepticism to flourish.

There are, nevertheless, some important aspects of the ongoing global climate change that are understandable in fairly simple basic physics terms. Global warming, the steadily increasing component of global climate change, is specifically linked to the growing strength of the greenhouse effect. Thus, it is the greenhouse effect that is at the very center of the global warming controversy, and it is also the component that is most readily understandable in basic physics terms.

6. Conclusion

There is a close analogy to be drawn between the way an ordinary thermostat maintains the temperature of a house, and the way that atmospheric carbon dioxide (and the other minor non-condensing greenhouse gases) control the global temperature of Earth. Atmospheric carbon dioxide performs a role that is similar to that of the house thermostat in setting the equilibrium temperature of the Earth. It differs from the house thermostat in that carbon dioxide itself is a potent greenhouse gas, warming the ground surface by means of the greenhouse effect. It is this sustained warming that enables water vapor and clouds to maintain their atmospheric distributions as the so-called feedback effects that amplify the initial warming provided by the non-condensing greenhouse gases. It is also important to keep in mind that the house thermostat merely turns the furnace on and off, and that the heat capacity of the house requires minutes before the house temperature responds to the thermostat setting. The climate system similarly has a delayed response to forcing.

Within only the past century, the carbon dioxide control knob has been turned sharply upward toward a much hotter global climate. The pre-industrial level of atmospheric carbon dioxide was about 280 ppm, which is representative of the inter-glacial maximum level of atmospheric carbon dioxide. During ice age extremes, the level of carbon dioxide drops to near 180 ppm, for which the global temperature is about 5 °C colder. The rapid recent increase of atmospheric carbon dioxide has been attributed to human industrial activity, primarily due to the burning of fossil fuels has pushed the carbon dioxide level to near the 390 ppm, far beyond the inter-glacial maximum. The climate system is trying to respond to the new setting of the global thermostat, and this response has been the rise in global surface temperature by about 0.2 °C per decade for the past three decades.

It has been suggested that we are well past the 300 to 350 ppm target level for atmospheric carbon dioxide beyond which dangerous anthropogenic interference in the climate system would be expected to exceed the 25% risk tolerance for impending degradation of land and ocean ecosystems, sea level rise, and inevitable disruption of the socio-economic and food-producing infrastructure (Hansen et al., 2008). This prospect of a rising risk of triggering unacceptable environmental consequences makes reduction and control of atmospheric carbon dioxide a serious and pressing issue for humanity, one that is worthy of real-time attention.

The bottom line is that atmospheric carbon dioxide has been a thermostat in regulating the temperature of Earth throughout the entire geological history of Earth. The present-day exceedingly rapid increase in atmospheric carbon dioxide due to human industrial activity is unprecedented in the geological record. It is setting the course for continued inevitable global warming that will eventually melt the polar ice caps to produce a catastrophic sea level rise if left unchecked. The large heat capacity of the ocean provides ample time for humans to forestall a climate disaster. Since humans have been responsible for changing the level of atmospheric carbon dioxide, they are then also in control over the thermostat that controls the global temperature of the Earth. Humans are at a difficult crossroad. Carbon dioxide is the lifeblood of civilization as we know it. It is also the direct cause fueling an impending climate disaster. There is no other viable alternative that will counteract global warming except direct human effort to reduce the atmospheric carbon dioxide level.

7. References

Arrhenius, S. (1896). On the influence of carbonic acid in the air upon the temperature of the ground, *Philosophical Mag*., 41: 237-276.

Berner, R.A. (2004). *The Phanerozoic Carbon Cycle: CO_2 and O_2*. Oxford U Press, New York.

Christianson, G.E. (1999). *Greenhouse*, Walker & Company.

Fleming, J.R. (1998). *Historical Perspectives on Climate Change*, Oxford University Press.

Fourier, J. (1824). Remarques générales sur les températures du globe terrestre et des spaces planétaires, *Annales de Chemie et de Physique*, 27: 136-167.

Hansen, J., et al., (2007). Dangerous human-made interference with climate: A GISS modelE study. *Atmos. Chem. Phys*., 7, 2287-2312, doi:10.5194/acp-7-2287-2007.

Hansen et al., J.E. (2008). Target atmospheric CO_2: Where should humanity aim? *Open Atmos. Sci. J*., 2: 217-231.

Hansen, J.E. (2009). *Storms of my Grandchildren*, Bloomsbury USA, New York.

Kirschvink, J. L. (1992). In *The Proterozoic Biosphere: A Multidisciplinary Study*. D. Des Maris, ed., Cambridge U Press, Cambridge, U.K. 51.

Lacis et al., A. A. (2010). Atmospheric CO_2: Principal control knob governing Earth's temperature, *Science*, 300: 356-359, doi:10.1126/science.1190653.

Lacis, A.A., and M.I. Mishchenko, (1995). Climate forcing, climate sensitivity, and climate response: A radiative modeling perspective on atmospheric aerosols. In *Aerosol Forcing of Climate: Report of the Dahlem Workshop on Aerosol Forcing of Climate, Berlin 1994, April 24-29*. R.J. Charlson and J. Heintzenberg, Eds. John Wiley Sons.

Lacis, A.A. and V. Oinas (1991) . A description of the correlated k distributed method for modeling nongray gaseous absorption, thermal emission, and multiple scattering in vertically inhomogeneous atmospheres. *J. Geophys. Res*., 96: 9027-9063.

Manabe S. and F. Moller (1961). On the radiative equilibrium and heat balance of the atmosphere, *Mon. Wea. Rev.* 89: 503-532.

Manabe S. and R.F. Strickler (1964). Thermal equilibrium of the atmosphere with a convective adjustment, *J. Atmos. Sci.* 21: 361-376.

Manabe S. and R.T. Wetherals (1967). Thermal equilibrium of the atmosphere with a given distribution of relative humidity, *J. Atmos. Sci*. 24: 241-259.

McKay, C.P., J.B. Pollack and R. Courtin (1991). The greenhouse and anti-greenhouse effects on Titan, Science, 253: 118-1121.

Rothman, L.S. et al., (2009). The HITRAN 2008 molecular spectroscopic database. *J. Quant. Spectrosc. Radiat. Transfer*, 110: 533–572.

Schmidt et al., G.A. (2010). Attribution of the present-day total greenhouse effect, *J. Geophys. Res*., 115: D20106, doi:10.1029/2010JD014287.

Solomon, S. et al. (2007). *Contribution of Working Group I to the Fourth Assessment Report of the Intergovernmental Panel on Climate Change*, Cambridge University Press.

14

Regional-Scale Assessment of the Climatic Role of Forests Under Future Climate Conditions

Borbála Gálos[1] and Daniela Jacob[1,2]
[1]*Max Planck Institute for Meteorology, Hamburg*
[2]*Climate Service Center–eine Einrichtung am Helmholtz-Zentrum Geesthacht*
Germany

1. Introduction

1.1 Regional climate projections for Europe

Several natural and anthropogenic processes influence the climate of the Earth. Human affect climate through increasing greenhouse gas concentrations, changing aerosol compositions as well as by land surface changes (IPCC, 2007). There are several recent EU-projects carried out in the last decade, to provide high-resolution climate change projections with focus on future climate changes and their impacts in Europe (Christensen et al., 2007; Jacob et al., 2008; van der Linden & Mitchell, 2009). These studies are based on the results of regional climate model simulations driven by different predefined greenhouse gas emission scenarios. The difference between the simulated climatic conditions for the future and for the present time period is the climate change signal. For the 21st century, projected climate change signals for temperature and precipitation show seasonal and spatial differences in Europe and also vary depending on the applied greenhouse gas emission scenario.

For the period 2021-2050 all regional climate models predict a quite robust (i.e. above the noise generated by the internal model variability and consistent across multiple climate models – Hagemann et al., 2009) surface warming in central and eastern Europe. The annual precipitation shows an increase in the northeastern and a decrease in the southwestern regions. The transition (neutral) zone (e.g. Hungary, Rumania) can be characterized by the largest spread between models (Christensen & Christensen, 2007; Kjellström et al., 2011), where precipitation changes are quite small.

At the end of the 21st century, a warming is expected in all seasons over Europe, which is stronger than in the first half of the 21st century. All models agree that the largest warming for summer is projected to occur in the Mediterranean area, southern France and over the Iberian Peninsula. Less warming is projected over the Scandinavian regions. For winter the maximum warming occurs in eastern Europe (Giorgi et al., 2004; Christensen & Christensen, 2007). For precipitation, the largest increase is projected in winter, whereas the decrease is the strongest in summer. Changes in the intermediate seasons (spring and autumn) are less pronounced. Results of the regional model simulations show a north-south gradient of annual precipitation changes over Europe, with positive changes in the north (especially in winter) and negative changes in the south (especially over the Mediterranean area in summer). The line of zero change moves with the seasons (Kjellström et al., 2011). For

southern and central Europe the spatial distribution of the projected temperature and precipitation changes in summer refer to a marked shift towards a warmer and drier climate (Vidale et al., 2007; Beniston, 2009). Recent results from enhanced greenhouse gas emission scenario simulation over Europe suggest that not only the climatic means are changing, but there is also an increase in the inter-annual variability of the future temperature and precipitation values, which leads to higher probability of extremes compared to the present-day conditions (Schär et al., 2004; Giorgi et al., 2004; Seneviratne et al., 2006; Beniston et al., 2007; Kjellström et al., 2007; Vidale et al., 2007; Fischer & Schär 2010).

The most commonly used IPCC-SRES (Intergovernmental Panel on Climate Change – Special Report on Emission Scenarios) emission scenarios for these studies are the B1, A1B, A2. In the first half of the 21st century, the climatic impact of these greenhouse gas emission scenarios are quite similar (van der Linden & Mitchell, 2009). But the temperature difference increases by mid-century with greatest warming in A2 and least warming in B1 (IPCC, 2007).

1.2 Climatic effects of land use and land cover change

Temperature and precipitation play an important role in determining the distribution of the terrestrial ecosystems that in turn interact with the atmosphere through biogeophysical and biogeochemical processes. Vegetation affects the physical characteristics of the land surface, which control the surface energy fluxes and hydrological cycle (biogeophysical feedbacks; Pielke et al., 1998; Brovkin, 2002; Pitman, 2003; Betts, 2007; Anderson et al., 2010). Through biogeochemical effects, ecosystems alter the biogeochemical cycles, thereby change the chemical composition of the atmosphere (Betts, 2001; Bonan, 2002; Pitman, 2003; Bonan, 2004; Feddema et al., 2005). Forests have larger leaf areas and aerodynamic roughness lengths, lower albedo and deeper roots compared to other vegetated surfaces. They sequester carbon thereby alter the carbon storage of land.

Depending on the region, biogeophysical and biogeochemical feedbacks of land cover on climate can amplify or dampen each other (Arora & Montenegro, 2011). Through these land-atmosphere interactions changes of the land cover and land use due to natural and human influence alter climate and hence can lead to the enhancement or reduction of the projected climate change signals expected from increased atmospheric CO_2 concentration (Feddema et al., 2005; Bonan, 2008). Long term studies show that land use and land cover changes have much weaker influence on the atmospheric circulation compared to greenhouse-gas forcings (Betts, 2007; Göttel et al., 2008; Wramneby et al., 2010; Arora & Montenegro, 2011). However, in smaller areas and in regions with strong land-atmosphere interactions the feedback processes can significantly affect and modify the weather and climate, the temperature and precipitation variability (Seneviratne et al., 2006; Seneviratne et al., 2010).

This section focuses on studies of the biogeophysical processes, which represent the contrasting climatic effects of forest cover changes on different regions, seasons and time scales. Changes of vegetation cover under future climate conditions enhance the warming trend in Scandinavian Mountains as well as the drying trend in southern Europe, but mitigate the projected increase of temperature in central Europe (Wramneby et al., 2010). Boreal forests have the greatest biogeophysical effect of all biomes on annual mean global temperature, which is larger than their effect on the carbon cycle (Bonan, 2008). If snow is present, the darker coniferous forest masks the snow cover. It is resulting in lower surface albedo compared to tundra vegetation or bare ground, which leads to higher winter and spring air temperatures (Bonan et al., 1992; Brovkin, 2002; Kleidon et al., 2007; Göttel et al., 2008).

Consequently, the change of vegetation from tundra to taiga under future climate conditions amplifies the global warming. Tropical forests maintain high rates of evapotranspiration. In this region, surface warming arising from the low albedo of forests is offset by the strong evaporative cooling that reduces global temperature increase (Bonan, 2008).

In temperate forests the albedo and evaporative forcings are moderate compared to boreal and tropical forests (Bala et al., 2007; Bonan, 2008; Jackson et al., 2008). Climate model studies for the temperate regions showed that replacing forests with agriculture or grasslands reduces the surface air temperatures (Bonan, 1997; Bounoua et al., 2002; Oleson et al., 2004) and the number of summer hot days (Anav et al., 2010). Other studies show opposite results, where temperate forests cool the air compared to grasslands and croplands and contribute to higher precipitation rates in the growing season (Copeland et al., 1996; Hogg et al., 2000; Sánchez et al., 2007). In the Mediterranean region climatic effects of forest cover change can also vary during the summer months (Heck et al., 2001). In the period from April until mid-July potential vegetation cover conditions led to cooler and moister conditions due to the increase of evapotranspiration. In mid-July soil moisture dropped below the critical value and transpiration was almost completely inhibited. It resulted in dryer and warmer summer accelerating the projected climate change. Teuling et al. (2010) pointed out that the role of the forests in the surface energy and water budget is depending on the selected time scale: in the short term, forests contribute to the increase of temperature, but on longer time scales they can reduce the impact of extreme heat weaves.

These studies indicate that forests can enhance or dampen the climate change signal depending on various contrasting vegetation feedbacks, which can diminish or counteract each other. Furthermore the variability of the climatic, soil and vegetation characteristics as well as the description of the land surface processes in the applied climate model also have an influence on the simulated vegetation-atmosphere interactions.

1.3 Research foci

The climatic feedbacks of land cover changes due to climate change and the regional land use politics as well as the role of the forests in the climate change mitigation on country scale are still unknown. Fine scale studies are essential not only for the assessment of the climate protecting effects of forests, but also for the development of adaptation strategies in forestry, agriculture and water management for the next decades.

In order to address this topic, our sensitivity study is focusing on the climatic effects of afforestation in Europe under future climate conditions based on the following research questions:

- In which regions does the increase of forest cover enhance/reduce the projected climate change?
- How big are the effects of forest cover change on the summer precipitation and temperature relative to the climate change signal?
- Which are the regions, where afforestation is the most beneficial from a climatic point of view?

On country scale, a more detailed case study has been carried out for Hungary. For the end of the 21st century, regional climate model simulations project a significant increase of summer temperature and a decrease of summer precipitation (Bartholy et al., 2007; Gálos et al., 2007;

Jacob et al., 2008; Szépszó, 2008; Radvánszky & Jacob, 2009). From ecological point of view Hungary (in the southeastern part of central Europe) has been selected as study region because here, many of the zonal tree species have their lower limit of distribution (Mátyás et al., 2009; Mátyás, 2010; Mátyás et al., 2010), which are especially sensitive and vulnerable to the increase of the frequency of climatic extremes, primarily droughts. In these forests the more frequent and severe droughts at the end of the 20th century already resulted in growth decline, loss of vitality and the decrease of the macroclimatically suitable area of distribution (Berki et al., 2009). Under the projected climate conditions these species may disappear from this region (Berki et al., 2009; Mátyás et al., 2010; Czúcz et al., 2011).

In the last 50 years, large scale afforestation was carried out in Hungary, which is planned to continue also in the near future. The influence of the historical land cover change on weather and climate has been investigated by Drüszler et al. (2011). For the future, forests can also have an important role in the adaptation to climate change. Therefore this case study is concentrating on the possible mitigation of the strong warming and drying of summers projected for the second half of the 21st century. The assessment of the maximal climatic effects of afforestation is addressing the following research questions:

- Which regions are the most affected by climate change for the end of the 21st century?
- In which part of the country can forests play an important role in reducing the projected tendency of drying?

In order to answer the scientific questions the chapter is organized as follows: in section 2 the applied model and experimental set up and the main steps of the analyses are described. Results are presented in section 3: in 3.1 the sign of the climatic effect of emission change and potential afforestation has been studied for precipitation and temperature. In section 3.2 the most climate change affected regions as well as the areas characterized by the largest climatic effects of forest cover increase have been determined. In section 3.3 the magnitude of the climatic feedbacks of afforestation is analyzed relative to the magnitude of the climate change signal. Section 3.4 introduces the country scale effects of maximal afforestation in Hungary. Results are summarized, conclusions are drawn and the possibilities for the practical application are stressed in section 4.

2. Methods

Regional climate models have the potential to provide detailed information about the future climate on fine horizontal resolution. For studying the climatic feedbacks of land cover change in Europe regional scale analyses are essential because of the differences in the climate sensitivity among regions and the large spatial variability of the land surface properties and the related processes.

2.1 The regional climate model REMO – General characteristics and land surface parameterization

In this study the REgional climate MOdel (REMO) has been applied for Europe, with horizontal resolution 0.22°. REMO (Jacob, 2001; Jacob et al., 2001; Jacob et al., 2007) is a regional three-dimensional numerical model of the atmosphere. It is based on the 'Europamodell', the former numerical weather prediction model of the German Weather Service, DWD (Majewski, 1991). The calculation of the prognostic variables is based on the

hydrostatic approximation. The physical parameterizations from the global climate model ECHAM4 are implemented at the Max Planck Institute for Meteorology in Hamburg (Roeckner et al., 1996) in the regional model.

Land surface processes in REMO are controlled by physical vegetation properties. For each land cover type the parameter values of leaf area index and fractional vegetation cover for the growing and dormancy season, background albedo, surface roughness length due to vegetation, forest ratio, plant-available soil water holding capacity and volumetric wilting point are allocated in the global dataset of land surface parameters (Hagemann et al., 1999; Hagemann, 2002). In the current model version the vegetation phenology is represented by the monthly varying values of the leaf area index and vegetation ratio. The mean climatology of the annual cycle of background albedo is also implemented (Rechid & Jacob, 2006, Rechid et al., 2008a, 2008b). The other land surface parameters remain constant throughout the year. Land cover change in REMO can be implemented by modification of the characteristic land surface parameters.

2.2 Experimental setup

The simulations have been carried out for Europe (figure 1), with 0.22° horizontal grid resolution. REMO was driven with lateral boundary conditions from the coupled atmosphere–ocean GCM ECHAM5/MPI-OM (Roeckner et al., 2006; Jungclaus et al., 2006).

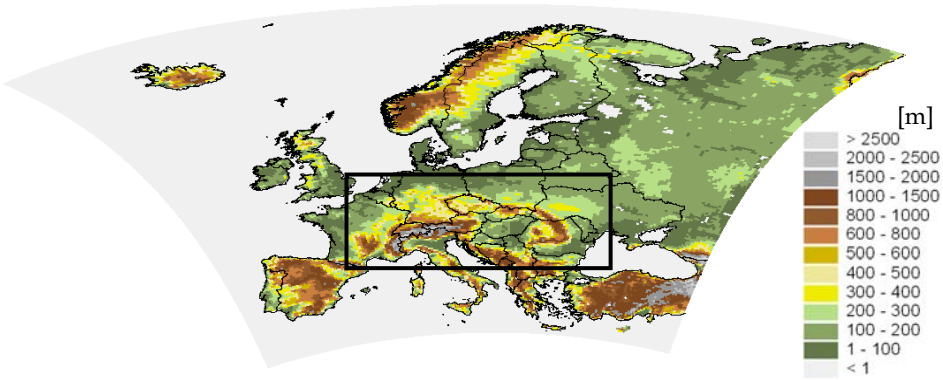

Fig. 1. Simulation domain. The smaller domain applied for the Hungarian case study is marked with rectangle

The following experiments have been performed (table 1):

- *Reference simulation* for the past (1971-1990) with present (unchanged) forest cover.
- *Emission scenario simulation* for the future (2071-2090) with present (unchanged) forest cover applying the A2 IPCC-SRES emission scenario[1] (Houghton et al., 2001; Nakicenovic et al., 2000). This experiment was the reference simulation to the land cover change study.

[1] A2: continuously increasing global population and regionally oriented economic growth that is more fragmented and slower than in other storylines.

- *Potential afforestation* experiment for 2071-2090. The forest cover increase (figure 2) is based on the net primary production map for Europe derived from remotely sensed MODIS (Moderate-Resolution Imaging Spectroradiometer) products, precipitation and temperature conditions from the Wordclim database and soil conditions from the International Institute for Applied Systems Analysis (Kindermann, pers. comm.). The new afforested areas were assumed to be deciduous.

Experiment	*Reference simulation*	*Potential afforestation simulation*
Characteristics	Present forest cover	Afforestation over all vegetated area [a]
Time period	1971-1990 2071-2090	2071-2090
Greenhouse gas forcing	IPCC-SRES emission scenario A2	
Horizontal resolution	0.22°	
Lateral boundaries	ECHAM5/MPI-OM[b]	

[a] based on Kindermann (pers. comm.)
[b] Roeckner et al., 2006; Jungclaus et al., 2006

Table 1. Analyzed data and time periods

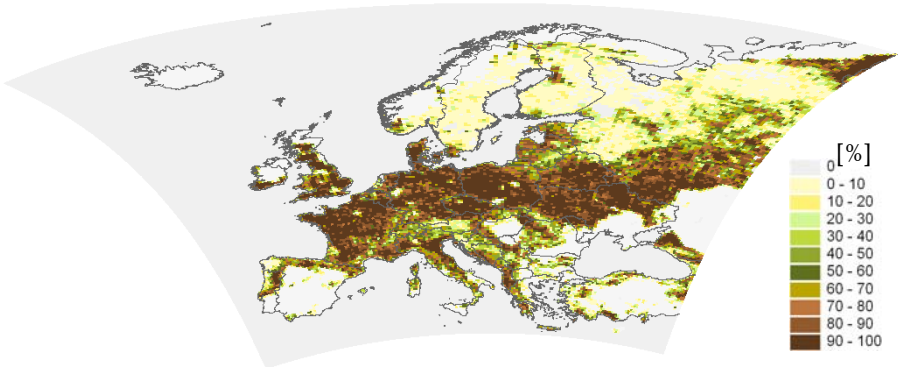

Fig. 2. Increase of the forest cover in the potential afforestation simulation compared to the present forested area in the model

2.3 Main steps of the analyses

These analyses are focusing on the biogeophysical feedbacks of afforestation on the climate. Corresponding to the forest cover increase in all grid boxes the new distribution of the land cover categories has been determined and a new land surface parameter set has been calculated. Simulation results have been analyzed for May, June, July and August. In this study the mean of this period is considered '*summer*' (MJJA), because in these months water availability is especially important for the vegetation growth. The leaf area index of the deciduous forests reaches its maximum, which has a strong control on the land-atmosphere interactions.

Climate change due to emission change has been investigated analyzing the summer precipitation sums and 2m-temperature means for 2071-2090 (without any land cover changes) compared to 1971-1990.

Climate change due to potential afforestation has been calculated comparing the simulation results with- and without forest cover increase for the future time period (2071-2090).

Climate changes due to emission changes and potential afforestation has been determined comparing the results of the potential afforestation experiment (2071-2090) to the reference study in the past (1971-1990). The sign and the magnitude climatic effects of potential afforestation have been analyzed relative to the climate change signal. Regional differences in the climate change altering effect of afforestation have been determined and investigated for two selected regions.

For more detailed analyses, a case study has been prepared for Hungary over a smaller simulation domain (figure 1), applying the same regional climate model and the same steps for data analyses. Climate change due to emission change has been calculated for 2071-2100 compared to the 30-year time period in the past (1961-1990). The A1B IPCC-SRES emission scenario[2] (Houghton et al., 2001; Nakicenovic et al., 2000) has been applied, which represents the average estimation for the analyzed region. To get information about the maximum climatic effects of afforestation and its regional differences, the whole vegetated area of Hungary was assumed to be forest and the new afforested areas are all deciduous. Over the simulation domain (marked in figure 1), forest cover has been changed only in Hungary. The assumed maximal afforestation takes approximately 75 % increase of forest cover in country mean additionally to the existing 20 % forested area (figure 3).

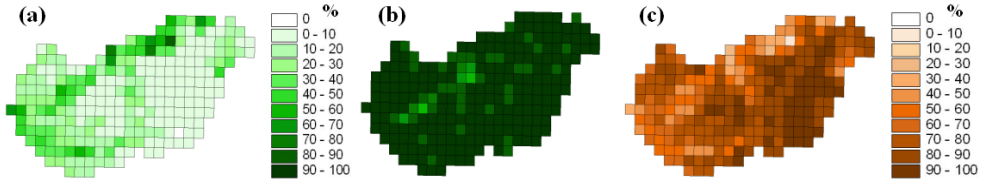

Fig. 3. Forest cover in Hungary in the reference simulation (a) and in the maximal afforestation experiment (b). Increase of forest cover in the maximal afforestation experiment compared to the reference (c). Adapted from: Gálos et al., 2011

A Mann-Whitney–U-Test (Mann & Whitney, 1947) was applied to test the significance of the climatic effects of afforestation and emission change. This is a ranking test, which does not assume a normal distribution.

3. Results

3.1 Sign of the climatic effects of emission change and potential afforestation

The climate change signals without any land cover changes have been analyzed for summer temperature means and precipitation sums in the time period 2071-2090 compared to 1971-1990. Based on the simulation results a positive temperature signal is expected in whole Europe (figure 4a). Increase of temperature is projected to occur with precipitation decrease

[2] A1: very rapid economic growth, global population peaks in mid-century and declines thereafter, and rapid introduction of new and more efficient technologies. The A1 scenario family develops into three groups that describe alternative directions of technological change in the energy system; A1B means a balance across all sources.

in southern and central Europe and in the southern part of Scandinavia, whereas Northeast Europe can be characterized with warmer and wetter conditions (figure 4a).

Figure 4b represents the direction of the temperature and precipitation changes due to afforestation only. Comparing the simulation results with- and without forest cover changes for the future (2071-2090), the cooling and moistening effects of afforestation are dominant in most parts of the temperate zone. Here, the largest amount of forest cover increase has been assumed. Forests have large leaf area and they are aerodynamically rough, that support the more intense vertical mixing compared to other vegetated surfaces. It leads to enhanced ability of evapotranspiration and thereby to the decrease of temperature compared to the reference simulation.

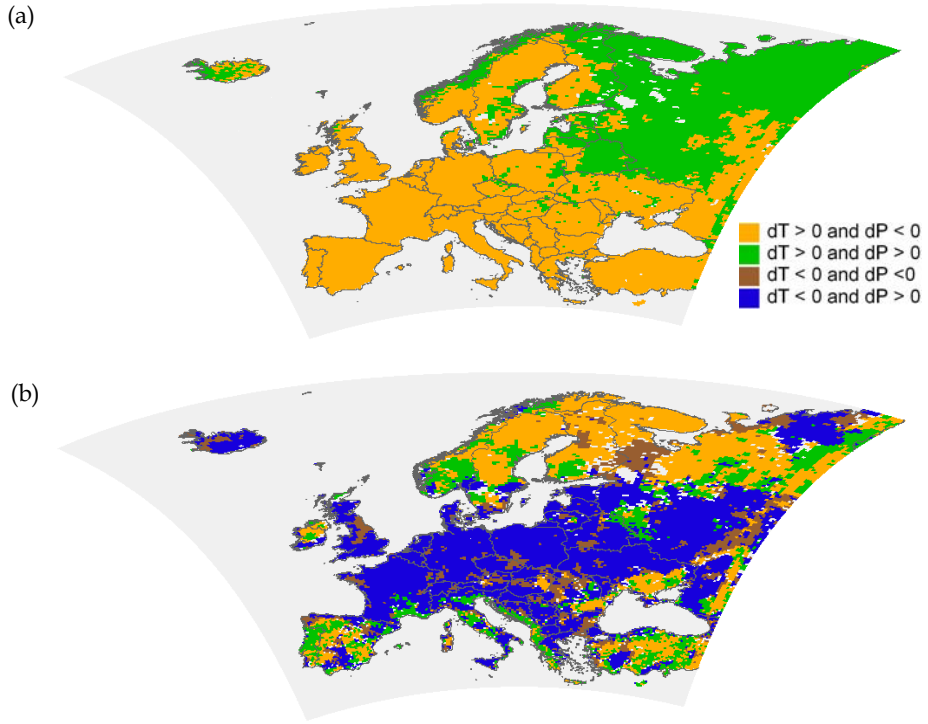

Fig. 4. Climate change signal for temperature (dT) and precipitation (dP) due to emission change (a) and due to potential afforestation (b)

Smaller patches in central and southeast Europe can be characterized also by colder but dryer conditions. Portugal, the Mediterranean coasts and the southern part of the boreal zone show a shift into the warmer and wetter direction (figure 4b). For the Mediterranean region a possible reason for it can be that in this dry area vegetation has deeper roots in the reference simulation than forests in the afforestation experiment. It means in the model that less water is available for cooling through evapotranspiration. Increase of forest cover resulted in higher temperatures and less precipitation in the northern part of Scandinavia and Russia as well as in smaller areas in Spain and around the Black Sea (figure 4b).

From the figure 4 it can be concluded that there are regions, where temperature and/or precipitation changes due to emission change and afforestation show the same sign so that they can enhance each other. In other areas they have the opposite sign, thus depending on their magnitude, afforestation can reduce or fully compensate the effects of the emission change.

3.2 Magnitude of the climatic effect of emission change and potential afforestation

First, those regions have been determined, which are the most affected by climate change for the end of the 21st century. Without any forest cover changes the strongest warming and drying are projected to the Mediterranean area, southern France and over the Iberian Peninsula (figure 5). These signals are in a good agreement with the simulation results of other regional climate models for the same region.

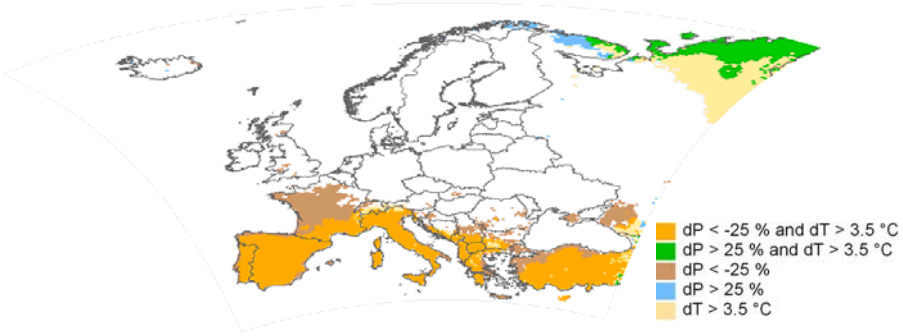

Fig. 5. The regions the most affected by climate change due to emission change (dT: temperature change, dP: precipitation change)

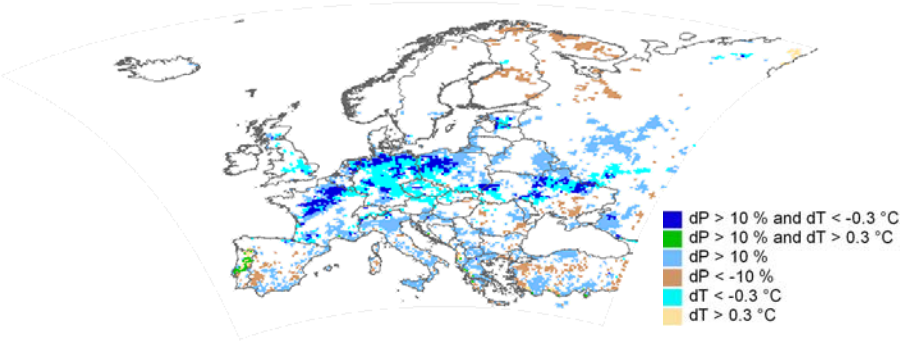

Fig. 6. The regions with the largest effects of forest cover increase on temperature and precipitation (dT: temperature change, dP: precipitation change)

Second, regions, where forest cover increase (without any emission change) has the largest effects on temperature and precipitation have been also identified. For the northern part of central and western Europe temperature decrease due to afforestation can exceed 0.3 °C additionally to more than 10 % increase of the summer precipitation sum (figure 6). The

regions characterized by largest cooling and moistening effects of afforestation do not correspond to the areas with the strongest warming and drying due to emission change (figure 5). In many southern European areas afforestation can result in larger than 10 % increase/decrease of summer precipitation sums but these are not statistically significant.

3.3 Sign and magnitude of the climatic feedbacks of potential afforestation relative to the magnitude of the climate change signal

The magnitude of the climatic effects of afforestation has also been analyzed relative to the effect of the enhanced greenhouse gas emissions in order to determine the regions, where forests can play a major role in altering the climate change signal. In figure 7 the values represent the temperature as well as the precipitation signals for afforestation divided by the climate change signal. The reddish colours are referring to the areas, where the changes of the analyzed climatic variables have the same sign for both afforestation and emission change. Whereas in the regions marked with bluish colours they show opposite sign.

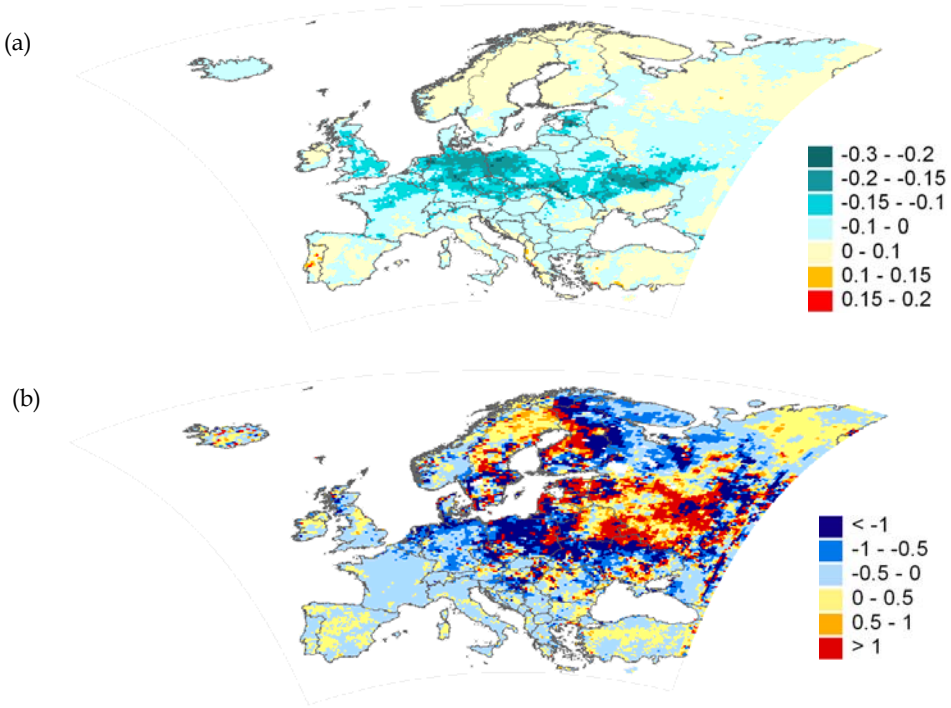

Fig. 7. Climate change signal due to potential afforestation divided by the climate change signal due to emission change for temperature (a) and precipitation (b)

The temperature change signal for potential afforestation is smaller than for emission change in the entire continent (figure 7a). Increase of the forest cover can enhance the climate change signal in the boreal and in the Mediterranean regions but its magnitude is

relatively small compared to the effect of the emission change. In the temperate zone afforestation can reduce the projected warming. In northern part of central Europe and Ukraine the effect of afforestation can be 15-20 % of the climate change signal.

The increase of forest cover can amplify the projected precipitation change in Sweden, Spain, Belarus and Russia (figure 7b). Whereas in the northern part of central Europe, Ukraine and eastern Finland the precipitation change signal due to emission change can be reduced by afforestation in more than 50 %. Figure 4 shows a border area between the projected precipitation increase and decrease due to emission change. Here the projected precipitation change is relatively small and not significant. In this zone the magnitude of the precipitation change due to afforestation can exceed the magnitude of the climate change signal (figure 7b).

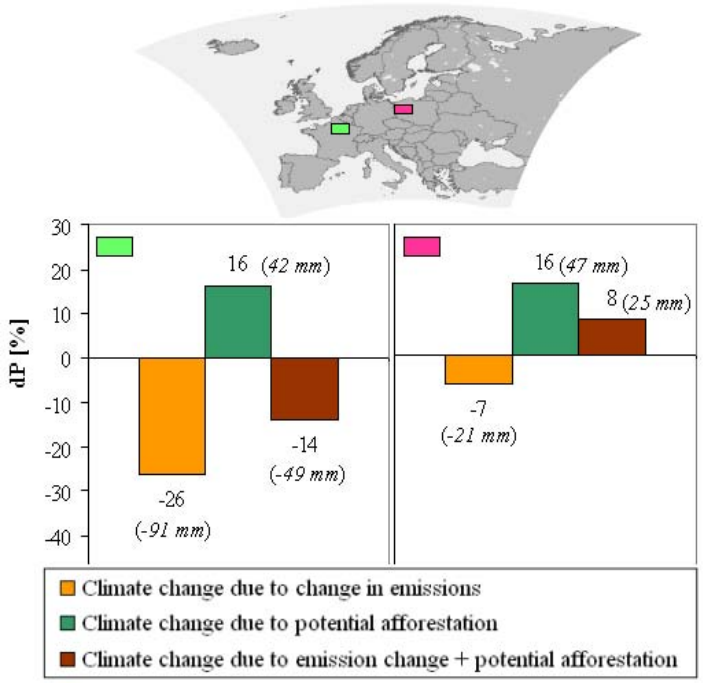

Fig. 8. Change of the summer precipitation sum (dP) due to emission change (2071-2090 vs. 1961-1990), due to potential afforestation (2071-2090) and due to emission change + potential afforestation for the two selected 30 box-regions in France (left) and in northern Poland (right)

Two smaller regions with similar amount of forest cover increase have been selected to represent the regional differences. In the northern part of Poland the changes of the physical properties of the land cover resulted in an increase of evapotranspiration. Due to the increase of latent heat of vaporization, the simulated climate change signal for temperature (2 °C) may decrease by 0.3 °C during the summer months (not shown). This effect of the afforestation is 17 % of climate change signal. Potential afforestation may result in

significant increase of the summer precipitation sum by 16 % (47 mm) compared to the reference simulation (figure 8). Due to the enhanced greenhouse gas emissions, a relatively small (-7 %; -21 mm) decrease of precipitation is projected for the period 2071-2090 compared to 1971-1990. Thus the combined effect of afforestation and emission changes led to 8 % (25 mm) increase of precipitation compared to the past time period without any land cover changes (figure 8).

In France, the precipitation change signal for emission change is projected to be larger (-26% -91 mm). Here, the 16 % (42 mm) increase of precipitation due to afforestation can diminish but not fully compensate the significant decrease of precipitation due to emission change (figure 8). If emission changes occur together with potential afforestation, the summer precipitation sum might decrease by 14 % (-49 mm).

3.4 Country scale effects of maximal afforestation in Hungary

A more detailed case study has been carried out for Hungary to assess the regional differences of the climatic role of afforestation within the country. These analyses concentrated on the possible mitigation of the strong warming and drying tendency of summers projected for this region.

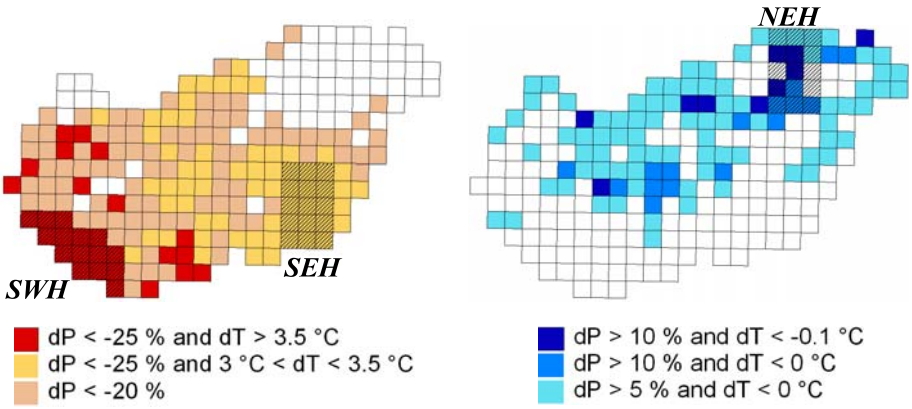

Fig. 9. The areas the most affected by climate change (left) and the spatial distribution of the precipitation-increasing (dP) and temperature-decreasing (dT) effect of maximal afforestation compared to the reference (right). The three investigated regions are hatched: the area the most affected by climate change (southwestern part of Hungary: SWH), the region with the largest amount of afforestation (southeastern part of Hungary: SEH) and the area, where the effect of maximal afforestation on precipitation is the largest (northeastern part of Hungary: NEH)

Based on the applied threshold values for temperature and relative precipitation the southwestern part of Hungary (SWH) can be the most affected by warming and drying. In this area the projected increase of summer temperature can exceed the 3.5 °C and the decrease of the summer precipitation sum the 25 % for the time period 2071-2100 compared to 1961-1990. The least affected are the northeastern areas.

Similarly the region has been determined, which can be characterized by the largest precipitation increase and temperature decrease due to maximal afforestation (figure 9).

Figure 9 shows that the climatic effects of the maximal afforestation are the largest in the northeastern part of Hungary (NEH), which does not correspond to the area with the largest amount of afforestation.

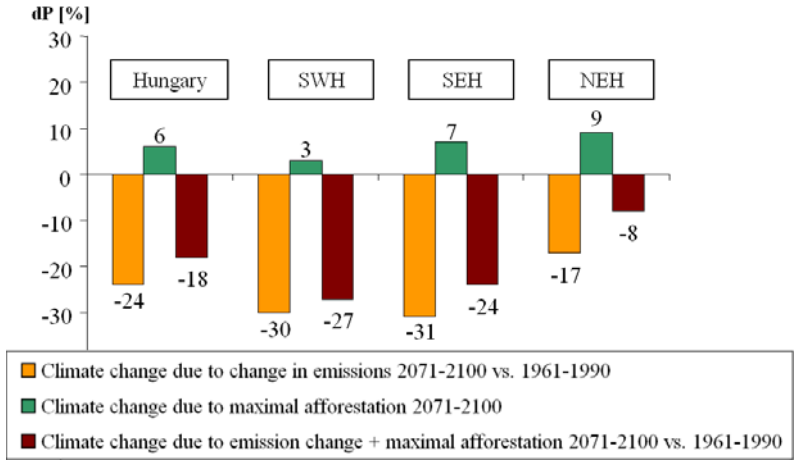

Fig. 10. Change of the summer precipitation sum (dP) due to emission change (2071-2100 vs. 1961-1990), due to maximal afforestation (2071-2100) and due to emission change + maximal afforestation in Hungary and in the three investigated regions (SWH: southwestern part of Hungary, SEH: southeastern part of Hungary, NEH: northeastern part of Hungary). Adapted from: Gálos et al., 2011

For the regions SWH and NEH as well as for the area with the largest increase of forest cover (SEH) the magnitude of the effects of forest cover increase on the summer precipitation sum has been compared to the magnitude of the projected climate change signal. For all three regions and for the whole area of Hungary the precipitation change due to emission changes and the precipitation change due to maximal afforestation have opposite effect (figure 10). This means that the projected climate change signal for precipitation can be reduced by the increase of the forest cover. The magnitude of the climate change altering effect of the maximal afforestation differs among regions. The area of SWH can be characterized by 30 % relative precipitation decrease due to emission change (2071-2100 vs. 1961-1990), which could be hardly compensated by the forest cover increase. In SEH, the significant decrease of summer precipitation can be weakened through the afforestation. In the mountainous region NEH, the projected drying in summer is the mildest (17 %). But also this is the area, where the largest precipitation-increasing (9 %) effect of maximal afforestation is observable. Here, for precipitation, more than half of the projected climate change signal can be relieved with enhanced forest cover (figure 10). These effects can play a major role in mitigating of the probability and severity of droughts in this region (Gálos et al., 2011).

4. Conclusions

A regional scale sensitivity study has been carried out to assess the climatic effects of forest cover increase for Europe, for the end of the 21st century. Applying the regional climate

model REMO, the projected temperature and precipitation tendencies have been analyzed for summer, based on the results of the A2 IPCC-SRES emission scenario simulation. For the end of the 21st century it has been studied, whether the effects of the emission changes could be reduced or enhanced by the increased forest cover. The magnitude of the biogeophysical effects of afforestation on temperature and precipitation has been determined relative to the magnitude of the climate change signal due to emission change. The regions have been determined, in which forests play a major role in altering of the projected climate change.

Simulation results of this sensitivity study can be summarized as follows:

a. *Climate change signal due to emission change:*
   - *Sign of the effects:* For the A2 emission scenario, a positive temperature signal is expected in whole Europe, which is projected to occur together with precipitation decrease in southern and central Europe and in the southern part of Scandinavia.
   - *Magnitude of the effects:* The strongest warming and drying are projected for the Mediterranean area, southern France and over the Iberian Peninsula.

b. *Climate change signal due to potential afforestation:*
   - *Sign of the effects:* In most parts of the temperate zone the cooling and moistening effect of afforestation dominates. Portugal, the Mediterranean coasts and the southern part of the boreal zone show a shift into the warmer and wetter direction. Warmer and dryer conditions over larger areas may occur in the boreal region.
   - *Magnitude of the effects:* Afforestation has the largest climatic effects in the northern part of central and western Europe, where the temperature decrease due to afforestation may exceed 0.3 °C additionally to more than 10 % increase of the summer precipitation sum.

c. *Climate change signal due to potential afforestation relative to the emission change:*
   - *Sign of the effects:* In the largest part of the temperate zone precipitation and temperature anomalies due to forest cover increase show the opposite sign than due to emission change, which means that the climate change signal can be reduced by afforestation. Whereas in Sweden, in Spain and in some regions in the eastern part of the continent afforestation can amplify the climate change signal for both investigated variables.
   - *Magnitude of the effects:* The largest climate change mitigating effects of afforestation can be expected in northern Germany, Poland and Ukraine, which is 15-20 % of the climate change signal for temperature and more than 50 % for precipitation. These changes are significant at the 90 % confidence level.

d. *Based on the detailed case study for Hungary:*
   - *Sign of the effects:* The projected climate change signal for precipitation can be reduced assuming maximal afforestation.
   - *Magnitude of the effects:* The strong warming and drying tendency projected for southwest Hungary could be hardly compensated by forest cover increase. But in the northwestern region more than half of the projected climate change signal for precipitation can be relieved with enhanced forest cover.

For Hungary results represent the first regional scale assessment of the climatic role of forests for a long future time period and its role in adapting to climate change.

Based on the simulation results it can be concluded that only large, contiguous forest blocks have robust effect on the climate on regional scale. The climate change altering effects of forest cover change show large spatial differences. In the most climate change affected regions climatic effects of afforestation are relatively small. But in other regions they can play an important role in reducing the probability and severity of climatic extremes (Gálos et al., 2011). These sensitivity studies confirm, that at the end of the 21st century in the regions, which are the most affected by climate change, vegetation feedbacks have weaker influence on the atmospheric circulation in comparison to the greenhouse gas forcing (Betts, 2007; Wramneby et al., 2010) and afforestation is not a substitute for reduced greenhouse gas emissions (Arora & Montenegro, 2011).

For each of the introduced sensitivity studies, one regional climate model has been applied driven by one emission scenario. For the climate change signal, results are in general agreement with earlier studies from the EU-projects PRUDENCE and ENSEMBLES. For the land cover change experiments the simulated sign and magnitude of the climatic effects can largely depend on the description of the land surface properties and processes in the applied climate model as well as the variability of the climatic and soil conditions and vegetation characteristics of the studied region. Therefore more similar fine-scale pilot studies are essential to reduce the uncertainties and to draw appropriate conclusions for decision makers about the role of the forests in the climate change mitigation on country scale.

Practical application of the results

From practical point of view, the investigation of the role of the land surface in the climate system gets even more important with the expected land cover change due to climate change and land use politics that differ among regions. Research into forestry's effect on climate is still relatively new and requires a major expansion to support policy development (Anderson et al., 2010). Our results also pointed out that the changes of forest cover could enhance and reduce the projected regional climate change. Therefore regional scale information is substantial about the climatic feedbacks of the future land cover and land use for the adaptation to the climate change in agriculture, forestry and water management.

Results of these sensitivity experiments contribute to the assessment of the climate change altering effects of forest cover change. It helps to identify the areas, where forest cover increase is climatically the most beneficial and should be supported to reduce the projected climate change. Here, the existing forests should be maintained. Thus the present study provides an important basis for the future adaptation strategies.

Outlook

Further research is essential to get information about the internal model variability and for studying the robustness of the results applying an ensemble of regional climate model simulations. In these sensitivity studies the spatial and temporal changes of vegetation cover due to climate change was not considered. Although the projected precipitation and temperature changes may have severe impacts on the spatial distribution of forests. Especially in the case-study region Hungary the drastic reduction of the macroclimatically suitable area for forests is expected at the forest/steppe limit (Berki et al., 2009; Mátyás et al., 2010; Czúcz et al., 2011). Therefore for the long-term investigation of forest-climate

interactions in the future, regional climate modelling is essential with dynamic vegetation scheme and more detailed and improved description of the forest related processes and parameters combining the biogeophysical and biogeochemical effects.

5. Acknowledgements

The authors give special thanks to the Regional Modelling Group of the Max Planck Institute for Meteorology, Hamburg for the fruitful scientific discussions about the simulation results. We thank to Prof. Dr. Csaba Mátyás for his expertise and suggestions regarding to the practical importance of this topic. The authors would like to thank to Georg Kindermann (IIASA, International Institute for Applied Systems Analysis Austria) for providing the forest cover database as well as to Kevin Sieck and Claas Teichmann for the technical guidance during the simulations. The REMO simulations without land cover changes have been carried out in the frame of the EU-project ENSEMBLES. This research was supported by the EC-FP7 project CC-TAME (www.cctame.eu; grant agreement n° 212535) and the TÁMOP 4.2.2-08 joint EU-national research project.

6. References

Anav A., Ruti P.M., Artale V. & Valentini R. (2010). Modelling the effects of land-cover changes on surface climate in the Mediterranean region. *Clim. Res.*, 41, 91-104

Anderson R.G., Canadel J.G., Randerson J.T., Jackson R.B., Hungate B.A., Baldocchi D.D., Ban-Weiss G.A., Bonan G.B., Caldeira K., Cao L., Diffenbaugh N.S., Gurney K.R., Kueppers L.M., Law B.E., Luyssaert S., & O'Halloran T.L. (2010). Biophysical considerations in forestry for climate protection. *Front Ecol Environ*; doi:10.1890/090179

Arora V.K. & Montenegro A. 2011. Small temperature benefits provided by realistic afforestation efforts. *Nature Geoscience* ,doi: 10.1038/NGEO1182, 5pp

Bala G., Caldeira K., Wickett M., Phillips T.J., Lobell D.B. , Delire C. & Mirin A. (2007). Combined climate and carbon-cycle effects of large-scale deforestation. *Proc Natl Acad Sci USA* 104, 6550–6555

Bartholy J., Pongrácz R. & Gelybó Gy. (2007). Regional climate change expected in Hungary for 2071-2100. *Applied Ecology and Environmental Research*, 5, 1-17

Berki I., Rasztovits E., Móricz N. & Mátyás Cs. (2009). Determination of the drought tolerance limit of beech forests and forecasting their future distribution in Hungary. *Cereal Research Communations,* 37, 613-616

Beniston M., Stephenson D.B., Christensen O.B., Ferro C.A.T., Frei C., Goyette S., Halsnaes K., Holt T., Jylhä K., Koffi B., Palutikof J., Schöll R., Semmler T. & Woth K. (2007). Future extreme events in European climate: an exploration of regional climate model projections. *Clim. Change,* 81, 71–95, doi:10.1007/s10584-006-9226-z

Beniston M. (2009). Trends in joint quantiles of temperature and precipitation in Europe since 1901 and projected for 2100. *Geophys. Res. Lett.*, 36, L07707, doi:10.1029/2008GL037119

Betts R.A. (2001). Biogeophysical impacts of land use on present-day climate: near-surface temperature change and radiative forcing. *Atmospheric Science Letters* 1, 23pp, doi: 10.1006/asle.2001.0023

Betts R. (2007). Implications of land ecosystem-atmosphere interactions for strategies for climate change adaptation and mitigation. *Tellus,* 59B, 602-615, doi: 10.1111/j.1600-0889.2007.00284.x

Bonan G.B., Pollard D. & Thompson S.L. (1992). Effects of boreal forests on global climate. *Nature,* 359, 716-718, doi: 10.1038/359716a0

Bonan G.B. (1997). Effects of land use on the climate of the United States. *Climatic Change,* 37, 449–486

Bonan G.B., Levis S., Kergoat L. & Oleson K.W. (2002). Landscapes as patches of plant functional types: an integrating concept for climate and ecosystem models. *Global Biogeochemical Cycles,* 16, 30pp,10.1029/2000GB001360

Bonan G.B. (2004). Biogeophysical feedbacks between land cover and climate. In: *Ecosystems and Land Use Change.*, DeFries R.S., Asner G.P., & Houghton R.A. (eds), 153, 61-72, Geophysical Monograph American Geophysical Union, Washington, D.C.

Bonan G.B. 2008. Forests and climate change: forcings, feedbacks, and the climate benefits of forests. *Science,* 320, 1444–1449, doi: 10.1126/science.1155121

Bounoua L., Defries R., Collatz G.J., Sellers P., & Khan H. (2002). Effects of land cover conversion on surface climate. *Climatic Change,* 52, 29-64

Brovkin V. (2002). Climate-vegetation interaction. *J. Phys.* IV France 12, 57-82, doi: 10.1051/jp4:20020452

Christensen J.H., Carter T.R., Rummukainen M., & Amanatidis G. (2007). Evaluating the performance and utility of regional climate models: the PRUDENCE project. *Clim. Change*, 81, 1-6, DOI 10.1007/s10584-006-9211-6

Christensen J.H. & Christensen O.B. (2007). A summary of the PRUDENCE model projections of changes in European climate by the end of this century. *Clim. Change,* 81, 7-30, doi: 10.1007/s10584-006-9210-7

Copeland J.H., Pielke R.A. & Kittel T.G.F. (1996). Potential climatic impacts of vegetation change: A regional modelig study. *Journal of Geophysical Research,* 101, 7409-7418 doi: 10.1029/95JD02676

Czúcz B., Gálhidy L. & Mátyás Cs. (2011). Present and forecasted xeric climatic limits of beech and sessile oak distribution at low altitudes in Central Europe. *Ann. For. Sci.,* 68(1), 99-108

Drüszler Á., Vig P. & Csirmaz K. (2011). Effects of Historical Land Cover Changes on the Precipitation Distribution in Hungary. *Riscuri Si Catastrofe (Risks and Disasters)*, ISSN: 15845273; I/2011 (in print)

Feddema J.J., Oleson K.W., Bonan G.B., Mearns L.O., Buja L.E., Meehl G.A. & Washington W.M. (2005). The Importance of Land-Cover Change in Simulating Future Climates. *Science,* 310, 1674 –1678, doi: 10.1126/science.1118160

Fischer E.M. & Schär C. (2010). Consistent geographical patterns of changes in high-impact European heatwaves. *Nature Geoscience,* 3, 398-403, doi: 10.1038/NGEO866

Gálos B., Lorenz Ph., & Jacob D. (2007). Will dry events occur more often in Hungary in the *future? Environ. Res. Lett.,* 2, 034006 (9pp), doi: 10.1088/1748-9326/2/3/034006

Gálos B., Mátyás Cs. & Jacob D. (2011). Regional characteristics of climate change altering effects of afforestation. *Environ. Res. Lett.* 6, 044010 (9pp), doi:10.1088/1748-9326/6/4/044010

Giorgi F., Bi X. & Pal J.S. (2004). Mean, interannual variability and trends in a regional climate change experiment over Europe. II: climate change scenarios (2071–2100). *Climate Dynamics,* 23, 839–858, doi: 10.1007/s00382-004-0467-0

Göttel H., Alexander J., Keup-Thiel E., Rechid D., Hagemann S., Blome T., Wolf A. & Jacob D. (2008). Influence of changed vegetation fields on regional climate simulations in the Barents Sea Region Climatic Change. *BALANCE Special Issues,* 87, 35-50

Hagemann S., Botzet M., Dümenil L. & Machenhauer M. (1999). Derivation of global GCM boundary conditions from 1 km land use satellite data. *Report 289* Max-Planck-Institute for Meteorology, Hamburg

Hagemann S. (2002). An improved land surface parameter dataset for global and regional climate models. *Report 336*, Max-Planck-Institute for Meteorology, Hamburg

Hagemann S., Göttel H., Jacob D., Lorenz P. & Roeckner E. (2009). Improved regional scale processes reflected in projected hydrological changes over large European catchments. *Climate Dynamics,* 32, 767–781

Heck P., Lüthi D., Wernli H. & Schär Ch. (2001). Climate impacts of European-scale anthropogenic vegetation changes: A sensitivity study using a regional climate model. *Journal of Geophysical Research,* 106, 7817-7835, doi: 10.1029/2000JD900673

Hogg E.H., Price D.T., & Black T.A. (2000). Postulated feedbacks of deciduous forest phenology on seasonal climate patterns in the Western Canadian interior. *Journal of Climate* ,13, 4229-4243

Houghton J. et al. (ed) (2001). *Climate change 2001 The Scientific Basis.* Intergovernmental Panel on Climate Change (Cambridge: Cambridge University Press)

IPCC (2007). Climate change 2007: Synthesis Report. Contribution of Working Groups I, II and III to the Fourth Assessment Report of the Intergovernmental Panel on Climate Change http//:www.ipcc.ch

Jackson R.B., Randerson J.T., Canadell J.G., Anderson R.G., Avissar R., Baldocchi D.D., Bonan G.B., Caldeira K., Diffenbaugh N.S., Field C.B., Hungate B.A., Jobbágy E.G., Kueppers L.M., Nosetto M.D., & Pataki D.E. (2008). Protecting climate with forests *Environ. Res. Lett.,* 3, 044006 (5pp), doi: 10.1088/1748-9326/3/4/044006

Jacob D., Andrae U., Elgered G., Fortelius C., Graham L.P., Jackson S.D., Karstens U., Koepken Chr., Lindau R., Podzun R., Rockel B., Rubel F., Sass H.B., Smith R.N.D., van den Hurk B.J.J.M. & Yang X. (2001). A Comprehensive Model Intercomparison Study Investigating the Water Budget during the BALTEX-PIDCAP Period. *Meteorology and Atmospheric Physics,* 77(1-4), 19-43

Jacob D. (2001). A note to the simulation of the annual and inter-annual variability of the water budget over the Baltic Sea drainage basin. *Meteorology and Atmospheric Physics,* 77, 61-73

Jacob D., Bärring L., Christensen O.B., Christensen J.H., de Castro M., Déqué M., Giorgi F., Hagemann S., Hirschi M., Jones R., Kjellström E., Lenderink G., Rockel B., Sánchez E., Schär C., Seneviratne S.I., Sommot S., van Ulden A. & van den Hurk B. (2007). An inter-comparison of regional climate models for Europe: model performance in present-day climate. *Climatic Change*, 81, 31-52, doi: 10.1007/s10584-006-9213-4

Jacob D., Kotova L., Lorenz P., Moseley Ch. & Pfeifer S. (2008). Regional climate modeling activities in relation to the CLAVIER project. *Quarterly Journal of the Hungarian meteorological Service (Időjárás),* 112, 141-153

Jungclaus J.H., Keenlyside N., Botzet M., Haak H., Luo J-J., Latif M., Marotzke J., Mikolajewicz U. & Roeckner E. (2006). Ocean circulation and tropical variability in the coupled model ECHAM5/MPI-OM. *J. Climate,* 19, 3952–3972

Kjellström E., Bärring L., Jacob D., Jones R., Lenderink G. & Schär C. (2007). Modelling daily temperature extremes: Recent climate and future changes over Europe. *Climatic Change*, 81, 249-265, doi: 10.1007/s105800692205

Kjellström E., Nikulin G., Hansson U., Strandberg G. & Ullerstig A. (2011). 21st century changes in the European climate: uncertainties derived from an ensemble of regional climate model simulations. *Tellus,* 63A(1), 24-40, doi:10.1111/j.1600-0870.2010.00475

van der Linden P. & Mitchell J.F.B. (eds.) (2009). *ENSEMBLES: Climate Change and its Impacts: Summary of research and results from the ENSEMBLES project*. 160pp, Met Office Hadley Centre, FitzRoy Road, Exeter EX1 3PB, UK

Majewski D. (1991). The Europa-Modell of the Deutscher Wetterdienst ECMWF. *Seminar on numerical methods in atmospheric models,* 2, 147-191

Mátyás Cs. (2009). Ecological perspectives of climate change in Europe's continental, drought-threatened Southeast In: *Regional aspects of climate-terrestrial-hydrologic interactions in non-boreal Eastern Europe,* Groisman P.Y., Ivanov S.V. eds, pp 31-42, NATO Science Series, Springer Verl.

Mátyás Cs. (2010). Forecasts needed for retreating forests (Opinion). *Nature*, 464, 1271 doi: 10.1038/4641271a

Mátyás Cs., Berki I., Czúcz B., Gálos B., Móricz N. & Rasztovits E. (2010). Future of beech in Southeast Europe from the perspective of evolutionary ecology. *Acta Silv. & Lign. Hung.*, 6, 91-110

Nakicenovic N. et al. (2000). IPCC Special Report on Emission Scenarios. Cambridge: Cambridge University Press, p 599

Oleson K.W., Bonan G.B., Levis S. & Vertenstein M. (2004). Effects of land use change on North American climate: impact of surface datasets and model Biogeophysics. *Climate Dynamics,* 23, 117–132, doi: 10.1007/s00382-004-0426-9

Pielke R.A., Avissar Sr R., Raupach M., Dolman A.J., Zeng X. & Denning A.S. (1998). Interactions between the atmosphere and terrestrial ecosystems: influence on weather and climate. *Global Change Biology,* 4, 461–475

Pitman A.J. (2003). The evolution off, and revolution in, land surface schemes designed for climate model. *Int. J. of Climatol.* 23, 479-510, doi: 10.1002/joc.893

Radvánszky B. & Jacob D. (2009). The Changing Annual Distribution of Rainfall in the Drainage Area of the River Tisza during the Second Half of the 21st Century. *Zeitschrift für Geomorphologie*, 53, 171195(25)

Rechid D. & Jacob D. (2006). Influence of monthly varying vegetation on the simulated climate in Europe. *Meteorol Z.,* 15, 99-116

Rechid D., Raddatz T.J. & Jacob D. (2008a). Parameterization of snow-free land surface albedo as a function of vegetation phenology based on MODIS data and applied in climate modelling. *Theor. Appl. Climatol.*, 95, 245-255 doi: 10.1007/s00704-008-0003-y

Rechid D., Hagemann S. & Jacob D. (2008b). Sensitivity of climate models to seasonal variability of snow-free land surface albedo *Theor. Appl. Climatol.,* 95, 197-221 doi: 10.1007/s00704-007-0371-8

Roeckner E., Arpe K., Bengtsson L., Christoph M., Claussen M., Dümenil L., Esch M., Giorgetta M., Schlese U. & Schulzweida U. (1996). The atmospheric general circulation model ECHAM-4: Model description and simulation of the present day climate. *Report 218 Max-Planck-Institut für Meteorologie, Hamburg*

Roeckner E., Brokopf R., Esch M., Giorgetta M., Hagemann S., Kornblueh L., Manzini E., Schlese U. & Schulzweida U. (2006). Sensitivity of simulated climate to horizontal and vertical resolution in the ECHAM5 atmosphere model. *J. Clim.* 19, 3771–3791

Sánchez E., Gaertner M.A., Gallardo C., Padorno E., Arribas A. & Castro M. (2007). Impacts of a change in vegetation description on simulated European summer present-day and future climates. *Clim. Dyn.* 29, 319–332, doi: 10.1007/s00382-007-0240-2

Schär C., Vidale P.L., Lüthi D., Frei C., Häberli C., Liniger, M.A. & Appenzeller C. (2004). The role of increasing temperature variability in European summer heatwaves. *Nature* 427, 332–336, doi: 10.1038/nature02300

Seneviratne S.I., Lüthi D., Litschi M. & Schär C. (2006). Land-atmosphere coupling and climate change in Europe. *Nature,* 443, 205–209, doi: 10.1038/nature05095

Seneviratne S.I. et al. (2010). Investigating soil moisture-climate interactions in a changing climate: A review. *Earth. Sci. Rev.*, 99, 125-161

Szépszó G. (2008). Regional change of climate extremes in Hungary based on different regional climate models of the PRUDENCE project. *Időjárás,* 112, 265-283

Teuling A.J., Seneviratne S.I., Stoeckli R., Reichstein M., Moors E., Ciais P., Luyssaert S., van den Hurk B., Ammann C., Bernhofer C., Dellwik E., Gianelle D., Gielen B., Gruenwald T., Klumpp K., Montagnani L., Moureaux C., Sottocornola M., & Wohlfahrt G. (2010). Contrasting response of European forest and grassland energy exchange to heatwaves. *Nature Geoscience* 3(10), 722-727

Vidale P.L., Lüthi D., Wegmann R., & Schär C. (2007). European summer climate variability in a heterogeneous multi-model ensemble. *Climatic Change*, 81, 209–232. doi: 10.1007/s10584-006-9218-z

Wramneby A., Smith B. & Samuelsson P. (2010). Hot spots of vegetation-climate feedbacks under future greenhouse forcing in Europe. *J. Geophys. Res.*, 115, D21119, doi:10.1029/2010JD014307

15

Climate Change in the Upper Atmosphere

Ingrid Cnossen
High Altitude Observatory, National Center for Atmospheric Research
USA

1. Introduction

Studies of climate change traditionally focus on long-term changes taking place in the troposphere. This is understandable, as this is the part of the atmosphere that most directly affects life on the surface. However, long-term trends higher in the atmosphere can have important consequences as well. The middle and upper atmosphere consist of the stratosphere (~15-50 km), the mesosphere (~50-90 km), the thermosphere (~90-800 km), and the embedded ionosphere, the ionized part of the upper atmosphere (see figure 1).

Many satellites operate within the thermosphere. Since the drag exerted upon them is proportional to the ambient atmospheric density, long-term changes in the density in the thermosphere can affect their trajectories and orbital lifetimes. Also, long-term trends in the ionosphere can affect radio wave propagation, and therefore the performance of the Global Positioning System (GPS) and other space-based navigation and communication systems that rely on radio waves (Laštovička et al., 2006a). In addition to these in-situ effects, there is evidence that perturbations in the upper atmosphere may propagate downward (e.g. Haynes et al., 1991), and that the state of the middle and upper atmosphere has an influence on the troposphere (e.g. Baldwin & Dunkerton, 2001; Sassi et al., 2010). There is thus a possibility that long-term trends in the upper atmosphere could play a role in tropospheric climate too. For these reasons it is important to gain a good understanding of the processes that cause long-term trends in this part of the atmosphere.

As in the lower atmosphere, the increase in carbon-dioxide concentration is thought to be one of the main causes for climatic changes in the upper atmosphere (Laštovička et al., 2006a). However, it has become clear in recent years that several other mechanisms for long-term change must be considered as well (e.g. Qian et al. 2011). These include changes in ozone, methane and water vapour concentration, the secular variation of the Earth's magnetic field, and long-term changes in solar and geomagnetic activity. Also climate change in the lower atmosphere could have an effect.

The aim of this chapter is to review our current knowledge of the processes mentioned above and their role in causing climate change in the upper atmosphere. A brief overview of observed trends in several variables is given first (section 2), followed by a discussion of the possible responsible mechanisms (sections 3-6). Estimates of trends caused by each of the mechanisms as determined from model simulations are compared to observed trends where possible.

2. Observed long-term trends in the upper atmosphere

2.1 Introduction

When talking about climate change, we generally are referring to quasi-linear changes or "trends" that occur over a period of ~30 years or more (by the definition of the World Meteorological Organization). In practice, climate change is not necessarily linear, and trends can (and eventually will) change over time. However, for the purposes of this chapter we will assume that trends that have been observed over the last 50-60 years, or subsets of that time frame, can be meaningfully described in terms of a linear change per decade.

To measure trends, we need high quality, long-term datasets, which are much sparser in the upper atmosphere than they are in the troposphere. In addition, the upper atmosphere is strongly influenced by the 11-year solar cycle, as well as fluctuations in geomagnetic activity (see section 5). This shorter-term variability must be corrected for to be able to detect a long-term trend. Various studies have shown that this is a non-trivial task, as different methodologies may yield different results (Laštovička et al., 2006b), and residual solar signals can remain, especially if the dataset is not sufficiently long (Clilverd et al., 2003).

Trends in the height of the peak electron density of the ionospheric F_2 layer, h_mF_2 (see figure 1), suffer from an additional complication when ionosonde data are used. In that case h_mF_2 is not directly measured, but calculated from the $M(3000)F_2$ parameter, which is a transmission factor related to the highest frequency that can be propagated between two sites 3000 km apart by ionospheric propagation alone. There are different empirical formulas to calculate h_mF_2 from $M(3000)F_2$, and unfortunately these can result in different trends from the same dataset, sometimes even with a different sign (Ulich, 2000; Jarvis et al., 2002). When incoherent scatter data are used, h_mF_2 can be directly measured, but the data record is much shorter, and far fewer sites are available.

Despite these difficulties, considerable progress has been made in building a global picture of long-term trends in the upper atmosphere. In this chapter we focus on a few selected variables for which both observational and theoretical trend estimates are available, so that the two can be directly compared. These are temperature, density, h_mF_2, and the critical frequency of the F_2 layer, f_oF_2, which is directly related to the peak electron density N_mF_2 as:

$$N_mF_2 = 1.24 \times 10^{10} (f_oF_2)^2 \quad (1)$$

where N_mF_2 is in m^{-3} and f_oF_2 is in MHz.

2.2 Temperature

Figure 1 gives a schematic overview of the observed trends in the temperature and the electron density profile, and also labels the various regions of the atmosphere. Trends in temperature have been determined from a large number of studies and a variety of measurement techniques (e.g. rocketsonde, lidar, radar, satellite data). Trends in the upper atmosphere are mostly negative, except in the mesopause/lower thermosphere region.

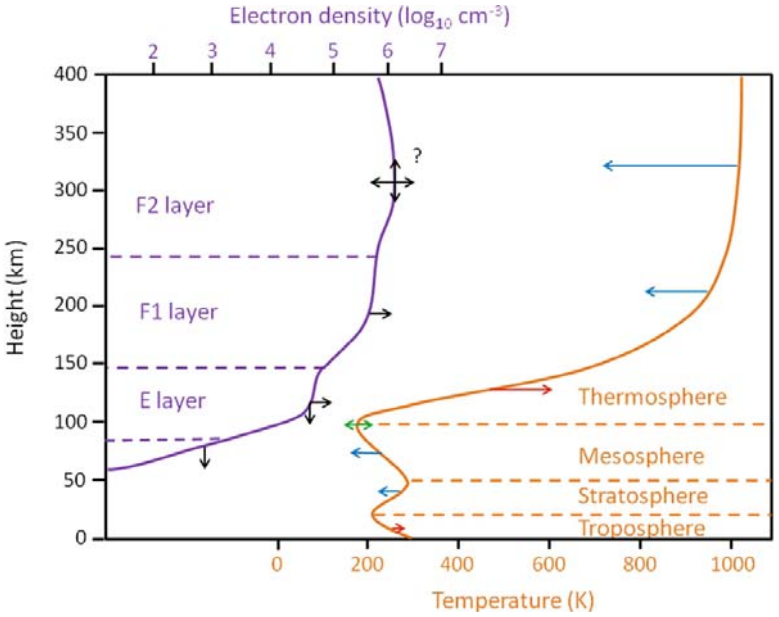

Fig. 1. Schematic summary of observed global mean trends in the atmosphere, after Laštovička et al. (2006a). Changes in the temperature profile (orange) are indicated by red (warming), blue (cooling) and green (no clear trend) arrows. Changes in the electron density profile (purple) are indicated by black arrows. Vertical arrows indicate the movement of the height of the peak electron density of the layer, while horizontal arrows indicate changes in the peak electron density itself. Trends in the F_2 layer vary strongly with location, season, and local time, so that no meaningful global mean can be defined. They are further discussed in section 2.4.

Beig et al. (2003) summarized temperature trends in the mesosphere. They reported that the lower and middle mesosphere has cooled on average by ~2-3 K/decade and at tropical latitudes the cooling trend increases with height in the upper mesosphere. However, near the mesopause the general consensus is that there is no significant trend. Some dependency of trends on latitude has been noted, but due to a limited number of sites, no clear pattern has yet emerged.

For the thermospheric temperature, only a few long-term trend studies are available. Semenov (1996) inferred a temperature trend of -30 K/decade based on changes in the atomic oxygen 630 nm emission layer, which is normally located at ~270 km. Holt & Zhang (2008) and Zhang et al. (2011) used incoherent scatter radar data from Millstone Hill (46.2°N, 288.5°E) to determine the long-term trend in ion temperature, which should be similar to the trend in neutral temperature, due to close thermal coupling between neutrals and ions. Zhang et al. (2011) showed that a warming trend is found between ~110 and 200 km altitude, and a cooling trend above 200 km, which increases with height and is stronger for lower solar activity. At 375 km the trend is as strong as -47±11 K/decade (Holt & Zhang, 2008). Donaldson et al. (2010), in a similar analysis of incoherent scatter

data from Saint Santin (44.1°N, 2.3°E), also found a warming at ~120-130 km of ~10 K/decade, and a cooling of -30 K/decade at 350 km, increasing with height. They also noted that negative trends were much larger at noon (up to -60 K/decade) than at midnight (nearly zero). For both locations trends were larger for the period from ~1980 onward.

2.3 Density

Because the atmosphere is nearly in hydrostatic equilibrium, a decrease in temperature results in contraction of the upper atmosphere, and a downward displacement of constant pressure surfaces. This means that the thermospheric density at a fixed height is expected to decrease. The same principle also explains why a warming is found in the lower thermosphere: as the thermosphere contracts the temperature profile essentially moves down. This results in an apparent warming at fixed height in the lower thermosphere due to the strong positive vertical gradient in temperature there (Akmaev & Fomichev, 1998).

Information about thermospheric density can be obtained from the orbits of near-Earth objects. Keating et al. (2000), Emmert et al. (2004, 2008), Emmert & Picone (2011), Marcos et al. (2005) and Saunders et al. (2011) used this technique and confirmed that the thermospheric density at fixed height is indeed decreasing. Observed trend magnitudes range from about -2%/decade to about -6%/decade, and generally increase with altitude. Trends are again larger for solar minimum conditions than for solar maximum conditions (Emmert et al., 2004). Emmert et al. (2008) reported that there is also a dependence on season, with trends being strongest in October and weakest in January and February. No dependence on local time or latitude was found.

2.4 Ionospheric trends

Another consequence of atmospheric contraction as a result of global cooling is that ionospheric layers are expected to move downward, as they tend to stay on the same pressure level. On the other hand, ion and electron densities should not be affected much as a result of global cooling, as both ion production rates and recombination coefficients are expected to be affected in a similar way (Rishbeth, 1990). Any increase in ion production should therefore mostly be offset by a similar increase in ion loss. Still, both long-term changes in the height of ionospheric layers and in their critical frequencies have been found.

Trends in the F_2 layer vary strongly with location, season, and local time. Bremer et al. (2004) reported median trends in f_oF_2 and h_mF_2, derived from over 50 ionospheric stations, of -0.01 MHz/decade and -0.09 km/decade, respectively. However, local trends tend to be much stronger and can be either positive or negative. Figure 2 shows trends in h_mF_2 at noon for May-June-July, colour-coded by strength, and demonstrates that trends of the order of ±1-5 km/decade are the most common of the trends that are considered reliable (filled circles). Both trends in h_mF_2 and f_oF_2 depend on the season and time of day (even switching sign), but this dependence is different for different stations (e.g. Elias & Ortiz de Adler, 2006). Similarly, no consistent dependence on solar activity level has been found (based on calculations by Th. Ulich, pers. comm., 2007).

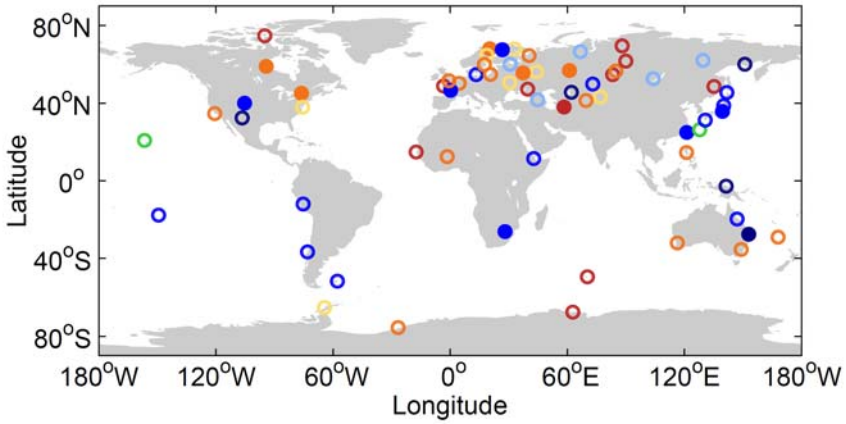

Fig. 2. Trends in h_mF_2 for May-June-July at noon hours (10-14 LT) colour-coded for strength. Dark blue: <-5 km/decade, medium blue: -5 to -1 km/decade, light blue: -1 to -0.2 km/decade, green: -0.2 to +0.2 km/decade, yellow: +0.2 to + 1 km/decade, orange: +1 to +5 km/decade, red: >5 km/decade. Filled circles represent trends that are larger than the standard deviation and were calculated based on at least 80 data points. They are therefore the most reliable. All other trends are represented by open circles. Trends were calculated using the Shimazaki (1955) formula by Th. Ulich (pers. comm., 2007).

Some studies have found regional patterns in F_2 layer trends. Danilov & Mikhailov (1999) found that the magnitude of trends in f_oF_2 increases with magnetic latitude. However, Bremer (1998) argued against this, and instead found a dependence on longitude: trends in both h_mF_2 and f_oF_2 were in general negative west of 30°E, but positive east of 30°E. Jarvis (2009) confirmed this finding. Bencze (2007, 2009) found that ionospheric stations showing negative trends in h_mF_2 are mostly located near seashores, while stations in continental areas usually exhibit positive trends.

3. Greenhouse gases and ozone

3.1 Background and mechanisms

3.1.1 Greenhouse gases

The CO_2 concentration in the Earth's atmosphere has increased from its estimated level of ~280 ppm before the industrial revolution to 317 ppm in 1960 and 390 ppm in 2010 as measured at ground level in Mauna Loa, Hawaii (P. Tans & R. Keeling, data obtained from www.esrl.noaa.gov/gmd/ccgg/trends, June 2011). The concentration of methane has also increased, from 1151 ppb in 1985 to 1355 ppb in 2008 as observed in the lower stratosphere (Rinsland et al., 2009). Partly as a result of the increase in methane, stratospheric water vapour has increased as well, by ~2 ppmv from 1945 to 2000, with its present-day level at ~4-6 ppmv (Rosenlof et al., 2001; Hurst et al., 2011).

CO_2, methane and water vapour all act as greenhouse gases. In the troposphere, greenhouse gases absorb outgoing infrared radiation, and emit it back to the surface, which results in warming. In the upper atmosphere they have the opposite effect. Greenhouse gases cool the

upper atmosphere, because they emit infrared radiation mostly to space upon relaxation from an excited state induced by collisions. This way they act to remove thermal energy from the upper atmosphere. This process overcomes the effects of extra absorption of radiation in the lower atmosphere, resulting in a net cooling effect. CO_2 is by far the most important contributor to infrared cooling in the middle atmosphere, followed by water vapour, while methane makes only a very small contribution (e.g. Fomichev, 2009). In the thermosphere both cooling by CO_2 and by nitric oxide (NO) is important.

3.1.2 Ozone

Ozone is also an important gas for the radiative budget of the stratosphere and mesosphere. Ozone absorbs solar ultraviolet (UV) radiation in the Chappuis (450-750 nm), Huggins (310-360 nm), and Hartley (450-750 nm) bands, which results in heating. The maximum heating occurs near the stratopause. Ozone also contributes to infrared cooling, but this is a much smaller effect (e.g. Fomichev, 2009).

The total ozone concentration decreased from ~375 Dobson units (DU) in 1970 to ~325 DU in 2000 as measured in Switzerland, with much stronger decreases occurring over the polar regions (Solomon, 1999). While the downward trend in ozone concentration may have slowed or even reversed in recent years (Stolarski & Frith, 2006; Salby et al., 2011), any data from the 1970s to the present-day will contain the effects that may have arisen from the original decrease in ozone concentration. A decrease in ozone results in less heating (i.e. cooling), and so acts in the same way as an increase in greenhouse gases. Note that while ozone is most important in the stratosphere and mesosphere, the cooling influence may still be felt in the thermosphere through the effect of atmospheric contraction.

3.1.3 Indirect effects

Once changes in temperature occur, whether they are caused by changes in greenhouse gases, ozone, or another process, this induces further indirect effects. We already noted that global cooling leads to thermal contraction, which has consequences for the density at a fixed height and the vertical electron density distribution. Changes in horizontal temperature structure can lead to changes in dynamics through changes in pressure gradients. The changes in dynamics can then cause further changes in temperature structure, and so on.

Not only the neutral atmosphere can be affected this way; ionospheric plasma transport is affected by changes in the neutral winds via ion-neutral collisions. Because the ionospheric plasma tends to be "frozen-in" to the magnetic field lines, meaning that it tends to flow along magnetic field lines, horizontal neutral winds can induce a vertical component in the plasma motion due to the inclination of magnetic field lines, as shown schematically in figure 3 (see also Rishbeth, 1998; Cnossen & Richmond, 2008). Due to the configuration of the Earth's magnetic field, ionospheric plasma is forced up magnetic field lines when neutral winds blow towards the magnetic equator, which acts to increase h_mF_2, and vice versa when neutral winds blow poleward. Because the geographic equator does not exactly coincide with the magnetic equator, not only the meridional wind, but also the zonal wind can contribute to the plasma transport taking place this way, although the contribution from

the meridional wind is dominant. Qian et al. (2009) have shown that this mechanism may be responsible for some of the spatial variation in trends in h_mF_2, as discussed in section 3.2.3.

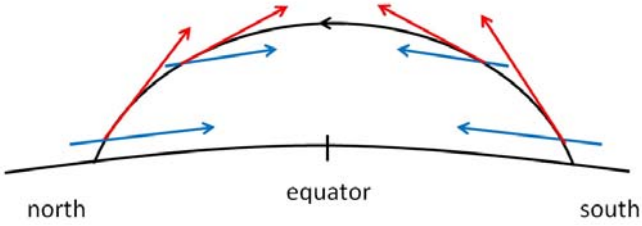

Fig. 3. Schematic illustration of the ionospheric plasma motion (red arrows) along a magnetic field line (black line with arrow) induced by horizontal neutral winds (blue arrows) blowing equatorward. In this case the ionospheric plasma is forced up magnetic field lines, resulting in an increase in h_mF_2. The opposite is true in case of poleward neutral winds. Note that the vertical component of the plasma motion becomes smaller near the equator, where the magnetic field makes a smaller angle with the Earth's surface.

3.2 Effect estimates and comparison to observations

3.2.1 Temperature

Roble & Dickinson (1989) were the first to quantify the effect of an increase in greenhouse gases on the upper atmosphere. They used a 1-D model of the upper atmosphere to show that a doubling of the CO_2 and methane concentration would cause a cooling of the thermosphere of up to 50 K. Since this initial pioneering study, many more have followed, using increasingly sophisticated numerical models of the upper atmosphere.

Most modelling studies employed a doubling of the CO_2 concentration, like Roble & Dickinson (1989). This can make it somewhat difficult to make direct quantitative comparisons between observed and modelled trends, as a doubling has not yet occurred. When variables depend more or less linearly on the CO_2 concentration, such as the thermospheric temperature or h_mF_2 (Cnossen, 2009; Cnossen et al., 2009), modelling results can be linearly interpolated. However, the response in thermospheric density decreases with increasing CO_2 concentration, so that linear interpolation results in an underestimate of trends (Cnossen, 2009).

Akmaev & Fomichev (2000) avoided such problems by performing simulations with the Spectral Mesosphere/Lower Thermosphere Model (SMLTM; Akmaev et al., 1992), using the CO_2 concentrations of 1955 and 1995 (313 and 360 ppm, respectively). The global mean vertical profile of the thermal response they found was in qualitative agreement with observations, showing cooling in the mesosphere, little change near the mesopause, a slight warming in the lower thermosphere, and a cooling from ~120-125 km that increased with height. However, their mesospheric cooling was about -0.8 K/decade, ~3 times smaller than observed. Also the thermospheric cooling was smaller than observed, and the turning point from warming to cooling in the lower thermosphere occurred at too low altitude.

Akmaev et al. (2006) therefore performed additional model simulations with the SMLTM which included also changes in water vapour and ozone concentration. The inclusion of

ozone resulted in a much stronger modelled cooling in the mesosphere of nearly 2 K/decade, almost as strong as the observed trend. The addition of ozone, and to a lesser extent water vapour, also produced a more pronounced warming in the lower thermosphere of up to 3 K/decade at ~115 km, which turned into a cooling again above ~150 km.

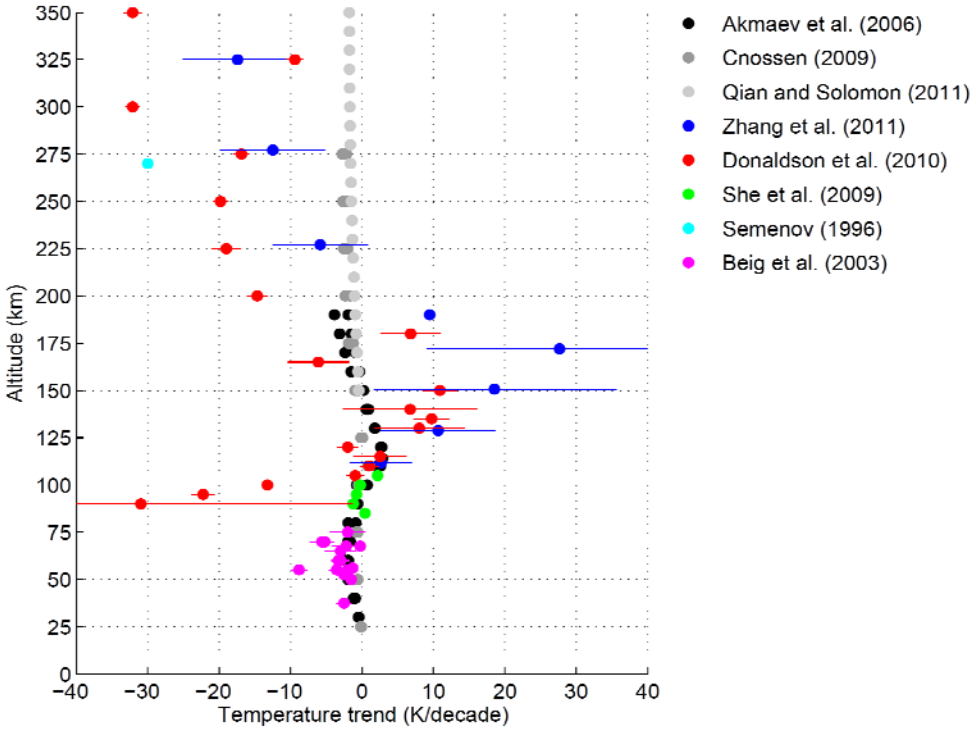

Fig. 4. Observed and modelled temperature trends (dots) with error bars where available (lines). Note that modelling results are in black/grey while observational results are in colour. For Akmaev et al. (2006) both January and March results are shown (stronger trends are for January) and for Cnossen (2009) both March and June results are shown (stronger trends are for June, though there is only a small difference). All other results are seasonal averages.

Cnossen (2009) obtained results similar to those of Akmaev et al. (2006) using simulations with the Coupled Middle Atmosphere and Thermosphere Model 2 (CMAT2; Harris, 2006), studying the combined effects of changes in CO_2 and ozone concentration between 1965 and 1995. Qian et al. (2006) and Qian & Solomon (2011) used a global mean model to investigate trends higher up in the thermosphere, but considered only changes in the CO_2 concentration from 1970 to 2000.

The temperature trends calculated by Akmaev et al. (2006), Cnossen (2009) and Qian & Solomon (2011) are compared to observed trends in figure 4. There is good agreement

between the Akmaev et al. (2006) and Cnossen (2009) model estimates and observed trends in the middle atmosphere and lower thermosphere (25-120 km). However, at ~130-180 km, most observations show a strong apparent warming, which is not reproduced by the models. Also, the strong cooling observed higher up in the thermosphere (>200 km) is underestimated by the modelling studies by Cnossen (2009) and Qian & Solomon (2011). Both studies predict a cooling that remains more or less constant with increasing altitude (>200 km), while observations indicate a strengthening of the trend with increasing altitude.

Akmaev et al. (2006) argued that the lack of a strong warming in the lower thermosphere in their results might be due to an overestimate of the amount of CO_2 present in the upper mesosphere and lower thermosphere in the SMLTM. Still, this does not explain why too little cooling is predicted by modelling studies above ~200 km. Although the observed thermospheric temperature trends are based on data from just two sites, it does appear that changes in CO_2 and ozone concentration cannot fully explain those trends.

3.2.2 Density

The same modelling studies described in the previous section also provided trends in density, which are compared to each other and to observations in figure 5. The density trends modelled by Akmaev et al. (2006) are about twice as strong as those modelled by Cnossen (2009). However, there is also a large spread in observed trends. At ~200 km, the Akmaev et al. (2006) trends seem to agree quite well with trends observed by Saunders et al. (2011), while the Cnossen (2009) trends agree better with Emmert & Picone (2011) and Emmert et al. (2004). The trends modelled by Qian & Solomon (2011) at higher altitude also tend to agree best with Emmert & Picone (2011) and Emmert et al. (2004), as well as Marcos et al. (2005).

Depending on which observations and modelling results are chosen for comparison, it may be argued that trends in density show better agreement between models and observations than trends in temperature. However, this may be partly so because the density at a certain height responds to the temperature structure of the entire atmosphere below. That means that the effects of insufficient warming below 200 km and insufficient cooling above 200 km could to some extent cancel each other out at altitudes above 200 km.

The modelled seasonal dependence of trends in density does not match with observations. Emmert et al. (2008) found that density trends are weakest in January and February, while the modelled trends by Akmaev et al. (2006) are stronger for January than for March. Changes in CO_2 and ozone concentration can therefore not explain the observed seasonal dependence.

There is however an explanation for the dependence of trends in density and temperature on the solar activity level. Qian et al. (2006) showed that stronger trends during solar minimum are due to CO_2 cooling being a relatively more important cooling mechanism at solar minimum, while cooling by nitric oxide (NO) becomes more important at solar maximum. A change in CO_2 concentration therefore has a larger impact on the radiative balance in the upper atmosphere during solar minimum than during solar maximum.

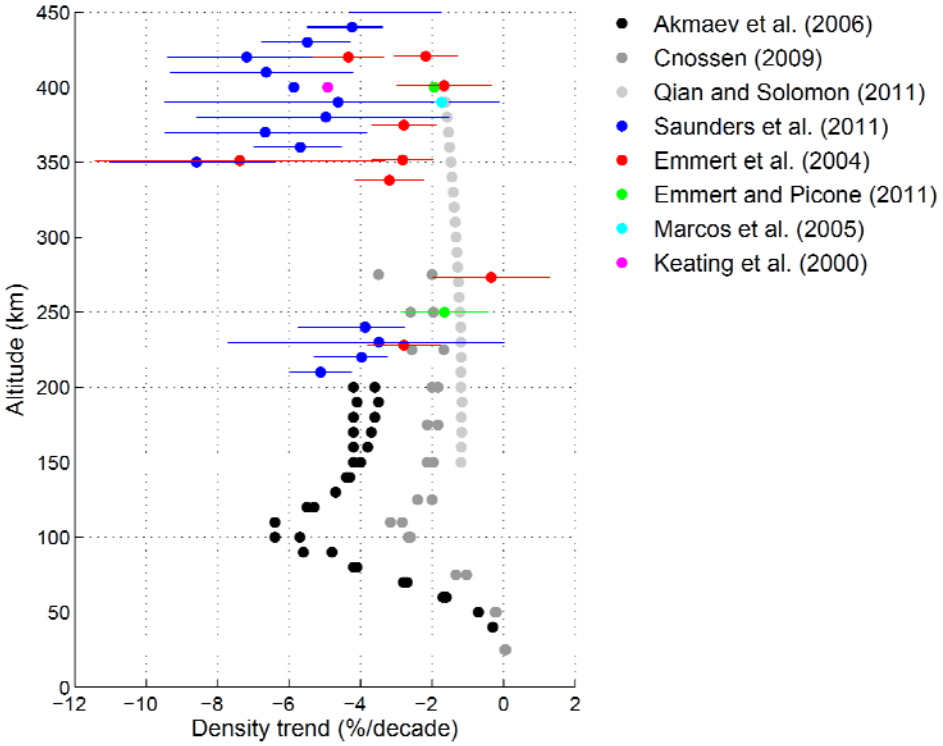

Fig. 5. Observed and modelled density trends (dots) with error bars where available (lines) Note that modelling results are in black/grey while observational results are in colour. For Akmaev et al. (2006) both January and March results are shown (stronger trends are for January) and for Cnossen (2009) both March and June results are shown (stronger trends are for June). All other results are seasonal averages.

3.2.3 The ionospheric F_2 layer

Qian et al. (2009) performed simulations with the Thermosphere-Ionosphere-Electrodynamics General Circulation Model (TIE-GCM; Roble et al., 1998; Richmond et al., 1992), focusing more on the effects of CO_2 cooling on the F_2 layer ionosphere. They doubled the CO_2 concentration from 365 ppmv to 730 ppmv and noted that certain features of the changes in N_mF_2 and h_mF_2 followed the magnetic equator, indicating the role of electrodynamics in generating these trends.

Qian et al. (2009) showed that changes in both the meridional and zonal neutral wind affected the transport of ionospheric plasma by neutral winds, through the mechanism described in section 3.1.3. This was an important contributor to changes in h_mF_2, especially under solar minimum conditions. At solar maximum, they found that the changes in N_mF_2 matched quite well with the pattern of changes in the O/N_2 ratio, which is proportional to the balance of ion production and loss rates. This result indicated a less important role for

changes in dynamics, and Qian et al. (2009) found indeed that changes in neutral winds were smaller at solar maximum. The smaller changes found under solar maximum conditions could again be linked to the smaller contribution to the radiative budget of CO_2 cooling relative to NO cooling at solar maximum (Qian et al., 2006).

The changes in h_mF_2 modelled by Qian et al. (2009) were mostly negative, as expected, but they were occasionally positive for solar minimum, usually after midnight. To compare the magnitude of the changes they found to observed trends, figure 6 shows trends in h_mF_2 and f_oF_2 in km/decade and MHz/decade, linearly interpolated from their results for 3 LT. The interpolation was done based on the actual change in CO_2 concentration between 1960 and 2010 (73 ppm; 14.6 ppm/decade), so that their original numbers were divided by 25 (365/14.6).

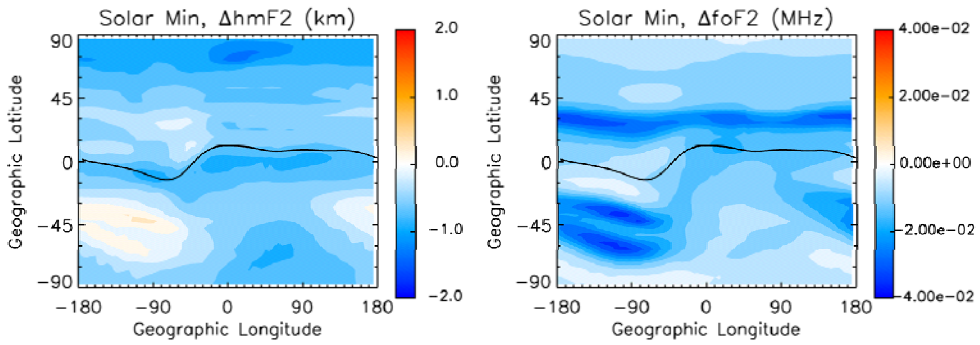

Fig. 6. Trends in h_mF_2 in km/decade (left) and f_oF_2 in MHz/decade (right) at 3 LT linearly interpolated from the model simulations by Qian et al. (2009) at June solstice.

A typical interpolated trend in h_mF_2 is -1 km/decade, while maximum negative trends go up to about -2 km/decade (at 12 LT; not shown) and maximum positive trends up to 0.5 km/decade. These values are somewhat larger than the median change in h_mF_2 reported by Bremer et al. (2004), but ~2-5 times smaller than typical changes at individual stations. Modelled trends for solar maximum conditions are even smaller. Estimated trends in f_oF_2 vary between 0 and -0.04 MHz/decade. The strongest trend of -0.04 MHz/decade is also larger than the median change in f_oF_2 of -0.01 MHz/decade reported by Bremer et al. (2004), but again underestimates changes observed at many individual stations. Positive trends that have been reported in some locations are not explained at all. From these results we can conclude that the change in CO_2 concentration has contributed to long-term trends in the F_2 layer, but it is unlikely to be the sole cause.

4. Secular variation of the Earth's magnetic field

4.1 Background and mechanism

The Earth's magnetic field varies slowly in strength and in orientation over time, and also the relative contributions of the main dipole component and higher order field components vary. We are currently at a time of relatively strong change in terms of field intensity, as the Earth's dipole moment has decreased by about 5% per century since 1840, while little

change in field strength occurred from 1590 to 1840 (Gubbins et al., 2006). The angle between the geomagnetic dipole and the Earth's rotation axis, the tilt angle, has changed also over the last half century, from ~11.7° in 1960 to ~10.5° in 2005, following more than a century where it remained nearly constant (Amit & Olson, 2008).

The Earth's magnetic field plays a role in the state of the upper atmosphere in various ways. First of all, it is what shapes the Earth's magnetosphere, and controls to some extent the interactions of the magnetosphere with the solar wind and the ionosphere. This determines the flux and energy of energetic particles precipitating into the upper atmosphere, as well as the high-latitude electric field and ionospheric convection pattern (see e.g. Kivelson & Russell (1995) for further details).

Secondly, the orientation of the Earth's magnetic field influences the transport of ionospheric plasma by neutral winds. This process has been described in section 3.1.3 in the context of indirect effects of changes in circulation. However, even if there were no changes in the neutral wind, changes in the inclination and declination of the Earth's magnetic field could still cause changes in the plasma motion. The inclination is the angle between the magnetic field and the Earth's surface and the declination is the angle with geographic North. A change in the inclination I directly affects the vertical component of the plasma motion driven by neutral winds, which is equal to the component of the horizontal neutral wind parallel to the magnetic field, $v_{n,par}$, times the factor $\sin(I)\cos(I)$. A change in declination changes the magnitude of $v_{n,par}$, as it changes the projection of the neutral wind onto magnetic field lines. The changes in magnetic field orientation also cause changes to the ion drag acting on the neutral wind, so that neutral winds are likely to change as well.

The neutral wind is also responsible for the generation of the dynamo electric field $\mathbf{E}_{dyn}$ through $\mathbf{E}_{dyn} = \mathbf{v}_n \times \mathbf{B}$, where $\mathbf{v_n}$ is the neutral wind and $\mathbf{B}$ the magnetic field. Both changes in the neutral wind and changes in declination and inclination alter the component of $\mathbf{v}_n$ perpendicular to $\mathbf{B}$. In addition, a change in the magnitude of $\mathbf{B}$ changes the ionospheric Pedersen and Hall conductivities, and these combined effects induce a change in the electrostatic field $\mathbf{E}$. The change in $\mathbf{E}$ and $\mathbf{B}$ does not only cause changes to the ion drag exerted on the neutral wind, further modifying $\mathbf{v}_n$, but also modifies the $\mathbf{E}\times\mathbf{B}$ drift of ions and electrons. The vertical component of this drift can be expected to change h_mF_2 and f_oF_2 too.

While the ionosphere is expected to be most directly affected by changes in the magnetic field, changes to the neutral atmosphere can occur as well. Possible effects on the neutral wind via ion-neutral collisions have already been mentioned, and as noted before, any changes in circulation can have secondary effects on for instance the neutral temperature structure. The neutral temperature in the thermosphere may also be directly affected through changes in Joule heating.

4.2 Effect estimates and comparison to observations

Cnossen & Richmond (2008) quantified the global effects of magnetic field changes on the ionospheric F_2 layer using simulations with the Thermosphere-Ionosphere-Electrodynamics general circulation model (TIE-GCM). They found that changes in the Earth's magnetic field from 1957 to 1997 had a substantial effect on h_mF_2 and f_oF_2 in some parts of the world, primarily South America and the southern Atlantic Ocean (see figure 7). In these regions,

the inclination of the magnetic field changed the most. The changes in inclination were the dominant cause of the trends in the F_2 layer, by changing plasma transport up and down magnetic field lines driven by neutral winds. Neutral winds also changed somewhat, but no significant effects on the thermospheric temperature were found.

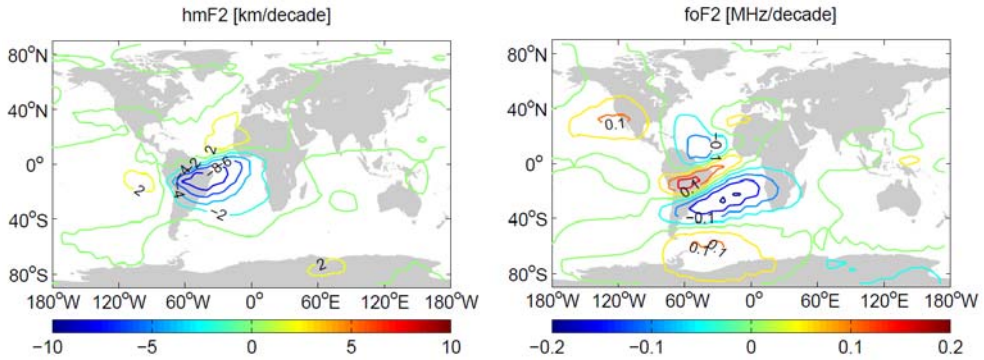

Fig. 7. Trends in h_mF_2 in km/decade (left) and f_oF_2 in MHz/decade (right) at 12 LT at June solstice due to changes in the Earth's magnetic field, interpolated from the model simulations by Cnossen & Richmond (2008).

Figure 7 shows the average trends in h_mF_2 and f_oF_2 in km/decade and MHz/decade, respectively, linearly interpolated from the change between 1957 and 1997. Over South America and the southern Atlantic Ocean, modelled trends in h_mF_2 and f_oF_2 are of the order of -5 to +2 km/decade and ±0.1 MHz/decade, respectively. Trends show a strong spatial dependence, and also vary (even in sign) depending on the season and time of day.

The magnitudes of the trends due to magnetic field changes in the regions that are most strongly affected are quite similar to the magnitudes of typical observed trends, and 2-5 times larger than the maximum changes predicted to be caused by changes in the CO_2 concentration. Still, a direct comparison between modelled and observed trends at specific stations indicated that modelled trends were usually smaller. At Concepción (36.8°S, 73.0°W) and Argentine Islands (65.2°S, 64.3°W), both located in the region where modelled trends were strongest, changes in the magnetic field could account for ~30-50% and ~20% of the observed trends. The observed and modelled seasonal-diurnal patterns of trends for these stations did not match.

The predicted changes outside the region of South America and the southern Atlantic Ocean were very small. However, the spatial pattern of modelled trends, showing a marked change at a longitude of ~0-20°, with weak trends east of that line, and much stronger trends to the west, was somewhat similar to the findings of Bremer (1998) and Jarvis (2009), although they found positive trends west of 30° and negative trends east of 30°. An increase of f_oF_2 trends with geomagnetic latitude, as found by Danilov & Mikhailov (1999), was not found.

Based on the study by Cnossen & Richmond (2008) we can conclude that long-term changes in the magnetic field are important in some regions, but do not explain observed trends elsewhere. However, Cnossen & Richmond (2008) had to neglect any effects of changes in

the high-latitude coupling between the magnetosphere and ionosphere-thermosphere system that might arise, as their model did not include a magnetosphere. This could have resulted in an underestimation of the effects of magnetic field changes, especially at high latitudes.

Recently the TIE-GCM has been successfully coupled to the Lyon-Fedder-Mobarry (LFM) MHD code, forming the Coupled Magnetosphere-Ionosphere-Thermosphere (CMIT) model (Wiltberger et al., 2004; Wang et al., 2004, 2008). With this model it is now possible to include the effects of changes in high-latitude magnetosphere-ionosphere coupling, and Cnossen et al. (2011) have started to use this to re-assess the effects of changes in the magnetic field on the ionosphere and thermosphere.

Cnossen et al. (2011) started with a simplified experiment, investigating the effect of changes in magnetic field strength only. They reduced the magnetic field strength to 75% of its present-day value, which caused changes in h_mF_2 of up to -40 and +60 km and changes in f_oF_2 of up to -3 to +1 MHz. If a linear response is assumed, considering a 5% decrease in magnetic field strength per century, these would be equivalent to trends of -0.8 to +1.2 km/decade and -0.06 to +0.02 MHz/decade. While clearly smaller than the trends predicted from the full magnetic field changes between 1957 and 1997, as expected, this rough estimate indicates that changes in magnetic field strength alone could still make a significant contribution to long-term trends. The trends in h_mF_2 and f_oF_2 predicted in this way appear to be of similar order of magnitude as those due to changes in CO_2 concentration.

The spatial pattern of changes simulated by CMIT is different from that simulated with TIE-GCM for the full magnetic field changes between 1957 and 1997, which is perhaps not surprising, as they were caused (predominantly) by different mechanisms. The new experiments show strong changes in h_mF_2 over Australia, the Pacific Ocean, and the northern Indian Ocean, and smaller changes over the Atlantic Ocean. This opens up the possibility that effects of changes in the magnetic field are present over different and more widespread areas than previously thought. A detailed comparison between the changes modelled by CMIT and observed trends will be done once CMIT simulations with historic magnetic fields have been performed, which are planned for the near future.

5. Changes in solar and geomagnetic activity

5.1 Solar activity

The solar activity level varies over an approximately 11-year cycle, and there are indications that there are longer-term variations too (e.g. Pap & Fox, 2004). When the Sun is more active, it is brighter and emits more radiation, especially in the shorter wavelengths, such as the ultraviolet (UV) and extreme ultraviolet (EUV), which are important for the radiative budget of the middle and upper atmosphere. Absorption of EUV radiation also results in ionization of O, O_2, and N_2. Any long-term changes in solar activity may therefore be expected to cause long-term trends in the temperature and electron density distribution in the upper atmosphere.

Lean (2001) used EUV satellite measurements and proxies (proxies only before 1974) to study long-term trends in EUV irradiance, and found an increase over the first half of the 20th century, with no clear trend after 1950. Since most observed trends in the upper atmosphere have been derived from data collected after 1950, a long-term trend in solar

activity is unlikely to have contributed much to those (Laštovička, 2005). However, for other time intervals (e.g. 1900-1950) it could be a contributor.

5.2 Geomagnetic activity

Geomagnetic activity is a manifestation and measure of "space weather", arising from the interaction between the solar wind and the Earth's magnetosphere. This interaction generates currents in the ionosphere and magnetosphere which cause small perturbations to the main magnetic field of the Earth that can be measured at the surface. These magnetic perturbations form the basis of indices of geomagnetic activity, such as the Ap, aa, and Kp indices. Each of these indices is derived from the K index, which is related to the maximum fluctuations of the horizontal components of the observed geomagnetic field, relative to a quiet day (a day with few disturbances due to the solar wind), during a three-hour interval.

Various studies have indicated the presence of a long-term trend in geomagnetic activity over the past ~50-150 years. Clilverd et al. (1998) and Stamper et al. (2002) found that the geomagnetic activity in terms of the aa-index was increasing throughout the 20th century, and Clilverd et al. (2002) found that the number of geomagnetic storms per solar cycle had also been increasing until it stabilized in the last few cycles. Long-term changes in the solar quiet-time day variation, Sq, have been found as well. Macmillan & Droujinina (2007) reported a weak upward trend of on average 1.3 nT per century (~10%) in the Sq amplitude based on records from 14 magnetic observatories. Elias et al. (2010) analysed data from three stations, and found also positive trends in Sq of 5-10%/century.

High geomagnetic activity indicates disturbed space weather conditions, usually resulting from disturbances in the solar wind. This tends to lead to stronger energetic particle precipitation and ionospheric convection at high latitudes, stronger ionospheric currents, and an enhancement of the Joule heating in the upper atmosphere, eventually leading to higher temperatures and stronger neutral winds. Variations in geomagnetic activity occur on short timescales from minutes to days, and are responsible for part of the large natural variability in the thermosphere-ionosphere system. A gradual, long-term change in the background level of geomagnetic activity could therefore cause a long-term trend in the upper atmosphere.

Because geomagnetic activity is a measure of the interaction between the solar wind and the Earth's magnetosphere-ionosphere-thermosphere system, the origin of long-term changes in geomagnetic activity could be associated either with the Sun (e.g. Stamper et al., 1999) or with the terrestrial system (or both). Clilverd et al. (2002) concluded from a simple calculation that involved various assumptions and approximations that changes in the Earth's magnetic field would have little effect on geomagnetic activity. However, a detailed analysis has not been done yet, and the simulations by Cnossen et al. (2011) indicate that the effect may be larger than previously thought, due to a stronger dependence of the ionospheric conductance on the magnetic field strength than was assumed by Clilverd et al. (2002). When considering the effects of changes in geomagnetic activity on the upper atmosphere, it is therefore possible that these may ultimately be due to changes in the Sun and/or changes in the Earth's magnetic field. Nevertheless, the effect of the observed change in geomagnetic activity on the upper atmosphere, regardless of which processes may have contributed to it, can still be investigated.

Laštovička (2005) claims that the role of geomagnetic activity in causing long-term trends was small for the second half of the 20th century, just like that of solar activity. However, there has been little effort so far to actually quantify the effect of reported long-term changes in geomagnetic activity on the upper atmosphere. No detailed modelling study exists, so this may be an area for future studies to explore.

6. Influences from the lower atmosphere

The lower atmosphere influences the upper atmosphere through upwardly propagating planetary waves, gravity waves and tides, and acts in general as a boundary condition for the middle and upper atmosphere. Any long-term changes in the lower atmosphere therefore have the potential to induce long-term changes in the upper atmosphere.

Jarvis (2009) argued that the longitudinal variation in h_mF_2 trends over Eurasia found by himself and Bremer (1998) suggests the influence of a stationary wave-like feature between 3°W and 104°E, and that the fact that it is a geo-stationary feature implies a cause linked to the troposphere or solid Earth. On this basis, he proposed that the longitudinal variation in F_2 region trends might be caused via long-term changes in non-migrating tides, originating in the troposphere. Bencze (2007, 2009) also proposed an influence of non-migrating tides to explain differences in h_mF_2 trends between continental regions and oceans/seashores. Note that "non-migrating" in this context means "not moving with the apparent motion of the Sun".

It has been found that in particular the eastward propagating zonal wavenumber-3 diurnal tide (DE-3) has a strong influence on the ionosphere and thermosphere, especially at low latitudes (Hagan & Forbes, 2002). The DE-3 tide originates in the tropical troposphere primarily through latent heat release associated with deep convective cloud systems. Forbes et al. (2006) explained that this process is intimately connected with the predominant wavenumber-4 longitudinal distribution of topography and land-sea differences at low latitudes. The interaction of the diurnal harmonic of solar radiation with the characteristics of the Earth's surface, roughly displaying a wavenumber-4 pattern, generates the DE-3 tide. From a Sun-synchronous perspective, this appears to the observer as a wavenumber-4 feature mimicking the longitudinal surface heating pattern (Forbes & Hagan, 2000).

Wavenumber-4 patterns in the thermosphere and ionosphere have indeed been observed (e.g. Immel et al., 2006; Häusler et al., 2007). Hagan et al. (2007) performed simulations with the TIME-GCM, using a lower boundary tidal forcing from the Global Scale Wave Model (GSWM; Hagan & Forbes, 2002), which includes only latent heat release as a source of non-migrating tides. This confirmed that the DE-3 tide generated this way propagates all the way up into the thermosphere, where it excites a wavenumber-4 longitudinal structure, similar to observations. Jarvis (2009) noted that observed wavenumber-4 patterns in the thermosphere have a scale size similar to that of the longitudinal variations found in long-term trends in h_mF_2. It may therefore be that long-term changes in tropical convection could be ultimately responsible for at least part of the long-term change in the ionosphere.

Unfortunately, the ionospheric data currently available are not evenly spread over the globe, and therefore are insufficient to determine whether the longitudinal variation found between 3°W and 104°E is part of a global wavenumber-4 pattern. In addition, there is insufficient information on non-migrating tides to determine whether they exhibit long-term trends, let alone whether these would be large enough to produce the ionospheric trends

that are observed. A direct test of this hypothesis is therefore not yet possible, but it remains an intriguing possibility.

7. Conclusion

Temperature trends in the mesosphere can be explained largely by changes in CO_2 and ozone concentration. The effect of changes in water vapour concentration is much smaller. Observed changes in the thermospheric temperature have not been fully explained by model simulations of compositional changes. They mostly have the expected sign, but are not strong enough. Estimated trends in h_mF_2 and f_oF_2 are also 2-5 times smaller than what is typically observed.

There are several possible explanations for the discrepancies between modelled and observed trends in the thermosphere. There are errors associated with the data (see section 2.1 and figures 3 and 4), and also the models do not represent reality perfectly. There is for instance some uncertainty over the collisional excitation rate between CO_2 and atomic oxygen, which determines the efficiency of CO_2 cooling. The value chosen will affect the sensitivity in the model to changes in the CO_2 concentration, and there are many other factors that can have an influence too. Still the difference in magnitude between modelled and observed trends in the thermosphere is sufficiently large to suggest that thermospheric trends are not caused by changes in CO_2 and ozone concentration alone.

Indeed, simulations have shown that changes in the Earth's magnetic field also affect the F_2 layer. An initial study by Cnossen & Richmond (2008) showed that this is primarily important over South America and the southern Atlantic Ocean, while more recent simulations indicate that other regions may be affected too, even if only changes in magnetic field strength are considered. Detailed comparisons between modelled and observed trends are needed to determine to what extent changes in the magnetic field can explain the observations in the F_2 layer. Changes in the magnetic field do not explain trends in neutral temperature and density.

Further work is needed to get quantitative estimates of the effects of changes in geomagnetic activity level, and possible influences of long-term changes in the lower atmosphere. Also, in order to reduce the error bars on observed trends and detect any changes in trends that may occur over time, continued monitoring of the upper atmosphere, with as much global coverage as possible, is essential.

8. Acknowledgment

I would like to thank Shunrong Zhang, Bill Oliver, John Emmert, Arrun Saunders and Rashid Akmaev for sending me their data used in creating figures 4 and 5, Liying Qian for creating figure 6 for me, and Thomas Ulich for calculating the trends in h_mF_2. I am also grateful to Bill Oliver, Art Richmond, John Emmert, and Liying Qian for helpful feedback on an earlier version of this manuscript. The National Center for Atmospheric Research is sponsored by the National Science Foundation.

9. References

Akmaev, R.A., Fomichev, V.I., Gavrilov, N.M., & Shved, G.M. (1992). Simulation of the zonal mean climatology of the middle atmosphere with a 3-dimensional spectral

model for solstice and equinox conditions. *J. Atmos. Solar-Terr. Phys.*, Vol. 54, No. 2, pp. 119-128.

Akmaev, R.A., & Fomichev, V.I. (1998). Cooling of the mesosphere and lower thermosphere due to doubling of CO_2. *Ann. Geophys.*, Vol. 16, pp. 1501-1512.

Akmaev, R.A., & Fomichev, V.I. (2000). A model estimate of cooling in the mesosphere and lower thermosphere due to the CO_2 increase over the last 3-4 decades. *Geophys. Res. Lett.*, Vol. 27, No. 14, pp. 2113-2116.

Akmaev, R.A., Fomichev, V.I., & Zhu, X. (2006). Impact of middle-atmospheric composition changes on greenhouse cooling in the upper atmosphere. *J. Atmos. Solar-Terr. Phys.*, Vol. 68, No. 17, pp. 1879-1889.

Amit, H. & Olson, P. (2008). Geomagnetic dipole tilt changes induced by core flow. *Phys. Earth Plan. Interiors*, Vol. 166, No. 3-4, pp. 226-238.

Baldwin, M.P., & Dunkerton, T.J. (2001). Stratospheric harbingers of anomalous weather regimes. *Science,* Vol. 294, No. 5542, pp. 581-584.

Beig, G., Keckhut, P., Lowe, R.P., et al. (2003). Review of mesospheric temperature trends. *Rev. Geophys.*, Vol. 41, No. 4, 1015.

Bencze, P. (2007). What do we know of the long-term change of the Earth's ionosphere? *Adv. Space Res.*, Vol. 40, pp. 1121-1125.

Bencze, P. (2009). Geographical distribution of long-term changes in the height of the maximum electron density of the F region: A nonmigrating tide effect? *J. Geophys. Res.*, Vol. 114, A06304.

Bremer, J. (1998). Trends in the ionospheric E and F regions over Europe. *Ann. Geophys.*, Vol. 16, pp. 986-996.

Bremer, J., Alfonsi, L., Bencze, P., Laštovička, J., Mikhailov, A.V., & Rogers, N. (2004). Long-term trends in the ionosphere and upper atmosphere parameters, *Annals of Geophysics*, Vol. 47 (supplement), No. 2-3, pp. 1009-1029.

Clilverd, M.A., Clark, T.D.G., Clarke, E., & Rishbeth, H. (1998), Increased magnetic storm activity from 1868 to 1995, *J. Atmos. Solar-Terr. Phys.*, Vol. 60, pp. 1047-1056.

Clilverd, M.A., Clark, T.D.G., Clarke, E., Rishbeth, H., & Ulich, T. (2002). The causes of long-term changes in the aa index. *J. Geophys. Res.*, Vol. 107, No. A12, 1441.

Clilverd, M.A., Ulich, T., & Jarvis, M.J. (2003). Residual solar cycle influence on trends in ionospheric F2-layer peak height. *J. Geophys. Res.*, Vol. 108, No. A12, 1450.

Cnossen, I., & Richmond, A.D. (2008). Modelling the effects of changes in the Earth's magnetic field from 1957 to 1997 on the ionospheric hmF2 and foF2 parameters. *J. Atmos. Solar-Terr. Phys.*, Vol. 70, No. 11-12, pp. 1512-1524.

Cnossen (2009). *Modelling of long-term trends in the middle and upper atmosphere.* PhD thesis, University of Leicester, Leicester, UK.

Cnossen. I., Harris, M.J., Arnold, N.F., & Yiğit, E. (2009). Modelled effect of changes in the CO_2 concentration on the middle and upper atmosphere: Sensitivity to gravity wave parameterization, *J. Atmos. Solar-Terr. Phys.*, Vol. 71, pp. 1484-1496.

Cnossen, I., Richmond, A.D., Wiltberger, M., Wang, W., & Schmitt, P. (2011). The response of the coupled magnetosphere-ionosphere-thermosphere system to a 25% reduction in the dipole moment of the Earth's magnetic field. *J. Geophys. Res.,* in press.

Danilov, A.D. & Mikhailov, A.V. (1999). Spatial and seasonal variations of the foF2 long-term trends. *Ann. Geophys.*, Vol. 17, No. 9, pp. 1239-1243.

Donaldson, J.K., Wellman, T.J., & Oliver, W.L. (2010), Long-term change in thermospheric temperature above Saint Santin, *J. Geophys. Res.*, Vol. 115, A11305.

Elias, A.G., de Artigas, M.Z., & de Haro Barbas, B.F. (2010), Trends in the solar quiet geomagnetic field variation linked to the Earth's magnetic field secular variation and increasing concentrations of greenhouse gases, *J. Geophys. Res.*, Vol. 115, No. 8, A08316, doi: 10.1029/2009JA015136.

Elias, A.G., & Ortiz de Adler, N. (2006). Earth magnetic field and geomagnetic activity effects on long-term trends in the F2 layer at mid-high latitudes. *J. Atmos. Solar-Terr. Phys.*, Vol. 68, No. 17, 1871-1878.

Emmert, J.T., Picone, J.M., Lean, J.L., & Knowles, S.H. (2004). Global change in the thermosphere: compelling evidence of a secular decrease in density. *J. Geophys. Res.*, Vol. 109, No. A2, A02301.

Emmert, J.T., Picone, J.M., & Meier, R.R. (2008). Thermospheric global average density trends, 1967-2007, derived from orbits of 5000 near-Earth objects. *Geophys. Res. Lett.*, Vol. 35, No. 5, L05101.

Emmert, J.T. & Picone, J.M. (2011). Statistical uncertainty of 1967-2005 thermospheric density trends derived from orbital drag. *J. Geophys. Res.*, in press, doi.: 10.1029/2010JAO16382.

Fomichev, V.I. (2009). The radiative energy budget of the middle atmosphere and its parameterization in general circulation models. *J. Atmos. Solar-Terr. Phys.*, Vol. 71, pp. 1577-1585.

Forbes, J.M, & Hagan, M.E. (2000). Diurnal Kelvin wave in the atmosphere of Mars: Towards an understanding of 'stationary' density structures observed by the MGS accelerometer. *Geophys. Res. Lett.*, Vol. 27, No. 21, pp. 3563-3566.

Forbes, J.M., Russell, J., Miyahara, S., Zhang, X., Palo, S., Mlynczak, M., Mertens, C.J., & Hagan, M.E. (2006). Troposphere-thermosphere tidal coupling as measured by the SABER instrument on TIMED during July-September 2002. *J. Geophys. Res.*, Vol. 111, A10S06.

Gubbins, D., Jones, A.L., & Finlay, C.C. (2006). Fall in Earth's magnetic field is erratic. *Science*, Vol. 312, pp. 900-902.

Hagan, M.E., & Forbes, J.M. (2002). Migrating and nonmigrating diurnal tides in the middle and upper atmosphere excited by tropospheric latent heat release. *J. Geophys. Res.*, Vol. 107, No. D24, 4754.

Hagan, M.E., Maute, A., Roble, R.G., Richmond, A.D., Immel, T.J., & England, S.L. (2007). Connections between deep tropical clouds and the Earth's ionosphere. *Geophys. Res. Lett.*, Vol. 34, L20109.

Harris, M.J. (2001). *A new coupled middle atmosphere and thermosphere general circulation model: studies of dynamic, energetic and photochemical coupling in the middle and upper atmosphere*, PhD thesis, University College London, London, UK.

Häusler, K., Lühr, H., Rentz, S., & Köhler (2007). A statistical analysis of longitudinal dependences of upper thermospheric zonal winds at dip equator latitudes derived from CHAMP. *J. Atmos. Solar-Terr. Phys.*, Vol. 69, No. 12, pp. 1419-1430.

Haynes, P.H., Marks, C.J., McIntyre, M.E., Shepherd, T.G., & Shine, K.P. (1991). On the downward control of extratropical diabatic circulations by eddy-induced mean zonal forces. *J. Atmos. Sci.,* Vol. 48, No. 4, pp. 651-679.

Holt, J.M., & Zhang, S.R. (2008). Long-term temperature trends in the ionosphere above Millstone Hill. *Geophys. Res. Lett.*, Vol. 35, No. 5, L05813.

Hurst, D.F., Oltmans, S.J., Vömel, H., Rosenlof, K.H., Davis, S.M., Ray, E.A., Hall, E.G., & Jordan, A.F. (2011). Stratospheric water vapor trends over Boulder, Colorado: Analysis of the 30 year Boulder record. *J. Geophys. Res.*, Vol. 116, D02306.

Immel, T.J., Sagawa, E., England, S.L., Henderson, S.B., Hagan, M.E., Mende, S.B., Frey, H.U., Swenson, C.M., & Paxton, L.J. (2006). Control of equatorial ionospheric morphology by atmospheric tides. *Geophys. Res. Lett.*, Vol. 33, L15108.

Jarvis, M.J., Clilverd, M.A., & Ulich, Th. (2002). Methodological influences on F-region peak height trend analyses, *Phys. Chem. Earth*, Vol. 27, pp. 589-594.

Jarvis, M.J. (2009). Longitudinal variation in E- and F-region ionospheric trends. *J. Atmos. Solar-Terr. Phys.*, Vol. 71, 1415-1429.

Keating, G.M., Tolson, R.H., & Bradford, M.S. (2000). Evidence of long term global decline in the Earth's thermospheric densities apparently related to anthropogenic effects. *Geophys. Res. Lett.*, Vol. 27, No. 10, pp. 1523-1526.

Kivelson, M.G. & Russell, C.T. (Eds.) (1995). *Introduction to space physics*. Cambridge University Press, ISBN 0-521-45714-9, Cambridge, UK.

Laštovička, J. (2005). On the role of solar and geomagnetic activity in long-term trends in the atmosphere-ionosphere system. *J. Atmos. Solar Terr. Phys.*, Vol. 67, No. 1-2, pp. 83-92.

Laštovička, J., Akmaev, R.A., Beig, G., Bremer, J., & Emmert, J.T. (2006a). Global change in the upper atmosphere. *Science,* Vol. 314, No. 5803, pp. 1253-1254.

Laštovička, J., Mikhailov, A.V., Ulich, T., Bremer, J., Elias, A.G., Ortiz de Adler, N., Jara, V., Abaraca del Rio, R., Foppiano, A.J., Ovalle, E., & Danilov, A.D. (2006b). Long-term trends in foF2: A comparison of various methods. *J. Atmos. Solar-Terr. Phys.*, Vol. 68, pp. 1854-1870.

Lean, J.L., White, O.R., Livingstone, C., & Picone, J.M. (2001). Variability of a composite chromospheric irradiance index during the 11-year activity cycle and over longer time periods. *J. Geophys. Res.,* Vol. 106, No. A6, pp. 10645-10658.

Macmillan, S., & Droujinina, A. (2007). Long-term trends in geomagnetic daily variation. *Earth Planets Space*, Vol. 59, pp. 391-195.

Marcos, F.A., Wise, J.O., Kendra, M.J., Grossbard, N.J., & Bowman, B.R. (2005). Detection of a long-term decrease in thermospheric neutral density. *Geophys. Res. Lett.*, Vol. 32, L04103.

Pap, J.M., & Fox, P. (Eds.). (2004). *Solar variability and its effects on climate*, Geophysical Monograph 141, American Geophysical Union, ISBN 0-87590-406-8, USA.

Qian, L., Roble, R.G., Solomon, S.C., & Kane, T.J. (2006). Calculated and observed climate change in the thermosphere, and a prediction for solar cycle 24. *Geophys. Res. Lett.*, Vol. 33, L23705.

Qian, L., Burns, A.G., Solomon, S.C., & Roble, R.G. (2009). The effect of carbon dioxide cooling on trends in the F2-layer ionosphere. *J. Atmos. Solar-Terr. Phys.,* Vol. 71, pp. 1592-1601.

Qian, L., & Solomon, S.C. (2011). Thermospheric density: an overview of temporal and spatial variations, *Space Sci. Rev.*, in press, doi.: 10.1007/s11214-011-9810-z.

Qian, L., Laštovička, J., Roble, R.G., & Solomon, S.C. (2011). Progress in observations and simulations of global change in the upper atmosphere. *J. Geophys. Res.*, Vol. 116, A00H03.

Richmond, A.D., Ridley, E.C., & Roble, R.G. (1992). A thermosphere-ionosphere general circulation model with coupled electrodynamics. *Geophys. Res. Lett.*, Vol. 19, No. 6, pp. 601-604.

Rinsland, C.P., Chiou, L., Boone, C., Bernath, P., Mahieu, E., & Zander, R. (2009). Trend of lower stratospheric methane (CH_4) from atmospheric chemistry experiment (ACE) and atmospheric trace molecule spectroscopy (ATMOS) measurements, *J. Quant. Spectr. Rad. Transfer*, Vol. 110, pp. 1066-1071.

Rishbeth, H. (1990). A greenhouse effect in the ionosphere? *Plan. Space Sci.*, Vol. 38, No. 7, pp. 945-948.

Rishbeth, H. (1998). How the thermospheric circulation affects the ionospheric F2-layer. *J. Atmos. Solar-Terr. Phys.*, Vol. 60, 1385-1402.

Roble, R.G., Ridley, E.C., Richmond, A.D., Dickinson, R.E. (1988). A coupled thermosphere ionosphere general circulation model. *Geophys. Res. Lett.*, Vol. 15, No. 12, pp. 1325-1328.

Roble, R.G., & Dickinson, R.E. (1989). How will changes in carbon-dioxide and methane modify the mean structure of the mesosphere and thermosphere? *Geophys. Res. Lett.*, Vol. 16, No. 12, pp. 1441-1444.

Rosenlof, K.H., Oltmans, S.J., Kley, D., Russell III, J.M., Chiou, E.W., Chu, W.P., Johnson, D.G., Kelly, K.K., Michelsen, H.A., Nedoluha, G.E., Remsberg, E.E., Toon, G.C., & McCormick, M.P. (2001). Stratospheric water vapour increases over the past half-century. *Geophys. Res. Lett.*, Vol. 28, No. 7, pp. 1195-1198.

Sassi, F., Garcia, R.R., Marsh, D., & Koppel, K.W. (2010). The role of the middle atmosphere in simulations of the troposphere during northern hemisphere winter: differences between high- and low-top models. *J. Atmos. Sci.,* Vol. 67, No. 9, pp. 3048-3064.

Salby, M., Titova, E., & Deschamps, L. (2011). Rebound of Antarctic ozone. *Geophys. Res. Lett.*, Vol. 38, L09702.

Saunders, A., Lewis, H., & Swinerd, G. (2011). Further evidence of long-term thermospheric density change using a new method of satellite ballistic coefficient estimation. *J. Geophys. Res.*, in press, doi.: 10.1029/2010JAO16358.

Semenov, A.I. (1996). Temperature regime of the lower thermosphere from emission measurements during the last decades. *Geomagn. Aeron.*, Vol. 36, No. 5, pp. 90-97.

She, C.-Y., Krueger, D.A., Akmaev, R.A., Schmidt, H., Talaat, E., & Yee, S. (2009). Long-term variability in mesopause region temperatures over Fort Collins, Colorado (41°N, 105°W) based on lidar observations from 1990 through 2007.

Shimazaki, T. (1955). World-wide variations in the height of the maximum electron density of the ionospheric F2 layer. *J. Radio Res. Labs. Japan*, Vol. 2, pp. 85-97.

Solomon, S. (1999). Stratospheric ozone depletion: a review of concepts and history. *Rev. Geophys.*, Vol. 37, No. 3, pp. 275-316.

Stamper, R., Lockwood, M., Wild, M.N., & Clark, T.D.G. (1999). Solar causes of the long-term increase in geomagnetic activity. *J. Geophys. Res.*, Vol. 104, pp. 28325-28342.

Stolarski, R. & Frith, S.M. (2006). Search for evidence of trend slow-down in the long-term TOMS/SBUV total ozone data record: the importance of instrument drift uncertainty. *Atmos. Chem. Phys.*, Vol. 6, pp. 4057-4065.

Ulich, Th. (2000). *Solar variability and long-term trends in the ionosphere.* PhD thesis, Sodankylä Geophysical Observatory Publications, No. 87, Sodankylä, Finland.

Wang, W., Wiltberger, M., Burns, A.G., Solomon, S.C., Killeen, T.L., Maruyama, N., & Lyon, J.G. (2004). Initial results from the coupled magnetosphere-ionosphere-thermosphere model: thermosphere-ionosphere responses. *J. Atmos. Solar-Terr. Phys.*, Vol. 66, No. 15-16, pp. 1425-1441.

Wang, W.B., Lei, J.H., Burns, A.G., Wiltberger, M., Richmond, A.D., Solomon, S.C., Killeen, T.L., Talaat, E.R., & Anderson, D.N. (2008). Ionospheric electric field variations during a geomagnetic storm simulated by a coupled magnetosphere ionosphere thermosphere (CMIT) model, *Geophys. Res. Lett.*, Vol. 35, No. 18, L18105.

Wiltberger, M., Wang, W., Burns, A.G., Solomon, S.C., Lyon, J.G., & Goodrich, C.C. (2004). Initial results from the coupled magnetosphere ionosphere thermosphere model: magnetospheric and ionospheric responses. *J. Atmos. Solar-Terr. Phys*., Vol. 66, No. 15-16, pp. 1411-1423.

Zhang, S.-R., Holt, J.M., & Kurdzo, J. (2011), Millstone Hill ISR observations of upper atmospheric long-term changes: Height dependency, *J. Geophys. Res*., Vol. 116, A00H05.

16

Projecting Changes in Extreme Precipitation in the Midwestern United States Using North American Regional Climate Change Assessment Program (NARCCAP) Regional Climate Models

Shuang-Ye Wu
University of Dayton, USA

1. Introduction

Based on the physics of global circulation, many expect an enhanced greenhouse effect to lead to a more active hydrological cycle with more precipitation on average (Hennessy et al. 1997). This expected increase has been found in observations (Zhang et al. 2007) and has also been suggested by climate models, although these models are not consistent with respect to the spatial and temporal variability about this change. An increase in mean precipitation depth, assuming no change in the shape of the frequency distribution, would imply an increased frequency of heavy-precipitation events. However, some studies (Hennessy et al. 1997, Allen and Soden, 2008) also suggest the increase in these extreme events could be disproportionate to the change in the mean, with a greater fraction of the total precipitation being delivered by such heavy precipitation events. Such a shift towards heavy events is a common conclusion of climate models (Cubasch et al. 2001, Meehl et al. 2007) as well as analyses of observed rainfall data at the continental scale (Easterling 2000, Kunkel 2003, Groisman 2005, Min et al. 2011). However, there is great spatial variation of this average pattern. This study aims to establish likely future projections for how extreme precipitation frequency and magnitude could change in the Midwestern region of the United States, and investigate the spatial variation of such changes within the area.

Present global climate models (GCMs) typically produce results at the spatial resolution of 150-300 km. This level of spatial resolution of GCMs is insufficient for establishing localized future climate projections and examining their spatial variations at the scale of a state. For increased spatial resolution, we used a set of Regional Climate Models (RCMs) run by National Center for Atmospheric Research (NCAR) under the North American Regional Climate Change Assessment Program (NARCCAP). RCMs involve nesting a higher resolution climate models within a coarser resolution GCM. The GCM output is used to define boundary conditions around a limited domain, within which RCM further models the physical dynamics of the climate system. These RCMs are designed to produce high resolution climate change simulations in order to investigate uncertainties in regional scale

projections of future climate and generate climate change scenarios for use in regional and local impacts research (Mearns et al, 2009).

This study aims to achieve two main objectives. First, we evaluate the performance of NARCCAP models in terms of whether they capture the frequency distribution of daily precipitation data. This evaluation is based on a comparison of retrospective model runs with observed station-based daily precipitation data. Second, based on the evaluation, we correct the bias in mean precipitation and frequency distribution of precipitation output from RCMs. After the model biases have been corrected, we then project future changes of mean and extreme precipitation patterns in the Midwest Region.

2. The Midwestern Region

The definition of the Midwestern region of the USA differs in literature. The Midwestern U.S. defined for the National Climate Change Assessment program (Easterling and Karl, 2000) includes the upper eight states south of the Great Lakes (Figure 1). We expanded the region to include Kentucky because of its similarities in both physical and socio-economic characters to the rest of the region. Based on 2010 census, the nine states contain about 21% of the nation's population. Their cumulative gross state product is approximately 20% of national gross domestic product of 2010. Therefore it is an area of great economic importance. Situated at the heart of the Corn Belt, the region's economy is dominated by farming, with 89% of the land area being used for agricultural purposes. As a result, climate variability and extreme weather play a key role in the economic productivity of the region. In recent decades, the Midwest region has observed a noticeable increase in average temperatures despite the strong year-to-year variations (Union of Concerned Scientists, 2009). The largest increase has occurred in winter. Both summer and winter precipitation has been above average for the last three decades, making it the wettest period in a century. Heavy rainfall events are also significantly more frequent than a century ago. The Midwest has experienced two record-breaking floods in the past 15 years (Union of Concerned Scientists, 2009). It can be seen from these already observed changes that climate change will have a profound impact on the region. As a result it is very important to investigate how precipitation pattern will change for the region in the near future.

The Midwestern region has a typical continental climate, although the Great Lakes have a great influence on nearby areas for both temperature and precipitation. The total annual precipitation of the region averages at 950 mm (1895-2005). In fall and winter, the precipitation is largely produced by mid-latitude wave cyclones. In spring and summer, it is dominated by varying amount of convective thunderstorm rainfall. In most part of the region, precipitation is highly seasonal, with most of the rainfall concentrated in spring and summer. However in the Ohio River Valley in the southeastern part of the region, the amount of precipitation is fairly constant throughout the year. Spatially, annual precipitation ranges from 600 mm in northwest to 1200 mm in southeast, because of the increasing proximity to the Gulf of Mexico source of moisture (Figure 1). The slight deviation to this precipitation gradient is leeway shores of the Great Lakes, where lake effect precipitation, particularly from August to December, generates relatively wet conditions that lead to an annual precipitation depth around 900 - 1000 mm (Huff and Angel, 1992). Most of extreme precipitation events occur in spring and summer. Heavy precipitation in spring, when evaporation is relatively low due to lower temperature, can lead to severe flooding.

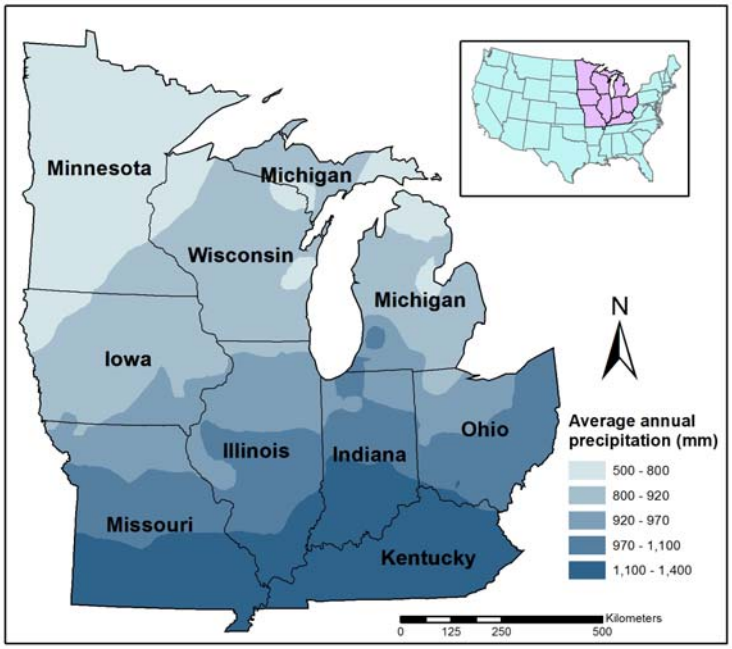

Fig. 1. Study area: annual mean precipitation in the Midwest United States

3. Data and methodology

3.1 Data

For model evaluation, observed daily precipitation data 1971-2000 were obtained from US Historical Climatology Network (USHCN) for climate stations in the Midwest Region. The time period was selected because it was the temporal domain of retrospective runs carried out by NARCCAP RCMs. We excluded years with less than 350 days of records to preserve frequency distribution of the data series, and any station with less than 25 complete years of records. We finally had 204 stations, with an average of 28.5 complete years of record per station.

NARCCAP includes 6 RCMs driven by 4 GCMs over the domain of North America, and they typically have the spatial resolution of 50 km. Not all simulations are completed. At the time of this study, 6 of the 24 RCM-GCM combinations are finished and data distributed. Table 1 shows the RCM-GCM combinations used in this study. For model evaluation, we used RCM retrospective runs (1971-2000), which produce 3-hourly precipitation data series. This data was summarized into daily precipitation data series 1971-2000. For projecting future precipitation patterns, we summarized RCM output for 2040-2070 into future daily precipitation data series. All model runs are driven with A2 emission scenario defined by the Intergovernmental Panel on Climate Change (IPCC) Special Report on Emission Scenarios (SRES) (IPCC, 2000). A2 assumes a medium high level of CO_2 emission based on a development pattern close to business-as-usual.

RCMs	GCMs			
	CCSM	CGCM3	GFDL	HADCM3
CRCM		X	X	
MM5I	X			
HRM3				X
RCM3		X		
WRFG	X			

Table 1. GCM-RCM combinations used in this study

3.2 Model evaluation methodology

In order to examine the frequency and magnitude of extreme events, it is important for a model to capture an accurate distribution of the data series. We first computed and compared the statistics that describe the shape of distribution for observed and modeled daily precipitation data. We chose to use L-moments to characterize the frequency distributions based on methods developed in Hosking (1990). L-moments are similar to conventional moments in that they are calculated to summarize the shape of a probability distribution. L-mean is identical to the conventional mean, whereas L-scale, L-skewness and L-kurtosis are analogous to conventional standard deviation, skewness and kurtosis. L-moments however are often considered superior to conventional moments in characterizing distribution shapes, because they are less sensitive to outliers (Ulrych et. al, 2000, Elamir et.al, 2003, and Hosking 2006).

We then attempted to quantify the deviation of the distributions of daily data output from 6 NARCCAP RCMs from observed daily precipitation distribution based on the following steps:

- Establish the empirical cumulative distribution function (F_{obs}) for observed precipitation series for each station: x_i , $i=1,2\ldots n$

$$F_{obs}(t) = \frac{1}{n}\sum_{i=1}^{n} 1\{x_i \le t\} \tag{1}$$

  Where 1{A} is the indicator function of event A.
- Based on F_{obs}, calculate the probability (p) for each observed precipitation value P_j

$$p(P_j) = F_{obs}(P_j) = \frac{1}{n}\sum_{i=1}^{n} 1\{x_i \le P_j\} \tag{2}$$

- Find the corresponding value in the modeled daily precipitation data for the grid point closest to that station ($P_j{}^m$) that has the same probability. That is, calculate the quantile (Q^m)value at p in the modeled precipitation data series

$$P_j^m = Q^m(p(P_j)) = x^m_{\lceil n_m p(P_j)\rceil} \tag{3}$$

  Where n_m is the number of data points in the modeled precipitation data series; x^m is the sorted modeled precipitation data series where $x_1^m \le x_2^m \ldots \le x_n^m$; $\lceil\rceil$ is the ceiling function.

- Calculate the model error (E) for each station as the root mean squared difference between P_j and P_j^m

$$E = \sqrt{\frac{\sum_{j=1}^{n}(P_j - P_j^m)^2}{n}} \tag{4}$$

Based this method, we evaluated E for complete precipitation data series, as well as the error for observed dry days (E_d) and wet days (E_w) separately at each climate station. We then calculated the mean error for all stations in the state for each model.

3.3 Method for projecting future mean and extreme precipitation

A Common approach to studying extreme events is to establish their probability distributions, upon which the magnitude and return intervals (frequency) of extreme events can be established. This can be achieved either by fitting a theoretical distribution functions, or based on the empirical distribution of the data. The advantage of using theoretical distributions is that they can smooth out outliers, particularly when data is only available for short time frame, and they can project beyond the time period when data is available.

Before we can apply this approach, however, we need to correct biases of RCMs in the frequency distribution of their output daily precipitation data series (as evaluated based on the methods outlined in 3.2). It is important to correct the entire distribution, not just mean values. We propose a quantile mapping method to achieve this correction.

3.3.1 Bias correction through quantile mapping

This involves the following steps:

- Establish an empirical cumulative distribution function (F_{mf})for modeled future daily precipitation data series x_i^{mf}

$$F_{mf}(t) = \frac{1}{n}\sum_{i=1}^{n} 1\{x_i^{mf} \le t\} \tag{5}$$

- For each modeled future precipitation value P_j^{mf}, find the corresponding quantile values of same probability in the observed and modeled current daily precipitation data series: P_j^{obs} and P_j^{mc}

$$P_j^{obs} = Q^{obs}(F_{mf}(P_j^{mf})) = x^{obs}_{\lceil n_{obs} F_{mf}(P_j^{mf}) \rceil} \tag{6}$$

Where n_{obs} is the number of data points in the observed precipitation data series; x^{obs} is the sorted observed precipitation data series where $x_1^{obs} \le x_2^{obs} \ldots \le x_i^{obs}$.

$$P_j^{mc} = Q^{mc}(F_{mf}(P_j^{mf})) = x^{mc}_{\lceil n_{mc} F_{mf}(P_j^{mf}) \rceil} \tag{7}$$

Where n_{mc} is the size of the modeled current precipitation data series; x^{mc} is the sorted modeled current precipitation data series where $x_1^{mc} \le x_2^{mc} \ldots \le x_i^{mc}$.

- We then use the ratio of P_j^{obs} and P_j^{mc} to correct the bias in future precipitation data series.

$$\hat{P}_j^{mf} = P_j^{mf} \frac{P_j^{obs}}{P_j^{mc}} = P_j^{mf} \frac{x^{obs}_{\lceil n_{obs} F_{mf}(P_j^{mf}) \rceil}}{x^{mc}_{\lceil n_{mc} F_{mf}(P_j^{mf}) \rceil}} \tag{8}$$

Based on this bias-correction, we derived a future daily precipitation data series from RCMs for each of the climate station.

3.3.2 Frequency analysis

After the bias in the distribution is corrected, we then fit a theoretical distribution function to both the observed and future modeled data, based on which the magnitude of precipitation events of certain return intervals can be established for comparison. A variety of distribution functions have been used to study extreme precipitation events, such as generalized extreme value (GEV), Weibull and Pearson III distributions for annual maxima data, generalized Pareto (GP) distribution for excesses over a high threshold, and generalized Logistic (GL), lognormal (LN) and Gamma distributions for full precipitation records. We used the L-moment ratio (L-skewness vs. L-kurtosis) diagram (Rao and Hamed, 1999) to help select the best distribution for our data. Figure 2 plot the L-skewness and L-kurtosis ratios for both observed and modeled data for all stations. Results show that Gamma distribution best approximate the distribution of daily precipitation totals. This selection is also supported by many previous studies (Crutcher et al. 1977, Buishand 1978, Guttman et al. 1993, Groisman et al. 1999). Gamma distribution has the following density function:

$$f(x) = \frac{1}{\alpha^{\beta}\Gamma(\beta)} x^{\beta-1} e^{-(\frac{x}{a})} \tag{9}$$

The variable x has lower bound of zero, $0< x < \infty$. For this family of distributions, the α-parameter defines the shape of the distribution, while β-parameter characterizes the scale. Since it does not rain every day, a mixed distribution model is sometimes considered for daily precipitation totals (Groisman et al, 1999). Under this model, it is assumed that the occurrence of daily precipitation events has a binary distribution with the probability of a single event p_{pr}, and the precipitation amount during this event is considered to have a gamma-distribution. The cumulative distribution function of precipitation totals $F(x)$ is expressed as:

$$F(x) = P(X \le x) = (1 - p_{pr}) + p_{pr} \int_0^x f(\alpha, \beta, t) dt \tag{10}$$

with $f(\alpha,\beta,t)dt$ being the probability density function of gamma-distribution. p_{pr} can be estimated as the percentage of wet days in the data series. The maximum likelihood method is used to estimate the parameters α and β for each of the observed and future modeled

daily precipitation data series. After the cumulative probably density function $F(x)$ is established we can derive the magnitude of precipitation events of various return intervals as:

$$P_y = F^{-1}(1 - \frac{1}{365y}) \tag{11}$$

Where P_y is the precipitation value with the return interval of y years, $F^{-1}(x)$ is the inverse function of the cumulative probability function $F(x)$.

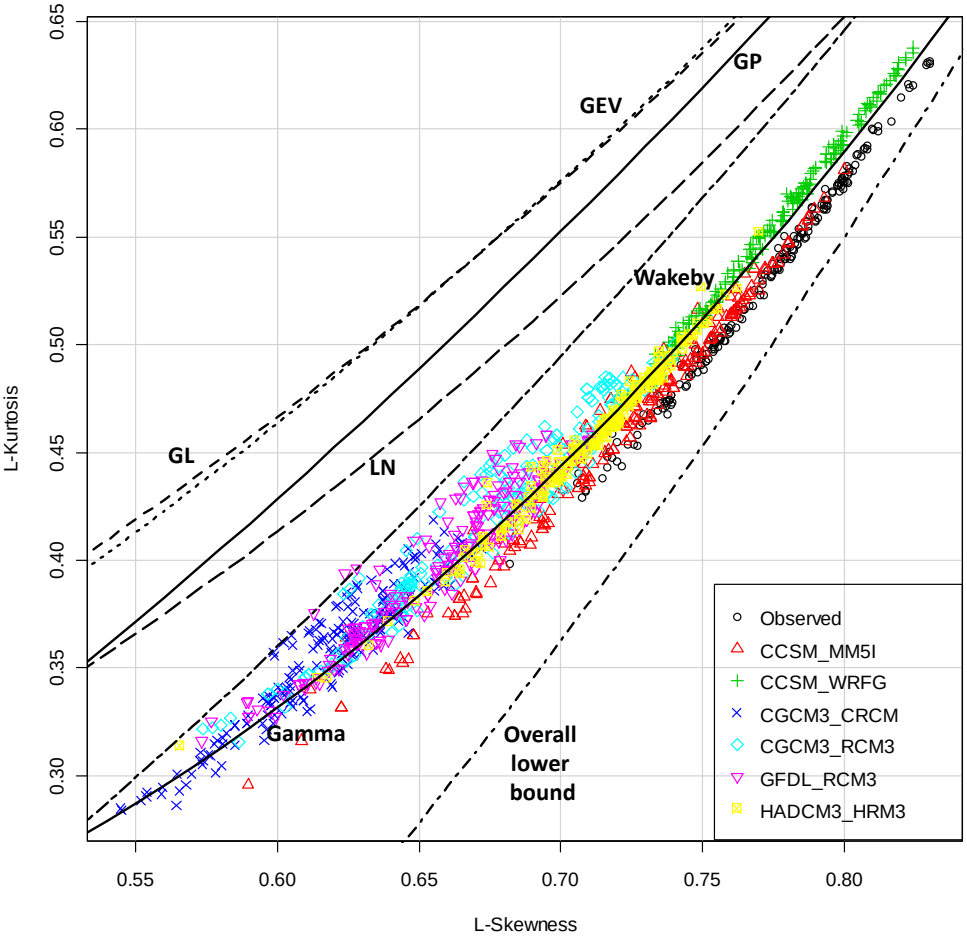

Fig. 2. L-moment ratio diagram for observed and modeled daily precipitation data in comparison to the L-moment ratio curves of theoretical distributions

4. Results and discussions

4.1 Model evaluation: Frequency distributions of observed and modeled daily precipitation data

Summary L-moment statistics for frequency distributions of observed and modeled daily precipitation data series are presented in Table 2. It can be seen that CCSM_WRFG daily precipitation series deviate most from the observed distribution of daily precipitation. The remaining models have comparable biases. They all have greater mean (except for CCSM_MM5I), less variance, skewness and kurtosis. This seems to indicate that the modeled data is less spread out, have higher values in small precipitation events and lower values in large events (hence less skewed than observed).

Figure 3 illustrates the correlation between observed and modeled mean daily precipitation at all stations. The correlation coefficient (Pearson's r) values are also presented in the figure. It should be noted that to evaluate a model's performance at estimating mean precipitation, we should not only look at the correlation coefficient, but also how closely the points follow the x=y line. It can be seen that CCSM_WRFG model consistently under-estimate the mean daily precipitation. Most models slightly over estimate the mean daily precipitation (such as CGCM_RCM3, GFDL_RCM3 and HADCM3_HRM3). The model that performs best in terms of mean precipitation is CGCM3_CRCM, which has the highest correlation coefficient (0.81), and follows x=y line most closely. However, close estimate in mean precipitation does not mean the model also simulates well the whole distribution of daily precipitation data series. Figure 4 presents the quantile-quantile (Q-Q) plots between observed and modeled data for all stations for each of the 6 RCMs in order to show the deviation from observed distribution as well as the spread of different models. It can be seen from figure 4 that despite its close estimate of mean precipitation, CGCM3_CRCM performs the worst in estimating the complete distribution. It consistently underestimates most of the wet day quantile values. The close estimate of the mean is a result of over-estimation of small precipitation events offsetting this underestimation of larger quantile values. Figure 4 shows that majority of models underestimate large quantile values. All models overestimate days with no or small amount of precipitation. This can also be illustrated by the dry day quintile errors (E_d) presented in table 3. To some extent, this could be attributable to the fact that RCMs output average precipitation of a whole grid, which covers an area of 50 by 50 km, whereas station data are point-based.

Table 3 summarizes root mean squared error of modeled quantile values for all data (E), dry days (E_d) and wet days (E_w) respectively. Based on RMSE, it seems that HADCM3_HRM3 performs best in estimating the observed frequency distribution of daily precipitation data, as it has lowest E and E_w, and fairly low E_d. The calculated model errors again confirm that CCSM_WRFG and CGCM3_CRCM have the poorest performance in simulating the frequency distribution, and its model errors are above the other models. The rest of the models have comparable performance. The average RMSE for full record quantiles for all models is about 1 mm, or about 40% of mean precipitation amount. This ranges from 0.78 to 1.65 mm, or 30 to 63% of mean daily precipitation. The average RMSE for wet day quantile values for all models is 3.04 mm, or 35% of the mean wet day precipitation. It ranges between 25-54% of mean wet day precipitation among different models.

Model	Mean (mm/day)		L-scale		L-skewness		L-kurtosis	
	Value	% diff.	Value	% diff.	Value	% diff.	Value	% diff.
Observed	2.62		0.88		0.77		0.53	
CCSM_MM5I	2.40	-8.38	0.84	-3.58	0.72	-6.18	0.46	-12.05
CCSM_WRFG	1.96	-25.39	0.87	-0.73	0.77	0.14	0.55	4.17
CGCM3_CRCM	2.65	0.92	0.76	-13.28	0.62	-19.55	0.36	-32.03
CGCM3_RCM3	3.09	18.01	0.80	-8.28	0.67	-12.36	0.42	-19.97
GFDL_RCM3	2.90	10.52	0.79	-9.56	0.66	-14.52	0.40	-24.14
HADCM3_HRM3	2.95	12.49	0.83	-4.94	0.71	-7.71	0.46	-13.37
Model mean	2.66	1.36	0.82	-6.73	0.69	-10.03	0.44	-16.23

Table 2. Summary statistics for frequency distributions of observed and modeled daily precipitation data series

Model	E	E as % of mean daily precipitation	E_d	E_w	E_w as % of mean wet day precipitation
CCSM_MM5I	0.93	36	0.07	2.95	34
CCSM_WRFG	1.11	42	0.05	3.63	42
CGCM3_CRCM	1.65	63	0.36	4.65	54
CGCM3_RCM3	0.85	32	0.27	2.16	25
GFDL_RCM3	1.02	39	0.29	2.69	31
HADCM3_HRM3	0.78	30	0.15	2.18	25
Model mean	1.06	40	0.20	3.04	35

Table 3. Root mean squared error of modeled quantile values for all data (E), dry days (E_d) and wet days (E_w)

4.2 Projecting future precipitation patterns in the Midwest Region

4.2.1 Mean daily precipitation

After applying bias correction based on quantile mapping method, we calculated future mean daily precipitation for the Midwest region for the time period 2040-2070. Table 4 summarizes how daily mean precipitation might change for the study area based on climate models. With the exception of CCSM_WRFG (which projects very slight decrease), all other models project increase in mean precipitation in the region. The average change for all models is 7.7%, ranging from 0-12%. Figure 5 shows the spatial pattern of precipitation change based on mean projection of all models. It seems that mean precipitation is likely to increase more in north and less in the south. This is likely due to increased evaporation from the Great Lakes under a warmer temperature. Spatial pattern of mean precipitation change varies among different models (Figure 6), but most models project increase in the northern part of the region. CCSM_WRFG is the only model that project decrease of precipitation in the south at the similar magnitude as the increase in the north. All other models project increase in all Midwest region.

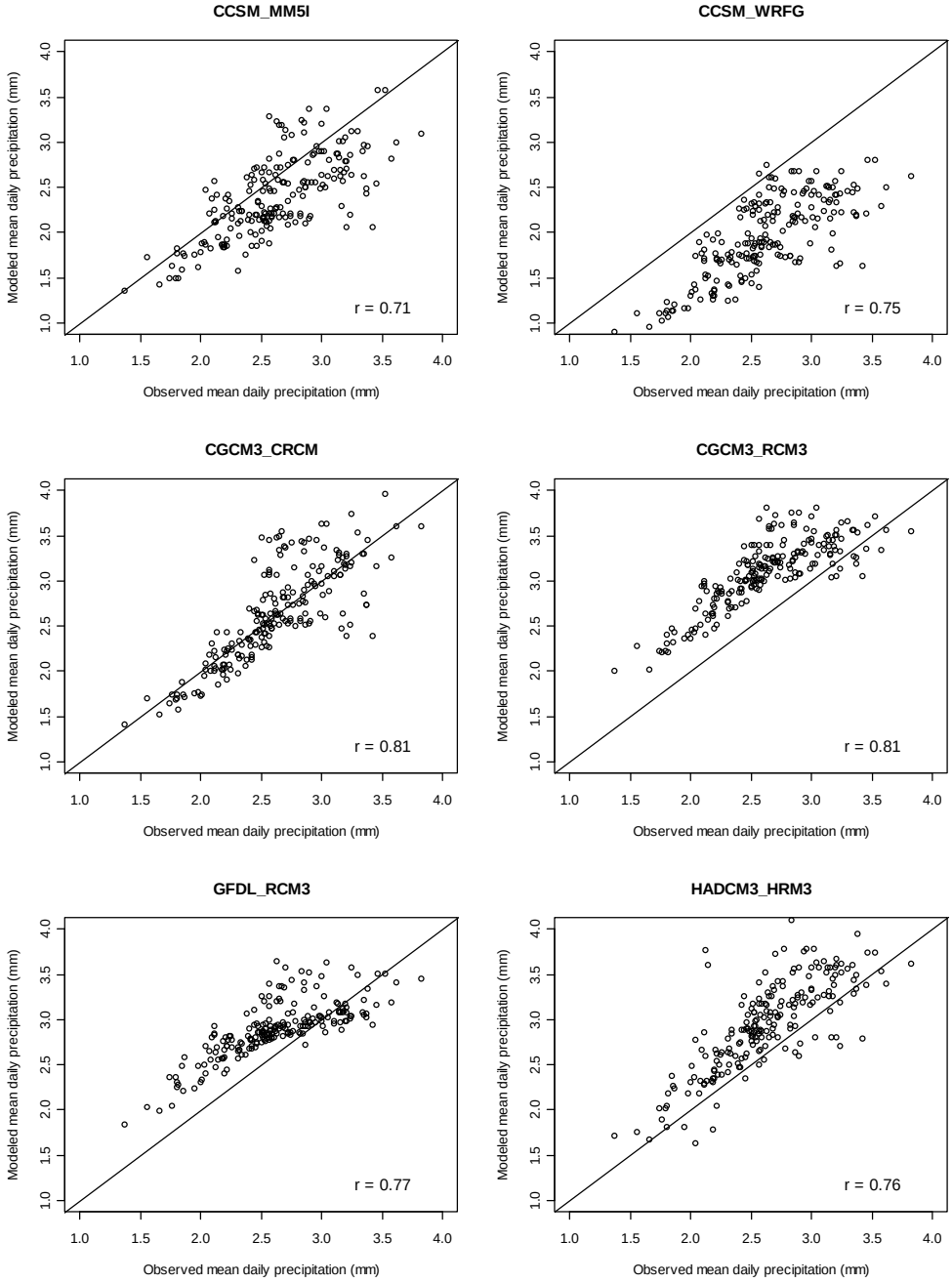

Fig. 3. Correlation between observed and modeled mean daily precipitation at all stations.

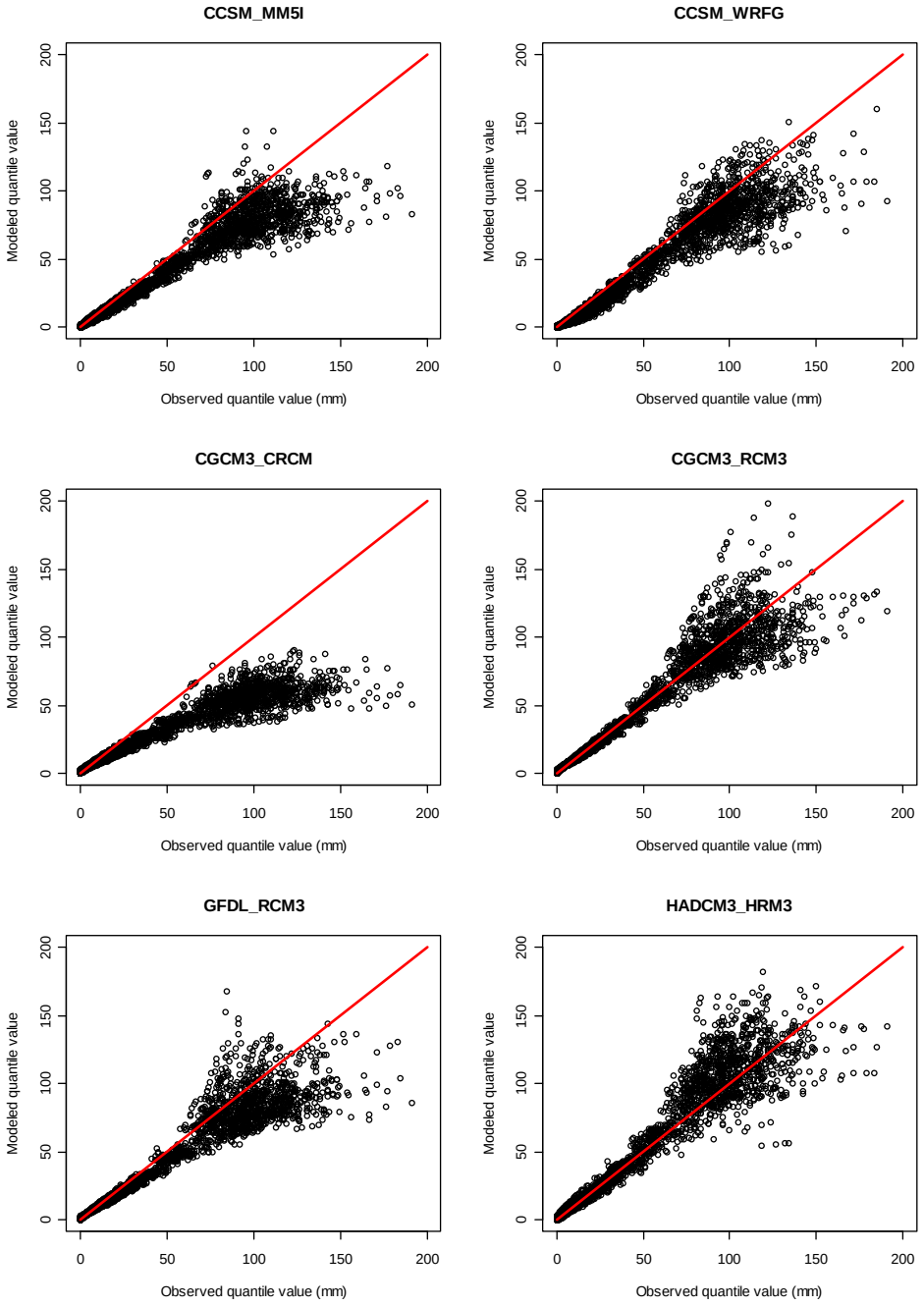

Fig. 4. Q-Q plots for all stations for each of the RCMs

Models	Mean daily precipitation (mm/d)	% change
Observed (1971-2000)	2.62	
Future (2040-2070)		
CCSM_MM5I	2.87	9.51
CCSM_WRFG	2.61	-0.44
CGCM3_CRCM	2.79	6.59
CGCM3_RCM3	2.89	10.11
GFDL_RCM3	2.86	8.95
HADCM3_HRM3	2.93	11.67
Model mean	2.82	7.73

Table 4. Changes in the Midwest mean daily precipitation in 2040-2070

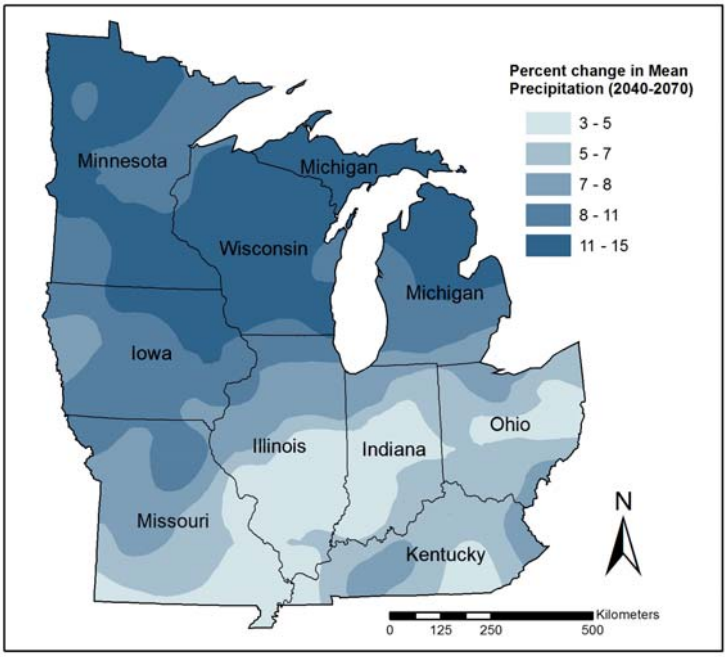

Fig. 5. Changes in mean daily precipitation in 2040-2070 (model mean).

4.2.2 Extreme precipitation events

We used the mixed probability model (eq. 10) to project extreme precipitation events. We used the wet day frequency as an estimate for precipitation probability (p_{pr}), and fit a Gamma distribution to the wet day precipitation data using maximum likelihood method. Applying the same methodology on the observed and bias-corrected future daily precipitation data, we derived the magnitudes of extreme events of return interval of 1, 5, 10, 15, 20 and 25 years for both present (1970-2000) and future (2040-2070). Table 5 summarized the results. All models show increase in precipitation depths of extreme events. In general, extreme precipitation events increase at greater magnitudes than mean precipitation. The increase is greater for more extreme events. For average results of all models, compared with 8% increase in mean precipitation, precipitation event of 1 year return interval is likely to increase by 13%, and that of 25 year could increase by 19%. There are variations among models in how they project spatial distribution of such changes. Our model evaluation suggests that mean of all models seems to capture the spatial variation of precipitation best. Based on this observation, we used mean values of all models to interpolate the spatial distribution of how extreme precipitation could change in the Midwest (Figure 7). It can be seen that in general the intensity for extreme precipitation increase disproportionately

Return interval		1 year	5 year	10 year	15 year	20 year	25 year
Observed (1970-2000)	mm/day	55	82	96	103	108	112
Future (2040-2070)							
CCSM_MM5I	mm/day	62	93	108	117	124	128
	% change	12.59	13.26	13.19	13.72	14.51	14.70
CCSM_WRFG	mm/day	62	93	108	116	124	129
	% change	11.80	12.70	12.90	12.87	14.31	14.86
CGCM3_CRCM	mm/day	61	91	106	114	121	125
	% change	9.90	10.96	10.94	10.86	11.82	12.11
CGCM3_RCM3	mm/day	64	100	117	127	135	141
	% change	16.11	20.86	22.45	23.21	24.98	25.69
GFDL_RCM3	mm/day	61	94	111	122	132	137
	% change	9.72	13.61	16.01	18.56	21.43	22.76
HADCM3_HRM3	mm/day	64	98	114	126	134	139
	% change	15.94	19.44	19.48	22.15	23.75	24.37
Model mean	mm/day	62	95	111	120	128	133
	% change	12.68	15.14	15.83	16.90	18.47	19.08

Table 5. Present and future magnitudes of extreme precipitation events.

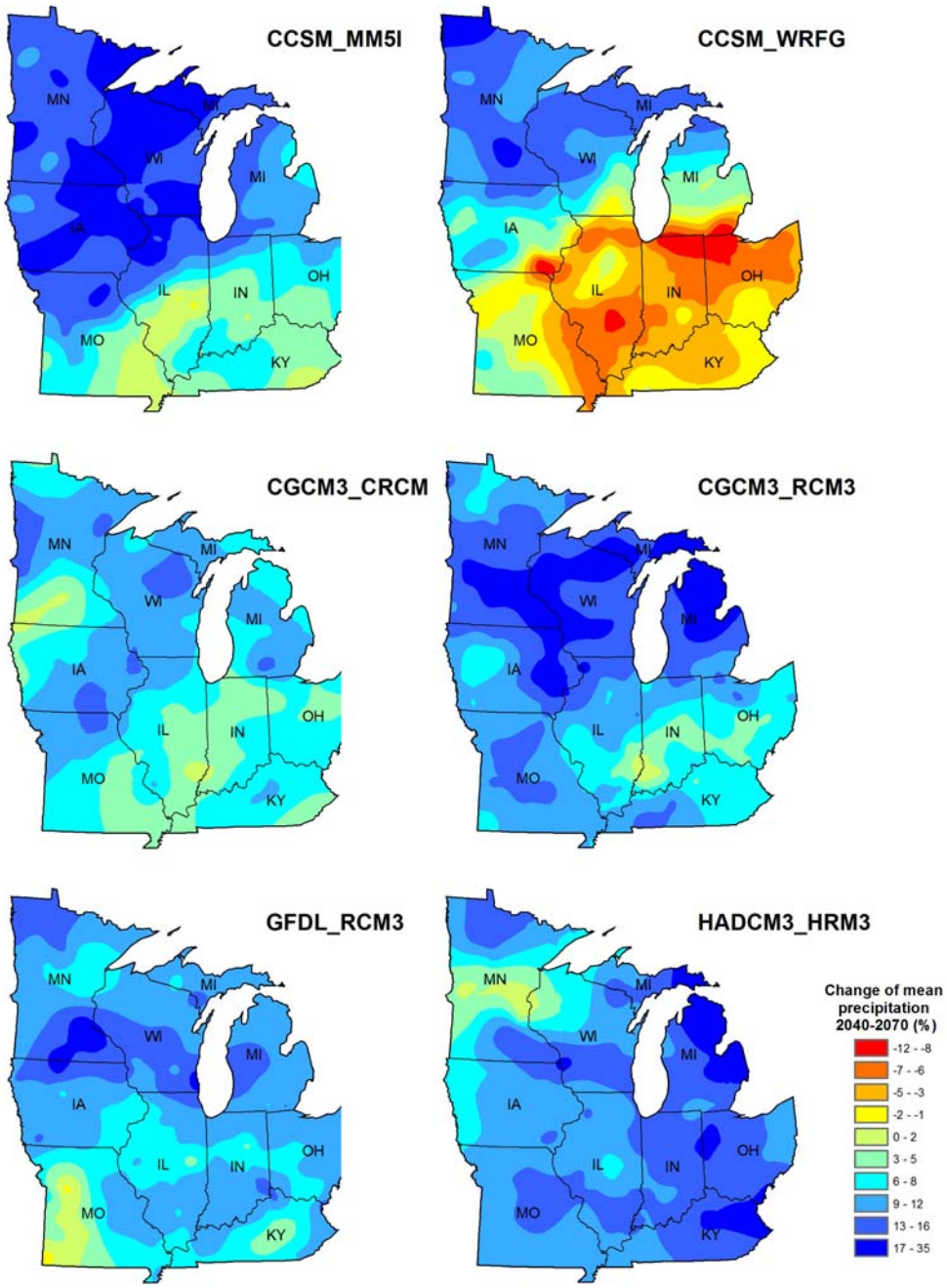

Fig. 6. Changes in mean daily precipitation in 2040-2070 from 6 RCMs

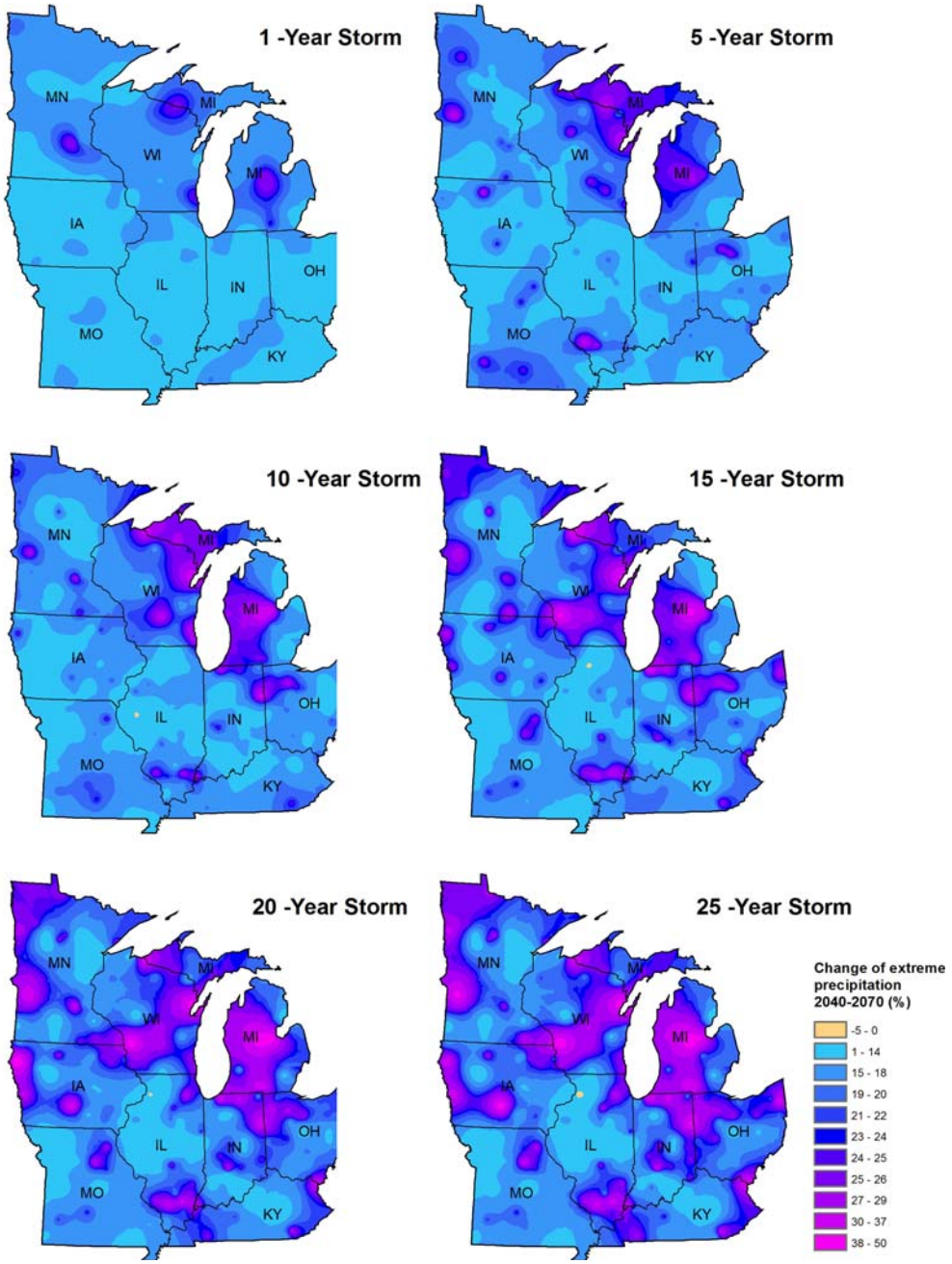

Fig. 7. Changes in extreme precipitation (2040-2070).

more for more extreme events. Similar to the pattern of mean precipitation change, there seems to be more increase in extreme events in the northern part of the region. Since a lot of extreme precipitation events occur in spring, this increase could be attributed to decreased ice cover during the winter, early melt of lake ice, and consequent increased evaporation of the great lakes under a warmer climate.

5. Conclusion

In this study, we first evaluated the performance of NARCCAP regional climate models in terms of its ability to capture the frequency distribution of daily precipitation data in the Midwest region of the United States. We found all models have biases. In general, they tend to overestimate small events, and underestimate large events. Based on such evaluation, we corrected model biases based on quantile-mapping method. We then used the bias-corrected future daily precipitation output from NARCCAP RCMs to project future changes in precipitation using a mixed probability model based on Gamma distribution. Based on the models, on average, the mean precipitation could increase by 7.7% by 2040-2070 for the Midwestern Region. Magnitudes of extreme precipitation are likely to increase more than average. The increase could be disproportionately larger for more extreme precipitation events. Spatially, northern part of the study area could see more increase in both mean and extreme precipitation, likely due to increased evaporation of the Great Lakes from a combination of higher temperature and less ice cover both spatially and temporally under a warmer climate.

6. References

Allan RP, Soden B J. 2008. Atmospheric warming and the amplification of precipitation extremes. *Science* 321:1481–1484.

Buishand, TA. 1978. Some remarks on the use of daily rainfall models. *Journal of Hydrology*, 36:295-308.

Crutcher, HL, McKay, GF, Fullbright, DC. 1977. A note on a gamma distribution computer program and computer produced graphs. NOAA Technical Report EDS24, Environmental Data Service, NOAA, Department of Commerce, Washington DC.

Cubasch U, Boer GJ, Stouffer RJ, Dix M, Noda A, Senior CA, Raper S, Yap KS. 2001. Projections of future climate change, in *Climate Change 2001: The Scientific Basis. Contribution of Working Group I to the Third Assessment Report of the Intergovernmental Panel on Climate Change.* Edited by J.T. Houghton et al., pp. 525-582. Cambridge University Press, New York.

Easterlin DR and Karl TR. 2000 Potential consequences of climate variability and change for the Midwestern United States. In *Climate Change Impacts on the U.S.: The Potential Consequences of Climate Variability and Change*, ed. National Climate Assessment Team, p 167-188.

Easterling DR, Evans JL, Ya P, Groisman PY, Karl TR, Kunkel KE, Ambenje P. 2000. Observed variability and trends in extreme climate events: a brief review. *Bulletin of the American Meteorological Society* 81(3): 417-425.

Elamir, EAH, Seheult, AH. 2003. "Trimmed L-moments". *Computational Statistics & Data Analysis* 43 (3): 299–314. doi:10.1016/S0167-9473(02)00250-5.

Groisman PY, Karl TR, Easterling DR, Knight RW, Jamason, PF, Hennessy, KJ, Suppiah, R. Page, CM, Wibig, J, Fortuniak, K, Razuvaev VN, Douglas A. Forland, E, Zhai PM. 1999. Changes in the probability of heavy precipitation: Important indicators of climate change. *Climatic Change* 42:243-283.

Groisman PY, Knight RW, Easterling DR, Karl TR, Hegerl GC, Razuvaev VN. 2005. Trends in intense precipitation in the climate record. *Journal of Climate* 18:1326-1350.

Guttman, NB, Hosking, JRM, Wallis, JR. 1993. Regional precipitation quantile values for the Continental United States computed from L-moments. *Journal of Climate*, 6:2326-2340.

Hennessy KJ, Gregory JM, Mitchel JFB. 1997. et al. 1995. Changes in daily precipitation under enhanced greenhouse conditions. *Climate Dynamics* 13: 667-680.

Hosking JR. 1990. L-moments: analysis and estimation of distributions using linear combinations of order statistics. *Journal of Royal Statistical Society B*, 52: 105-124.

Hosking, JRM. 2006. "On the characterization of distributions by their L-moments". *Journal of Statistical Planning and Inference* 136: 193–198.

Huff, FA, Angel JR. 1992. *Rainfall Frequency Atlas of the Midwest*. Midwestern Climate Center Bulletin 71.

Intergovernmental Panel on Climate Change. 2000. Special Report on Emission Scenarios. UN Environment Program, Nairobi, Kenya.

Kunkel KE. 2003. North American trends in extreme precipitation. *Natural Hazards* 29: 291–305.

Mearns LO, Gutowski WJ, Jones R, Leung L-Y, McGinnis S, Nunes AMB, and Qian, Y. 2009. A regional climate change assessment program for North America. *EOS* 90(36): 311-312.

Meehl GA, Stocker TF, Collins WD, Friedlingstein P, Gaye AT, Gregory JM, Kitoh A. Knutti R, Murphy JM, Noda A, Raper SCB, Waterson IG, Weaver AJ, Zhao Z-C. 2007. Global climate projections. In: *Climate Change 2007: The Physical Science Basis. Contribution of Working Group I to the Fourth Assessment Report of the Intergovernmental Panel on Climate Change.* Edited by S. Solomon et al. pp. 749-845. Cambridge University Press, New York.

Min SK, Zhang X, Zwiers FW, Hegerl GC. 2011 Human contribution to more-intense precipitation. *Nature* 470:378-381. doi:10.1038/nature09763.

Rao, AR, Hamed KH. 2000 *Flood Frequency Analysis.* CRC Press, Boca Raton, Florida.

Ulrych, T J, Velis, DR, Woodbury, AD, Sacchi, MD. 2000. "L-moments and C-moments". *Stochastic Environmental Research and Risk Assessment*, 14 (1), 50–68.

Union of Concerned Scientists. 2009. Confronting Climate Change in the U.S. Midwest. http://www.ucsusa.org/global_warming/science_and_impacts/impacts/climate-change-midwest.html. Accessed Nov. 1, 2011.

Zhang X, Zwiers FW, Hegerl BC, Lambert FG, Gillett NP, Solomon S, Stott PA, Nozawa T. 2007. Detection of human influence on twentieth-century precipitation trends. *Nature* 448: 461-465. doi:10.1038/nature06025

17

Future Changes in the Quasi-Biennial Oscillation Under a Greenhouse Gas Increase and Ozone Recovery in Transient Simulations by a Chemistry-Climate Model

Kiyotaka Shibata and Makoto Deushi
Meteorological Research Institute, Tsukuba
Japan

1. Introduction

In the equatorial stratosphere, the zonal wind direction changes from westward to eastward and vice versa at intervals of from less than two to about three years and centered at about 28 months (Reed et al., 1961; Veryard & Ebdon, 1961). This phenomenon is called the quasi-biennial oscillation (QBO) from the length of its period (Angell & Korshover, 1964). The QBO initiates in the upper stratosphere, then descends gradually at a rate of about 1 km per month with an amplitude of about 20 ms^{-1}, and diminishes near the tropopause (~16 km). The QBO structure for zonal wind and temperature is highly symmetric in longitude and latitude with a half-width of about 12° latitude, and the QBO dominates the annual and semiannual cycles in the equatorial stratosphere (e.g., Baldwin et al., 2001; Pascoe et al., 2005). The QBO can also be seen in changes in the abundances of ozone (e.g., Angell & Korshover, 1964; Randel & Wu, 1996) and other trace gases (e.g., Luo et al., 1997; Dunkerton, 2001) because their transport and chemistry are strongly dependent on the wind and temperature fields, respectively.

The QBO plays a very important role in the stratosphere not only because the QBO is the largest variation in the equatorial stratosphere but also because its effects significantly extend to the northern extratropical stratosphere (e.g. Holton & Tan, 1980, 1982), with the result that the stratospheric polar vortex tends to be weaker (stronger) during the QBO easterly (westerly) phase in the lower stratosphere. In addition, the QBO effect can also be seen in the extratropical troposphere at or near the surface not only in the Northern Hemisphere (NH) (e.g., Coughlin & Tung, 2001; Marshall & Scaife, 2009) but also in the Southern Hemisphere (SH) (Kuroda & Yamazaki, 2010), indicating that it has dynamical impacts on the tropospheric circulation even though the physical mechanism is still unknown.

The QBO effect on the polar vortex, which has been confirmed by many statistical analyses, is referred to as the Holton-Tan relation (e.g., Labitzke, 1982; Naito & Hirota, 1997; Lu et al., 2008). The Holton-Tan relation is ascribed to modulation by the QBO of the strength of the effective waveguide for the mid-latitude planetary waves propagating through the winter

stratosphere (e.g., Holton & Tan, 1980, 1982). Although the Holton-Tan relation has been reproduced by general circulation models (GCM) (e.g., Niwano & Takahashi, 1998; Hamilton 1998, Anstey et al., 2010) and chemistry-climate models (CCM) (Naoe & Shibata, 2010), the details of its mechanism are not yet well understood because the Eliassen-Palm (EP) flux diagnostics do not show a more poleward propagation in the mid-latitude stratosphere during the easterly QBO phase. Rather, planetary waves propagate more equatorward as well as more upward during the easterly QBO phase in both 25-year (1980-2004) data of the reanalysis and a CCM ensemble simulation (Naoe & Shibata, 2010) under the REF-1 scenario of CCM validation phase 1 (CCMVal-1) activity for stratospheric processes and their role in climate (SPARC) (Eyring et al., 2005). Furthermore, the polar vortex intensity depends not only on the QBO but also on the 11-year solar cycle (e.g., Labitzke & van Loon, 1999); as a result, the Holton-Tan relation varies irregularly or non-stationarily with the solar activity (e.g., Gray et al., 2001; Labitzke, et al., 2006; Lu et al., 2009), making the circumstances of the Holton-Tan relation more complicated than what Holton & Tan (1980, 1982) first suggested.

The mechanism of the QBO is generally explained with a wave-mean flow interaction, wherein gravity waves and/or equatorial waves excited in the troposphere deposit their westward or eastward momentum, depending on the mean flow direction during their vertical propagation in the stratosphere, as has been demonstrated with numerical models (e.g., Lindzen & Holton 1968; Plumb 1977). This mechanism, which has also been reproduced in a laboratory experiment of Plumb & McEwan (1978), is one reason why the oscillation does not have a narrow annual or semiannual period but a peculiar, broad 28-month period. The QBO is hence strongly dependent on the wave source and the propagation conditions, that is, the wave generation in the troposphere and the background wind field in the troposphere and stratosphere.

Under the changing climate resulting from increases in greenhouse gases (GHG), the stratosphere is projected to continue to cool because of strong CO_2 longwave emission, in a sharp contrast to the tropospheric warming caused by the sea surface temperature (SST) rise driven by the enhancement of downward longwave radiation by CO_2 and H_2O. This raises the question as to how the QBO might behave in the future under global warming caused by increased GHGs. To date, two equilibrium GCM simulations under doubled CO_2 levels have projected the future QBO. Giorgetta & Doege (2005) investigated the effect of variations in the source strength of parameterized gravity wave forcing (GWF) with a middle atmosphere GCM (Roeckner et al., 2003) at the T42L90 resolution and showed that the QBO period is shortened when the source strength of GWF increases. The future QBO periods are 26, 22, and 17 months for a 0%, 10%, and 20% increase in source strength, respectively, against a 29-month period under the current CO_2 conditions. Kawatani et al. (2011) carried out a similar experiment with a GCM (Hasumi & Emori, 2004) at the T106L72 resolution. They did not employ a parameterized GWF, so that the wave forcing of the QBO was by resolved waves alone. In their simulation, the future QBO has a period that is 1-5 months longer than that of the control QBO, which has a period of 24 months. Moreover, the future QBO amplitude is smaller than the control; in particular, the amplitude is much smaller below 50 hPa. Thus, the two GCM results show an opposite change in the QBO period, although both Giorgetta & Doege (2005) and Kawatani et al. (2011) attributed the future QBO change mainly to changes in the residual circulation (mean tropical upwelling) and to the enhanced wave forcings. Aside from the use of a parameterized or resolved GWF, the difference in the QBO

period response may reside partly in the change in the mean tropical upwelling (i.e., the Brewer-Dobson circulation (BDC)), which is weakening in the simulation by Giorgetta & Doege (2005) and strengthening in that by Kawatani et al. (2011). Either way, it indicates the importance of the vertical momentum transport to the future QBO momentum budget.

Climate change is driven not only by increases in GHGs but also by changes in the ozone layer, because the stratospheric thermal structure is substantially affected by the stratospheric ozone through solar heating. The quasi-global (60°S-60°N) stratospheric ozone abundances decreased from the 1970s to the mid-1990s (e.g., WMO, 2011) because of increases in emissions of anthropogenic ozone-depleting substances (ODSs) such as Chlorofluorocarbons (CFCs) and halons. Since the mid-1990s, stratospheric ozone has been stable or slightly increasing (e.g., WMO, 2011) because of international regulation of ODS production. ODS-originated halogens cause severe ozone depletion through the gas-phase reactions in the upper stratosphere, which in turn induces stratospheric cooling (e.g., WMO, 2007). The CO_2 increase also causes cooling in the stratosphere through emission of longwave radiation to space; in particular, it causes strong cooling in the upper stratosphere, which in turn increases ozone abundances through chemical reactions. Hence, radiation and chemistry interaction between ozone and CO_2 (e.g., Shepherd & Jonsson, 2008) should be included in a model to obtain realistic simulations of climate change, at least, in the stratosphere. Accordingly, CCMs have advantage over GCMs because the interaction between dynamics, radiation, and chemistry for radiatively active gases such as O_3, CH_4, N_2O, and CO_2 is included in CCMs.

In the polar regions, ODS increases led to severe ozone depletion in spring through the heterogeneous reactions on the polar stratospheric clouds (PSCs), which manifested as the Antarctic ozone hole (Chubachi, 1984; Farman et al., 1985), defined as an area with less than 220 Dobson Units (DU) of total ozone. The ozone hole developed rapidly from about 1980 to the mid-1990s; since then, the area with severely depleted ozone has remained nearly constant, except during a few years, when wave activity was unusually active (e.g., WMO, 2011). Severe ozone depletion also occurs in the northern polar region if the winter stratospheric temperature is cold enough for PSCs to form (e.g. Rex et al., 2006), though not as frequently as in the southern polar region.

Here, to address future QBO behavior under climate changes due to increasing GHGs and decreasing ODSs, Meteorological Research Institute (MRI) CCM transient simulation data from 1960 to 2100 are analyzed focusing on the QBO trend and its forcings. The future QBO effect on the polar vortex, that is, the future Holton-Tan relation, in MRI-CCM simulations is described in another paper (Naoe & Shibata, 2012). Three simulations, using the three scenarios of CCMVal phase 2 (CCMVal-2, Eyring et al., 2008; SPARC, 2010) for the future projection of the stratospheric ozone and related species, are used. The scenarios used in this study specify only anthropogenic forcings of GHGs/SST and/or ODSs, and include no natural forcings, that is, neither the 11-year solar cycle nor volcanic aerosols. The simulation data are thereby free from the complicated overlapping effects among the QBO, solar cycle, and volcanic aerosols (e.g., Lee & Smith, 2003; Yamashita et al., 2011), which would otherwise reduce the confidence level of each detected signal.

The rest of this paper is organized as follows. Section 2 describes the model and simulation conditions, and section 3 presents past and future climatologies of zonal wind and temperature. Section 4 describes the QBO and its forcings in the past, and section 5 treats the

evolutions of the QBO and of its forcings. The results are discussed in section 6, and section 7 is a conclusion.

2. Model simulation and data

2.1 MRI-CCM

MRI-CCM is an upgraded version of the MRI chemistry transport model (Shibata et al., 2005), and its details are described by Shibata & Deushi (2008a, b) and references therein. The dynamics module of MRI-CCM is a spectral global model with triangular truncation, a maximum total wavenumber 42 (about 2.8° by 2.8° in longitude and latitude), and 68 layers in the eta-coordinate extending from the surface to 0.01 hPa (about 80 km). The vertical spacing is about 500 m in the stratosphere between 100 and 10 hPa, with tapering below and above. Non-orographic gravity wave (GW) forcing by Hines (1997) is incorporated, and GW source strength is enhanced symmetrically with respect to latitudes between 30°S and 30°N by superimposing a Gaussian function (15° e-folding latitude) source (0.7 ms^{-1}) on an isotropic source (2.3 ms^{-1}). The gravity wave spectrum is isotropically launched toward eight equally spaced azimuths (north, northwest, west etc) at the lowest level with horizontal wavenumber $k_* = 5.0 \times 10^{-6}$ (m^{-1}).

Biharmonic (Δ^2) horizontal diffusion is weakened only in the middle atmosphere from that in the troposphere in order to spontaneously reproduce the QBO in zonal wind while minimizing the changes in the troposphere (Shibata & Deushi, 2005a, b). The e-folding time at the maximum total wavenumber (n = 42) is 18 h below 100 hPa, 100 h above 150 hPa, and intermediate values in between. This e-folding time of 100 h in the middle atmosphere results in an e-folding time of about 3.6 years at n = 10; almost all of the power (>99%) is included within this total wavenumber for a representative equatorial wave of Gaussian meridional structure centered at the equator with a 15° e-folding latitude (Shibata & Deushi, 2005a). In addition, vertical diffusion is not applied in the middle atmosphere in order to keep the sharp vertical shear in the QBO.

The chemistry-transport module employs a hybrid semi-Lagrangian transport scheme compatible with the continuity equation to satisfy the mass conservation. The horizontal form is an ordinary semi-Lagrangian scheme, and the vertical form is equivalent to a mass-conserving flux form in the transformed pressure coordinate specified by the vertical velocity. The vertical procedure employs the piecewise rational method (Xiao & Peng, 2004), and the horizontal procedure uses quintic interpolation. The chemistry scheme treats 36 long-lived species including 7 families, and 15 short-lived species with 80 gas-phase reactions, 35 photochemical reactions and 9 heterogeneous reactions on PSCs and sulfate aerosols. Since MRI-CCM does not include all of the chlorine species, the chlorine species (CCl_4, $CFCl_3$, CF_2Cl_2, and CH_3Cl) are lumped, except for BrCl, such that the modeled total chlorine corresponds to the input total chlorine at the surface.

2.2 Simulations with the CCMVal-2 scenarios

Two scenarios in CCMVal-2 are used for reference simulations (Eyring et al., 2008): REF-B1 is used for simulations of the past, from 1960 to 2006, with all observed forcings of GHGs, ODSs, SST, solar spectral irradiance variability, and (volcanic) aerosols in the stratosphere, and REF-B2 is used for both past and future simulations, from 1960 to 2100, with time-

evolving forcings of GHGs, ODSs, and SST and with fixed solar minimum and background aerosol conditions. Fixed conditions are used because plausible specification of future solar variability and volcanic aerosols is very difficult. SST/sea-ice data for the entire period from the spin-up (covering the 1950s) to 2100 are taken from a transient simulation (1%/year CO_2 increase) by the MRI coupled ocean-atmosphere model MRI-CGCM2.3.2 (Yukimoto et al., 2006), in which the atmospheric GCM is nearly the same as in MRI-CCM. Note that even the past simulation from the 1950s uses not observed but simulated SST/sea-ice data in order to avoid gap in SST/sea-ice data, stemming from model SST biases, in the vicinity of the present condition.

GHG and ODS abundances are assumed to be geographically uniform and specified at the surface (Eyring et al., 2008). The future scenarios for GHGs and ODSs are taken from the Special Report on Emissions Scenarios (SRES) A1B GHG scenario (IPCC, 2000) and the adjusted A1 halogen scenario. The A1B GHG scenario represents a future world of very rapid economic growth, a global population that peaks in the mid-twenty-first century and declines thereafter, and the rapid introduction of new and more efficient technologies, balanced across all GHG sources. On the other hand, the adjusted A1 halogen scenario includes the earlier phase-out of hydrochlorofluorocarbons (HCFCs) that was agreed to by the Parties to the Montreal Protocol in 2007, with other species such as CFCs, halons, and other non-HCFCs remaining identical to the original A1 scenario (WMO, 2007). In the original A1 scenario, future production of ODSs is determined from the Montreal Protocol limitations or the most recent annual estimates, whichever is less; future emissions are determined in order to yield banks consistent with those of IPCC/TEAP (2005); and the future annual fractional bank release is adjusted so as to attain the IPCC/TEAP (2005) bank for 2015.

Beside the two reference simulations, two other simulations were performed by fixing either ODSs or GHGs at those values at 1960 levels; these simulations correspond to two of the eight sensitivity simulations of CCMVal-2 (Eyring et al., 2008). The first simulation (SCN-B2b, i.e., fixed halogens) uses fixed ODSs and the same time-evolving GHGs and SST/sea-ice data as REF-B2, whereas the second (SCN-B2c, i.e., no-climate-change) uses fixed GHGs and annually repeating SST/sea-ice data and the same time-evolving ODSs as REF-B2. Note that the SST/sea ice at 1960 levels is the 10-year average centered on 1960.

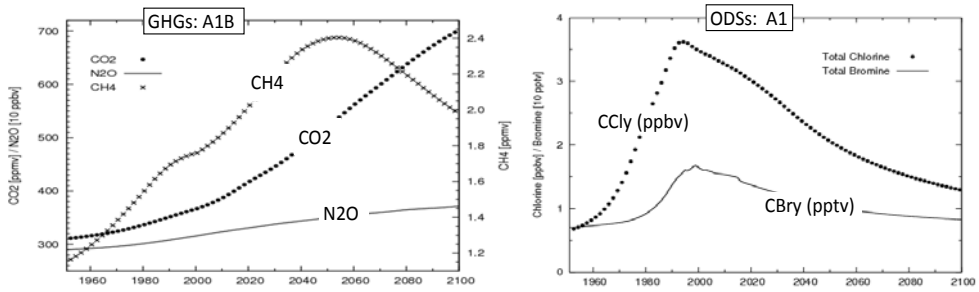

Fig. 1. Evolutions of GHGs and ODSs. Time evolutions of the (a) SRES A1B GHGs scenario for CO_2 (ppmv), CH_4 (ppmv), and N_2O (10 pptv) from 1950 to 2100, and (b) total halogens as CCl_y (ppbv) and total bromine as CBr_y (10 pptv) of the SRES A1 adjusted ODSs scenario.

Figure 1 exhibits time evolutions of GHGs (CO_2, CH_4, and N_2O) in the A1B scenario and ODSs (as total chlorine, CCl_y, and total bromine, CBr_y) in the A1 adjusted scenario for 1960 to 2100. CO_2 and N_2O abundances increase monotonically throughout the entire period, reaching maxima of about 700 ppmv and 370 ppbv, respectively, in 2100, whereas CH_4 abundances attains a maximum of about 2.4 ppmv around the 2050s and then decreases to about 2.0 ppmv in 2100. We henceforth refer to this GHGs evolution simply as the GHG increase, neglecting the non-monotonic behavior of CH_4. CCl_y increases rapidly from 0.8 ppbv around 1960 to a maximum of about 3.7 ppbv in the first half of the 1990s and then gradually decreases to about 1.3 ppmv in 2100. CBr_y also behaves qualitatively like CCl_y but it starts to increase much later (from about 1980) and attains a maximum of about 17 pptv around 2000.

To reduce noise stemming from internal variability among simulations, REF-B2 simulations were performed for three members, in which different initial conditions were taken from the spin-up runs of the REF-B1 simulations. The three members are henceforth referred to as B21, B22, and B23. On the other hand, single-member simulations were made for SCN-B2b and SCN-B2c, referred to as Sb and Sc, respectively. These simulations can be combined into different ensembles, depending on the key variables; for example, a realistic forcing (B21, B22, B23), or idealized forcing (Sb, Sc) ensemble, or GHG increase (B21, B22, B23, Sb) or time-varying ODS (B21, B22, B23, Sc) ensembles.

2.3 Data processing

As observed data, for comparison with past simulations, we used reanalysis data sets compiled by the European Centre for Medium-Range Weather Forecasts (ECMWF): namely, ERA40 (Uppala et al., 2005) from 1958 to 1988, and ERA-Interim (Dee et al., 2011) from 1989 to 2009. The two reanalysis data sets are smoothly merged such that the data for 1989 overlap, without any gap in any month, thus producing a long, continuous time series of data from 1958 to 2009, which is henceforth referred to simply as ERA-Interim. Monthly-mean data are used in this study for both the observation and the simulations.

A Lanczos filter (e.g., Duchon, 1979) was applied to the monthly-mean time series to get band-passed data within the QBO period (20-40 months) or low-passed data in low-frequency ranges, with periods much longer than the QBO period. The cut-off for the low frequency data period was set at 120 months. The running-mean was used as an alternative way of deriving low-frequency data. Student's *t*-test was used to evaluate the linear trend in the QBO and related quantities over the entire integration period, and results were considered statistically significant at the 95% or 99% confidence level.

3. Simulated global atmosphere

3.1 Zonal mean climatology

Simulated annual- and zonal-mean temperature and zonal wind in the past 30 years (1970-1999) are displayed for B21, Sb, and Sc in Figs. 2 and 3, together with observed values. Although the overall features of temperature are very similar between the observation and the simulations, the simulated temperatures show common biases in the mid- and high-latitude stratosphere in both the NH and SH, which are substantially due to biases during the winter. In the NH, the simulated temperatures show local minima at around 200 hPa in the polar lower stratosphere, above which temperatures increase monotonically upward to

the stratopause. On the other hand, observed temperatures exhibit a local warm maximum at around 200 hPa and a local cold minimum at around 30 hPa, in the polar lower stratosphere, indicating that MRI-CCM simulations show a cold bias in the lower stratosphere and a warm bias in the upper stratosphere at high latitudes.

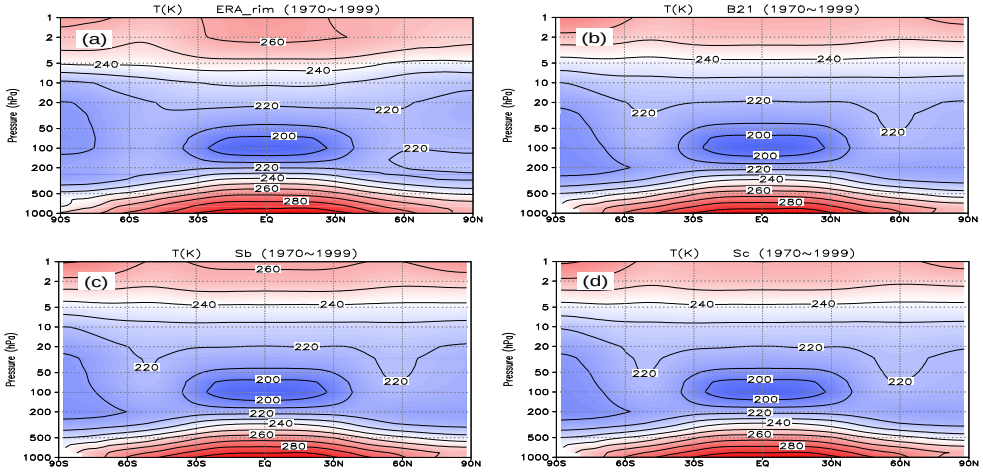

Fig. 2. Annual- and zonal-mean temperature. Latitude-pressure cross sections for annual- and zonal-mean temperature (K) in the past 30-year (1970-1999) are for (a) ERA-Interim, (b) B21, (c) Sb, and (d) Sc. The contour interval is 10 K, and blue colors represent lower temperatures and red colors higher temperatures.

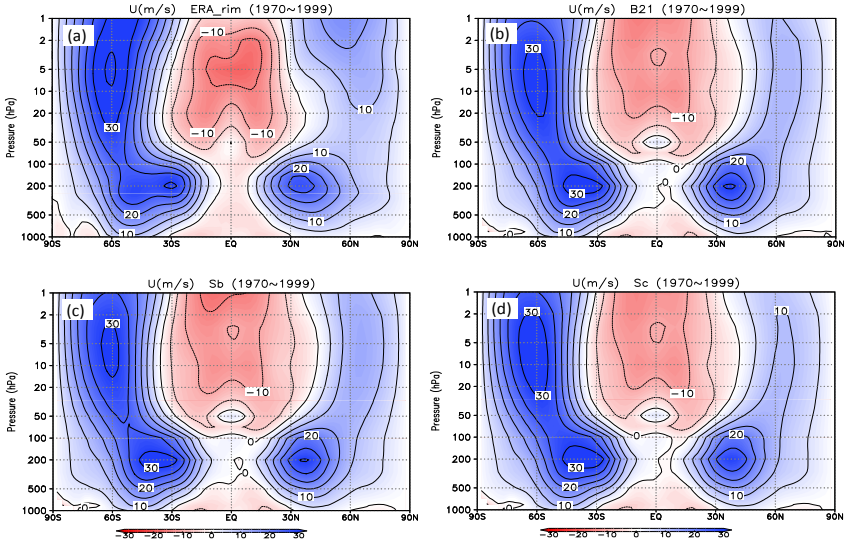

Fig. 3. Annual- and zonal-mean zonal wind. Same as Fig.2 except for zonal wind (ms^{-1}). The contour interval is 5 ms^{-1}, and blue colors represent positive (westerly) winds and red colors negative (easterly) winds.

Consistent with these temperature biases, the simulated zonal winds also show common biases in the subtropical jet and the polar night jet as a result of the thermal wind balance. The core velocity of the subtropical jet is too strong, and its separation from the polar night jet is too weak; that is, the zonal wind at around 50 hPa and 60°N is too strong, and the polar night jet in the upper stratosphere is too weak. In the SH, there are also cold biases in the mid- and high-latitude lower stratosphere at around 200 hPa. Similar to the NH, in the SH the simulated subtropical jet is stronger than the observed one, but the simulated polar night jet is weaker.

3.2 Future climate change in temperature and zonal wind

Figures 4 and 5 display the changes in the future 30-year period (2070-2999, 100 years later than the past 30-year period (1970-1999)) in annual- and zonal-mean temperature and zonal wind. During this future period, the ODS abundances are almost restored to pre-1970s levels (Fig. 1), so that the forcing is almost entirely due to GHGs alone. The temperature changes in the three B2 members (B21, B22, and B23) and in the fixed-halogen simulation Sb exhibit very similar CO_2- (GHG-) induced patterns (e.g., Yukimoto et al., 2006; IPCC, 2007): warming in the troposphere through SST warming (indirect CO_2 effect) and cooling in the stratosphere (direct CO_2 effect) (Kodama et al., 2007). In addition, weak but substantial cooling is seen in the tropical lower stratosphere. The tropospheric warming reaches a maximum of about 4 K in the tropical upper troposphere, reflecting the enhanced latent heat release resulting from intensified convective activity caused by the SST rise. In the B2 simulations, the maximum stratospheric cooling, to about -6 K, in the upper stratosphere is caused both by enhanced CO_2 terrestrial radiation and by recovered ozone solar radiation as described below.

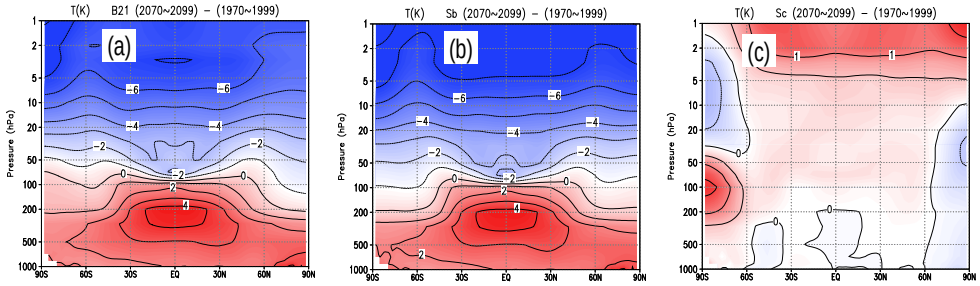

Fig. 4. Future changes in temperature. Latitude-pressure cross sections of future changes (difference between 2070-2099 and 1970-1999) in annual- and zonal-mean temperature (K) for (a) B21, (b) Sb, and (b) Sc. The contour interval is 1 K for B21 and Sb and 0.5 K for Sc, and blue colors represent cooling and red colors warming.

In the no-climate-change simulation Sc, on the other hand, strong warming occurs in the upper stratosphere above about 5 hPa in both hemispheres, except in the southern high latitudes, where prominent warming occurs in the lower stratosphere at 300-30 hPa, centered at 100 hPa, and the cooling above 30 hPa. This temperature change pattern is completely different from the CO_2-induced pattern and is due solely to the ODS decrease, or equivalently, the ozone recovery, because the average ODS concentration was higher in the past 30 years (1970-1999) than in the future 30 years (2070-2099) (Fig. 1). In fact, stratospheric

ozone abundances were projected to recover to or exceed pre-1980 levels globally in the future, except for the tropical lower stratosphere due to the increased inflow of ozone-poor tropospheric air mass (e.g., SPARC, 210). In other words, the upper stratospheric cooling in the past 1970-1999 was due to an ozone decrease caused by gas-phase reactions with reactive chlorine and bromine atoms photodissociated from ODSs under strong ultraviolet solar radiation, whereas the pattern in the southern high latitudes was associated with severe ozone depletion (i.e., the ozone hole) caused by heterogeneous reactions on PSCs (e.g., SPARC, 2010). This ODS-decrease effect is also included in the B2 simulations; thus, temperature changes similar to those in Sc can be obtained by subtracting the changes in Sb from those in the B2 members (not shown).

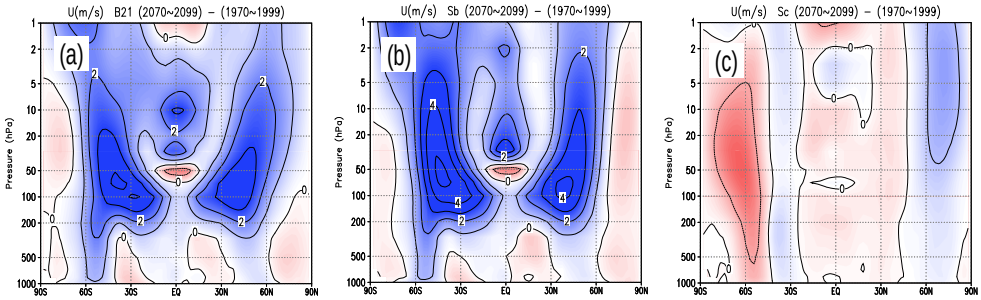

Fig. 5. Future changes in zonal wind. Same as Fig.4 except for zonal wind (ms^{-1}). The contour interval is 1 ms^{-1}, and blue colors represent positive (westerly/eastward) acceleration and red colors negative (easterly/westward) acceleration.

Zonal wind changes in the three B2 members and Sb display a very similar pattern in the polar night jet regions in both hemispheres and in the equatorial lower stratosphere. Westerly wind intensification extends from the upper region of the subtropical jet upward along the equatorward flank of the polar night jet axis, reaching a maximum at around 70 hPa and 40° in both hemispheres. In the SH, the westerly wind intensification also extends down to the surface at around 55°S, resulting in poleward spreading of the subtropical jet. In the tropics, westerly wind strengthening (eastward acceleration) occurs above 30 hPa and weakening (westward acceleration) at 50 hPa, below which very weak westerly wind strengthening occurs down to the surface. In the no-climate-change simulation Sc, on the other hand, the zonal wind change pattern is completely different. In the SH, weakening of the polar night jet and both weakening of the poleward and strengthening of the equatorward flank of the subtropical jet down to the surface occur, changes which are almost opposite to those in B2 and Sb in the troposphere above southern high latitudes. This change in the subtropical jet in Sc means that the equatorward shift of the jet is associated with ozone recovery (e.g., Son et al., 2008). In the NH, the poleward flank of the polar night jet is slightly intensified above the middle stratosphere. In the tropics, there is almost no change in the troposphere and stratosphere, consistent with the temperature results.

3.3 Evolution of the Brewer-Dobson circulation and the ozone hole area

The GHG increase affects the mass exchange between the troposphere and the stratosphere, which can be evaluated as the upward mass flux across the tropopause. Most GCMs and

CCMs (e.g., Butchart et al., 2006; Austin & Li, 2006; Garcia & Randel, 2008) show an acceleration of BDC resulting from an increase in GHGs, but balloon measurements do not necessarily support these model results, even given the large uncertainties and sparse observations in both time and space (Engel et al., 2009). Figure 6 depicts the evolution of the global upward mass flux anomaly (49-month running mean) at 100 hPa, calculated from the residual mass stream function. It is evident that the simulations with the GHG increase scenarios (B21, B22, B23, and Sb) result in a nearly linear increase of the upward mass flux across 100 hPa, and the trend slopes are very similar at about 8×10^9 kgs^{-1} per century. On the other hand, the simulation results for the no-climate-change scenario Sc exhibit no trend at all. This feature can be also analyzed in the equatorial stratosphere, as displayed in Fig. 7, which depicts the low-frequency (period longer than 10 years) components of the residual vertical velocity $\overline{w}^*$ (in units of 10^{-4} ms^{-1}, averaged from 10°S to 10°N) from 70 to 1 hPa. Note that some high-frequency components remain, due to leakage of the Lanczos filter. The magnitude of $\overline{w}^*$ is very small in the lower stratosphere, with a minimum at 50 hPa; above 50 hPa it increases with altitude, gradually up to about 5 hPa and steeply above that. This vertical structure does not change in the GHG-increase simulations or in the no-climate-change simulation during the whole integration period, consistent with equilibrium CO_2-doubling simulations (e.g., Kawatani, et al., 2011).

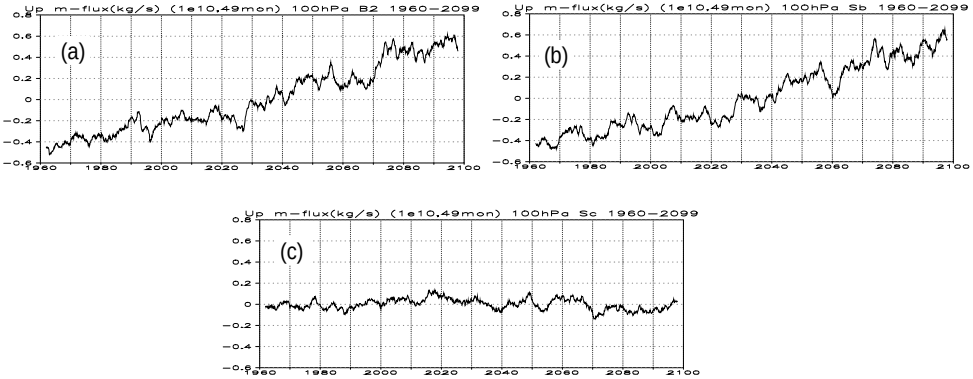

Fig. 6. Upward mass flux at 100 hPa. Evolution of the upward mass flux (10^{10} kgs^{-1}) at 100 hPa for (a) B21, (b) Sb, and (c) Sc. The 49-month running mean is applied to eliminate short-term variations.

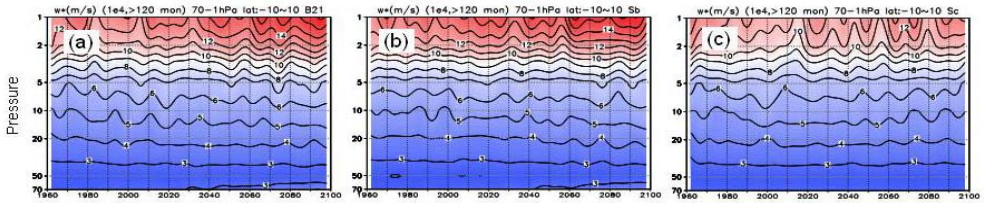

Fig. 7. Low-frequency residual vertical velocity. Time-pressure cross section of the low frequency (period longer than 120 months) component of the residual vertical velocity (averaged between 10S and 10N) from 70 to 1 hPa. Units are 10^{-4} ms^{-1}.

ODSs will continue to induce an ozone hole over the Antarctic from late winter to spring in the future, as long as their abundances exceed certain values (e.g., SPARC, 2010). Figure 8 exhibits the evolutions of the annual maximum ozone hole area in the ODS time-evolving simulations (B21, B22, B23, and Sc). Different from these simulations, no ozone hole appears in the fixed-ODS simulation Sb, even if the GHGs-induced climate change progresses. Even though the inter-simulation variation is not especially small, the features of all of these simulations are very similar with regard to the long-term evolution of the ozone hole area: (1) initial appearance around 1980, (2) followed immediately by a rapid increase until the later 1990s, (3) then nearly saturated values until about 2010, and (4) followed by a gradual decrease, with disappearance around 2070. Features 1-3 qualitatively correspond to the observed features (e.g., WMO, 2011), aside from the short-term variations. The fact that the evolution of the ozone hole area in Sc is similar to that in the three B2 members indicates that the effect of the GHG increase on the ozone hole in the SH is limited.

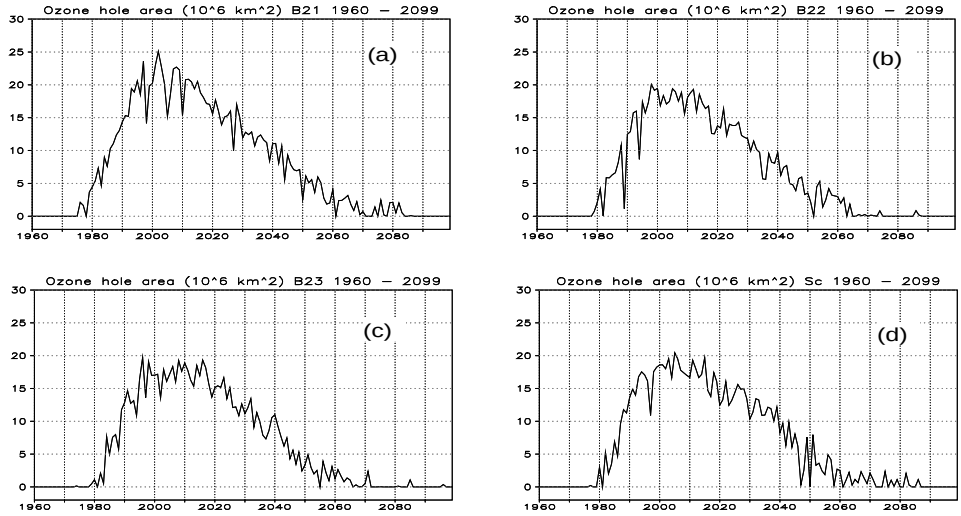

Fig. 8. Ozone hole area in SH. Evolution of the annual maximum ozone hole area in the SH in (a) B21, (b) B22, (c) B23, and (d) Sc. Units are 10^6 km^2.

4. Characteristics of the QBO

4.1 Vertical structure and power spectrum of the QBO

Figure 9 shows the observed and simulated zonal-mean zonal wind (averaged from 10°S to 10°N) between 100 and 5 hPa for the 20 years from 1990 to 2009. Monthly averages are subtracted from the values of each month to extract anomalies from the seasonal cycle, so that the semi-annual oscillation (SAO) in the upper stratosphere becomes smaller than or similar to the QBO. It is evident that all of the simulations reproduced the overall features of the observed QBO, such as the stronger westerly shear than easterly shear during the phase transition as well as the stalling of the descent of the easterly winds. Empirical orthogonal function (EOF) analysis revealed that EOF 1 and 2 explain major parts of the variance as in observations (e.g., Wallace et al.,1993) (not shown). The simulated QBOs realistically

descend to as low as 100 hPa, whereas their amplitudes are smaller than the observed amplitude, particularly below about 50 hPa in the lower stratosphere, a common bias among three-dimensional models (Takahashi, 1999; Hamilton et al., 1999; Scaife et al., 2000; Giorgetta et al., 2002; Butchart et al., 2003; Shibata & Deushi, 2005a; Watanabe et al., 2008; Kawatani et al., 2011). The differences among the simulations are not necessarily discernible in Fig. 9.

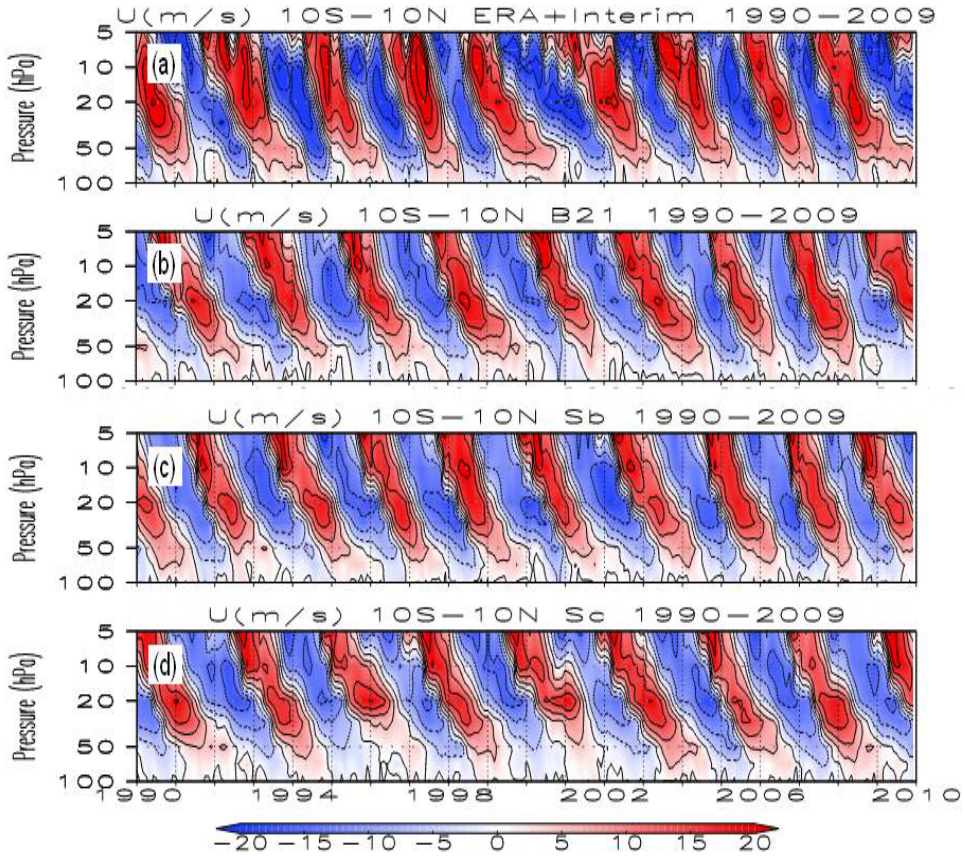

Fig. 9. Zonal wind evolution in the tropics. Evolution of zonal-mean zonal wind (averaged between 10S and 10N) from 100 to 5 hPa for the 20 years from 1990 to 2009: (a) ERA-Interim, (b) B21, (c) Sb, and (d) Sc.

Figure 10 depicts the power spectrum in the low-frequency domain (periods longer than 16 months) for the observed and simulated wind averaged 10°S to 10°N from 100 to 1 hPa. The observed power, extending from about 18 to 240 months, is evidently much broader than the simulated power. This is because the simulations include only the anthropogenic forcing of GHGs and ODSs without the natural forcings of the solar 11-year cycle and volcanic aerosols. The broad spectral peaks at around 28 months, which represent the QBO, are distributed similarly between the observation and the simulations, though the observed

QBO has less power than the simulated QBO in the upper stratosphere. On the basis of the power spectrum distribution, we defined the QBO as the components with a period between 20 and 40 months. In the higher frequency domain (periods shorter than 16 months), the power spectrum is a narrow monomodal distribution concentrated at an annual frequency below 10 hPa, and a bimodal distribution sharply concentrated at annual and semiannual frequencies above 10 hPa, in both the observation and the simulations (not shown). The QBO power is the largest of these two or three peak powers below the middle stratosphere.

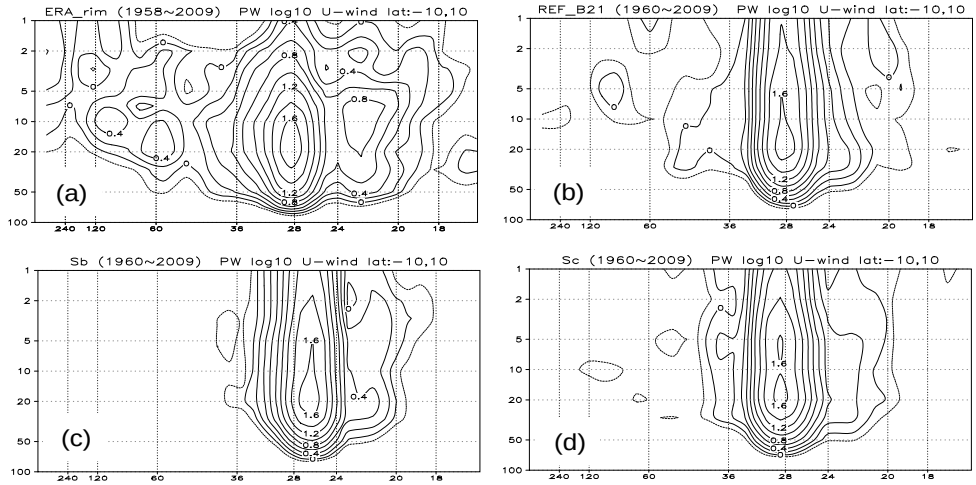

Fig. 10. Power spectra of zonal wind. Power spectra (ms^{-1}) of zonal-mean zonal wind averaged from 10°S to 10°N for periods > 16 months: (a) ERA-Interim, (b) B21, (c) Sb, and (d) Sc. The analysis period was from 1958 to 2009 for ERA-Interim, and from 1960 to 2009 for the simulations.

4.2 Forcings of the QBO

Figure 11 displays the composite relations within the QBO cycle at 30 and 70 hPa for B21 between the QBO zonal wind and the three major forcings, parameterized gravity-wave forcing (GWF), resolved-wave forcing (Eliassen-Palm flux divergence, EPD), and vertical advection of zonal momentum ($\overline{w}^{*}(\partial u/\partial z)$, WUZ), calculated for the entire period of 1960-2099. Note that all of the forcing terms and the zonal wind are band-passed (20-40 months) values with the QBO components extracted by a Lanczos filter. In making the composite figures, we assumed that each cycle expands in 2π phase space with a peak power period of 28 months, even though each cycle had a different period. Although the fine structures such as steep gradient during the phase transitions disappear due to the band-pass filtering, basic configuration among the QBO and its forcings are represented in Fig. 11.

AT 30 hPa, GWF is retarded by about one-seventh cycle relative to zonal wind, so that positive (eastward acceleration) GWF occurs approximately from after the initial stage of the westerly shear descent (equivalently, $\partial u/\partial t > 0$) to the initial stage of the easterly shear descent ($\partial u/\partial t < 0$); conversely, negative (westward acceleration) GWF continues from after

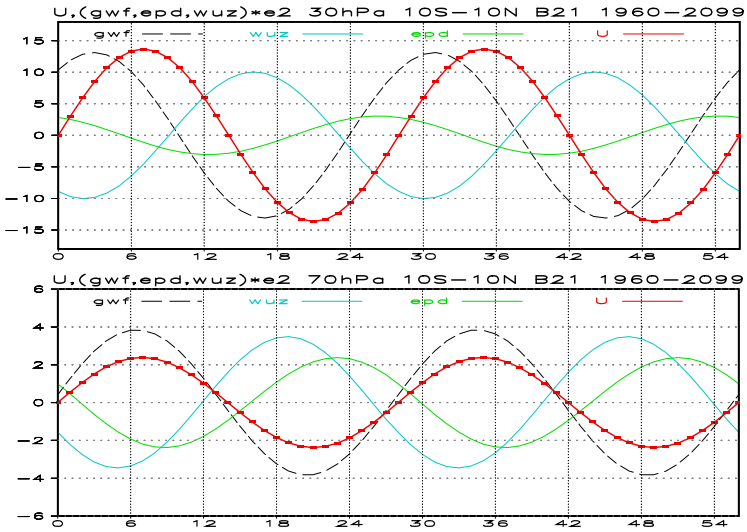

Fig. 11. Composite relations among the QBO and its forcings. Composite relations among zonal wind (U, red solid curve with closed circles), parameterized gravity wave forcing (GWF, black dashed curve), resolved wave forcing (EPD, green solid curve), and vertical advection (WUZ, cyan solid curve) at (upper) 30 hPa and (lower) 70 hPa over two cycles for an average QBO cycle (28 months). All quantities are averaged from 10°S to 10°N and band-pass filtered (20-40 months). Units are ms^{-1} for U, 10^{-2} ms^{-1} day^{-1} for forcing/advection.

the initial stage of the easterly shear descent to the initial stage of the westerly shear descent. The amplitude of WUZ is three-quarters that of GWF amplitude and is almost of opposite phase, thus partially cancelling GWF. Therefore, GWF promotes the descent of the vertical shear, and WUZ hinders it. EPD lags GWF by about one-seventh cycle, and thus lags the zonal wind by approximately one-quarter cycle. Of these three forcings, GWF and WUZ are the largest and second largest terms, but as a result of the partial cancellation due to their being of almost opposite phase, the sum of GWF and WUZ has a similar amplitude to that of EPD. At other altitudes, a similar relation quantitatively holds true, particularly at 20 hPa and above, although the deviation from the relation at 30 hPa increases in the lower stratosphere (50-70 hPa). AT 50 hPa, GWF is nearly in-phase with zonal wind, whereas WUZ and EPD lag the zonal wind by about four- and three-sevenths cycle, respectively, and are thus out of phase with zonal wind. In addition, the amplitudes of GWF and WUZ decrease from around 0.13 and 0.10 ms^{-1} day^{-1}, respectively, at 30 hPa to 0.04 and 0.03 ms^{-1} day^{-1}, respectively, at 70 hPa, resulting in similar amplitudes among GWF, WUZ, and EPD at 70 hPa. The Differences in the phase relation among all of the simulations were very small.

The vertical advection WUZ consists of two terms. One is associated with low-frequency (<< the QBO frequency) vertical wind, and the other with the vertical wind from the secondary circulation of the QBO (e.g., Plumb & Bell, 1982). This is because WUZ is the product of the residual vertical wind and the vertical shear of zonal wind, both of which have two major peaks in power spectrum at the QBO and annual frequencies below the middle stratosphere,

similarly to zonal wind as stated before. Thus, since cross terms with annual or semiannual component cannot create the QBO term of broad-period range, the QBO acceleration of zonal wind due to WUZ is expressed as

$$\left(\frac{\partial u}{\partial t}\right)^{Q}_{WUZ} = -\left(\overline{w}^{*}\left(\frac{\partial u}{\partial z}\right)\right)^{Q} \sim -\left(\overline{w}^{*}\right)^{L}\left(\frac{\partial u}{\partial z}\right)^{Q} - \left(\overline{w}^{*}\right)^{Q}\left(\frac{\partial u}{\partial z}\right)^{L} \quad (1)$$

where the superscripts Q and L represent the QBO and the low-frequency components, respectively. The first term on the right-hand side of the approximation sign represents the contribution of the lower-frequency (background) vertical wind, corresponding to the interaction with BDC, and the second term is the interaction between the background zonal wind shear and the QBO secondary circulation. Henceforth the first term is referred to as BDT and the second term as SCT. Just below the maximum power altitude at 30 hPa, the magnitude of each term on the right hand side of Eq. (1) is, on average, as will be demonstrated later

$$\left(\frac{\partial u}{\partial z}\right)^{L} \sim -1.5\times10^{-3}(s^{-1}),\ \left|\left(\frac{\partial u}{\partial z}\right)^{Q}\right| \sim +3.5\times10^{-3}(s^{-1})$$

$$\left(\overline{w}^{*}\right)^{L} \sim +0.35\times10^{-3}(ms^{-1}),\ \left|\left(\overline{w}^{*}\right)^{Q}\right| \sim +0.1\times10^{-3}(ms^{-1})$$

where $|(X)^{Q}|$ represents the QBO amplitude of X.

It is evident that the residual vertical velocity is one order smaller than the vertical shear of zonal wind for both the QBO and the low-frequency components. Because the QBO vertical shear of zonal wind is almost of opposite phase to the QBO vertical wind (e.g., Plumb & Bell, 1982; Andrews et al., 1987), and the low-frequency term of vertical shear of zonal wind and that of vertical wind are negative- and positive-definite, respectively, at 30 hPa throughout the whole period from 1960 to 2100, BDT and SCT exert acceleration in approximately the same direction with a ratio of about 8 to 1, indicating that BDT is the major acceleration term of the vertical momentum advection. The magnitude of BDT is also much larger than that of SCT at other altitudes, in particular in the lower stratosphere, because the vertical shear is larger in the QBO than in the low-frequency and the residual vertical wind is larger in the low-frequency than in the QBO. However, other features such as acceleration direction and trend differ depending on altitude and latitude. In the lower stratosphere at 50 hPa and below, for example, BDT and SCT do not always exert acceleration in the same direction because the low-frequency vertical shear did not hold but, in the middle of the integration period (1960-2099), changes its sign from negative to positive at 50 hPa and from positive to negative at 70 hPa over the equator as a result of the climate change caused by the GHG increase.

5. Evolution of the QBO

5.1 Future change of the zonal wind forcing in the tropical stratosphere

Changes in the zonal wind forcings affect the background zonal wind, which in turn modifies the QBO through the interactions between the background zonal wind and the

QBO; thus, such changes are one of the crucial factors affecting the future QBO. Figures 12-14 depict annual mean GWF, WUZ, and EPD in the past (30 years, 1970-1999) and their changes after 100 years (30 years, 2070-2099) in the low-latitude (30°S-30°N) stratosphere from 70 to 5 hPa. GWF and EPD generally exert negative (westward) acceleration in this domain, except in some regions: namely, in the upper stratosphere around 15° in both hemispheres, and at 50 hPa in the deep-tropics (10°S-10°N) for GWF, and at 30 hPa south of the equator for EPD. On the other hand, WUZ exerts positive (eastward) acceleration almost everywhere in this domain.

It is evident that the distributions of the forcing magnitude are commonly very different between the mid-tropics (15°S-15°N) and higher latitudes. In the mid-tropics, the magnitude of GWF is minimal below 50 hPa, and above 50 hPa it is maximal and more concentrated south of the equator. The magnitude of WUZ shows a similar pattern with a broader maximum above 50 hPa. The magnitude of EPD is also minimal in the mid-tropics, and the width of the minimum area becomes narrower with altitude; the magnitude is largest at 50 hPa, and then the minimum area becomes more concentrated downward toward the equator. The EPD minimum over the tropics reflects the suppression of the propagation of Rossby waves from the mid-latitudes and subtropics against the easterly background zonal wind (Fig. 3).

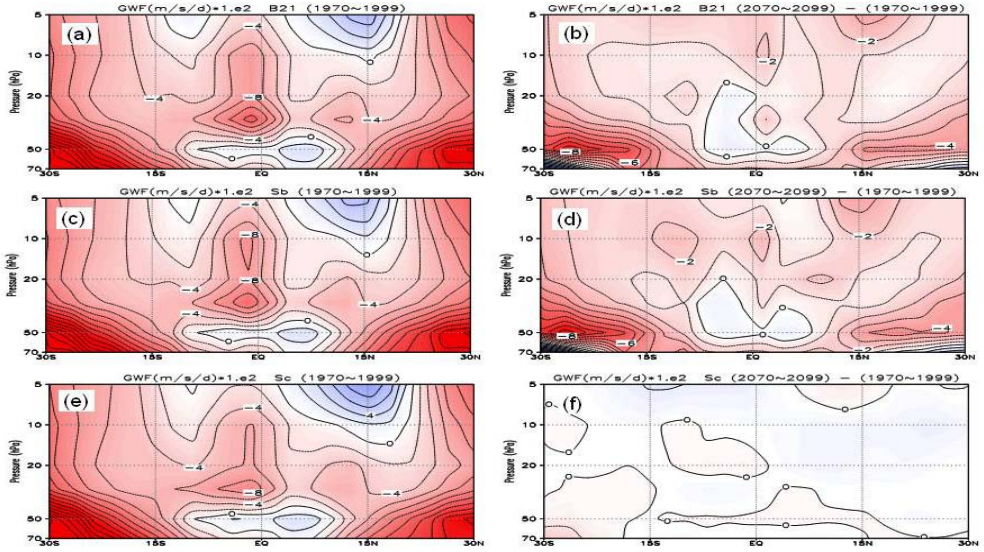

Fig. 12. GWF in the past and future. Annual and zonal mean GWF (left) in the past 30-year period (1970-1999) and (right) the changes in the future 30-year period (2070-2099) for (upper) B21, (middle) Sb, and (lower) Sc. The contour interval is 2×10^{-2} ms^{-1} per day for the left panels and 1×10^{-2} ms^{-1} per day for the right panels.

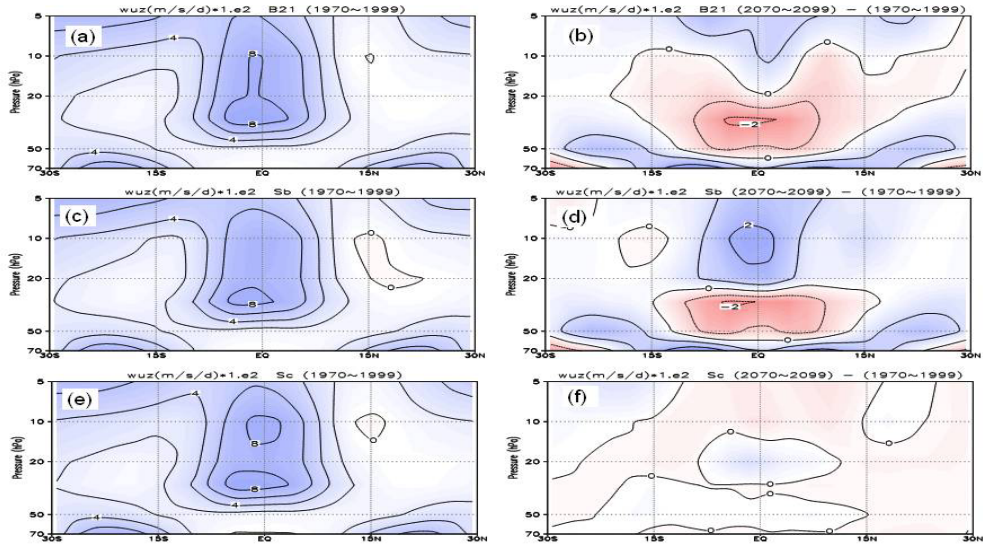

Fig. 13. WUZ in the past and future. Same as Fig.12 except for WUZ.

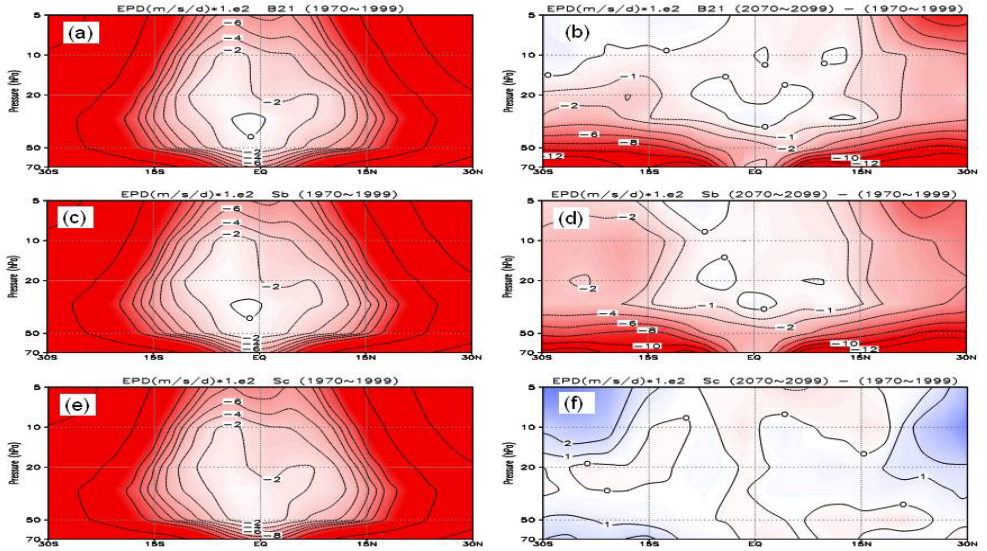

Fig. 14. EPD in the past and future. Same as Fig.12 except for EPD. Units are 10^{-2} ms^{-1} per day. The contour interval is 2 for the values greater than -12, except that the outer contours in the left panels have the values -16, -32, and -64. The contour interval is 1 for values greater -2, but for values less than -2, the contour interval is 2 in the right panels.

Future changes in GWF and EPD are larger outside of the mid-tropics below the middle stratosphere in GHG-increase simulations, owing to the shift of the zero line of zonal wind (e.g., Deushi & Shibata, 2011). In contrast, future GWF and EPD changes are small in the

mid-tropical middle stratosphere, in particular at around 30 hPa, in GHG-increase simulations. On the other hand, in the mid-tropical middle stratosphere, the future WUZ changes are larger negative values with a large cell structure. In the no-climate-change simulation, the future changes in the QBO forcings are very small everywhere.

5.2 Trend of the QBO zonal wind

Figure 15 exhibits the QBO zonal wind (averaged from 10°S to 10°N) at 30 hPa for the whole period from 1960 to 2099 in simulations for B21, Sb, and Sc. It is evident that the QBO zonal winds show long-term decreasing trends in all of the GHG-increase simulations, whereas in the no-climate-change simulation Sc, the QBO zonal wind shows no long-term trend at all. To quantify the trends, the QBO amplitude was calculated by two independent methods, that is, direct and wavelet methods. The direct method assumes that the QBO amplitude is $\sqrt{2}\sigma$, analogous to a monochromatic wave, where σ is the root mean square of the QBO time series over three cycles, even though the QBO time series is not a single sinusoidal wave (Pascoe et al., 2005; Baldwin & Gray, 2005). The cycles are defined as periods from one zero point to the third consecutive zero point, and the QBO amplitude is assigned to the center time of the three cycles. In this way, the QBO amplitudes are first calculated discretely in time, about a half (14 months) cycle apart, and then monthly amplitudes are obtained through cubic interpolation with Lagrange polynomials. This procedure results in a QBO amplitude that is a low-passed (> 3 cycles~7 years) data with a temporal resolution of about 14 months. The wavelet method used a Morlet mother wavelet (plane wave modified by a Gaussian envelope) with non-dimensional frequency ω_0=6 (e.g., Torrence & Compo, 1998), so the result of the wavelet analysis incorporates a mean information within approximately three cycles centered at time and frequency concerned.

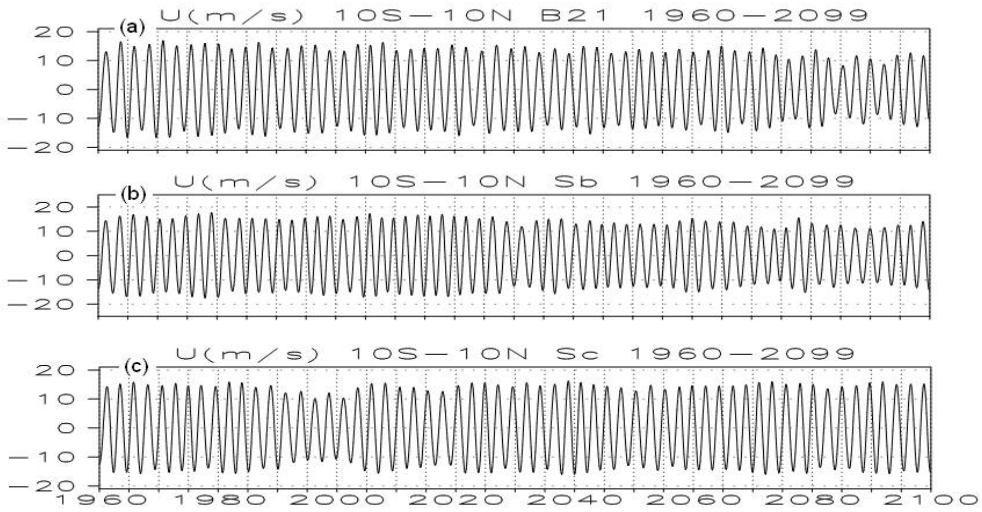

Fig. 15. QBO wind evolution. Zonal-mean zonal wind averaged from 10°S to 10°N at 30 hPa for the whole period 1960-2099 for (a) B21, (b) Sb, and (c) Sc. A band-pass filter (20-40 months) was applied to obtain the QBO component.

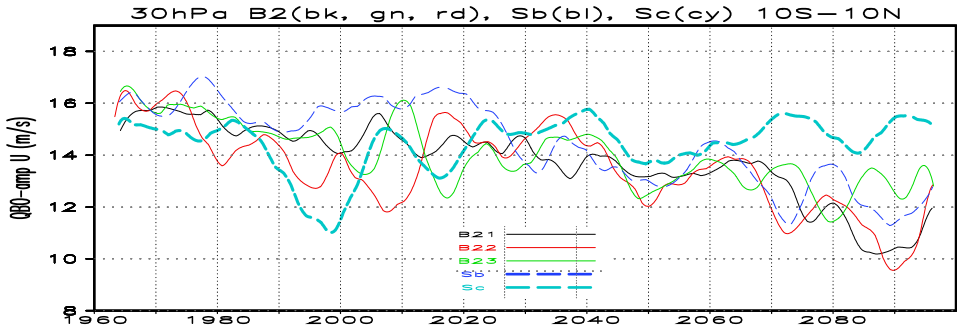

Fig. 16. QBO amplitude evolution. Evolution of the QBO amplitude of zonal-mean zonal wind at 30 hPa in B21 (black solid), B22 (green solid), B23 (red solid), Sb (blue dashed), and Sc (cyan dashed).

Figure 16 depicts the QBO amplitude of the zonal-mean zonal wind (averaged from 10°S to 10°N) at 30 hPa in all simulations. The QBO amplitudes of the GHG-increase simulations steadily decreases from about 16 ms^{-1} in the 1960s and 70s to about 12 ms^{-1} in the 2080s and 90s, resulting in, on average, a linear trend of about 0.3 ms^{-1} per decade. On the other hand, in the no-climate-change simulation Sc, the QBO amplitude does not seem to show a distinct trend. Nevertheless, close inspection reveals that the amplitude, like the GHG-increase simulations, decreases until about year 2000, and thereafter gradually increases. As a result, the overall trend is a small positive slope. Among all simulations, other features such as decadal variations are very different from one simulation to another, even within the B2 three members.

Different from the distinct decreasing trend of the QBO amplitude, the QBO period does not exhibit any significant trend as depicted by the local wavelet power spectrum of the QBO zonal wind at 20 hPa, where the power maximizes (Fig. 17). The QBO powers are mainly confined to between 22 and 32 months, and the peak power frequencies (periods) stabilize at 28 months, in spite of some excursions toward 20-24 months in the GHG-increase simulations. Similarly to the direct evaluation, the QBO powers show a common decreasing trend in the GHG-increase simulations. The no-climate-change simulation Sc, on the other hand, shows a very stable QBO without a substantial trend in either frequency or power magnitude.

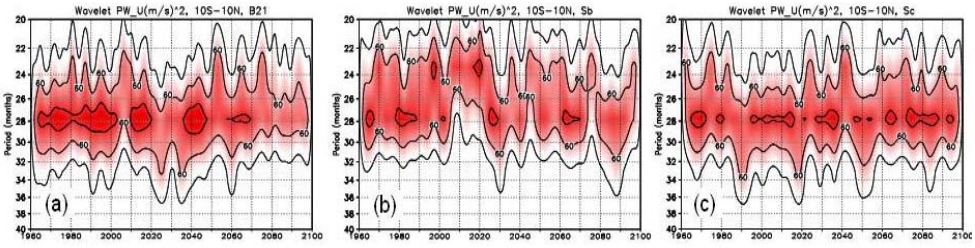

Fig. 17. QBO local wavelet power spectrum at 20 hPa. Evolution of the local wavelet power spectrum of the zonal-mean zonal wind averaged from 10°S to 10°N at 20 hPa in the QBO period for (a) B21, (b) Sb, and (c) Sc. Units are m^2s^{-2} and the contour interval is 20.

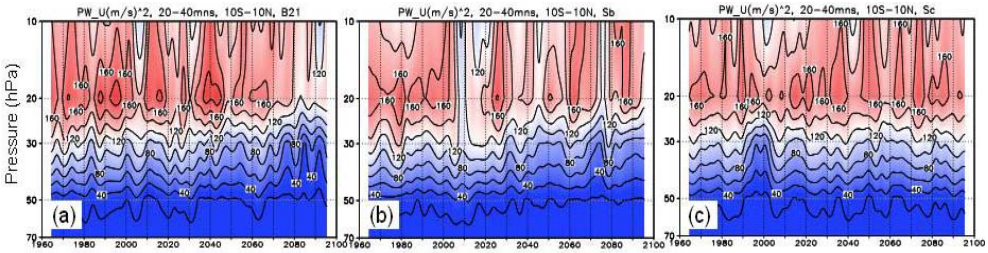

Fig. 18. Vertical profile of the QBO local wavelet power spectrum. Evolution of the wavelet power of the QBO zonal-mean zonal wind (averaged from 10°S to 10°N) from 70 to 10 hPa for (a) B21, (b) Sb, and (c) Sc. Units are m^2s^{-2} and the contour interval is 20.

Figure 18 exhibits the evolution of the QBO local wavelet power from 70 to 10 hPa for B21, Sb, and Sc simulations. Below 30 hPa, the QBO powers show an apparent decreasing trend in the GHG-increase simulations, whereas they do not at 10 hPa. The no-climate-change simulation Sc, on the other hand, does not seem to show a discernible trend for the QBO zonal wind at any altitude. To quantify linear trends in the QBO amplitude, the linear regression is calculated not for the monthly interpolated amplitude but for the original about half-cycle (~14 months) interval amplitude using the least squares method at each altitude.

Figure 19 depicts the vertical profile of the linear trend in the QBO zonal wind amplitude from 70 to 10 hPa for all simulations. The GHG-increase simulations all exhibit a statistically significant (at the 99% confidence level) negative trend below 20 hPa, except for that of B23 at 20 hPa. The maximum negative trends at 30 hPa are about 0.3 ms^{-1} per decade, and negative trend below and above 30 hPa are 0.2-0.1 ms^{-1} per decade. In the upper stratosphere, the trends are near zero or small positive, but the differences among the simulations are not small. The no-climate-change simulation exhibits a near-zero trend in the lower stratosphere below 50 hPa, and a small but statistically significant positive trend above 30 hPa. These results demonstrate that the GHG increase is responsible for the decrease in the QBO amplitude below 20 hPa and that ODS changes alone cause the increase above 30 hPa.

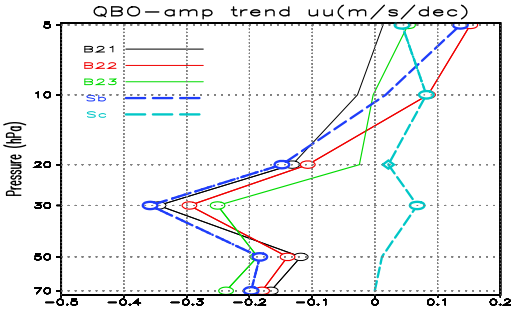

Fig. 19. Trends of the QBO amplitude. Vertical profiles of the linear trends (ms^{-1} per decade) in the QBO amplitude for the zonal-mean zonal wind (averaged from 10°S to 10°N) from 70 to 5 hPa in all simulations. Open circles and diamonds represent the trend being different from zero at the 99% and 95% confidence levels (*t*-test), respectively. The QBO amplitude was calculated by the direct method.

5.3 Trends in the forcings of the QBO zonal wind

The QBO trends of the zonal wind amplitude are statistically significant below 20 hPa in the GHG-increase simulations and above 30 hPa in the no-climate-change simulation; therefore, the forcings of the QBO zonal wind themselves show similar trends. Figure 20 exhibits the evolutions of the QBO forcing terms, GWF, WUZ, and EPD, at 30 hPa in all simulations. As shown by the composite relations among the QBO and its forcings (Fig. 11), GWF has the largest amplitude and EPD the smallest amplitude during the whole period (1960-2099). Although the short-term variations are considerable, it is evident that the forcings show decreasing trends in the GHG-increase simulations and that they do not in the no-climate-change simulation. Similarly to the quantification of the trend of the QBO zonal wind amplitude, linear regression was used to calculate the trends of the forcings. In addition, to include different responses at different frequencies, that is, a larger response at a smaller frequency, even in the QBO narrow-frequency domain (period of 20-40 months) and to get more direct contribution to the trend of the QBO zonal wind, each raw forcing was integrated over time and band-passed to yield the corresponding zonal wind response (see Eq. (1)). For example, u_{GWF} is the integrated QBO zonal wind (response wind) due to GWF. Following this procedure, the linear regressions were calculated. Note that the trends in the forcing amplitudes are not additive, even though forcings are additive in the temporal space, owing to their different phases (Fig. 11).

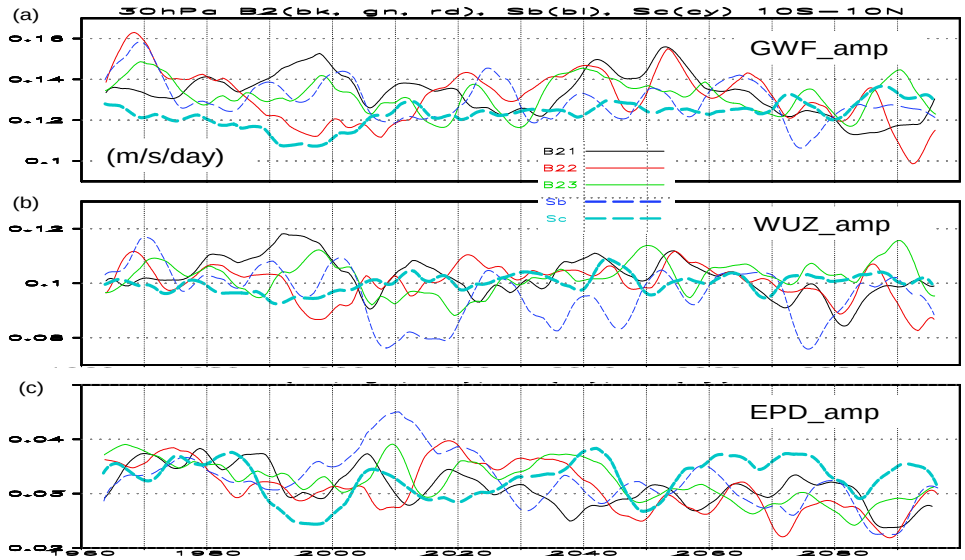

Fig. 20. QBO forcing evolution. Same as Fig. 16 except for (a) the parameterized gravity forcing (GWF), (b) the momentum vertical advection (WUZ), and (c) the resolved wave forcing (EPD).

Figure 21 displays the vertical profiles of GWF and u_{GWF} from 70 to 5 hPa for all simulations. The GHG-increase simulations exhibit the same statistically significant negative trend at 30 ant 70 hPa and, in most cases, at 50 hPa as well, with a maximum of about 0.2×10^{-2} ms^{-1} day^{-1}

per decade for GWF at 70 hPa. At 20 hPa the trends are dispersed around zero, and at 10 and 5 hPa, the GWF shows statistically significant positive values of nearly the same magnitude. The trends of integrated zonal wind u_{GWF} are qualitatively similar to those of GWF but the statistically significances are not necessarily so.

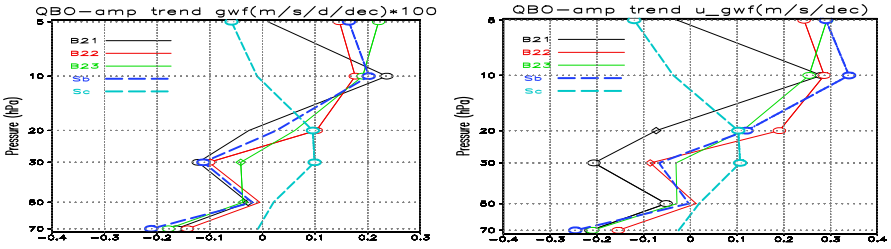

Fig. 21. GWF amplitude evolution. Same as Fig.19 except for (left) GWF and (right) the GWF-induced zonal wind $u_{GWF,}$ which was calculated by time-integration of GWF. Units are 10^{-2} ms^{-1}day^{-1} per century for GWF and ms^{-1} per decade for u_{GWF}.

For example, while most GHG-increase simulations show a statistical significant negative trend at 70 hPa and positive trend above 10 hPa both in u_{GWF} and in GWF, the number of statistically significant trends decreases at 50 and 30 hPa and increases at 20 hPa in u_{GWF} compared with GWF. The no-climate-change simulation exhibits statistically significant positive trends of about 0.1x10^{-2} ms^{-1} day^{-1} per decade at 20 and 30 hPa, and a negative trend of similar magnitude at 5 hPa for GWF.

The vertical transport of zonal momentum WUZ shows a statistically significant trend at almost all altitudes in the GHG-increase simulations (Fig. 22). A negative trend of about 0.1x10^{-2} ms^{-1} day^{-1} per decade is seen at 30 and 50 hPa, and a positive trend of nearly the same magnitude at 70 hPa and above 20 hPa. The no-climate-change simulation exhibits almost no trends at any altitude in both WUZ and u_{WUZ}, and most apparent trends are thus not statistically significant. The resolved-wave forcing EPD and u_{EPD} exhibit a vertically flat structure (Fig. 23), and the trend magnitudes are smaller than those of the other forcings in all simulations; nevertheless, most of the trends are statistically significant.

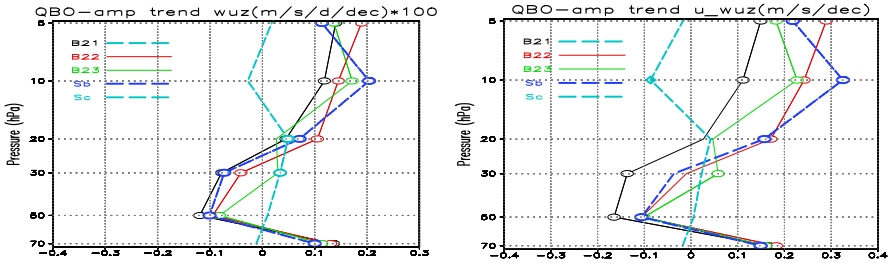

Fig. 22. WUZ amplitude evolution. Same as Fig.19 except for (left) WUZ and (right) the WUZ-induced zonal wind u_{WUZ}.

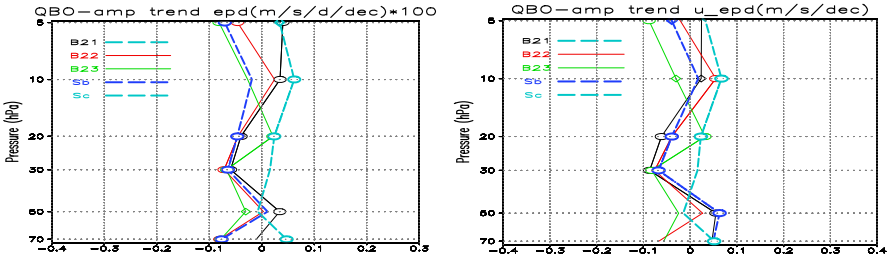

Fig. 23. EPD amplitude evolution Same as Fig.19 except for (left) EPD and (right) the EPD-induced zonal wind u_{EPD}.

6. Discussion

The GHG-increase simulations have thus far demonstrated that the QBO amplitude decreases linearly below 20 hPa with rates of 0.1-0.3 m s^{-1} per decade and increases above 10 hPa with rates of 0-0.1 m s^{-1} per decade (Fig. 19). As shown by the difference between the B2 and Sb simulations, the trends of the B2 members tend to be smaller below 20 hPa than the Sb trend, but the difference between them is not substantial. That is, the inter-member variations are too large to ascribe the difference between the B2 members and Sb to the forcing difference, that is, ODSs. On the other hand, the small but statistical significant increasing trends of less than 0.1 m s^{-1} per decade at 30 hPa and above exhibited by the no-climate-change simulation is likely an effect of the ODS decrease, although to confirm this result , an Sc ensemble simulation should be performed.

The cause of the QBO trend should reflect the trends of the forcings, GWF, EPD, and WUZ. However, because the forcings include not only external quantities but also internal ones related to the QBO, separating the forcings from the responses is not straightforward. For example, the propagation of the resolved waves and that of the parameterized gravity waves strongly depend on the background QBO wind, as does the deposition of their momentum on the QBO. The vertical advection WUZ is also affected by the QBO, because WUZ is explicitly expressed as the product of the QBO and the background wind field (Eq. (1)). In addition, the trends in the forcing amplitude are not additive because of the phase differences as stated before; thus, evaluation of their total effects is not straightforward either, if the signs of the forcing trends are not the same.

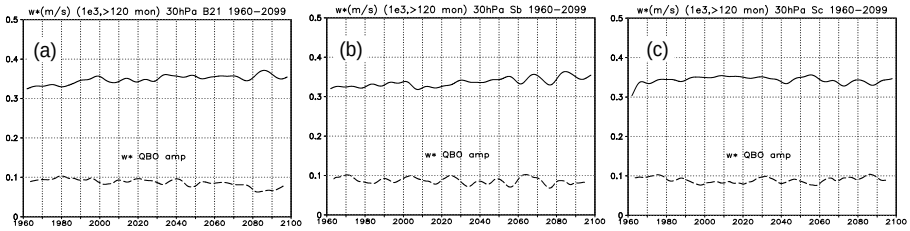

Fig. 24. Residual vertical velocity evolution at 30 hPa. Evolutions of the residual vertical velocity for the low-frequency component (period longer than 120 months, solid) and the amplitude of the residual vertical velocity of the QBO frequency (dashed) at 30 hPa in simulations for (a) B21, (b) Sb, and (c) Sc. Units are 10^{-3} ms^{-1}.

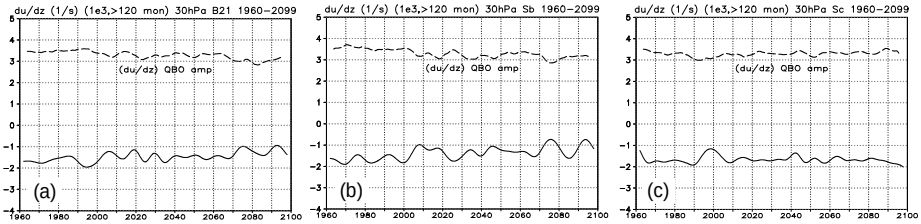

Fig. 25. Zonal wind vertical shear evolution at 30 hPa. Same as Fig.24 except for the vertical shear of zonal wind. Units are 10^{-3} s^{-1}.

Almost all of the trends in the forcings and their response winds in the GHG-increase simulations exhibit negative trends at 30 hPa, where the trend of the QBO wind is the largest negative; therefore, the forcings and responses are qualitatively consistent. At 50 hPa, the magnitude of the negative trend in WUZ is significantly larger than that of the GWF (small negative) or the EPD trend (nearly zero or small positive), which is also consistent with the negative trend in the QBO wind. At 20 hPa, the trends are on average nearly zero in GWF, have small positive values in WUZ, and small negative values in EPD, as are those of their responses, which is not consistent with the small but significant negative trend in the QBO wind. At 70 hPa, GWF exhibits a statistically significant negative trend, and its magnitude is largest compared with the magnitudes of the trends at other altitudes. WUZ, on the other hand, exhibits a statistically significant positive trend, the magnitude of which is about three-fourths that of GWF. EPD tends to have a small negative trend, but its response is nearly zero in the ensemble mean, indicating that EPD plays a minor role at 70 hPa.

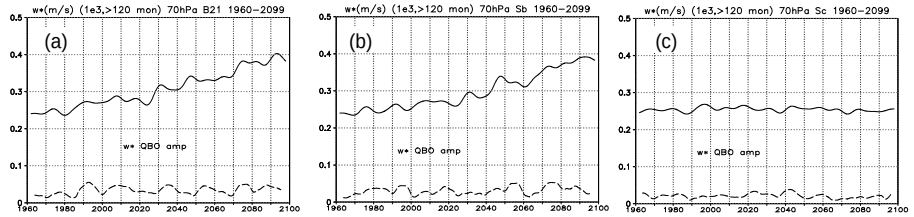

Fig. 26. Residual vertical velocity evolution at 70 hPa. Same as Fig.24 except at 70 hPa.

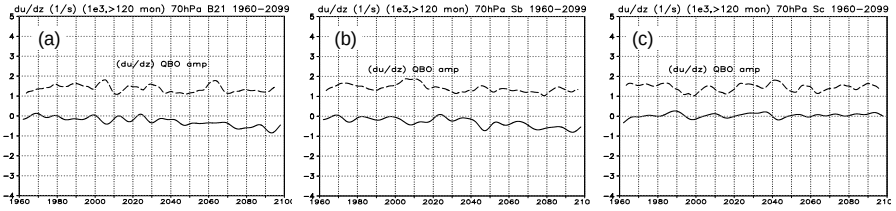

Fig. 27. Zonal wind vertical shear evolution at 70 hPa. Same as Fig.25 except at 70 hPa.

WUZ trends in the GHG-increase simulations are statistically significant below the middle stratosphere but they show sharp contrasts in sign, being negative at 70 hPa and positive at 50 and 30 hPa, although their magnitudes are almost the same at 0.1×10^{-2} $ms^{-1}day^{-1}$ per

decade (Fig. 22). To explore the cause of this, we evaluated the trend of each component, that is, BDT and SCT, of WUZ (Eq. 1). Figure 24 depicts the evolution of the residual vertical velocities of the low-frequency and the QBO at 30 hPa in simulations for B21, Sb, and Sc, and Fig. 25 displays the evolution of the vertical shears. The tendencies of the residual vertical velocity and the vertical shear at 50 hPa are very similar to those at 30 hPa, aside from the background levels. Figures 26 and 27 depict the same evolutions as Figs. 25 and 26, but at 70 hPa. The tendency of WUZ depends on those of BDT and SCT (Eq. (1)), each of which is further decomposed into two terms. As a result, to evaluate of the tendency of WUZ it is necessary to know the tendencies of four terms: low-frequency residual vertical velocity $\overline{w}^{*L}$, QBO vertical shear $(\partial u/\partial z)^{Q}$, QBO residual vertical velocity $\overline{w}^{*Q}$, and low-frequency vertical shear $(\partial u/\partial z)^{L}$. It should be noted that $\overline{w}^{*L}$ always shows an increasing trend in all of the GHG-increase simulations, but the trends of the other three terms depend on altitude. At 30 hPa in the GHG-increase simulations, they are decreasing; thus, SCT also has a negative trend because of the decrease in $\overline{w}^{*Q}$ and $(\partial u/\partial z)^{L}$. On the other hand, BDT has both an increasing component $\overline{w}^{*L}$ and a decreasing component $(\partial u/\partial z)^{Q}$, resulting in a decreasing trend comparable to that of SCT. At 50 hPa the tendencies of the four terms are qualitatively similar to those at 30 hPa, but the SCT tendency is much smaller than the BDT tendency, in which the decrease in $(\partial u/\partial z)^{Q}$ is much larger than the increase in $\overline{w}^{*L}$. As a result, BDT shows a slightly larger decreasing trend at 50 hPa than at 30 hPa.

At 70 hPa, the BDT components are a rapidly increasing $\overline{w}^{*L}$ and a very slowly decreasing $(\partial u/\partial z)^{Q}$, leading to an increasing trend in BDT. The SCT components are both increasing but very small, so SCT is much smaller than BDT. At 20 hPa, both SCT components are increasing, so SCT has a positive trend. Although $(\partial u/\partial z)^{Q}$ is decreasing, BDT has a positive trend comparable to the SCT trend. These results indicate that the BDT trend is of similar magnitude to the SCT trend at 30 and 20 hPa, while the SCT trend is much smaller than the BDT trend at 50 and 70 hPa. This altitude dependence of SCT derives mainly from the low-frequency vertical shear, which is very small as well as its tendency in the lower stratosphere.

In this study the source strength of GWF was fixed in all simulations, irrespective of the ODS evolution and/or the GHG-induced global warming, wherein convective precipitation increased (e.g., Yukimoto et al., 2006; IPCC, 2007) as manifested in the strong warming in the tropical upper troposphere (Fig. 4). This fixation of source strength is different from the precedent simulations of equilibrium CO_2 doubling. Giorgetta & Doege (2005) varied the GWF source by 0% to 20% and showed that a statistically significant reduction in the QBO period occurred in runs with a 10% or 20% increase. Kawatani et al. (2011) demonstrated that wave momentum fluxes increase by 10%–15% in the equatorial lower stratosphere, though those relevant to the QBO forcing do not increase as much. Since tropical convective precipitation is closely linked to gravity and equatorial wave generation (e.g., Horinouchi et al., 2003), we assume that the fixation of the GWF source differs more or less from reality. Thus, to specify appropriate changes in the GWF source, observations of relations between the QBO and other independent quantities such as SST/precipitation or outgoing longwave radiation are needed.

For example, Taguchi (2010) demonstrated a connection between the QBO and El Niño-Southern Oscillation (ENSO): the QBO signals have a weaker amplitude and faster phase

propagation under El Niño conditions, when the west-east contrast of SST and precipitation drastically changes in the tropical Pacific (e.g., Philander, 1990). However, since the tropical upwelling is also enhanced (Randel et al., 2009) during El Niño conditions, isolation of the SST/precipitation effect is required for evaluation of the GWF source in the troposphere. On the other hand, according to Fischer and Tung (2008), the QBO period does not show any trend but has been stable within 24-32 months for five decades (from 1953 to 2007) despite period variations due mainly to stalling of the westerly phase. These findings indicate that further investigation is required to identify the tropospheric factors affecting the QBO.

7. Conclusion

To investigate future changes in the QBO in the tropical stratosphere, transient simulations were carried out for the period from 1960 to 2100 with MRI-CCM by inputting observed and projected GHGs and/or ODSs at the surface. SST/sea ice, generated by an MRI coupled ocean-atmosphere model, was also specified so as to be compatible with the GHGs abundances. Three types of simulations were performed to evaluate the effects of a GHGs increase and an ODSs decrease, both in combination and separately: The first type used the REF-B2 scenario of CCMVal-2, in which both GHGs and ODSs evolve following observed values for past simulations, and specified SRES A1B scenario for GHGs and the adjusted A1 scenario for ODSs for future simulations. The second type of simulation used an SCN-B2b scenario, in which GHGs were the same as in REF-B2 but ODSs were fixed at 1960 levels. The third type used an SCN-B2c scenario, in which ODSs were the same as in REF-B2 but GHGs/SST were fixed at 1960 levels. The REF-B2 simulation was carried out with three members, and the other two were performed with a single member.

The future climate change due to increasing GHGs was characterized as tropospheric warming as a result of SST warming (indirect CO_2 effect), with maximum warming in the tropical upper troposphere, and cooling in the stratosphere (direct CO_2 effect), with maximum cooling in the upper stratosphere. Zonal wind changes were characterized by westerly wind intensification from the upper region of the subtropical jet upward along the equatorward flank of the polar night jet axis, reaching a maximum at around 70 hPa and 40° in both hemispheres. In the SH, the westerly wind intensification also extends down to the surface at around 55°S, resulting in poleward spreading of the subtropical jet. In the tropics, westerly wind strengthening (eastward acceleration) occurred above 30 hPa and weakening (westward acceleration) at 50 hPa, below which very weak strengthening occurred down to the surface. The Brewer-Dobson circulation was similarly intensified in all of the GHG-increase simulations.

The future climate change in the no-climate-change simulation was characterized by strong warming in the upper stratosphere above about 5 hPa in both hemispheres, except in the southern high latitudes, where prominent warming occurred in the lower stratosphere at 300-30 hPa, centered at 100 hPa, with cooling above 30 hPa. This pattern of temperature change was due solely to the ODSs decrease, or, equivalently, ozone recovery. The zonal wind change characterized by slight intensification of the polar night jet in the poleward flank above the middle stratosphere in the NH. In the SH, weakening of the polar night jet and both weakening of the poleward and strengthening of the equatorward flank of the subtropical jet down to the surface occurred. In the tropics, there was almost no change, including in the Brewer-Dobson circulation.

The QBO was spontaneously generated with a period of about 28-month period in the equatorial stratosphere by MRI-CCM under both past and current conditions in all simulations. The QBO frequency was very stable without any substantial trend in all simulations, and the QBO amplitude showed a small but statistically significant decreasing trend below 20 hPa with a maximum (~0.3 ms^{-1} per decade) at 30 hPa in GHG-increase simulations. ODS decreases in the future (i.e., ozone recovery) led to very small increasing trend (<0.1 ms^{-1} per decade) in the QBO amplitude above 20 hPa. The causes of the QBO amplitude trend were largely changes in the parameterized gravity wave forcing and the vertical advection of zonal wind momentum. In the QBO trend, the vertical advection was brought about not only by the Brewer-Dobson circulation but also by the QBO secondary circulation above the middle stratosphere, while the Brewer-Dobson circulation was dominant in the lower stratosphere, mainly because of the very weak vertical shear and the very small vertical shear trend of the background wind.

The QBO effects globally extend from the stratosphere to the troposphere, and thus the projected decreasing trend of the QBO amplitude in the CCM simulations would likely cause, more or less, changes in various phenomena in the whole atmosphere. However, since the current CCM simulations included only forcings of SST, GHGs, and ODSs, other forcings such as solar irradiance variability and volcanic aerosols would induce different responses in the QBO, depending on the timescale of these forcings. In addition, different scenarios in GHGs result in different SSTs, and thereby likely in different QBO trends. Therefore, there are larger uncertainties in the effects of the QBO in the future than in the QBO itself.

8. Acknowledgements

Some of the MRI-CCM simulations were performed by using the supercomputer at the National Institute for Environmental Studies, Japan. This work was supported in part by a Grant-in-Aid (20340129, 20340131, and 20244076) for Scientific Research (KAKENHI) from the Ministry of Education, Culture, Sports, Science, and Technology of Japan. Wavelet software was provided by C. Torrence & G. Compo, and is available at the URL: http://paos.colorado.edu/research/wavelets/.

9. References

Andrews, D. G., Holton, J. R. & Leovy, C. B. (1987). *Middle Atmosphere Dynamics,* Academic Press.

Angell, J. K. & Korshover, J. (1964). Quasi-biennial variations in temperature, total ozone, and tropopause height. *J. Atmos. Sci.*, 21, 479– 492.

Anstey, J. A., Shepherd, T. G., Scinocca, J. F. (2010). Influence of the quasi-biennial oscillation on the extratropical winter stratosphere in an atmospheric general circulation model and in reanalysis data, *J. Atmos. Sci.*, 67, 1402-1419, doi: 10.1175/2009JAS3292.1, 2010.

Austin, J. & Li, F. (2006). On the relationship between the strength of the Brewer-Dobson circulation and the age of stratospheric air. Geophys. Res. Lett., 33, L17807, doi:10.1029/2006GL026867.

Baldwin, M. P. & Gray, L. J. (2005). Tropical stratospheric zonal winds in ECMWF ERA-40 reanalysis, rocketsonde data, and rawinsonde data. *Geophys. Res. Lett.*, 32, L09806, doi:10.1029/2004GL022328.

Baldwin, M. P., Gray, L. J., Dunkerton, T. J., Hamilton, K., Haynes, P. H., Randel, W. J., Holton, J. R., Alexander, M. J., Hirota, I., Horinouchi, T., Jones, D. B. A., Kinnersley, J. S. Marquardt, C., Sato, K. & Takahashi, M. (2001). The quasi-biennial oscillation, *Rev. Geophys.*, 39, 179–229.

Butchart, N., Scaife, A. A., Austin, J., Hare, S. H. E. & Knight, J. R. (2003). Quasi-biennial oscillation in ozone in a coupled chemistry-climate model, *J. Geophys. Res.*, 108(D15), 4486, doi:10.1029/2002JD003004.

Butchart, N., Scaife, A. A., Bourqui, M., de Grandpre, J., Hare, S. H. E., Kettleborough, J., Langematz, U., Manzini, E., Sassi, F., Shibata, K., Shindell, D. & Sigmond, M. (2006). Simulation of anthropogenic change in the strength of the Brewer-Dobson circulation, *Climate Dynamics*, 27, doi:10.1007/s00382-006-0162-4, 727-741.

Chubachi, S. (1985). A special ozone observation at Syowa Station, Antarctica from February 1982 to January 1983. *Proceedings of the Quadrennial Ozone Symposium 1984*, 285-289.

Coughlin, K. & Tung, K. -K. (2001). QBO signal found at the extratropical surface through northern annular modes. *Geophys. Res. Lett.*, 28, 4563–4566.

Dee, D. P., Uppala, S. M., Simmons, A. J., Berrisford, P., Poli, P., Kobayashi, S., Andrae, U., Balmaseda, M. A., Balsamo, G., Bauer, P., Bechtold, P., Beljaars, A. C. M., van de Berg L., Bidlot J., Bormann N., Delsol C., Dragani R., Fuentes M., Geer A.J., Haimberger L., Healy S.B., Hersbach H., Hólm E.V., Isaksen L., Kållberg P., Köhler M., Matricardi M., McNally A. P., Monge-Sanz B. M., Morcrette J.-J., Park B-K, Peubey C., de Rosnay P., Tavolato C., Thépaut J.-N. & Vitart F. (2011). The ERA-Interim reanalysis: configuration and performance of the data assimilation system. *Q. J. R. Meteorol. Soc.* 137: 553–597. DOI:10.1002/qj.828.

Deushi, M. & Shibata, K. (2011). Impacts of increases in greenhouse gases and ozone recovery on lower stratospheric circulation and the age of air: Chemistry-climate model simulations up to 2100. *J. Geophys. Res.*, 116, D10302, doi:10.1029/2010JD015361.

Duchon, C. E. (1979). Lanczos filtering in one and two dimensions. *J. Appl. Meteorol.*, 18, 1016–1022.

Dunkerton, T. (2001). Quasi-biennial and subbiennial variations of stratospheric trace constituents derived from HALOE observations. *J. Atmos. Sci.*, 57, 7-25.

Engel, A., Möbius, T., Bönisch, H., Schmidt, U., Heinz, R., Levin, I., Atlas, E., Aoki, S., Nakazawa, T., Sugawara, S., Moore, F., Hurst, D., Elkins, J., Schauffler, S., Andrews, A. & Boering, K. (2009). Age of stratospheric air unchanged within uncertainties over the past 30 years. *Nat. Geosci.*, 2, 28–31, doi:10.1038/NGEO388.

Eyring, V., Harris, N. R. P., Rex, M., Shepherd, T. G., Fahey, D. W., Amanatidis, G. T., Austin, J., Chipperfield, M. P., Dameris, M., Forster, P. M. De F., Gettelman, A., Graf, H. F., Nagashima, T., Newman, P. A., Pawson, S., Prather, M. J., Pyle, J. A., Salawitch, R. J., Santer, B. D. & Waugh, D. W. (2005). A strategy for process oriented validation of coupled chemistry-climate models. *Bull. Am. Meteorol. Soc.*, 86, 1117–1133.

Eyring, V., Chipperfield, M. P., Giorgetta, M. A., Kinnison, D. E., Manzini, E., Matthes, K., Newman, P. A., Pawson, S., Shepherd, T. G. & Waugh, D. W. (2008). Overview of the New CCMVal reference and sensitivity simulations in support of upcoming ozone and climate assessments and the planned SPARC CCMVal. *SPARC Newsletter*, No. 30, p.20–26.

Farman, J. C., Gardiner, B. G. & Shanklin, J. D. (1985). Large losses of total ozone in Antarctica reveal seasonal ClOx/NOx interaction. *Nature*, 315, 207-210.

Fischer, P. & Tung, K. K. (2008). A reexamination of the QBO period modulation by the solar cycle. *J. Geophys. Res.*, 113, D07114, doi:10.1029/2007JD008983.

Garcia, R. R. & Randel, W. J. (2008). Acceleration of the Brewer-Dobson circulation due to increases in greenhouse gases. *J. Atmos. Sci.*, 65, 2731-2739.

Giorgetta, M. A. & Doege, M. C. (2005). Sensitivity of the quasi-biennial oscillation to CO_2 doubling. *Geophys. Res. Lett.*, 32, L08701, doi:10.1029/2004GL021971.

Giorgetta, M. A., Manzini, E. & Roeckner, E. (2002). Forcing of the quasi-biennial oscillation from a broad spectrum of atmospheric waves. *Geophys. Res. Lett.*, 29(8), 1245, doi:10.1029/2002GL014756.

Gray, L. J., Drysdale, E. F., Lawrence, B. N. & Dunkerton, T. J. (2001). Model studies of the interannual variability of the northern-hemisphere stratospheric winter circulation: The role of the quasi-biennial oscillation. *Q. J. R. Meteorol. Soc.*, 127, 1413–1432, doi: 10.1002/qj.49712757416.

Hamilton, K. (1998). Effects of an imposed quasi-biennial oscillation in a comprehensive troposphere–stratosphere–mesosphere general circulation model. *J. Atmos. Sci.,* 55, 2393–2418.

Hamilton, K., Wilson, R. J. & Hemler, R. S. (1999). Middle atmosphere simulated with high vertical and horizontal resolution versions of a GCM: Improvements in the cold pole bias and generation of a QBO-like oscillation in the tropics. *J. Atmos. Sci.*, 56, 3829– 3846.

Hasumi, H. & S. Emori, Eds. (2004). K-1 coupled GCM (MIROC) description. *K-1 Tech. Rep. 1*, University of Tokyo.

Hines, C. O. (1997). Doppler-spread parameterization of gravity-wave momentum deposition in the middle atmosphere. 2. Broad and quasi-monochromatic spectra, and implementation. *J. Atmos. Sol. Terr. Phys.*, 59, 387–400.

Holton, J. R. & Tan, H. -C. (1980). The influence of the equatorial quasi-biennial oscillation on the global circulation at 50 mb. *J. Atmos. Sci.*, 37, 2200–2208.

Holton, J. R. & Tan, H. -C. (1982). The quasi-biennial oscillation in the Northern Hemisphere lower stratosphere. *J. Meteorol. Soc. Japan*, 60, 140–148.

Horinouchi, T., Pawson, S., Shibata, K., Langematz, U., Manzini, E., Giorgetta, M. A., Sassi, F., Wilson, R. J., Hamilton, K., de Grandpre, J. & Scaife, A. A. (2003). Tropical cumulus convection and upward propagating waves in middle atmospheric GCMs. *J. Atmos. Sci.*, 60, 2765-2782.

IPCC (2000). Special Report on Emissions Scenarios: A Special Report of Working Group III of the Intergovernmental Panel on Climate Change (Nakicenovic, N. & R. Swart (eds)), Cambridge University Press, Cambridge, U.K.

IPCC (2007). Climate Change 2007: The Physical Science Basis. Contribution of Working Group I to the Fourth Assessment Report of the Intergovernmental Panel on Climate Change (Solomon, S., D. Qin, M. Manning, Z. Chen, M. Marquis, K.B. Averyt, M. Tignor & H.L. Miller (eds.)). Cambridge University Press, Cambridge, United Kingdom and New York, NY, USA.

IPCC/TEAP (2005). IPCC/TEAP Special Report on Safeguarding the Ozone Layer and the Global Climate System: Issues Related to Hydrofluorocarbons and Perfluorocarbons. *Summary for Policymakers and Technical Summary*, WMO and UNEP.

Kawatani, Y., Hamilton, K. & Watanabe, S. (2011). The quasi-biennial oscillation in a double CO_2 climate. *J. Atmos. Sci.*, 68, 265–283, doi: 10.1175/2010JAS3623.1.

Kodama, C., Iwasaki, T., Shibata, K. & Yukimoto, S. (2007). Changes in the stratospheric mean meridional circulation due to increased CO_2: Radiation- and sea surface temperature-induced effects. *J. Geophys. Res.*, 112, D16103, doi:10.1029 /2006JD008219.

Kuroda, Y. & Yamazaki, K. (2010). Influence of the solar cycle and QBO modulation on the Southern Annular Mode. *Geophys. Res. Lett.*, 37, L12703, doi:10.1029/2010GL043252.

Labitzke, K. (1982). On the interannual variability of the middle stratosphere during the northern winters. *J. Meteorol. Soc. Japan*, 60, 124–139.

Labitzke, K. & van Loon, H. (1999). *The Stratosphere: Phenomena, History, and Relevence.* Springer-Verlag.

Labitzke, K., Kunze, M. & Brönnimann, S. (2006). Sunspots, the QBO, and the stratosphere in the north polar region––20 years later. *Meteor. Z.*, 3, 355–363.

Lee, H. & Smith, A. K. (2003). Simulation of the combined effects of solar cycle, quasi-biennial oscillation, and volcanic forcing on stratospheric ozone changes in recent decades. *J. Geophys. Res.*, 108, 4049, doi:10.1029/2001JD001503.

Lindzen, R. S. & Holton, J. R. (1968). A theory of the quasibiennial oscillation. *J. Atmos. Sci.*, 25, 1095–1107.

Lu, H., Baldwin, M. P., Gray, L. J. & Jarvis, M. J. (2008). Decadal-scale changes in the effect of the QBO on the northern stratospheric polar vortex. *J. Geophys. Res.*, 113, D10114, doi:10.1029/2007JD009647.

Lu, H., Gray, L. J., Baldwin, M. P., & Jarvis, M. J. (2009). Life cycle of the QBO-modulated 11-year solar cycle signals in the Northern Hemispheric winter. *Q. J. R. Meteorol. Soc.*, 135, 1030-1043. DOI: 10.1002/qj.419.

Luo, M., Russell III, J. M. & Huang, T. Y. W. (1997). Halogen Occultation Experiment observations of the quasi-biennial oscillation and the effects of Pinatubo aerosols in the tropical stratosphere. *J. Geophys. Res.*, 102, 19187–19198.

Marshall, A. G. & Scaife, A. A. (2009). Impact of the QBO on surface winter climate. *J. Geophys. Res.*, 114, D18110, doi:10.1029/2009JD011737.

Naito, Y. & Hirota, I. (1997). Interannual variability of the northern winter stratospheric circulation related to the QBO and the solar cycle. *J. Meteorol. Soc. Japan*, 75, 925–937.

Naoe, H. & Shibata, K. (2010). Equatorial quasi-biennial oscillation influence on northern winter extratropical circulation, *J. Geophys. Res.*, 115, doi:10.1029/2009JD012952.

Naoe, H. & Shibata, K. (2012). Future changes in the influence of the quasi-biennial oscillation on the northern polar vortex simulated with an MRI chemistry climate model. *J. Geophys. Res.*, D03102, doi:10.1029/2011JD016255, 2012.

Niwano, M. & Takahashi, M. (1998). The influence of the equatorial QBO on the Northern Hemisphere winter circulation of a GCM. *J. Meteor. Soc. Japan*, 76, 453–461.

Pascoe C. L., Gray, L. J., Crooks, S. A., Juckes, M. N. & Baldwin, M. P. (2005). The quasi-biennial oscillation: Analysis using ERA-40 data. *J. Geophys. Res.*, 110, D08105, doi:10.1029/2004JD004941.

Philander, S. G. (1990). *El Niño, La Niña and the Southern Oscillation*, Academic Press, New York, 293pp.

Plumb, R. A. (1977). The interaction of two internal waves with the mean flow: Implications for the theory of the quasi-biennial oscillation. *J. Atmos. Sci.*, 34, 1847–1858.

Plumb, R. A. & McEwan, D. (1978). The instability of a forced standing wave in a viscous stratified fluid: A laboratory analogue of the quasi-biennial oscillation. *J. Atmos. Sci.*, 35, 1827–1839.

Plumb, R. A. & Bell, R. C. (1982). A model of the quasi-biennial oscillation on an equatorial beta-plane. *Q. J. Roy. Meteorol. Soc.*, 108, 335–352.

Randel, W. J. & Wu, F. (1996). Isolation of the ozone QBO in SAGE II data by singular value decomposition. *J. Atmos. Sci.,* 53, 2546-2559.

Randel, W. J., Garcia, R. R., Calvo, N. & Marsh, D. (2009). ENSO influence on zonal mean temperature and ozone in the tropical lower stratosphere. *Geophys. Res. Lett.*, 36, L15822, doi:10.1029/2009GL039343.

Reed, R. J., Campbell, W. J., Rasmussen, L. A. & Rogers, D. G. (1961). Evidence of a downward propagating annual wind reversal in the equatorial stratosphere. *J. Geophys. Res.*, 66, 813– 818.

Rex, M., Salawitch, R. J., Deckelmann, H., von der Gathen, P., Harris, N. R. P., Chipperfield, M. P., Naujokat, B., Reimer, E., Allaart, M., Andersen, S. B., Bevilacqua, R., Braathen, G. O., Claude, H., Davies, J., De Backer, H., Dier, H., Dorokhov, V., Fast, H., Gerding, M., Godin-Beekmann, S., Hoppel, K., Johnson, B., Kyrö, E., Litynska, Z., Moore, D., Nakane, H., Parrondo, M. C., Risley Jr., A. D., Skrivankova, P., Stübi, R., Viatte, P., Yushkov, V. & Zerefos, C. (2006). Arctic winter 2005: Implications for stratospheric ozone loss and climate change. *Geophys. Res. Lett.*, 33, L23808, doi:10.1029/2006GL026731.

Roeckner, E., Bäuml, G., Bonaventura, L., Brokopf, R., Esch, M., Giorgetta, M., Hagemann, S., Kirchner, I., Kornblueh, L., Manzini, E., Rhodin, A., Schlese, U., Schulzweida, U. & Tompkins, A. (2003). *The atmospheric general circulation model ECHAM 5. part I: Model description.* MPI-Rep. 349, Max-Planck-Inst., Hamburg, Germany.

Scaife, A. A., N. Butchart, C. D. Warner, D. Stainforth, W. A. Norton & J. Austin (2000). Realistic quasi-biennial oscillations in a simulation of the global climate. *Geophys. Res. Lett.*, 27, 3481–3484.

Shepherd, T. G. & Jonsson, A. I. (2008). On the attribution of stratospheric ozone and temperature changes to changes in ozone-depleting substances and well-mixed greenhouse gases. *Atmos. Chem. Phys.,* 8, 1435-1444.

Shibata, K., Deushi, M., Sekiyama, T. T., & Yoshimura, H. (2005). Development of an MRI chemical transport model for the study of stratospheric chemistry. *Papers in Meteorology and Geophysics*, 55, 75-119.

Shibata, K. & Deushi, M. (2005a). Partitioning between resolved wave forcing and unresolved gravity wave forcing to the quasi-biennial oscillation as revealed with a coupled chemistry-climate model. *Geophys. Res. Lett.*, 32, L12820, doi:10.1029/ 2005GL022885.

Shibata, K. & Deushi, M. (2005b). Radiative effect of ozone on the quasi-biennial oscillation in the equatorial stratosphere. *Geophys. Res. Lett.*, 32, L24802, doi:10.1029/ 2005GL023433.

Shibata, K. & Deushi, M. (2008a). Long-term variations and trends in the simulation of the middle atmosphere 1980-2004 by the chemistry-climate model of the Meteorological Research Institute. *Annales Geophysicae*, 26, 1299-1326.

Shibata, K. & Deushi, M. (2008b). *Simulation of the stratospheric circulation and ozone during the recent past (1980-2004) with the MRI chemistry-climate model.* CGER's Supercomputer Monograph Report, Vol.13, National Institute for Environmental Studies, Japan.

SPARC, V. Eyring, T. G. Shepherd, D. W. Waugh (Eds.) (2010). *SPARC CCMVal Report on the Evaluation of Chemistry-Climate Models*, SPARC Report No.5, WCRP-132, WMO/TD-No.1526.

Son, S. -W., Polvani, L. M., Waugh, D. W., Akiyoshi, H., Garcia, R., Kinnison, D., Pawson, S., Rozanov, E., Shepherd, T. G., & Shibata, K. (2008). The impact of stratospheric ozone recovery on the southern hemisphere westerly jet. *Science*, 320, 1486-1489, doi:10.1126/science.1155939.

Taguchi, M. (2010). Observed connection of the stratospheric quasi-biennial oscillation with El Niño–Southern Oscillation in radiosonde data. *J. Geophys. Res.*, 115, D18120, doi:10.1029/2010JD014325.

Takahashi, M. (1999). Simulation of the stratospheric quasi-biennial oscillation in a general circulation model. *Geophys. Res. Lett.*, 26, 1307–1310.

Torrence, C. & Compo, G. P. (1998). A Practical Guide to Wavelet Analysis. *Bull. Amer. Meteor. Soc.*, 79, 61-78.

Uppala, S. M., Kållberg, P. W., Simmons, A. J., Andrae, U., da Costa Bechtold, V., Fiorino, M., Gibson, J. K., Haseler, J., Hernandez, A., Kelly, G. A., Li, X., Onogi, K., Saarinen, S., Sokka, N., Allan, R. P., Andersson, E., Arpe, K., Balmaseda, M. A., Beljaars, A. C. M., van de Berg, L., Bidlot, J., Bormann, N., Caires, S., Chevallier, F., Dethof, A., Dragosavac, M., Fisher, M., Fuentes, M., Hagemann, S., Holm, E., Hoskins, B. J., Isaksen, L., Janssen, P. A. E. M., Jenne, R., McNally, A. P., Mahfouf, J.-F., Morcrette, J.-J., Rayner, N. A., Saunders, R. W., Simon, P., Ster, A., Trenberth, K. E., Untch, A., Vasiljevic, D., Viterbo, P., & Woollen, J. (2005). The ERA-40 Reanalysis. *Q. J. Roy. Meteor. Soc.*, 131, 2961–3012, doi:10.1256/qj.04.176.

Veryard, R. G. & Ebdon, R. A. (1961). Fluctuations in tropical stratospheric winds. *Meteorol. Mag.*, 90, 125–143.

Wallace, J. M., Panetta, R. L. & Estberg, J. (1993). Representation of the equatorial stratospheric quasi-biennial oscillation in EOF phase space. *J. Atmos. Sci.*, 50, 1751–1762.

Watanabe, S., Kawatani, Y., Tomikawa, Y., Miyazaki, K., Takahashi, M. & Sato, K. (2008). General aspects of a T213L256 middle atmosphere general circulation model. *J. Geophys. Res.*, 113, D12110, doi:10.1029/2008JD010026.

WMO (2007). *Scientific Assessment of Ozone Depletion: 2006*, World Meteorological Organization, Global Ozone Research and Monitoring Project, Report No. 50, Geneva, Switzerland.

WMO (2011). *Scientific Assessment of Ozone Depletion: 2010,* World Meteorological Organization, Global Ozone Research and Monitoring Project, Report No. 52, Geneva, Switzerland.

Xiao, F. and Peng, X. (2004). A convexity preserving scheme for conservative advection transport. *J. Comput. Phys.*, 198, 389–402, doi:10.1016/j.jcp.2004.01.013.

Yamashita, Y., Akiyoshi, H. & Takahashi, M. (2011). Dynamical response in the Northern Hemisphere midlatitude and high-latitude winter to the QBO simulated by CCSR/NIES CCM. *J. Geophys. Res., 116*, D06118, doi:10.1029/2010JD015016.

Yukimoto, S., Noda, A., Kitoh, A., Hosaka, M., Yoshimura, H., Uchiyama, T., Shibata, K., Arakawa, O. & Kusunoki, S. (2006). Present-day climate and climate sensitivity in the Meteorological Research Institute coupled GCM version 2.3 (MRI-CGCM2.3). *J. Meteorol. Soc. Japan*, 84, 333-363.

18

Regional Pattern of Trends in Long-Term Precipitation and Stream Flow Observations: Singularities in a Changing Climate in Mexico

Luis Brito Castillo
Centro de Investigaciones Biológicas del Noroeste
Mexico

1. Introduction

The Intergovernmental Panel on Climate change has concluded that global warming is unequivocal (IPCC, 2007). However, there is still a debate regarding whether global warming is mainly due to anthropogenic greenhouse gas emissions (Zhao, 2011), particularly because, as Lindzen (2007) states, current models fail to describe many known climate changes, and because some sources of anthropogenic forcing contribution (like surface albedo, total aerosol, etc) are essentially unknown (Lindzen, 2007). It has been stated that the warming has penetrated into the world's oceans (Barnett et al., 2005) increasing sea surface temperatures (SSTs) by approximately 0.5°C since the mid-nineteenth century (Houghton et al. 2001). Higher SSTs are associated with increased water vapor in the lower troposphere (Trenberth, 2005) implying that perturbations in the global water cycle are expected to accompany this warming (Milly et al., 2005). The understanding of specific regional changes (i.e. trend analysis) in temperature, rainfall, and streamflow is very necessary for supporting the needs of an ever-broadening spectrum of decision-makers as they strive to deal with influences of Earth's climate at global to local scales. Trend analyses have revealed the existence of temperature trends with different signs in Mexico in general (Englehart & Douglas, 2004; Pavia et al., 2009), central Mexico (Brito-Castillo *et al*., 2009), and northwestern Mexico (Gutierrez-Ruacho et al., 2010; Weiss & Overpeck, 2005), which is partly associated with regional land use, changes in land cover (Englehart & Douglas, 2004), and changes in large-scale atmospheric flow patterns (Brito-Castillo *et al*., 2009). These studies have shown that, while significant trends do exist, they are at times in line with warming hypotheses and at times they are not. The complete understanding of these changes is particularly important, especially for river discharges, since availability of water is vital for human health, economic activity, ecosystem functions, and geophysical processes (Milly et al., 2005). In Mexico, trend analyses have mostly focused on maximum and minimum temperatures, while trend analyses of precipitation and streamflow have only partly been studied. Knowledge remains scarce, partly attributed to lack of long-term data (both in space and time), the difficulties encountered in providing a correct interpretation of changes attributed to human disturbances, such as diversion of water for irrigation of cropland and control of water for generating electric power, as well as the complexity of the processes that externally force hydroclimate variability (natural changes and low-frequency

internal variability, such as Pacific decadal oscillation (PDO) and Atlantic multidecadal oscillation (AMO). Given the limited knowledge of streamflow and precipitation trend structures in Mexico, in this chapter, we analyzed overall trends in Mexico and described the regional structures of the trends for the period 1920–2008. Evidence of real trends over different regions of Mexico is provided, sometimes revealing that oscillations of long-term high and low humid periods (depending on their arrangement) force the fitted linear trend model. This implies that declining or increasing trends are restrained by the length of the records. However, there are also cases of unambiguous multi-decadal trends in rainfall and streamflow time series that require more detailed analysis. Section 2 explains the statistical approaches used in the study of trends, with some real examples from precipitation and streamflow variables in Mexico. In Section 3, we describe seasonal precipitation characteristics over Mexico to illustrate the main climate differences across the country. Section 4 provides an introduction to the most recent findings related to global warming and changes in tropical cyclones, including a brief description of tropical cyclone contribution to rainfall in Mexico. In the remaining sections, we explain the main procedures for detecting trends used in this work. In Section 5 we describe climate data and quality control; in Section 6, we show a regionalization of Mexico by simply fractioning the territory into several domains with specific climatic conditions. Finally, in Sections 7 and 8, we discuss the main regional structures of trends detected in precipitation variables and their correspondence to trends in streamflow datasets. We hope that this chapter provides a useful introduction to problems related to trends in precipitation and streamflow variables in Mexico.

2. The study of trends

If data show continuous increase or decline change over time, we refer to this change as a trend (Figure 1). Linear trends are an example of data "statistics" like the average (or mean) and "standard deviation values", which is a measure of the variability within a data set around the mean value. Sometimes, to allow comparisons between the series having different scales of variability results, it is necessary to change the data scores to standardized values or z scores, which is the number of standard deviations away from the mean:

$$z_i = (x_i - \mu) / \sigma \quad (1)$$

where: z_i, is the standard score; x_i is the observed score; μ is the mean value; σ is the standard deviation; i = 1…n; and n is the sample size.

When all the scores from a variable are transformed into standard scores (z scores), a new variable is obtained with a mean of zero and standard deviation of one.

Fitting a linear trend model to data is a common practice; however linear trends may be deceptive, particularly when datasets show non-linear changes over time (Wigley, 2006), which is a property of precipitation and streamflow time series. An example of this situation is displayed in Figure 1 for three different series expressed as z scores: (1) Total annual days with precipitation >0 mm (i.e. annual TDP > 0) (Figure 1a); (2) Total annual precipitation (mm) (Figure 1b & Figure 2) and (3) mean annual streamflow (m^3/s) (Figure 1c). All variables show an initial declining trend (though incomplete), followed by a large upward step after 1958 that results in an overall increasing trend. It is evident that inter-annual variability of the time

series is superimposed on multi-decadal variability with substantial deviations from linearity (i.e., the trend) in some years (1956 and 2000 in Figure 1b and in 1959 and 2004 in Figure 1c.). In these situations a detailed inspection of the series can help show more complex changes that are evident in data; still, linear trends provide the simplest and most convenient way to describe the overall change over time in a dataset (Wigley, 2006).

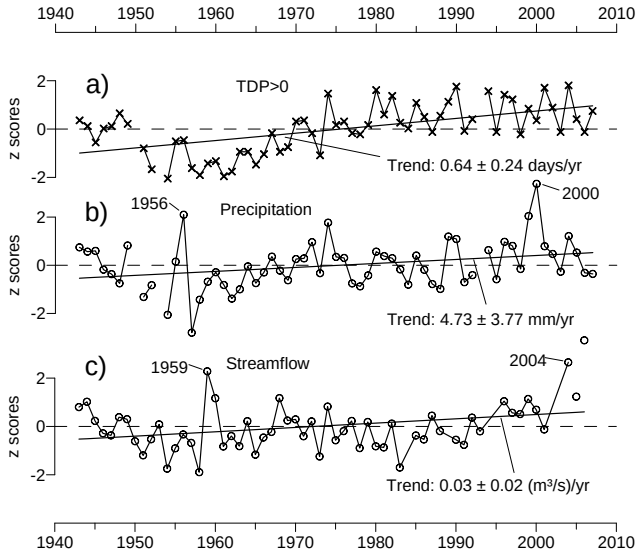

Fig. 1. Long-term fluctuations of different data sets: (a) Total annual days with precipitation >0 mm (TDP >0); (b) total annual precipitation (mm) and (c) mean annual streamflow (m^3/s). a-b are from Ocozonautla, Chiapas weather station (Code: 07123; –93.374°W; 16.751°N; 838 masl); c is from La Y-Rio Lerma gauging station (Code: 12374; –99.5894°W; 19.40611°N; basin area 1582 km^2). The line is the trend and the ± values define the 95% confidence intervals for the trends. For comparison all variables are expressed in standardized values (i.e., z scores; see text for definitions).

In this work, linear trends were quantified as the change of TDP > 0, precipitation, and streamflow per year by fitting a straight line to the data using the method of minimal least squares errors, with years (T) as the independent values and serial data (Y) within each year as the dependent values. The "best-fit" straight line to data is obtained by linear regression analysis:

$$Y_{est} = b + T \tag{2}$$

$$b = [\sum\{(T_i - T_{avg})\,(Y_i - Y_{avg})\}] \,/\, [\sum\{(T_i - T_{avg})^2\}], \tag{3}$$

where $\sum$ represents the summation over i = 1…n; the subscripts "est" and "avg" are the estimate of Y (TDP > 0, precipitation or streamflow) by the fitted regression line and the mean value, respectively, and b is the slope of the fitted line (the trend value).

Estimates of the linear trend are sensitive to points at the start or end of the dataset. This is more a problem with small sample sizes (for trends over short time periods). For example, if

we considered streamflow data points in Figure 1c from 1959 through 1983 (25 years), because there was an unusual increase in 1959 (which is also recorded at other gauging stations downstream along the river), the calculated trend may be an overestimate of the true underlying trend.

Other uncertainties that can be found in trend analysis is related to the presence of gaps in datasets and the apparently multi-decadal variability that seems to be "incomplete" in some series (Figure 2), giving the impression that the trends might not be real. In both cases shown in Figure 2, there are clear trends, upward trend in Figure 2a and downward trend in Figure 2b. However, after the 1970s, the overall trend in Figure 2a assumes a decreasing trend. Unfortunately, the dataset finished very early at the middle of the 1990s without enough data to prove if this second trend is statistically significant (see below for definition). In Figure 2b, on the contrary, there is an overall decreasing trend, but before 1970, it seems to be an increasing trend or no trend at all. Unfortunately, the dataset beginning in 1950 cannot prove this. Around the 1970s, the scores are greater than the mean value in both datasets (Figures 2a & b). Comparing the overall behavior between both data sets, it seems as though both datasets were complementary to each other, indicating the possibility that, if observations were available for both time series over the 1920-2010 period, it might be possible to calculate no trend at all. So far, we can say that, with this information, increasing (Figure 2a) or declining (Figure 2b) trends might be restrained by the length of the records.

For examples, given in Figure 2, results necessary to explore the behavior of surrounded stations is more certain.

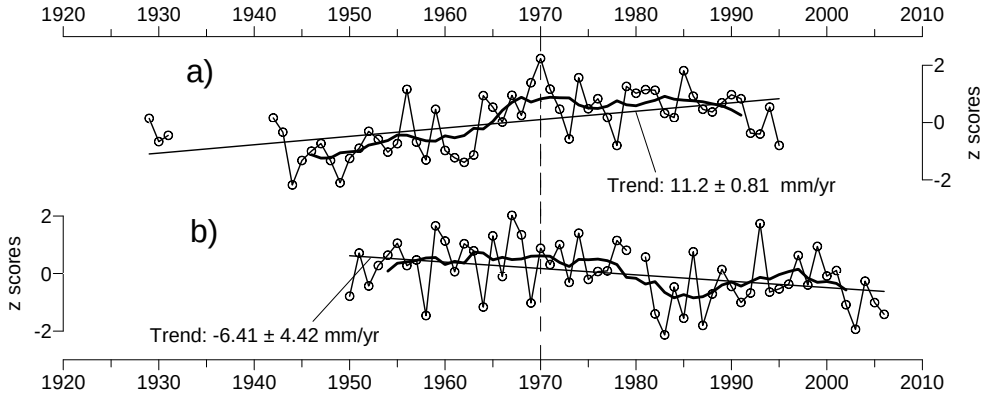

Fig. 2. The same as Figure 1, but for total annual precipitation (mm). (a) Matías Romero (Code: 20068; –95.03°W; 16.88°N; 201 masl); (b) Paso de Arocha, Nayarit Code: 18025; –105.10°W; 21.83°N; 30 masl). Heavy lines are 9-yr running means.

A measure of how well the straight line fits the data is the average value of the squares of the residuals (i.e. deviations about the fitted line) or the standard deviation of the trend estimate, or its squares, the variance of the distribution of b (Var(b)). The smaller this is, the better is the fit:

$$\mathrm{Var}(b) = (\mathrm{SE})^2 = \mathrm{MSE} \,/\, [\sum\{(T - T_{avg})^2\}] \quad (4)$$

$$MSE = [\sum((Y-Y_{est})^2)] / (n-2) \quad (5)$$

where MSE is the mean square error and SE is the standard error of the trend estimate.

To decide if upward or downward trends are an indication of some underlying cause or merely a chance fluctuation, in this work, we use two approaches: (1) confidence intervals: b ± 2 SE (often called the two-sigma confidence interval) and (2) significance testing. The range b ± 2 SE is a good approximation to represent the 95% confidence interval and is used as a signed error magnitude. If –2SE < b < 2SE, it means that the 95% confidence interval includes the zero trend value and the null hypothesis that "there is no trend in data sets or b = 0" is true; otherwise (i.e. b > 2SE or b < –2SE), we say that the null hypothesis is unlikely to be true and we must accept the alternate hypothesis that "data show a real, externally forced upward or downward trend (Wigley, 2006).

The second approach consists in trying to decide whether an observed data trend that is noticeably different from zero is sufficiently different that it could not have occurred by chance or that the probability (known as p-level) that it could have occurred by chance is very small. If the null hypothesis is rejected, then we say that the observed trend is "statistically significant" at some level of confidence. In this study, the confidence level we used to reject the null hypothesis is alpha level = 0.05. If the probability that the null hypothesis is true is small (i.e. p-level < 0.05), then the null hypothesis is unlikely to be correct. Such a low probability would mean that the observed trend is highly unusual and therefore a "significant result". The significance test used here is a "two-tailed" test, meaning that we are concerned only with whether the trend is different from zero, with no specification of whether the trend should be increasing (positive) or declining (negative) trend.

The significance of a trend and its confidence intervals depend on the standard error of the trend estimate. Equation (4) given above is, however, only correct if the individual scores are unrelated. The dependence between scores is referred to as "temporal autocorrelation" or "serial correlation". When data are auto-correlated, many statistics behave as if the sample size was less than the number of data points, n, so it is necessary to determine an "effective sample size" (n_{eff}). In this study, n_{eff} was estimated by Equation (6):

$$n_{eff} = n(1-r_1) / (1 + r_1) \quad (6)$$

where r_1 is the lag-1 autocorrelation coefficient calculated from the time series of residuals about the fitted line of the observed data.

If r_1 is statistically significant (i.e. p-level of r_1 is < 0.05), then in Equation (5), n_{eff} is used instead of n. It can be seen from Equation (5) that if n_{eff} is noticeably smaller than n, then the standard error of the trend estimate may be much larger than one would otherwise expect. This means that results that may show a significant trend if autocorrelation is ignored; it is frequently found to be non-significant when autocorrelation is accounted for.

3. Rainfall distribution over Mexico

The climate of Mexico is influenced by the strength and position of the subtropical high pressure systems of the Northeast Pacific (the East Pacific High) and the North Atlantic (the Bermuda High) (Wang et al., 2007), and the variations in the location of the Intertropical Convergence Zone (ITCZ), which lies south of Mexico. The formation of the high pressure

systems is related to global scale circulations that function to move excess energy from the equatorial regions to poles affecting precipitation variability across Mexico on seasonal to decadal time scales. An unusually strong East Pacific High during the winter can steer storm systems far to the north, limiting cloud formation and precipitation with a drying effect over the river basins in much of northern Mexico (Brito-Castillo et al., 2003), while an unusually strong Bermuda High during the summer can enhance monsoon circulation and numerous transient disturbances (e.g. tropical storms, tropical easterly waves, inverted troughs, the Madden Julian Oscillation, and mid-latitude troughs) and bring above-average precipitation across much of Mexico (Douglas et al., 2007; Wang et al., 2007). Subtle changes to the position and strength of these circulation features appear to be connected to global scale shifts in circulation patterns related to changes in sea surface temperature patterns (e.g., El Niño-Southern Oscillation) affecting rainfall variability of Mexico at inter-annual timescales and can persist for years (e.g., the Pacific Decadal Oscillation, PDO), bringing extended periods of unusually wet or dry conditions at decadal timescales (Magaña et al., 2003; Pavia et al., 2006).

3.1 Seasonality of precipitation

Mexico receives most of its annual rainfall during the summer, with a secondary peak occurring during the winter. From November through March (Figure 3 left maps), winter precipitation is associated with large-scale low pressure systems that traverse northern Mexico, drawing in moisture from the Pacific Ocean and producing widespread rain and snow at higher elevations of the Sierra Madre Occidental in northwestern Mexico, the northwestern portion of the Baja California Peninsula, the coastal plains of the Gulf of Mexico (CPGM), the Yucatan Peninsula (YP), and some portions of central Mexico (mainly in December and January), while the rest of the country generally experiences dry conditions. The effects of cold fronts coming from the northwest also cause lower temperatures in most of Mexico, but are more evident in the highlands of north and central Mexico, and on the CPGM, and the YP, where they are associated with strong northerly winds (nortes; outbreaks of cold weather), occasionally producing intense precipitation in the southeast, when the cold air masses are modified by the warm waters from the Gulf of Mexico. The large-scale forcing (1000 km-global) of regional climate variability, such as the location and strength of the subtropical westerly jet, determines the succession of weather events during winter in eastern Mexico. A change from zonal to more frequent meridional circulation has been linked to increased winter precipitation over the region. At the end of March, the strong midlatitude westerlies (jet stream) begin their northward retreat, and more tropical conditions affect the region, restraining wet conditions mostly over the CPGM and YP during April (Figure 3 left maps).

Summer precipitation in Mexico (May through October, see Figure 3 right maps) is, in large part, controlled by the North American Monsoon (NAM) system (Higgins et al., 2003), which is associated with thermal contrasts between the continent and adjacent eastern Pacific Ocean (Giovannettone & Barros, 2008; Higgins et al., 2003; Turrent & Cavazos, 2009).

Initially, greater rainfall occurs in southern Mexico in May, as the ITCZ assumes a northerly position during the Northern Hemisphere summer. This position, combined with modulation by easterly waves from the Caribbean Sea and the lower branch of easterly flow from over the Gulf of Mexico have a direct influence on the mountain ranges in southern Mexico (Giovannettone & Barros, 2007), initiating precipitation over the southern slopes and

propagating northward as the convective activity and easterlies strengthened in May-June. In southern and central Mexico, precipitation peaks in June and September with a decline in convective activity in late July-early August, causing a break period known as canicula (midsummer drought) (Magaña et al., 1999), as a result of the presence of an anticyclone southwest of Mexico over the ITCZ (Giovannettone & Barros, 2007).

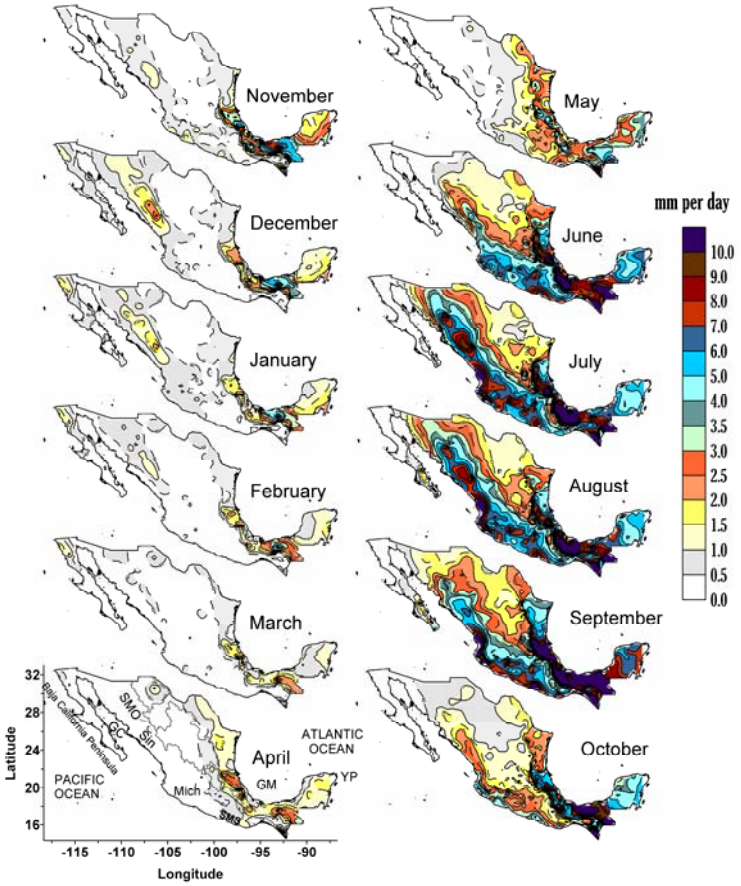

Fig. 3. Distribution of long-term mean values of daily precipitation per month. The mean value is calculated for individual stations with larger than 40 yrs of records over the 1948–2000 period. In lower left map, GC = Gulf of California; Sin = Sinaloa; Mich = Michoacan; SMO = Sierra Madre Occidental; SMS = Sierra Madre del Sur, GM = Gulf of Mexico, YP = Yucatan Peninsula.

Poleward extension of the summer precipitation regime in northwest Mexico starts with an abrupt onset of precipitation in late June or early July and quickly spreads northward along the western slopes of the Sierra Madre Occidental. Precipitation increases coincide with increased vertical transport of moisture by convection and southerly winds through the Gulf of California. During July through early September, the monsoon system is fully developed

and the heaviest rainfalls occur west of the Sierra Madre Occidental. In late September to October, precipitation over northwest Mexico diminishes in response to a southward movement of the NAM upper level anticyclone to weakening of land surface heating and southerly flow and to the retraction of the North Atlantic Subtropical High eastward.

Other sources of moisture in Mexico during summertime are mesoscale convective systems (Farfan & Zhender, 1994) and tropical cyclones (Farfan, 2011; Jáuregui, 2003).

4. Tropical cyclones and their contribution to rainfall

It has been established that sea surface temperature (SST) is increasing all over the world (Barnett et al., 2005). For tropical SSTs, the total increase has been on the order of 0.5°C since the mid-nineteenth century (Houghton et al. 2001). Warming signals have been found to be far stronger than would be expected from natural internal variability (i.e., external forcing such as solar variability or volcanic activity), attributing ocean warming signal to anthropogenic forcing (Barnett et al., 2005). A warmer tropical ocean brings increased water vapor in the lower troposphere and both tend to enhance moisture convergence for a given amount of mass convergence. This increases the energy available for atmospheric convection and rainfall rates in systems, such as thunderstorm and cyclones (Knutson et al., 2010) where moisture convergence is an important component of the water-vapor budget. However, the issue of attribution of increased hurricane frequency to increasing SST has been a matter of academic debate, since there is no sound theoretical basis for drawing any conclusions about how anthropogenic climate change affects hurricane number or tracks (Trenberth, 2005). It is known than over the 20th century, there is a nonlinear upward trend in SSTs with domination of multi-decadal variability being a pronounced trend in the past three to four decades (Trenberth, 2005). The study by Webster et al. (2005), analyzing global hurricane data, shows that, opposed to increasing SST, no global trend has yet emerged in the number of tropical storms or hurricanes, although model results and observations suggest a shift in hurricane intensities toward extreme hurricanes (Knutson et al., 2010; Webster et al., 2005; Yu et al., 2010).

With extensive coastline bordering both oceans, Mexico is particularly vulnerable to hurricanes. Moreover, the eastern Pacific Ocean is the most productive in hurricane activity of any basin per unit area worldwide (McBride, 1995). From May through October, an average of 15 named tropical cyclones (TC) form every summer season and provide changes in moisture content to western Mexico (Farfan, 2011). According to Jáuregui (2003), from 1951–2000, Pacific hurricane hits were more frequent on coastal areas of Sinaloa, southern Baja California Peninsula, and Michoacan. More recently, analysis by Farfan (2011) states that, from 1970 through 2009, the Baja California Peninsula was the most affected area, with 97% probability of being affected by at least one TC each season and 46% probability of having at least one TC move inland. On the Atlantic side, the Yucatan Peninsula and the northern state of Tamaulipas were the most exposed to these storms (Jáuregui, 2003). September is the month with the highest rate (33% compared to the eastern Pacific Ocean) of landfall in Mexico (Diaz et al., 2008; Farfan, 2011; Jáuregui, 2003). The study made by Jáuregui (2003) indicates that during 1951–2000, landfall hurricane trends are declining for both coasts of the country. Attempts to understand the links between SST changes and inter-annual variations of cyclone formations in western Mexico indicate that the strong El Niño

decades of the 1980s and 1990s appear to have favored fewer storms passing into the central part of the Baja California Peninsula. Diaz et al. (2008), indicate that tropical cyclone contributions to rainfall in the Baja California Peninsula and the State of Sinaloa display a statistically significant correlation with PDO, suggesting a larger contribution of tropical cyclones on annual precipitation in both areas occurs during the positive phase of the PDO than the negative phase.

5. Climate data and quality control

Perhaps, the main difficulty that one encounters when trying to discern regional structures of trends is the lack of sufficient quality records in space and time; this is not an exception in Mexico. According to available information, a little more than 6000 weather stations (Quintas, 2000) and 1475 gauging stations (Banco Nacional de Datos de Aguas Superficiales-BANDAS, 1997) have been put in operation around the country. Unfortunately, only 20% of both kinds of stations have > 40 yrs of records, with datasets on runoff within a river basin (Milly et al., 2005) even smaller than precipitation records (Table 1). The highest density of stations is from 1960 through 2004 (Figure 4) with an abrupt decline at the beginning of the 1980s in both sources of data and slight recovery in rainfall datasets in the 1990s. Considering just those stations with more than four decades of daily observations (between 1920 and 2008), it is still possible to have sufficient information to include all the country (Figure 5) and preserve the longest time series for analysis: 1161 for precipitation and 141 for streamflow data sets. The exception is the Baja California and Yucatan Peninsulas, northwestern Sonora (NWS), and the Altiplano Mexicano, where streamflow observations are scarce or non-existent (Figure 5). Selected basins range from very large (124,000 km²) to very small (25 km²), with an average of 14,500 km². For precipitation records, some parts of the central Baja California Peninsula; NWS; northern Mexico, and mid-level elevations of central Mexico in the Pacific drainage region (near 22° latitude) have no stations with long-term records.

Interval of observations (yr)	Number of stations having data	
	Gauging sites	Weather stations
Less than 1	101 (6.8)	732 (12.1)
1 - 10	442 (30.0)	1139 (18.8)
11 - 20	314 (21.3)	1065 (17.6)
21 - 30	241 (16.3)	1187 (19.6)
31 - 40	165 (11.2)	773 (12.8)
41 - 50	123 (8.3)	664 (11.0)
51 - 60	63 (4.3)	325 (5.4)
61 - 70	25 (1.7)	139 (2.3)
More than 70	1 (0.1)	37 (0.6)
Total	1475 (100)	6061 (100)

Table 1. Density of gauging sites and weather stations with measurements of streamflow and rainfall from 1920–2008. Percentages are shown in parentheses.

	N	C	SE	YP
Annual	402	899	1716	1220
Summer	311 (78)	791 (88)	1446 (84)	955 (79)
Winter	89 (22)	109 (12)	288 (16)	257 (21)

Table 2. The 1921–2008 mean annual and seasonal precipitation (in mm) over each of the domains derived from weather stations displayed in Figure 5. Shown in parentheses is the proportion of seasonal precipitation relative to annual precipitation. N = north domain; C = center domain; SE = southeast domain; YP = Yucatan Peninsula domain.

From daily observations, we calculated total annual (preceding May to following April, the year is of the last month) precipitation and seasonal accumulations for summer (May–October), and winter (November–April) because they are the main precipitation seasons in Mexico (see Figure 3). For each precipitation dataset, we also estimated TDP >0 (expressed in n-days – total days with precipitation >0 mm) for annual and seasonal components. For streamflow records, we estimated mean annual and seasonal streamflow for the same months as precipitation time series. The mean magnitudes of streamflow records, derived from the 141 gauging stations are 295 m^3/s, 374 m^3/s, and 59.1 m^3/s for mean annual, summer, and winter streamflow, respectively. In all variables, a year was considered valid if, at least 85% of the daily records were available (i.e., >310 daily observations for annual series; >156 for summer series, and >153 for winter series), otherwise the year was considered a gap.

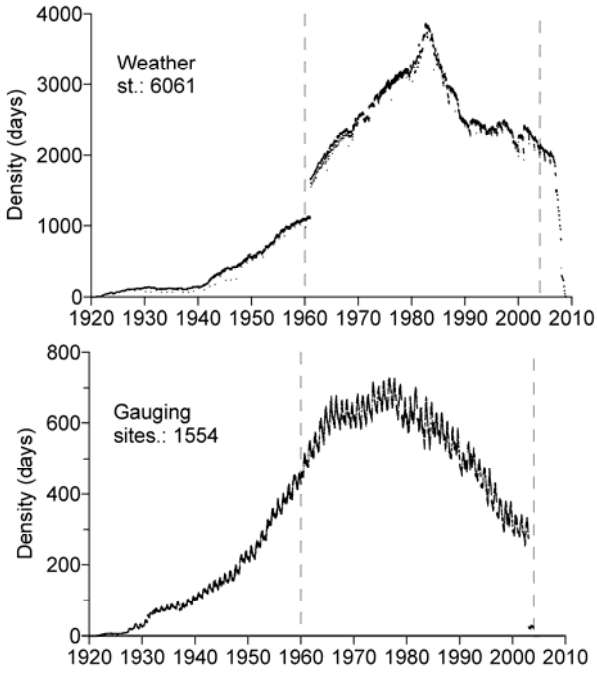

Fig. 4. Series displaying daily density observations of precipitation (a) and streamflow (b) from 1920–2008 derived from 6061 weather and 1554 gauging stations in Mexico.

For all selected datasets, quality control was performed to remove implausible values (i.e., values arising from data entry errors evident as data points with extreme deviations from the overall mean of the series without replication at surrounding station datasets). For streamflow time series, significance tests for variances (*F* distribution) and means (*t*-test distribution) were performed to test for the null hypothesis about the similarity of these parameters inside the series. Hypothesis testing was performed for each series, dividing the series in two equally long parts and comparing the mean and variance of each part. Then, the results were accepted if there were statistically significant differences between the parameters at the 0.05 alpha level. When the series showed significant differences between the parameters, this was considered an indication of change in the long term period.

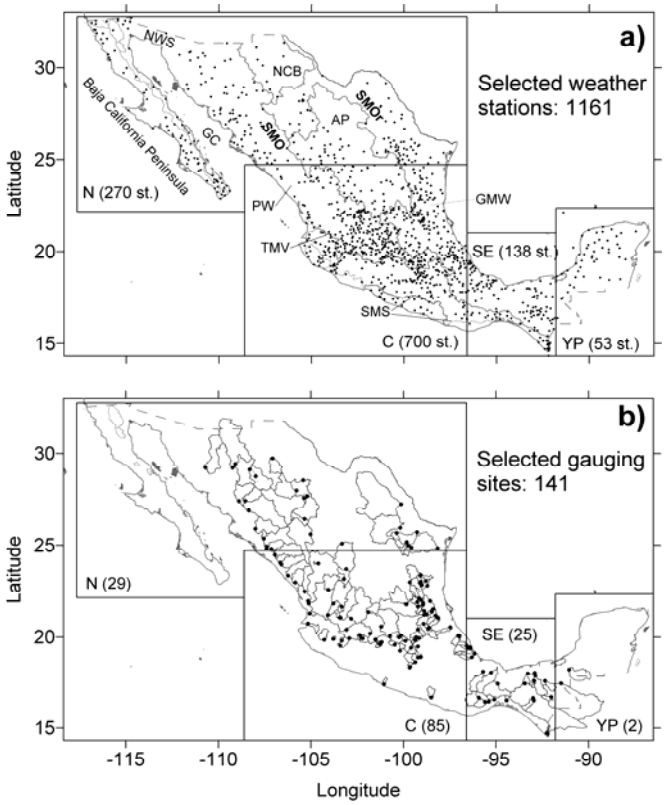

Fig. 5. Spatial distribution of 1161 selected weather stations (a), and 141 selected gauging sites (b) having more than 40 years of records. The maps are divided in domains: N = North; C = Center; SE = Southeast, and YP = Yucatan Peninsula. Density of stations is displayed in parentheses over each domain. Lines in (a) divide the main drainage areas of Mexico: PW = Pacific watershed; GMW = Gulf of Mexico watershed; NCB = northern closed basins; AP = Altiplano Mexicano, and main mountain arrangements: SMO = Sierra Madre Occidental; SMOr = Sierra Madre Oriental; TMVB = Trans-Mexican Volcanic Belt, and SMS = Sierra Madre del Sur. Polygons displayed inside the map in (b) are the catchment areas of each identified gauge point.

Trend analysis was performed for precipitation (total annual and total seasonal observations and their correspondent TDP >0) and streamflow data sets over Mexico from 1161 weather stations and 141 gauging stations (shown in Figure 5), using the procedure explained above. For precipitation time series, our interest was on trends observed in the sequence of days with recorded rainfall (TDP >0). This was done to prove if a station had a declining or increasing trend in total annual and seasonal precipitation corresponding to a downward or upward trend in TDP >0.

6. Regionalization

To simplify the analysis of the regional structure of the trends observed in precipitation and streamflow, the country was divided into polygons of different sizes in the domains (N, C, SE, and YP). Density of weather stations across the domains is displayed in Figure 5. The C domain has the highest density of stations (700 weather stations and 85 gauging sites), while N domain, the largest area, has the lowest density (270 and 29). Climate conditions are different across each of the domains, with a gradient from arid and semi-arid climates over the N domain; sub-humid climates over the C domain, except over the Altiplano Mexicano and middle-to-high elevations in the southeastern part of the C domain, where semi-arid and humid climates dominate, respectively; humid climate over the SE domain, and sub-humid climates over the YP domain (Garcia, 2004). The 1921–2008 mean annual and seasonal precipitation over each domain displays the intra-seasonal differences inside and among the domains (Table 2). As can be seen in Table 2, the arid and semi-arid N domain (annual mean = 402 mm) contrasts with the humid SE domain (1716 mm). The larger winter contribution to annual total is observed over the N domain (22%) followed by the YP domain (21%), the SE domain (16%), and the C domain (12%). This agrees with the larger influence of the intrusion of cold fronts that produce winter precipitation over the N, SE, and YP domains (Figure 3). Each domain is characterized by high annual and seasonal inter-annual variability that is superimposed on multi-decadal variability (Figure 6). Length and magnitude of long-term (multi-decadal) wet and dry periods have been different between the domains, although they overlap in some years. For example (see Figures 6a & b), the prolonged 1940–55 and 1996-onward dry periods in mean total annual precipitation over the C and N domains (early dry period lasting longer in the N domain until 1960, while the actual dry period started earlier in the C domain in 1980); the moderate 1960–1980 wet period between dry periods and the earlier wet period that ended in 1940 over both domains are evidence that wet and dry periods can affect more than half of the country at the same time, affecting not only mean total annual precipitation but also mean total seasonal precipitation (see Figures 6e, f, i & j). These multi-decadal annual and seasonal fluctuations in time series of N and C domains are linked to the PDO shifts, from cold to warm PDO in the mid-1970s and from warm to a temporarily cold PDO at the end of the 1990s (Pavia et al., 2006). Moreover, in the northwestern portion of the N-domain (known as the monsoon region, Higgins et al., 2003), it is known that winter precipitation is in phase with the PDO (Brito-Castillo et al., 2002; Pavia et al., 2006). Stahle et al. (2009) propose that the recent drought (or the 2000s drought) that has affected the N and C domains (Figures 6a, b, e, f, i & j), is associated with a downward trend in precipitation projected for the regions (Seager et al., 2007), based on anthropogenic global warming.

The multi-decadal behavior observed over the SE and YP domains display different structures. Over both domains, dry and wet periods in mean total annual and seasonal precipitation, (see Figures 6c, d, g, h, k & l), appear to last longer, a situation that is unfavorable for Mexico, since over precipitation in both domains is larger (see Table 2) and the effects over the country's national economy might be large, as occurred in the past (Mendoza & Velasco, 2006). Over the SE domain, for example, the early dry period that started in 1926 lasted almost three decades (until the 1950s) and is evident in mean total annual (Figure 6c) and summer (Figure 6g) precipitation. In mean total winter precipitation (Figure 6k), this early dry period ended some years before (mid 1940s). The dry period was followed by a prolonged wet period that occurred from the 1950s onward (Figures 6c, g, k) with a near-normal period at the end of the 1980s-beginning of the 1990s. Comparing the multi-decadal variability between N and SE domains (i.e., Figures 6a, c, e, g, i & k), an apparent opposite pattern emerges (i.e., droughts in the N domain generally coincide with anomalously wet conditions in the SE domain and vice versa) that is related to tropical SST conditions (Matias & Magaña, 2009). The interaction between easterly waves and trade winds over the Gulf of Mexico and the Caribbean Sea appears to be crucial to explain spatial patterns of droughts that affected Mexico (Matias & Magaña, 2009).

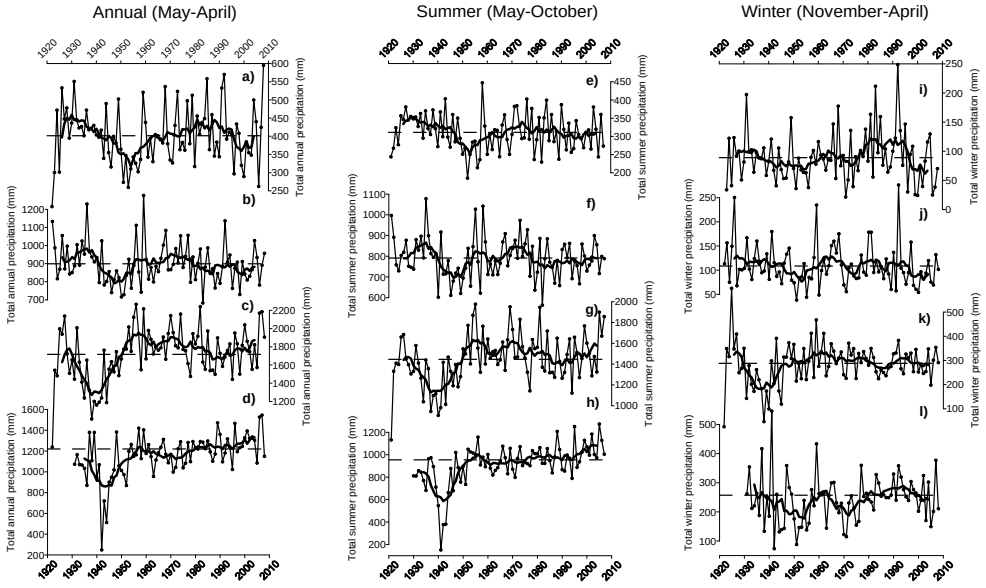

Fig. 6. Mean total annual (May–April) precipitation (left series: a–d; mm), and mean total seasonal precipitation in Mexico for summer (May–October; middle series: e-h) and winter (November–April: right series: i–l), from weather stations displayed in Figure 6 over N-domain (a, e, i); C-domain (b, f, j); SE-domain (c, g, k) and YP-domain (d, h, l). Heavy lines are 9-yr running means and horizontal lines display the mean values over the period for each variable (see Table 2). Note the different ranges in Y-scales due to differences in magnitude and variability in each data set.

7. Regional structures of precipitation trends

The primary goal in detecting trends in streamflow is to identify changes associated with specific physical processes (causal factors) or combinations of processes. But this procedure requires a complete knowledge of the components of the balance equation. Instead, in this study, we start identifying regional trends in precipitation records and then corroborate the corresponding regional trends in streamflow to confirm if they are spatially consistent with one another. This procedure helps, in some way to avoid misleading interpretations, particularly in streamflow datasets where diversion of water for irrigation, control of rivers by damming (when the gauge station is located downstream), or pumping of underground water results in a strong (non-climatic) decline of surface water through time, implying that the causal factor for the declining trend is mostly anthropogenic, and probably with very localized (i.e., non-regional) effects.

Tables 3–5 show the mean magnitude of annual and seasonal trends over each of the domains. In all cases, except in the C domain, total annual precipitation showed a larger number of statistically significant trends than seasonal accumulations. Throughout Mexico, the number of stations displaying downward precipitation trends is larger than stations displaying upward trends, resulting in overall mean annual and summer declining trends. However, the statistical uncertainty in the mean winter trend, based on the 95% confidence interval, includes the zero trend (–0.30 ± 0.54 mm/yr; Table 5). The decrease number of stations having significant trends in winter and their high and uneven spread over the domains (i.e. N, SE and YP) are factors resulted in increasing error in estimating the mean trend, therefore the magnitude of the standard error of trends, derived from weather stations having statistically significant trends in total winter precipitation is very large, indicating that with the available information there is not sufficient evidence to conclude there is an overall mean winter declining trend in Mexico. This conclusion is also valid for the N, SE, and YP domains for mean winter trends (Table 5) and for the SE and YP domains for mean annual (Table 3) and summer (Table 4) trends. In all these cases, the standard error of the trends exceeds the mean magnitude of their respective trends. A different situation occurs over the N and C domains, where the statistical uncertainty of mean annual (Table 3) and summer (Table 4) trends and over the C domain for mean winter trend (Table 5) is smaller than the mean magnitude of the trend. In these cases, we conclude that the mean annual and summer trends are toward increasing precipitation over the N domain and, on the contrary, toward declining precipitation over the C domain (including the mean winter precipitation trend). This last conclusion can be easily verified in Figure 7 that shows the distribution of weather stations over each of the domains that display statistically significant annual (Figure 7a) and seasonal (Figures 7b & c) trends. In all maps of Figure 7, some basic coherent regional trend patterns can be identified for annual and seasonal accumulations over the N domain, such as the tendency for higher precipitation over the high elevations of northeastern Mexico (verified by the line indicating the position of the continental divide, i.e., the limits of the Sierra Madre Oriental), and over middle to high elevations of northwestern Mexico, including the Baja California Peninsula; a tendency for downward precipitation trends over the C domain, with a larger number of stations displaying declining trends over the middle-to-high elevations of the Gulf of Mexico drainage area

than over the Pacific drainage area (except in total winter precipitation, where there is no increasing precipitation trends on either side of the main drainage areas), and over the main drainage area of the Rio Lerma-Santiago basin; a tendency for upward mean seasonal precipitation and downward mean annual precipitation trends over the western half of the YP domain; and finally, a tendency for mean annual and mean summer downward precipitation trends and a mean upward winter precipitation trend over the SE domain. Over the SE domain, individual stations located through the high mountain areas show a tendency for upward trends in annual and seasonal accumulations.

Domain	N(+)	N(-)	Total	Mean Trend (mm/yr)
N	28	7	35	2.54 ± 1.36
C	26	75	101	–3.79 ± 1.57
SE	9	14	23	–3.99 ± 5.40
YP	6	7	13	–0.40 ± 3.76
Overall	69	103	172	–2.38 ± 1.31

Table 3. Mean annual precipitation trends derived from all weather stations having statistically significant trends and located in the North (N), Central (C), Southeast (SE), and Yucatan Peninsula (YP) domains, respectively. N(+) and N(-) are the number of stations displaying upward and downward trends, respectively; the ± values define the 95% confidence intervals for the trends.

Domain	N(+)	N(-)	Total	Mean Trend (mm/yr)
N	22	3	25	2.39 ± 0.26
C	38	69	107	–2.14 ± 1.47
SE	8	12	20	–3.03 ± 4.93
YP	6	3	9	1.90 ± 3.86
Overall	74	87	161	–1.32 ± 1.22

Table 4. Mean summer precipitation trends derived from all the weather stations having statistically significant trends and located in the North (N), Central (C), Southeast (SE), and Yucatan Peninsula (YP) domains respectively. N(+) and N(-) are the number of stations displaying upward and downward trends, respectively; the ± values define the 95% confidence intervals for the trends.

Domain	N(+)	N(-)	Total	Mean Trend (mm/yr)
N	16	6	22	–0.68 ± 0.74
C	10	36	46	–1.13 ± 0.65
SE	9	2	11	0.68 ± 2.03
YP	4	1	5	–0.91 ± 2.14
Overall	39	45	84	–0.30 ± 0.54

Table 5. Mean winter precipitation trends derived from all the weather stations having statistically significant trends located in the North (N), Central (C), Southeast (SE), and Yucatan Peninsula (YP) domains, respectively. N(+) and N(-) are the number of stations displaying upward and downward trends, respectively; the ± values define the 95% confidence intervals for the trends.

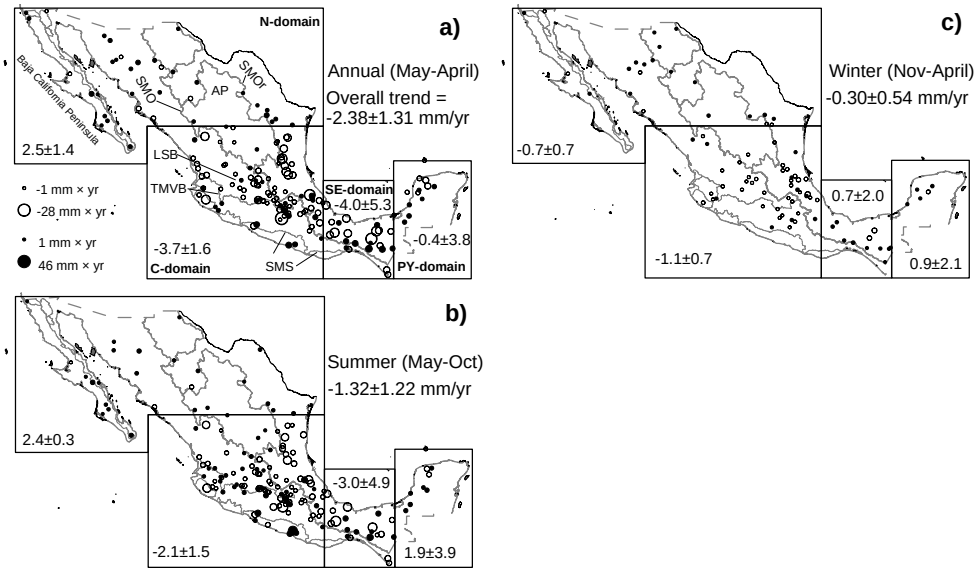

Fig. 7. Maps displaying the distribution of weather stations having statistically significant total annual (a) total summer (b) and total winter (c) precipitation trends in Mexico. Points indicate the position of stations having an increasing precipitation trend while open circles indicate the position of those stations having a declining precipitation trend. Symbols inside the maps are proportional to the magnitude of the trends displayed in the bottom left corner scale of the upper map. The mean trends, derived from the total number of stations overall Mexico, are shown outside the maps, while the mean trends, derived from the stations over each domain, are displayed inside the polygon of each domain (in mm/yr). The ± values define the 95% confidence intervals for the trends. Lines inside the maps show the continental divides with the Pacific drainage areas to the left and Gulf of Mexico drainage areas to the right. Abbreviations in upper left map are the same as in Figure 5a. LSB= Lerma Santiago basin.

To clarify the internal structure of the series, Figures 8–10 show observed time series (expressed as z scores) of selected variables having general significant upward and downward trends. A couple of series have been plotted from each selected station: (1) TDP >0 and (2) total precipitation. Total annual precipitation series are displayed in Figure 8 and total seasonal precipitation time series are displayed in Figures 9 and 10. All series display large inter-annual variability with substantial deviations from linearity in several years. The correspondence between TDP >0 and total annual precipitation trends (having both variables similar general upward or downward trend) is evident in Figure 8 for each station, indicating that an overall upward or downward precipitation trend matches a similar upward or downward trend in TDP >0 (i.e., the decline in total annual precipitation corresponds to a decline in the number of rainy days and vice versa). What is the cause of the overall increasing rainy (dry) days over the N and C domains? It is clear that, if a change of TDP >0 is underway, then a change in annual rainfall accumulation in the same direction

as TDP >0 changes is highly possible and the occurrence of heavy rainfall (from tropical cyclones, for example) only temporarily changes the total annual precipitation without affecting the overall trend.

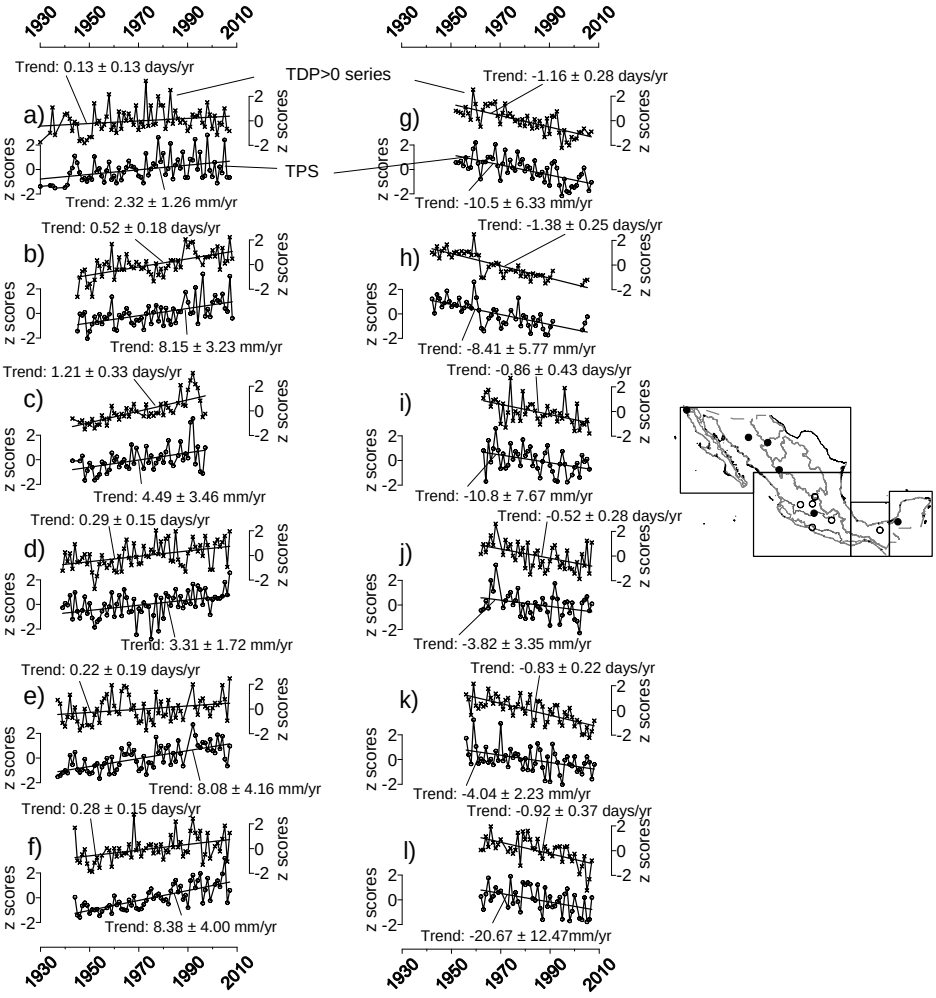

Fig. 8. Examples of observed time series of selected variables (expressed as z scores) displaying upward (left series) and downward (right series) total annual precipitation trends. A couple of series have been plotted from the same selected station, i.e., an upper – TDP >0 (total days with rainfall > 0 mm; lines with ×s) series, and lower TPS-total precipitation series (lines with •). For each variable, the magnitude of the trend with the 95% confidence intervals with their respective units is shown. The map to the right displays the position of the selected stations corresponding to the variables with upward (points) and downward (circles) trends.

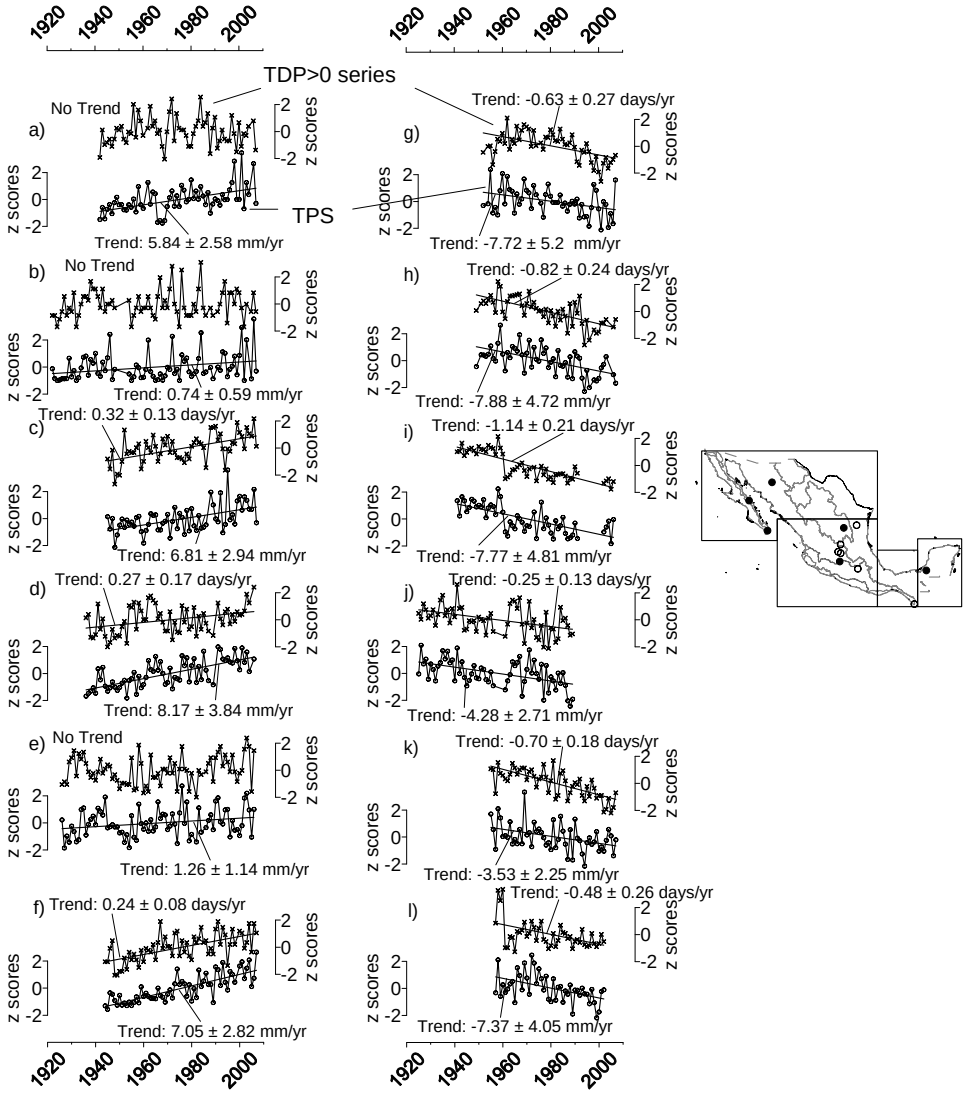

Fig. 9. The same as Figure 8, but for total summer precipitation series. No Trend indicates that for the particular time series the trend is not statistically significant.

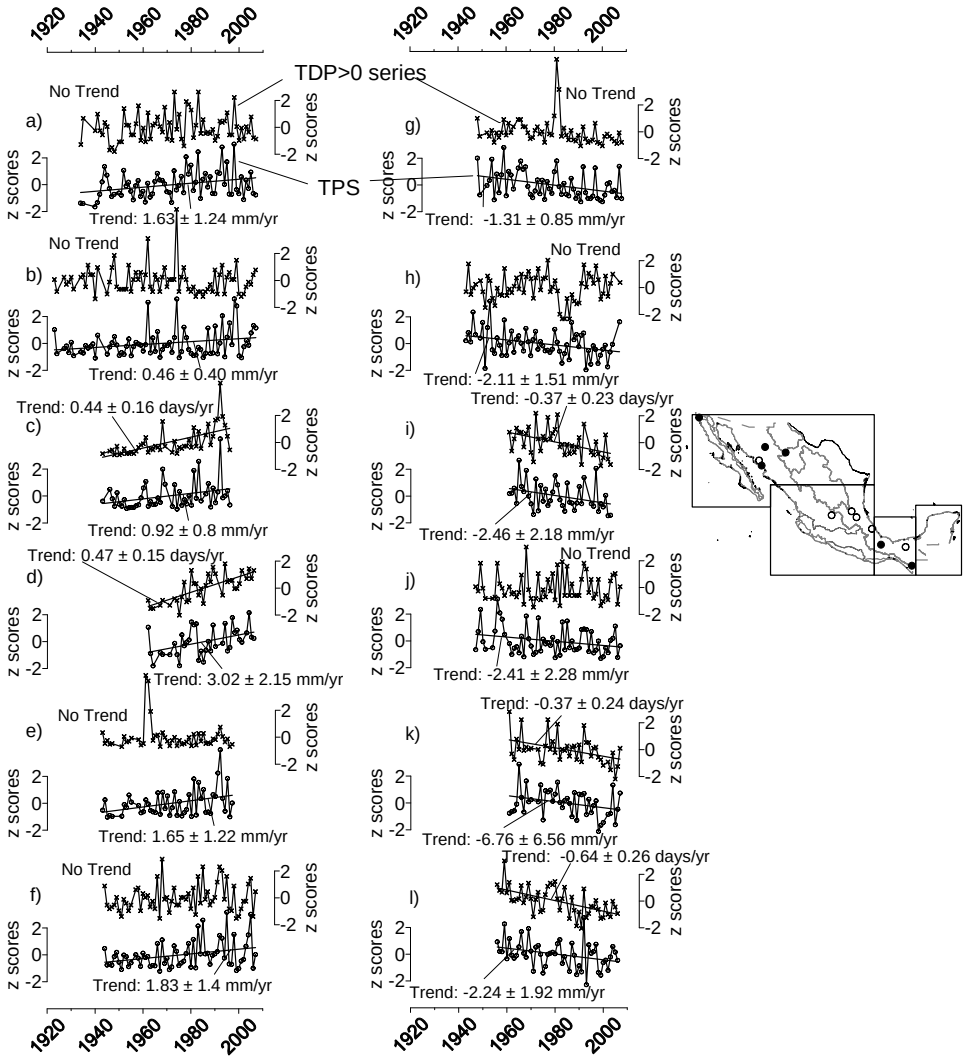

Fig. 10. The same as Figure 8, but for total winter precipitation series. No Trend indicates that for the particular time series the trend is not statistically significant.

This conclusion is not completely valid for total summer (Figure 9) and total winter (Figure 10) precipitation variables because some stations have a general upward or downward seasonal precipitation trend that does not match the corresponding behavior in TDP >0 variables for the same station. This occurs for example, in Figures 9a, 9b, & 9e. Note that the

upper TDP >0 time series in each case does not display statistically significant trends (indicated in Figure 9 by the legend "No Trend"). This is in contrast with the upward trend in the lower total summer precipitation series. In Figures 9a & 9b, a group of years with high precipitation values occurred in recent years, while the corresponding TDP >0 point values show a declining trend in the last two decades, an indication that some external source of humidity has provided the complementary rainfalls for the high summer values recorded in these stations (i.e., less summer rainy days correspond to higher summer rainfalls). This source of precipitation might derive from tropical cyclones, as suggested by Arriaga-Ramírez & Cavazos (2010).

The situation is a little different in winter, where the main source of precipitation proceeds from the passage of cold fronts, enhanced by the southern movement of the subtropical westerly jet stream, which is sometimes associated with El Niño events (Magaña et al., 2003). It is established that there is a direct link between warm SSTs during El Niño years and high winter precipitation in Mexico and vice versa (a cold SSTs during La Niña years and low winter precipitation). In this sense, the high values of winter precipitation during the 1990s, evident in some series (Figures 10a, b, e & f) that display an upward total winter precipitation trend and no trend at all in corresponding the TDP >0 time series might be a reflection of the strong-to-moderate El Niño years of 1991, 1994, 1997, and 2002 that provided necessary atmospheric conditions for production of the complementary winter precipitations in the datasets, since the corresponding TDP >0 time series decreases during the same period. The situation is a little harder to explain in series displaying a decreasing total winter precipitation trend (Figures 10g, h & j), and no trend at all in corresponding TDP >0 time series. The low winter precipitation observed in recent years in these time series might have been influenced by the strong-to-moderate La Niña conditions of 1988, 1998, 1999, and 2007 enhancing the overall decreasing trend, i.e., similar number of rainy days experienced lower precipitation values in recent years.

8. Annual and seasonal regional trends observed in streamflow series

8.1 Hypothesis testing

The results of hypothesis testing (not shown) indicate that changes in variances of all datasets are more common in winter than in summer or annual components. However, a significant change in means or variances of the two halves of the series do not necessarily result in a significant general trend for the series since the number of stations with significant changes in means or variances are always larger than those stations displaying a significant trend. This conclusion is also valid for each domain. On the contrary, similar means or similar variances inside the series do not necessarily mean that the corresponding series does not display a significant overall trend.

8.2 Significant trends in streamflow

Mean winter streamflow show a larger number of stations displaying significant trends than mean summer or mean annual components. Upward trends in streamflow are more common in winter, while downward trends are more common in summer, than the other components.

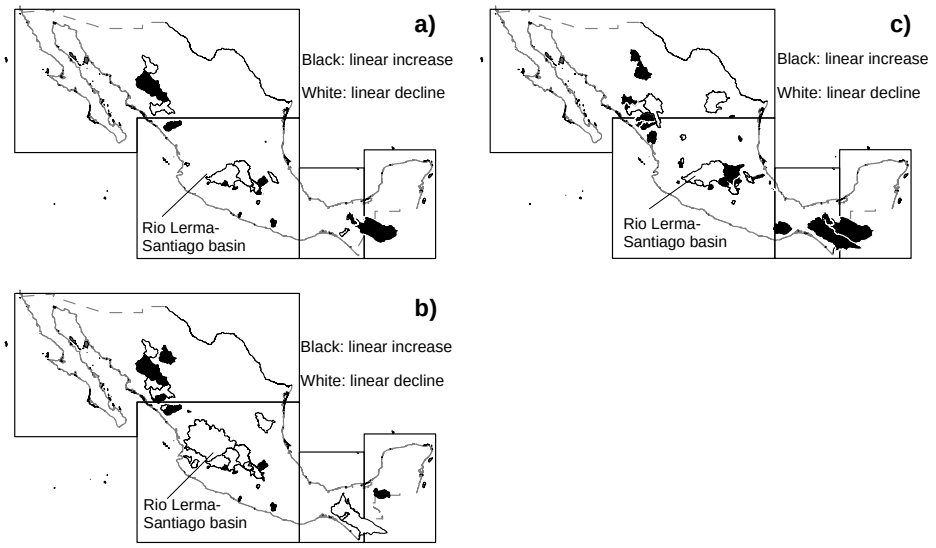

Fig. 11. Maps showing the distribution of river basin polygons displaying significant upward (black polygons) and downward (white polygons) streamflow trends for mean annual (a) mean summer (b) and mean winter (c) components.

The distribution of river basins having significant upward and downward mean annual and mean seasonal streamflow trends is shown in Figure 11. A tendency for a large number of drainage areas to have downward annual and seasonal trends is evident in basins located in the C domain, particularly those in the Lerma-Santiago river basin in central Mexico. This result matches downward trends observed in total annual and seasonal precipitation over the C domain, indicating that overall decreases in rainfall over the C domain have resulted in lower values for streamflow, mainly over Pacific drainage areas. Small basins surrounding the Lerma-Santiago river basin display upward trends in mean annual and seasonal streamflow. Although in the C domain, there are also weather stations displaying significant upward annual and summer trends (See Figures 7a & b), the position of those stations does not necessarily correspond to the position of the small basins. Moreover, mean winter streamflow in some basins display upward trends (Figure 11c), while no weather station displays similar significant upward trends over those areas (Figure 7c). These results suggest that the significant annual and seasonal upward trends in precipitation and streamflow over the C domain might be a reflection of local rather than regional factors. In addition it may be also due to there are 1161 for precipitation and only 141 for streamflow data sets. Not enough streamflow datasets and the large dataset ratio for precipitation to streamflow may cause some errors in the analysis. Over northwestern Mexico in the N domain, large drainage areas display upward and downward mean annual and mean seasonal trends with no obvious regionally coherent pattern (Figures 11a-c). Although we established that the middle-to-high elevations in northwestern Mexico in the N domain have upward mean annual and mean seasonal precipitation trends (Figures 7a-c), the decreasing trends observed in streamflow over these areas do not match this pattern.

Unfortunately, over the drainage areas where significant downward streamflow trends are evident in northwestern Mexico, there are no weather stations (See Figure 5). This makes it impossible to prove a correspondence between precipitation and streamflow variables in western part of the mainland in the N domain.

Finally, some selected time series with significant upward and downward mean annual streamflow trends are displayed in Figure 12. As occurred with total precipitation series, streamflow series also show high inter-annual variability, with substantial deviations from the linear trend. From the time series, it is evident that the dry period during the 1950s (Figures 12a, b, e, i, j & l), and the dry period during the 1990s (Figure 12a, c, h & i) affected a large part of Mexico.

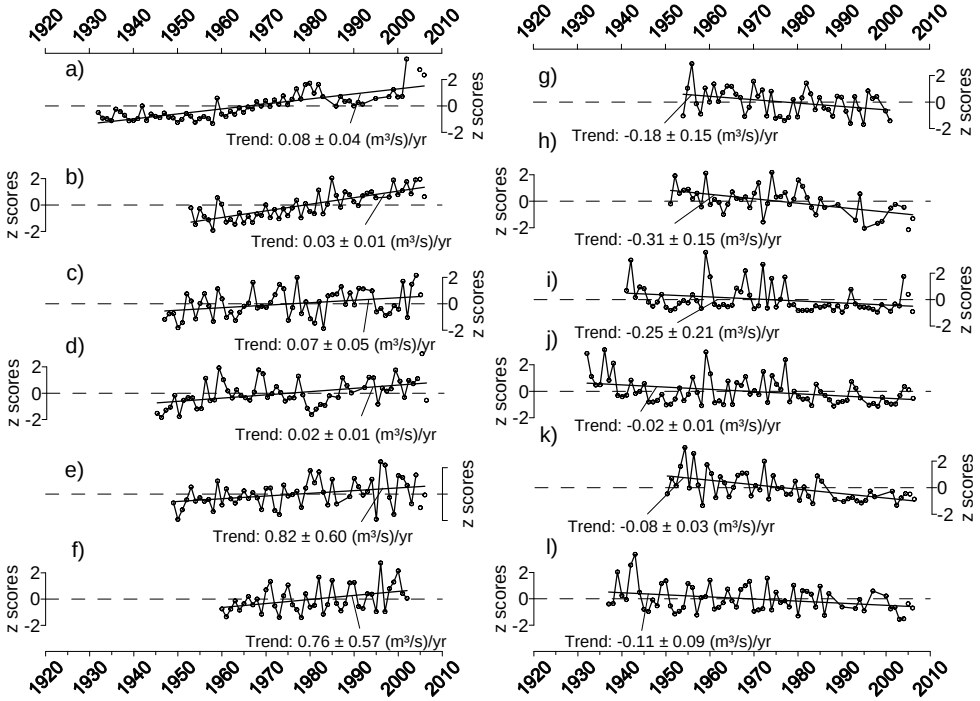

Fig. 12. Examples of observed time series (expressed as z scores) of selected gauging stations displaying upward (left series) and downward (right series) mean annual streamflow trends (lines). The magnitude of each trend with 95% confidence intervals is shown for each variable.

9. Conclusions

Regional changes in rainfall and streamflow in Mexico have significant trends of different sign (Figures 7 & 11), both declining and increasing trends. While isolated differences in trends occur in rainfall and streamflow over large areas, some basic coherent patterns can be identified, such as the trend for lower precipitation in the C domain and a trend for higher precipitation in the N domain. In the C domain, decreasing annual and seasonal trends

match the mean annual and seasonal trends in streamflow. However, we also see that trend structures exhibit some spatial patterns that are not readily explained, such as the trend for declining streamflow in the N domain over large drainage areas of the western mainland and increasing streamflow in the C domain that does not match the opposite behavior of the trends observed in precipitation. The possibility that these differences might be related to more localized external factor and errors resulted from not enough streamflow data sets and the large dataset ratio for precipitation are suggested. However, more detailed analyses are necessary to prove these.

Finally, we conclude that over the last nine decades, Mexico has experienced an overall decrease in mean total annual and summer precipitation, based on analysis of 1161 weather stations across Mexico. Mean total precipitation changes were derived from 172 annual precipitation series and 161 summer rainfall series, displaying significant trends in both directions, declining trends for 103 annual and 87 summer series and increasing trends for 69 annual and 74 summer series. The total change from 1920–2008 has been about 21 mm in mean annual accumulation and 9 mm in mean summer accumulation. The most affected areas from declining precipitation are the middle-to-high elevations in the Gulf of Mexico drainage areas in eastern Mexico and over the upper Rio Lerma-Santiago basin in central Mexico. Several stations in northern and northwestern Mexico (including the Baja California Peninsula), have an overall increase in mean annual and mean summer rainfall accumulations with large variations over the areas. Although the number of stations having declines in mean total winter precipitation is larger than those having increases in mean total winter precipitation, the uncertainties among the trends are so large that the double mean square trend error overpasses the mean magnitude of the trends. In essence, the data does not provide evidence for regional mean changes in winter. The analysis of 141 streamflow series provided more evidence for declines in total annual and summer precipitation, mainly in the Río Lerma-Santiago Basin, although some river basins in northwestern Mexico also display declining trends that do not match the upward trend observed in precipitation. Unfortunately, no weather stations with long datasets are available there, mainly in the highlands of those basins. This makes it difficult to relate streamflow and precipitation changes in northwestern Mexico.

10. Acknowledgments

This work was carried out with the support of the National Council on Science and Technology of Mexico (CONACYT grant J50757-F) and of the Centro de Investigaciones Biologicas del Noroeste (CIBNOR grant PC 0.3). Ira Fogel provided editorial services.

11. References

Arriaga-Ramírez, S. & Cavazos, T. (2010). Regional trends of daily precipitation indices in northwest Mexico and southwest United States. *Journal of Geophysical Research*, Vol. 115, D14111, doi:10.1029/2009JD013248, ISSN 0148-0227

BANDAS (Banco Nacional de Datos de Aguas Superficiales). (1997). Instituto Mexicano de Tecnología del Agua, Período 1997-2004, CD-rom data base, Morelos, México. Available from:<http://www.imta.gob.mx>

Barnett, T.P., Pierce, D.W., AchutaRao, K.M., Gleckler, P.J., Santer, B.D., Gregory, J.M. & Washington, W.M. (2005). Penetration of human-induced warming into the world´s oceans. *Science*, Vol. 309, (July 2005), pp. 284-287, ISSN 0036-8075

Brito-Castillo, L., Díaz, C.S.C. & Ulloa-Herrera, R.S. (2009). Observed tendencies in maximum and minimum temperatures in Zacatecas, Mexico and possible causes. *International Journal of Climatology,* Vol. 29, No. 2, (February 2009), pp. 211-221, ISSN: 1097-0088

Brito-Castillo, L., Douglas, A.V., Leyva-Contreras, A. & Lluch-Belda, D. (2003). The effect of large-scale circulation on precipitation and streamflow in the Gulf of California continental watershed. *International Journal of Climatology*, Vol. 23, No. 7, (June 2003), pp. 751-768, ISSN: 1097-0088

Brito-Castillo, L., Leyva-Contreras, A., Douglas, A.V. & Lluch-Belda, D. (2002). Pacific Decadal Oscillation and the filled capacity of dams on the rivers of the Gulf of California continental watershed. *Atmosfera*, Vol. 15, No. 2, (April 2002), pp. 121-136, ISSN 0187-6236

Díaz, S.C., Salinas-Zavala, C.A. & Hernández-Vázquez, S. (2008). Variability of rainfall from tropical cyclones in northwestern Mexico and its relation to SOI and PDO. *Atmosfera*, Vol. 21, No. 2, (April 2008), pp. 213-223, ISSN 0187-6236

Douglas, A.V. & Englehart, Ph. J. (2007). A Climatological perspective of transient synoptic features during NAME 2004. *Journal of Climate*, Vol. 20, No. 9, (May 2007), pp. 1947-1954, ISSN 0894-8755

Englehart, Ph.J. & Douglas, A.V. (2004). Characterizing regional-scale variations in monthly and seasonal surface air temperature over Mexico. *International Journal of Climatology,* Vol. 24, No. 15, (December 2004), pp. 1897-1090, ISSN: 1097-0088

Farfan, L.M. & Zehnder J.A. (1994). Moving and stationary mesoscale convective systems over Northwest Mexico during the southwest area monsoon project. *Weather and Forecasting*, Vol. 9, No. 4, (December 1994), pp. 630-639, ISSN: 0882-8156

Farfan, L.M. (2011). Eastern Pacific tropical cyclones and their impact over western Mexico. In: *Experimental and Theoretical Advances in Fluid Dynamics*, Klapp et al. (eds.), Environmental Science and Engineering, pp. 135-148, doi: 10.1007/978-3-642-17958-7_9. ISBN: 978-3-642-17957-0, Springer-Verlag Berlin Heidelberg

Garcia, E. (2004). *Modificaciones al sistema de clasificación climática de Koppen (para adaptarlo a las condiciones climáticas de México)*. 5ta edición, Instituto de Geografía, UNAM, ISBN: 970-32-1010-4, México, D.F.

Giovannettone, J.P. & Barros, A.P. (2008). A remote sensing survey of the role of landform on the organization of orographic precipitation in Central and southern Mexico. *Journal of Hydrometeorology*, Vol. 9, No. 6, (December 2008), pp. 1257-1283, ISSN: 1525-7541

Gutierrez-Ruacho, O.G., Brito-Castillo, L., Díaz, C.S.C. & Watts Ch. (2010). Trends in rainfall and extreme temperatures in Northwestern Mexico. *Climate Research,* Vol. 42, No. 2, (July 2010),pp. 133-142, ISSN: 1616-1572

Higgins, R.W., Douglas, A.V., Hahmann, A., Berbery, E.H., Gutzler, D., Shuttleworth, J., Stensrud, D., Amador J., Carbone, R., Cortez, M., Douglas, M., Lobato, R., Meitin, J., Ropelewski, Ch., Schemm, J., Schubbert, S. & Zhang, Ch. (2003). Progress in Pan American CLIVAR research: the North American monsoon system. *Atmosfera*, Vol. 16, No. 1, (January 2003), pp. 29-65, ISSN 0187-6236

Houghton, J.T., Ding, Y., Griggs, D.J., Noguer, M., van der Linden, P.J., Dai, X., Maskell, K. & Johnson, C.A. (2001). *Climate Change 2001: The Scientific Basis*, Cambridge University Press, ISBN: 9780521014953, Cambridge, U.K.

IPCC (2007). Intergovernmental Panel on Climate Change. In *Climate Change 2007: The physical science basis. Contribution of working group I to the fourth assessment report of the IPCC (AR4)*, Solomon, S., Qin, D., Manning, M., Chen, Z., Marquis, M., Avery, K.B., Tignor, M. & Miller, H.L. (eds). Cambridge University Press, New York, http://www.ipcc.ch/press/index.htm

Jáuregui, E. (2003). Climatology of landfalling hurricanes and tropical storms in Mexico. *Atmosfera*, Vol. 16, No. 4, (October 2003), pp. 193-204, ISSN 0187-6236

Knutson, Th.R., McBride, J.L Greenhouse Gases / Book 1., Chan, J., Emanuel, K., Hollan, G., Landsea, Ch., Held, I., Kossin, J.P., Srivastava A.K. & Sugi, M. (2010). Tropical cyclones and climate change. *Nature*, Vol. 3, (March 2010), pp. 157-163, ISSN: 0028-0836

Lindzen, R.S. (2007). Taking greenhouse warming seriously. *Energy & Environment*, Vol. 18, No. 7+8, pp. 937-950, ISSN: 0958-305X

Magaña, V., Amador, J. & Medina, S (1999). The midsummer drought over Mexico and Central America. *Journal of Climate*, Vol. 12, No. 6, (June 1999), pp. 1577-1588, ISSN 0894-8755

Magaña, V.O., Vázquez, J.L, Pérez, J.L. & Pérez, J.B. (2003). Impact of El Niño on precipitation in Mexico. *Geofísica Internacional*, Vol. 42, No. 3, pp. 313-330, ISSN: 0016-7169

Matías, M. & Magaña, V. (2010). Regional aspects of prolonged meteorological droughts over Mexico and Central America. *Journal of Climate*, Vol. 23, No. 5 (March 2010), pp. 1175-1188, ISSN 0894-8755

McBride, J.L. (1995). *Tropical cyclone formation, global perspective on tropical cyclones*. Elsberry, R.L. (ed.). World Meteorological Organization, pp. 106-197

Mendoza, B. & Velasco, V. (2006). A study of historical droughts in southeastern Mexico. *Journal of Climate*, Vol. 19, No. 12 (June 2006), pp. 2916-2934, ISSN 0894-8755

Milly, P.C.D., Dunne, K.A & Vecchia, A.V. (2005). Global pattern of trends in streamflow and water availability in a changing climate. *Nature*, Vol. 438, (November 2005), pp. 347-350, ISSN: 0028-0836

Pavia, E.G., Graef F. & Reyes, J. (2009). Annual and seasonal surface air temperature trends in Mexico. *International Journal of Climatology,* Vol. 29, No. 9, (July 2009), pp. 1324-1329, ISSN: 1097-0088

Pavia, E.G., Graef, F. & Reyes, J. (2006). PDO-ENSO effects in the climate of Mexico. *Journal of Climate*, Vol. 19, pp. 6433-6438, doi:10.1175/JCL14045.1, ISSN 0894-8755

Quintas, I. (2000). ERIC II. In: *Documentación de la base de datos climatológica y del programa extractor (ERIC II: Documentation of the climatologic database anda data extraction program)*. Instituto Mexicano de Tecnología del Agua (IMTA). 54 pp.

Seager, R., Tign, M., Held, I., Kushnir, Y., Lu, J., Vecchi, G., Huan, H., Harnik, N., Leetmaa, A., Lau, N., Li, C. Velez, J. & Naik, N. (2007). Model projections of an imminent transition to a more arid climate in southwestern North America. *Science*, Vol. 316, (May 2007), pp. 1181-7784, ISSN 0036-8075

Stahle, D.W., Cook, E.R., Villanueva-Diaz, J., Fye, F.K, Burnette, D.J., Griffin, R.D., Acuña-Soto, R., Seager, R. & Heim, Jr., R.R. (2009). Early 21st-century drought in Mexico, *Eos Translational*, AGU, Vol. 90, No. 11, pp. 89-100, doi:10.1029/2009EO110001

Trenberth, K. (2005). Uncertainty in Hurricane and global warming. *Science*, Vol. 308, (June 2005), pp. 1753-1754, ISSN 0036-8075

Turrent, C. & Cavazos, T. (2009). Role of the land-sea thermal contrast in the interannual modulation of the North American Monsoon. *Geophysical Research Letters*, Vol. 36, L02808, doi:10.1029/2008GL036299, ISSN: 0094-8276

Wang, C., Lee, S.K & Enfield, D.B. (2007). Impact of the Atlantic warm pool on the summer climate of the western hemisphere. *Journal of Climate*, Vol. 20, No. 20, (October 2007), pp. 5021-5040, ISSN 0894-8755

Webster, P.J., Hollan, G.J., Curry, J.A. & Chang, H.-R. (2005). Changes in tropical cyclone number, duration and intensity in a warming environment. *Science*, Vol. 309, (September 2005), pp. 1844-1846, ISSN: 0036-8075

Weiss, J.L. & Overpeck, J.T. (2005). Is the Sonoran Desert losing its cool?. *Global Change Biology*, Vol. 11, No. 12, (December 2005), pp. 2065-2077., ISSN: 1365-2486

Wigley, T.M.L. (2006). Appendix A: Statistical Issues Regarding Trends. *In Temperature Trends in the Lower Atmosphere: Steps for Understanding and Reconciling Differences*. TR Karl, SJ Hassol, CD Miller, and WL Murray (Eds.). A Report by the Climate Change Science Program and the Subcommitttee on Global Change Research,Washington, DC. 165 pp.

Yu, J., Wang, Y. & Hamilton, K. (2010). Response of tropical cyclone potential intensity to al global warming scenario in the IPCC AR4 CGCMs. *Journal of Climate*, Vol. 23, No. 6, (March 2010), pp. 1354-1373, ISSN: 0894-8755

Zhao, X. (2011). Is global warming mainly due to anthropogenic greenhouse gas emissions?. *Energy Sources, Part A: Recovery, Utilization, and Environmental Effects*, Vol. 33, No. 21, (August 2011), pp. 1985-1992, ISSN: 1556-7036

19

The Environmental and Population Health Benefits of Active Transport: A Review

Richard Larouche
Children's Hospital of Eastern Ontario
Canada

1. Introduction

In 2007, the prestigious medical journal *The Lancet* published a series of papers entitled *Energy and Health*. In his commentary, Richard Horton argued that "*The current debate about the impact of human beings on our planet – especially with respect to climate change – is one of the most important issues of our time. But that debate is presently unbalanced and too narrow*." He considered that the relationship between energy and health had been clearly neglected by governments and international institutions such as the World Health Organization and the World Bank. One of the proposed pathways to reduce our global footprint while improving our health is to switch from an automobile-dependent transportation system to a low-carbon system characterized by an increased utilization of modes of transportation such as walking, cycling and public transport (Horton, 2007; Woodcock et al., 2007).

On a worldwide basis, transport activities account for 23% of CO_2 emissions and this proportion is steadily increasing (International Transport Forum, 2010). Moreover, worldwide CO_2 emissions from transport have increased by 45% from 1990 to 2007 (International Transport Forum, 2010). In parallel with their rapid economic growth, transport-related CO_2 emissions are increasing markedly in developing countries such as China and India (Woodcock et al., 2007). For example, in China, total motorized travel distance has increased almost five-folds between 1980 and 2003 (Zhou & Szyliowicz, 2006).

Within the transport sector, private vehicles represent the second most important contributor to greenhouse gases (GHG) emissions behind road freight (Chapman, 2007). Existing road infrastructure cannot cope with the rapid increase in the number of vehicles; thereby generating traffic jams which, aside from the increased GHG emissions, have dire economic consequences. For example, Levy et al. (2010) estimated that fuel wasted and time lost in traffic jams in 83 American cities cost 60 billion US$. Moreover, they evaluated that mortality associated with ambient exposure to fine particulate matter ($PM_{2.5}$) cost an additional 31 billion US$ in these cities. Although technological innovations may contribute to reduce the intensity of CO_2 emissions from transport in a long term perspective, more immediate changes in transport behaviors are crucial to achieve a stabilization of the absolute emissions in order to mitigate climate change (Chapman, 2007).

Data from the 1995 Nationwide Personal Transportation Survey in the US indicate that private cars were used for about 90% of trips of 0.5 to 3 miles, of which an important

proportion could be substituted by walking, cycling and public transport (de Nazelle et al., 2010). This would represent an interesting strategy to reduce GHG emissions considering the disproportionate contribution of short trips to pollutant emissions due notably to cold starts (Frank et al., 2000). Further, since most individuals must travel to work or to school on a daily basis, active transport (e.g. using active modes of transportation such as walking and cycling) is increasingly regarded as a promising alternative to increase physical activity (PA) levels (Larouche & Trudeau, 2010; Shephard, 2008).

From a public health perspective, there is clear evidence of a strong relationship between PA and several health-related illnesses including cardiovascular diseases (Manson et al., 2002), diabetes (Sigal et al., 2006), cancer (Friedenreich & Orenstein, 2002), and all-cause mortality (Paffenbarger et al., 1993). Moreover, the prevalence of obesity has increased throughout the world to such an extent that it is now considered a pandemic (Lobstein et al., 2004; Wang & Lobstein, 2006). Recent research has also shown that the majority of the population fails to accumulate enough daily PA (Colley et al 2011a, b; Troiano et al., 2008). During the last decades, the rates of AT to/from school in children and adolescents has decreased markedly in several countries (Buliung et al, 2009, Grize et al., 2010; McDonald, 2007; van der Ploeg et al., 2008). Further, exposure to ambient air pollution is associated with respiratory and cardiovascular morbidity and mortality (Brook et al., 2010; Brunekreef & Holgate, 2002).

To implement more effective strategies to promote active transport (AT), it is necessary to develop a greater understanding of the factors associated with individuals' mode of transport, that is the correlates of AT[1]. Current theoretical models suggest that the choice of travel mode is based on several factors including characteristics of the individual (i.e. perceived barriers to active transport), of the social environment (i.e. social support), of public policies (i.e. laws and taxes) and of the built environment (i.e. population density and land-use mix) (Panter et al., 2008; Sallis et al., 2006). These models are typically based on the social ecological theory (i.e. Bronfenbrenner, 1979) which predicts that human behavior result from the interactions within and between these multiple "levels of influence".

Consequently, the current review is organized in four main sections. First, the impact of various transportation strategies to reduce emissions of GHG and other pollutants are described. Second, the impacts of AT on physical activity, physical fitness and other health-related outcomes are summarized. Third the correlates of AT are briefly examined to identify key variables to consider for the promotion of AT as a strategy to reduce GHG emissions and increase physical activity. Finally, the fourth section examines the inter-relationships between the environmental and public health impacts of AT.

2. Methods

Potentially relevant articles were identified through databases including Medline, PsychInfo, Google Scholar and the National Transportation Library. Keywords such as "active transport*", "active commuting", "active travel" were used in addition to the following exposures or outcomes: "greenhouse gas*", "carbon dioxide", "climate change",

[1] As detailed in the current review, most of the research that has examined the factors associated with AT have used a cross-sectional methodology. Therefore, the term "correlates" is used rather than the term "determinants" which involves a causal relationship (Bauman et al., 2002).

"traffic", "physical activity", "physical fitness", "obes*", "overweight", "diabetes", "cardiovascular disease*", "cancer", "hypertension", "all-cause mortality", "correlates", "determinants". Other articles were added from the author's personal library. In addition, reference lists of previous reviews were scanned to identify potentially relevant literature.

Articles were selected on the basis that they provide additional elements to the comprehension of the explored phenomena. To be included in the review, articles generally needed to have examined AT, either as an outcome variable or as an exposure. However, in some cases, studies that examined the association between environments recognized as conductive to AT were also considered eligible. There were no restriction with respect to date of publication; however, most included studies were published during the last 10 years. Studies published in English or French were considered eligible.

For the section on the impact of transport practices on pollution and GHG, priority was given to the natural experiments in which the impact of transport policies was rigorously examined before and after the intervention. To complement this rather scarce literature, simulations and cross-sectional studies were also included. For the section on the health-related outcomes of AT, priority was given to the studies that used an experimental design, which provide the highest level of evidence. These studies were complemented by prospective cohort studies, large cross-sectional studies and systematic reviews. Finally, as a systematic examination of the correlates of AT was beyond the scope of this book chapter, a simplified ecological model was used to categorize the most important factors into five levels of influence, as illustrated in Figure 1.

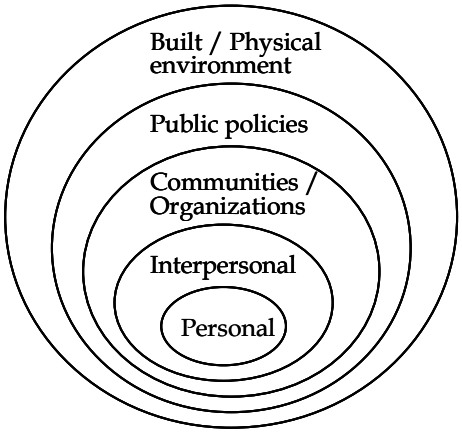

Fig. 1. Simplified ecological model for categorizing the correlates of active transport into the different levels of influence.

3. Impact of transport practices on pollution and greenhouse gases

3.1 Natural experiments

In central London, a congestion charging scheme was introduced by the mayor in February 2003. Drivers are charged £8 (about US$16) to enter the downtown core during working hours. While the scheme had little impact on the concentrations of CO_2 and PM_{10} in Greater

London, small decreases were observed in the central wards. Estimated years of life gained were 183 per 100 000 individuals. Interestingly, air pollution and mortality reductions were greater in more deprived areas, but emissions nevertheless remained higher in these areas compared to the more affluent areas (Tonne et al., 2008). A similar scheme was implemented in Stockholm and it resulted in a 15% decrease in vehicle miles travelled accompanied by 8.5-14% reductions of the emissions of nitric oxides, PM_{10} and CO_2 in the inner city (Johansson et al., 2009). However, as in London, changes in emissions were lower in the Greater Stockholm (1-3%), suggesting that the impact of congestion charging schemes is mostly localized.

For the 1996 Summer Olympic Games in Atlanta, a transportation strategy was developed to minimize traffic congestion and to ensure that spectators could commute to the Olympic events in a reasonable amount of time. This strategy included the development of a public transportation system operating 24 hours a day, the addition of 1000 buses for park-and-ride services, the closure of the downtown core to private automobile travel, and modified delivery schedules (Friedman et al., 2001). Local businesses were also encouraged to implement alternative work schedules. Using an ecological study design, Friedman and colleagues (2001) examined the impact of these changes in traffic on air quality and childhood asthma events. They observed a 22.5% reduction in weekday peak traffic that was correlated ($r = 0.36$) with a 27.9% reduction in ozone concentration. Reductions in concentrations of carbon monoxide, PM_{10} and nitrogen dioxide were also noted. Lower rates of childhood asthma acute care events were also reported.

Similarly, a combination of aggressive measures was put in place in order to improve air quality for the 2008 Beijing Olympic Games. Private vehicles with odd-numbered license plates were allowed to circulate on Beijing's roads one day and those with even numbers were allowed on the next day, while vehicles that failed to meet the European No. 1 standard for exhaust emissions were banned. Power plants and large factories were also required to reduce their emissions (Wang et al., 2009). These measures have led to reductions in the concentration of sulfur oxide, carbon monoxide, nitric oxides and ozone of 61%, 25%, 21% and 26% respectively. It is however unclear whether such policies could be implemented at a larger scale and for longer periods of time.

3.2 Simulations

Woodcock and colleagues (2009) examined the impact of different transportation scenarios on carbon emissions and public health for the year 2030. Using the cities of London and Delhi as examples, they modeled the impact of five scenarios: 1) Business as usual; 2) Lower carbon-emission motor vehicles; 3) Increased active travel; 4) "Towards sustainable transport (e.g. a combination of scenarios 2 and 3); and 5) Increased active travel, but shorter distances travelled. In London, the scenario #1 would lead to a 4% increase in CO_2 emissions from 1990 levels while scenarios 2 to 5 would lead to 35-60% reductions of emissions. In Delhi, due to the projected increases in population and in the level of motorization, the predicted CO_2 emissions from all scenarios would represent major increases in comparison with 1990 levels. However, with scenario #4, the increase would be 199% compared to 526% for the business as usual scenario. The "Towards sustainable transport" scenario would have the greatest impact on mortality in London (7 439 disability-adjusted life-years) and Delhi (12 995 disability-adjusted life-years). Increasing the mode share of AT would have a greater impact than relying on technology (e.g. lower-emissions motor vehicles).

Similarly, American researchers examined the impact of five different education policy scenarios on vehicle emissions during children's school commuting in St-Paul, Minnesota using data from a school travel survey and a school enrollment data set (Marshall et al., 2010). In the first scenario, children where modeled as attending the school that they actually attended. The second scenario randomly assigned children to any school in the district. In the third scenario, children were assigned to the closest school in their neighborhood. In the fourth scenario, the district was subdivided into three regions and most children were assigned to a school in the district where they lived. Finally, the fifth scenario is similar to the first one, except that all children living within 1 mile of school were modeled as active commuters. Emissions of CO_2, CO, NO_x, PM_{10} and volatile organic compounds were predicted using the US Environmental Protection Agency's MOBILE6 model[2]. The third scenario would be the most effective, achieving 3- to 8-fold reductions in the pollutant emissions with a 7-fold reduction in transport costs. Further, because only 27% of children lived within 1 mile of their actual school, this scenario would achieve an even greater mode share of AT. However, this scenario would go against the habit of free choice; thus, it would likely be a challenge to gather public acceptability.

Using data from the 1995 Nationwide Personal Transportation Survey, de Nazelle et al. (2010) estimated the impact of conversing short car trips (defined as < 3 miles) to alternative modes of transportation on pollutant emissions. Their estimates suggest that, across the US, daily emissions reductions would amount to 30-70 tons for volatile organic compounds, 15-35 tons for nitrogen oxides, and 400-900 tons for carbon monoxide. Daily reductions in GHG emissions would vary between 20 000 to 46 000 tons of CO_2 equivalent. This simulation is based on a very small decrease in vehicle miles travelled (0.8% to 1.8%), while it is estimated for example that a 10% increase in the price of gas can reduce consumption by 2.5% (Kaza et al., 2011). Thus, one could argue that there is a potential for greater reductions of driving.

3.3 Observational studies

Combining data from the Neighborhood Quality of Life Study and the King County Land Use, Transportation, Air Quality, and Health Study, Frank and colleagues (2006) examined the interactions between land use, pollution and health. Their analyses indicate that a 5% increase in the index of walkability[3] was associated with decreases in vehicle miles travelled (6.5%), NO_x emissions (5.6%) and volatile organic compounds (5.5%). Such an increase in walkability was also associated with lower body mass indices (-0.228 kg/m^2) and with 32.1% more minutes of weekly AT. Similar analyses based on the SMARTRAQ study in the Atlanta area have shown that increased residential density, street connectivity and transit accessibility were associated with increased walking and decreased driving (Frank et al., 2010). In contrast, increasing the land-use mix was associated with reductions in both driving and walking, probably because individuals travel shorter distances in this type of environment (Frank et al., 2010).

Further, a study from the US Environmental Protection Agency (1999) compared the impact of new residences in already built-up areas (e.g. infill development) vs. new residences built

[2] This model can be found at www.epa.gov/otaq/mobile.htm

[3] Walkability refers to the ability to walk to certain destinations within the neighborhood. This concept is further described in section 5.1 of this book chapter.

in the suburbs and exurbs (e.g. greenfield development) in San Diego (CA), Montgomery County (MD) and West Palm Beach (FL). In the denser "infill" developments, vehicle miles travelled were 40-50% lower, emissions of CO_2 and NO_x were about 50% lower and public infrastructure costs were also markedly lower.

However, the concentrations of NO_x can nevertheless be higher in more "walkable" areas, which are characterized by higher population density and land-use mix (Marshall et al., 2009), emphasizing the need to distinguish emissions and concentrations. For example, in Vancouver (Canada), a strong correlation was noted between neighborhoods walkability and NO_x concentrations. High walkability areas were mostly located in the more densely populated city center through which residents of the suburbs are likely to commute to work. However, ozone is a secondary pollutant formed in the atmosphere rather than emitted directly from traffic exhaust, so high concentrations generally occur downwind from the high density areas; hence ozone concentrations in Vancouver where higher in the suburbs (Marshall et al., 2009).

Altogether, these studies suggest that the design of more walkable neighborhoods could lead to a decrease in the mode share of driving that should, in turn, lead to reductions of GHG emissions. However, because these studies have used a cross-sectional design, their findings must be interpreted with caution. There may be an underlying self-selection issue such that individuals choose to live in a neighborhood that meets certain preferences (Frank et al., 2007). To address this issue, Handy and colleagues (2005) compared the travel behaviors of residents who had moved during a 1-year period to others that did not while controlling for neighborhood preferences. They found that changes in neighborhood characteristics were associated with changes in walking and driving. In their model, accessibility of destinations was the strongest predictor of changes in driving, emphasizing the importance of land-use mix.

Another study explored the relationship between urban form and the ecological footprint associated with commuting patterns in the 163 municipalities of the Barcelona metropolitan region, Spain (Muniz & Galindo, 2005). Between 1986 and 1996, per capita ecological footprint increased by 95% driven by increases in the average trip distance (from 4.6 km to 6.7 km), and the mode share of car trips (22 to 35%). The mean trip distance and the ecological footprint of commuting increased systematically as distance from the city center increased reflecting higher car use. In addition, population density and accessibility of destination were negatively associated with ecological footprint.

4. Health-related outcomes of active transport

4.1 Controlled trials

A recent systematic review identified 2 randomized controlled trials in which individuals were randomly assigned either to an AT or a passive transport (PT) group (Oja et al., 2011). Specifically, in the first study, 68 Finnish adults who were classified as insufficiently active before the study were assigned either to a PT or an AT (walking or cycling) group. Individuals from the latter group were asked to engage in AT to work on every workday for 10 consecutive weeks (Oja et al., 1991). Participants accumulated an average of 1 hour of daily AT. Cardiovascular fitness (VO_2max) increased by 4.5% in the AT group, while cycling led to a greater improvement than walking (7% vs. 2%). Statistically significant

improvements were also noted for HDL cholesterol, blood lactate concentration during exercise and cardiovascular endurance in the AT group (Oja et al., 1991). In the second randomized controlled trial, 122 Dutch adults were assigned either to a PT or a cycling group for a 6 months period (Hendriksen et al., 2000). Maximal power output increased by 13% in both men and women, and VO_2max increased by 6% in men while, in the PT group, VO_2max decreased by 5-10%. In addition, despite no changes in body mass, there was a reduction in the percentage of body fat in the cycling group (Hendriksen et al., 2000).

In a Belgian non-randomized controlled trial, 65 middle-aged men and women were asked to cycle to work at least three times a week for a one year period, while the 15 participants from the control group were asked not to change their travel patterns (de Geus et al., 2009). Participants from the experimental group cycled 2.5 days per week for 45 minutes per day. Their maximal power output increased by 5%, but their VO_2max decreased by 1%, while corresponding figures in control participants were 2% and -7%. Albeit small, differences between groups were significant for both maximal power output and VO_2max, and individuals who cycled the most had greater improvements in fitness. As hypothesized by Oja et al. (2011), the smaller effect observed in this study compared to the 2 randomized controlled trials could be explained by lower cycling frequency and lower daily cycling time.

4.2 Prospective studies

Andersen and colleagues (2000) assessed the relationship between cycling to work and all-cause mortality among a cohort of 6 954 Danish adults. The relative risk of mortality was 0.72 (95% CI 0.57-0.91) among the cyclists, even after adjusting for physical activity, cholesterol and triglyceride levels, body mass index, blood pressure, education level, smoking status, gender, and age at the beginning of the study. Similarly, a prospective study of 75 221 women aged 40-70 from seven communities in Shanghai has shown lower rates of all-cause mortality after 5.7 years of follow-up. The relative risk of mortality was 0.66 (95% CI 0.40-1.07) among the women who cycled the most when adjusted for a similar range of potential confounders (Matthews et al., 2007).

Gordon-Larsen and colleagues (2009) examined the prospective impact of AT to work on body composition, cardiovascular disease risk factors and cardiovascular fitness among 2364 participants from the Coronary Artery Risk Development in Young Adults that were followed for 20 years. When controlling for age, race, income, education, smoking, examination center and physical activity index, men who used AT to work had a reduced risk of obesity (OR = 0.50; 95% CI = 0.33-0.76), lower triglyceride levels (OR = 0.88; 99% CI = 0.80-0.98), fasting insulin (OR = 0.86; 95% CI = 0.78-0.93) and diastolic blood pressure (OR = -1.67; 95% CI = -3.20;-0.15). Furthermore, both men and women who used AT had greater cardiovascular fitness as measured by time to exhaustion on a treadmill test.

Hu and colleagues (2005) prospectively followed a cohort of 47 721 Finnish adults aged 25-64 and without history of coronary heart disease, stroke or cancer at baseline. They found that compared to participants who did not used AT, those who used AT for 1-29 minutes per day (RR = 0.92; 95% CI = 0.84-1.01) and those who engaged in 30 minutes of more of daily AT (RR = 0.89; 95% CI = 0.80-0.98) were less likely to have suffered a stroke during the 19 years of follow-up. In the same cohort, AT to work was also associated with a reduced risk of coronary heart disease in women, but not in men (Hu et al., 2007).

Using a prospective case-control study design, Wennberg et al. (2010) found that car commuting was associated with a markedly increased risk of myocardial infarction (OR = 1.77; 95% CI = 1.05-2.99), even when adjusting for smoking, education level, leisure time physical activity, occupational physical activity, hypertension and diabetes. The effect of AT was partly mediated by variables such as BMI, the ratio of apolipoprotein B/apolipoprotein A-1 and other inflammatory and hemostatic biomarkers.

In line with these findings, a meta-analysis of prospective epidemiological studies has indicated that individuals who use AT have an 11% lower risk of cardiovascular events including mortality, coronary heart disease, stroke, hypertension and diabetes (Hamer & Chida, 2008). However, differences were more pronounced in women (RR = 0.87; 95% CI = 0.77-0.98) than in men (RR = 0.91; 95% CI = 0.80-1.04) and direct comparison of studies is complicated by the inclusion of different endpoints.

Wen and Rissel (2008) examined the association between different modes of transport to work and the risk of overweight and obesity in a representative sample of 6810 Australian adults. The prevalence of overweight (39.8% vs. 60.8%; OR=0.49; 95% CI 0.31-0.76) and obesity (5.4% vs. 15.5%; OR = 0.34; 95% CI = 0.13-0.87) was significantly lower among men who cycled to work. No such differences were seen in women, of whom only 0.33% cycled to work. There were also no difference between individuals who walked to work and those who drove.

Among children, data from the 322 children that participated to the 6-year follow-up of the Danish arm of the European Youth Heart Study indicated a positive relationship between cycling to school and cardiovascular fitness (Cooper et al., 2008). Children who cycled at both time points and those who changed from non-cycling to cycling had a 9% greater maximal aerobic power than those who did not cycle at any time point and those who stopped cycling. However, no difference in BMI was observed in this study, and children who walked to school did not have greater fitness than those who were driven. A more recent analysis of the same dataset revealed longitudinal associations between cycling to school and lower waist circumference, serum glucose and insulin (Andersen et al., 2011). Cyclists were less resistant to insulin according to the homeostasis model assessment (e.g. HOMA), and their ratio of HDL to total cholesterol was also lower. Differences in other risk factors were not significant, but overall, the clustered risk of cardiovascular disease was markedly lower among cyclists.

4.3 Cross-sectional studies and literature reviews

Pucher and colleagues (2010) assessed whether the mode share of AST was associated with the prevalence of obesity and diabetes and with the proportion of individuals meeting the PA guidelines in 14 different countries, all 50 states in the US, and 47 of the 50 largest American cities. They found large negative correlations (r = -0.45 to -0.8) between the mode share of AT and obesity rates at the country, state and city levels. They also found that the prevalence of diabetes was markedly lower and that more individuals were sufficiently active in cities and states with higher mode share of AT.

Using data from the Montréal Origin-Destination survey, Morency and Demers (2009) determined the number of trips of less than 1 km made by children aged 5-14 (N = 16 837) and estimated the number of steps per day that these trips would involve if they were

substituted by walking. Their findings indicate that 31.2% of the daily trips were < 1 km and that 33.0%of these trips were motorized. Overall, these trips would require an average of 2238 steps per child, which translates into 16.6% of the recommended volume of daily physical activity.

Faulkner and colleagues' (2009) systematic review has shown that AT to and from school was associated with a higher level of objectively measured physical activity level among children and adolescents in 11 out of 13 studies. A more recent systematic review has evaluated the associations between AT to and from school, PA, body composition and cardiovascular fitness (Larouche et al., submitted). Currently, 78% of studies have shown that active commuters accumulate significantly more daily PA than passive commuters. A dose-response relationship such that active commuters who lived further away from school accumulated more PA than those who lived closer has been found in two of the reviewed studies (Panter et al., 2011; van Sluijs et al., 2009).

However, there remains inconclusive evidence regarding the association between AT to and from school and body composition outcomes (Larouche et al., submitted). This is not very surprising because body weight regulation is a very complex phenomenon (Jéquier & Tappy, 1999; Keith et al., 2006) and even the evidence on the association between overall physical activity levels and body weight remains conflicting (Harris et al., 2009). Further, the energy expenditure associated with AT can be compensated by changes in other energy-balance related behaviors during the day (i.e. by eating more or by spending more time in sedentary behaviors). However, all reviewed studies have shown that cycling was associated with greater physical fitness, while associations were less consistent for walking or AT in general (e.g. combined walking and cycling) (Larouche et al., submitted).

5. Correlates of active transportation

Despite the potential of AT to reduce GHG emissions while improving many indicators of public health, the proportion of individuals using active modes of transportation remains very low in several countries. While several initiatives have been implemented to promote utilitarian walking and cycling, few of these have been evaluated rigorously. Systematic reviews of interventions to promote walking and cycling as an alternative to driving have indicated modest positive changes (Ogilvie et al., 2004; Yang et al., 2010). Furthermore, few studies have sought to determine the factors associated with changes in travel mode (Hume et al., 2009; Owen et al., 2004).

Altogether, these limitations in current knowledge highlight the importance of examining more carefully the correlates of AT. While a detailed review of the correlates of AT is beyond the scope of this book, a brief description of the main correlates is provided for five different levels of influence according to the ecological model: the built and physical environment[4], public policies, communities and organizations, interpersonal factors, and personal factors.

[4] The built environment refers to "the physical features of the urban landscape (i.e. alterations to the natural landscape) that collectively define the public realm, which might be as modest as a sidewalk or an in-neighborhood retail shop or as large as a new town." (Cervero & Kockelman, 1997).

5.1 Built and physical environment correlates

Several reviews highlight strong associations between elements of the built environment, the mode share of active transport and the number of vehicle miles travelled (Larouche & Trudeau, 2010; Saelens & Handy, 2008; Sallis et al., 2006). The term "walkability" is often used by urban planners and researchers to refer to the ability to walk to certain destinations within the neighborhood (Sallis et al., 2006). The 3D model proposed by Cervero and Kockelman (1997) is a central component in most indices of walkability (Sallis et al., 2006). The three components of this model are: 1) Density (e.g. the amount of individuals or households within a given area); 2) Diversity (often referred to as land-use mix or the variety of destination within a given area); and 3) Design (which includes various attributes such as street connectivity, sidewalks and cycling infrastructure, aesthetics, etc.).

There is consistent evidence supporting the associations between density and land-use mix with adults' travel mode (Ewing et al., 2003; Frank et al., 2006; Saelens & Handy, 2008). Pooling data from the 206 992 adult participants to the 1998, 1999 and 2000 Behavioral Risk Factor Surveillance System, Ewing et al. (2003) assessed the relationship between urban sprawl and physical activity, obesity and morbidity in 448 counties and 83 metropolitan areas in the US. The county sprawl index was positively associated to body mass index and hypertension, and negatively associated with time spent walking. Another American study reported that individual who lived in neighborhoods characterized by high walkability accumulated 70 more minutes of weekly PA than those who lived in less walkable neighborhoods (Saelens et al., 2003). However, studies that examined the impact of design on travel mode have found conflicting results (Saelens & Handy, 2008; Sallis et al., 2006). Another caveat of the walkability construct is neighborhood self-selection; i.e. active individuals may decide to live in walkable areas (Handy et al., 2006).

Amongst children and adolescents, a systematic review of 14 studies which measured environmental correlates of AT to/from school with geographic information systems has shown that distance was the only consistent correlate (Wong et al., 2011). There was conflicting evidence regarding the impact of density and diversity, suggesting that these constructs may not be as relevant as for adults. The mode share of AT to/from school also tends to be lower in secondary schools students who generally need to travel greater distances (Pabayo et al., 2008, 2011).

5.2 Public policies

Differences between countries in the mode share of cycling are particularly striking. For example, the proportion of trips made by bicycle varies from about 1% in countries such as USA, UK, Australia and Canada to 18% in Denmark and 27% in the Netherlands (Pucher & Buehler, 2008). Further the mode shares of cycling for distances < 2.5 km, 2.5-4.4 km and 4.5-6.4 km in the Netherlands are respectively 37%, 37% and 24%, while corresponding figures in the US are 2%, 1% and 0.4%. These large variations can be partly explained by differences between countries in factors such as the provision of cycling infrastructure, the quality of public transit networks, gas prices and other expenses associated with car ownership, and urban planning practices (Banister, 2008; Chapman, 2007).

From an historical perspective, the industrial revolution has led to a major increase in the population of cities and infectious diseases spread rapidly in overcrowded neighborhoods

in which individuals were exposed to high concentrations of coal and other pollutants (Frumkin et al., 2004). To address this public health issue, urban planning policies were implemented to segregate factories from households. Nevertheless, urban areas of the early 20th century were still generally favorable to AT: density was moderate to high, land-use mix was the norm and streets were built in a grid-like fashion which facilitates navigation. Then, after World War II, urban planning policies primarily focused on car-oriented development which has led to increasing urban sprawl and decreasing density, land-use mix and street connectivity. Hence, Turcotte (2008) reported that newer homes where located further away from the city center based on findings from the 2006 Canadian census. This type of development has led to major reductions in the mode share of AT (Frumkin et al., 2004; King et al., 2002).

In contrast, to address the environmental and public health issues associated with car-oriented development, Northern European countries adopted a series of policies to promote AT and reduce car travel in the middle of the 1970s, as described by Pucher and Buehler (2008). These policies have led to 20-43% increases in the mode share of AST in cities such as Amsterdam and Groningen (Netherlands), Copenhagen and Odense (Denmark) and Berlin and Muenster (Germany), and large reductions in the relative risk of traffic injuries were observed.

5.3 Communities and organizations

Local communities can promote AT through different strategies, including the provision of walking and cycling infrastructure (Dill & Carr, 2003; Pucher et al., 2010), bike-sharing schemes (DeMaio, 2009), parking restrictions (Pucher & Buehler, 2008) and Safe Routes to School and/or walking school buses schemes (Heelan et al., 2009; Hinckson & Badland, 2011). Moreover, Giles-Corti (2006) argues that the inclusive or exclusive nature of the social environment fosters the social norm that may increase or decrease the likelihood of PA in general or AT specifically – and that car-oriented development favors social exclusion. It has also been proposed that increasing social cohesion could lead to more "eyes on the street" (Jacobs, 1961), which could favor children's independent mobility and AT.

Workplaces can also play a role in the promotion of AT. For example, a workplace-based social marketing campaign in a large Finnish factory (N = 1256 employees) achieved a 7% increase in the proportion of workers using AT (Oja et al., 1998). Australian researchers examined the influence of workplaces on travel mode among 888 adults (Wen et al., 2010). Respondents whose workplace encouraged AT were significantly less likely to drive to work than those without such encouragement (49% vs. 73%; OR = 0.41; 95% CI = 0.23-0.73). In contrast, participants who had access to convenient parking near their workplace were almost 5 times more likely to drive. In Belgium, a similar survey revealed that individuals who reported that their workplace offered safe bicycle parking spots and showers were more likely to cycle to work (de Geus et al., 2008).

5.4 Interpersonal factors

According to Bandura's (1986) social cognitive theory, human behavior is strongly influenced by modeling and by social interactions with significant others. In support of this theory, researchers have found that individuals whose friends and/or family members

engaged in AT were more likely to walk or cycle for utilitarian purposes (de Geus et al., 2007; Titze et al., 2007). Similarly, social support has been shown to be positively related to AT (Ball et al., 2007; Titze et al., 2008).

In addition, current theoretical frameworks assume that parents are the key decision makers for their children's mode of transportation to school (McMillan, 2005; Panter et al., 2008). To further explore this decision making process, Faulkner et al. (2010) conducted semi-structured interviews with 37 parents. Their findings suggest that, after deciding if their children needed to be escorted, parents typically chose the mode of transport that they perceived to be the quickest and most convenient. Other studies have shown that parental concerns about road safety are inversely related with children's likelihood of walking or cycling to school (Davison et al., 2008; Panter et al., 2008).

5.5 Personal factors

Several studies have shown that men were more likely than women to use AT and this gender difference tends to be much greater for cycling (Bell et al., 2006; Davison et al., 2008; Garrard et al., 2008). Interestingly, in countries with higher mode shares of cycling, no gender differences were observed whereas in Australia, US, UK and Canada, less than 30% of bike trips are made by women (Pucher & Buehler, 2008). Australian researchers suggested that this situation may reflect higher risk aversion among women; underscoring the importance of developing safe cycling infrastructure to promote commuter cycling among women (Garrard et al., 2008). Perceptions of lack of time (Oja et al., 1998; Shannon et al., 2006), car ownership (Ogilvie et al., 2008; Wen et al., 2010), road safety concerns (Garrard et al., 2008; Panter et al., 2008; Titze et al., 2007) and hilly routes (Troped et al., 2003) have also been associated with lower rates of AT. While weather conditions are often cited as a barrier to AT (Humpel et al., 2004), it is noteworthy that the Scandinavian countries all have cycling mode shares above 10%, while cycling is much less common in Mediterranean countries, US and Australia (Pucher & Buehler, 2008).

In contrast, studies have consistently shown a positive association between self-efficacy perceptions and AT (Ball et al., 2007; de Geus et al., 2008; Sallis et al., 2006; Troped et al., 2003). Other personal factors that may favor AT include the desire to be physically active or to increase fitness (Oja et al., 1998; Shannon et al., 2006; Titze et al., 2007), intentions and habits to walk or cycle (Lemieux & Godin, 2009), and environment-friendly attitudes (Bopp et al., 2011; de Geus et al., 2008).

6. The nexus between the environment and public health

As highlighted by McMichael and Butler (2011), there is currently a paradox between the increasing disruptions of the global environments (i.e. rising GHG emissions, oversized ecological footprint, acidification of the oceans, destruction of stratospheric ozone, degradation of arable land, depletion of freshwater supplies, loss of biodiversity, etc.) and the improvement in indices of population health (especially life expectancy). They further explain: "*The factors that have historically underpinned population health gains are now, by dint of their much increased scale, scope, and intensity undermining sustainable good health as we exceed Earth's capacity to renew, replenish, provide and restore*" (McMichael and Butler, 2011). Hence, profound changes in lifestyle will likely be required to avoid widespread societal collapse,

like it has happened several times in history, albeit at a much smaller scale (Weiss & Bradley, 2001).

As the transport sector is currently one of the most important contributors of climate change (Unger et al., 2010) while PT represents a significant health risk, it is fair to consider that transport practices represent a major nexus between the environment and public health. In other words, interventions promoting AT as a source of physical activity also have important environmental implications and, inversely, GHG emissions policies aiming to reduce car use would have major public health implications.

One factor that may play a determinant role with respect to both GHG emissions and indicators of public health is the likely occurrence of "peak oil" which is defined as "*the maximum rate of the production of oil in any area under consideration, recognizing that it is a finite natural resource subject to depletion*"[5] While some authors perceive peak oil as a great opportunity to promote healthier modes of transport (Demers, 2008; Frumkin et al., 2004; Younger et al., 2008), others are less optimistic (Hanlon & McCartney, 2008; Kaza et al., 2011). Nevertheless, the impacts of peak oil are difficult to forecast given the uncertainty associated with its occurrence, its impact on gas price, the rapidly increasing oil demand from developing countries, the availability of alternative fuels and their actual impact on pollutant emissions, the public policies that will be implemented by different countries, etc.

The gas embargo of the 1970s show that countries can use different strategies in order to adapt to the rising price of gas (Mapes, 2009). In the US, sales of bicycles literally doubled in the 2 years following the embargo, but once gas prices dropped, bicycle sales plummeted, and the mode share of cycling remained very low thereafter. In contrast, this crisis made Dutch policy makers realize that they did not have control over their gas supplies so, after the embargo was over, they maintained high fuel taxes and invested massively in the development of infrastructure for alternative modes of transportation (Mapes, 2009).

Another insightful example in this regard is the fuel shortage experienced during Cuba's "special period" following the collapse of the Soviet Union in the early 1990s (Franco et al., 2008) which has led to a major increase in the mode share of AT. The proportion of physically active individuals increased from 30 to 67%, while the prevalence of obesity declined from 14 to 7% and large reductions in mortality from diabetes (-51%), coronary heart disease (-35%), stroke (-20%) and all-cause mortality (-18%) were observed. However, a neuropathy outbreak affected 50 000 individuals in 1992-1993, but its impact amongst children, pregnant women and the elderly was minimized by a special rationing system. These historical examples suggest that different countries will implement different strategies in response to peak oil, and these strategies may have markedly different environmental and public health impacts.

6.1 The case for health impact assessment studies

Health impact assessment studies represent a promising strategy to simultaneously assess the environmental and health-related impacts of AT policies and interventions (de Nazelle et al., 2011). As illustrated in Figure 2, a comprehensive framework has been proposed to integrate the impact of policies/interventions on: 1) the behavioral changes (including

[5] For more details, see: http://www.peakoil.net/about-peak-oil

changes in modes of transport); 2) the environment (i.e. air pollution, greenhouse gases); and 3) the health risks and benefits resulting from the interaction between behavioral changes and environmental exposures. It is anticipated that such an approach could allow researchers and policy-makers to examine if a given intervention can achieve improvements in the health status of individuals while providing environmental co-benefits.

However, only a few such assessments have been conducted to date (de Nazelle et al., 2011). First, Dutch researchers simulated the impact on all-cause mortality if 500 000 individuals would switch from car travel to cycling for short trips on a daily basis (de Hartog et al., 2010). Their findings indicate that the benefits from increased PA (3-14 months gained) would be much greater than the mortality resulting from greater doses of inhaled air pollution (0.8-40 days lost) and the potential increase in traffic accidents (5-9 days lost). Furthermore, such a change in mode of transportation would result in air quality improvements that would benefit the whole population.

A second health impact assessment study was conducted for the Bicing bike-sharing scheme in Barcelona, Spain which was implemented in 2007 as a strategy to reduce traffic congestion (Rojas-Rueda et al., 2011). By August 2009, 182 062 residents had subscribed (about 11% of the population), of which 28 251 were considered regular users (Rojas-Rueda et al., 2011). It was estimated that the Bicing initiative led to an annual reduction of 9 062 344 kg of CO_2. The health impact assessment predicts that Bicing would cause 0.16 deaths/year because of traffic accidents and inhalation of air pollution, but it would prevent 12.46 deaths/year due to increased physical activity (benefit-risk ratio = 77). Considering that bike-sharing schemes have been implemented in several cities in Europe, Asia and North America (DeMaio, 2009), these initiatives could have positive impacts both for population health and climate change mitigation.

The findings of these health impact assessment studies are coherent with the "safety in number" principle which suggests that a mode of transport becomes safer as more people use it (Jacobsen, 2003; Tin Tin et al., 2011). This principle also has its corollary: when less people use a mode of transport, it tends to become more dangerous. In this regard, the number of cycling injuries has increased while per capita time spent cycling decreased during the last decade in New Zealand (Tin Tin et al., 2011).

Jacobsen's (2003) power law model predicts that, if a community was to double its mode share of AT, the relative risk of injury for each walker or cyclist would drop to 0.66. At the community level, the rate of injury would increase by 32% for a 100% increase in the mode share of AT. It is noteworthy that the relationship between the mode share of AT and rates of injuries is non-linear and tends to vary between communities. Furthermore, Elvik (2009) argued that due to the non-linearity of risk, very large transfers of trips from motorized modes to AT could lead to a reduction in the absolute number of reported accidents.

Among children and adolescents, various schemes such as "Safe Routes to School" and walking school buses have been implemented to promote AT while reducing the risk of injuries (Davison et al., 2008). In the mid-1970s, Denmark had the highest child pedestrian accident rate in Europe (Appleyard, 2003). To address this issue, the city of Odense invested in the creation of an extensive network of pedestrian and bicycle paths, narrowed roads, added traffic islands, and mandated all of its 45 schools to identify specific road-safety issues. After ten years, child pedestrian and cyclist casualties had decreased by 80% and this

program was implemented at the national level. Moreover, studies have repetitively shown that more than 60% of Danish adolescents cycle to school (Andersen et al., 2011). School travel planning was also very successful in the UK where pedestrian and cyclist casualties felt by 77% and 28% respectively (Appleyard, 2003).

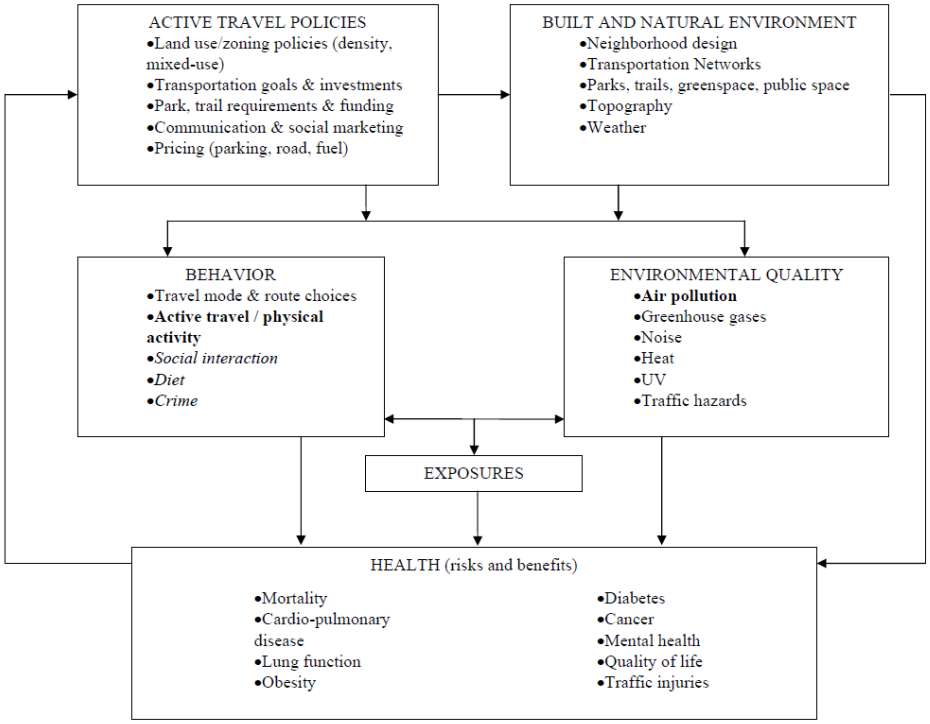

Fig. 2. Conceptual model of health impacts of active travel policies. In bold are shown behavioral and environmental quality variables recognized as having strongest exposure-health quantifications available, while variables in italics are the most uncertain to quantify. (Reproduced with permission from de Nazelle et al., 2011).

A recent systematic review of interventions promoting AT to school reported that most were effective in increasing the mode share of AT and/or decreasing driving (Chillón et al., 2011). However, the majority of these studies reported small effect sizes and most did not assess the broader impacts of the interventions on environmental and health-related outcomes.

These studies provide preliminary evidence to suggest that a transition from PT to AT could have rather positive environmental and health impacts. The magnitude of these impacts will likely depend on the degree of behavior change. For example, larger reduction in driving would achieve greater reductions in exhaust emissions and could decrease walkers' and cyclists' risk of accident to a greater extent. However, further studies will need to take into account socio-economic status because individuals living in deprived neighborhoods are typically exposed to higher concentration of pollutants (Marshall et al., 2009; Tonne et al.,

2008). Moreover, low income households and families with young children are likely to be more affected by a potential increase in the cost of food transportation caused by fuel scarcity (Kaza et al., 2011).

7. Limitation and strengths of present review

Overall, this review is limited by the lack of prospective intervention studies that examined the impact of policies aimed at reducing greenhouse gases emissions. In the absence of such studies, simulations provide an interesting alternative to examine the impact of large-scale changes in transportation practices. However, simulations are limited by their reliance on highly uncertain assumptions about factors such as the potential for behavioral change, the occurrence of peak oil, the confounding variables not accounted for, and the magnitude of technological innovations.

While there has been a lot of studies on the correlates of AT, few of these have rigorously examined the factors associated with changes in travel mode. This may partly explain the modest success of interventions that sought to increase the mode share of AT. The findings of the current review nevertheless suggest that more comprehensive interventions tend to be more effective, highlighting the need for better integrated policies to promote AT and reduce the mode share of PT.

In addition the use of the social-ecological approach for the description of the correlates of AT can be perceived both as a strength and as a limitation. This model allows the consideration of a wide range of factors located at different levels of influence emphasizing the interactions between different variables (McLeroy et al., 1988; Sallis et al., 2006). However, ecological models can be criticized for being too complicated; rendering the identification of intervention targets more difficult (Stokols, 1996).

The main strength of the current review is the broadness of its scope which allowed a simultaneous examination of both the environmental and the public health impacts of AT. Further, this review summarizes the increasing evidence supporting the positive association between AT and several indicators of public health including increased PA and physical fitness, and decreased morbidity and all-cause mortality. This body of evidence should therefore be useful for policy-makers to justify investments to promote AT by the perspective of combined environmental and public health benefits. Haines et al. (2010) argue that such policies should be more cost-effective and socially attractive than strategies addressing climate change or public health separately.

8. Conclusion

The share of the global CO_2 emissions attributable to the transport sector is increasing steadily while the level of motorization is rising rapidly in developing countries (International Transport Forum, 2010). In this context, the present review sought to examine the impact of transportation strategies to reduce emissions of GHG and other pollutants. Few studies have used a rigorous experimental or natural experiment design and current investigations assessed localized interventions (i.e. the congestion schemes in central London and Stockholm) or exceptional measures taken for reducing traffic congestion during the Olympic Games in Atlanta and Beijing. However, simulations and observational

studies provide preliminary evidence suggesting that transport policies could achieve considerable reductions in GHG emissions.

The second objective of this chapter was to summarize the literature on the health benefits of AT. Altogether, the reviewed studies suggest that increasing the mode share of AT may lead to multiple health benefits (i.e. declines in the risk of obesity, cardiovascular diseases, diabetes, hypertension, cancer, etc.). The benefits vary across studies, but importantly, all available health impact assessment studies have concluded that the benefits of increasing the mode share of AT largely outweighed the risks (de Hartog et al., 2010; de Nazelle et al., 2011; Rojas-Rueda et al., 2011). Moreover, controlled trials have consistently shown that commuter cycling led to improved cardiovascular fitness. The findings from another randomized controlled trial suggest that lifestyle-oriented physical activity (such as AT) can result in greater compliance than structured physical activity programs (Dunn et al., 1999).

Despite this wide range of potential benefits, the mode share of AT is exceedingly low in most industrialised countries except The Netherlands, Germany and the Scandinavian countries. This highlights the necessity of developing a better understanding of the correlates of AT in order to increase the effectiveness of interventions to promote AT.

Current models that predict the choice of travel mode (i.e. Panter et al., 2008; Sallis et al., 2006) are rooted in the social ecological theory. Based on this theory, intervening only by trying to convince individuals to change their transport behaviors would likely be effective only among individuals who are highly receptive to this message (i.e. those who have a high degree of concerns about environmental issues). In this context, Banister (2008) argues that a paradigm shift from the "conventional approach" to transport planning (or car-oriented development) towards a sustainable mobility paradigm (or people-oriented development) is urgently needed. However, to achieve such a paradigm shift, it is necessary to gain public acceptability in order to drive social and political action (Banister, 2008).

The example of Northern European countries suggests that it is feasible to achieve public acceptability. Furthermore, the cities that had the most success in increasing the mode share of AT are those that implemented comprehensive multi-level strategies (Pucher et al., 2008, 2010). Such strategies can include a combination of incentives to individuals who adopt active transportation (i.e. tax credits), an increased availability of sidewalks, cycle paths, improved public transport systems, an increased community/organizational support for active transportation (i.e. provision of safe places to store bicycles, showers in workplaces), traffic calming strategies, policies to increase the cost of car use (e.g. increased fuel taxes or reduced availability of car parking), and well-designed social marketing campaigns (Oja & Vuori, 2000; Pucher et al., 2010).

As noted in the 'limitations and strengths' section, there is a clear need for more prospective intervention studies in order to increase the overall quality of evidence. In this regard, future studies should: 1) assess in a more comprehensive fashion the effectiveness of AT interventions and their impact on environmental variables (including GHG emissions) and health-related outcomes; and 2) identify key variables associated with changes in travel modes to inform the design of more effective interventions.

Although stronger proof of effectiveness from experimental studies and natural experiments would increase the quality of evidence and may potentially increase public acceptability, it

should not be viewed as a reason to maintain car-oriented development. First, large increases of motorization in developing countries such as China and India, coupled with the status quo in developed countries are expected to lead to major increases in GHG emissions (Woodcock et al., 2007, 2009). The transport sector already accounts for 23% of worldwide CO_2 emissions. Second, exposure to vehicle exhaust gases is strongly associated with cardiovascular morbidity and mortality (Brook et al., 2010). Third, there is already strong evidence supporting that commuter cycling leads to significant increases in cardiovascular fitness, which is an important cardiovascular disease risk factor (Oja et al., 2011). Fourth, due to the safety in number principle, an increase in the mode share of AT typically leads to a decrease in the relative risk of traffic injury for each commuter (Jacobsen, 2003).

Further, there are economic reasons supporting a shift to the sustainable mobility paradigm. First, Stern's (2006) review illustrated that if we do not act now to reduce the magnitude of climate change, the price to pay would approximate 5 to 20% of the global GDP each year. In contrast, reducing greenhouse gas emissions to avoid the worst consequences of climate change would cost only 1% of the global GDP per year. Second, current evidence suggests that investments in AT-related infrastructure are highly cost-effective (Cavill et al., 2008; Gotschi, 2011). Therefore, by attacking several of today's most important environmental and health problems, AT is a powerful strategy that should not be overlooked by policy-makers. Hence, "*Levels of cycling can be seen as a measure of progress towards a healthier sustainable future in both the developed and the developing world*" (Woodcock et al., 2007).

9. Acknowledgements

Richard Larouche is a member of the Healthy Active Living and Obesity Research Group at the Children's Hospital of Eastern Ontario and a doctoral student at the University of Ottawa. He holds a Frederick Banting and Charles Best Canada Graduate Scholarship from the Canadian Institutes of Health Research. Publication of this book chapter was supported by the University of Ottawa Author Fund.

10. References

Andersen, L.B., Schnohr, P., Schroll, M. & Hein, H.O. (2000). All-cause mortality associated with physical activity during leisure time, work, sports, and cycling to work *Archives of Internal Medicine*, Vol.160, No.11 (June 2000), pp. 1621-1628, ISSN 0003-9926

Andersen, L.B., Wedderkopp, N., Kristensen, P., Moller, N.C., Froberg, K. & Cooper, A.R. (2011). Cycling to school and cardiovascular risk factors: a longitudinal study. *Journal of Physical Activity and Health*, Vol.8, No. (November 2011), pp. 1025-1033. ISSN 1543-3080

Appleyard, B. (2003). Planning Safe Routes to School. *Planning*, Vol.69, No.5 (May 2003), pp.34-37. ISSN 0001-2610

Ball, K., Timperio, A., Salmon, J., Giles-Corti, B., Roberts, R. & Crawford, D. (2007). Personal, social and environmental determinants of educational inequalities in walking. *Journal of Epidemiology and Community Health*, Vol.61, No.2 (February 2007), pp. 108-114. ISSN 0143-005X

Bandura, A. (1986) *Social foundations of thought and action: a social cognitive theory*. Englewoods Cliff, New Jersey: Prentice Hall. ISBN 013815614X

Banister, D (2008). The sustainable mobility paradigm. *Transport Policy*, Vol.15, No.2 (March 2008), pp. 73-80, ISSN 0967-070X

Bauman, A., Sallis, J. F., Dzewaltowski, D. A. & Owen, N. (2002). Toward a better understanding of the influences on physical activity: the role of determinants, correlates, causal variables, mediators, moderators, and confounders. *American Journal of Preventive Medicine*, Vol.23 No.2 (August 2002), pp. S5-S14, ISSN 0749-3797

Bell, C., Garrard, J., & Swinburn, B. (2006). Active transport to work in Australia: is it all downhill from here? *Asia Pacific Journal of Public Health*, Vol.18, No.1 (March 2006), pp. 62-68, ISSN 1010-5395

Bopp, M., Kaczynski, A.T., & Wittman, P. (2011). The relationship of eco-friendly attitudes with walking and biking to work. *Journal of Public Health Management and Practice*, Vol.17, No.5 (September/October 2011), pp. E9-E17, ISSN 1078-4659

Bronfenbrenner, U. (1979). The ecology of human development: Experiments by nature and design. Cambridge, Mass: Harvard University Press. ISBN 0674224566.

Brook, R.D., Rajagopalan, S., Pope III, A., Brook, J.R., Bhatnagar, A. et al. (2010). Particulate matter air pollution and cardiovascular disease: an update to the scientific statement from the American Heart Association. *Circulation*, Vol.121 (June 2010), pp. 2331-2378, ISSN 0009-7322

Brunekreef, B., & Holgate, S.T. (2002). Air pollution and health. *Lancet*, Vol.360, No.9341 (October 2002), pp. 1233-1242, ISSN 0140-6736

Buliung, R.N., Mitra, R., & Faulkner, G. (2009). Active school transportation in the Greater Toronto Area, Canada: An exploration of trends in space and time (1986-2006). *Preventive Medicine*, Vol.48, No.6 (June 2009), pp. 507-512, ISSN 0091-7435

Cavill, N., Kahlmeier, S., Rutter, H., Racioppi, F. & Oja, P. (2008). Economic analyses of transport infrastructure and policies including health effects related to cycling and walking: A systematic review. *Transport Policy*, Vol.15, No.5 (September, 2008), pp. 291-304, ISSN 0967-070X

Cervero, R. & Kockelman, K. (1997). Travel demands and the 3Ds: Density, diversity and design. *Transportation Research Part D: Transport and Environment*, Vol.2, No.3 (September 1997), pp. 199-219, ISSN 1361-9209

Chapman, L. (2007). Transport and climate change: A review. *Journal of Transport Geography*, Vol.15, No.5 (September 2007), pp. 354-367, ISSN 0966-6923

Chillón, P., Evenson, K.R., Vaughn, A. & Ward, D.S. (2011). A systematic review of interventions for promoting active transportation to school. *International Journal of Behavioral Nutrition and Physical Activity*, Vol.8, No.10, ISSN 1479-5868 http://www.ijbnpa.org/content/pdf/1479-5868-8-10.pdf

Colley, R.C, Garriguet, D., Janssen, I., Craig, C.L., Clarke, J. & Tremblay, M.S. (2011). Physical activity of Canadian children and youth: Accelerometer results from the 2007 to 2009 Canadian Health Measures Survey. *Health Reports*, Vol.22, No.1 (March 2011), pp. 15-23, ISSN 0840-6529

Colley, R.C, Garriguet, D., Janssen, I., Craig, C.L., Clarke, J. & Tremblay, M.S. (2011). Physical activity of Canadian adults: Accelerometer results from the 2007 to 2009

Canadian Health Measures Survey. *Health Reports*, Vol.22, No.1 (March 2011), pp. 7-14, ISSN 0840-6529

Cooper, A.R., Wedderkopp, N., Jago, R., Kristensen, P.L., Moller, N.C., et al. (2008). Longitudinal associations of cycling to school with adolescent fitness. *Preventive Medicine*, Vol.48, No.3 (September 2008), pp. 324-328, ISSN 0091-7435

Davison, K.K., Werder, J.L, & Lawson, C.T. (2008). Children's active commuting to school: current knowledge and future directions. *Preventing Chronic Diseases*, Vol.5, No.3 (July 2008), pp. 1-11, ISSN 1545-1151

de Geus, B., de Bourdeaudhuij, I., Jannes, C., & Meeusen, R. (2008). Psychosocial and environmental factors associated with cycling for transport among a working population. *Health Education Research*, Vol.23, No.4 (August 2008), pp. 697-708, ISSN 0268-1153

de Geus, B., Joncheere, J., & Meeusen, R. (2009).Commuter cycling: effect on physical performance in untrained men and women in Flanders: minimum dose to improve indexes of fitness. *Scandinavian Journal of Medicine & Science in Sports*, Vol. 19, No.2 (April 2009), 179-187, ISSN 1600-838

de Hartog, J.J., Boogaard, H., Nijland, H. & Hoek, G. (2010). Do the health benefits of cycling outweigh the risks? *Environmental Health Perspectives*, Vol.118, No.8 (August 2010), pp. 1109-1116, ISSN 0091-6765

de Nazelle, A., Morton, B.J., Jerret, M., & Crawford-Brown, D. (2010). Short trips: an opportunity for reducing mobile-source emissions? *Transportation Research Part D*, Vol.15, No.8 (December 2010), pp.451-457, ISSN 1361-9209

de Nazelle, A., Nieuwenhuijsen, M.J., Anto, J.M., Brauer, M., Briggs, D., et al. (2011). Improving health through policies that promote active travel: A review of evidence to support health impact assessment. *Environment International*, Vol.37, No.4 (May 2011), pp. 766-777, ISSN 0160-4120

DeMaio, P. (2009). Bike-sharing: History, impacts, models of provision and future. *Journal of Public Transport*, Vol.12, No.4, pp. 41-56, ISSN 1077-291X

Demers, M., (2008) Pour une ville qui marche: Aménagement urbain et santé. Montréal, Québec : Écosociété ISBN 978-2-923165-35-6

Dill, J., & Carr, T. (2003). Bicycle commuting and facilities in major U.S. cities: if you build them, commuters will use them. *Transportation Research Record*, Vol.1828 (January, 2003), pp. 116-123, ISSN 0361-1981

Dunn, A.L., Marcus, B.H., Kampert, J.B., Garcia, M.E., Kohl III, H.W. & Blair, S.N. (1999). Comparison of lifestyle and structured interventions to increase physical activity and cardiorespiratory fitness: a randomized controlled trial. *Journal of the American Medical Association*, Vol.281, No.4 (January 1999), 327-334. ISSN 1538-3598

Elvik, R. (2009). The non-linearity of risk and the promotion of environmentally sustainable transport. *Accident Analysis & Prevention*, Vol.41, No.4 (July 2009), pp. 849-855, ISSN 0001-4575

Ewing, R., Schmid, T., Killingsworth, R., Zlot, A., & Raudenbush, S. (2003). Relationship between urban sprawl and physical activity, obesity and morbidity. *American Journal of Health Promotion*, Vol.18, No.1 (January 2003), pp. 47-57 ISSN 0890-1171

Faulkner, G.E.J., Buliung, R.N., Flora, P.K. & Fusco, C. (2009). Active school transport, physical activity levels and body weight of children and youth: A systematic Review. *Preventive Medicine*, Vol.48, No.1 (January 2009), pp. 3-8, ISSN 0091-7435

Faulkner, G.E.J., Richichi, V., Buliung, R.N., Fusco, C., & Moola, F. (2010). What's "quickest and easiest"?: parental decision making about school trip mode. *International Journal of Behavioral Nutrition and Physical Activity*, Vol.7, No.62, ISSN 1479-5868. http://www.biomedcentral.com/content/pdf/1479-5868-7-62.pdf

Franco, M., Ordunez, P., Caballero, B., & Cooper, R.S. (2008). Obesity reduction and its possible consequences : what can we learn from Cuba's special period? *Canadian Medical Association Journal*, Vol.178, No.8 (April 2008), pp.1032-1034, ISSN 0820-3946

Frank, L.D., Stone, B.J., & Bachman, W. (2000). Linking land use with household vehicle emissions in the central Puget Sound: Methodological framework and findings. *Transportation Research Part D*, Vol.5, No.3 (May 2000), pp. 173-190, ISSN 1361-9209

Frank, L.D., Sallis, J.F., Conway, T.L., Chapman, J.E., Saelens, B.E. & Bachman, W. (2006). Many pathways from land use to health – associations between neighborhood walkability and active transportation, body mass index, and air quality. *Journal of the American Planning Association*, Vol.72, No.1 (Winter 2006), pp. 75-87. ISSN 0194-4363

Frank, L.D., Saelens, B.E., Powell, K.E. & Chapman, J.E. (2007). Stepping towards causation: do built environments or neighborhood and travel preferences explain physical activity, driving, and obesity? *Social Science & Medicine*, Vol.65, No.9 (November 2007), pp.1898-1914. ISSN 0277-9536

Frank, L.D., Greenwald, M.J., Winkelman, S., Chapman, J. & Kavage, S. (2010). Carbonless footprints: promoting health and climate stabilization through active transportation. *Preventive Medicine*, Vol.50, No.1 (Suppl.) (January 2010), pp.99-105, ISSN 0091-7435

Friedenreich, C. M., & Orenstein, M. R. (2002). Physical activity and cancer prevention: Etiologic evidence and biological mechanisms. *Journal of Nutrition*, Vol.132, No.11 (November 2002), pp. 3456S-3364S, ISSN 0022-3166

Friedman, M.S., Powell, K.E., Hutwagner, L., Graham, L.M. & Teague, W.G. (2001). Impact of changes in transportation and commuting behaviors during the 1996 Summer Olympic Games in Atlanta on air quality and childhood asthma. *Journal of the American Medical Association*, Vol.285, No.7 (July 2001), pp. 897-905. ISSN 0098-7484

Frumkin, H., Frank, L. & Jackson, R. *Urban sprawl and public health: Designing, planning, and building for healthy communities*. Washington, DC: Island Press. ISBN 1-55963-305-0

Garrard, J., Rose, G., Lo, S.J. (2008). Promoting transportation cycling for women: the role of bicycle infrastructure. *Preventive Medicine*, Vol.46, No.1 (January 2008), pp.55-59, ISSN 0091-7435

Giles-Corti, B. (2006). People or places: what should be the target? *Journal of Science and Medicine in Sports*, Vol.9, No.5 (October 2006), pp. 357-366, ISSN 1440-2440

Gordon-Larsen, P., Boone-Heinonen, J., Sidney, S., Sternfeld, B., Jacobs, D.R. Jr. & Lewis, C.E. (2009). Active commuting and cardiovascular disease risk: The CARDIA study. *Archives of Internal Medicine*, Vol.169, No.13 (July 2009), pp. 1216-1223, ISSN 0003-9926

Gotschi, T. (2009). Costs and benefits of bicycling investments in Portland, Oregon. *Journal of Physical Activity and Health*, Vol.8, No.1 (Suppl.) (January 2010), pp. S49-S58, ISSN 1543-3080

Grize, L., Bringolf-Isler, B., Martin, E., Braun-Fahrländer, C. (2010). Trends in active transport to school among Swiss school children and its associated factors: three

cross-sectional surveys 1994, 2000 and 2005. *International Journal of Behavioral Nutrition and Physical Activity*, Vol.7, No.28, ISSN 1479-5868. http://www.ijbnpa.org/content/7/1/28.

Haines, A., McMichael, A.J., Smith, K.R., Roberts, I., Woodcock, J. et al. (2010). Public health benefits of strategies to reduce greenhouse-gas emissions: Overview and implications for policy makers. *Lancet*, Vol.374, No.9707 (January 2010), pp. 2104-2114, ISSN 0140-6736

Hamer, M. & Chida, Y. (2008). Active commuting and cardiovascular risk: a meta-analytic review. *Preventive Medicine*, Vol.46, No.1 (January 2008), pp. S9-S13, ISSN 0091-7435

Handy, S.L., Cao, X. & Mokhtarian, P.L. (2005). Correlation or causality between the built environment and travel behavior? Evidence from Northern California. *Transportation Research Part D*, Vol.10, No.6 (November 2005), pp. 427-444, ISSN 1361-9209.

Handy, S.L., Cao, X., & Mokhtarian, P.L. (2006). Self-selection in the relationship between the built environment and walking. *Journal of the American Planning Association*, Vol.72, No.1 (Winter 2006), pp.55-74. ISSN 0194-4363

Hanlon, P., & McCartney, G. (2008). Peak oil: will it be public health's greatest challenge. *Public Health*, Vol.122, No.7 (July 2008), pp. 647-652, ISSN 0033-3506

Harris, K.C., Kuramoto, L.K., Schulzer, M, & Retallack, J.E. (2009). Effect of school-based physical activity interventions on body mass index in children: a meta-analysis. *Canadian Medical Association Journal*, Vol.180, No.7 (July 2008), pp. 719-726, ISSN 0820-3946

Heelan, K.A., Abbey, B.M., Donnely, JE., Mayo, M.S. & Welk, G.J. (2009). Evaluation of a walking school bus for promoting physical activity in youth. *Journal of Physical Activity and Health*, Vol.6, No.5 (September 2009), pp. 560-567, ISSN 1543-3080

Hendriksen, I.J.M., Zuiderveld, B., Kemper, H.C.G. & Bezemer, P.D. (2000). Effect of commuter cycling on physical performance of male and female employees. *Medicine & Science in Sports and Exercise*, Vol.32, No.2 (February 2000), pp. 504-510. ISSN 0195-9131

Hinckson, E.A. & Badland, H.M. (2011). School travel plans: Preliminary evidence for changing school-related travel patterns in elementary school children. *American Journal of Health Promotion*, Vol.25, No.6 (July 2011), pp.368-371, ISSN 0890-1171

Horton, R. (2007). Righting the balance: energy for health. *Lancet*, Vol.370, No.9591 (September 2007), pp. 921, ISSN 0140-6736

Hu, G., Sarti, C., Jousilahti, P., Silventoinen, K., Barengo, N.C. & Tuomilehto, J. (2005). Leisure time, occupational, and commuting physical activity and the risk of stroke. *Stroke*, Vol.36, No.9 (September 2005), pp. 1994-1999, ISSN 0039-2499

Hu, G., Jousilahti, P., Borodulin, K., Barengo, N.C., Lakka, T.A., Nissinen, A. & Tuomilehto, J. (2007). Leisure time, occupational, and commuting physical activity in relation to coronary heart disease among middle-aged Finnish men and women. *Atherosclerosis*, Vol.194, No.2 (October 2007), pp. 490-497, ISSN 0021-9150

Hume, C., Timperio, A., Salmon, J., Carver, A., Giles-Corti, B. & Crawford, D. (2009). Walking and cycling to school: Predictors of increase among children and adolescents. *American Journal of Preventive Medicine*, Vol.36, No.3 (March 2009), pp. 195-200, ISSN 0749-3797

Humpel, N., Owen, N, Iverson, D., Leslie, E. & Bauman, A. (2004). Perceived environmental attributes, residential location, and walking for particular purposes. *American Journal of Preventive Medicine*, Vol.26, No.2 (February 2004), pp. 119-125, ISSN 0749-3797

Jacobs, J. (1961). The death and life of great American cities. New York: Random House. ISBN 9780679741954

Jacobson, P.L. (2003). Safety in numbers: more walkers and bicyclists, safer walking and bicycling. *Injury Prevention*, Vol.9, No.3 (September 2003), pp. 205-209, ISSN 1353-8047

Jéquier, E. & Tappy, L. (1999). Regulation of body weight in humans. *Physiological Reviews*, Vol.79, No.2 (April 1999), pp. 451-480, ISSN 0031-9333

Johanssen, C., Burman, L. & Forsberg, B. (2009). The effects of congestions tax on air quality and health. *Atmospheric Environment*, Vol.43, No.31 (October 2009), pp. 4843-4854, ISSN 1352-2310

Kaza, N., Knaap, G.J., Knaap, I., & Lewis, R. (2011). Peak oil, urban form, and public health: exploring the connections. *American Journal of Public Health*, Vol.101, No.9 (September 2011), pp.1598-1606, ISSN 1541-0048

Keith, S.W., Redden, D.T., Katzmarzyk, P.T., Boggiano, M.M., Hanlon, E.C. et al. (2006). Putative contributors to the secular increase in obesity: exploring the roads less travelled. *International Journal of Obesity*, Vol.30, No.11 (June 2006), pp. 1585-1594, ISSN 0307-0365

King, A.C., Stokols, D., Tahen, E., Brassington, G.S. & Killingsworth, R. (2002). Theoretical approaches to the promotion of physical activity: forging a transdisciplinary paradigm. *American Journal of Preventive Medicine*, Vol.22, No.2 (February 2002), pp. S15-S25, ISSN 0749-3797

International Transport Forum (2010). *Reducing transport greenhouse gas emissions: Trends and data 2010*. Leipzig, Germany. http://www.internationaltransportforum.org/Pub/pdf/10GHGTrends.pdf

Larouche, R. & Trudeau, F. (2010). Étude des impacts du transport actif sur la pratique d'activités physiques et la santé et de ses principaux déterminants. *Science & Sports*, Vol.25, No.5 (November 2010), pp. 227-237. ISSN 0765-1597

Larouche, R., Saunders, T.J., Faulkner, G.E.J., Colley, R.C. & Tremblay, M.S. (submitted). Associations between active school transport and physical activity, body composition and cardiovascular fitness: a systematic review of 57 studies. *Journal of Physical Activity and Health*. ISSN 1543-3080

Lemieux, M., & Godin, G. (2009). How well do cognitive and environment variables predict active commuting? *International Journal of Behavioral Nutrition and Physical Activity*, Vol.6, No.12, ISSN 1479-5868 http://www.biomedcentral.com/content/pdf/1479-5868-6-12.pdf

Levy, J.I., Buonocore, J.J., & von Stackelberg, K. (2010). Evaluation of the public health impacts of traffic congestion: A health risk assessment. *Environmental Health*, Vol.9, No.65, ISSN 1476-069X http://www.ehjournal.net/content/9/1/65

Lobstein, T., Baur L. & Uauy, R. (2004). Obesity in children and young people: a crisis in public health. *Obesity Reviews,* Vol.5 No.1 Suppl. (May 2004), 4-85, ISSN 1467-7881

Manson, J.E., Greenland, P.E., LaCroix, A.Z., Stefanick, M.L., Mouton, C.P., et al. (2002). Walking compared with vigorous exercise for the prevention of cardiovascular

events in women. *New England Journal of Medicine*, Vol.347, No.10 (September 2002), pp. 716-725. ISSN 0028-4793

Mapes, J. (2009). Pedaling revolution: how cyclists are changing American cities. Corvallis, OR: Oregon State University Press, ISBN 978-0-87071-419-1

Marshall, J.D., Brauer, M. & Frank, L.D. (2009). Healthy neighborhoods: walkability and air pollution. *Environmental Health Perspectives*, Vol.117, No.11 (November 2009), pp.1752-1759, ISSN 0091-6765

Marshall, J.D., Wilson, R.D., Meyer, K.L., Rajangam, S.K., McDonald, N.C. & Wilson, E.J. (2010). Vehicle emissions during children's school commuting: Impact of education policy. *Environmental Science & Technology*, Vol.44, No.5 (January 2010), pp. 1537-1543, ISSN 0013-936X

Matthews, C.E., Juri, A.L., Shu, X.O., Li, H.L., Yang, G., Li, Q., Gao, Y.T. & Zheng, W. (2007). Influence f exercise, walking, cycling, and overall nonexercise physical activity on mortality in Chinese women. *American Journal of Epidemiology*, Vol.165, No.12 (June 2007), pp.1343-1350, ISSN 0002-9262

McDonald, N.C. (2007). Active transportation to school: Trends among U.S. schoolchildren, 1969-2001. *American Journal of Preventive Medicine*, Vol.32, No.6 (June 2007), pp. 509-516, ISSN 0749-3797

McLeroy, K.R., Bibeau, D., Steckler, A. & Glanz, K. (1988). An ecological perspective on health promotion programs. *Health Education Quarterly*, Vol.15, No.4 (Winter 1988), pp. 351-377, ISSN 0195-8402

McMichael, A.J., Butler, C.D. (2011). Promoting global population health while constraining the environmental footprint. *Annual Reviews of Public Health*, Vol.32, (April 2011), pp. 179-197, ISSN 0136-9529

McMillan, T.E. (2005). Urban form and a child's trip to school: The current literature and a framework for future research. *Journal of Planning Literature*, Vol.19, No.4 (May 2005), pp. 440-456, ISSN 0885-4122

Morency, P. & Demers, M. (2009). Active transportation as a way to increase physical activity among children. *Child: Care, Health and Development*, Vol. 36, No.3 (May 2010), pp. 421-427, ISSN 1365-2214

Muniz, I., & Galindo, A. (2005). Urban form and the ecological footprint of commuting. The case of Barcelona. *Ecological Economics*, Vol.55, No.4 (December 2005), pp. 499-514, ISSN 0921-8009

Ogilvie, D., Egan, M., Hamilton, V. & Petticrew, M. (2004). Promoting walking and cycling as an alternative to using cars: systematic review. *British Medical Journal*, Vol.329, No.7469 (October 2004), pp.763-766, ISSN 0959-8146

Ogilvie, D., Mitchell, R., Mutrie, N., Petticrew, M., & Platt, S. (2008). Personal and environmental correlates of active travel and physical activity in a deprived urban population. *International Journal of Behavioral Nutrition and Physical Activity*, Vol.5, No.43, ISSN 1479-5868 http://www.ijbnpa.org/content/5/1/43

Oja, P., Mänttäri, A., Heinonen, A., Kukkonen-Harjula, K., Laukanen, R., Pasanen, M. & Vuori, I. (1991). Physiological effects of walking and cycling to work. *Scandinavian Journal of Medicine & Science in Sports*, Vol.1, No.3 (September 1991), pp. 151-157, ISSN 1600-838

Oja, P. & Vuori, I., & Paronen, O. (1998). Daily walking and cycling to work: their utility as health enhancing physical activity. *Patient Education and Counselling*, Vol.33, No.1 (April 1998), pp. S87-S94, ISSN 0738-3991

Oja, P. & Vuori, I. (2000). *Promotion of transport walking and cycling in Europe: strategy directions*. Tampere, Finland: UKK Institute for Health Promotion Research. http://www.panh.ch/hepaeurope/materials/HEPA%20Walking%20and%20Cycling%20Strategy%20.pdf

Oja, P., Titze, S., Bauman, A., de Geus, A., Krenn, P., Reger-Nash, B., & Kohlberger, T. (2011). Health benefits of cycling: Systematic review. *Scandinavian Journal of Medicine & Science in Sports*, Vol.21, No.4 (August 2011), pp.496-509, ISSN 1600-838

Owen, N., Humpel, N., Leslie, E., Bauman, A. & Sallis, J.F. (2004). Understanding environmental influences on walking: Review and research agenda. *American Journal of Preventive Medicine*, Vol.27, No.1 (July 2004), pp. 67-76, ISSN 0749-3797

Paffenbarger, R.S. Jr., Hyde, R.T., Wing, A.L., Lee, I., Jung, D.L. & Kampert, J.B. (1993). The association of changes in physical activity level and other lifestyle characteristics with mortality among men. *New England Journal of Medicine*, Vol.328, No.8 (February 1993), pp.538-545, ISSN 0028-4793

Pabayo, R. & Gauvin, L. (2008). Proportion of students who use various modes of transportation to and from school in a representative population-based sample of children and adolescents, 1999. *Preventive Medicine*, Vol.46, No.1 (January 2008), pp. 63-66, ISSN 0091-7435

Pabayo, R., Gauvin, L. & Barnett, T.A. (2011). Longitudinal changes in active transportation to school in Canadian youth aged 6 through 16 years. *Pediatrics*, Epub 2011 Jul 4. ISSN 0031-4005

Panter, J.R., Jones, A.P., van Sluijs & E.M.F. (2008). Environmental determinants of active travel in youth: A review and framework for future research. *International Journal of Behavioral Nutrition and Physical Activity*, Vol.5, No.34, ISSN 1479-5868 http://www.ijbnpa.org/content/5/1/34/

Panter, J.R., Jones, A.P., van Sluijs, E.M.F. & Griffin, S.J. (2011). The influence of distance to school on the association between active commuting and physical activity. *Pediatric Exercise Science*, Vol.23, No.1 (March 2011), pp. 72-86, ISSN 1541-0048

Pucher, J. & Buehler, R. (2008). Making cycling irresistible: Lessons from The Netherlands, Denmark and Germany. *Transport Reviews*, Vol.28, No.4 (July 2008), pp. 495-528, ISSN 0899-8493

Pucher, J., Dill, J. & Handy, S. (2010). Infrastructures, programs and policies to increase bicycling: an international review. *Preventive Medicine*, Vol.50, No.1 (January 2010), pp. S106-S125, ISSN 0091-7435

Pucher, J., Buehler, R., Bassett, D.R. Jr. & Dannenberg, A.L. (2010). Walking and cycling to health: A comparison of recent evidence from cities, states, and international studies. *American Journal of Public Health*. Vol.100, No.10 (October 2010), pp. 1986-1992, ISSN 1541-0048

Rojas-Rueda, D., de Nazelle, A., Tainio, M. & Nieuwenhuijsen, M.J. (2011). The health risks and benefits of cycling in urban environments compared with car use: health impact assessment study. *British Medical Journal*. Epub ahead of print, August 4, 2011, ISSN 0959-8138

Saelens, B.E., Sallis, J.F., Black, J.B., & Chen, D. (2003). Neighborhood-based differences in physical activity: an environment scale evaluation. *American Journal of Public Health*, Vol.93, No.9 (September 2003), pp. 1552-1558, ISSN 1541-0048

Saelens, B.E. & Handy, S.L. (2008). Built environment correlates of walking: A review. *Medicine and Science in Sports & Exercise*, Vol.40, No.7 (Supplement 7) (July 2008), pp. S550-S566, ISSN 0195-9131

Sallis, J.F., Cervero, R.B., Ascher, W., Henderson, K.A., Kraft, M.K. & Kerr, J. (2006). An ecological approach to creating active living communities. *Annual Reviews of Public Health*, Vol.27, (April 2006), pp. 297-322, ISSN 0163-7525

Shannon, T., Giles-Corti, B., Pikora, T., Bulsara, M., Shilton, T., & Bull, F. (2006). Active commuting in a university setting: assessing commuting habits and potential for modal change. *Transport Policy*, Vol.13, No.3 (May 2006), pp. 240-253, ISSN 0967-070X

Sigal, R.J., Kenny, G.P., Wasserman, D.H., Castaneda-Sceppa, D. & White, R.D. (2006). Physical activity / Exercise and type 2 diabetes: A consensus statement from the American Diabetes Association. *Diabetes Care*, Vol.29, No.6 (June 2006), pp. 1433-1438, ISSN 0149-5992

Stern, N. (2006). *Stern review on the economics of climate change*. London: HM Treasury. http://mudancasclimaticas.cptec.inpe.br/~rmclima/pdfs/destaques/sternreview_report_complete.pdf

Stokols, D. (1996). Translating social ecological theory into guidelines for community health promotion. *American Journal of Health Promotion*, Vol.10, No.4 (March-April 1996), pp. 282-298, ISSN 0890-1171

Tin Tin, S., Woodward, A., Thornley, S. & Ameratunga, S. (2011). Regional variations in pedal cyclist injuries in New Zealand: safety in numbers or risk in scarcity? *Australian and New Zealand Journal of Public Health*, Vol.35, No.4 (August 2011), pp.357-363. ISSN 1753-6405

Titze, S., Stronneger, W.J., Janschitz, S., & Oja, P. (2007). Environmental, social and personal correlates of cycling for transportation in a student population. *Journal of Physical Activity and Health*, Vol.4, No.1 (January 2007), pp. 66-79, ISSN 1543-3080

Titze, S., Stronneger, W.J., Janschitz, S., & Oja, P. (2008). Association of built-environment, social-environment and personal factors with bicycling as a mode of transportation among Austrian city dwellers. *Preventive Medicine*, Vol.47, No.3 (September 2008), pp. 252-259, ISSN 0091-7435

Tonne, C., Beevers, S., Armstrong, B., Kelly, F. & Wilkinson, P. (2008). Air pollution and mortality benefits of the London Congestion Charge: spatial and socioeconomic inequalities. *Occupational Environmental Medicine*, Vol.65, No.9 (September 2008), pp. 620-627, ISSN 1470-7926

Troiano, R.P., Berrigan, D., Dodd, K.W., Mâsse, L.C., Tilert, T. & McDowell, M. (2008). Physical activity in the United States measured by accelerometers. *Medicine & Science in Sports & Exercise*. Vol.40, No.1 (January 2008), pp. 181-188, ISSN 0195-9131

Troped, P., Saunders, R.P., Pate, R.R., Reininger, B., & Addy, C.L. (2003). Correlates of recreational and transportation physical activity among adults in a New England community. *Preventive Medicine*, Vol.37, No.4 (October 2003), pp.304-310, ISSN 0091-7435

Turcotte, M. (2008). Dépendance à l'automobile dans les quartiers urbains. Tendances Sociales Canadiennes, Vol.1, No.1, p.21-32, ISSN 1481-1642 http://www.statcan.gc.ca/pub/11-008-x/2008001/article/10503-fra.pdf

Unger, N., Bond, T.C., Wang, J.S., Koch, D.M., Menon, S. et al. (2010). Attribution of climate forcing to economic sectors. *Proceedings of the National Academy of Science*, Vol.107, No.8 (February 2010), pp. 3382-3387, ISSN 1091-6490

US Environmental Protection Agency. (1999). *The transportation and environmental impacts of infill vs. greenfield development: a comparative case study analysis*. Washington, DC: Urban and Economic Development Division, U.S. Environmental Protection Agency. http://www.epa.gov/smartgrowth/pdf/infill_greenfield.pdf

van der Ploeg, H.P., Merom, D., Corpuz, G., & Bauman, A.E. (2008). Trends in Australian children travelling to school 1971-2003: Burning petrol or carbohydrates? *Preventive Medicine*, Vol.46, No.1 (January 2008), pp. S60-S62, ISSN 0091-7435

van Sluijs, E.M.F., Fearne, V.A., Mattocks, C., Riddoch, C., Griffin, S.J., Ness, A. (2009). The contribution of active travel to children's physical activity levels: Cross-sectional results from the ALSPAC study. *Preventive Medicine*, Vol.48, No.6 (June 2009), pp. 519-524, ISSN 0091-7435

Wang, Y., Hao, J., McElroy, M.B., Munger, J.W., Ma, H., Chen, D., Nielsen, C. P. (2009). Ozone air quality during the 2008 Beijing Olympics: effectiveness of emission restrictions. *Atmospheric Chemistry and Physics*, Vol.9, No.3 (January 2007), pp.5237-5251, ISSN 1352-2310

Wang, Y. & Lobstein, T. (2006). Worldwide trends in childhood overweight and obesity. *International Journal of Pediatric Obesity*, Vol.1, No.1, pp. 11-25, ISSN 1747-7166

Weiss, H. & Bradley, R.S. (2001). What drives societal collapse? *Science*, Vol.291, No.5504 (January 2001), pp.609-610, ISSN 0036-8075

Wen, L.M. & Rissel, C. (2008). Inverse associations between cycling to work, public transport, and overweight and obesity: findings from a population based study in Australia. *Preventive Medicine*, Vol.46, No.1 (January 2008), pp.29-32, ISSN 0091-7435

Wen, L.M., Kite, J., & Rissel, C. (2010). Is there a role for workplaces for reducing employees' driving to work? Findings from a cross-sectional survey from inner-west Sydney, Australia. *BMC Public Health*, Vol.10, No.50, ISSN 1471-2458 http://www.biomedcentral.com/content/pdf/1471-2458-10-50.pdf

Wennberg, P., Wensley, F., Johansson, L., Boman, K., Di Angelantonio, E., et al. (2010). Reduced risk of myocardial infarction related to active commuting: inflammatory and haemostatic effects are potential major mediating mechanisms. *European Journal of Cardiovascular Prevention and Rehabilitation*, Vol.17, No. 1 (February 2010), pp.56-62, ISSN 1741-8267

Woodcock, J., Banister, D., Edwards, P., Prentice, A.M. & Roberts, I. (2007). Energy and transport. *Lancet*, Vol.370 No.9592 (September 2007), pp. 1078-1088, ISSN 0140-6736

Woodcock, J., Edwards, P., Tonne, C., Armstrong, B.G., Ashiru, O. et al. (2009). Public health benefits of strategies to reduce greenhouse-gas emissions: urban land transport. *Lancet*, Vol.374, No.9705, pp.1930-1943 (December 2009), ISSN 0140-6736

Wong, B.Y.M., Faulkner, G. & Buliung, R. (2011). GIS measured environmental correlates of active school transport: A systematic review of 14 studies. *International Journal of*

Behavioral Nutrition and Physical Activity, Vol.8, No.39, ISSN 1479-5868 http://www.ijbnpa.org/content/pdf/1479-5868-8-39.pdf

Yang, L., Sahlqvist, S., McMinn, A., Griffin, S.J. & Ogilvie, D. (2010) Interventions to promote cycling: systematic review. *British Medical Journal*, Vol.341, No.5293 (October 2010), ISSN 0959-8146

Younger, M., Morrow-Almeida, H.R., Vindigni, S.M., & Dannenberg, A.L. (2008). The built environment, climate change, and health: opportunities for co-benefits. *American Journal of Preventive Medicine*, Vol.35, No.5 (November 2008), 517-526, ISSN 0749-3797

Zhou, W. & Szyliowicz, J.S. (2006). The development and current status of China's transportation system. *World Transport Policy & Practice*, Vol.12 No.4 (Setember 2006), pp. 10-16, ISSN 1352-7614

20

Arctic Sea Ice Decline

Julienne C. Stroeve and Walter Meier
National Snow and Ice Data Center, Cooperative Institute for Research in Environmental Sciences, University of Colorado, Boulder, CO, USA

1. Introduction

The Arctic is currently undergoing rapid environmental changes (ACIA, 2005; IPCC, 2007). One of the most striking of these changes is the decline in the floating sea ice cover. Sea ice is frozen sea water that forms in winter as temperatures drop and darkness sets over the northern high latitudes. At its winter maximum, roughly 14 to 16 million km^2 of the Northern Hemisphere ocean surface is covered by sea ice, extending as far south as Newfoundland, Canada (at 50^o latitude) along the eastern coast of Canada and as far south as Bohai Bay, China (at 38^o latitude) on the Eurasian side. During summer as temperatures warm, the ice cover shrinks to about half its winter size by September, covering on average 6 million km^2 (Figure 1).

Arctic sea ice is an important regulator of the exchange of heat and moisture between the atmosphere and the ocean. The presence of the sea ice cover insulates the relatively warm ocean from the colder atmosphere and because of its high reflectivity, its presence helps to keep the northern high latitudes cool by reflecting a large portion of the sun's energy back to space. Sea ice also exerts a strong influence on global atmospheric and oceanic circulation. Because of the Earth's orientation relative to the sun, the equator receives more incoming solar radiation than the poles. The inequality in the amount of solar radiation received gives rise to a temperature gradient that drives the circulation of air in the atmosphere that transports heat from the tropics to the poles.

During winter, there is little solar energy and sea ice acts as a very effective insulator, preventing heat in the Arctic Ocean from warming the lower atmosphere. During early spring, as the sun rises in the Arctic, but temperatures remain cold, the snow-covered sea ice remains frozen and may reflect more than 80 percent of the sun's energy back to space. As temperatures rise through the spring and summer, the snow melts, bare ice is exposed and melt ponds form, allowing for more of the sun's energy to be absorbed by the surface. However, even under these melt conditions the ice surface usually reflects 50% or more of the sun's energy. Additionally, since most of the solar energy absorbed by the ice in summer is used to melt ice, near surface air temperatures stay fixed near the freezing point. As the ice melts out completely in summer, the exposed darker ocean surface absorbs roughly 90 percent of the sun's incoming energy. This causes the oceans to warm up. Before the ice can once again reform in autumn, the ocean must first release the heat gained in summer back to the atmosphere, warming the lower troposphere.

The strong seasonal cycle of the Arctic sea ice cover not only affects our weather patterns, it also affects human activities and biological habitats. For example, hunters in the Arctic depend on the ice cover as a platform to hunt for Arctic mammals, such as seals, whales, walruses and polar bears. These species themselves depend on sea ice for their habitat, using the ice as places to breed, feed and hunt for food. The timing of the phytoplankton bloom, which supplies energy to the entire Arctic ecosystem, is also regulated by the timing of the ice retreat. Shipping companies are starting to take advantage of less sea ice in the summer to ship materials through the Arctic and the potential for extraction of natural resources, such as oil and natural gas, is also drawing increasing attention.

Over the past few decades, the Arctic has warmed at about twice the rate as the rest of the planet. As a result, significant changes are happening in the Arctic sea ice cover, with potentially large implications not only regionally but also for the global climate. This chapter discusses recent Arctic sea ice changes, the factors responsible for these changes, what climate models project for the future, and our current understanding of the climatic impacts of continued sea ice loss.

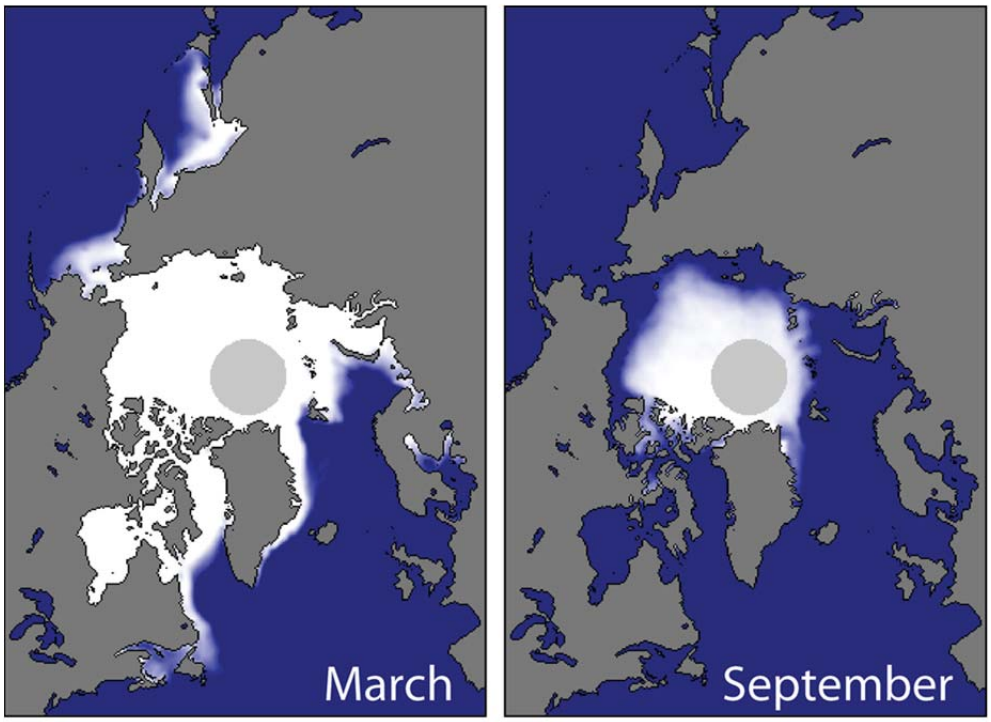

Fig. 1. March (left) and September (right) mean seasonal ice cover. The area in grey near the pole is the area not seen by the satellite sensor.

2. Recent changes in the Arctic sea ice cover

2.1 Ice extent

Before the satellite era, it was not easy to obtain reliable measurements of Arctic sea ice. The Arctic is remote and can be an inhospitable place. Early ship, submarine and aircraft observations provide some local information, but it wasn't until the late 1960s/early 1970s that satellites were able to provide the first broad look at changes in the sea ice cover. The modern passive microwave satellite data record further allowed for monitoring of ice conditions regardless of sunlight or cloud cover. Starting with the launch of NASA's Scanning Multichannel Microwave Radiometer (SMMR) satellite in October 1978, and continuing on with a series of Special Sensor Microwave/Imager (SSM/I) instruments on the Defense Meteorological Satellite Program (DMSP) satellites, scientists now have a consistent time-series of sea ice changes that spans nearly 34 years.

Analysis of this data record shows that since the late 1970s, the amount of sea ice covering the ocean has declined during all calendar months (Serreze et al., 2007). The trends are smallest in winter and strongest in late summer and early autumn (Figure 2). However, in recent years, the trend in the end-of-summer ice extent has accelerated. Every year since 2002 has been characterized by extreme September ice extent minima (Stroeve et al., 2008; Comiso et al., 2008; Stroeve et al., 2011a). Through 2001, the linear trend in September ice extent over the satellite record stood at -7.0% per decade. By 2010, it increased to -12.4% per decade. Yet another record or near-record low is expected for September 2011. This represents a ~40% reduction in the surface area of the Arctic Ocean covered by sea ice.

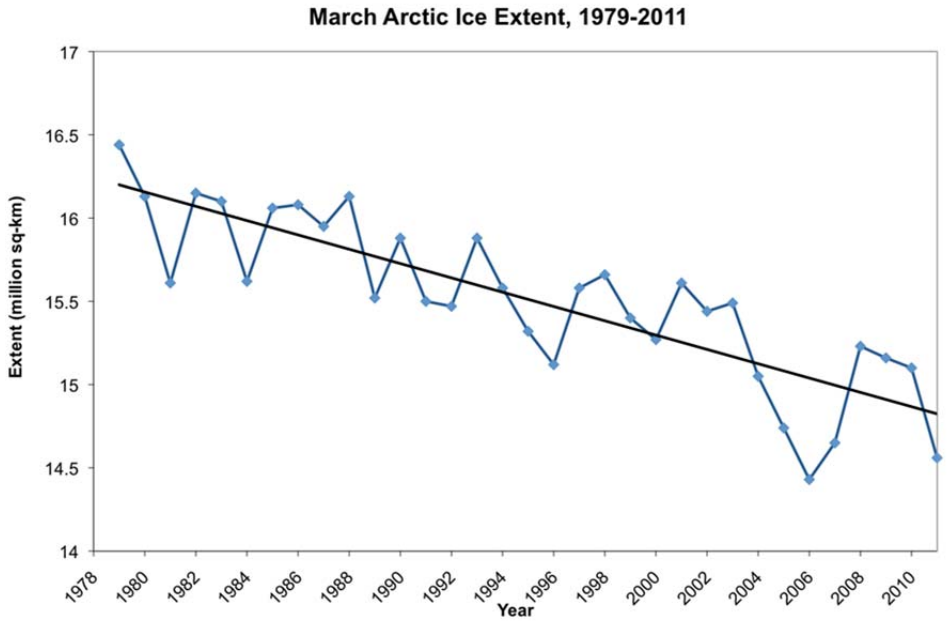

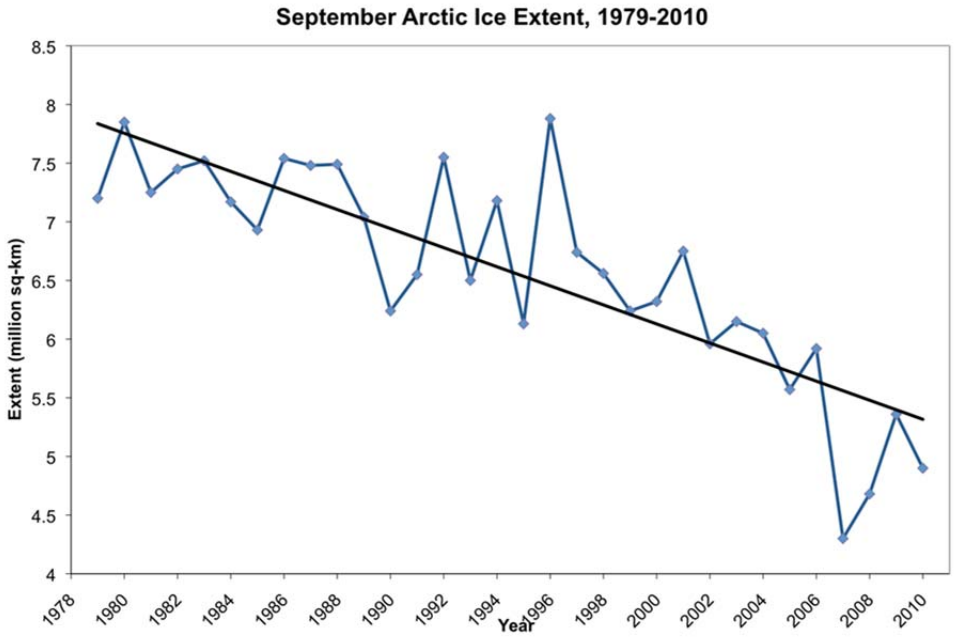

Fig. 2. Monthly mean March (top) and September (bottom) sea ice extent from 1979 through present derived from the passive microwave satellite data record and using the NASA Team sea ice algorithm.

During the 1980s and the 1990s, a low summer sea ice year would often be followed the next year by higher summer extents. In addition, the Arctic-wide low sea ice anomalies tended to be characterized by less ice the Eurasian side (i.e. Laptev or E. Siberian seas) with average or anomalously more sea ice on the Alaskan side (i.e. Chukchi and Beaufort seas) or vice versa. However, ice losses during the past decade have been characterized by pronounced sea ice retreat from both the Alaska and Siberia shores (Figure 3). The last several years have also seen opening up of the northern shipping routes. The last four summers saw opening of the Northern Sea Route, a shipping route that runs along the Russian Arctic coast from Murmansk on the Barents Sea to the Bering Strait and the Far East. Additionally, the Northwest Passage southern route, a waterway amidst the Canadian Arctic Archipelago was open the past five summers.

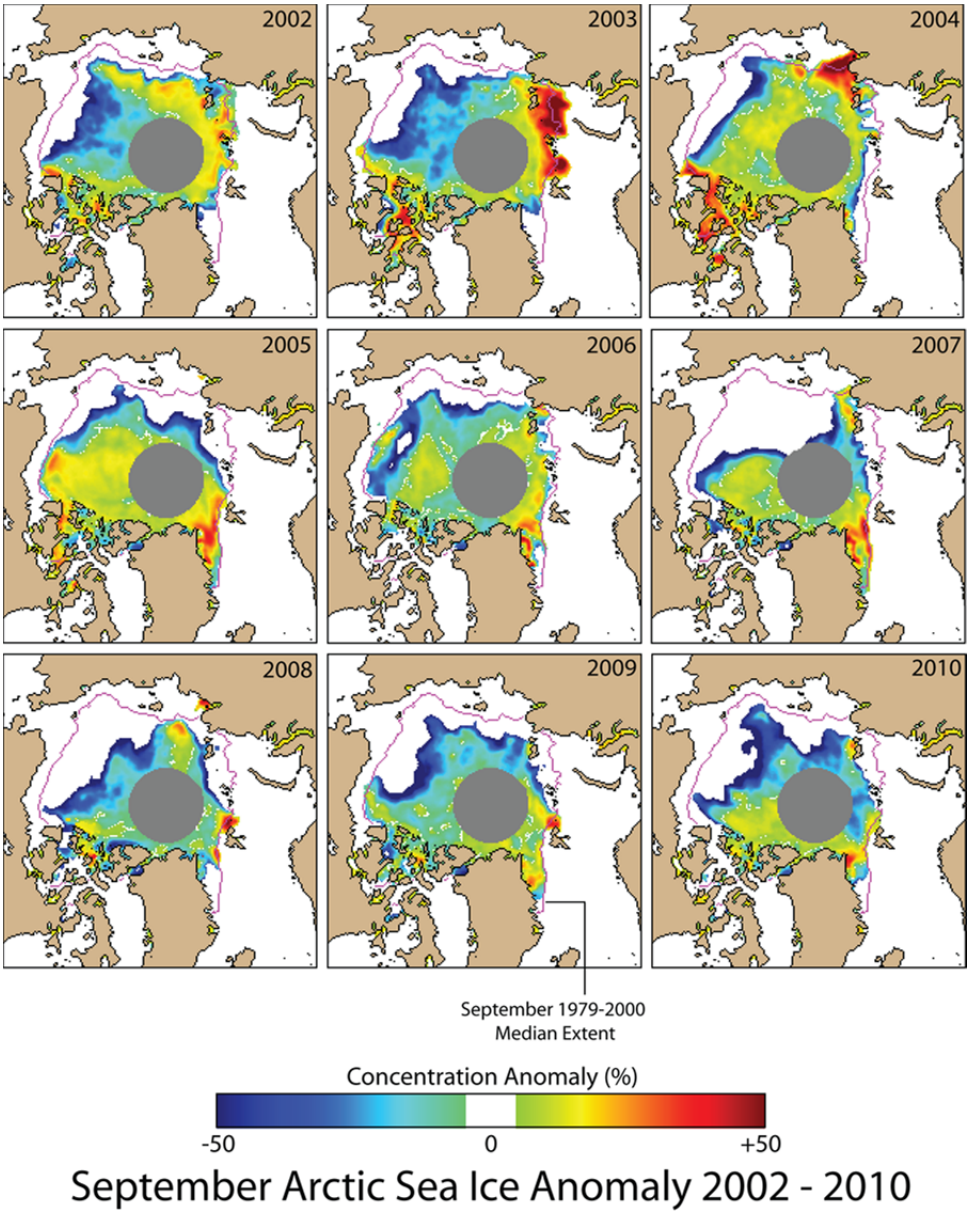

Fig. 3. Sea ice extent anomaly maps, 2002-2010: Sea ice conditions for the month of September, 2002 through 2010, derived from the NSIDC Sea Ice Index. Each image shows the concentration anomaly (see color key) and the 1979-2000 mean September ice edge (pink line). Nearly every year, the ice edge is well north of its mean position off the coasts of Alaska and Siberia. Image provided by National Snow and Ice Data Center, University of Colorado, Boulder.

2.2 Ice thickness

At the same time that the spatial coverage of the summer ice cover is shrinking, the ice cover is also thinning. Comparisons between early upward looking sonar aboard submarines (1958-1976) and those from 1993 to 1997 suggested a reduction of 1.3 m in the mean late summer ice thickness over much of the central Arctic Ocean [(Rothrock et al., 1999)]. However, sparse sampling has complicated the interpretation of wide-spread changes in the Arctic ice thickness. Rothrock et al. [(2003)] further analyzed the submarine data in conjunction with model simulations and found that there was a modest recovery in ice thickness after 1996. *In situ* measurements of thickness have been collected during short field experiments at scattered locations. These measurements have proven valuable for validation of submarine and satellite data, but do not provide useful information on the Arctic-wide sea ice thickness.

In recent years, satellites have allowed for further assessment of sea ice thickness changes. Giles et al. [(2008)] and Laxon et al. [(2003)] demonstrate the ability to derive ice thickness estimates from satellite radar altimetry (i.e., from the European Space Agency's (ESA) ERS1/2, Envisat) to an accuracy of 4 to 6 cm, excluding regions thin ice (below 0.5 m). These satellites have a latitudinal limit of 81.5°N but have proven valuable in assessing changes in ice thickness, with high correlations between derived ice thickness fields and submarine estimates of ice thickness (r=0.99) [(Laxon et al., 2003)]. Thickness estimates based on measurements taken by NASA's Ice, Cloud and land Elevation Satellite (ICESat) laser altimeter launched in January 2003 provide a further update on thickness changes during the time when large changes in the summer ice cover have occurred (satellite mission ended In 2009). Using this data in conjunction with the submarine thickness record, Kwok and Rothrock [(2009)] determined that the Arctic mean ice thickness declined from 3.64 meters in 1980 to 1.89 meters in 2008, or a total decline of 1.75 meters. CryoSat-2 is another radar altimeter instrument that was launched in April 2010 by ESA, but covers higher latitudes than the earlier radar altimeter satellites and has a 250 m resolution along the track. ICESat-2 is planned for launch early 2016. Together CryoSat-2 and ICESat-2 are expected to achieve improved accuracy in sea ice thickness retrievals over a broad spatial scale.

2.3 Ice age

The large decreases in summer sea ice extent in recent years [(e.g., Comiso et al., 2008; Stroeve et al., 2008; Stroeve et al., 2005)] further manifest a fundamental transition from a largely perennial ice cover where ice persists from year to year, to a seasonal coverage with substantial open water during summer [(e.g., Kwok, 2007; Maslanik et al., 2007a; Kwok and Cunningham, 2010)]. Using satellite-derived ice motion fields, the age of an individual ice parcel can be tracked by treating each grid cell that contains ice as an independent Lagrangian particle and advecting the particles at weekly time steps [(Fowler et al., 2004)]. In cases where particles of different ages fall within a single grid cell, the age of the grid cell is assigned to the oldest particle. These fields reveal a dramatic decline during the past 30 years in the Arctic's multiyear ice cover [(Figure 4]). The fraction of total ice extent made up of multiyear ice in March decreased from about 75% in the mid-1980s to 45% in 2011, while the proportion of the oldest ice (i.e. ice 5 years or older) declined from 50% of the multiyear ice pack to 10% [(Maslanik et al., 2011)]. Reductions in old ice now extend into the central Arctic Ocean and adjacent to the Canadian Archipelago, areas where the ice cover was

relatively stable prior to 2007 and where long-term survival of sea ice through summer is considered to be most likely.

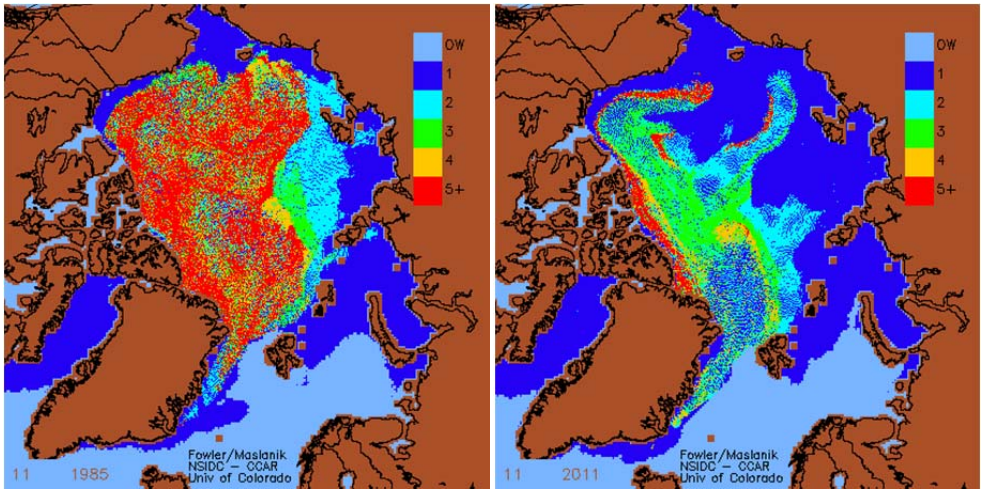

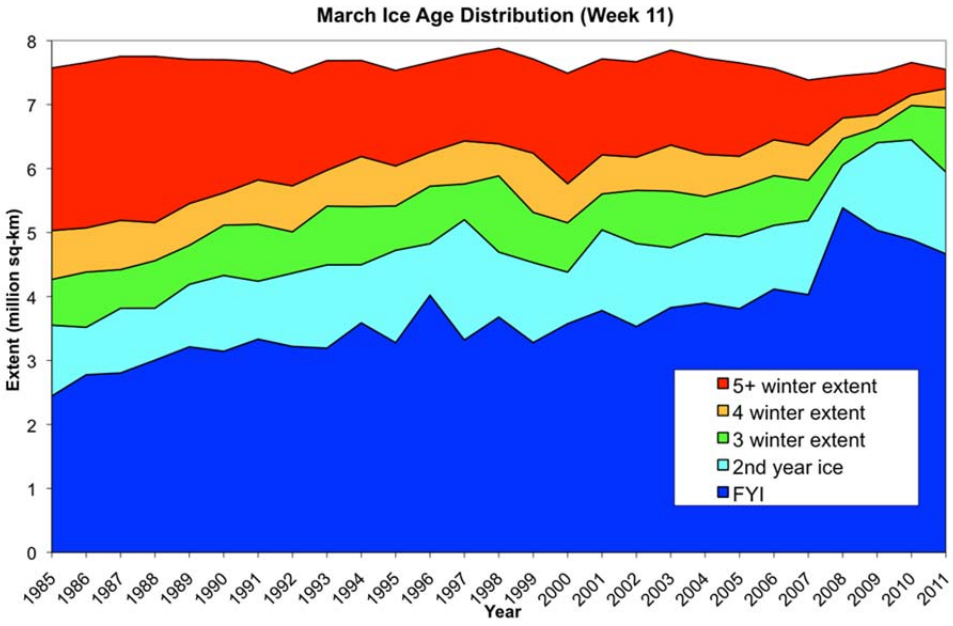

Fig. 4. Spatial distribution of ice of different age classes during March (week 11) in 1985 (top, left) and 2011 (top, right). Bottom figure shows the total extent of ice of different age classes for the Arctic Ocean domain. Data from C. Fowler and J. Maslanik, CCAR, University of Colorado.

Mapping the age of the sea ice not only provides a measure of how much the ice cover has transitioned from a largely perennial ice cover, where ice persists from year to year, to more of a seasonal coverage, it also provides an additional indication of sea ice thickness. Using February and March ICESat-derived thickness fields for the years 2003 and 2006, Maslanik et al. [(2007)] calculated mean ice thickness as a function of ice age. This comparison suggested a nearly linear relationship between age and thickness, with a 0.19 m yr^{-1} increase in thickness with age up to thickness values about 3 m, the approximate limit for thermodynamic ice growth. Thus, substituting these mean thicknesses for age at each grid cell provides an approximation of thickness, with the advantage of offering extended time coverage versus the ICESat data alone. Maslanik et al. [(2007)] suggested that using the ice age as a proxy for thickness shows that the Arctic has experienced significant thinning between the 1980s and 2006, corresponding to a ~40% reduction in ice volume.

3. Factors behind the sea ice decline

The decline in Arctic sea ice can be best explained from a combination of natural climate variability, such as variability in air temperature, atmospheric and oceanic circulation, and from external forcing due to rising concentrations of atmospheric greenhouse gases (GHGs) [(e.g. Serreze et al., 2007; Kay et al., 2011)]. Global climate models have long predicted the rise in atmospheric air temperatures as GHG concentrations in the atmosphere increase [(e.g. IPCC, 2007 and references therein)]. In the 2007 Intergovernmental Panel on Climate Change (IPCC) Fourth Assessment Report (AR4), hindcast simulations from the coupled GCMs that incorporate the observed record of GHGs show that the increase in global temperature results in a decline in the Arctic sea ice cover. However, while these model simulations were found to reasonably simulate the seasonal cycle in the sea ice cover [(e.g. Zhang and Walsh, 2006)], Stroeve et al. [(2007)] found that the observed winter (March) and summer (September) rates of decline were triple the respective model ensemble means, and for September the observed rate of decline was larger than all of the individual model runs. While the qualitative agreement between the GCM simulations and the observations provides evidence for a role of GHG forcing on the observed decline, the disagreement on the rate of decline could indicate a substantial natural variability component or an underestimation of the sea ice sensitivity in the models.

3.1 Changes in atmospheric circulation

An important contribution towards the recent decline in extent and thickness of the sea ice cover came from an atmospheric shift in the late 1980s, early 1990s, when the Arctic Oscillation (AO), also referred to as the Northern Annual Mode (NAM), was predominately in a positive phase [(Rigor and Wallace, 2004)]. The AO is defined as the leading stationary mode of variability in the northern hemisphere sea level pressure (SLP) field based on Empirical Orthogonal Function (EOF) analysis. As such, the AO can be interpreted as an exchange of atmospheric mass between the Arctic and the mid-latitudes [(Thompson and Wallace, 1998)]. When the AO is in its positive phase, SLP over the Icelandic region and extending into the Arctic is anomalously low, promoting a cyclonic (counter-clockwise) sea ice circulation anomaly. This results in decreased ice transport from the Beaufort Sea westward across the date line into the Chukchi Sea, increased ice transport out of the Arctic Ocean through Fram Strait, and increased transport of ice away from the Siberian coast,

leaving open water areas that foster new ice formation [(Rigor et al., 2002)]. By promoting more thin ice in spring, the positive AO sets the stage for negative anomalies in summer ice extent in the Siberian Arctic. It is widely believed that the late 1980s through the mid 1990s positive winter AO state led to significant export of old, thick ice out of the Arctic via Fram Strait, leaving behind thinner ice that is more vulnerable to summer melt [(e.g. Rigor and Wallace, 2004; Lindsay and Zhang, 2005; Maslanik et al., 2007; Nghiem et al., 2007)].

Another key driver for recent record low summer ice extents has been persistence of a summer atmospheric circulation pattern defined by anomalously high SLP over the Beaufort Sea and Canada Basin and unusually low SLP over eastern Siberia, termed the Arctic Dipole Anomaly (DA) [(Wu et al., 2006; Overland et al., 2008; Wang et al., 2009)]. This circulation pattern leads to warm southerly winds in the Chukchi and East Siberian seas, favoring melt and transporting ice northwards towards the pole. In 2007 the DA was particularly well developed throughout the entire summer [(Figure 5])*, resulting in very strong southerly winds that transported ice away from the coasts of Siberia and Alaska, as well as enhanced transport of ice out of the Arctic Ocean and into the North Atlantic through Fram Strait [(Wang et al., 2009)]. Another feature of the anomalously high pressure over the Beaufort Sea in 2007 was unusually clear skies that enhanced surface and basal melt [(Kay et al., 2008)]. While the DA has not been as strong or persistent in the summers following 2007, it has been a common feature of the summer circulation pattern [(Stroeve et al., 2011a)].

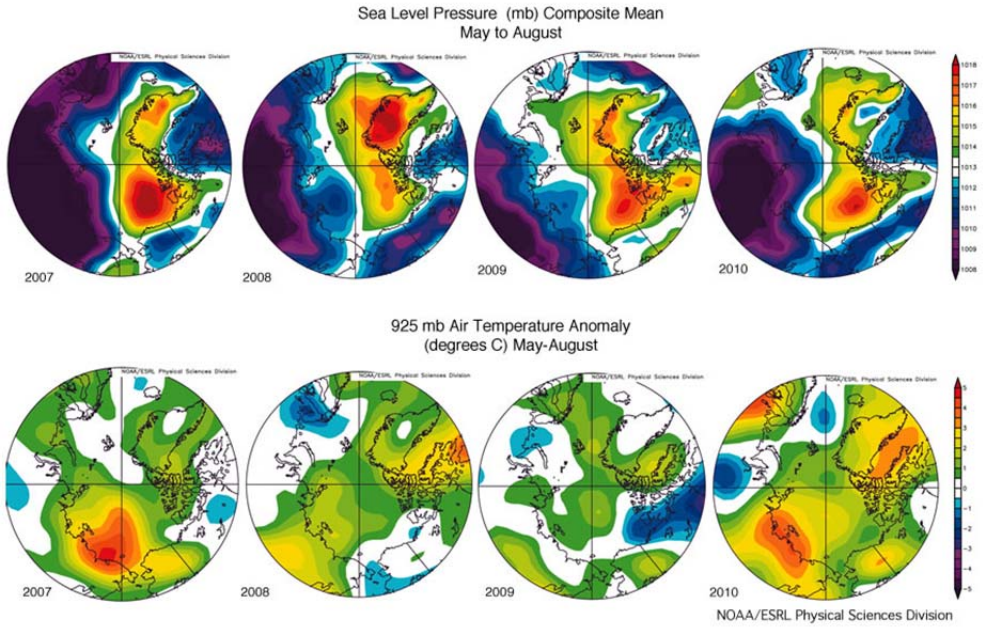

Fig. 5. Composite mean sea level pressure from May through August for 2007 through 2010 (top) and corresponding 925 hPa air temperature anomaly (bottom). Data are from the NOAA/ESRL Physical Sciences Division. Figure from Stroeve et al. (2011a).

3.2 A warming climate

Another important factor behind the decline in the sea ice cover is that Arctic air temperatures are rising [(e.g. ACIA, 2005 and references therein)]. Figure 6 shows temperature anomalies by year and month at the 925 hPa level for the Arctic Ocean domain from JRA-25 atmospheric reanalysis, a product of the Japan Meteorological Agency [(Onogi et al., 2007]). Anomalies are computed with respect to means for the period 1979-2010. In the earlier part of the record, it was common for an anomalously warm summer, contributing to a negative September ice extent anomaly, to be followed by an anomalously cold winter or summer, helping to bring about recover in the ice cover. However, since about 2000, positive air temperature anomalies dominate all months, making it more difficult for the ice cover to rebound from an anomalously low sea ice year. The warmer air temperatures during the past decade have been linked to increased concentrations of black carbon aerosols [(e.g. Shindell and Faluvegi, 2009]), increased spring cloud cover that leads to increased downward longwave radiation at the surface [(Francis and Hunter, 2006]), changes in atmospheric circulation patterns that transports warm air into the Arctic [(*Yang et al*., 2010]), and changes in oceanic heat transport [(Polykov et al., 2005; Shimada et al., 2006]). Other factors include the loss of the ice cover itself as well as increases in atmospheric GHGs (discussed shortly).

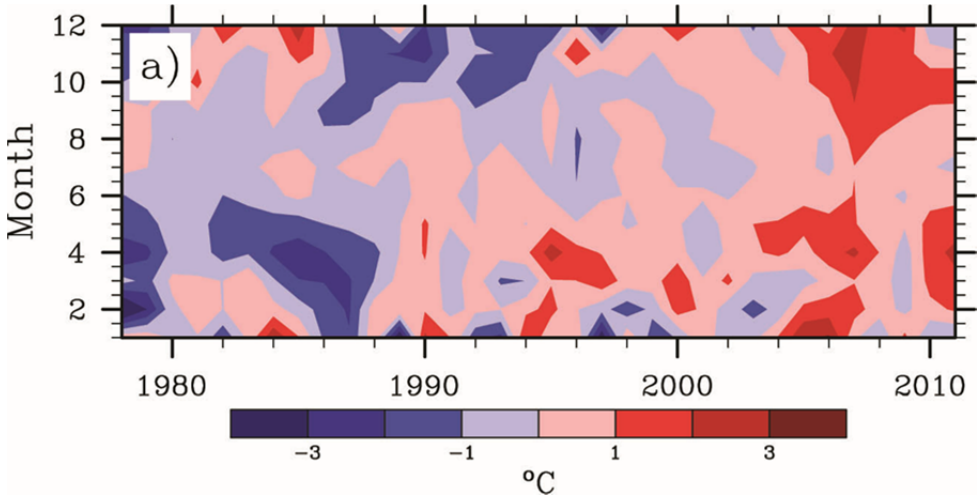

Fig. 6. Near surface air temperature anomalies (925 hPa) for all regions north of 60°N by year (x-axis) and by month (y-axis). Temperature anomalies are derived relative to the 1979 to 2010 mean.

Warmer spring temperatures have led to earlier melt onset in recent years [(e.g. Markus et al., 2009; Belchansky et al., 2004]). The earlier the ice begins to melt, the earlier the albedo drops, leading to increased absorption of solar radiation that further melts the ice and helps to cause open water areas to develop earlier during summer. These expanding open water areas absorb even more of the sun's energy, leading to enhanced basal and lateral melt. Deposition of black carbon and other impurities on the ice cover further increases the absorption of solar radiation, leading to enhanced ice melt.

Warmer autumn temperatures have correspondingly led to later autumn freeze-up and a lengthening of the melt season by 20 days over the last three decades [(Markus et al., 2009]). Temperature anomalies are especially strong in October, a month after the seasonal sea ice minimum. This has been linked to more open water areas in September, leading to strong transfer of heat from the ocean mixed layer (the top 50 meters of the ocean) to the atmosphere as the ocean refreezes [(e.g. Serreze et al., 2009; Screen and Simmonds, 2010a, 2010b; Serreze et al., 2011]). Because it takes time for the ocean to lose its mixed layer sensible heat, the ice that grows will not be as thick as it used to be in spring. This represents a feedback in that the thinner ice will more readily melt out the next summer. Other factors towards warmer autumn temperatures include increased horizontal atmospheric heat flux convergence [(e.g. Yang et al., 2010]), increased ocean heat flux convergence [(Chylek et al., 2009]) and changes in cloud cover and atmospheric water vapor that augment the downwelling longwave radiation flux to the surface [(Francis and Hunter, 2008]).

3.3 Enhanced ice-albedo feedback

As mentioned in the introduction, snow-covered sea ice has a high albedo, reflecting much of the incoming sun's radiation back out to space. As the snow begins to melt, the bare ice is exposed which absorbs more of the sun's energy. During advanced melt, melt ponds and areas of dark open water (low albedo) form, which readily absorb solar radiation, fostering further ice melt. Without this "ice-albedo" feedback, the amplitude of the seasonal cycle in ice extent (the change from March through September) would be smaller than is observed.

The continued decline in the summer ice cover has in part been attributed to a growing importance of the ice-albedo feedback [(Perovich et al., 2007; Lindsay et al. 2005]). With thinner first-year ice replacing thick multiyear ice, dark open water areas form earlier in spring, leading to increased sensible heat content of the ocean mixed layer, fostering further melt [(Stroeve et al., 2011a]). The shift towards more first-year ice also has large implications for the amount of solar energy absorbed by the sea ice itself since multiyear ice tends to have a higher albedo than first-year ice [(Perovich et al., 2000]). This in turn affects the strength of the ice-albedo feedback and hence the sea ice and upper ocean energy balance. The growing albedo feedback appears to be especially strong in the Beaufort and Chukchi seas, such that it is now warm enough that multiyear ice drifting into the region tends to melt out [(Stroeve et al., 2011b; Maslanik et al., 2011, Kwok and Cunnigham, 2010]).

It has been thought that this feedback could lead to a "tipping point" where the Arctic reaches a point of no return making summer ice-free conditions inevitable and to some extent irreversible [(e.g. Holland et al., 2006; Lindsay and Zhang, 2005]). However, more recent model results indicate that such a tipping point is unlikely [(Amstrup et al., 2010; Tietsche et al., 2011]). After the additional heat in the ocean is dissipated in the autumn, the sea ice can grow rapidly under the cold atmosphere, and because ice growth is fastest when ice is thin and then slows as the ice thickens through the winter, the final spring thickness of seasonal ice is only slightly thinner than normal. This mitigates some of the effects of the ice-albedo feedback. Thus, if temperatures stabilize or decrease, the summer sea ice will quickly recover to an equilibrium state determined by the temperature. Another implication of this is that the sea ice decline may be interrupted by several-year periods of little decline or even short-term increases in extent due to natural variability in the climate system [(Kay et al., 2011]).

3.4 Warmer ocean temperatures

There is growing evidence that the waters of the Arctic are warming. Since the 1990s, there has been an overall increase in the temperature and transport of warm Atlantic water through Fram Strait [(Schauer et al., 2004; Polyakov et al., 2005; Dmitrenko et al., 2008]). However it is unclear how much of this heat can be brought to the surface to melt the ice cover. This is because the warm Atlantic water exists below the colder, fresher (less dense) Arctic surface water. A more recent study found that the Atlantic water flowing north into the Arctic Ocean is the warmest that it has been in at least 2,000 years [(Spielhagen et al., 2011]). This large heat input into the Arctic appears to have caused an enhanced heat flux to the surface, concurrent with the decreasing sea ice cover.

On the Pacific side of the Arctic there is also indication of warm water inflow that is capable of reaching the surface and melting the ice from below. Shimada et al. [(2006]) find increases in Pacific Surface Water temperature in the Arctic Ocean beginning in the late 1990s that appear to have helped melt ice in the Chukchi and Beaufort seas. Jackson et al. [(2010]) finds that near surface (20-25 m depth) ocean temperatures in the Canada Basin have increased and moved further northward between 1993 and 2007.

3.5 Atmospheric greenhouse gases

All models participating in the IPCC 2007 AR4 report show declining sea ice extent over the period of observations when forced with the observed record of atmospheric GHGs [(e.g. Stroeve et al., 2007; Bo et al., 2009; Zhang and Walsh, 2006; Overpeck, 2005]). This is not the case when the models are run using pre-industrial levels of atmospheric greenhouse gasses and provides strong evidence that GHGs are in part responsible for the observed decline. Stroeve et al. [(2007]) estimated that 47-57% of the decline from 1979-2006 could be explained by GHG-forcing assuming that the multi-model ensemble mean was an accurate representation of the forced change by GHGs. Min et al. [(2008]) examined the observed changes from 1953-2006 together with the AR4 models and concluded that since the 1990s there has been a detectable anthropogenic forcing on the sea ice trends. A more recent paper by Kay et al. [(2011]) analyzed the influence of anthropogenic forcing on the late 20th and early 21st century Arctic sea ice extent trends using the latest version of the Community Climate System Model version 4 (CCSM4). They concluded that the observed ice losses could not be explained by natural climate variability alone.

Another feature of the GCM simulations is that some of the models show that the decline becomes steeper with time, but not until much later into the 21st century [(e.g. Wang and Overland, 2009]). However, it appears that accelerated ice loss is already happening today. Stroeve et al. [(2011a]) argue that the recent steepening in the rate of decline of September ice extent points to a growing non-linear response to external climate forcing. This growing non-linear response is related to the following. First, because there is less sea ice in September, there is more open water in which new ice can form in winter. Since this ice is thinner than ice that has survived more than one melt season, the following spring ice cover is increasingly dominated by thinner ice that is more vulnerable to melting out in summer, especially when atmospheric forcing is conducive to ice loss [(e.g. Lindsay et al., 2009]). Second, the presence of more thin ice in spring, allows open water areas to develop earlier in the melt season, leading to increased importance of the ice-albedo feedback [(e.g. Stroeve et

al., 2011a, 2011]), though to some degree mitigated by the more rapid autumn ice growth, as discussed above. During the record ice loss year of 2007, the early development of large open water areas in the Beaufort and Chukchi seas led to sea surface temperature anomalies in excess of 2.5°C [(**Figure 7**]), leading to more than 2 m of basal melt by the end of summer [(Perovich et al., 2007]). Third, the Arctic has warmed in all seasons [(Serreze et al., 2009; Stroeve et al., 2011a]), leading not only to earlier melt onset and later autumn freeze-up [(Markus et al., 2009]), but also a reduced likelihood of unusually cold conditions that could bring about temporary recovery through natural climate variability.

However, even during decadal or multi-decadal periods of accelerated ice loss, climate model simulations such as those from CCSM3 and CCSM4 simulations [(Holland et al., 2007, Kay et al., 2011]), show there can be several-year periods of slow ice loss or even temporary increases in extent. Thus, while the observed trend is steeper over the past decade compared to the earlier part of the record, it is uncertain if this pattern will be sustained. The higher extent for September 2009 relative to 2007 and 2008 may have suggested a temporary recovery, yet September 2010 and 2011 saw less ice compared to 2009 despite a winter circulation pattern that should have helped to favor ice retention through the summer melt season in 2010 [(Stroeve et al., 2011b]), and generally less favorable summer conditions for substantial ice loss in summer of 2011.

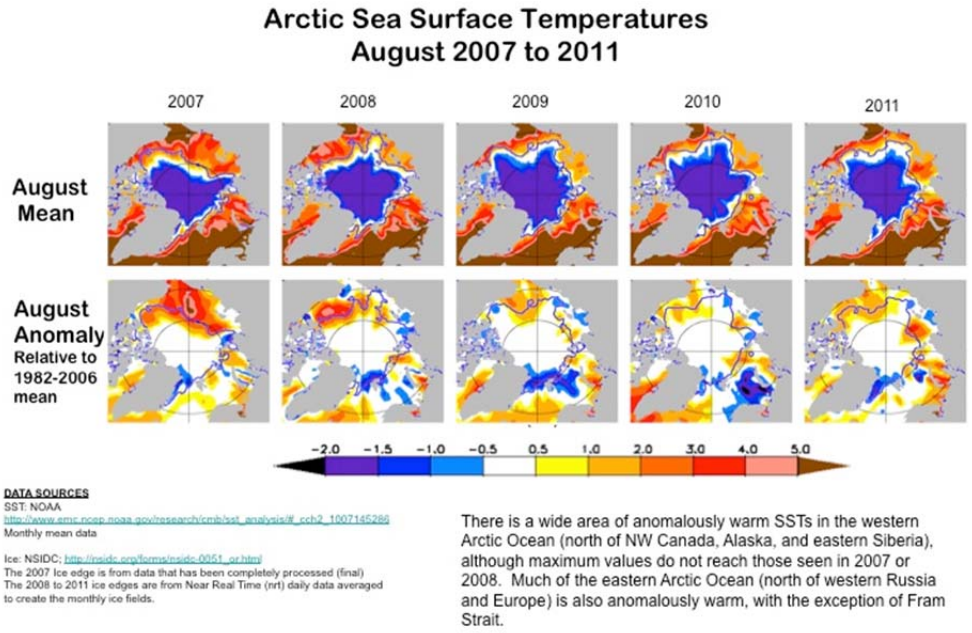

Fig. 7. Mean August sea surface temperatures and anomalies for 2007 through 2011. Anomalies are computed relative to the 1982-2006 mean. Credit: Michael Steele and Wendy Ermold, Polar Science Center, Applied Physics Laboratory, University of Washington.

4. Future ice conditions

Climate models have long suggested that as atmospheric greenhouse gas concentrations increase, the Arctic Ocean will likely become ice-free during. In some of the model projections, this seasonally ice-free Arctic state is expected to occur sometime after 2100 whereas in other models the estimate is as early as 2050 [(IPCC, 2007]). Figure 8 shows a comparison between the observed September ice extent from 1953 to 2010, based on a combination of early ship, aircraft, satellite and submarine records together with the modern satellite data record [(Stroeve et al., 2007; Stroeve et al., 2008]), and 15 models participating in the IPCC AR4 report using the "business as usual (A1B)" GHG scenario. It is clear that all models show declining September sea ice extent, with some models indicating that the Arctic will become ice-free sometime during the latter half of this century and others suggesting it will happen sometime after 2100. However, there is significant spread in the simulated September ice extents.

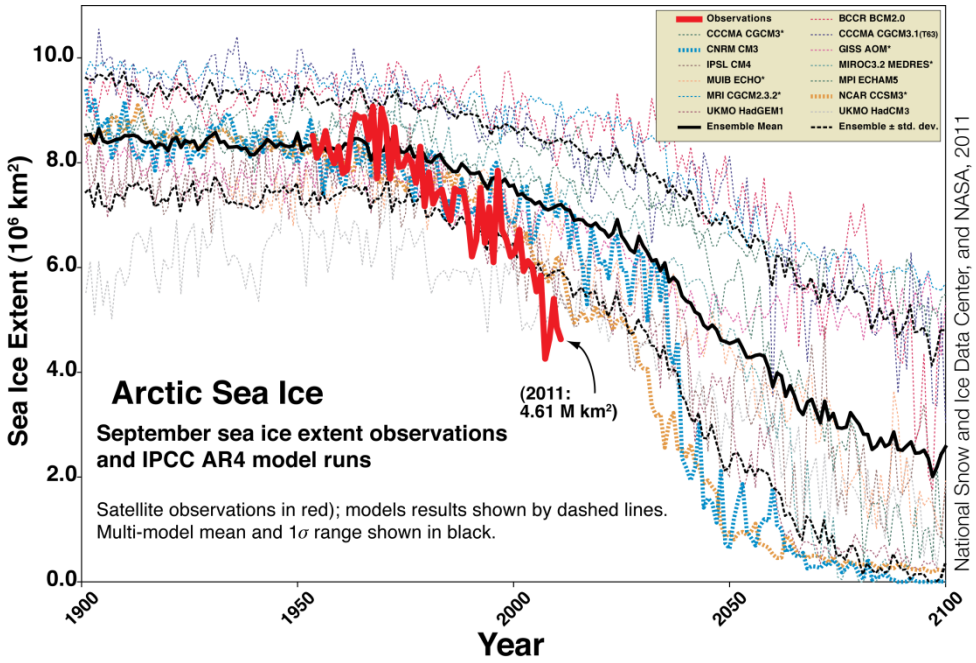

Fig. 8. Comparison between Global Climate Model (GCM) simulations of September sea ice extent (individual color lines) and observations (shown in red). The solid black line represents the ensemble mean and the dotted black lines are the +/- one standard deviation of the ensemble mean. Figure updated from Stroeve et al., 2007.

While the model simulated September ice extents are in qualitative agreement with the observations that the sea ice has been in declining during the observational record, it is clear that the models are failing to capture the rate of decline. From 1953 to 2010, the observed rate of decline in the September ice extent is -8.8 $\pm$ 0.6 percent per decade. The multi-model ensemble mean is only -2.8 $\pm$ 0.2 percent per decade. Over the modern satellite data record (e.g. 1979-2010) the model ensemble mean increases to -4.4 $\pm$ 0.2 percent per decade, but it remains three times less than the observed (-12.5 $\pm$ 1.6 percent per decade) trend. The inability of the climate models to accurately simulate the observed rate of decline has raised speculation that the Arctic may become seasonally ice-free sooner than the climate models predict.

As mentioned earlier, it appears that both anthropogenic forcing and natural climate variability are responsible for the observed decline. However it is clear from climate model simulations that as atmospheric GHGs continue to increase, the Arctic will transition towards a seasonally ice-free Arctic state. However, climate model simulations also suggest the natural climate model variability can exert a strong influence on the sea ice trends, especially on sub-20 year time-scales. Thus, while the Arctic ice cover appears to be on track to become ice-free in summers in the future, it is entirely possible to have periods of temporary recovery [Kay et al., 2011].

5. Climate Implications

5.1 Reduced sea ice amplifies warming

Except during summer, the sea ice cover insulates a relatively warm Arctic Ocean from a much colder atmosphere. As mentioned earlier, with less sea ice at summer's end and more open water, the ocean absorbs the suns energy that would normally be reflected by the ice cover and the ocean mixed layer heats up. As temperatures drop in autumn and the sun disappears for winter, the ocean will eventually lose the extra mixed layer heat that it gained in summer and the ice will form. This results in large heat transfers from the ocean back to the atmosphere in autumn, most pronounced at the surface but also extending upwards in the lower troposphere. This "amplified warming" is a prominent feature of climate models. **Figure 9** shows how the pattern of cold-season warming over the Arctic Ocean grows with time in the model simulations. Additionally, the warming is focused near the surface, but extends up to considerable height within the troposphere. Analysis of the GCMs participating in the IPCC 2007 report reveal consistency in the seasonality and vertical structure of this warming, but with different timings, magnitudes and spatial patterns of change [(Serreze et al., 2009]). This is in part a result of inter-model scatter in the timing of the sea ice cover retreat through the coming century as well as differences in patterns of atmospheric heat transport, vertical mixing, cloud processes and water vapor. Atmospheric circulation and precipitation patterns are one of the least robust signals in climate model simulations [(e.g. Deser et al., 2011]).

One implication of amplified Arctic temperatures is the potential to hasten permafrost degradation [(e.g. Lawrence et al., 2008]). Permafrost is frozen land that remains below 0^{o}C for at least two years. In the Northern Hemisphere, permafrost occupies approximately 22.79 million km^2 (about 24% of the exposed land surface) [(Zhang et al. 2003]). This permafrost contains a significant store of the Earth's deposits of organic carbon. Observations indicate that permafrost in the Arctic is warming [(e.g. Isaksen et al., 2007;

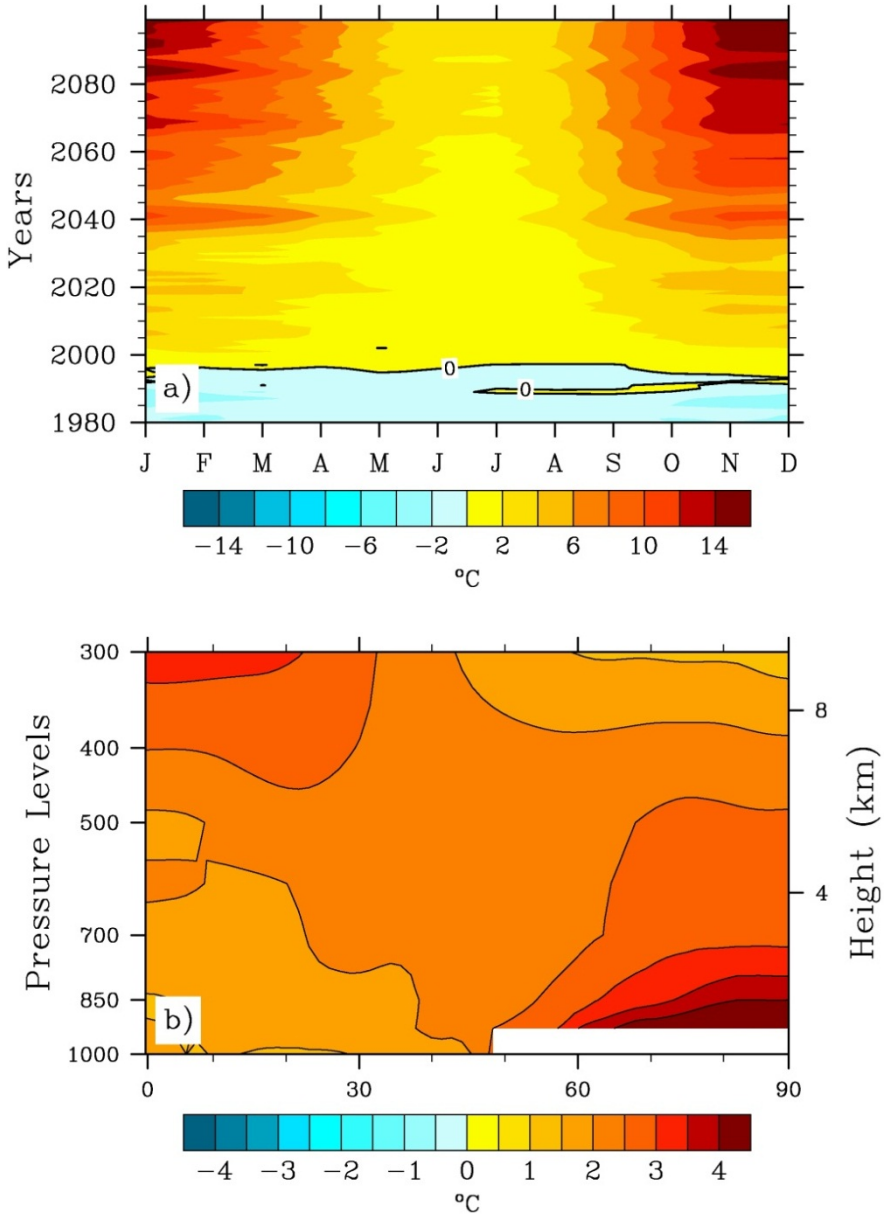

Fig. 9. Air temperature simulations from the NCAR CCSM3 global climate model using the IPCC A1B emission scenario. The top figure shows the near surface (2 meter) air temperature anomalies by month and year over the Arctic Ocean while the bottom figure shows the latitude by height plot of the October through March temperature anomalies for 2050-2059 relative to 1979-2007. Figure from Serreze et al., 2009.

Osterkamp, 2007; Jorgenson et al, 2001]), and this warming is already leading to increased emissions of carbon dioxide and methane [(e.g. Schuur et al., 2009]). Climate models suggest that as much as 90% of the near-surface permafrost may disappear by the end of this century [(Lawrence et al., 2008]). This has the potential to release large amounts of carbon into the atmosphere and contribute to further warming.

Another potential impact of Arctic amplification is the potential to melt more of the land ice in the Arctic, including the ice on the Greenland ice sheet. More melting of land ice in the Arctic has the potential to raise global sea level by several meters.

5.2 Altered weather patterns

Heating the atmosphere over the Arctic Ocean alters the temperature gradient from the equator to the poles. This impacts both the atmosphere's static stability and the atmospheric thickness gradient. A weaker thickness gradient toward the poles results in weaker vertical wind speed (or wind shear). This impacts on the development, tracks and strengths of storms and the precipitation they generate, that may well extend beyond the Arctic. For example, there is some evidence that autumn sea level pressure fields following summers with less sea ice exhibit higher pressures over much the Arctic Ocean and the North Atlantic, compensated by lower pressures in the mid-latitudes, otherwise known as the negative phase of the AO [(e.g. Francis et al., 2009]). This can have wide-spread impacts on temperatures and precipitation in the Northern Hemisphere [(e.g. Hurrell, 1995]).

There is broad agreement in climate models that warming will lead to increased precipitation in the northern high latitudes [(Kattsov et al., 2007; Finnis et al., 2007; Deser et al, 2010]). This is linked to the influence of more open water on atmospheric temperatures and the ability of a warmer atmosphere to hold more water vapor. However, different modeling studies have come to vastly different conclusions as to the spatial distribution of these precipiation changes. While many models suggest a decrease in cyclone frequency, but more intense storms, other studies suggest increased frequency of intense storms [(Lambert and Fyfe, 2006]), while other studies suggest precipitation increases are a result of poleward shifts in storm tracks (Yin, 2005).

Simmonds and Kaey (2009) suggest the loss of the summer Arctic sea ice cover has led to increased strength of September cyclones. This link is associated with increased sensible and latent heat fluxes associated with more open water. Stroeve et al. [(2011c]) further note there has been a corresponding increase in autumn precipitation associated with more frequent and stronger cyclones in years that had anomalously low September sea ice extent [(**Figure 10**]). However cause and effect remain unclear. While there has been anomalously more sensible and latent heat fluxes, as well as more precipitable water vapor over the regions where the ice cover has retreated, the increase in precipitation is primarily linked to a shift in atmospheric circulation towards more frequent and intense cyclones in the Atlantic sector of the Arctic. Thus, the absence of a clear link between the spatial patterns of recent precipitation changes and sea ice extent anomalies may suggest the link between recent changes in cyclone activity and sea ice loss is premature.

However, it is entirely possible that the recent declines in the sea ice cover have in part forced the observed circulation changes [(Francis et al., 2009; Overland and Wang, 2010]). As changes in the temperature structure in the Arctic atmosphere become more pronounced in the coming decades as the summer sea ice cover continues to decline, a clearer link between corresponding atmospheric circulation and precipitation changes should emerge.

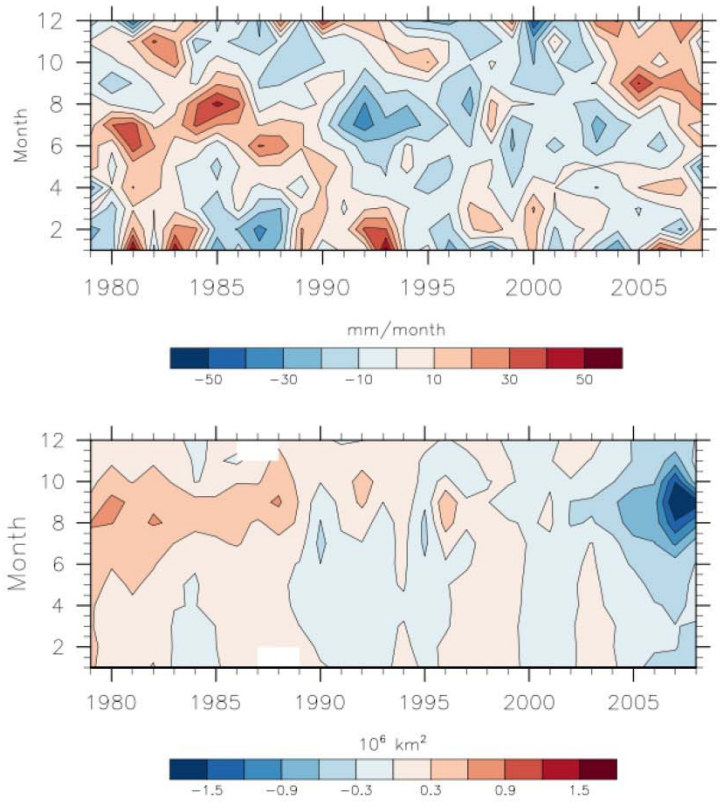

Fig. 10. Cyclone associated precipitation anomalies averaged for all regions north of 60°N (top) and corresponding sea ice extent anomalies (bottom). Anomalies are computed with respect to the 1979 to 2009 mean. Figure from Stroeve et al., 2011c.

6. Summary

The Arctic sea ice is currently in a state of accelerated decline. This decline has been linked to a combination of natural climate variability and anthropogenic forcing linked to rising concentrations of atmospheric greenhouse gases. Global climate models suggest that as the amount of atmospheric CO_2 continues to increase, the Arctic will eventually transition towards ice-free conditions in summer, though there could be periods of temporary recovery on that trajectory. Given the fact that the currently observed rate of decline exceeds that simulated by our most advanced climate models, it is entirely possible that a seasonally ice-free Arctic state may be achieved within the next 20 to 30 years. The loss of the Arctic summer sea ice cover will have profound implications for our climate. Today we are already seeing the impacts of amplified warming over the Arctic linked to the loss of the summer ice cover, with the potential to further amplify warming by releasing carbon stored in the permafrost and further melting of the Arctic's ice caps and glaciers. This warming will additionally invoke changes in atmospheric circulation. While there is at the moment no universal consensus regarding the changes in weather patterns expected, a common thread in the climate model simulations is that the changes will be significant and affect areas well beyond the boundaries of the Arctic.

7. References

Amstrup, S.C., E.T. DeWeaver, D.C. Douglas, B.G. Marcot, G.M. Durner, C.M. Bitz, and D.A. Bailey (2010), Greenhouse gas mitigation can reduce sea-ice loss and increase polar bear persistence, *Nature*, 468, 955-958.

Arctic Climate Impact Assessment (ACIA) (2004), *Impacts of a Warming Arctic*. Cambridge University Press, Cambridge, UK, pp139.

Belchansky, G.I., D.C. Douglas, and N.G. Platonov, (2004), Duration of the Arctic sea ice melt season: Regional and interannual variability, 1979-2001, *J. Clim., 17*, 67-80.

Bo, J.; Hall, A.; Qu, X, (2009), September sea-ice cover in the Arctic Ocean projected to vanish by 2100, *Nature Geoscience* 2 (5), 341, doi:10.1038/ngeo467

Chylek, P., C.K. Folland, G. Lesins, M.K. Dubey, and M-Y. Wang (2009), Arctic air temperature change amplification and the Atlantic Multidecadal Oscillation, *Geophys. Res. Lett*. 36, L14801, doi:10.1029/2009GL038777.

Comiso, J. C., C. L. Parkinson, R. Gersten, and L. Stock, (2008), Accelerated decline in the Arctic sea ice cover, *Geophys. Res. Lett*., 35, L01703,doi:10.1029/2007GL031972.

Deser, C., A. S. Phillips, V. Bourdette, and H. Teng, (2011), Uncertainty in climate change projections: The role of internal variability. Climate Dyn., DOI 10.1007/s00382-010-0977-x.

Deser, C., Tomas, R., Alexander, M. and Lawrence, D. (2010), The seasonal atmospheric response to projected Arctic sea ice loss in the late twenty-first century. *J. Climate* 23, 333-351.

Dimitrenko, I.A., I.V., Polyakov, S.A. Krillov, L.A. Timokhov, I.E. Frolov, V.T. Sokolov, H.L. Simmons, V.V. Ivnov, and D. Walsh (2008), Toward a warmer Arctic Ocean: Spreading the early 21st century Atlantic Water warm anomaly along the Eurasian Basin margins, *J. Geophys. Res*., 113, C05023, doi:10.1029/2007JC004158.

Finnis, J., Holland, M.M., Serreze, M.C. and Cassano, J.J. (2007), Response of Northern Hemisphere extratropical cyclone activity and associated precipitation to climate

change, as represented by the Community Climate System Model. *J. Geophys. Res.* 112, G04S42, doi: 10.1029/2006JG000286.

Francis, J.A., W. Chan, D.J. Leathers, J.R. Miller and D.E. Veron, (2009), Winter Northern Hemisphere weather patterns remember summer Arctic sea ice extent, *Geophys. Res. Lett.*, 36, L07503, doi:10.1029/2009GL037274.

Francis, J.A., and E. Hunter (2006), New insight into the disappearing Arctic sea ice, *EOS, Trans. Am. Geophys. Union*, 87, 509-511.

Gillett, Nathan P.; Stone, Dáithí A.; Stott, Peter A.; Nozawa, Toru; Karpechko, Alexey Yu.; Hegerl, Gabriele C.; Wehner, Michael F.; Jones, Philip D. (2008), Attribution of polar warming to human influence", *Nature Geoscience*, 1, 750, doi:10.1038/ngeo33.

Holland, M.M., C.M. Bitz, and B. Tremblay, (2006), Future abrupt reductions in the summer Arctic sea ice. *Geophys. Res. Lett., 33*, L23503, doi:10.1029/2006GL028024.

Hurrel, J.W., (1995), Decadal trends in the North Atlantic Oscillation: Regional tempeatures and precipitation, *Science*, 269, 676-679.

Intergovernmental Panel on Climate Change (IPCC) (2007), Climate Change 2007: The Physical Science Basis. Contribution of Working Group I to the Fourth Assessment Report of the Intergovernmental Panel on Climate Change, edited by S. Solomon et al., Cambridge Univ. Press, Cambridge, U. K.

Isaksen, K., R.E. Benestad, C. Harris, and J.L. Sollid, (2007), Recent extreme near-surface permafrost temperatures on Svalbard in relation to future climate scenarios. Geophysical Research Letters doi:10.1029/2007GL031002.

Jackson, J.M., E.C. Carmack, F.A. Mc Laughlin, S.E. Allen, and R.G. Ingram (2010), Identification, characterization, and change of the near-surface temperature maximum in the Canada Basin, 1993-2008, *J. Geophys. Res.*, 115, C05021, doi:10.1029/2009JC005265.

Jorgenson, M.T., C.H. Racine, J.C. Walters, and T.E. Osterkamp, (2001), Permafrost degradation and ecological changes associated with a warming climate in central Alaska, *Climatic Change*, 48, 551-579.

Kattsov, V.M., Walsh, J.E., Chapman, W.L., Govorkova, V.A., Pavlova, T.V. and Zhang, X. 2007. Simulation and projection of Arctic freshwater budget components by the IPCC AR4 Global Climate Models. *J. Hydrometeorol*. 8, 571-589, doi:10.1175/JHM575.1.

Kay, J.E., M. M. Holland, and A. Jahn (2011), *Inter-annual to multi-decadal Arctic sea ice extent trends in a warming world*, *Geophys. Res. Lett.*, 38, L15708, doi:10.1029/2011GL048008.

Kay, J.E., T. L'Ecuyer, A. Gettelman, G. Stephens, and C. O'Dell (2008), The contribution of cloud and radiation anomalies to the 2007 Arctic sea ice extent minimum, *Geophys. Res. Lett.*, 35, L08503, doi:10.1029/2008GL033451.

Kwok, R., and G. F. Cunningham, (2010), Contribution of melt in the Beaufort Sea to the decline in Arctic multiyear sea ice coverage: 1993–2009, *Geophys. Res. Lett.*, 37, L20501, doi:10.1029/2010GL044678.

Lambert, S.J. and Fyfe, J.C. (2006), Changes in winter cyclone frequencies and strengths simulated in enhanced greenhouse warming experiments: Results from models participating in the IPCC diagnostic exercise. *Clim. Dynam.*, 26, 713-728.

Lindsay, R.W. and J. Zhang (2005), The thinning of Arctic sea ice, 1988-2003: have we passed a tipping point*? J. Climate*, 18, 4879-4894.

Markus, T., J. C. Stroeve, and J. Miller, (2009), Recent changes in Arctic sea ice melt onset, freeze-up, and melt season length, *J. Geophys. Res.*, doi:10.1029/2009JC005436.

Maslanik, J.A., C. Fowler, J. Stroeve and W. Emery (2011), Distribution and trends in Arctic sea ice age through spring 2011, *Geophys. Res. Lett.*, 38, L13502, doi:10.1029/2011GL047735.

Maslanik, J.A., C. Fowler, J. Stroeve, S. Drobot, J. Zwally, D. Yi and W. Emery, (2007), A younger, thinner Arctic ice cover: Increased potential for rapid, extensive sea-ice loss. *Geophys. Res. Lett.*, 34, L24501, doi:10.1029/2007GL032043.

Min, S.-K., X. Zhang, F. W. Zwiers, and T. Agnew (2008), Human influence on Arctic sea ice detectable from early 1990s onwards, *Geophys. Res. Lett.*, 35, L21701, doi:10.1029/2008GL035725.

Nghiem, S.V., I.G. Rigor, D.K. Perovich, P. Clemente-Colón, J. Richter-Menge, J. W. Weatherly, and G. Neumann, Rapid reduction of Arctic perennial sea ice, (2007), *Geophys. Res. Lett.*, 24, L19504, doi:10.1029/2007GL031128.

Onogi, K., J. Tsutsui, H. Koide, M. Sakamoto, S. Kobayashi, H. Hatsushika, T. Matsumoto, S. Yamazaki, H. Kamahori, K. Takahashi, S. Kadokura, K. Wada, K. Kato, R. Oyama, T. Ose, N. Mannoji, and R. Taira (2007), The JRA-25 reanalysis, *J. Met. Soc. Japan*, 85, 369-432.

Overpeck, Jonathan T. (2005), Arctic System on Trajectory to New, Seasonally Ice-Free State, *Eos, Transactions, American Geophysical Union,* 86 (34), 309–316.

Osterkamp, T.E. (2007), Characteristics of the recent warming of permafrost in Alaska. *J. Geophys. Res.*, 112, doi:10.1029/2006JF000578.

Perovich, D. K., J. A. Richter-Menge, K. F. Jones, and B. Light, (2008), Sunlight, water, and ice: Extreme Arctic sea ice melt during the summer of 2007, *Geophys. Res. Lett.*, 35, L11501, doi:10.1029/2008GL034007.

Polyakov, I.V., et al. (2005), One more step toward a warmer Arctic, *Geophys. Res. Lett.*, 32, L17605, doi:10.1029/2005GL023740.

Rigor, I.G. and J.M. Wallace (2004), Variations in the age of Arctic sea ice and summer sea ice extent, Geophys. Res. Lett., 31, 109401, doi:10.1029/2004GL019492.

Rigor, I.G., J.M. Wallace and R.L. Colony (2002), Response of the sea ice to the Arctic Oscillation, *J. Clim.*, 15, 2648-2663.

Schauer, U., E. Fahrbach, S. Osterhus, and G. Rohardt (2004), Arctic warming through the Fram Strait – Oceanic heat transport from three years of measurements, *J. Geophys. Res.*, 109, C06026, doi:10.1029/203JC001823.

Schuur, E.A.G., J.G. Vogel, K.G. Crummer, H. Lee, J.O. Sickman and T.E. Osterkamp, (2009), The effect of permafrost thaw on old carbon release and net carbon exchange from tundra, *Nature*, 459, doi:10.1038/nature0831.

Screen, J.A., and I. Simmonds (2010a), The central role of diminishing sea ice in recent Arctic temperature amplification, Nature, 464, 1334-1337.

Screen, J.A., and I. Simmonds (2010b), Increasing fall-winter energy loss from the Arctic Ocean and its role in Arctic temperature amplification, *Geophys. Res. Lett.* 37, L16707, doi: 10.1029/2010GL044136.

Serreze, M.C., A.P. Barrett and J.J. Cassano (2011), Circulation and surface controls on the lower-tropospheric air temperature field of the Arctic, *J. Geophys. Res.*, 116, D07104, doi:10.1029/2010JD015127..

Serreze, M.C., A.P. Barrett, J.C. Stroeve, D.M. Kindig and M.M. Holland (2009), The emergence of surface-based Arctic amplification, *The Cryosphere*, 3, 1-9.

Serreze, M.C., M.M. Holland and J. Stroeve, 2007. Perspectives on the Arctic's shrinking sea ice cover, *Science*, 315, 1533-1536.

Shimada, K., T. Kamoshida, M. Itoh, S. Nishino, E. Carmack, F. McLaughlin, S. Zimmerman, and A. Proshutinsky, (2006), Pacific Ocean inflow: Influence on catastrophic reduction of sea ice cover in the Arctic Ocean, *Geophys. Res. Lett.,* 33, L08605, doi:10.1029/2005GL025624.

Simmonds, I. and Keay, K. (2009), Extraordinary September Arctic sea ice reductions and their relationships with storm behavior over 1979-2008. *Geophys. Res. Lett*. 36, L19715, doi:10.1029/2009GL039810.

Speilhagen, R.F., and others (2011), Enhanced modern heat transfer to the Arctic by warm Atlantic water, *Science*, 331 (6016), doi:10.116/science.1197397.

Stroeve, J.C., M.C. Serreze, J.E. Kay, M.M. Holland, W.N. Meier and A.P. Barrett, (2011a). The Arctic's rapidly shrinking sea ice cover: A research synthesis, *Climatic Change*, doi: 10.1007/s10584-011-0101-1.

Stroeve, J.C., J. Maslanik, M.C. Serreze, I. Rigor and W. Meier, (2011b), Sea ice response to an extreme negative phase of the Arctic Oscillation during winter 2009/2010, *Geophys. Res. Lett.*, doi: 2010GL045662.

Stroeve, J.C., M.C. Serreze and D.N. Kindig, (2011c), Attribution of recent changes in autumn cyclone associated precipitation in the Arctic, *Tellus*, DOI: 10.1111/j.1600-0870.2011.00515.x.

Stroeve, J., M. Serreze, S. Drobot, S. Gearheard, M. Holland, J. Maslanik, W. Meier, T. Scambos, (2008), Arctic sea ice extent plummets in 2007, *EOS Transactions, AGU*, 89(2), 13-14.

Stroeve, J.C., M.C. Serreze, F. Fetterer, T. Arbetter, W. Meier, J. Maslanik and K. Knowles, (2005), Tracking the Arctic's shrinking ice cover: Another extreme September minimum in 2004, *Geophys. Res. Lett.,* 32(4), L04501, doi:10.1029/2004GL021810, 2005.

Thompson, D.W.J., and J.M. Wallace, (1998), The Arctic Oscillation signature in the wintertime geopotential height and temperature fields, *Geophs. Res. Lett.*, 25(9), 1297-1300.

Tietsche, S., D. Notz, J. H. Jungclaus, and J. Marotzke (2011), Recovery mechanisms of Arctic summer sea ice, *Geophys. Res. Lett.*, *38*, L02707, doi:10.1029/2010GL045698.

Wang, M., and J. E. Overland (2009), A sea ice free summer Arctic within 30 years?, *Geophys. Res. Lett*., 36, L07502, doi:10.1029/2009GL037820.

Wang, J., J. Zhang, E. Watanabe, M. Ikeda, K. Mizobata, J.E. Walsh, X. Bai, and B. Wu, (2009). Is the dipole anomaly a major drier to record lows in Arctic summer sea ice extent?, *Geophys. Res. Lett*., 36, L05706, doi:10.1029/2008GL036706.

Wu, B., J. Wang, and J. E. Walsh (2006), Dipole anomaly in the winter Arctic atmosphere and its association with sea ice motion, *J. Climate*, 19, 210–225.

Yang, X-Y., J.C. Fyfe, and G.M. Flato (2010), The role of poleward energy transport in Arctic temperature evolution, *Geophys. Res. Lett*., 37, L14803, doi:10.1029/2010GL042487.

Yin, J.H. (2005), A consistent poleward shift of the storm tracks in simulations of 21st century climate. *Geophys. Res. Lett*. 32, L18701, doi:10.1029/2005GL023684.

Zhang, T., R.G. Barry, K. Knowles, F. Ling, and R.L. Armstrong, (2003), Distribution of seasonally and perennially frozen ground in the Northern Hemisphere. In Permafrost. Phillips, Springman, and Arenson, eds. Swets and Zeitlinger.

Zhang, X. D., and J. E. Walsh (2006), Toward a seasonally ice-covered Arctic Ocean: Scenarios from the IPCC AR4 model simulations, *J. Clim*., 19(9), 1730–1747.

21

Post-Combustion CO_2 Capture with Monoethanolamine in a Combined-Cycle Power Plant: Exergetic, Economic and Environmental Assessment[1]

Fontina Petrakopoulou[1,2], George Tsatsaronis[1],
Alicia Boyano[1,3] and Tatiana Morosuk[1]
[1]*Technische Universität Berlin, Institute for Energy Engineering,*
[2]*IMDEA Energy, Energy Systems Analysis Unit,*
[3]*Join Research Center-European commission,*
Institute for Prospective Technological Studies,
[1]*Germany*
[2,3]*Spain*

1. Introduction

Post-combustion capture through chemical absorption is the most technologically-mature CO_2 capture method, developed about 70 years ago to remove acid gases from natural gas streams (Herzog, 2001). The prominent disadvantage of the method is the significant amount of thermal energy required for the regeneration of the chemicals used, resulting in a considerable efficiency penalty. In recent years, many studies have reviewed different post-combustion technologies and compared the effectiveness of different types of absorbents for chemical absorption (e.g., Kothandaraman et al., 2009; Rubin & Rao, 2002). Analyses have yet to reveal any significant breakthrough, leaving chemical absorption as one of the most energy intensive methodologies for CO_2 capture. Nevertheless, the significant advantage of chemical absorption is that existing plants can be retrofitted with a capture unit without further rearrangements. This straightforward application of the technology makes it interesting from both a practical and an economic point of view.

This study evaluates the performance of a combined-cycle power plant with post-combustion CO_2 capture using monoethanolamine (MEA plant). The structure and operating conditions of the plant are based on a reference power plant that does not include CO_2 capture. The methods used in the evaluation process are exergy-based. In an exergetic analysis the physical and chemical exergies of process streams are calculated and the performance of the plant components is assessed using exergy destruction and exergetic efficiency. The combination of an exergetic analysis with an economic analysis and a life cycle assessment (LCA) constitutes an exergoeconomic and an exergoenvironmental

[1] The views expressed are purely those of the authors and may not in any circumstances be regarded as stating an official position of the European Commission

analysis, respectively. In an exergoeconomic analysis, costs are assigned to the exergy of the streams and to the exergy destruction, revealing trade-offs between capital investment and cost of exergy destruction within each component of an energy conversion system. Analogously, in an exergoenvironmental analysis, environmental impacts are assigned to the construction of the components and to the exergy destruction and trade-offs between the environmental impact of component construction and exergy destruction are identified. In all cases, the evaluation takes place both at the component and the plant level.

2. The power plants

2.1 The reference plant

The reference plant is a combined-cycle power plant without CO_2 capture that is used as the base case for the simulation of the MEA plant. A simplified flow diagram of the reference plant is shown in Figure 1, while its detailed diagram can be found in the Appendix (Figure A.1).

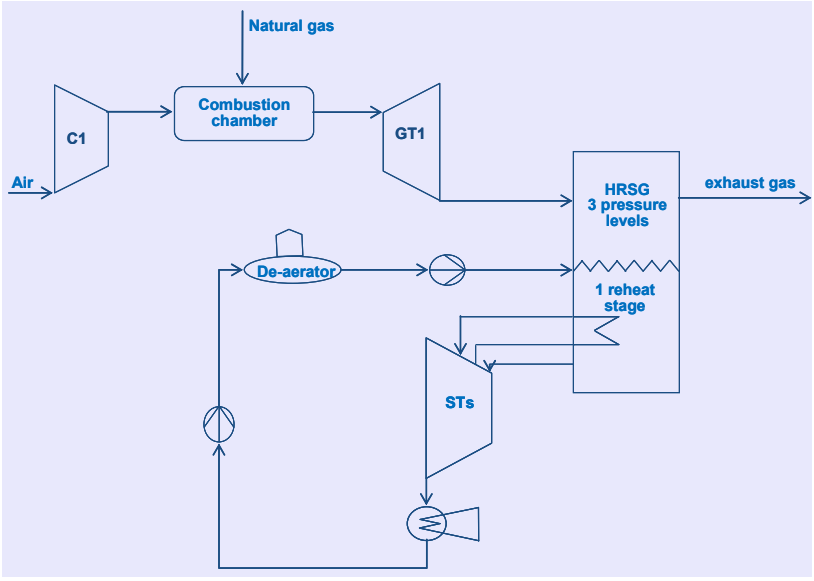

Fig. 1. Simplified diagram of the reference plant.

The plant includes a three-pressure-level heat-recovery steam generator (HRSG) and one reheat stage. A description of the operation and important operating parameters of the plant can be found in Petrakopoulou (2010) and Petrakopoulou et al. (2011a).

2.2 The plant with chemical absorption using monoethanolamine (MEA plant)

The plant with post-combustion capture bears minimal structural changes when compared to the reference plant. The modifications needed to incorporate CO_2 capture here are: (1) the addition of a chemical absorption unit (CAU) at the outlet of the exhaust gases, (2) the extraction of low-pressure steam to produce adequate thermal energy for the regeneration

of the chemical solvent used, and (3) the addition of steam turbines (STs) to drive the flue gas and compressors (C2 & C3-C6 in Figure A.2). The last two points result in a significant decrease in the power output and, consequently, in the efficiency of the overall system. A simple diagram of the plant with chemical absorption capture is shown in Figure 2. The grey box highlights the additional parts of this plant, when this is compared to the reference plant. The detailed flow diagram of the plant is shown in Figure A.2. The flue gas entering the CAU of the plant consists of 3.9% (v/v) CO_2, resulting in 38 kg/s of CO_2, 85% of which is captured. The solution used consists of 40% MEA (w/w).

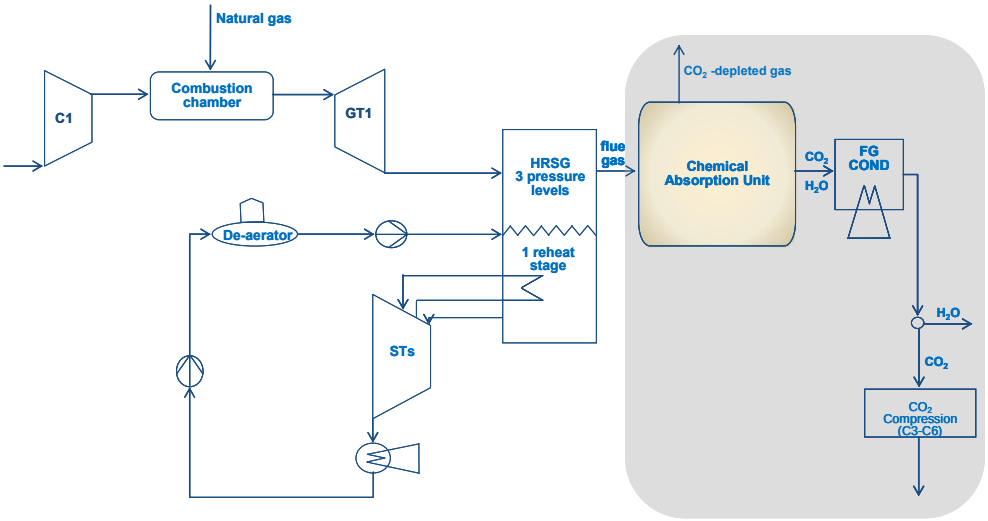

Fig. 2. Simplified diagram of the MEA plant (grey box highlights differences from the reference plant).

In the CAU, the CO_2-rich gas enters the absorber flowing upwards, counter-current to the lean MEA solution (Figure 3). After the CO_2 is absorbed, the clean gas is exhausted to the atmosphere and the CO_2–rich solution is heated in a heat exchanger (HX) and sent to a regenerator. In the regenerator, low-pressure steam extracted from the ST of the plant provides the necessary thermal energy ($\dot{Q}$) to regenerate the absorption medium. In this study, all of the components included in the CAU have been simulated as a black box with the embedded Equations (1)-(4) derived from Rubin & Rao (2002). Two input streams (the steam that provides the regeneration heat and the exhaust gas of the power plant) and three output streams (the exiting liquid water, the CO_2 stream and the stream containing the remaining elements of the flue gas) have been considered.

$$(L/G) = \exp\left(-1.4352 + 0.1239 \times y_{CO_2} + 3.4863 \times \varphi_{lean} + 0.0174 \times \eta_{CO_2} - 0.0397 \times C + 0.0027 \times T_{fg,in}\right) \quad (1)$$

$$\left(Q/L\right) = \exp\left(-2.4452 - 0.0037 \times y_{CO_2} - 6.2743 \times \varphi_{lean} + 0.0254 \times C\right) \times 100 \quad (2)$$

$$\left(T_{fg,out}\right) = 41.15 + 0.062 \times T_{fg,in} + 1.307 \times y_{CO_2} - 18.872 \times \varphi_{lean} + 0.270 \times C \quad (3)$$

$$\left(mw_{lean}\right) = 16.907 + 2.333 \times \varphi_{lean} + 0.204 \times C \quad (4)$$

Here, C is the MEA concentration in the sorbent (w/w, %), G is the total inlet flue gas flow rate (kmol/h), L is the total sorbent flow rate (kmol/h), mw_{lean} is the average molecular weight of the lean sorbent (kg/kmol), $\dot{Q}$ is the total sorbent regeneration heat requirement (GJ/h), $T_{fg,in}$ is the temperature of the flue gas entering the CO_2 absorber (°C), $T_{fg,out}$ is the temperature of the flue gas leaving the CO_2 absorber (°C), y_{CO_2} is the CO_2 concentration in the inlet flue gas (v/v, %) and φ_{lean} is the lean sorbent CO_2 loading that represents the part of the leftover CO_2 within the regenerated solvent (mol CO_2/mol MEA).

MEA is not included as a chemical compound in the simulation software (EBSILONProfessional), therefore its thermodynamic properties cannot be calculated. This leaves us with two choices: either no consideration of solvent losses (φ_{lean}=0) or consideration of losses that cause a minor violation of mass conservation because no MEA input stream is considered. Without lean solvent CO_2 loading, the MEA is assumed to be fully regenerated. This results in a relatively large amount of regeneration energy (6 MW/kg of CO_2 captured). Therefore, the lean solvent CO_2 loading has been varied from 0.0-0.3 mol CO_2/mol MEA. The influence of this variation on the exergetic efficiency and on the energy requirement of the plant is shown in Figure 4. As can be seen, with a mean value of the lean solvent CO_2 loading (0.2 mol CO_2/mol MEA), the energy requirement is reduced from 6 MW/kg of CO_2, calculated without losses, to 3.7 MW/kg of CO_2. In section 4, the MEA plant is evaluated with both 0.0 and 0.2 mol CO_2/mol MEA (MEA-0 and MEA-0.2), to further assess the effect of this parameter.

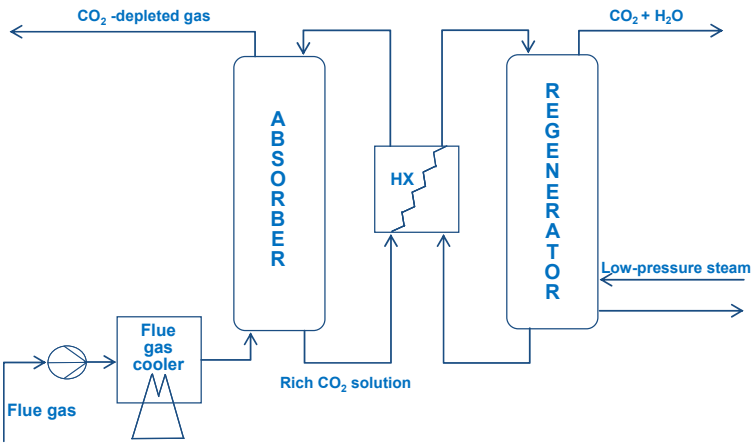

Fig. 3. Simplified diagram of a CAU.

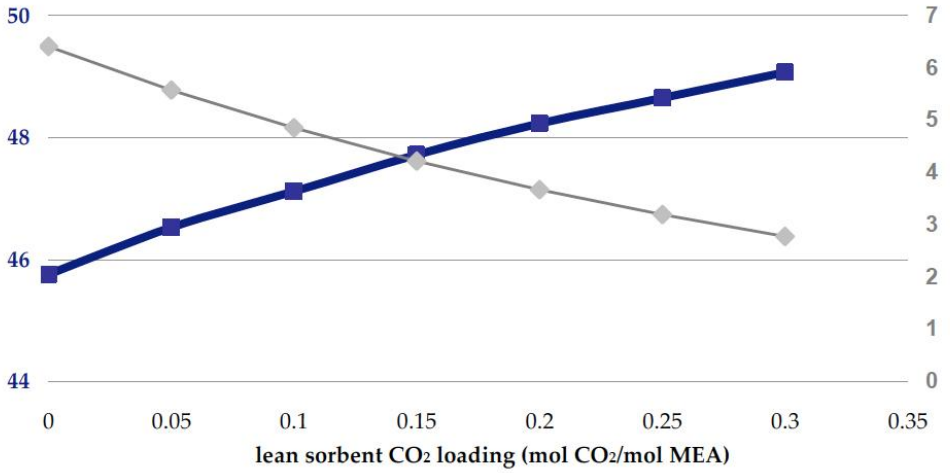

Fig. 4. Exergetic efficiency (%, blue line) and energy requirement (MJ/kg CO_2, grey line) relative to the lean sorbent CO_2 loading.

3. Methodology

3.1 Exergetic analysis

An exergetic analysis reveals the magitudes, locations and causes of inefficiencies and losses in an energy conversion system and provides insights that cannot be obtained from an energetic analysis. For a considered process, an exergetic analysis begins with a system of balance equations, formulated at the component level. The rate of exergy of product of component *k*, , is the exergy of the desired output resulting from the operation of the component, while the rate of exergy of fuel exergy of the same component, $\dot{E}_{F,k}$, is the expense in exergetic resources for the generation of the desired output. The rate of exergy destruction within component *k*, $\dot{E}_{D,k}$, is calculated as the difference between its rate of exergy of fuel and product ($\dot{E}_{D,k} = \dot{E}_{F,k} - \dot{E}_{P,k}$). For the analysis at the component level, streams exiting a component are considered either as part of the product, or they are used in the definition of the component's fuel. Thereafter, exergy loss is only defined for the overall system (tot): $\dot{E}_{L,tot} = \dot{E}_{F,tot} - \dot{E}_{P,tot} - \dot{E}_{D,tot}$.

The exergetic efficiency of component *k* and that of the overall system consisting of n-components are defined by Equations (5) and (6), respectively:

$$\varepsilon_k = \frac{\dot{E}_{P,k}}{\dot{E}_{F,k}} = 1 - \frac{\dot{E}_{D,k}}{\dot{E}_{F,k}} \tag{5}$$

$$\varepsilon_{tot} = \frac{\dot{E}_{P,tot}}{\dot{E}_{F,tot}} = 1 - \frac{\sum_{k=1}^{n} \dot{E}_{D,k} + \dot{E}_{L,tot}}{\dot{E}_{F,tot}} \tag{6}$$

General guidelines for the definition of exergetic efficiencies have been proposed in (Lazzaretto & Tsatsaronis, 2006). In dissipative components, such as condensers, intercoolers and throttling valves, exergy is destroyed without any useful product in the component itself; thus, no exergetic purpose can be defined (Bejan et al., 1996; Lazzaretto & Tsatsaronis, 2006). The essential role of these components is to serve other plant components, leading to a more efficient or cost effective operation of the overall system.

Variables related to exergy destruction and exergy loss are the exergy destruction ratio (defined both at the component level and the overall system with, Equations (7) and (8) and the exergy loss ratio (defined only for the overall plant with, Equation 9).

$$y_{D,k} = \frac{\dot{E}_{D,k}}{\dot{E}_{F,tot}} \tag{7}$$

$$y_{D,tot} = \frac{\dot{E}_{D,tot}}{\dot{E}_{F,tot}} \tag{8}$$

$$y_{L,tot} = \frac{\dot{E}_{L,tot}}{\dot{E}_{F,tot}} \tag{9}$$

The exergy destruction ratio is a measure of the contribution of the exergy destruction within each component to the reduction of the overall exergetic efficiency. It can be used to compare dissimilar components of the same system, while the ratios of total exergy destruction and exergy loss can be used to compare different thermodynamic systems.

With an exergetic analysis the main sources of thermodynamic irreversibilities within a plant are identified. If necessary, modifications to the plant can then be applied, in order to reduce these inefficiencies. Since the adoption and/or the development of systems are mainly driven by economics, the thermodynamically optimal design can be used as the starting point for cost reduction and eventually for cost minimization. Nowadays, the concept of *cost* could also be substituted with *environmental impact*, since a rapid increase in energy demand is foreseen that will impact the environment significantly.

3.2 Exergoeconomic analysis

An exergoeconomic analysis is an appropriate combination of an exergetic analysis with economic principles. This is achieved through exergy costing, by which a specific cost c is assigned to each exergy stream of the plant. The specific cost of stream i, c_i, multiplied by the exergy rate of the same stream, $\dot{E}_i$, provides the cost rate $\dot{C}_i$, associated with stream i:

$$\dot{C}_i = c_i \dot{E}_i \tag{10}$$

To perform an exergoeconomic analysis on a plant, cost balances are formulated at the component level resulting in a system of balance equations. For example, the cost balance of component k is stated as follows:

$$\sum_{i=1}^{l}\dot{C}_{i,k}-\sum_{j=1}^{m}\dot{C}_{j,k}+\dot{Z}_k=0 \tag{11}$$

Here, $\sum_{i=1}^{l}\dot{C}_{i,k}$ is the sum of the cost rates associated with the *l* steams entering component *k*, $\sum_{j=1}^{m}\dot{C}_{j,k}$ is the sum of the cost rates associated with the *m* streams leaving the component and Z_k is the rate of investment cost associated with the component.

In the system of balance equations, when the number of unknown stream costs is larger than the number of equations, auxiliary statements are required. For each component, streams entering are assumed to be known, while streams leaving the component are unknown. When the number of the outgoing exergy streams of a component is higher than one (m > 1), m-1 auxiliary equations are needed. The P-principle (on the product side) and the F-principle (on the fuel side) are used to determine the auxiliary equations (Lazzaretto & Tsatsaronis, 2006). The P-principle states that the cost per unit of exergy is supplied to all streams that belong to the definition of the product of the component at the same cost. The F-principle states that the cost, associated with the exergy removed from a component, has the same specific cost as the exergy supplied to the upstream components.

An important outcome of the exergoeconomic analysis is the relation of exergy destruction with costs:

$$\dot{C}_{D,k}=c_{F,k}\dot{E}_{D,k} \tag{12}$$

where, $c_{F,k}$ is the average specific cost of fuel of component *k*.

The calculation of the cost of exergy destruction facilitates the evaluation of plant components and allows comparisons between the cost of exergy destruction and the investment cost for the most important components. The components are first ranked and evaluated based on their total costs $\dot{C}_{D,k}+\dot{Z}_k$. The higher the sum of these costs is, the more significant the effect of the component on the overall plant. The contribution of the capital cost, $\dot{Z}_k$, to the sum of costs is expressed by the exergoeconomic factor f_k, defined by Equation (13).

$$f_k=\frac{\dot{Z}_k}{\dot{Z}_k+\dot{C}_{D,k}} \tag{13}$$

Another important variable in the exergoeconomic evaluation is the relative cost difference, r_k. For a given component *k*, the difference between the specific cost of product, $c_{P,k}$, and the specific cost of fuel, $c_{F,k}$, depends on the cost of exergy destruction, $\dot{C}_{D,k}$, and the related $\dot{Z}_k$.

$$r_k=\left(\frac{c_{P,k}-c_{F,k}}{c_{F,k}}\right)=\frac{\dot{C}_{D,k}+\dot{Z}_k}{c_{F,k}\dot{E}_{P,k}} \tag{14}$$

Information about compromises between the cost of exergy destruction and the investment cost of components, resulting from the exergoeconomic evaluation, can be used in an iterative design improvement of the plant. The objective is to reduce the cost associated with the product of the overall plant.

3.3 Exergoenvironmental analysis

In an exergoenvironmental analysis, the concepts of exergy and environmental impact are combined (Meyer et al., 2009). The component-related environmental impact of component k, $\dot{Y}_k$, is obtained in an LCA considering the entire life cycle of each plant component. It is the sum of the environmental impact of: (a) construction, $\dot{Y}_k^{CO}$, (including manufacturing, transport and installation), (b) operation and maintenance, $\dot{Y}_k^{OM}$ and (c) the disposal, $\dot{Y}_k^{DI}$, of component k:

$$\dot{Y}_k = \dot{Y}_k^{CO} + \dot{Y}_k^{OM} + \dot{Y}_k^{DI} \tag{15}$$

Similar to the exergoeconomic analysis, the exergoenvironmental analysis is performed with a system of equations written at the component level. The environmental impact balance for component k states that the sum of the environmental impacts associated with all input streams of the component equals the sum of the environmental impacts associated with all output streams of the same component:

$$\sum_{i=1}^{l} \dot{B}_{i,k} - \sum_{j=1}^{m} \dot{B}_{j,k} + \dot{Y}_k + \dot{B}_k^{PF} = 0 \tag{16}$$

Here, $\dot{B}_{i/j} = b_{i/j}\dot{E}_{i/j}$ (b: specific environmental impact of stream i/j), $\sum_{i=1}^{l} \dot{B}_{i,k}$ is the sum of the environmental impacts associated with the l steams entering component k, $\sum_{j=1}^{m} \dot{B}_{j,k}$ is the sum of the environmental impacts associated with the m streams leaving component k and $\dot{B}_k^{PF}$ is the impact of pollutant formation. The latter is related to the production of pollutants within a component and is charged to the specific component, representing the potential impact that could be caused if the generated pollutants were exhausted. Pollutant formation is defined only when a chemical reaction takes place; in any other case, it is zero. It is calculated as:

$$\dot{B}_k^{PF} = \sum_i b_i^{PF} \left(\dot{m}_{i,out} - \dot{m}_{i,in} \right) \tag{17}$$

where, $\dot{m}_{in}$ and $\dot{m}_{out}$ are the mass flow rates of pollutants entering and exiting component k, respectively. The pollutant streams that are taken into account here include CO_2 and NO_X.

When auxiliary equations need to be formulated, to make the number of the unknowns equal to the number of equations, the same principles are valid as for the exergoeconomic analysis. The environmental impact of the exergy destruction is calculated as:

$$\dot{B}_{D,k} = b_{F,k}\dot{E}_{D,k} \tag{18}$$

Here, $b_{F,k}$ is the specific environmental impact of the fuel provided to component k. $\dot{B}_{D,k}$ can then be compared to the component-related impact of component k, $\dot{Y}_k$.

The exergoenvironmental analysis not only identifies the components with the highest environmental impact, but also reveals the possibilities for improvement, in order to decrease the environmental impact of the overall plant. These improvement possibilities can be identified through the sum of the component-related environmental impact and the impact of exergy destruction, $\dot{Y}_k + \dot{B}_{D,k}$, the exergoenvironmental factor, $f_{b,k}$, and the relative environmental impact difference, $r_{b,k}$.

$$f_{b,k} = \frac{\dot{Y}_k}{\dot{Y}_k + \dot{B}_{D,k}} \tag{19}$$

$$r_{b,k} = \frac{\left(b_{F,k} - b_{P,k}\right)}{b_{F,k}} = \frac{\dot{B}_{D,k} + \dot{Y}_k}{b_{F,k}\dot{E}_{P,k}} \tag{20}$$

With the exergoenvironmental factor, the contribution of the component-related impact, $\dot{Y}_k$, to the total environmental impact, $\dot{Y}_k + \dot{B}_{D,k}$ is expressed at the component level. In theory, when the value of $f_{b,k}$ is relatively high, $\dot{Y}_k$ is dominant, whereas when the value of $f_{b,k}$ is low, exergy destruction is dominant. Thus, the higher the exergoenvironmental factor, the higher the influence of the component-related impact on the overall performance of the plant. In practice, when a system works with fossil fuels, the results of the exergoenvironmental factor differ from those of the exergoeconomic factor significantly: the component-related impact is very low when compared to the impact associated with the operation of the plant (exergy destruction).

The environmental impact difference of component k, $r_{b,k}$, depends on the impact of its exergy destruction and its component-related impact. Thus, it is an indicator of the environmental impact reduction potential of the component. After the calculation and evaluation of the mentioned variables, design changes are suggested, in order to reduce the environmental impact associated with the product of the overall process.

4. Results

4.1 Exergetic analysis

In the analysis it was assumed that all power plants are provided with the same amount of fuel. Thus, the derived rate of exergy of product ($\dot{E}_{P,tot}$) depends on the operating characteristics of the plant and the requirements of the CO_2 capture technology. Selected results of the analysis for the overall plants are presented in Table 1 and for the individual components in the Appendix.

As previously discussed, the MEA plant is considered with both zero and 0.2 lean sorbent CO_2 loading (MEA-0 and MEA-0.2). The results of MEA-0.2 agree better with published

work (Rubin & Rao, 2002). Therefore, although MEA-0 will sometimes be used for comparison purposes, MEA-0.2 is considered as the main representative plant for chemical absorption. If not otherwise stated, *MEA plant* refers to MEA-0.2.

	Ref. Plant	**MEA-0.2**[2]	**MEA-0**[1]
ε_{tot} *(%)*	56.5	48.4	45.8
$\dot{E}_{P,tot}$ *(MW)*	412.5	353.8	334.6
$\dot{E}_{D,tot}$ *(MW)*	300.4	349.1	368.3
$\dot{E}_{L,tot}$ *(MW)*	17.6	27.6	27.7
$y_{D,tot}$ *(%)*	41.1	47.8	50.4

Table 1. Selected results of the exergetic analysis.

The MEA plant results in an efficiency of eight percentage points lower than that of the reference plant. As expected, the main exergy destruction in the plant occurs within its combustion chamber (CC). When the reactants are preheated, the exergy destruction within the reactors decreases (Petrakopoulou, 2010). The exergy destruction within the CC of the MEA plant is the same as that of the reference plant, because the gas turbine (GT) systems of the two plants are identical. The CC is followed by the expander and the compressor of the GT system (GT1 and C1) in descending order of exergy destruction. Apart from the GT system that has a dominant influence due to its high values of $\dot{E}_{D,k}$, other components appear to be equally important. The CAU has the second highest value of exergy destruction among the plant components with 8% of the plant's $\dot{E}_{F,tot}$ being destroyed there. The high-pressure level of the HRSG (HPHRSG) is the most important part of the HRSG in the plant, followed by its respective low-pressure level part (LPHRSG). The low-pressure steam turbine (LPST) also presents relatively significant values of exergy destruction. Lastly, the exergy destruction within the CO_2 compression unit is approximately 2% of the $\dot{E}_{F,tot}$ of the plant.

4.2 Exergoeconomic analysis

The investment cost of the reference plant is calculated to be 213 € million (Petrakopoulou et al., 2011c). For the MEA plants the investment cost is increased by 50%, which is related to the cost of the CAU. Specifically, the investment cost of MEA-0.2 has been found to be 326 € million and that of MEA-0 319 € million. Comparing the two MEA plants, the regeneration requirement in MEA-0.2 is reduced and the CAU is smaller and, therefore, cheaper. However, since a smaller steam mass flow is needed for the CAU, more steam will flow through the condenser of the plant (COND, Figure A.2). Thus, the cooling water requirement of the plant increases, resulting in a larger condenser and a larger cooling tower (CT). Moreover, the first CO_2 compressor (C3) is larger in MEA-0.2 than in MEA-0, because the outlet temperature of the CAU is calculated to be higher. The CO_2 compression unit, i.e., the CO_2 compressors and coolers, is accountable for 13% of the investment cost in the MEA

[2] 0 and 0.2 stand for the assumed lean sorbent CO_2 loading (0 or 0.2 mol CO_2/mol MEA).

plant. Additionally, the cost of the HRSG of both MEA plants is similar to that of the reference plant. Detailed results of the economic analysis can be found in (Petrakopoulou, 2010).

An important outcome of the exergoeconomic analysis is the correlation of exergy destruction with costs. The cost rate of exergy destruction is calculated at the component level and is compared to the respective investment cost rates. In the reference plant, the three components with the highest cost rates are those constituting the GT system: CC, GT1 and C1. The components that follow the GT system in order of importance are the LPST and the HPHRSG. In the MEA plants, the CAU presents the second highest cost of exergy destruction and total cost, right after the CC of the plant. GT1, C1 and the group of the CO_2 compressors follow the CAU. In the MEA plants, the HPHRSG exceeds the STs in cost. Results for selected components of the exergoeconomic analysis are shown in Tables A.1 - A.3 of the Appendix, while the complete results at the component and the stream level can be found in Petrakopoulou (2010).

The relative cost difference, r_k, is found to be high for compressors and pumps, where electric power is used as fuel. This variable shows the theoretical improvement potential of the components. Nevetheless, the exergoeconomic factor, f_k, is the main tool for evaluating the cost effectiveness of a considered component. High values of the exergoeconomic factor for components with high total cost suggest that a reduction of the investment cost should be considered. On the other hand, low values of the factor suggest that a reduction in the exergy destruction should be considered, even if this would increase the investment cost of the component. The low exergoeconomic factors of the CCs of the plants show that most of the components' total cost is related to exergy destruction. This, however, is common for chemical reactors, due to the high level of irreversibilities present there. The exergoeconomic factor of reactors increases when a design with different, more expensive and/or rare materials is considered.

In general, the values of the exergoeconomic factor are within the expected value ranges for the most influential components (Bejan et al., 1996). Exceptions could be the high exergoeconomic factors calculated for the CO_2 compressors, suggesting that a decrease in the investment cost of these components (if less expensive components could be employed) should be considered in an attempt to improve the cost effectiveness of the overall plant. A low exergoeconomic factor is calculated for ST4 of the MEA plants. This is due to the exergy destruction within this component, which is found to be high both on its own and when it is compared to the other STs of the plants. Thus, to improve the overall operation of the plants, the efficiency of this ST should be increased. Additionally, for all plants, low factors are calculated in coolers and condensers, where relatively high exergy destruction is found.

Since the plants have the same c_F, the total cost rate of exergy destruction, $\dot{C}_{D,tot}$, depends on the exergy destruction ($\dot{E}_{D,tot}$) within the plants (i.e., $\dot{C}_{D,tot} = c_F \dot{E}_{D,tot}$). The cost of exergy destruction of the MEA plants is larger when compared to that of the reference plant. Specifically, the $\dot{C}_{D,tot}$ of MEA-0 is higher by 23% and that of MEA-0.2 by 16% (see Appendix). As expected, the cost differences are representative of the differences between the $\dot{E}_{D,tot}$ of the MEA plants and that of the reference plant.

Values for the overall plants are shown under *Total* in Tables A.1 - A.3. The overall exergoeconomic factor of the reference plant is calculated to be 40%, while the MEA plants result in overall exergoeconomic factors of 43 and 45%. Additionally, the overall relative cost difference is higher for the plants with CO_2 capture than for the reference plant. This is justified with the additional charges of the supplementary equipment used.

To further compare the costs of the plants, the COE and the cost of avoided CO_2 (COA-CO_2) are considered. The latter shows the added cost of electricity per ton of CO_2 avoided based on net plant capacity (Rubin & Rao, 2002):

$$\text{COA-CO}_2 = \frac{(€/kWh)_{capture} - (€/kWh)_{ref.plant}}{(t_{CO_2}/kWh)^{emitted}_{ref.plant} - (t_{CO_2}/kWh)^{emitted}_{plant+capture}} \quad (21)$$

The COA-CO_2 relates only to the capture of the CO_2 and it does not include transportation or storage costs.

The resulting levelized COE and the COA-CO_2 for the plants are shown in Table 2. Between the two MEA plants, a lower COE is achieved by MEA-0.2. The COE of this plant is 28% higher than that of the reference plant. When compared to other plants with CO_2 capture (Petrakopoulou et al., 2010b; Petrakopoulou et al., 2011a, 2011b, 2011c), the MEA plants present relatively high costs. These costs are mainly associated with the high energy demand of the solvent regeneration in the CAU and the relatively low percentage of CO_2 capture (85%).

	Ref. Plant	**MEA 0.2**	**MEA 0.0**
COE (€/MWh)	74.1	94.6	99.5
COA-CO_2 (€/t)	N/A	73.5	92.2

COA-CO_2: Cost of avoided CO_2, COE: Cost of electricity

Table 2. Overall results of the exergoeconomic analysis for the plants.

4.3 Results of the exergoenvironmental analysis

The component-related environmental impacts determined in the LCAs of the plants differ in relative magnitude from costs obtained in the economic analysis. While in the economic analysis, the cost rates (calculated in €/h), are relatively substantial, in the LCA, the component-related environmental impact rates, ($\dot{Y}_k$, in Pts/h) are much lower in scale. Relatively high values are calculated for components constructed with materials of higher environmental impact and for the CTs of the plants, due to their large size. As can be seen in Table 3, the MEA plants have a relatively low increase in relative total environmental impact (Pts/kW), when compared to the reference plant, because of the similar equipment used in both plants. Comparing MEA-0 with MEA-0.2, the differences are also small. While the absorber of MEA-0.2 is smaller and results in a lower impact, its COND and CT are larger. This happens because of the larger mass of steam flowing through the COND, which is a direct result of the lower mass of steam extracted and used in the CAU of this plant (Petrakopoulou, 2010).

For the LCA, the environmental impact of pollutant formation $\dot{B}^{PF}$ of the reactors of each plant has been calculated separately. The specific environmental impact associated with each pollutant and the results of the calculations, including the impact that is avoided due to CO_2 capture, are shown in Table 4. As can be seen, 60% of pollutant formation in the reference plant is related to the CO_2 emissions of the reference plant, while the remaining 40% is related to its NO_X emissions. The same NO_X emissions are considered for the MEA plants. The environmental impact of pollutants, such as CO_2, can affect the result of the overall analysis. A sensitivity analysis of the impact of CO_2 emissions for the reference and MEA-0.2 plants (with and without consideration of the environmental impact of CO_2 sequestration) is presented in Petrakopoulou (2010). It was found that CO_2 capture becomes meaningful when the environmental impact of CO_2 is higher than 20 Pts/t (when storage is also accounted for). This is a specific environmental impact of CO_2 approximately four times higher than that provided by Goedkoop & Spriensma (2000). Additionally, when CO_2 transport and sequestration are not accounted for, the limit for a positive environmental impact of CO_2 capture decreases the required specific environmental impact of CO_2 to 14 Pts/t.

	Ref. Plant	**MEA 0.2**	**MEA 0.0**
Total environmental impact (10^3 Pts)	2,592	3,223	2,871
Total environmental impact (Pts/kW)	6.3	9.1	8.6
EIE (mPts/kWh)	25.1	27.4	29.0

Table 3. Component-related environmental impact and environmental impact of electricity (EIE).

	CO_2		**NO_X**		$\dot{B}^{PF}$	$\dot{B}^{PF}_{CO_2\_capt}$
	(kg/s)	**(mPts/kg)**	**(kg/s)**	**(Pts/t)**	**(Pts/h)**	**(Pts/h)**
Ref. Plant	38.41		0.05		1259	0
MEA 0.2	38.42	**5.4**	0.05	**2749.4**	1270	-646
MEA 0.0	38.42		0.05		1268	-646

Table 4. Environmental impact of overall and avoided pollutant formation due to CO_2 capture.

The component-related impact ($\dot{Y}_{tot}$) differs among the plants. However, this difference is almost negligible and differences among the total impact ($\dot{B}_{D,tot}+\dot{Y}_{tot}$) of the plants are determined by the impact of exergy destruction (see Tables A.1 - A.3). This indicates that the construction is not the key area for reducing the environmental impact of the plants.

In the reference plant, the highest environmental impact ($\dot{B}_{D,k}+\dot{Y}_k$) corresponds to the CC, GT1, the LPST and C1. In the MEA plant, the CC is followed by the CAU, which presents a high environmental impact of exergy destruction. In the exergoenvironmental analysis, dissipative components become more important than in the exergoeconomic analysis: a high

impact is calculated for the condensers (COND and FG COND) of the plants. As already mentioned, in the exergoeconomic and exergoenvironmental analyses, the influence of the non-exergy related costs/impacts (investment cost rate and rate of the component-related impact) is different. Because in the exergoenvironmental analysis the component-related environmental impact is almost negligible, the exergy destruction and the specific environmental impact of fuel are the main deciding factors of the significance of a component. Differences between the results of the exergoenvironmental analysis and that of the exergetic analysis can be noted only for components with high environmental impacts (Petrakopoulou et al., 2010a; Petrakopoulou et al., 2011b).

The total exergoenvironmental factor is similar for the reference and MEA plants because of their similar component-related environmental impact. A reduction in the overall environmental impact could be achieved by increasing the exergetic efficiency of the GT system and of the reactors. In general, a significant decrease in the irreversibilities present in reactors is difficult to be achieved, because these irreversibilities are mostly unavoidable (Petrakopoulou et al., 2011d). However, the preheating of the reactants, as well as the use of different GT systems (e.g., steam-cooled expanders) would lead to better efficiencies, thus decreasing the incurred exergy destruction. In general, in order to reduce the overall impact of the plants, more attention should be given to the effectiveness of the component operation, thus to the exergetic efficiencies of the components.

To compare the overall environmental performance of the plants, the environmental impact of the electricity (EIE) has been calculated (Table 3). The EIE produced by the reference plant is found to be 25.1 Pts/MWh. This is comparable to the European average impact of low voltage electricity: 26 Pts/MWh (Goedkoop & Spriensma, 2000). When compared to the reference plant, the EIE of MEA-0.2 is higher by 2.3 Pts/MWh. Considering that no impact has been considered for pollutants generated by the processing of the solvent used in the plant, the case presented is considered the *best case scenario* of this plant.

5. Conclusion

In this study, a post-combustion CO_2 capture technology (chemical absorption with monoethanolamine) has been evaluated with two different possible energy requirements. A plant incorporating this technology (MEA plant) has been compared with a reference power plant of similar configuration that does not include CO_2 capture. The plants have been analyzed using conventional exergetic, exergoeconomic and exergoenvironmental analyses.

The plant with CO_2 capture presented an (exergetic) efficiency penalty of approximately eight percentage points (48.4%[3]), when compared to the reference plant (56.5%). The relatively high efficiency penalty of the MEA plant is caused by the high energy requirements of chemical absorption that decrease its net power output.

When comparing the cost of the plant with other CO_2 capture technologies (Petrakopoulou, 2010), the MEA plant presents the most economical relative costs based on its power output

[3] Here, only MEA-0.2 is considered.

(921 €/kW). Additionally, it was found that the cost of exergy destruction of the MEA plant is larger than that of the reference plant. It should be noted that this difference is mainly representative of the differences between the rates of exergy destruction of the plants. Larger differences between the overall costs of the reference and MEA plants are caused by the high investment cost of components used in the CO_2 separation and compression units. The cost of electricity of the MEA plant is found to be 28% higher that of the reference plant. When compared to other capture technologies, and on the basis of the cost of avoided CO_2, large cost differences are observed (Petrakopoulou, 2010). These differences are mainly associated with the high energy demand of the solvent regeneration and the relatively low percentage of CO_2 capture (85%).

In the exergoenvironmental analysis, it was found that the MEA plant presents a low unit increase of the component-related environmental impact (Pts/kW), when compared to the reference plant. However, the component-related environmental impact of the plants is negligible when compared to the impact associated with the exergy destruction that takes place during the operation phase of the plants. The calculation of the overall environmental impact is mainly influenced by the impacts of fuel processing (methane) and the impact of pollutant emission. With data provided by Goepkoop & Spiensma (2000), the environmental impact of the electricity generated in the MEA plant is found to be significantly higher than that of the reference plant (2.3 mPts/kWh higher), due its high efficiency penalty. This raises questions concerning the real environmental and cost viability of chemical absorption with MEA for CO_2 capture in power plants. A sensitivity analysis concerning the variation of the environmental impact of CO_2 emissions showed that post-combustion technology will not decrease the environmental impact of power production, unless a specific environmental impact approximately four times higher than the present estimate is assigned to the CO_2 emissions.

In general, CO_2 capture is a costly process, since it involves either expensive equipment that increases the overall investment cost of the facility or energy-demanding processes that decrease the efficiency, in turn increasing the fuel consumption (i.e., the fuel costs) of a plant. Moreover, the environmental analysis shows that high efficiency reductions result in significant environmental penalties. Thus, with present data, the environmental viability of post-combustion CO_2 capture with chemical absorption using monoethanolamine is questionable, especially when the associated cost expenditure of the technology is also considered.

6. Nomenclature

b	Environmental impact per unit of exergy (Pts/GJ)
$\dot{B}$	Rate of environmental impact (Pts/h)
c	Cost per unit of exergy (€/GJ)
$\dot{C}$	Cost rate associated with an exergy stream, (€/h)
$\dot{E}$	Exergy rate (MW)
f	Exergoeconomic factor (%)

$\dot{m}$ Mass flow (kg/s)
r Relative cost difference (%)
y Exergy destruction ratio (%)
$\dot{Y}$ Component-related environmental impact (Pts/h)
$\dot{Z}$ Cost rate associated with capital investment (€/h)

Subscripts

D Exergy destruction
F Fuel (exergy)
P Product (exergy)
i,j Stream
k Component
L Loss

Greek symbols

ε Exergetic efficiency (%)

Abbreviations

C (1-6) Compressor
CAU Chemical absorption unit
CC Combustion chamber
COA-CO_2 Cost of avoided CO_2
COE Cost of electricity
COND Condenser
CT Cooling tower
EC Economizer
EIE Environmental impact of electricity
EV Evaporator
FG Flue gas
GT Gas turbine
HP, IP, LP High pressure, intermediate pressure, low pressure
HRSG Heat recovery steam generator
HX Heat exchanger
LCA Life cycle assessment
MEA Monoethanolamine
NG Natural gas
PF Pollutant formation
PH Preheater
RH Reheater
SH Superheater
ST Steam turbine

7. Appendix

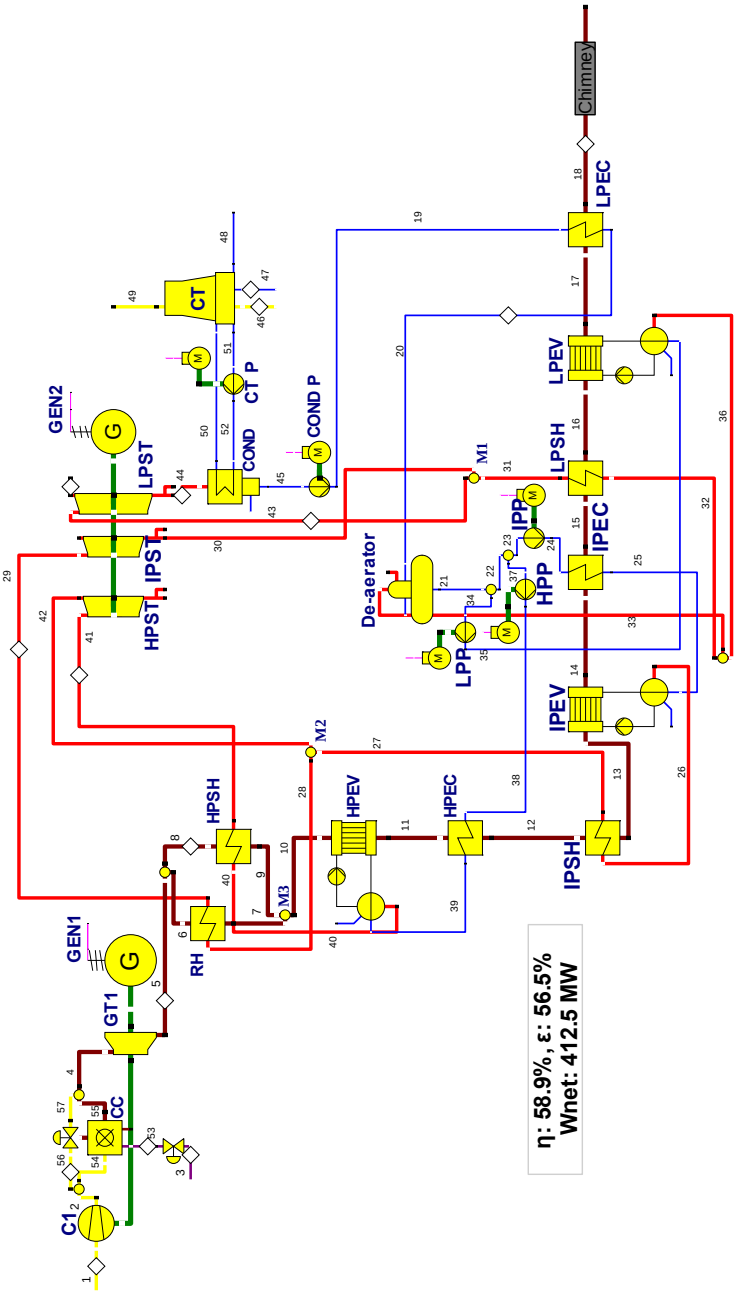

Fig. A.1. The reference plant.

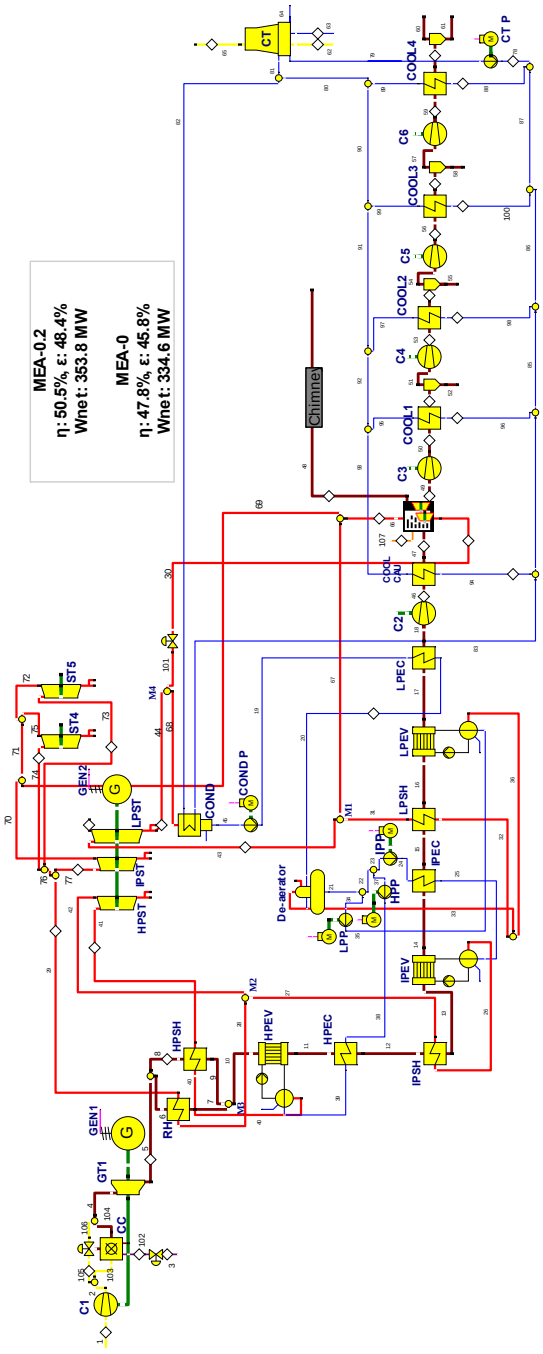

Fig. A.2. The MEA plant.

Component, k	$\dot{E}_{F,k}$ (MW)	$\dot{E}_{P,k}$ (MW)	$\dot{E}_{D,k}$ (MW)	ε_k (%)	$y_{D,k}$ (%)	$c_{F,k}$ (€/GJ)	$c_{P,k}$ (€/GJ)	$\dot{C}_{D,k}$ (€/h)	$\dot{Z}_k$ (€/h)	$\dot{C}_{D,k}+\dot{Z}_k$ (€/h)	f_k (%)	r_k (%)	$b_{F,k}$ (Pts/GJ)	$b_{P,k}$ (Pts/GJ)	$\dot{B}_{D,k}$ (Pts/h)	$\dot{Y}_k$ (Pts/h)	$\dot{B}_{D,k}+\dot{Y}_k$ (Pts/h)	$f_{b,k}$ (%)	$r_{b,k}$ (%)
C1	242.68	231.30	11.38	95.3	1.56	16.9	19.5	693	1,423	2,116	67.3	15.0	6.1	6.4	249.71	0.24	249.94	0.09	4.9
CC	729.62	508.76	220.87	69.7	30.23	9.2	13.7	7,276	1,017	8,293	12.3	49.5	3.5	5.6	2746.20	0.38	2746.58	0.01	63.3
GT	551.15	530.67	20.47	96.3	2.80	15.5	16.9	1,140	1,627	2,766	58.8	9.4	5.9	6.1	432.58	1.12	433.71	0.26	3.9
HPSH	35.07	31.72	3.35	90.5		15.5	19.4					25.6	5.9	6.8					15.5
HPEV	43.64	39.91	3.73	91.5		15.5	19.0					23.1	5.9	6.7					13.6
HPEC	28.92	24.91	4.00	86.2	1.52	15.5	20.4	617	432	1,049	41.2	31.8	5.9	7.2	234.07	1.42	235.49	0.60	23.3
RH	26.47	23.89	2.58	90.3		15.5	19.4					25.4	5.9	6.8					15.8
IPSH	0.18	0.12	0.06	69.0		15.5	35.4					128.8	5.9	9.7					65.2
IPEV	6.10	5.67	0.43	92.9		15.5	20.5					32.8	5.9	6.5					11.1
IPEC	1.06	0.87	0.19	82.5	0.44	15.5	22.3	181	186	367	50.7	44.3	5.9	7.7	68.64	0.85	69.49	1.22	30.9
LPSH	1.43	1.04	0.38	73.3		15.5	29.5					90.9	5.9	9.0					53.0
LPEV	19.03	15.48	3.55	81.4		15.5	24.2					56.4	5.9	7.8					33.3
LPEC	11.49	7.71	3.78	67.1	1.06	15.5	30.8	429	287	716	40.1	99.3	5.9	10.1	162.97	0.23	163.20	0.14	71.3
LPST	70.99	61.35	9.64	86.4	1.32	21.4	29.7	743	764	1,508	50.7	38.5	7.2	8.8	251.49	0.49	251.98	0.20	21.5
Total	**730.58**	**412.54**	**300.41**	**56.5**	**41.12**	**9.2**	**20.6**	**9,897**	**6,519**	**16,416**	**39.7**	**124.8**	**3.5**	**7.0**	**3735.22**	**17.33**	**3752.54**	**0.46**	**101.7**
Exergy loss	**17.63**																		
$\dot{B}_k^{PF}$ **(Pts/h)**	**1,259**																		

Table A.1. Selected results at the component level for the reference plant.

Component, k	$\dot{E}_{F,k}$ (MW)	$\dot{E}_{P,k}$ (MW)	$\dot{E}_{D,k}$ (MW)	ε_k (%)	$y_{D,k}$ (%)	$c_{F,k}$ (€/GJ)	$c_{P,k}$ (€/GJ)	$\dot{C}_{D,k}$ (€/h)	$\dot{Z}_k$ (€/h)	$\dot{C}_{D,k}+\dot{Z}_k$ (€/h)	f_k (%)	r_k (%)	$b_{F,k}$ (Pts/GJ)	$b_{P,k}$ (Pts/GJ)	$\dot{B}_{D,k}$ (Pts/h)	$\dot{Y}_k$ (Pts/h)	$\dot{B}_{D,k}+\dot{Y}_k$ (Pts/h)	$f_{b,k}$ (%)	$r_{b,k}$ (%)
C1	242.68	231.30	11.38	95.3	1.56	16.9	19.4	691	1,396	2,086	66.9	14.9	6.1	6.4	249.98	0.24	250.22	0.09	4.9
CC	729.62	508.76	220.87	69.7	30.23	9.2	13.7	7,276	997	8,273	12.0	49.4	3.5	5.6	2746.20	0.38	2746.59	0.01	63.5
GT	551.15	530.67	20.47	96.3	2.80	15.4	16.9	1,137	1,595	2,732	58.4	9.3	5.9	6.1	433.06	1.13	434.18	0.26	3.9
HPSH	35.06	31.72	3.34	90.5		15.4	18.9					22.6	5.9	6.7					13.5
HPEV	43.64	39.91	3.73	91.4		15.4	18.6					20.4	5.9	6.6					11.9
HPEC	28.92	24.91	4.01	86.1	1.52	15.4	19.6	615	424	1,040	40.8	27.3	5.9	7.1	234.36	1.46	235.82	0.62	20.4
RH	26.46	23.89	2.57	90.3		15.4	18.9					22.2	5.9	6.7					13.8
IPSH	0.18	0.12	0.06	69.0		15.4	33.3					115.7	5.9	9.2					57.1
IPEV	6.10	5.67	0.43	92.9		15.4	20.1					30.3	5.9	6.4					9.7
IPEC	1.06	0.87	0.19	82.5	0.44	15.4	21.3	180	182	362	50.3	38.2	5.9	7.5	68.58	0.83	69.41	1.19	27.0
LPSH	1.43	1.05	0.38	73.3		15.4	27.8					80.4	5.9	8.6					46.4
LPEV	19.02	15.47	3.54	81.4		15.4	23.1					49.8	5.9	7.6					29.1
LPEC	11.57	7.81	3.76	67.5	1.05	15.4	28.5	427	284	711	39.9	84.5	5.9	9.5	162.68	0.23	162.90	0.14	61.2
LPST	40.94	35.38	5.56	86.4	0.76	21.4	27.8	428	296	723	40.9	30.0	7.2	8.6	144.91	0.32	145.23	0.22	19.2
C2	18.53	16.93	1.59	91.4		22.5	43.6					94.0	7.2	8.0					10.3
C3	4.33	3.78	0.55	87.3		22.4	132.9					493.8	7.2	25.8					256.9
C4	3.45	2.86	0.59	82.9		22.4	100.1					347.2	7.2	16.3					125.2
C5	3.44	2.82	0.61	82.1	0.46	22.4	77.0	270	2,297	2,567	89.5	244.3	7.2	11.5	87.31	4.90	92.21	5.31	58.3
C6	3.49	2.83	0.66	81.1	0.09	22.4	77.4	53	354	406	87.0	245.7	7.2	11.4	17.13	0.20	17.34	1.18	57.5
CAU	59.28	-	40.59	-	5.56	23.7	-	3,463	1,023	4,486	22.8	-	6.9	-	1006.53	1.75	1008.28	0.17	-
Total	**730.58**	**353.82**	**349.14**	**48.4**	**47.79**	**9.2**	**26.3**	**11,502**	**9,440**	**20,942**	**45.1**	**187.0**	**3.5**	**7.6**	**4341.17**	**21.63**	**4362.80**	**0.50**	**120.7**
Exergy loss	**27.62**																		
$\dot{B}_k^{PF}$ **(Pts/h)**	**1,270**																		

Table A.2. Selected results at the component level for MEA-0.2.

Component, k	$\dot{E}_{F,k}$ (MW)	$\dot{E}_{P,k}$ (MW)	$\dot{E}_{D,k}$ (MW)	ε_k (%)	$y_{D,k}$ (%)	$c_{F,k}$ (€/GJ)	$c_{P,k}$ (€/GJ)	$\dot{C}_{D,k}$ (€/h)	$\dot{Z}_k$ (€/h)	$\dot{C}_{D,k}+\dot{Z}_k$ (€/h)	f_k (%)	r_k (%)	$b_{F,k}$ (Pts/GJ)	$b_{P,k}$ (Pts/GJ)	$\dot{B}_{D,k}$ (Pts/h)	$\dot{Y}_k$ (Pts/h)	$\dot{B}_{D,k}+\dot{Y}_k$ (Pts/h)	$f_{b,k}$ (%)	$r_{b,k}$ (%)
C1	242.68	231.30	11.38	95.3	1.56	19.4	690	1,395	2,086	66.9	14.9	19.4	6.1	6.4	249.94	0.24	250.17	0.09	4.9
CC	729.62	508.76	220.87	69.7	30.23	13.7	7,276	997	8,273	12.0	49.4	13.7	3.5	5.6	2746.20	0.38	2746.59	0.01	63.5
GT	551.15	530.67	20.47	96.3	2.80	16.9	1,137	1,595	2,732	58.4	9.3	16.9	5.9	6.1	432.98	1.13	434.11	0.26	3.9
HPSH	35.06	31.72	3.34	90.5		18.7	615				20.9	18.7	5.9	6.6					12.1
HPEV	43.64	39.91	3.73	91.4		18.4	18.7				19.0	18.4	5.9	6.5					10.6
HPEC	28.92	24.91	4.01	86.1	1.52	19.3	19.6	423	1,039	40.8	24.9	19.3	5.9	6.9	234.32	1.45	235.77	0.62	18.2
RH	26.46	23.89	2.57	90.3		18.6	180				20.6	18.6	5.9	6.6					12.3
IPSH	0.18	0.12	0.06	69.0		32.2	33.3				108.7	32.2	5.9	8.9					51.0
IPEV	6.10	5.67	0.43	92.9		19.9	20.4				29.2	19.9	5.9	6.4					8.7
IPEC	1.06	0.87	0.19	82.5	0.44	20.8	21.2	182	362	50.3	35.0	20.8	5.9	7.3	68.57	0.83	69.40	1.19	24.1
LPSH	1.43	1.05	0.38	73.3		27.0	427				74.7	27.0	5.9	8.3					41.4
LPEV	19.02	15.47	3.54	81.4		22.6	23.1				46.3	22.6	5.9	7.4					26.0
LPEC	11.57	7.81	3.76	67.5	1.05	27.3	28.0	284	711	39.9	77.3	27.3	5.9	9.1	162.65	0.23	162.87	0.14	54.6
LPST	17.84	15.42	2.42	86.4	0.33	29.3	200	134	334	40.1	27.9	29.3	7.5	8.8	65.52	0.19	65.71	0.29	17.4
C2	18.53	16.93	1.59	91.4		43.2	191				95.4	43.2	7.1	7.8					10.3
C3	3.54	3.00	0.54	84.6		153.7	161.9				594.8	153.7	7.1	30.2					325.7
C4	3.45	2.86	0.59	82.9		78.6	83.6				255.3	78.6	7.1	11.8					66.4
C5	3.44	2.82	0.61	82.1	0.33	77.2	82.2	1,435	1,626	88.2	249.1	77.2	7.1	11.3	61.40	1.32	62.72	2.11	58.7
C6	3.49	2.83	0.66	81.1	0.09	77.6	52	360	412	87.3	250.8	77.6	7.1	11.2	16.79	0.20	16.99	1.20	57.8
CAU	86.54	-	67.95	-	9.30	-	5,417	1,086	6,503	16.7	-	-	6.8	-	1658.02	3.50	1661.52	0.21	-
Total	**730.58**	**334.63**	**368.27**	**45.8**	**50.41**	**9.2**	**27.6**	**12,133**	**9,257**	**21,390**	**43.3**	**201.9**	**67.8**	**73.0**	**4579.01**	**19.27**	**4598.28**	**0.42**	**7.6**
Exergy loss	**27.68**																		
$\dot{B}_k^{PF}$ **(Pts/h)**	**1,268**																		

Table A.3. Selected results at the component level for MEA-0.

8. References

Bejan, A., Tsatsaronis, G., & Moran, M. (1996). *Thermal Design and Optimization* (p. 560). New York: Wiley-Interscience. Retrieved from http://www.amazon.com/Thermal-Design-Optimization-Adrian-Bejan/dp/0471584673

EBSILONProfessional. (n.d.) Retrieved August 8, 2011, from http://www.steag-systemtechnologies.com/ebsilon_professional.html

Goedkoop, M., & Spriensma, R. (2000). *Eco-indicator 99 impact assessment method for Life Cycle Impact Assessment*. Amersfoort. Retrieved from http://www.pre.nl/content/eco-indicator-99

Herzog, H. J. (2001). What future for carbon capture and sequestration? *Environmental science & technology*, *35*(7), 148A-153A. Retrieved from http://www.ncbi.nlm.nih.gov/pubmed/11348092

Kothandaraman, A., Nord, L., Bolland, O., Herzog, H. J., & McRae, G. J. (2009). Comparison of solvents for post-combustion capture of CO2 by chemical absorption. *Energy Procedia*, *1*(1), 1373-1380. Elsevier. doi:10.1016/j.egypro.2009.01.180

Lazzaretto, A., & Tsatsaronis, G. (2006). SPECO: A systematic and general methodology for calculating efficiencies and costs in thermal systems. *Energy*, *31*, 1257-1289.

Meyer, L., Tsatsaronis, G., Buchgeister, J., & Schebek, L. (2009). Exergoenvironmental analysis for evaluation of the environmental impact of energy conversion systems. *Energy*, *34*(1), 75-89. doi:10.1016/j.energy.2008.07.018

Petrakopoulou, F. (2010). *Comparative Evaluation of Power Plants with CO2 Capture: Thermodynamic, Economic and Environmental Performance*. Institut für Energietechnik. Retrieved from http://opus.kobv.de/tuberlin/volltexte/2011/2946/

Petrakopoulou, F., Boyano, A., Cabrera, M., & Tsatsaronis, G. (2010a). Exergy-based analyses of an advanced zero emission plant. *International Journal of Low-Carbon Technologies*, *5*(4), 231-238. doi:10.1093/ijlct/ctq028

Petrakopoulou, F., Tsatsaronis, G., Boyano, A., & Morosuk, T. (2010b). Exergoeconomic and exergoenvironmental evaluation of power plants including CO2 capture. *Chemical Engineering Research and Design*, *89*(9), 1469-1461. doi:10.1016/j.cherd.2010.08.001

Petrakopoulou, F., Boyano, A., Cabrera, M., & Tsatsaronis, G. (2011a). Exergoeconomic and exergoenvironmental analyses of a combined cycle power plant with chemical looping technology. *International Journal of Greenhouse Gas Control*, *5*(3), 475-482. doi:10.1016/j.ijggc.2010.06.008

Petrakopoulou, F., Tsatsaronis, G., & Morosuk, T. (2011b). Exergoeconomic Analysis of an Advanced Zero Emission Plant. *Journal of Engineering for Gas Turbines and Power*, *133*(11), 113001-12. ASME. Retrieved from http://link.aip.org/link/?GTP/133/113001/1

Petrakopoulou, F., Tsatsaronis, G., & Morosuk, T. (2011c). Conventional Exergetic and Exergoeconomic Analyses of a Power Plant with Chemical Looping Combustion for CO2 Capture. *International Journal of Thermodynamics*, *13*(3), 77-86. doi:10.5541/ijot.204

Petrakopoulou, F., Tsatsaronis, G., Morosuk, T., & Carassai, A. (2011d). Conventional and advanced exergetic analyses applied to a combined cycle power plant. *Energy*. doi:10.1016/j.energy.2011.05.028

Rubin, E. S., & Rao, A. B. (2002). *A Technical, Economic and Environmental Assessment of Amine-based CO2 Capture Technology for Power Plant Greenhouse Gas Control*. doi:10.2172/804932

22

The Greenhouse Stakes of Globalization

Sébastien Dente[1] and Troy Hawkins[2]
[1]*Université de Technologie de Troyes*
[2]*Environmental Protection Agency*
[1]*France*
[2]*USA*

1. Introduction

As 2012 approaches, twenty-five years have passed since the Brundtland report defining sustainable development as a progress that meets the needs of the present without compromising the ability of future generations to meet their own needs (United Nations). Currently, the fight against Climate change constitutes one of the main features of worldwide policies towards sustainable development. Furthermore, the global climate change issue benefits from an international discussion area through the United Nations framework convention on climate change (UNFCCC). This convention was created during the first Earth summit, which was held in Rio in 1992 and benefits from the scientific support of the Intergovernmental Panel on Climate Change (IPCC) created in November 1988. The ultimate objective of this convention is to achieve stabilization of greenhouse gas concentrations in the atmosphere at a level that would prevent dangerous anthropogenic interference with the climate system (United Nations, 1992). Thus far, the 1997 Kyoto protocol constitutes the main achievement of this convention of which we propose to briefly remind the objectives and analyze the policy patterns in **2.1**.

During the same period, the world is known to have experienced an unprecedented wave of globalization. Such globalization is characterized by the increasing number of countries taking part in international trade and the growing number of traded items both in variety, quantity, and value. **Figure 1** shows the world production and the associated globalization expressed in terms of world GDP fraction associated with exports have been respectively multiplied by 45 and 2.5 over the last fifty years. Nevertheless, over the 1960 – 2008 periods, it should be noted the same three regions[1] cover over half of the world GDP. It thus seems the globalization process has so far mainly consisted in a redistribution of GDP strength between these regions.

Another key point in the globalization process is the increasing sophistication of modern supply chains. Indeed, the application of modern management principles throughout the supply chain such as Just-In-Time, lean production and Efficient Consumer Response have led to more responsive, more flexible supply chains that enable firms to compete in a global

[1] **Western Europe**: Austria, Belgium, France, Germany, Luxembourg, Netherlands, Switzerland.
East Asia: China, Hong Kong, Macao, North Korea, Japan, Mongolia, South Korea.
Northern America: Bermuda, Canada, Greenland, Saint Pierre and Miquelon, USA.

market. Furthermore, the potential extension of trade partners encourages companies to experience global sourcing strategies and wider distribution of finished products (Cetinkaya, et al., 2011). All these new aspects of trade tend to increase the need for freight transportation and particularly for international freight transportation whose associated emissions were not addressed by the Kyoto Protocol. Indeed, the inclusion of these emissions constitutes the main debate of Post-Kyoto mitigation policies.

The objective of this chapter is thus to link globalization to global climate change via:

- A policy and macro-economic perspective in framing the stakes linked to the increasing importance of GHG emissions associated with trade and freight transportation for the definition of Post-Kyoto GHG reduction strategies.
- A micro-economic or trade perspective in framing the stakes and challenges of product carbon labeling policies and carbon accounting, notably those associated with freight transportation.

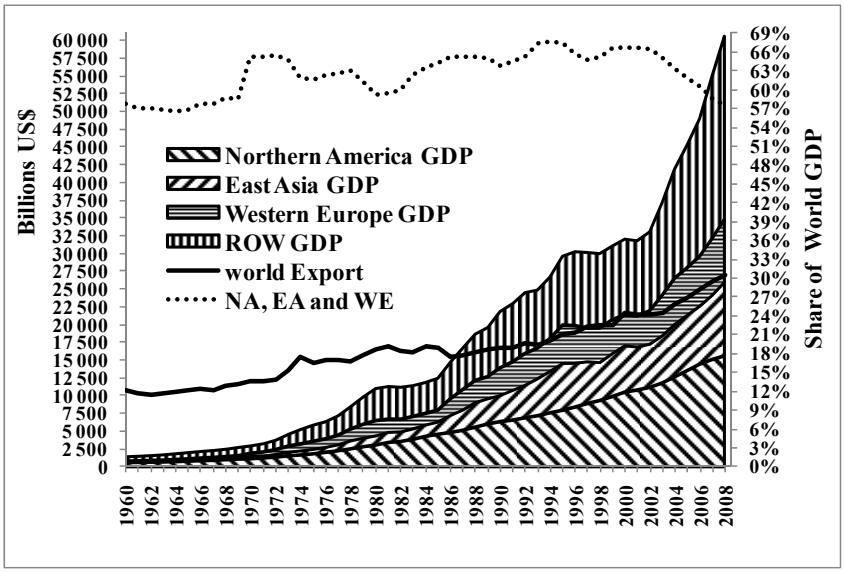

Fig. 1. The evolution of world, Northern America, East Asia and Western Europe GDP together with the corresponding fraction of world GDP in the 1960-2008 period

2. How to frame reduction of GHG emissions from freight transportation in a global economy?

2.1 Kyoto Protocol and GHG mitigation policy backgrounds

In 2011, the 193 member states of the United Nations have signed the Kyoto Protocol except Afghanistan, Andorra, and South Sudan (United Nations). Nevertheless, there are 193 signatories of the Kyoto Protocol as Cook Islands and Niue are considered as additional states and European Union as an added economic region. Among these 193 signatories, only the United States has not ratified the Protocol (United Nations). Being able to unify all these

countries around global climate change issue constitutes without doubt an international policy success but only 41 countries[2] grouped under the "Annex I" label are mandated with GHG emission reduction targets. Following the principles of historical responsibility and the right to development of developing and emerging countries, the UNFCCC determined on December 11th 1997 in Kyoto that reduction targets should first applied to developed countries. Therefore, Annex I countries are mainly developed countries and the Article 3 of the UNFCCC Kyoto protocol sets their GHG emissions must be at least 5 % below 1990 levels for the commitment period 2008 to 2012(United Nations). On the other hand, non-Annex I countries are only encouraged to elaborate and publish methodologies and datasets of the GHG emissions associated with their activities (United Nations). Therefore, build a comprehensive worldwide dataset of GHG emissions may be complicated due to the uncertainties associated with non-Annex I GHG emissions. Nevertheless, the 1990 reference emissions associated with Annex I countries represent as much as 63.7% of 1990 worldwide GHG emissions (United Nations). Furthermore, the Kyoto Protocol entered only into force on February 16th 2005 after more than 55% of 1990 GHG emissions of Annex I countries was concerned by the Protocol. These last figures means the lowest worldwide GHG emissions reduction target set by the Kyoto Protocol corresponds to a 1.8% reduction of the 1990 world GHG emissions[3]. Consequently, three main questions need to be addressed in regards to the Kyoto policy success:

- Has the reduction targets been reached for Annex I countries?
- How much represent Annex I countries GHG emissions in today's world?
- What has been the evolution of worldwide GHG emissions for the last twenty years?

The Annex I countries GHG emissions dropped from 18.73 $GtCO_2$ in 1990 to 17.76 $GtCO_2$ in 2008 thus achieving a 5.2% reduction in emissions. When comparing the average GHG annual emission level of the 1990-2008 periods with the 1990 emission level, the reduction achieved is 5.3%. Therefore, from the viewpoint of the reduction targets set for Annex I countries, the Kyoto protocol has reached its objectives. However, this success covers different stories as shown in **Figure 2**. Actually, Annex I countries without emission reduction targets has known a 10% increase of their average GHG annual emission while those with emissions reduction targets followed an opposite trend with a 13% decrease of average annual emission level. Consequently, Annex I countries without GHG emission targets of which the United States constitutes the main contributor (95%) represent 42% of total Annex I GHG emissions in 2008 against 34% in 1990. Furthermore, within the Annex I countries with targets, four main trends clearly appear:

- Countries with high increase in emission **(Canada , Oceania)**

[2] ***Non-EU Europe***: Belarus*, Croatia (-5%), Iceland (+10%), Liechtenstein (-8%), Monaco (-8%), Norway (+1%), Switzerland (-8%), Russian Federation (+0%), Ukraine (0%) ***EU27***: Bulgaria (-8%), Romania (-8%) ***EU25***: Czech Republic (-8%), Estonia (-8%), Hungary (-6%), Latvia (-8%), Lithuania (-8%), Malta*, Poland (-6%), Slovakia (-8%), Slovenia (-8%) ***EU15***: Austria (-8%), Finland (-8%), Sweden (-8%) ***EU12*** : Denmark (-8%), Greece (-8%), Ireland (-8%), Portugal (-8%), Spain (-8%), United Kingdom (-8%) ***EU6***: Belgium (-8%), France (-8%), Germany (-8%), Italy (-8%), Luxembourg (-8%), Netherlands (-8%) ***Oceania:*** Australia (+8%), New Zealand (+0%) ***Asia***: Japan (-6%), Turkey* ***America***: Canada (-6%), United States* (-7%)* ***Without target Annex I countries*** (United Nations)

[3] 5% reduction*55 % of Annex I GHG emissions*63.7% of world GHG emission=1.8% of world GHG emissions

- Countries with slow increase in emission **(Japan, Other EU6, EU12, EU15)**
- Countries with slow decrease in emission **(France)**
- Countries with high decrease in emission **(Russian Federation, Other Non-EU, Germany, EU25, EU27)**

Interestingly, while a 6.1% reduction of French GHG emissions is achieved in 2008 compared to 1990 level, this reduction drops to 0.9% when considering the average annual French GHG emissions of the 1990-2008 periods. Respectively, Japanese emissions increase from 1% to 4.7%. Therefore, though most statistics regarding climate change compares directly the 2008 emission level to those of 1990, we argue that considering the level of emissions averaged over the 1990-2008 periods better captures the historical evolution of GHG emissions. Indeed, the 2008 GHG emissions may correspond to a crisis year with low level of activities, thus setting a low GHG emission reference. Furthermore, in the perspective of an achievement of GHG emission reduction over the 2008-2012 periods and beyond, one needs to ensure the achieved GHG emission reduction are not cyclical and will not rise up as soon as the crisis period has ended.

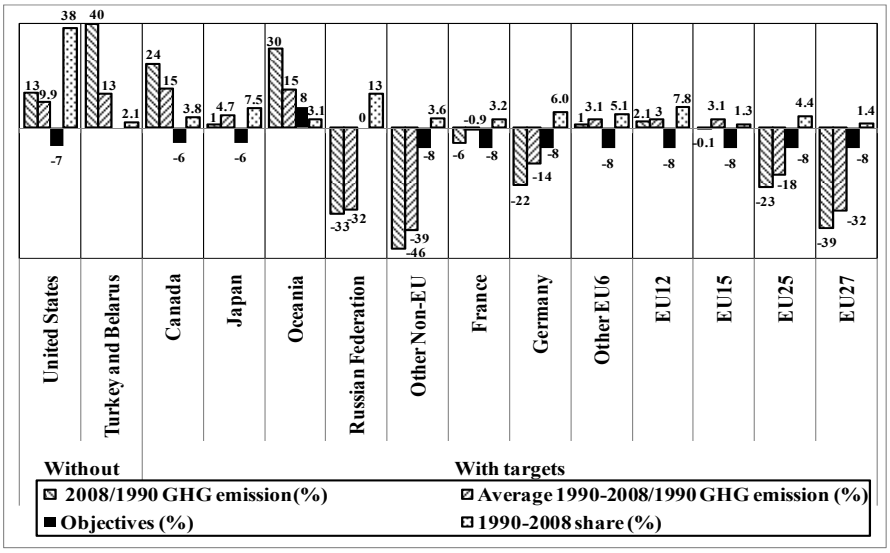

Fig. 2. Has the reduction targets been reached for Annex I countries? A direct ratio and cumulated ratio perspective

In this framework, as shown in **Figure 3a)**, the historical perspective of Russian federation emissions is straightforward: a huge decrease due to the former Soviet Union reconstruction until 1998 and a slow increase since then. The importance of the former Soviet Union reconstruction in the rapid decrease of European emissions is further confirmed by the profile of the evolution of German emissions[4]. Nevertheless, contrary to Russian federation,

[4] Indeed, the former DRG experienced a huge decrease of emission in the beginning of the nineties, 50% decrease in terms of CO_2 emission over the 1987 – 1993 period while the 1993 CO_2 emissions level of the former FRG is 2% more than 1987 level (United Nations, UNFCCC, 1994)

German decreasing emission trend has been going on after 1998 though at a slower pace. **Figure 3a)** allows a clearer distinction between Japan and Oceania historical evolution of emissions. While Oceania emissions are growing at a high rate especially in the 1995-2000 periods, Japan experienced their main rise in emission in the 1990-1994 periods before remaining around the same level until a huge drop in 2008 which may be due to financial crisis. Therefore, contrary to Oceania, Japan, though not fulfilling in 2008 its Kyoto target, seems to have at least stabilized its emissions. Finally, France, after some chaotic variation corresponding to the 1993-1994 recession period, experienced a slow decrease in its emissions between 1998 and 2005 followed by a higher decrease during the 2005-2008 periods. Interestingly, the beginning of this higher decrease period coincides with the introduction into the French Vth republic constitution of an environment charter (Digithèque MJP) and the entry into force of the Kyoto Protocol. Since then, environment has taken a stronger place in French policy debate but it should be noted that in spite of these late efforts, France has not in 2008 met its Kyoto targets.

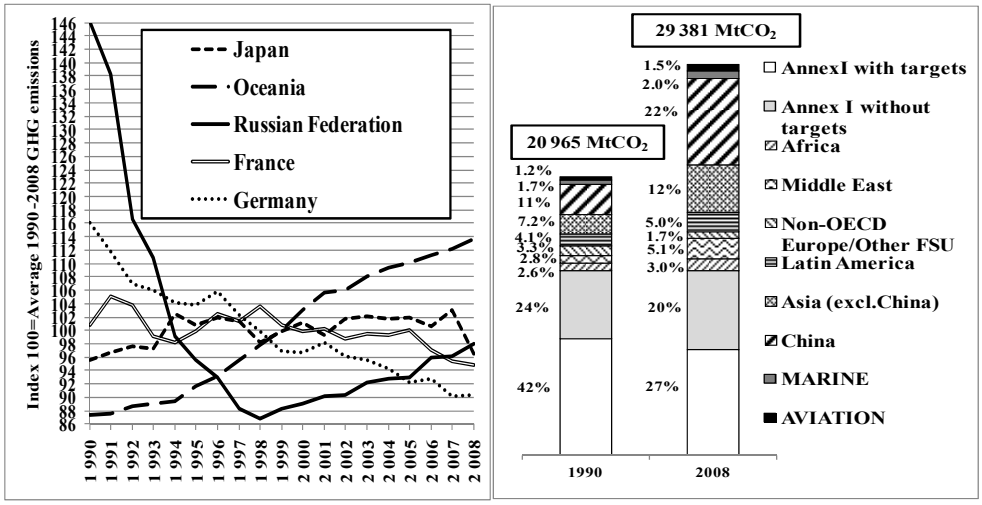

Fig. 3. a) A historical perspective of the evolution of GHG emissions compared to 2008 emission level.
b) Evolution of the structure worldwide energy-related emissions between 1990 and 2008

According to IEA report (IEA, 2010), the world carbon dioxide emissions associated with fuel combustion has increased by 40 percent during the period 1990 – 2008, from 21.0 $GtCO_2$ in 1990 to 29.4 $GtCO_2$ in 2008. During this period, the Annex I CO_2 emissions associated with fuel combustion has remained the same, thus showing the difficulties to implement CO_2 reduction when it comes to fuel combustion processes. Indeed, if the 2008 GHG emissions of Annex I countries are 5.2% less than those of 1990, their 2008 CO_2 emissions are only 2.2% less than those of 1990. This demonstrates that most of the GHG emission reduction achieved concerned GHGs other than CO_2 such as methane and nitrous oxide and that among CO_2 emission reduction, those concerning fuel combustion has particularly difficult to achieve. Furthermore, while Annex I countries represented 66% of world CO_2 emissions associated with fuel combustion in 1990, they represent only 47% of these in 2008.

Consequently, post-Kyoto policies must necessarily consider that more parties should get emission reduction targets and not only Annex I countries. As shown in **Figure 3b)**, Asian countries and particularly China should be among the first to get these emission reduction targets as their associated fuel combustion CO_2 emissions raised up from 19% of 1990 world emission to 34% of 2008 world emission. Indeed, when looking at the top20 CO_2 emitters in 2007, which alone cover 81% of the world CO_2 emissions, a worldwide pattern of CO_2 emissions clearly appear, Asia (35%), North America (23%), Europe (15%), Middle and Near Eastern countries (3.1%), Africa (1.5%), Oceania (1.3%) and South America (1.3%)[5]. Furthermore, among the top20 CO_2 emitters in 2007, Annex I countries represent 55% of the GHG emissions and only 30% if the United States who did not ratify the Kyoto protocol are taken out of Annex I countries emissions. Consequently, efficient post-Kyoto policies will have to deal with the increasing distribution of GHG emissions worldwide.

The globalization of trade and associated GHG emissions are logically connected to an increase of GHG emissions associated with international transportation. Actually, the 2008 CO_2 emission associated with international marine bunkers fuel combustion are 63% higher than those of 1990 while those of international aviation bunkers have increased by 76% over the same period. Moreover, transport represents 22% of world CO_2 emissions in 2008 thus constituting an important potential for mitigation policy. Nevertheless, global demand for transport appears unlikely to decrease in the foreseeable future as the *WEO 2009* projects that transport will grow by 45% by 2030(IEA, 2010). Noting that international bunkers emissions are not currently part of Kyoto protocol framework, the observed globalization of GHG emissions calls for the development of methodologies able to track down national and international bunkers emissions throughout the patterns of trade so as to ensure the best post-Kyoto GHG emission reduction international policy. However, current methodologies regarding GHG emission accounting framework mostly focus on national emission patterns and miss the trade perspective. Consequently, the next section presents the evolution of perspective required by the introduction of trade within the GHG emission accounting framework. Then section **2.3** focuses on the transportation aspects needed to frame a comprehensive macro-economic GHG emission accounting framework.

2.2 Production or consumption perspectives?

The GHG emission reduction targets of Annex I countries is based on a national GHG accounting framework which is thus production driven since all emissions resulting from national residents activities are assigned to the associated country. Particularly, this means that American companies, which are resident in France will contribute to French GHG emissions and not American ones. In the same perspective, French tourists visiting the United States contribute to American GHG emissions. This framework is thus in line with the Gross Domestic Product (GDP) framework which aggregates in monetary terms the results of residents' production but not with the Gross National Income (GNI) which would associate American companies in France with the United States.

[5] **Asia**: China (22%), India (5.5%), Japan* (4.3%), Republic of Korea (1.7%), Indonesia (1.4%) ; **Europe**: Russian Federation* (5.2%), Germany* (2.7%), United Kingdom* (1.8%), Italy* (1.6%), France* (1.3%), Spain* (1.2%), Ukraine* (1.1%) ; **North America**: United States* (20%), Canada* (1.9%), Mexico (1.6%) ; **Middle and Near Eastern countries**: Islamic republic of Iran (1.7%), Saudi Arabia (1.4%) ; **Africa**: South Africa (1.5%) ; **Oceania**: Australia* (1.3%) ; **South America**: Brazil (1.3%) ****Annex I countries***

The fact that GNI is generally different from GDP is a sign of the globalization process. However, even if imports and exports have roughly doubled between 2000 and 2009, the main contributing countries to globalization covering more than 50% of worldwide monetary exports and imports remain those of Western Europe, East Asia, and Northern America[1] thus creating three globalization driven attractive economic areas (dat). Nevertheless, the globalization process is still expanding and new globalization driven attractive economic areas will appear in the future. Notably, one of the consequences of this on-going process will result in an even more increasing inter-connection of countries GHG emissions than the one presented in section **2.1**. Consequently, two perspectives are offered to policy-makers:

- **The production perspective (PP)**: GHG emission reduction should be based on the amount produced by country as following the sovereignty principle, each state is the only one able to enforce emission reduction from its resident production activities. Therefore, the GHG emissions associated with the production perspective ($\mathbf{GHG_{PP}}$) is the sum of GHG emissions associated with resident production activities for their own consumption ($\mathbf{GHG_C}$) and those for exports ($\mathbf{GHG_E}$).
- **The consumption perspective (CP)**: GHG emission reduction should be based on the amount consumed by country as following the sovereignty principle, each state is the only one able to enforce emission reduction from its resident consumption activities. Therefore, the GHG emissions associated with the consumption perspective ($\mathbf{GHG_{CP}}$) is the sum of GHG emissions associated with resident production activities for their own consumption ($\mathbf{GHG_C}$) and those associated with imports ($\mathbf{GHG_I}$).

The difference between CP and PP results from the difference of GHG emissions embodied in exports and those embodied in imports. Therefore, while PP policy options only aims at improving national production GHG efficiency, CP policy options are dependent on the trade partners' production GHG efficiency. Consequently, the CP policy options would have to be more collaborative raising the issue of emission allocations between actors (Lenzen, et al., 2007).

For 2004, Davis and Caldeira determined that 23% of CO_2 worldwide emissions were traded internationally primarily as exports from china and other emerging markets to consumers in developed countries (Davis, et al., 2010). This result was further confirmed by Peters and Hertwich who determined that almost one-quarter of carbon dioxide emissions released to the atmosphere is emitted in the production of internationally traded goods and services (Peters, et al., 2008) thus calling for the introduction of trade within post-Kyoto policy debate (Peters, et al., 2008). Following this trade perspective at the Chinese national level, Ackerman determined that if Chinese exports and Chinese imports were produced with the U.S. carbon intensity, the CO_2 trade surplus would be close to zero as CO_2 emissions associated with Chinese exports would decreased by around 75%(Ackerman, 2009). Other studies regarding carbon embodied in trade were realized in developed countries[6]. All of these studies show as in **Figure 4** that CP leads to higher GHG emissions than PP for most of the developed Annex I countries.

On a policy level, this means the risk of carbon leakage is high as the developed countries could relocate GHG-intensive activities to a cheaper labor but less GHG efficient market and

[6] Austria (Kratena, et al., 2010), U.S (Weber, et al., 2007), France(Lenglart, et al., 2010)

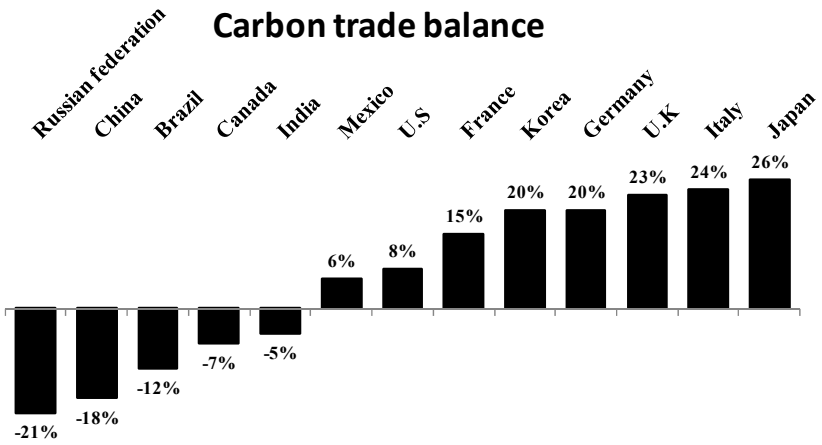

Fig. 4. Carbon trade balance for main GHG emitters' countries (Sustainable Consumption institute of the University of Manchester)

then import high GHG embodied goods, which are currently not accounted in the Kyoto framework. Therefore, it would be more politically sounded to evaluate CP emissions as it could help convince new emerging countries to join Annex I and get emission reduction targets. Furthermore, a comprehensive framework of the trade patterns is in line with the micro-economic perspective of life cycle assessment (LCA). Indeed, CP corresponds to the product perspective of carbon labeling policy, further explained in section **3.1**., and thus offers possibilities of bi or multi-lateral agreement between countries on the way to achieve reduction of GHG emissions for particular products or sectors.

Nevertheless, from a methodology perspective, CP is more data intensive than PP. Indeed, language, policy issues, non-recorded data, or data non-recorded at the same detailed level are examples of the barriers encountered to comprehensively associate data from trading countries. Furthermore, contrary to PP which only accounts in an aggregate way the national emissions, CP supposes to be able to track down imports, exports and production for national consumption separately thus raising the issue of data availability. Finally, though many environmental assessment methodologies are available such as material flow analysis (MFA), life cycle assessment (LCA) and input-output analysis (IOA) (Hertwich, 2005)(Wiedmann, et al., 2006), they do not cover the same perspectives. LCA and MFA are bottom-up approaches, consequently more suitable to micro-economic or company level, whereas IOA is a top-down approach more suitable to a macro-perspective. Particularly, multi-regional Input-Output analysis (MRIO) lies at the core of CP (Hertwich, et al., 2004), implemented in three ways depending on data availability:

- **The single region IO framework**: The analyst has been able to differentiate imports, exports, and national production for national consumption but has no data from other regions. A mirror-economy assumption is then used by giving the same economic structure and thus the same GHG efficiency to the trade partners which allows the distribution of GHG emissions to each import from and export to these countries. Nevertheless, the mirror economy assumption may be quite far from reality. Indeed, the

carbon efficiency of economies may vary a lot between developed and developing countries but between developed countries. For example, the French electricity carbon content is cleaner than the German one.

- **The without re-import/re-export MRIO framework**: IO tables from other countries with the associated emissions are available but it is supposed that direct trade predominates. Thus, it is assumed the production of imports for one country does not induce production within this country.
- **The comprehensive MRIO framework**: IO tables from all countries with full differentiation between imports and domestic technology matrices are available. Therefore, a comprehensive multi-lateral trade analysis can be made. This framework is data intensive.

In PP, national transportation analysis is straightforward as it can be associated with a particular country. However, it should be noted the transport sector is often not well represented within the national accounting framework leading to the making of IO tables. Moreover, international transport appears difficult to analyze, as they constitute by their international nature a complex allocation problem. To adopt CP changes the way to deal with the transportation allocation problem. Indeed, in this perspective, transportation is seen as part of a product story of life cycle. Consequently, the associated emissions go to the country that consumes the transported goods. However, may it be CP or PP, there is a need for the development of methodologies that better integrate freight transportation. Section 2.3 provides an overview of the last researches done in this direction. Sections 3.1 and 3.2 respectively present the carbon labeling policy framework within which transportation takes its full meaning and the related allocation issues.

2.3 Towards a better integration of GHG emissions from freight transportation

The MRIO framework explained in **2.2** though enabling the tracking of emissions embodied in trade with technology differentiations between nations misses to specifically address freight transportation. However, transportation key role in global trade and associated GHG emissions have been increasing ever since 1990. Therefore, new models have been developed to specifically address the issues associated with freight transportation such as food-miles and the connection between product, location of production, choice of transport mode and GHG emissions. These models are based on the IO framework but further differentiate transportation by applying a vector characterizing the Ton-kilometers (Tkm) driven for each sector before calculating the GHG emission associated through the application of physical based sounded ratio such as gCO_2/Tkm ratios.

For example, Webers and Matthews applied a single region IO framework to the U.S. together with an extended transport model to determine the impacts of transportation within the supply chain of food products (Weber, et al., 2008). They found the food-miles problem, namely the trade-off between buying locally or globally, was less important in terms of GHG emissions than the shifting diet problem. Therefore, they confirm the predominance of production climate impact over transportation climate impact for food products. Notably, their study pointed out red meat products top scoring on climate impact is only third when it comes to transportation GHG emissions. Indeed, transportation emissions associated with red mead was found within the same range of fruits, vegetable, and cereals products.

In their study on greenhouse gas emissions driven by the transportation of goods associated with French household consumption, Hawkins and Dente constructed a without re-import/re-export two regional IO model extended with a transportation model accounting for 116 sectors, 175 product types, 5 transport modes, 22 French regions and 42 foreign countries (Hawkins, et al., 2010). The imports coming from the 42 foreign countries were assumed to be produced using German technology, as IO tables were not available at a sufficient level of details for all the 42 countries. It was found that French household consumption was responsible for the emissions of 627 $MtCO_2e$ in 2004, 54% more than the 2005 French territorial CO_2 emissions and 14% more than the total CO_2 emissions driven by total 2005 French final demand as determined by the French National Institute of Statistics and Economic Studies (INSEE) through a six regional classical IO model including Germany, Italy, Belgium, U.K. and Spain in addition to France. Nevertheless, the INSEE study provided low values for agriculture since only dealing with CO_2 emissions and not GHG emissions contrary to the Hawkins and Dente study which showed that when dealing with GHG emissions, the agriculture sector accounted for as much as 23% of production and transport related emissions (cf. **Figure 5**). This difference in scope explains most of the result differences observed between the two studies, the rest of the difference being explained through a number of factors: better representation of national and international transportation with the specific transportation model for the Hawkins and Dente study, better representation of the technology differentiation for the INSEE studies as more regional IO tables are taken into account. Furthermore, it is interesting to notice the Hawkins and Dente study estimated to $14MtCO_{2e}$ the transportation occurring abroad for the purpose of French household consumption.

The above examples shows the use of transport specific models allows for a better tracking of flows within the supply chain of global economies and better represents the patterns of trade and international transportation, the fundamental features of globalization. Moreover, coupled with comprehensive MRIO models, these models allow for differentiation between indirect and direct emissions, transport modes emissions, sector and product differentiations, linkages between the final demand and the CO_2 global economic chain. **Figure 5** provides a good description of the achievement available through the application of such models, which provide important analyses and indications for national and supra-national policies such as national emission reduction planning and the Kyoto Protocol.

However, the application of transportation model supposes not only to have data to lead a comprehensive MRIO framework but data from transport satellite accounts for all countries. Therefore, the main problem is data availability and initiatives are made notably at the European level through the EXIOPOL project to offer harmonized detailed IO tables for all the EU-27 members (htt4). In this perspective, it should not be forgotten that non-Annex I Kyoto parties were encouraged to establish statistical competencies for the evaluation of their GHG emissions (United Nations). Moreover, the gCO_2/tkm ratio taken within transportation models can vary greatly depending on the goods transported and the upstream logistic choices, which determined load factor and empty trips ratio. Thus, take an average cross-technological gCO_2/tkm ratio can lead to errors in the determination of emissions and data from meso/micro levels are needed to address the problem of the greening of global supply chains. These questions are the purpose of section 3.

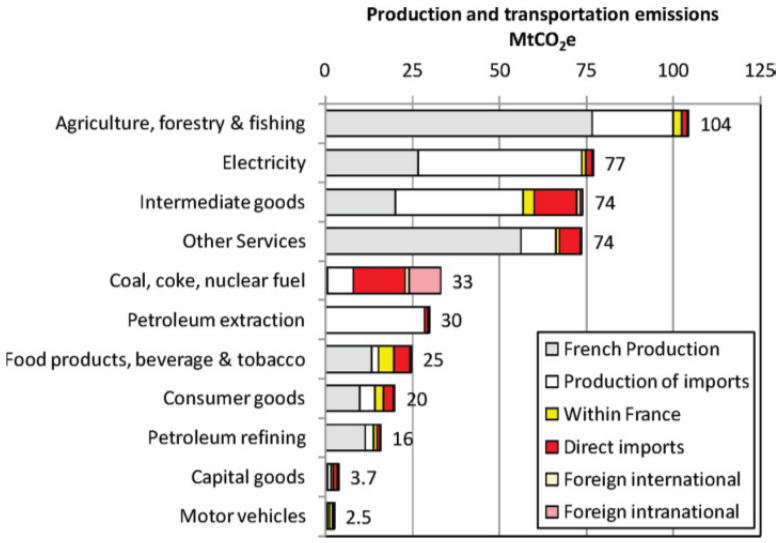

Fig. 5. Production and transportation emissions associated with French household consumption (Hawkins and Dente, 2010)

3. How to frame GHG reduction and ensure a greening of supply chains

3.1 The scientific, business and policy challenges of carbon labeling

At the most basic level carbon labeling involves associating an amount of CO_2 equivalent emissions with a product. Though seemingly simple in principle, carbon labeling schemes raise challenges upon application. These challenges make it difficult to standardize a method for quantifying CO2 equivalents for carbon labeling and open the possibility of litigation and controversy upon implementation.

Carbon labeling is closely tied to the complex relationship between companies, consumers, and policy makers. In section **2.2** we discussed two options for framing carbon labels, the producer perspective (PP) and the consumer perspective (CP). PP implies setting guidelines that move companies towards improving carbon efficiencies. These could take the form of thresholds, limitations, bans, externality-related taxation schemes, subsidies for cleaner production processes, and research efforts focused on improving or replacing dirty processes. CP shifts the focus to that of a consumer who is concerned with the overall impact of each product rather than the specific impacts of nodes in the supply network. In contrast to PP where policy actions focus on enhancing the carbon efficiency of individual actors or sectors based on their relevance to total territorial emissions, CP policy is focused on the community of actors involved in an individual product life cycle or basket of goods. From the perspective of a particular company, there are two strategic advantages to viewing their own environmental impacts from a consumer perspective and having policy-makers do so as well.

Quantifiable evidence of environmental performance is valued by customers:

Consumers choose products based on the information they receive. All else being equal, a consumer should choose the least costly option. However, the consumer's perception of

characteristics such as quality, durability, aesthetics, others' perceptions, and a number of other factors combine with price in the final decision of which items to purchase. In the absence of reliable environmental information, as is the case today, it might appear that consumers do not factor the environmental impacts of production processes into purchasing decisions (Llerena, et al., 2007). However, as rigorous environmental indicators find their way into the marketplace, the willingness to pay for improvements in the life cycle environmental quality of products will increase as a result of consumers' desire to convey a positive image to others through their choices and perhaps through an internal desire to view themselves as altruistic. When confronted by otherwise equivalent products resulting from different production processes, a well-informed consumer would not be as indifferent as might be predicted by a narrow interpretation of traditional economic theory. Within a society whose environmental conscience is growing, as is the case today, companies that provide information about environmental performance, demonstrate transparency, and continue to improve win market share over time to those that do not.

The enhanced efficiency of supply chains:

The usual framework to analyze competitiveness is to compare the cost structure and competitive advantage of actors producing similar products with the goal of becoming more cost-efficient while maintaining customer satisfaction. In the current globalized world, this framework still holds true but has evolved from the company level to the supply chain level. Each actor of the supply chain contributes to the comparative advantage of the entire network leading to product sales. In such a complex system often, local optimization does not correspond with the optimization of the global system and can even result in worsening the previous situation. First generation biofuels and the replacement of lead solder exemplify how a narrow approach to the optimization can result in global worsening. While biofuels were seen as attractive replacements for fossil fuels because carbon uptake by plant biomass would off-set the releases upon combustion, further analysis suggests the combined impacts of inputs to agricultural production, soil carbon loss, and other factors may well drive an overall higher carbon footprint. In the case of solder, lead was replaced by costlier substitutes such as silver, with greater extraction- and processing-related impacts, and potentially the same or higher toxicity considering exposure routes along their supply chains. Although these examples are controversial and dependent on which factors are considered in the optimization, we present them here for illustrative purposes.

Although the scope of decision-making for a company lies within its own operations, considering each company relies on the supply network within which it exists, the consumer perspective better addresses overall competitive advantage. Furthermore, CP does not exclude improvements in the carbon efficiency of individual actors, but through the broader perspective, it deals with offers the possibility to transform the investments made in these improvements into market strengths.

In spite of the expected benefits from the implementation of CP for companies, most of the efforts so far have been policy driven. For example, the EU sustainable consumption and production, which includes eco-labeling, aims at reducing the negative impact of consumption on the environment, health, climate, and natural resources. On 24th November 2009, the European parliament resolved to widen the EU eco-label scope in terms of impacts and product categories to avoid the proliferation of environmental labeling schemes and to encourage improvement in all sectors for which environmental impact affects consumer choice

(Reg11). More recently in France, the Operational Committee on Consumption, Ecological Price and Competitive Advantage of the "Grenelle de l'environnement" announced that environmental information will be required for each product beginning 1st January 2011 (Ministère de l'Ecologie, du Développement durable, des transports et du logement). Though this goal is still in the process of being realized a proposition within the consumption code approved by the French Senate (Article 85) requires carbon cost labeling (htt1). This will be provided on an experimental basis beginning in July 2011 (Afnor-Normalisation).

To answer the raising environmental awareness of their consumers and the compulsory labeling policies driven by policy makers, businesses nevertheless took actions towards the reporting of their emissions, as the increasing number of carbon accounting tools tends to prove. An international benchmarking of carbon accounting tools realized by the French Environment and Energy Management Agency (ADEME) shows that this new market of environmental accounting tools concerns mainly Annex I countries of the Kyoto Protocol[7] and the United Nations Environmental Program (UNEP)(ADEME, 2008). On the 62 accounting tools reviewed, 10 are ONG's, 39 related to private businesses activities and 13 are governments'. Consequently, there is seemingly some serious environmental commitment from business companies. Nevertheless, while governments' and ONG's solutions are oriented towards emission reduction, a large majority of private accounting tools corresponds to the needs of companies to compensate emissions thus not enabling exhaustive emission accounting. Furthermore, most of the solutions are site and territory oriented since only ten of the accounting tools reviewed includes a product orientation. This demonstrates that today's accounting tools are in line with the policy framework developed by nations to achieve their Kyoto targets but are not sufficient to embrace the policy objectives of carbon labeling neither those of sustainable consumption. They lack interconnection with the different aspects of their activities to comprehensively accumulate emissions from each node of the supply chain and allocate them to the final consumer products.

However, ideally, the link between PP carbon accounting and CP carbon labeling is straightforward. Actually, let us assume that each company implied in the making and delivery of a product to the final retailer[8] is able to provide for each of their products the associated amount of CO_2 equivalent emitted. If we consider that N companies are implied in the making and delivery of product i and M as the total number of different products produced by these N companies, our previous assumption allows us to build a M times N dimension table (CO_2). Coefficient $CO_{2_{i,j}}$ represents the amount of CO_2 equivalent associated with product i emitted by company j. In this mathematical framework, the PP carbon accounting framework appears as a sum across the rows $(CO_{2,j})$ while the CP carbon-labeling framework corresponds to a sum across the columns $(CO_{2,i})$.

$$CO_2 = \begin{pmatrix} CO_{2_{1,1}} & \cdots & CO_{2_{1,j}} & \cdots & CO_{2_{1,N}} \\ \vdots & \ddots & \vdots & \ddots & \vdots \\ CO_{2_{i,1}} & \cdots & CO_{2_{i,j}} & \cdots & CO_{2_{i,N}} \\ \vdots & \ddots & \vdots & \ddots & \vdots \\ CO_{2_{M,1}} & \cdots & CO_{2_{M,j}} & \cdots & CO_{2_{M,N}} \end{pmatrix} \quad (1)$$

[7] France, Germany, U.K., Australia, U.S.A, Canada, Netherlands, Japan

[8] The final retailer constitutes the final place of purchase but not of consumption. This distinction is important for future researches on the subject.

$$CO_{2,i} = \sum_{j=1}^{N} CO_{2_{i,j}} \quad \text{and} \quad CO_{2,j} = \sum_{i=1}^{M} CO_{2_{i,j}} \tag{2}$$

However, the establishment of these coefficients is rarely straightforward. Consequently, one of the major scientific challenges concerning carbon labeling lies in the allocation issues that are associated with the determination of these coefficients. The main features of these allocation issues are presented and analyzed in the next section **3.2**.

3.2 The allocation issues of carbon labeling

3.2.1 The allocation issue within a company

The scope of decision-making for a company lies within its own operations such as the transformation of purchased products, the business travels, the storing of raw materials, work-in-progress and finished products, the lightning and daily management of buildings and so on. The first challenge to ensure good management of GHG emissions at the company level is thus to allocate GHG emissions to each operation. This is not easy as different levels of complexity are intertwined within companies:

- Physical complexity linked to the industrial processes. Process engineering and management of complex physical systems constitute the main features of this complexity.
- Management complexity linked to the company objectives. Depending on the company business model, the complexity of management deals with socio-economic and physical indicators.

Regarding physical complexity, a first option would be to provide a continuous measurement of the emissions on every workstation. This would mean that each work station provide measurement of GHG emissions while delivering its work. Such framework is thus heavily based on electronic devices. The fact that many Annex I countries[9] have started implementation projects of smart meters as home energy monitors exemplifies how measurement device constitutes the understanding basis of the energy use at consumers' home. Notably, the United Kingdom counts on smart meters to address the greening of everyday energy-consuming behaviors through the completion of the smart meter roll-out in 2019 (Beh11). Nevertheless, smart meters are electronic devices and therefore consume non-renewable resources such as minerals and imply high-energy intensive processes in their making. Consequently, a trade-off between the environmental benefits that could be gained from the use of smart meters with the environmental costs associated with their life cycle must be found. A good way of avoiding the use of measurement systems is to base the determination of GHG emissions on explanatory variables through the use of physical models. One of the main advantages of using physical models is to adopt better manageable variables. For example, knowing that 1 toe corresponds to 1616 kg of coal, a company can at the same time track down their coal purchase in tons and calculate the energy they will use when burning it. Therefore, through calculation, physical models allow to multiply the benefits associated with a particular measurement. Nevertheless, the emissions associated with physical models are often determined in standardized conditions that may reveal quite far from reality. For instance, combustion process is sensitive to the environment

[9] Italy, Japan, Canada, United Kingdom, United States, Australia, New Zealand, Netherlands, Spain, France, Ireland, Italy, Malta, Sweden, Finland, Norway (Sma11)

temperature pressure and air/gasoline ratio and consequently would need to be associated with real-time measurements. Therefore, an uncertainty is always attached to the use of a physical model so that two companies using the same physical model and reporting two different GHG emission factor within the uncertainty range should be considered as having the same emission factor. Furthermore, direct measurement of GHG emissions should be preferred in the case of highly variable physical phenomena for which physical model are difficult to implement.

The management complexity consists in the organization of industry activities, the daily management of tasks and business travels together with the choices of processes. These decisions influence a lot the GHG efficiency of a company. Therefore, the allocation issue consists here in associating emissions with decision-making processes and is dependent on the time-framework chosen for the analysis. Electricity gives a good illustration of this point. Indeed, if we consider real-time measurement, assuming that $CO2^{j}_{k}$ is the per kWh emission factor determined for the power plant k based on primary energy source j, the carbon content of 1kWh delivered to the network is:

$$CO2_{\text{network}}(t) = \frac{\sum_{Network}\left(kWh_k^j(t) \times CO2^{j}_{k}(t)\right)}{\sum_{Network} kWh_k^j(t)} \quad (3)$$

Getting the level of carbon emission at the yearly level would imply to sum the previous framework over time. In this ideal case, we thus obtained a comprehensive framework of emission per energy source with a timeline result. However, in present days, these kind of accurate data are not easily available. The electricity productions for each power plant are often given at the yearly level. Furthermore, there is often only a simple distinction of emission factors based on energy sources. The carbon content of 1 kWh delivered by the network is thus constant over the year:

$$CO2^{\text{year}}_{\text{network}} = \frac{\sum_{Network}\left(kWh_k^{j,year} \times CO2^{j,year}\right)}{\sum_{Network} kWh_{k,year}^{j}} \quad (4)$$

The difference between (4) and (3) exemplifies how important the time-management framework chosen can influence a GHG analysis. Furthermore, one cannot differentiate electrons on the electric network and it is thus physically not possible to source the origin of electricity used on the network to a specific power plant. Therefore, no one on the network use cleaner energy than the other at a given time. The ways to get cleaner electricity delivered at one particular moment are thus:

- Replace old power plants by newer and more performing ones $\left(CO2^{j}_{k}\right)$
- Improve the electricity transformation process based on primary source j $\left(CO2^{j}_{k}\right)$
- Change the primary energy source structure of the electricity delivered to the network $\left(kWh_k^j\right)$

The example of electricity demonstrates the difficulty of an accurate calculation and allocation of GHG emissions. First in terms of physical complexity, there is a need for standardization of the assumptions used in physical models. The lack of standardization and the difference of scope between studies are indeed the main features of green washing. By green washing, we define any communication using abusively ecological argumentation

(Afnor Normalisation). The abusive character of green washing can be based on insufficient scientific methods in data collection, modeling, allocation methods, or the use of sounded GHG inventories outside their uncertainty ranges. All these issues can lead to the communication of wrong or not meaningful GHG emission figures. Furthermore, in addition to the previous difficulties in the determination of GHG emissions, the absence of transparency on the method used to calculate GHG emission is often the main obstacle to decide whether or not there is a risk of green washing. Therefore, the reproducibility of the calculation methodology is essential to provide a clear allocation of GHG emissions related to physically complex phenomena. Once the physical characteristics of GHG emissions allocation are solved, it becomes important to understand how to use this information to take decisions that enhance the carbon efficiency of the company and the supply chain within it exists. As said before, such decisions refer to management complexity, which is dependent on the number of actors involved in the decision-making process. Freight transportation is characterized by an important number of actors thus raising interesting allocation issues related to management complexity. Section **3.2.2** presents some of these aspects.

3.2.2 The allocation issues related to transportation

Transportation is a service allowing the physical connection between two companies through the moving of goods. It is thus characterized by a complex set of actors: 1st party logistic providers (shipper, consignee), 2nd party logistic providers (carriers), 3rd party logistic providers (freight forwarders), and 4th party logistics providers (consulting and IT activities). These actors may have different interests and may not search to optimize the same aspects of the transport chain. A good example is given in the railway sector.

- The shipper wants to optimize the delivery of the goods it provides in terms of cost, reliability, etc.
- The carrier wants to optimize the routing of all the goods received from different shippers to minimize costs such as fuel expenses.
- The owner of goods wagons wants the use optimization of his assets

Therefore, optimization trade-offs need to be found between these different perspectives. This would mean that all actors implied in the transportation process are willing to optimize the all process rather than the small part they are responsible for. This holds particularly true for the problem of empty trips, which correspond to the transport of empty wagons. This problem exists for the other transport mode such as road transportation where the term empty truck is used. Who should thus be responsible for the GHG emissions associated with empty trips?

One could take the position of the EcoTransIT world tool intended to be used by shippers that want to estimate the emissions associated with a particular transport activity or a set of different transport options: the shipper or freight owner takes responsibility for the vessel utilization factor that is averaged over the entire journey, from the starting point to the destination as well as the return trip or the entire loop respectively (Eco). This allocation process is coherent with an LCA perspective as it allows for the tracking of emission associated with a particular good. However, accuracy on the routing of empty wagons is

difficult to achieve as no commercial contract is linked to the moving of empty wagons. Furthermore, the decision regarding the management of empty wagons concerns as well the initial shipper, the owner of the wagon and the carrier. The latter must not only take into account the needs of the initial shipper but those of the other shippers to whom the empty wagons will be sent to be loaded.

Such complex patterns would not be a significant problem regarding allocation of GHG emissions if the level of empty trip did not have such an important effect on the GHG emission level. Indeed, according to a Mc Kinnon study (ECTA, Responsible Care and Cefic, 2011), the gCO_2/tonne-km emission factor for a 40-44 tonne trucks running 50% of its km empty is between 61% and 87% higher than when there is no vehicle-km run empty. Therefore, in the context of a carbon pricing, such differences will directly result in economic opportunity or losses. The same types of problems are encountered in the international maritime transportation area where the interdependencies of actors are even more complex. Indeed, the diversity of countries involved and notably the possibility to endorse a flag of convenience makes the determination of responsibility utterly complex. The term flag of convenience describes the business practice of registering a merchant ship in a sovereign state different from that of the ship's owners. The main interest for doing so is to reduce operating costs or avoid the regulations, notably taxes and environmental regulations, of the owner's country. Nevertheless, this situation makes it difficult to identify the ship owner and enforce a fair environmental post-Kyoto policy based on the allocation of emissions to the ship owner's state.

4. Conclusion

The present chapter has demonstrated the importance of globalization in regards to climate change and the necessity to include the trade perspective to enforce effective post-Kyoto policies. Such macro-policy framework is highly based on a better description of the GHG emissions associated with national and international freight transportation. Furthermore, the chapter revealed the difficulties of allocation associated with current policies notably in multi-actors sectors such as those of transport and logistics. **Figure 6** represents the hierarchy between the different allocation schemes explained in this chapter through an improvement loop. Doing so allows a clearer understanding of the distinction between scientific and policy driven procedures of allocation while maintaining the link between them. This framework shows where the opportunity for new researches stand:

- Improvement of measurement systems.
- Improvement of physical models so as to better capture the reality of physical processes.
- Improvement of collaboration between economic actors for the determination of environmental and market efficient allocation rules.
- Change in economic accounting practices and trade pattern through the implementation of more environmentally friendly business models such as Product Service System.

The non-exhaustive list above offers a glimpse of the path towards more sustainable grounds for supply chains and society.

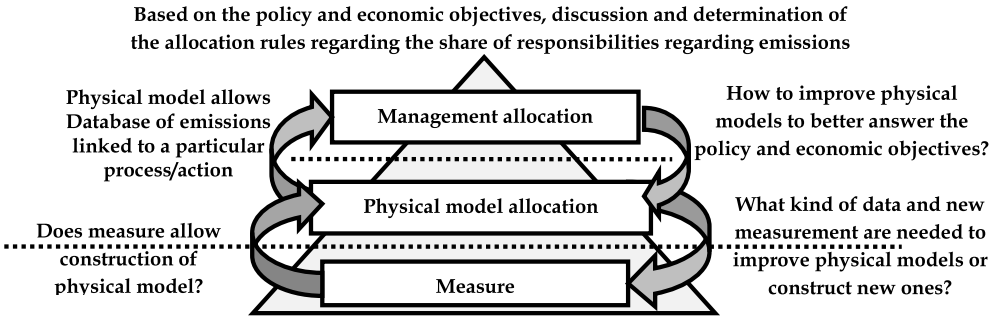

Fig. 6. The hierarchy between the different allocation steps and the on-going improvement process

5. References

[En ligne]. - http://www.feem-project.net/exiopol/.

[En ligne]. - http://www.senat.fr/rap/l08-552-1117.html.

Ackerman Franck Carbon Embedded in China's Trade [Rapport]. - Somerville - US : Stockholm Environment Institute, 2009.

ADEME Réalisation d'une veille internationale relative aux outils et méthodes d'évaluation globale des émissions de gaz à effet de serre et des démarches de réduction associées [Rapport]. - 2008.

Afnor Normalisation Guides pratique des allégations environnementales à l'usage des professionnels et des consommateurs [En ligne] // Affichage environnemental des produits de grande consommation - Actualités. - 04 08 2011. - http://affichage-environnemental.afnor.org/actualités.

Afnor-Normalisation Mission [En ligne] // Affichage environnemental des produits de grande consommation. - 05 08 2011. – http://affichage-environnemental.afnor.org/mission.

Behaviour change and energy use [En ligne] // Department of Energy and Climate Change. - 24 08 2011. - http://www.decc.gov.uk/en/content/cms/emissions/beh_change/beh_change.aspx.

Cetinkaya Balkan [et al.] Sustainable Supply Chain Management [Livre]. - Heidelberg Dordrecht London New York : Springer, 2011. - ISBN. data trade [En ligne].

Davis Steven J. et Caldeira Ken Consumption-based accounting of CO2- emissions [Article] // PNAS. - 2010. - 12 : Vol. 107.

Digithèque MJP Loi constitutionnelle n°2005-205 du 1er mars 2005 relative à la charte de l'environnement [En ligne] // Constitution de la Vème République. - 23 08 2011. - http://mjp.univ-perp.fr/france/co1958-19.htm.

EcoTransIT world methodology and data [En ligne] // Ecological Transport Information Tool for Worldwide Transport. – http://www.ecotransit.org/download/ecotransit_background_report.pdf.

ECTA, Responsible Care and Cefic Guidelines for measuring and managing CO2 emission from freight transport operaitons [Rapport]. - 2011.

Hawkins Troy R. et Dente Sébastien M.R. Greenhouse Gas Emissions Driven by the Transportation of Goods Associated with French Consumption [Article] // Environ. Sci. Technol.. - 2010.

Hertwich Edgar et Peters Glen Production factors and pollution embodied in trade - Theoretical Development [Rapport]. - Trondheim : NTNU - Program for industriell økologi, 2004.

Hertwich Edgar G. Life cycle approaches to Sustainable Consumption: A critical Review [Article] // Environmental Science & Technology. - 2005. - 13 : Vol. 39.

IEA CO2 emissions from fuel combustion - Highlights [Rapport]. - [s.l.] : IEA, 2010.

Kratena Kurt et Meyer Ina CO2 Emissions Embodied in Austrian International Trade [Rapport]. - [s.l.] : FIW, 2010.

Lenglart Fabrice, Lesieur Christophe et Pasquier Jean-Louis Les émissions de CO2 du circuit économique en France [Rapport]. - Paris : [s.n.], 2010.

Lenzen Manfred [et al.] Shared producer and consumer responsibility - Theory and practice [Article] // Ecological Economics. - 2007. - 61. - pp. 27-42.

Llerena Daniel et Michaud Céline Révélation des consentements à payer pour des produits remanufacturés [Section du livre] // Les systèmes de production applications interdisciplinaires et mutations / auteur du livre Boujut jean-François, Llerena Daniel et Brissaud Daniel. - [s.l.] : Lavoisier, 2007. - ISBN 978-2-7462-1819-2.

Ministère de l'Ecologie, du Développement durable, des transports et du logement Les 34 chantiers opérationnels (COMOP) [En ligne] // le Grenelle Environnement. - 05 08 2011. – http://www.legrenelle-environnement.fr/IMG/pdf/rapport_final_comop_23.pdf.

Noussair C., Robin S. et Ruffieux B. Do consumers really refuse to buy genetically modified food? [Article] // The Economic Journal. - 2004. - 114.

Peters Glen P. et Hertwich Edgar G. Post Kyoto greenhouse gas inventories: production versus consumption [Article] // Climatic Change. - 2008. - 86: 51-66.

Peters Glen P. et Hertwich Edgar G. Trading Kyoto [Article] // nature reports climate change. - 2008. - Vol. 2.

Regulation (EC) N°66/2010 of the European Parliamant and of the council of 25th November 2009 on the EU Ecolabel [En ligne] // EUR-Lex Access to European Union Law. - 04 08 2011. - http://eur-lex/europa.eu/LexUriServ/LexUriserv.do?uri=OJ:L:2010:027:0001:0019:EN:PDF.

Smart meter [En ligne] // Wikipédia. - 24 08 2011. – http://en.wikipedia.org/wiki/Smart_meter.

Sustainable Consumption institute of the University of Manchester Consumer, business and climate change [Rapport].

Ton of oil equivalent [En ligne] // National Institute of Statistic and Economic Studies. - 24 08 2011. – http://www.insee.fr/en/methodes/default.asp?page=definitions/tonne-equivalent-petrole.htm.

United Nations [En ligne]. - 1 08 2011. - http://www.un-documents.net/ofc-02.htm#I.

United Nations Member States of the United Nations [En ligne] // United Nations. - 19 08 2011. - http://www.un.org/en/members/#n.

United Nations Parties to the Convention and Observer States [En ligne] // UNFCCC. - 19 08 2011. - http://unfccc.int/parties_and_observers/parties/items/2352.php.

United Nations Protocole de Kyoto à la convention cadre des nations Unies sur les changements climatiques [En ligne]. - 1 08 2011. – http://unfccc.int/resource/docs/convkp/kpfrench.pdf.

United Nations Status of Ratification of the Kyoto Protocol [En ligne] // UNFCCC. - 19 08 2011. - http://unfccc.int/kyoto_protocol/status_of_ratification/items/2613.php.

United Nations United Nations Framework Convention on Climate Change [Rapport]. - 1992.

United Nations, UNFCCC Résumé analytique de la communication nationale de l'Allemagne [Rapport]. - 1994.

Weber C. et Matthews H.S. Embodied Environmental Emissions in U.S. International Trade, 1997 – 2004 [Article] // Environmental Science and Technology. - 2007. - 4875 – 4881 : Vol. 41.

Weber C. L. et Matthews H. S. Food-miles and the relative environmental impact of food choices in the United States [Article] // Environ. Sci. Technol. - 2008.

Wiedmann Dr. Thomas [et al.] Sustainable Consumption and Production - Development of an Evidence Base [Rapport]. - York : Stockholm Environment Institute, 2006.